# TUMOR MICROENVIRONMENT AND RESISTANCE TO CURRENT THERAPIES

EDITED BY: Ahmed Lasfar, Andrew Zloza, Karine A. Cohen-Solal and Murugabaskar Balan

PUBLISHED IN: Frontiers in Pharmacology and Frontiers in Oncology

frontiers Research Topics

# frontiers



ISSN 1664-8714
ISBN 978-2-88963-283-1
DOI 10.3389/978-2-88963-283-1

## About Frontiers

Frontiers is more than just an open-access publisher of scholarly articles: it is a pioneering approach to the world of academia, radically improving the way scholarly research is managed. The grand vision of Frontiers is a world where all people have an equal opportunity to seek, share and generate knowledge. Frontiers provides immediate and permanent online open access to all its publications, but this alone is not enough to realize our grand goals.

## Frontiers Journal Series

The Frontiers Journal Series is a multi-tier and interdisciplinary set of open-access, online journals, promising a paradigm shift from the current review, selection and dissemination processes in academic publishing. All Frontiers journals are driven by researchers for researchers; therefore, they constitute a service to the scholarly community. At the same time, the Frontiers Journal Series operates on a revolutionary invention, the tiered publishing system, initially addressing specific communities of scholars, and gradually climbing up to broader public understanding, thus serving the interests of the lay society, too.

## Dedication to Quality

Each Frontiers article is a landmark of the highest quality, thanks to genuinely collaborative interactions between authors and review editors, who include some of the world's best academicians. Research must be certified by peers before entering a stream of knowledge that may eventually reach the public - and shape society; therefore, Frontiers only applies the most rigorous and unbiased reviews.
Frontiers revolutionizes research publishing by freely delivering the most outstanding research, evaluated with no bias from both the academic and social point of view. By applying the most advanced information technologies, Frontiers is catapulting scholarly publishing into a new generation.

## What are Frontiers Research Topics?

Frontiers Research Topics are very popular trademarks of the Frontiers Journals Series: they are collections of at least ten articles, all centered on a particular subject. With their unique mix of varied contributions from Original Research to Review Articles, Frontiers Research Topics unify the most influential researchers, the latest key findings and historical advances in a hot research area! Find out more on how to host your own Frontiers Research Topic or contribute to one as an author by contacting the Frontiers Editorial Office: researchtopics@frontiersin.org

# TUMOR MICROENVIRONMENT AND RESISTANCE TO CURRENT THERAPIES

Topic Editors:
**Ahmed Lasfar,** Rutgers, The State University of New Jersey, United States
**Andrew Zloza,** Rush University Medical Center, United States
**Karine A. Cohen-Solal,** Rutgers, The State University of New Jersey, United States
**Murugabaskar Balan,** Boston Children's Hospital, Harvard Medical School, United States

**Citation:** Lasfar, A., Zloza, A., Cohen-Solal, K. A., Balan, M., eds. (2020). Tumor Microenvironment and Resistance to Current Therapies. Lausanne: Frontiers Media SA. doi: 10.3389/978-2-88963-283-1

# Table of Contents

frontiers in Oncology

EDITORIAL
published: 14 November 2019
doi: 10.3389/fonc.2019.01131

# Editorial: Tumor Microenvironment and Resistance to Current Therapies

*Ahmed Lasfar*[1,2*], *Murugabaskar Balan*[3], *Karine A. Cohen-Solal*[1†] *and Andrew Zloza*[4]

[1] Rutgers Cancer Institute of New Jersey, Rutgers, The State University of New Jersey, New Brunswick, NJ, United States, [2] Department of Pharmacology and Toxicology, Ernest Mario School of Pharmacy, Rutgers, The State University of New Jersey, New Brunswick, NJ, United States, [3] Harvard Medical School, Boston Children's Hospital, Boston, MA, United States, [4] Rush University Medical Center, Chicago, IL, United States

**Keywords: cancer resistance, tumor—targeting, tumor microenvironment, immunotherapy, therapy resistance, cancer cell signaling, targeted therapy**

## Editorial on the Research Topic

## Tumor Microenvironment and Resistance to Current Therapies

The tumor microenvironment (TME) constitutes an important component of any cancer. The histology of TME consists of a series of normal resident cells and a variety of recruited cells, which are involved in complex and dynamic interactions with cancer cells (**Figure 1**). These interactions, which occur via released factors or cell-to-cell contact, are fundamental in tumor-induced suppression and metastatic dissemination of cancer cells, ultimately leading to morbidity and/or mortality for the majority of cancer patients. Considerable progress has been made in understanding the mechanisms by which the TME contributes to the inhibition or promotion of cancer, enabling the emergence of a range of novel targeted therapies. In addition to stroma-targeted strategies, checkpoint inhibitor-based immunotherapy has emerged as a new treatment of choice for many advanced cancers. However, many cancer patients remain resistant to current therapies, necessitating the development of more innovative therapeutic strategies based on the identification of new targets and combining drugs that could counteract resistance. In the present issue, "Tumor microenvironment and resistance to current therapies," authors highlight this aspect in the included articles describing innovative and impactful studies.

In this Research Topic, diverse facets of the TME are addressed, including different tumor types and tissue specificity of TME (**Figure 1**). Recently, the TME has emerged as a key player in both drug efficacy and chemoresistance, impelling the development of novel therapeutic strategies. Despite constant progress in antitumor drug development, multidrug resistance (MDR) is still a major challenge for effective patient treatment. Sachs et al., describe a novel method for overcoming this problem by demonstrating, in different cancer models, the ability of new small molecules to reverse chemotherapy resistance. Munoz et al., address the problem of chemoresistance of glioblastoma multiforme (GBM), a fatal malignancy of the central nervous system. They show that MiR-93 and−193 are specifically expressed in temozolomide (TMZ) resistant glioblastoma cells (GBM), including resistant neurospheres from a patient with TMZ resistance. Part of the resistance occurs by miR-93 and−193 decreasing Cyclin D1 to reduce GBM cycling. This may open up avenues for new therapeutic approaches to reverse such chemoresistance (Munoz et al.). Besides chemoresistance in GBM, expansion of residual glioma cells is also a challenge in the context of chemotherapy. Work by Tsidulko et al., indicates that conventional anti-glioblastoma therapy such as TMZ affects proteoglycan structure and composition of normal brain tissue. Proteoglycan alteration may be involved in brain extracellular matrix (ECM) deterioration and the development of residual glioma cells (Tsidulko et al.).

Although immune checkpoint blockade therapy has afforded new hope for the durable treatment of many cancers, it has not provided yet substantial benefit to patients with glioblastoma. Utilizing a series of epidemiological, genome expression, and immunome databases,

OPEN ACCESS

***Edited and reviewed by:***
*Wafik S. El-Deiry,*
*Brown University, United States*

***Correspondence:**
*Ahmed Lasfar*
*ahmed.lasfar@pharmacy.rutgers.edu*

***†Present address:***
*Karine A. Cohen-Solal,*
*Lambda Pharmaceuticals,*
*Bridgewater, NJ, United States*

***Specialty section:***
*This article was submitted to Cancer Molecular Targets and Therapeutics, a section of the journal Frontiers in Oncology*

***Received:*** *24 June 2019*
***Accepted:*** *10 October 2019*
***Published:*** *14 November 2019*

***Citation:***
*Lasfar A, Balan M, Cohen-Solal KA and Zloza A (2019) Editorial: Tumor Microenvironment and Resistance to Current Therapies. Front. Oncol. 9:1131. doi: 10.3389/fonc.2019.01131*

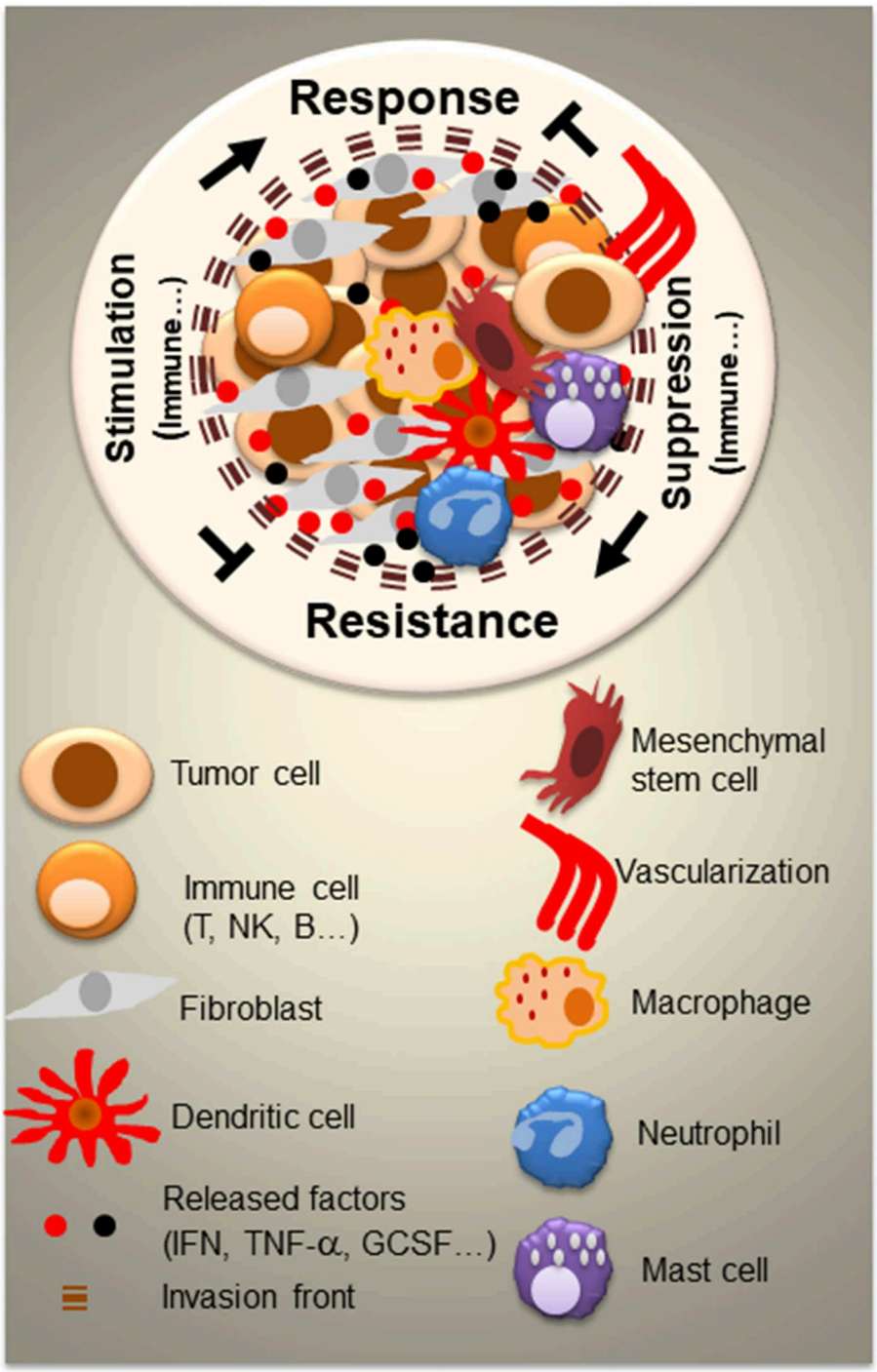


**FIGURE 1 |** Tumor microenvironment (TME) and the complexity of interactions between resident and recruited normal cells and tumor cells. Besides tumor cells, the tumor TME consists of a variety of normal cells and factors which can be serves as mediators for both cancer control and cancer outgrowth. Normal cells are either resident cells or recruited cells. They vary from each cancer type and level of cancer progression. In large part, they consist of immune cells (T, B, and NK cells, mast, dendritic cells, macrophages, and neutrophils) and non-immune cells such as fibroblasts and mesenchymal stem cells. All of the cells release and respond to a variety factors (IFN, TNF-α, GCSF,…) and engage in cell-to-cell contact. Cell signaling within the TME represents a crucial key for the design of successful therapeutic strategies.

Ladomersky et al., demonstrate a significant association between advanced age of patients and immunosuppression in the circulation and central nervous system. Based on their findings, the authors propose that normal human aging suppresses immune surveillance and immunotherapeutic efficacy against glioma, and thus, contributes to GBM initiation and progression (Ladomersky et al.).

Using a lung cancer model, Yang et al., focus their study on bronchoalveolar lavage fluid-derived exosomes, released in the TME and demonstrate their role in fueling inflammation and tumor invasiveness via mast cells/neutrophils activation and cytokines release in TME. In a gastric cancer study, Zhao et al., analyze the role of NEDD9 in cancer cell migration under hypoxia. They demonstrate that NEDD9 regulates MICAL1, which facilitates hypoxia-induced gastric cancer cell migration in a Rac1-dependent manner (Zhao et al.).

Tuo et al., address the role of the cytoplasmic isoform of phosphoenolpyruvate carboxykinase (PCK1) in the progression of hepatocellular carcinoma (HCC). PCK1 is a rate-limiting enzyme in gluconeogenesis which occurs mainly in the liver. The authors find that the expression of PCK1 is down regulated in HCC and associated with poor outcome. In hepatoma cells, the authors demonstrate that reactive oxygen species (ROS) production and nuclear translocation of Nrf2 and thioredoxin reductase 1 (TXNRD1) are suppressed during PCK1 overexpression. Furthermore, the authors show that targeting the TXNRD1 antioxidant pathway sensitizes PCK1-knockout hepatoma cells to sorafenib treatment *in vitro* (Tuo et al.).

The role of natural products in the modulation of the TME is likewise addressed in this Research Topic. Hu et al., investigate the effect of berberine (BBR) in gastric cancer (GC). BBR is a natural isoquinoline alkaloid, presumably involved in lipid metabolism and glucose homeostasis by regulating the expression of HNF4α. The authors show that BBR inhibits the proliferation, invasion, and migration of GC cell lines, and thus reduces GC tumor growth *in vivo*. The antitumor effect of BBR shown appears to involve the AMPK-HNF4α-WNT5A signaling pathway (Hu et al.). Using scutellarin, an active flavone extracted from *Erigeron breviscapus* Hand-Mazz (EBHM), Sun et al., investigate cisplatin resistance in non-small cell lung cancer (NSCLC). The authors find that scutellarin sensitizes tumor cells to cisplatin by enhancing apoptosis and autophagy via downregulation of p-AKT and c-Met in autophagy and caspase-3-dependent apoptosis. They suggest that the combination of cisplatin and scutellarin may be a novel therapeutic strategy for patients with NSCLC (Sun et al.).

The impact of DNA damage on TME is also investigated. Tirado-Hurtado et al., highlight the role of DNA Damage Inducible Transcript 4 (DDIT4) in cancer. The DDIT4 gene is expressed under stress situations, turning off the metabolic activity triggered by the mammalian target of rapamycin (mTOR). The authors propose targeting DDIT4 for the development of novel drugs that could be more specific and efficient than current mTOR inhibitors (Tirado-Hurtado et al.).

Mesenchymal stem cells (MCSs) play important role in the TME (**Figure 1**). Chulpanova et al., address the use of MCSs for drug delivery in oncology. The authors focus on MSC and tumor interactions, which are crucial for cancer control. They also describe novel therapeutic strategies using MSCs and MSC-derived membrane microvesicles for cancer therapy (Chulpanova et al.).

In conclusion, investigation of TME continues to be a vital focus toward the elaboration of novel strategies that produce more effective treatments for localized cancers and metastases. Findings presented in this Research Topic have the potential to make a major impact on this field and to inspire further discoveries.

## AUTHOR CONTRIBUTIONS

AL drafted the manuscript. AL, MB, KC-S, and AZ critically reviewed the manuscript for important intellectual content and approved it for publication.

## FUNDING

This work was supported by NIH/NCI: R01CA225993.

## ACKNOWLEDGMENTS

We thank all the authors of this Frontiers Research Topic for their excellent contribution. We also thank the reviewers for their valuable comments and Frontiers editorial team for their constant support, and Dr. Soumitro Pal for his input.

**Conflict of Interest:** AL and KC-S are Founders and Shareholders of Lambda Pharmaceuticals.

The remaining authors declare that the research was conducted in the absence of any commercial or financial relationships that could be construed as a potential conflict of interest.

frontiers in Pharmacology

ORIGINAL RESEARCH
published: 13 February 2018
doi: 10.3389/fphar.2018.00092

# Scutellarin Increases Cisplatin-Induced Apoptosis and Autophagy to Overcome Cisplatin Resistance in Non-small Cell Lung Cancer via ERK/p53 and c-met/AKT Signaling Pathways

*Chao-Yue Sun[1], Ying Zhu[1], Xiao-Feng Li[2], Xie-Qi Wang[1], Li-Peng Tang[1], Zu-Qing Su[1], Cai-Yun Li[1], Guang-Juan Zheng[1]* and Bing Feng[1]**

[1] Guangdong Provincial Hospital of Chinese Medicine, The Second Clinical College of Guangzhou University of Chinese Medicine, Guangzhou University of Chinese Medicine, Guangzhou, China, [2] Guangzhou Higher Education Mega Center, Clinical Medical College of Acupuncture and Rehabilitation, Guangzhou University of Chinese Medicine, Guangzhou, China

OPEN ACCESS

**Edited by:**
Karine A. Cohen-Solal,
Rutgers University, United States

**Reviewed by:**
Harikumar K. B.,
Rajiv Gandhi Centre for Biotechnology, India
Hiroyuki Seimiya,
Japanese Foundation for Cancer Research, Japan

***Correspondence:**
Guang-Juan Zheng
zhengguangjuan@163.com
Bing Feng
bing19831@163.com

**Specialty section:**
This article was submitted to Cancer Molecular Targets and Therapeutics, a section of the journal Frontiers in Pharmacology

**Received:** 13 November 2017
**Accepted:** 26 January 2018
**Published:** 13 February 2018

**Citation:**
Sun C-Y, Zhu Y, Li X-F, Wang X-Q, Tang L-P, Su Z-Q, Li C-Y, Zheng G-J and Feng B (2018) Scutellarin Increases Cisplatin-Induced Apoptosis and Autophagy to Overcome Cisplatin Resistance in Non-small Cell Lung Cancer via ERK/p53 and c-met/AKT Signaling Pathways. Front. Pharmacol. 9:92. doi: 10.3389/fphar.2018.00092

Cisplatin, as the first-line anti-tumor agent, is widely used for treatment of a variety of malignancies including non-small cell lung cancer (NSCLC). However, the acquired resistance has been a major obstacle for the clinical application. Scutellarin is a active flavone extracted from *Erigeron breviscapus Hand-Mazz* that has been shown to exhibit anticancer activities on various types of tumors. Here, we reported that scutellarin was capable of sensitizing A549/DDP cells to cisplatin by enhancing apoptosis and autophagy. Mechanistic analyses indicated that cisplatin-induced caspase-3-dependent apoptosis was elevated in the presence of scutellarin through activating extracellular signal-regulated kinases (ERK)-mediated p53 pathway. Furthermore, scutellarin also promoted cisplatin-induced cytotoxic autophagy, downregulated expression of p-AKT and c-met. Deficiency of c-met reduced p-AKT level, and inhibition of p-AKT or c-met improved autophagy in A549/DDP cells. Interestingly, loss of autophagy attenuated the synergism of this combination. *In vivo*, the co-treatment of cisplatin and scutellarin notably reduced the tumor size when compared with cisplatin treatment alone. Notably, scutellarin significantly reduced the toxicity generated by cisplatin in tumor-bearing mice. This study identifies the unique role of scutellarin in reversing cisplatin resistance through apoptosis and autophagy, and suggests that combined cisplatin and scutellarin might be a novel therapeutic strategy for patients with NSCLC.

**Keywords: scutellarin, cisplatin, NSCLC, apoptosis, autophagy**

## INTRODUCTION

Lung cancer is still the most prevalent malignant cancer worldwide with adverse clinical outcomes. Non-small cell lung cancer (NSCLC) accounts for 80–85% of lung cancer, with a low 5-years survival rate, approximately 13% (Siegel et al., 2016). Cisplatin is first-line anti-tumor drug for the treatment of advanced NSCLC (Miller et al., 2016). However, due to the frequent occurrence of acquired resistance, the use of cisplatin is limited (Galluzzi et al., 2012). Also, the molecular mechanisms by which cisplatin leads to resistance is not fully clear. Therefore,

investigating the underlying mechanism involved in cisplatin resistance, and searching for an effective component that can reverse the resistance are clinically necessary.

Apoptosis is a form of cell death, and as such it has been frequently induced by chemotherapy agents (Zhu et al., 2017). Autophagy, also called "self-eating," is an evolutionarily conserved catabolic process that sequesters unnecessary proteins and organelles to keep cell homeostasis (Yang and Klionsky, 2010). It is well studied that autophagy functions as a key factor in the tumorigenesis and cancer chemotherapy (Li Y.J. et al., 2017). To date, however, there are still a troublesome question: autophagy is a friend or foe for cancer treatment? Recently, accumulating evidence has been demonstrated that autophagy protects cancer cells when treated by chemotherapy, resulting in drug resistance (Wang et al., 2013). Accordingly, autophagy inhibitors are often recognized as a potential therapeutic strategy to enhance the cytotoxicity of chemotherapeutic drug (McAfee et al., 2012; Jin et al., 2017). However, unlike above reports, drug-induced autophagy can sensitize cancer cells to chemotherapy (Li and Zhang, 2017). Thus, the role of autophagy in cancer therapy remains not completely understood.

Extracellular signal-regulated kinases (ERK) plays a crucial role in the regulation of tumorigenesis, cell proliferation and cancer chemotherapy (Fremin and Meloche, 2010). Paradoxically, overexpression of ERK in advanced lung adenocarcinoma, is associated with worse chemotherapeutic outcome and a poor prognosis (Tsujino et al., 2016). However, on the other hand, ERK can be activated by many anti-cancer drugs, such as cucurbitacin to induce high autophagy, resulting tumor cell death (Wu et al., 2016). Thus, it is of paramount importance to explore the role of ERK pathway in cancer chemotherapy.

The c-met signaling is hyperactivated in a number of malignancies including NSCLC, and has been implicated in cancer initiation, progression and therapeutic resistance (Gozdzik-Spychalska et al., 2014). Recent study has demonstrated that cisplatin resistance cells A549/DDP exerted up-regulation of c-met, and suppression of the c-met by salvianolic acid A could reverse cisplatin resistance (Tang et al., 2017). Notably, the c-met signaling has an important role in the regulation of autophagy (Akl et al., 2015). For example, in lung adenocarcinoma, loss of c-met contributed to the induction of autophagy (Liu et al., 2013). Unfortunately, in cisplatin resistance, the role of c-met in regulating autophagy remains unresolved.

Scutellarin (4′,5,6-trihydroxyflavone-7-*O*-glucuronide), is a active flavone extracted from Chinese traditional herb *Erigeron breviscapus Hand-Mazz*, which was generally used for treatment of cerebral vascular diseases (Wang et al., 2017). Recently, scutellarin has been shown to exhibit anticancer activities on various types of tumors, such as hepatocellular carcinoma, colorectal cancer and tongue squamous carcinoma (Li et al., 2013; Ke et al., 2017; Yang et al., 2017), although the underlying mechanisms have not been fully determined. However, little is known about whether scutellarin can potentiate antitumor activity of cisplatin in NSCLC. In this study, we aimed to explore the mechanisms underlying synergistic interactions between scutellarin and cisplatin, and provided a new therapeutic target for reversing cisplatin resistance.

# MATERIALS AND METHODS

## Reagents and Antibodies

Scutellarin (purity ≥ 98%) was obtained from Sigma–Aldrich (St. Louis, MO, United States), and dissolved in PBS (PH 7.4). Cisplatin was provided by Yangtze River Pharmaceutica, and diluted in culture medium. U0126, hydroxychloroquine (HCQ), MK-2206, pifithrin-μ (PFT) and crizotinib were purchased from Selleckchem (Houston, TX, United States). Primary antibodies against β-actin (catalog number: 4970S), LC3 (catalog number: 12741S), p62 (catalog number: 39749S), p53 (catalog number: 2527S), caspase-3 (catalog number: 9662S), cleavaged caspase-3 (catalog number: 9664S), PARP (catalog number: 9454S), ERK1/2 (catalog number: 4695S), p-ERK1/2 (catalog number: 8544S), c-met (catalog number: 4560S), AKT (catalog number: 2920S), P-AKT (catalog number: 4060P), together with secondary HRP-conjugated goat anti-rabbit antibody were purchased from Cell Signaling Technology (Danvers, MA, United States).

## Cell Culture

The human lung adenocarcinoma cell lines A549, PC-9, H1975, and A549/DDP were obtained from the Chinese Academy of Sciences (Shanghai, China). A549/DDP cell line was generated from its parental A549 by step-dose selection *in vitro*. A549 cells were exposed to increasing concentrations ranging from 1 to 8 μM for 4 months. After establishment, the resistant index of the A549/DDP at 48 h was 37.37. Cells were maintained in RPMI 1640 supplemented with 10% fetal bovine serum (FBS; Gibco Laboratories, Grand Island, NY, United States). In addition, the culture medium for A549/DDP cells contained 2 mg/L cisplatin to keep its drug-resistant phenotype.

## MTT Assay and Synergy Analyses

To validate chemosensitivity of A549/DDP cells to cisplatin, the MTT assay was firstly performed. In summary, cells were seed into 96-well plates ($5 \times 10^3$ cells/well), and cultured overnight for adherence. Cells were exposed to different concentrations of cisplatin (0.625, 1.25, 2.5, 5, 10, and 20 μg/ml), scutellarin (10, 20, 40, 80, 120, and 160 μM), or their combination. After treatment for 24 or 48 h, 20 μL MTT (5 mg/ml) was added to each well and incubated for another 4 h. Subsequently, the medium was discarded and replaced with 150 μL DMSO. The absorbance at 490 nm wavelength was measured using a multiwell spectrophotometer (Bio-Rad, Hercules, CA, United States). To calculate the combination index (CI) of cisplatin and scutellarin, CalcuSyn software package (version 2.1) was used (Omar et al., 2016).

## Flow Cytometry

For apoptosis studies, cells were treated with cisplatin, or scutellarin, or in combination for 48 h. Following the cell collection after being centrifuged, cells were subsequently re-suspended with 500 μL binding buffer. Cells were stained with 5 μL Annexin V-FITC and 10 μL PI solution provided in an Annexin V-FITC apoptosis detection kit (MultiSciences Biotech

Co., Ltd.). The apoptotic cells were detected by a flow cytometer (BD Biosciences, San Jose, CA, United States).

## Western Blot Analysis

Total protein was harvested using standard RIPA buffer that contained 1% protease and phosphatase inhibitors (Thermo Fisher Scientific, Canoga Park, CA, United States). Equal proteins were subjected to electrophoresis on a 8 or 12% SDS-polyacrylamide gel, then transferred into PVDF membrane. After blocked in 5% skim milk for an hour, the membrane was incubated in primary antibodies overnight at 4°C. Then, the membrane were hybridized with the secondary horseradish peroxidase-conjugated antibodies at room temperature for an hour. Finally, protein bands were visualized by the enhanced chemiluminescence (ECL) system (Millipore, United States), and the expression of protein was measured using the ImageJ software. Here, β-actin was used as an internal control.

## Transmission Electron Microscopy (TEM)

Cells were collected and washed by PBS, and promptly immersed in a fixative solution of 2.5% glutaraldehyde for 4 h at 4°C. The samples were postfixed in 1.5% osmium tetroxide, and then dehydrated in a graded series of ethanol. Ultrathin sections (50 nm) were cut, followed by dyed with 2.5% uranyl acetate and 1% lead citrate. The samples were examined with a electron microscope (Hitachi H-7650, Tokyo, Japan) at 80 kV, and the images were captured using a Veleta TEM camera.

## Establishment of A549/DDP-Luc Cells

For establishment of A549/DDP-Luciferase (A549/DDP-Luc) cells, a Hind-III and Xba-I fragment of the luciferase was prepared for pGL4.13-Promoter (Promega, Fitchburg, WI, United States) and inserted into the PRC/$CMV_2$ vectors. The resulting PRC/$CMV_2$-Luc recombinant plasmid was transfected into A549/DDP cells to establish A549/DDP-Luc, followed by G418 screening to obtain unicellular resistant clones. The clone cells stably expressing strong luciferase were selected for animal experiment by luciferase activity test.

## *In Vivo* Xenograft and Treatment Experiments

The animal procedures were approved by the Animal Care and Use Committee of Guangdong Provincial Hospital of Chinese Medicine (the Ethics Approval Number 2016023) and the Declaration of the National Institutes of Health Guide for Care and Use of Laboratory Animals. A549/DDP-Luc cells ($4 \times 10^6$) were subcutaneously injected into the right flank of 4-to-6 week-old female BALB/c nude mice, which were purchased from Guangdong Medical Laboratory Animal Center (Fushan, Guangdong, China) when the tumor reached approximately 100 $mm^3$, mice were randomly divided into four groups ($n = 8$ each): the vehicle; the cisplatin alone; the scutellarin alone; and cisplatin + scutellarin. Cisplatin (5 mg/kg) were intraperitoneally given every 3 days, while scutellarin (60 mg/kg) were orally administered daily. Cisplatin was diluted using normal saline for the certain dosage, and scutellarin was dissolved in PBS (PH 7.4). The tumor dimensions and body weight were measured per 3 days, and tumor volume was calculated as follows: Volume = (Length × $width^2$) × 0.5. After treatment for 21 days, mice were humanely euthanized, and the tumor tissues were subsequently harvested for further analysis.

## Statistical Analysis

Data are depicted as the mean ± SEM. One-way analysis of variance (ANOVA) was used for multiple comparisons among three or more groups, while sample *t*-test was utilized for comparisons between two groups. $p < 0.05$ was interpreted to indicate statistical significance.

# RESULTS

## Scutellarin Enhanced the Drug Susceptibility of Cisplatin in A549/DDP Cells

Previously, we found that scutellarin potently suppressed the cell viability of NSCLC parental cells including A549, PC-9, H1975 (**Supplementary Figure S1B**), whereas the cytotoxic effect of scutellarin on cisplatin-resistant A549/DDP cells was dismal (**Figure 1A**). However, co-treatment of scutellarin and cisplatin significantly sensitized A549/DDP cells to cisplatin (**Figure 1B**). Here, we compared cisplatin-resistant cells A549/DDP with the parental A549 cells, A549/DDP showed high resistance to the DDP challenge. The IC50 of A549 and A549/DDP cells was 0.43 and 16.07 μg/ml, respectively, and the resistant index was 37.37 (**Figure 1C**). A CI was used to assess synergistic effects of cisplatin with scutellarin. Combinated cisplatin and scutellarin at 80, 120 μM showed a abvious synergism (**Figure 1D**). Thus, cisplatin and scutellarin yield a synergistic effect in killing A549/DDP cells. Specifically, 120 μM scutellarin did not yield measurable impact on cell viability of A549/DDP cells, but clearly enhanced the sensitivity of A549/DDP to cisplatin. Also, as shown in **Figure 1C**, the efficiency of 10 μg/ml cisplatin combined with 120 μM scutellarin peaked at 48 h. Of note, 120 μM scutellarin obviously reduced the IC50 of cisplatin in A549/DDP cells. Thus, 10 μg/ml cisplatin and 120 μM scutellarin were used for further study.

## Scutellarin Enhanced Cisplatin-Induced p53-Dependent Apoptosis

We next examined whether scutellarin could enhance cisplatin-induced apoptosis using flow cytometry. Scutellarin increased cisplatin-induced apoptosis by greater than 24%, when compared with cisplatin alone (**Figures 2A,B**). Caspase-3 is cleaved and activated during apoptosis, and in turn, caspase-3 cleaves PARP (Xu et al., 2016). In addition to flow cytometry, we tested the expression of caspase-3, cleavage of caspase-3 and PARP. Combination of cisplatin and scutellarin significantly increased cleavage of caspase-3 and PARP when compared with cisplatin alone (**Figure 2C** and **Supplementary Figure S2A**).

Given that p53 plays a distinct role in cisplatin-mediated apoptosis in cancer cells (Li et al., 2015), we examined

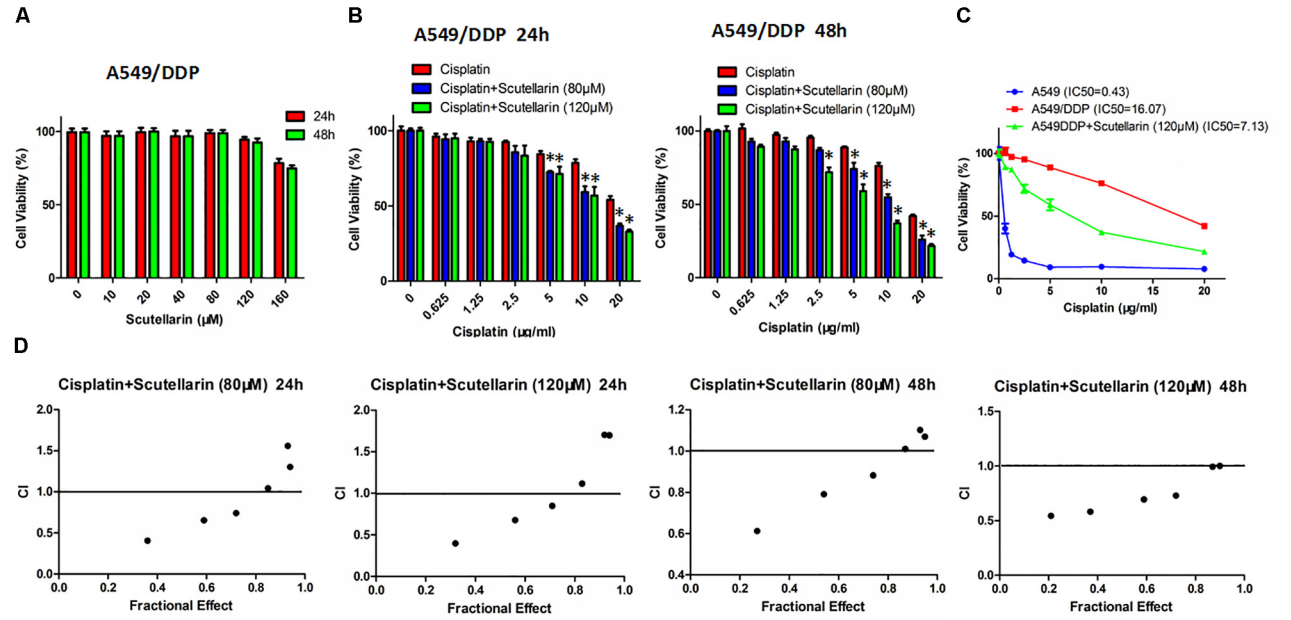


**FIGURE 1 |** Scutellarin enhanced the drug susceptibility of cisplatin in A549/DDP cell. **(A)** A549/DDP cells were treated with different concentrations of scutellarin for 24 or 48 h, the cell viability was determined by the MTT assay. **(B)** Cells were treated with cisplatin combined with scutellarin (80 or 120 μM), cell viability was measured by the MTT assay. **(C)** The sensitivity of A549 and A549/DDP to cisplatin was measured by MTT assay, and 120 μM scutellarin reduced IC50 of cisplatin in A549/DDP cells. **(D)** Drug synergism are expressed as fraction affected (Fa) curves and combination index (CI) plots. CI as a indicator of synergistic effects of cisplatin and scutellarin (additive effect, CI = 0.9–1.1; slight synergism, CI = 0.7–0.9; synergism, CI = 0.3–0.7; strong synergism, CI = 0.1–0.3). *$p < 0.05$.

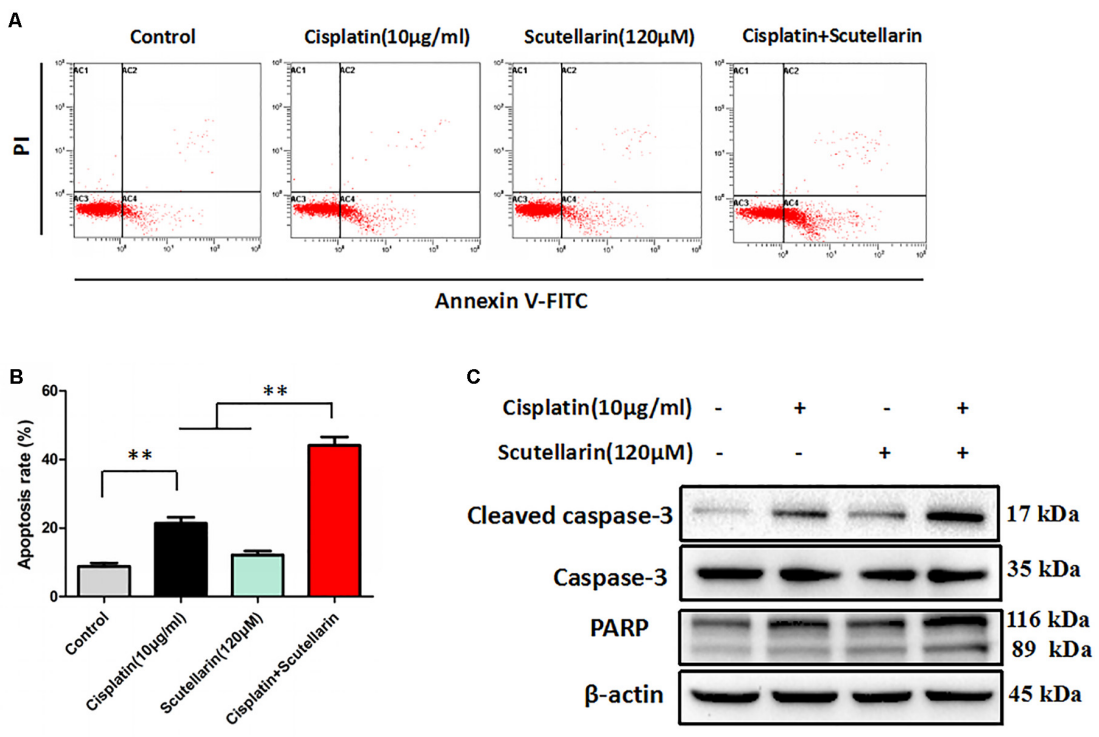


**FIGURE 2 |** Scutellarin enhanced cisplatin-induced apoptosis. **(A)** Cells were exposed to cisplatin with or without scutellarin for 48 h, cell apoptosis was measured by flow cytometric analysis. **(B)** Apoptosis rate in each group. **(C)** Western blot analysis showing caspase-3, cleaved caspase-3 and PARP expression levels in A549/DDP cells treated as indicated. Actin was used as loading control. Data are representative of three independent experiments (mean ± SEM). **$p < 0.01$.

p53 expression by western blots. In this study, cisplatin-resistant A549/DDP cells still retain the wild-type p53. In the presence of scutellarin, the cisplatin-induced expression of p53 was markedly enhanced (**Figure 3A** and **Supplementary Figure S3A**). To identify whether the heightened apoptotic response was p53-dependent, we next treated A549/DDP cells with a specific p53 inhibitor, pifithrin-μ (PFT). As expected, inhibition of p53 by PFT blocked cisplatin plus scutellarin-induced cleavage of caspase-3 and PARP (**Figure 3B** and **Supplementary Figure S3B**). Moreover, PFT markedly reduced cell apoptosis induced by co-treatment of cisplatin and scutellarin (**Figures 3C,D**). Thus, scutellarin enhanced cisplatin-induced apoptosis through activation of p53 signaling pathway.

## Scutellarin Enhanced Cisplatin-Induced p53-Dependent Apoptosis through Activating the ERK1/2 Signaling Pathway

It is well known that ERK pathway has been reported to regulate p53-dependent apoptosis (Lv et al., 2013). In line with this, we found that p-ERK1/2 level showed a very obvious increase in response to cisplatin plus scutellarin treatment in A549/DDP cells (**Figure 3E** and **Supplementary Figure S3C**). Similarly, we used a ERK inhibitor, U0126 to determine whether ERK pathway participated in scutellarin and cisplatin-induced apoptosis. Western blot analysis revealed that U0126 reversed the high expression of p53 induced by the combination treatment in A549/DDP cells (**Figure 3F** and **Supplementary Figure S3D**). Thus, scutellarin enhanced cisplatin-induced p53-dependent apoptosis through activating the ERK1/2 signaling pathway.

## Scutellarin Increased Cisplatin-Induced Autophagy

Autophagy plays a central role in governing chemotherapy resistance, yet its involved mechanisms are largely unknown. Here, we tested autophagy-related proteins, LC3 and p62, using western blot analysis. In the presence of scutellarin, the level of LC3-II was greatly increased in A549/DDP cells treated with cisplatin, whereas p62 was degraded (**Figure 4A** and **Supplementary Figure S4A**). Meanwhile, we employed TEM to verify the autophagy induced by cisplatin, or scutellarin, or in combination. As observed, the number of autophagic vacuoles was elevated in A549/DDP cells exposed to co-treatment of cisplatin and scutellarin, compared with cisplatin alone, or scutellarin alone (**Figure 4C**), indicating scutellarin indeed enhanced cisplatin-induced autophagy. In addition, autophagy inhibition achieved by using autophagy inhibitor HCQ, dramatically impaired autophagic flux (**Figure 4B** and **Supplementary Figure S4B**). Interestingly, MTT assay results revealed that HCQ treatment slightly contributed to cisplatin

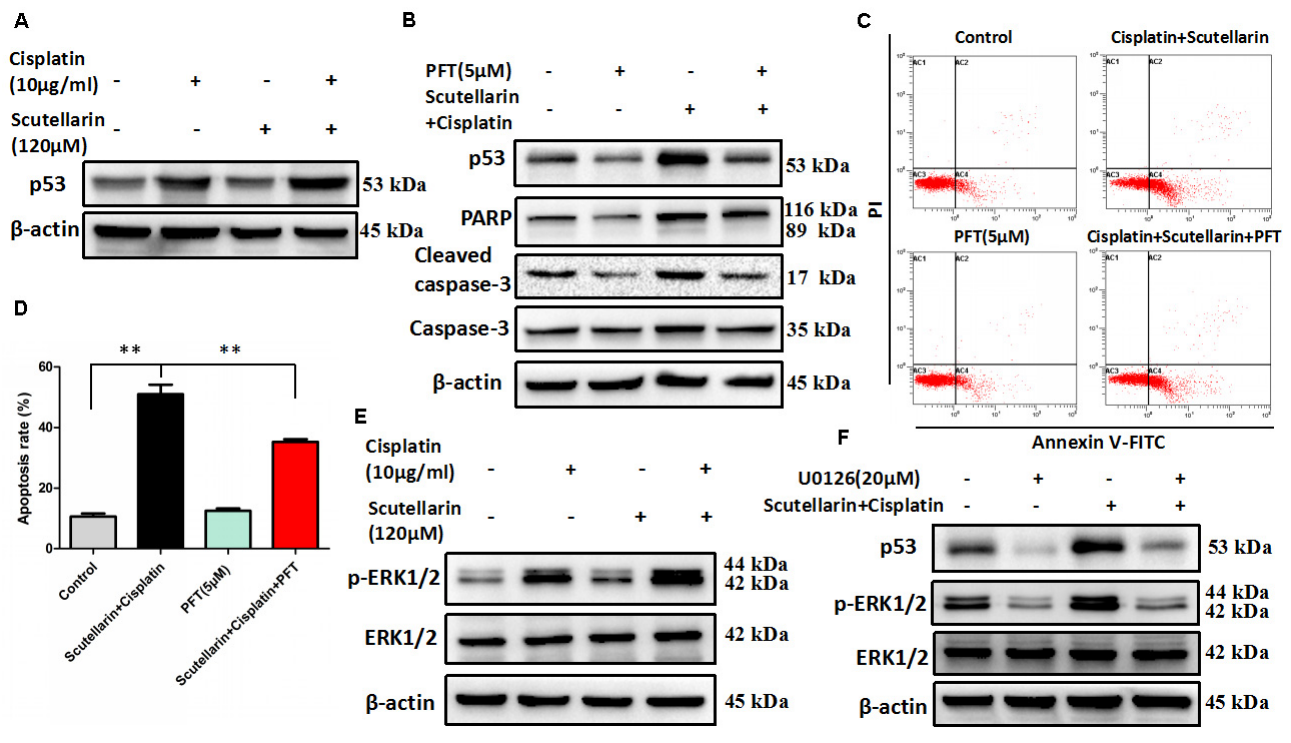


**FIGURE 3 |** Scutellarin enhanced cisplatin-induced apoptosis through the ERK1/2-mediated p53 signaling pathways. **(A)** Western blot analysis of p53 protein in A549/DDP cells treated by cisplatin, or scutellarin, or the combination. **(B)** The effect of p53 inhibitor PFT on p53, caspase-3, cleaved caspase-3 and PARP expression levels was measured by western blot analysis. **(C,D)** Flow cytometric analysis showing apoptosis in cells treated by cisplatin plus scutellarin, or PFT, or the combination. **(E)** The expression of p-ERK1/2, ERK1/2 were determined by western blot analysis. **(F)** The level of p-ERK1/2, ERK1/2, p53 in A549/DDP cells were measured in the presence of ERK1/2 specific inhibitor U0126. Data are representative of three independent experiments (mean ± SEM). $^{**}p < 0.01$.

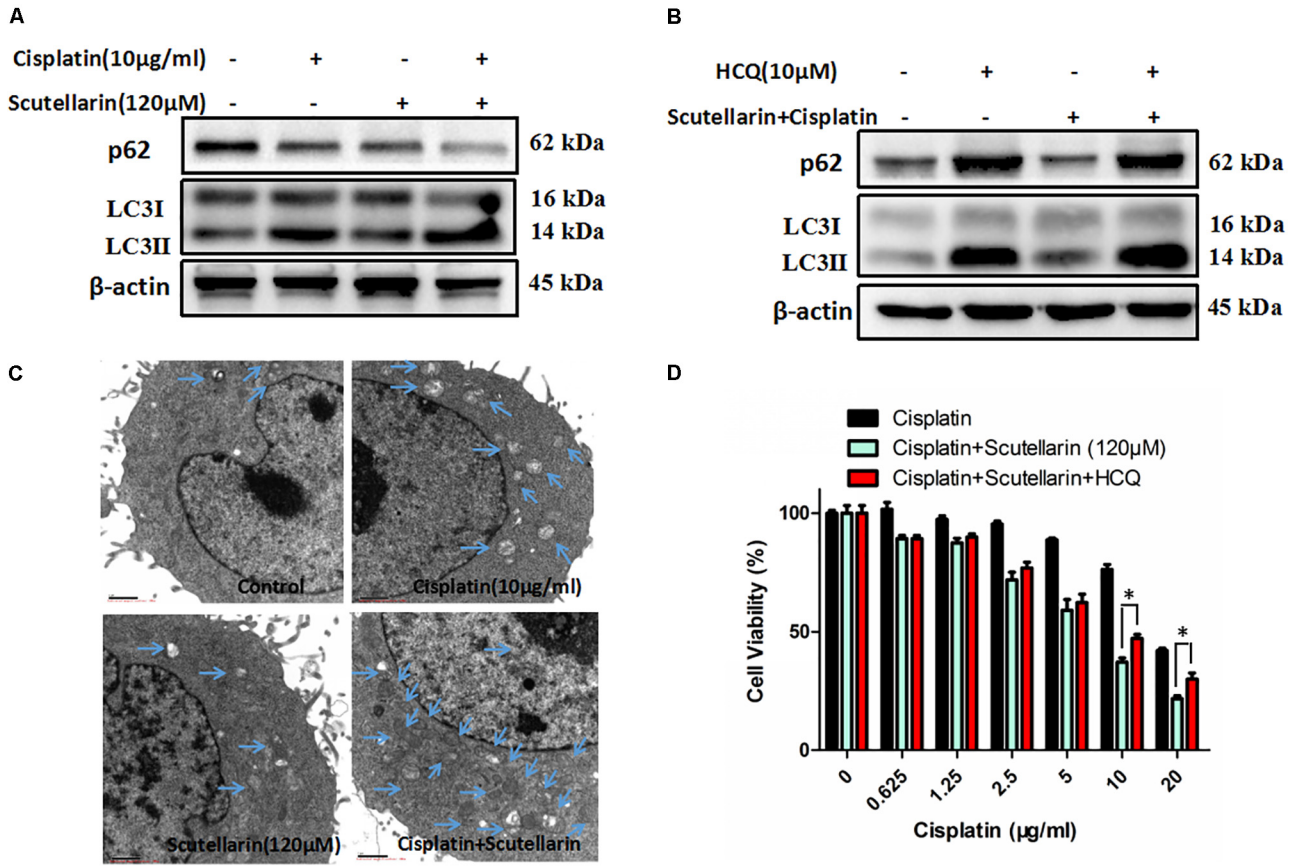


**FIGURE 4 |** Scutellarin increased cisplatin-induced autophagy. **(A)** A549/DDP cells were treated with the indicated concentrations of cisplatin or scutellarin, or the combination for 48 h, the expression of p62 and conversion of LC3-I to LC3-II were measured by western blotting. **(B)** Western blot analysis of p62 and LC3 in A549/DDP cells incubated with autophagy inhibitor HCQ. **(C)** Quantification of autophagic vacuoles in A549/DDP cells was analyzed by TEM. **(D)** The effect of HCQ on sensitivity of cisplatin and scutellarin was detected by MTT assay. Data are representative of three independent experiments (mean ± SEM). $*p < 0.05$, $**p < 0.01$.

resistance in A549/DDP cells (**Figure 4D**). Together, these findings suggested that scutellarin was able to promote cisplatin-induced autophagy, of which was not cytoprotective, but lead to cell death.

## Scutellarin Increased Cisplatin-Induced Autophagy through Suppressing c-met/AKT Signaling Pathway

Previous researches have been shown that c-met and AKT both play an important role in regulating autophagy (Heras-Sandoval et al., 2014; Li N. et al., 2017). Here, we also found that the expression of c-met and p-AKT was higher in cisplatin-resistant A549/DDP than A549 cells (**Supplementary Figure S1A**). In addition, hence, we question whether the increased autophagy was associated with above pathways, and we profiled AKT and c-met using western blot analysis. Comparatively, combined treatment with cisplatin and scutellarin reduced the expression of p-AKT, whereas the AKT level showed no significant difference (**Figure 5A** and **Supplementary Figure S5A**). In addition, inhibition of AKT by pharmacological inhibitor MK-2206 decreased p-AKT, but significantly enhanced autophagy marker expression LC3-II, and attenuated the level of p62 (**Figure 5B** and **Supplementary Figure S5B**). Moreover, in the presence of scutellarin, cisplatin caused significant suppression of c-met in A549/DDP cells (**Figure 5C** and **Supplementary Figure S5C**). Crizotinib is a potent and specific small-molecule inhibitor of c-met that binds to the hinge region of c-met in a bidentate manner and competes with ATP binding in c-met (Gandhi and Jänne, 2012). Here, the addition of c-met inhibitor, crizotinib abolished c-met expression, impaired p-AKT, and promoted high autophagy (**Figure 5D** and **Supplementary Figure S5D**). Taken together, these data showed that scutellarin enhanced cisplatin-induced autophagy by suppressing c-met/AKT pathways.

## Scutellarin Enhanced Antitumor Efficacy of Cisplatin *in Vivo*

To verify our previous conclusions, we established xenograft mouse model. The A549/DDP-Luc cells were subcutaneously implanted into BALB/c nude mice, and the mice were treated

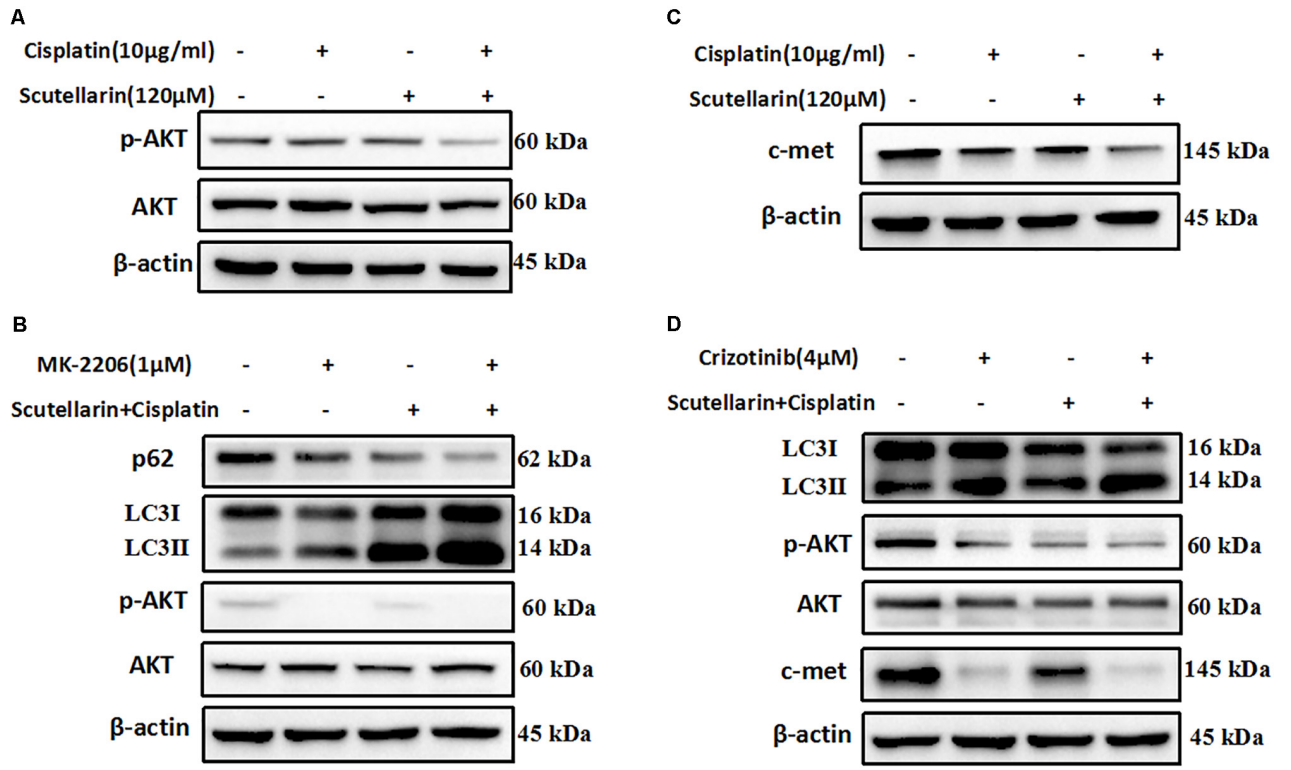


**FIGURE 5 |** Scutellarin increased cisplatin-induced autophagy through suppressing c-met/AKT signaling pathways. **(A)** Cells were treated by cisplatin with or without scutellarin, the protein expressions of AKT and p-AKT were determined by western blotting. **(B)** The expression levels of LC3, AKT, p-AKT were detected by western blotting in A549/DDP cells coincubated with MK-2206. **(C)** Western blot analysis of the protein of c-met. **(D)** The effect of crizotinib on the expression of LC3, AKT, p-AKT, c-met was analyzed by western blot analysis.

with cisplatin with or without scutellarin. As shown in **Figures 6A,B,D,E**, cisplatin significantly inhibited tumor growth, and this efficiency was significantly enhanced by scutellarin treatment, whereas the anti-tumor activity of scutellarin alone was dismal. Furthermore, due to the toxicity of cisplatin, the body weight of mice treated by cisplatin was decreased. However, in the presence of scutellarin, the weight reduction was recovered (**Figure 6C**). Moreover, the combination of cisplatin with scutellarin increased the expression of LC3-II, p53, p-ERK1/2, and reduced p-AKT and c-met, compared with cisplatin alone (**Figure 6F** and **Supplementary Figure S6A**). Collectively, scutellarin could notably improve anti-tumor effect of cisplatin, and reduce the toxicity generated by cisplatin *in vivo*.

## DISCUSSION

Cisplatin, one of the most commonly chemotherapeutic agent, has been widely used to treat different types of cancer including NSCLC (Kim et al., 2017). However, its tumoricidal efficacy is often limited due to the rapid emergence of acquired resistance. Multiple mechanisms contributed to cisplatin resistance have been documented, such as decreased drug absorption, DNA repair, inactivated apoptosis programs (Fang et al., 2017). Unfortunately, there remains a lack of targeted treatment strategies focusing on reversing cisplatin resistance. To circumvent this difficulty, we focused on looking for novel drugs to suppress chemotherapy resistance. Our results offer the first evidence, to our knowledge, that scutellarin improved the sensitivity of cisplatin-resistant cells A549/DDP to cisplatin. In addition to A549/DDP cells, our study shows that scutellarin could potentiate antitumor activity of cisplatin in NSCLC line PC-9, suggesting the synergism of scutellarin and cisplatin was applied to NSCLC cells (**Supplementary Figure S1C**).

Apoptosis is the predominant manner of cisplatin-induced cell death. However, cancer cells can develop its own specific strategies to evade apoptosis, which facilitates their survival and promote resistance to anticancer therapies (Ravegnini et al., 2017). Caspase-3 is a apoptotic effector that has been well studied to be involved in cisplatin-induced apoptosis (Shen et al., 2007). In this study, cisplatin markedly induced caspase-3-dependent apoptosis, of note, its efficiency was enhanced by scutellarin. Accumulating evidence has shown that p53 serves as a key tumor suppressor, which is essential for induction of cisplatin-induced apoptosis (Yang et al., 2012). It has been proposed that the presence of functional p53 facilitates the cytotoxic effects of chemotherapeutic drugs including cisplatin (Herudkova et al., 2017). For instance,

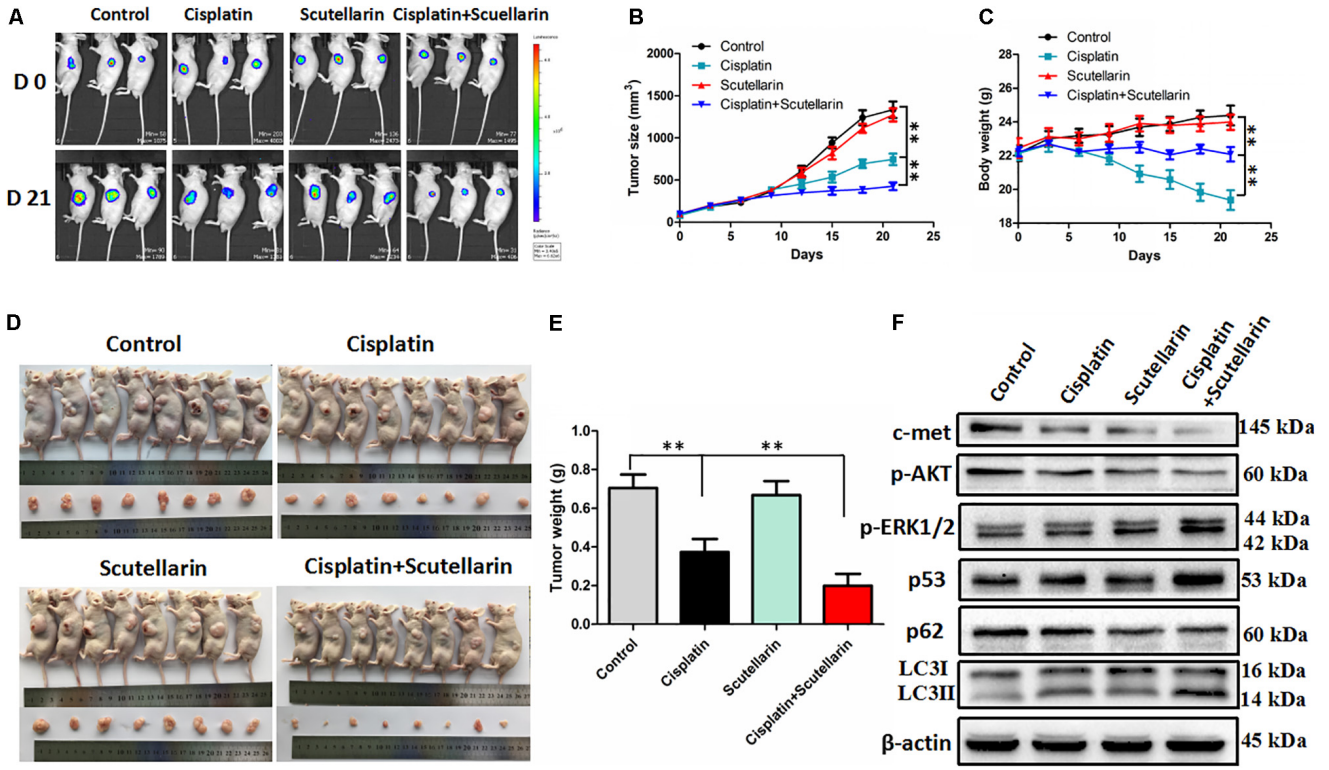


**FIGURE 6 |** Scutellarin enhanced antitumor efficacy of cisplatin *in vivo*. The A549/DDP-Luc cells were subcutaneously implanted BALB/c nude mice, and the mice were treated with cisplatin with or without scutellarin. **(A)** Tumor growth was monitored by IVIS, representative bioluminescence images of tumor in mice are shown. **(B)** The tumor dimensions were measured per 3 days using a digital caliper, tumor size in each group is shown. **(C)** Body weight of each group ($n = 8$). **(D)** After treatment for 21 days, mice were humanely euthanized, and the tumor tissues were subsequently harvested. **(E)** Tumor weight of each group ($n = 8$). **(F)** The expression levels of LC3, p62, p53, p-ERK1/2, p-AKT, c-met in mice tumor were detected by western blot analysis. Data are representative of three independent experiments (mean ± SEM). $^{**}p < 0.01$.

in head and neck squamous cell carcinoma, small molecules targeted p53-reactivation have been shown to induce apoptosis and enhance chemotherapeutic cytotoxicity (Roh et al., 2011). Here, we demonstrated that scutellarin increased cisplatin-induced p53 activation, resulting in apoptotic cell death. This is especially important given that p53 activation is mainly responsible for enhancement of cisplatin-induced apoptosis by scutellarin.

Extracellular signal-regulated kinases, an prototypic MAPK (mitogen-activated protein kinase), is involved in Ras/Raf/ERK pathway that is hyperactivated in a high many types of tumors, which drives cancer growth, inhibits apoptosis, promotes angiogenesis and invasion (Miyake et al., 2015). As such, small-molecule inhibitors targeting ERK signaling, such as RAF or MEK inhibitors, have shown to promise as efficient cancer therapeutics (Samatar and Poulikakos, 2014). However, ERK pathway also can be activated by antitumor agents to trigger its downstream tumor suppressor proteins (Lv et al., 2013). Meanwhile, cisplatin-induced ERK activation is an key regulator of the p53 response to DNA damage caused by cisplatin (Persons et al., 2000). Our data show that scutellarin serves an ERK inducer that potentiated cisplatin-induced ERK activation. Inhibition of ERK by U0126 suppressed p53 expression. Thus, co-treatment of cisplatin and scutellarin induced p53-mediated apoptosis via activating ERK pathway.

Autophagy or "self-eating," has been vividly regarded as janus-faced player due to its dual function in cancer progression (Gugnoni et al., 2016). The role of autophagy in cancer, however, is still paradoxical. On the one hand, autophagy plays a central role in suppressing tumor initiation by inhibiting necrosis and immune cell infiltration during tumorigenesis (Eritja et al., 2017). However, on the other side, autophagy can confer cancer cells the ability to protect itself in response to new hostile environments, such as hypoxic and nutrient-deficient (Zhan et al., 2016). Notably, some tumor cells are able to hijack the adaptation cues to cope with autophagy triggered by anti-tumor therapy (Kondo et al., 2005). In certain condition, autophagy inhibition can enhance the efficacy of anticancer treatments. Thus, the role of autophagy in cancer therapy has not been clear. During autophagy activation, lots of double-membrane electron-dense autophagosomes that capture unnecessary contents fuse with lysosomes or vacuoles to form autolysosomes, where these dysfunctional organelles are degraded (Li Y. et al., 2017). Meanwhile, in particular, accumulation of LC3-II and p62 degradation are regarded as

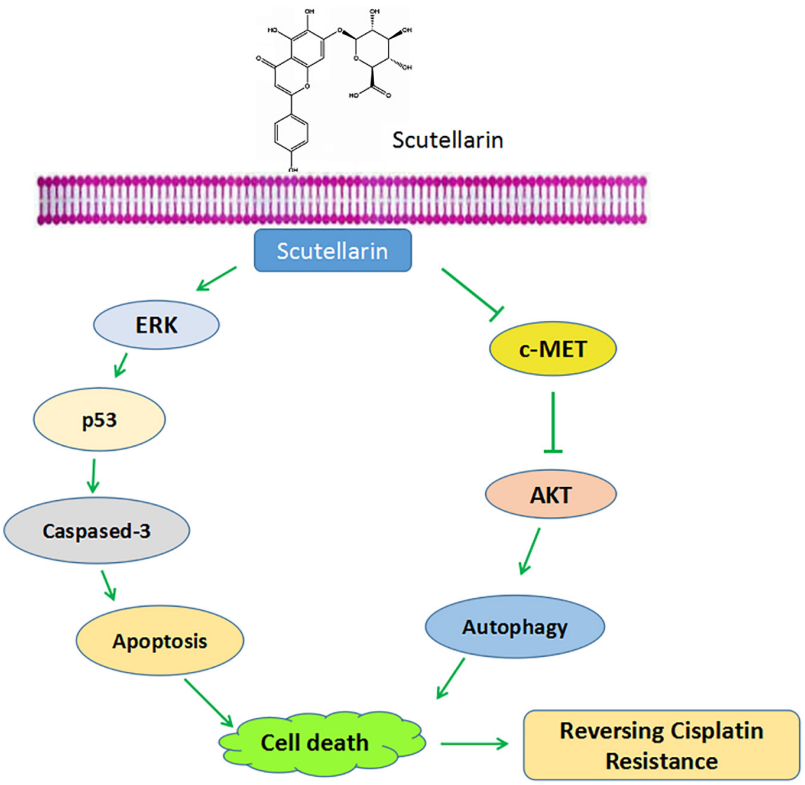


**FIGURE 7 |** Schematic diagram shows scutellarin increases the sensitivity of non-small cell lung cancer to cisplatin via ERK/p53 and c-met/AKT signaling pathways.

the induction of autophagy (Guo et al., 2013). Western blots and TEM results demonstrated combination of cisplatin and scutellarin markedly increased the induction of autophagy. Interestingly, deficiency of autophagy slightly contributed to cisplatin resistance in A549/DDP cells. These observations elucidated that scutellarin was able to promote cisplatin-induced autophagy, of which was not cytoprotective, but lead to cell death.

It is well established that PI3K/AKT/mTOR pathway is emerging as important player in the regulation of autophagy in various types of cancers (Chen et al., 2017). For example, in prostate cancer, inhibition of the PI3K/AKT/mTOR pathway is sufficient to activate autophagy (Butler et al., 2017). Indeed, co-treatment of cisplatin and scutellarin significantly decreased the level of phosphorylated AKT in A549/DDP cells, and the AKT inhibitor MK-2206 enhanced the induction of autophagy. The c-met oncogene has been identified as a potential target for cancer therapy. Activation of c-met contributes to the proliferation and invasion of cancer cells, and has been also considered as a biomarker in several tumor types (Blumenschein et al., 2012). Of note, AKT is regarded as a downstream factor of the c-met pathway (Peters and Adjei, 2012). Here, we found that cisplatin or scutellarin alone could suppressed c-met level, however, the efficiency of combination treatment was stronger. Inhibition of c-met by crizotinib attenuated p-AKT level, but induced high autophagy. These findings clearly indicated that scutellarin enhanced cisplatin-induced autophagy via suppressing the c-met/AKT signaling pathway. Furthermore, our *in vivo* experiment indicated that scutellarin significantly enhanced cisplatin-suppressed tumor growth, and reduced the toxicity generated by cisplatin.

In sum, our results showed that scutellarin reversed cisplatin resistance in NSCLC cells. Mechanically, scutellarin enhanced cisplatin-induced apoptosis and autophagy via ERK/p53 or c-met/AKT signaling pathways, suggesting that ERK and c-met signalings were the direct target of scutellarin (**Figure 7**). Notably, scutellarin can reduce the toxicity associated with repeated administration of cisplatin in tumor-bearing mice. These findings suggest that the combination of cisplatin treatment with scutellarin can be effectively applied for the treatment of NSCLC. In this study, A549/DDP cells still retain the wild-type p53, it is not clear whether the combination therapy is effective to p53-mutant lung cells. Thus, further experiments should performed to demonstrate whether scutellarin can enhance the sensitivity of p53-mutant cells to cisplatin.

## AUTHOR CONTRIBUTIONS

C-YS designed the experiments and drafted the manuscript. YZ and X-FL revised the manuscript. X-QW and L-PT carried out western blots and statistical analyses. Z-QS and C-YL performed the animal experiments. G-JZ and BF supervised the study.

## ACKNOWLEDGMENTS

This work was supported by the National Natural Science Foundation of China (Grant No. 81403142), the Special Fund of Guangdong Provincial Hospital of Chinese Medicine for Scientific and Technological Research of Traditional Chinese Medicine (Grant No. YK2013B2N09), the Terry Fox Foundation Cancer Research Funding (Grant No. YN2014TF04), and the Science and Technology Planning Project of Guangdong Province (Grant No. 2016A020226048).

## SUPPLEMENTARY MATERIAL

The Supplementary Material for this article can be found online at: https://www.frontiersin.org/articles/10.3389/fphar.2018.00092/full#supplementary-material

**FIGURE S1 | (A)** The expression levels of c-met, p-AKT in A549 and A549/DDP cells were detected by western blot analysis. **(B)** PC-9 cells were treated with different concentrations of scutellarin, cell viability was measured by the MTT assay. **(C)** PC-9 cells were treated with cisplatin combined with scutellarin (40 μM), cell viability was measured by the MTT assay. $^*p < 0.05$.

**FIGURE S2 | (A)** Western blot analysis showing caspase-3, cleaved caspase-3 and PARP expression levels in A549/DDP cells treated with cisplatin, or scutellarin, or the combination. Actin was used as loading control.

**FIGURE S3 | (A)** Western blot analysis of p53 protein in A549/DDP cells treated by cisplatin, or scutellarin, or the combination. **(B)** The effect of p53 inhibitor PFT on p53, caspase-3, cleaved caspase-3 and PARP expression levels were measured by western blot analysis. **(C)** The expression of p-ERK1/2, ERK1/2 were determined by western blot analysis. **(D)** The level of p-ERK1/2, ERK1/2, p53 in A549/DDP cells were measured in the presence of ERK1/2 specific inhibitor U0126.

**FIGURE S4 | (A)** A549/DDP cells were treated with cisplatin or scutellarin, or the combination for 48 h, the expression of p62 and conversion of LC3-I to LC3-II were measured by western blotting. **(B)** Western blot analysis of p62 and LC3 in A549/DDP cells incubated with autophagy inhibitor HCQ.

**FIGURE S5 | (A)** Cells were treated by cisplatin with or without scutellarin, the protein expressions of AKT and p-AKT were determined by western blotting. **(B)** The expression levels of LC3, AKT, p-AKT were detected by western blotting in A549/DDP cells coincubated with MK-2206. **(C)** Western blot analysis of the protein of *c-met*. **(D)** The effect of crizotinib on the expression of LC3, AKT, p-AKT, c-met was analyzed by western blot analysis.

**FIGURE S6 | (A)** The expression levels of LC3, p62, p53, p-ERK1/2, p-AKT, c-met in mice tumor were detected by western blot analysis.

## REFERENCES

Akl, M. R., Ayoub, N. M., Ebrahim, H. Y., Mohyeldin, M. M., Orabi, K. Y., Foudah, A. I., et al. (2015). Araguspongine C induces autophagic death in breast cancer cells through suppression of c-Met and HER2 receptor tyrosine kinase signaling. *Mar. Drugs* 13, 288–311. doi: 10.3390/md13010288

Blumenschein, G. R. Jr., Mills, G. B., and Gonzalez-Angulo, A. M. (2012). Targeting the hepatocyte growth factor-cMET axis in cancer therapy. *J. Clin. Oncol.* 30, 3287–3296. doi: 10.1200/JCO.2011.40.3774

Butler, D. E., Marlein, C., Walker, H. F., Frame, F. M., Mann, V. M., Simms, M. S., et al. (2017). Inhibition of the PI3K/AKT/mTOR pathway activates autophagy and compensatoryRas/Raf/MEK/ERK signalling in prostate cancer. *Oncotarget* 8, 56698–56713. doi: 10.18632/oncotarget.18082

Chen, L. M., Song, T. J., Xiao, J. H., Huang, Z. H., Li, Y., and Lin, T. Y. (2017). Tripchlorolide induces autophagy in lung cancer cells by inhibiting the PI3K/AKT/mTOR pathway and improves cisplatin sensitivity in A549/DDP cells. *Oncotarget* 8, 63911–63922. doi: 10.18632/oncotarget.19201

Eritja, N., Chen, B. J., Rodriguez-Barrueco, R., Santacana, M., Gatius, S., Vidal, A., et al. (2017). Autophagy orchestrates adaptive responses to targeted therapy in endometrial cancer. *Autophagy* 13, 608–624. doi: 10.1080/15548627.2016.1271512

Fang, Y., Zhang, C., Wu, T., Wang, Q., Liu, J., and Dai, P. (2017). Transcriptome sequencing reveals key pathways and genes associated with cisplatin resistance in lung adenocarcinoma A549 cells. *PLOS ONE* 12:e0170609. doi: 10.1371/journal.pone.0170609

Fremin, C., and Meloche, S. (2010). From basic research to clinical development of MEK1/2 inhibitors for cancer therapy. *J. Hematol. Oncol.* 3:8. doi: 10.1186/1756-8722-3-8

Galluzzi, L., Senovilla, L., Vitale, I., Michels, J., Martins, I., Kepp, O., et al. (2012). Molecular mechanisms of cisplatin resistance. *Oncogene* 31, 1869–1883. doi: 10.1038/onc.2011.384

Gandhi, L., and Jänne, P. A. (2012). Crizotinib for ALK-rearranged non-small cell lung cancer: a new targeted therapy for a newtarget. *Clin. Cancer Res.* 18, 3737–3742. doi: 10.1158/1078-0432.CCR-11-2393

Gozdzik-Spychalska, J., Szyszka-Barth, K., Spychalski, L., Ramlau, K., Wojtowicz, J., Batura-Gabryel, H., et al. (2014). C-MET inhibitors in the treatment of lung cancer. *Curr. Treat. Options Oncol.* 15, 670–682. doi: 10.1007/s11864-014-0313-5

Gugnoni, M., Sancisi, V., Manzotti, G., Gandolfi, G., and Ciarrocchi, A. (2016). Autophagy and epithelial-mesenchymal transition: an intricate interplay in cancer. *Cell Death Dis.* 7:e2520. doi: 10.1038/cddis.2016.415

Guo, J. Y., Karsli-Uzunbas, G., Mathew, R., Aisner, S. C., Kamphorst, J. J., Strohecker, A. M., et al. (2013). Autophagy suppresses progression of K-ras-induced lung tumors to oncocytomas and maintains lipid homeostasis. *Genes Dev.* 27, 1447–1461. doi: 10.1101/gad.219642.113

Heras-Sandoval, D., Perez-Rojas, J. M., Hernandez-Damian, J., and Pedraza-Chaverri, J. (2014). The role of PI3K/AKT/mTOR pathway in the modulation of autophagy and the clearance of protein aggregates in neurodegeneration. *Cell. Signal.* 26, 2694–2701. doi: 10.1016/j.cellsig.2014.08.019

Herudkova, J., Paruch, K., Khirsariya, P., Soucek, K., Krkoska, M., Vondalova Blanarova, O., et al. (2017). Chk1 inhibitor SCH900776 effectively potentiates the cytotoxic effects of platinum-based chemotherapeutic drugs in human colon cancer cells. *Neoplasia* 19, 830–841. doi: 10.1016/j.neo.2017.08.002

Jin, F., Wang, Y., Li, M., Zhu, Y., Liang, H., Wang, C., et al. (2017). MiR-26 enhances chemosensitivity and promotes apoptosis of hepatocellular carcinoma cells through inhibiting autophagy. *Cell Death Dis.* 8:e2540. doi: 10.1038/cddis.2016.461

Ke, Y., Bao, T., Wu, X., Tang, H., Wang, Y., Ge, J., et al. (2017). Scutellarin suppresses migration and invasion of human hepatocellular carcinoma by inhibiting the STAT3/Girdin/Akt activity. *Biochem. Biophys. Res. Commun.* 483, 509–515. doi: 10.1016/j.bbrc.2016.12.114

Kim, E. Y., Jung, J. Y., Kim, A., Chang, Y. S., and Kim, S. K. (2017). ABT-737 synergizes with cisplatin bypassing aberration of apoptotic pathway in non-small cell lung cancer. *Neoplasia* 19, 354–363. doi: 10.1016/j.neo.2017.02.008

Kondo, Y., Kanzawa, T., Sawaya, R., and Kondo, S. (2005). The role of autophagy in cancer development and response to therapy. *Nat. Rev. Cancer* 5, 726–734. doi: 10.1038/nrc1692

Li, H., Huang, D., Gao, Z., Chen, Y., Zhang, L., and Zheng, J. (2013). Scutellarin inhibits the growth and invasion of human tongue squamous carcinoma through the inhibition of matrix metalloproteinase-2 and -9 and alphavbeta6 integrin. *Int. J. Oncol.* 42, 1674–1681. doi: 10.3892/ijo.2013.1873

Li, N., Tang, B., Jia, Y. P., Zhu, P., Zhuang, Y., Fang, Y., et al. (2017). *Helicobacter pylori* CagA protein negatively regulates autophagy and promotes inflammatory

response via c-Met-PI3K/Akt-mTOR signaling pathway. *Front. Cell. Infect. Microbiol.* 7:417. doi: 10.3389/fcimb.2017.00417

Li, N., and Zhang, W. (2017). Protein kinase C beta inhibits autophagy and sensitizes cervical cancer Hela cells to cisplatin. *Biosci. Rep.* 37:BSR20160445. doi: 10.1042/BSR20160445

Li, X., Huang, J. M., Wang, J. N., Xiong, X. K., Yang, X. F., and Zou, F. (2015). Combination of chrysin and cisplatin promotes the apoptosis of Hep G2 cells by up-regulating p53. *Chem. Biol. Interact.* 232, 12–20. doi: 10.1016/j.cbi.2015.03.003

Li, Y., Zhang, Y., Wang, L., Wang, P., Xue, Y., Li, X., et al. (2017). Autophagy impairment mediated by S-nitrosation of ATG4B leads to neurotoxicity in response to hyperglycemia. *Autophagy* 13, 1145–1160. doi: 10.1080/15548627.2017.1320467

Li, Y. J., Lei, Y. H., Yao, N., Wang, C. R., Hu, N., Ye, W. C., et al. (2017). Autophagy and multidrug resistance in cancer. *Chin. J. Cancer* 36:52. doi: 10.1186/s40880-017-0219-2

Liu, Y., Liu, J. H., Chai, K., Tashiro, S., Onodera, S., and Ikejima, T. (2013). Inhibition of c-Met promoted apoptosis, autophagy and loss of the mitochondrial transmembrane potential in oridonin-induced A549 lung cancer cells. *J. Pharm. Pharmacol.* 65, 1622–1642. doi: 10.1111/jphp.12140

Lv, C., Hong, Y., Miao, L., Li, C., Xu, G., Wei, S., et al. (2013). Wentilactone A as a novel potential antitumor agent induces apoptosis and G2/M arrest of human lung carcinoma cells, and is mediated by HRas-GTP accumulation to excessively activate the Ras/Raf/ERK/p53-p21 pathway. *Cell Death Dis.* 4:e952. doi: 10.1038/cddis.2013.484

McAfee, Q., Zhang, Z., Samanta, A., Levi, S. M., Ma, X. H., Piao, S., et al. (2012). Autophagy inhibitor Lys05 has single-agent antitumor activity and reproduces the phenotype of a genetic autophagy deficiency. *Proc. Natl. Acad. Sci. U.S.A.* 109, 8253–8258. doi: 10.1073/pnas.1118193109

Miller, K. D., Siegel, R. L., Lin, C. C., Mariotto, A. B., Kramer, J. L., Rowland, J. H., et al. (2016). Cancer treatment and survivorship statistics, 2016. *CA Cancer J. Clin.* 66, 271–289. doi: 10.3322/caac.21349

Miyake, M., Goodison, S., Lawton, A., Gomes-Giacoia, E., and Rosser, C. J. (2015). Angiogenin promotes tumoral growth and angiogenesis by regulating matrix metallopeptidase-2 expression via the ERK1/2 pathway. *Oncogene* 34, 890–901. doi: 10.1038/onc.2014.2

Omar, H. A., Tolba, M. F., Hung, J. H., and Al-Tel, T. H. (2016). OSU-2S/Sorafenib synergistic antitumor combination against hepatocellular carcinoma: the role of PKCdelta/p53. *Front. Pharmacol.* 7:463. doi: 10.3389/fphar.2016.00463

Persons, D. L., Yazlovitskaya, E. M., and Pelling, J. C. (2000). Effect of extracellular signal-regulated kinase on p53 accumulation in response to cisplatin. *J. Biol. Chem.* 275, 35778–35785. doi: 10.1074/jbc.M004267200

Peters, S., and Adjei, A. A. (2012). MET: a promising anticancer therapeutic target. *Nat. Rev. Clin. Oncol.* 9, 314–326. doi: 10.1038/nrclinonc.2012.71

Ravegnini, G., Sammarini, G., Nannini, M., Pantaleo, M. A., Biasco, G., Hrelia, P., et al. (2017). Gastrointestinal stromal tumors (GIST): facing cell death between autophagy and apoptosis. *Autophagy* 13, 452–463. doi: 10.1080/15548627.2016.1256522

Roh, J. L., Kang, S. K., Minn, I., Califano, J. A., Sidransky, D., and Koch, W. M. (2011). p53-Reactivating small molecules induce apoptosis and enhance chemotherapeutic cytotoxicity in head and neck squamous cell carcinoma. *Oral Oncol.* 47, 8–15. doi: 10.1016/j.oraloncology.2010.10.011

Samatar, A. A., and Poulikakos, P. I. (2014). Targeting RAS-ERK signalling in cancer: promises and challenges. *Nat. Rev. Drug Discov.* 13, 928–942. doi: 10.1038/nrd4281

Shen, J., Huang, C., Jiang, L., Gao, F., Wang, Z., Zhang, Y., et al. (2007). Enhancement of cisplatin induced apoptosis by suberoylanilide hydroxamic acid in human oral squamous cell carcinoma cell lines. *Biochem. Pharmacol.* 73, 1901–1909. doi: 10.1016/j.bcp.2007.03.009

Siegel, R. L., Miller, K. D., and Jemal, A. (2016). Cancer statistics, 2016. *CA Cancer J. Clin.* 66, 7–30. doi: 10.3322/caac.21332

Tang, X. L., Yan, L., Zhu, L., Jiao, D. M., Chen, J., and Chen, Q. Y. (2017). Salvianolic acid A reverses cisplatin resistance in lung cancer A549 cells by targeting c-met and attenuating Akt/mTOR pathway. *J. Pharmacol. Sci.* 135, 1–7. doi: 10.1016/j.jphs.2017.06.006

Tsujino, I., Nakanishi, Y., Hiranuma, H., Shimizu, T., Hirotani, Y., Ohni, S., et al. (2016). Increased phosphorylation of ERK1/2 is associated with worse chemotherapeutic outcome and a poor prognosis in advanced lung adenocarcinoma. *Med. Mol. Morphol.* 49, 98–109. doi: 10.1007/s00795-015-0130-3

Wang, J., Tan, J., Luo, J., Huang, P., Zhou, W., Chen, L., et al. (2017). Enhancement of scutellarin oral delivery efficacy by vitamin B12-modified amphiphilic chitosan derivatives to treat type II diabetes induced-retinopathy. *J. Nanobiotechnology* 15:18. doi: 10.1186/s12951-017-0251-z

Wang, P., Zhang, J., Zhang, L., Zhu, Z., Fan, J., Chen, L., et al. (2013). MicroRNA 23b regulates autophagy associated with radioresistance of pancreatic cancer cells. *Gastroenterology* 145, 1133–1143.e12. doi: 10.1053/j.gastro.2013.07.048

Wu, Y., Chen, H., Li, R., Wang, X., Li, H., Xin, J., et al. (2016). Cucurbitacin-I induces hypertrophy in H9c2 cardiomyoblasts through activation of autophagy via MEK/ERK1/2 signaling pathway. *Toxicol. Lett.* 264, 87–98. doi: 10.1016/j.toxlet.2016.11.003

Xu, P., Cai, X., Zhang, W., Li, Y., Qiu, P., Lu, D., et al. (2016). Flavonoids of Rosa roxburghii Tratt exhibit radioprotection and anti-apoptosis properties via the Bcl-2(Ca(2+))/Caspase-3/PARP-1 pathway. *Apoptosis* 21, 1125–1143. doi: 10.1007/s10495-016-1270-1

Yang, M., Yuan, F., Li, P., Chen, Z., Chen, A., Li, S., et al. (2012). Interferon regulatory factor 4 binding protein is a novel p53 target gene and suppresses cisplatin-induced apoptosis of breast cancer cells. *Mol. Cancer* 11:54. doi: 10.1186/1476-4598-11-54

Yang, N., Zhao, Y., Wang, Z., Liu, Y., and Zhang, Y. (2017). Scutellarin suppresses growth and causes apoptosis of human colorectal cancer cells by regulating the p53 pathway. *Mol. Med. Rep.* 15, 929–935. doi: 10.3892/mmr.2016.6081

Yang, Z., and Klionsky, D. J. (2010). Mammalian autophagy: core molecular machinery and signaling regulation. *Curr. Opin. Cell Biol.* 22, 124–131. doi: 10.1016/j.ceb.2009.11.014

Zhan, L., Zhang, Y., Wang, W., Song, E., Fan, Y., Li, J., et al. (2016). Autophagy as an emerging therapy target for ovarian carcinoma. *Oncotarget* 7, 83476–83487. doi: 10.18632/oncotarget.13080

Zhu, J., Yu, W., Liu, B., Wang, Y., Shao, J., Wang, J., et al. (2017). Escin induces caspase-dependent apoptosis and autophagy through the ROS/p38 MAPK signalling pathway in human osteosarcoma cells *in vitro* and *in vivo*. *Cell Death Dis.* 8:e3113. doi: 10.1038/cddis.2017.488

**Conflict of Interest Statement:** The authors declare that the research was conducted in the absence of any commercial or financial relationships that could be construed as a potential conflict of interest.

frontiers in Pharmacology

MINI REVIEW
published: 20 March 2018
doi: 10.3389/fphar.2018.00259

# Application of Mesenchymal Stem Cells for Therapeutic Agent Delivery in Anti-tumor Treatment

*Daria S. Chulpanova[1], Kristina V. Kitaeva[1], Leysan G. Tazetdinova[1], Victoria James[2], Albert A. Rizvanov[1] and Valeriya V. Solovyeva[1]**

[1] OpenLab Gene and Cell Technologies, Institute of Fundamental Medicine and Biology, Kazan Federal University, Kazan, Russia, [2] School of Veterinary Medicine and Science, University of Nottingham, Nottingham, United Kingdom

Mesenchymal stem cells (MSCs) are non-hematopoietic progenitor cells, which can be isolated from different types of tissues including bone marrow, adipose tissue, tooth pulp, and placenta/umbilical cord blood. There isolation from adult tissues circumvents the ethical concerns of working with embryonic or fetal stem cells, whilst still providing cells capable of differentiating into various cell lineages, such as adipocytes, osteocytes and chondrocytes. An important feature of MSCs is the low immunogenicity due to the lack of co-stimulatory molecules expression, meaning there is no need for immunosuppression during allogenic transplantation. The tropism of MSCs to damaged tissues and tumor sites makes them a promising vector for therapeutic agent delivery to tumors and metastatic niches. MSCs can be genetically modified by virus vectors to encode tumor suppressor genes, immunomodulating cytokines and their combinations, other therapeutic approaches include MSCs priming/loading with chemotherapeutic drugs or nanoparticles. MSCs derived membrane microvesicles (MVs), which play an important role in intercellular communication, are also considered as a new therapeutic agent and drug delivery vector. Recruited by the tumor, MSCs can exhibit both pro- and anti-oncogenic properties. In this regard, for the development of new methods for cancer therapy using MSCs, a deeper understanding of the molecular and cellular interactions between MSCs and the tumor microenvironment is necessary. In this review, we discuss MSC and tumor interaction mechanisms and review the new therapeutic strategies using MSCs and MSCs derived MVs for cancer treatment.

**Keywords: mesenchymal stem cells, tumor microenvironment, membrane vesicles, cytokines, suppressor genes, oncolytic viruses, chemotherapy resistance**

OPEN ACCESS

***Edited by:***
*Ahmed Lasfar, Rutgers University, The State University of New Jersey, United States*

***Reviewed by:***
*Pranela Rameshwar, Rutgers Biomedical and Health Sciences, United States*
*Sujuan Guo, Dana–Farber Cancer Institute, United States*

****Correspondence:***
*Valeriya V. Solovyeva*
*solovyovavv@gmail.com*

***Specialty section:***
*This article was submitted to Cancer Molecular Targets and Therapeutics, a section of the journal Frontiers in Pharmacology*

***Received:*** *21 December 2017*
***Accepted:*** *08 March 2018*
***Published:*** *20 March 2018*

***Citation:***
*Chulpanova DS, Kitaeva KV, Tazetdinova LG, James V, Rizvanov AA and Solovyeva VV (2018) Application of Mesenchymal Stem Cells for Therapeutic Agent Delivery in Anti-tumor Treatment. Front. Pharmacol. 9:259. doi: 10.3389/fphar.2018.00259*

## INTRODUCTION

Due to their tropism to the tumor niche, mesenchymal stem cells (MSCs) are promising vectors for the delivery of antitumor agents. The isolation of MSCs from adult tissues poses circumvents many of the ethical and safety concerns which surround the use of embryonic or fetal stem cells, as these have been comprehensively discussed elsewhere (Herberts et al., 2011; Volarevic et al., 2018), this review focuses on the anti-tumor and therapeutic potential of MSCs. It is believed that the migration of MSCs toward the tumor is determined by inflammatory signaling similar to a chronic non-healing wound (Dvorak, 1986). It has been shown that MSCs are actively attracted to hepatic carcinoma (Xie et al., 2017), breast cancer (Ma et al., 2015), glioma (Smith et al., 2015)

and pre-metastatic niches (Arvelo et al., 2016). However, the mechanism and factors responsible for the targeted tropism of MSCs to wounds and tumors microenvironments remain unclear. MSCs can migrate to sites of trauma and injury following the gradient of chemo-attractants in the extracellular matrix (ECM) and peripheral blood (Son et al., 2006) and local factors, such as hypoxia, cytokine environment and Toll-like receptors ligands, where upon arrival these local factors promote MSCs to express growth factors that accelerate tissue regeneration (Rustad and Gurtner, 2012).

It is believed, that following accumulation at the sites of tumor formation and growth, MSCs differentiate into pericytes or tumor-associated fibroblasts (TAF) thereby forming a growth supporting microenvironment and secreting such trophic factors as vascular endothelial growth factor (VEGF), interleukin 8 (IL-8), transforming growth factor β (TGF-β), epidermal growth factor (EGF), and platelet-derived growth factor (PDGF). (Nwabo Kamdje et al., 2017). For example, it has been shown that MSCs stimulate tumor growth and vascularization within the colorectal cancer xenograft model *in vivo* and can also induce activation of Akt and ERK in endothelial cells, thereby increasing their recruitment and angiogenic potential (Huang et al., 2013). Whilst in co-culture *in vitro* experiments, MSCs stimulated the invasion and proliferation of breast cancer cells (Pinilla et al., 2009).

However, besides tumor progression, MSCs can also supress tumor growth by cell cycle arrest and inhibition of proliferation, as well as blocking of PI3K/AKT pathway and tumor suppressor gene expression (Ramdasi et al., 2015). Anti-tumor properties are described for MSCs isolated from various sources in experiments both *in vitro* and *in vivo* of various tumor models (different tumor models are discussed in (Blatt et al., 2013a,b). For instance, MSCs injected into an *in vivo* model of Kaposi's sarcoma suppressed tumor growth (Khakoo et al., 2006). Similar results have been reported for hepatoma (Qiao et al., 2008), pancreatic cancer (Cousin et al., 2009; Doi et al., 2010), prostate cancer (Chanda et al., 2009) and melanoma (Otsu et al., 2009) in both *in vitro* and *in vivo* models.

Thus, there are contradictory reports about the role of MSCs in tumor formation and development. The differences in the anticancer activity of MSCs reported by different group might be due to their activation status, which is discussed elsewhere (Rivera-Cruz et al., 2017). Nevertheless, there is a consensus that MSCs have enhanced tropism toward tumors which make them ideal vector candidates for targeted anti-tumor therapy.

## MSCs MIGRATE TOWARD IRRADIATED TUMORS

Mesenchymal stem cells migration in the context of radiation therapy may also be very promising for cancer therapy. In fact, MSCs migrate better to irradiated 4T1 mouse mammary tumor cells in comparison to non-irradiated 4T1 cells (Klopp et al., 2007). Irradiated 4T1 cells are characterized by increased expression levels of TGF-β1, VEGF, and PDGF-BB. The activation of chemokine receptor CCR2 in MSCs interacting with irradiated 4T1 cells was also observed, as well as higher expression of MCP-1/CCL2 in the tumor parenchyma of 4T1 mice. Thus, MCP-1/CCL2/CCR2 signaling is important in the attraction of MSCs to irradiated tumor cells. Furthermore, CCR2 inhibition resulted in a significant decrease in MSC migration *in vitro* (Klopp et al., 2007). In irradiated glioma cells Kim et al. (2010) reported increased IL-8 expression, which led to an upregulation of IL-8 receptor by MSCs and an increase in their migration potential and tropism to glioma cells.

Once at the irradiated tumor site, MSCs can suppress immune cell activation directly through cell-cell interactions by binding the membrane protein PD-1 with PD-L1 and PD-L2 ligands on the T-lymphocyte surface. Moreover, MSCs can induce T-lymphocyte agonism by suppressing the expression of CD80 and CD86 on antigen-presenting cells (Yan et al., 2014a,b). Thus, the increased MSCs tropism to irradiated tumors may have the opposite effect in cancer therapy.

The described data clearly illustrate the correlation between tissue damage and MSCs recruitment. Due to an increase in tropism to the tumor, genetically modified MSCs can be an effective therapeutic tool. However, such therapeutic strategies can be risky for cancer patients since MSCs can potentially stimulate cancer progression within certain contexts.

## MSCs CHEMOTAXIS MEDIATING FACTORS

Mesenchymal stem cells migrate to damaged tissue, trauma or sites of inflammation in response to secreted cytokines. Similarly, the tumor environment consists of a large number of immune cells, which alongside tumor cells, secrete soluble factors such as VEGF, PDGF, IL-8, IL-6, basic fibroblast growth factor (bFGF or FGF2), stromal cell-derived factor 1 (SDF-1), granulocyte colony-stimulating factor (G-CSF), granulocyte-macrophage colony stimulating factor (GM-CSF), monocyte chemoattractant protein 1 (MCP1), hepatocyte growth factor (HGF), TGF-β and urokinase-type plasminogen activator receptor (UPAR), attracting MSCs (Ponte et al., 2007).

Soluble factors CCL21 (Sasaki et al., 2008), IL-8 (Birnbaum et al., 2007), CXC3L1 (Sordi et al., 2005), IL-6 (Liu et al., 2011), macrophage inflammatory protein 1δ (MIP-1δ) and MIP-3α (Lejmi et al., 2015) directly mediate MSCs chemotaxis and recruitment to damaged tissues. IL-6 mediates chemotaxis, which facilitates MSC attraction into the main tumor growth sites (Rattigan et al., 2010). Ringe et al. (2007) observed the dose-dependent chemotactic activity of bone marrow-derived MSCs in relation to SDF-1α and IL-8. IL-8 dependent recruitment of MSCs was also detected in glioma. A multitude of angiogenic cytokines secreted by glioma cells, including IL-8, actively attract MSCs to tumor tissue (Ringe et al., 2007). Experiments with conditioned medium from Huh-7 hepatoma cell (Huh-7 CM) showed that MIP-1δ and MIP-3α induced MSC migration. Moreover, after cultivation of MSCs in Huh-7 CM the expression of matrix metalloproteinase 1 (MMP-1), necessary for migration, was significantly increased (Lejmi et al., 2015). It was also shown that PDGF-BB, VEGF and TGF-β1 can induce MSC

migration (Schar et al., 2015). Experiments using MSCs modified with CXCR4, showed that increased expression of the CXCR4 receptor enhances MSC migration toward tumor cells in both *in vitro* and *in vivo* models (Kalimuthu et al., 2017). In osteosarcoma models, it was described that SDF-1α is involved in MSCs recruitment to tumor areas. MSCs in turn stimulate the migration of osteocarcinoma cells by CCL5/RANTES secretion (Xu et al., 2009), thereby promoting tumor invasion and metastatic colonization by providing metastatic osteosarcoma cells with a suitable microenvironment (Tsukamoto et al., 2012).

## GENETICALLY ENGINEERED MSCs WITH ANTICANCER ACTIVITY

In early studies MSCs genetically modified with interferon β (IFN-β) were injected into human melanoma mouse xenotransplantation models which resulted in decreased tumor growth and increased (2-times) survival of mice in comparison with controls (Studeny et al., 2002). In addition, it was shown in a melanoma xenograft mouse model that additional loading of IFN-β-modified canine MSCs with low amounts of cisplatin significantly increased the effectiveness of the antitumor therapy (Ahn et al., 2013).

Currently, besides IFN-β there are several other cytokines and tumor-suppressor genes with anticancer activity which are used for genetic modification of MSCs (**Table 1**). One of the most promising therapeutic pro-apoptotic cytokines is tumor necrosis factor (TNF)-related apoptosis-inducing ligand (TRAIL), which selectively induces apoptosis in cancer cells. The antitumor effect of TRAIL-modified MSCs has been described for different types of tumors, within which TRAIL has not been found to be cytotoxic for normal mammalian cells and tissues (Szegezdi et al., 2009; Yuan et al., 2015). It is interesting that recombinant TNF-α-activated MSCs in combination with radiation exposure are able to significantly increase expression level of endogenous TRAIL (Mohammadpour et al., 2016). Long-lasting expression of endogenous TRAIL can also be observed in IFN-γ-modified MSCs (Yang X. et al., 2014). To increase the therapeutic potential of TRAIL-modified MSCs, it has been suggested they could be used in combination with chemotherapeutic agents, such as cisplatin (Zhang et al., 2012). However, some tumors have mechanism of TRAIL resistance through overexpression of X-linked inhibitory of apoptosis protein (XIAP), which inhibits caspase 3 and 9 activation. Anti-apoptotic properties of XIAP are under control of the second mitochondria-derived activator of caspase (Smac), which prevents physical interaction of XIAP and caspases thereby preventing apoptosis inhibition (Srinivasula et al., 2001). Khorashadizadeh et al. (2015) used MSCs for the delivery and simultaneous expression of novel cell penetrable forms of Smac and TRAIL. The effectiveness of this approach was shown in TRAIL-resistant breast cancer cell line MCF-7 (Khorashadizadeh et al., 2015).

Besides IFN-β and TRAIL as anti-tumor agents, interleukins are also under consideration because they regulate inflammation and immune responses For instance, IL-12-modified MSCs decrease metastasis and induce cancer cell apoptosis in mice with melanoma, lung cancer and hepatoma by 75, 83, and 91%, respectively. The activation of immune cells [cytotoxic T-lymphocytes and natural killers (NK)] was also reported (Chen et al., 2008). You et al. (2015) showed that injection of genetically modified amniotic fluid-derived MSCs expressing IL-2 resulted in induction of apoptosis in ovarian cancer cells in an *in vivo* mouse model.

PTEN (phosphatase and tensin homolog deleted on chromosome 10) is one of the main human tumor-suppressors. Yang Z.S. et al. (2014) showed that PTEN expressing MSCs are able to migrate toward DBTRG (brain glioblastoma) tumor cells *in vitro*. PTEN-modified MSCs anti-cancer activity in co-culture with U251 glioma cells *in vitro* was also described (Guo et al., 2016). MSC-mediated delivery and anti-tumor properties were described for other proteins (IFN-α, IFN-γ, CX3CL1, apoptin, PEDF) and ncRNAs (miR-124 and miR-145) (**Table 1**). Modification of MSCs for the co-expression of several therapeutic proteins can increase their anti-cancer potential. It was shown that TRAIL and herpes simplex virus thymidine kinase (HSV-TK) modified MSCs in the presence of ganciclovir (GCV) significantly reduced tumor growth and increased survival of mice with highly malignant glioblastoma multiform (GBM) (Martinez-Quintanilla et al., 2013).

The effect of direct administration of many of these agents in cancer treatment is often limited due to their short half-life in the body and pronounced toxicity in relation to normal, non-cancerous cells. The use of MSCs for delivery of the above mentioned therapeutic proteins can help to minimize such problems because MSCs can selectively migrate to tumor sites and exert therapeutic effects locally thereby significantly increasing the concentration of the agent in the tumor and reducing its systemic toxicity.

Another promising approach is delivery of oncolytic viruses with MSCs. For instance, Du et al. (2017) used MSCs as a vector for the delivery of oncolytic herpes simplex virus (oHSV) [approved by Food and Drug Administration (FDA) for melanoma treatment] in human brain melanoma metastasis models in immunodeficient and immunocompetent mice. Authors noted that the introduced MSCs-oHSV migrated to the site of tumor formation and significantly prolonged the survival of mice. In the immunocompetent model a combination of MSCs-oHSV and PD-L1 blockade increases IFNγ-producing $CD8^+$ tumor-infiltrating T lymphocytes and results in a significant increase of the median survival of treated animals (Du et al., 2017).

## MSCs PRIMED WITH ANTICANCER DRUGS

Mesenchymal stem cells relative resistance to cytostatic and cytotoxic chemotherapeutic drugs and migration ability opens new ways to use them for targeted delivery of therapeutic drugs directly to tumor sites. Pessina et al. (1999) showed that SR4987 BDF/1 mouse bone marrow stromal cells can be a reservoir for doxorubicin (DOX) which can subsequently be released not only in the form of DOX metabolites but also in its original form.

**TABLE 1 |** The usage of genetically engineered Mesenchymal stem cells for target delivery of therapeutic agents with anti-tumor activity.

| Agent | Mechanism of action | Model | Reference |
|---|---|---|---|
| IFN-α | Immunostimulation, apoptosis induction, angiogenesis suppression | Immunocompetent mouse model of metastatic melanoma | Ren et al., 2008a |
| IFN-β | Increased activity of NK cells, inhibition of Stat3 signaling | Mouse 4T1 breast tumor model | Ling et al., 2010 |
| | | Mouse prostate cancer lung metastasis model | Ren et al., 2008b |
| | | PC-3 (prostate cancer) xenograft model | Wang et al., 2012 |
| | | PANC-1 (pancreatic carcinoma) xenograft model | Kidd et al., 2010 |
| IFN-γ | Immunostimulation, apoptosis induction | *In vitro* human leukemia cell line K562 | Li et al., 2006 |
| TRAIL | Caspase activation, apoptosis induction | Orthotopic model of Ewing sarcoma | Guiho et al., 2016 |
| | | Subcutaneous model of lung cancer | Mohr et al., 2008; Yan et al., 2016 |
| | | Xenograft model of human malignant mesothelioma | Sage et al., 2014; Lathrop et al., 2015 |
| | | Colo205 (colon cancer) xenograft tumor model | Marini et al., 2017 |
| | | Xenograft model of human myeloma | Caffario et al., 2017 |
| | | Xenograft model of human tongue squamous cell carcinoma (TSCC) | Xia et al., 2015 |
| | | Eca-109 (esophageal cancer) xenograft model | Li et al., 2014 |
| | | Xenograft model of human glioma | Kim et al., 2010; Choi et al., 2011; Wang et al., 2017 |
| IL-2 | Immunostimulation | Rat glioma model | Nakamura et al., 2004 |
| IL-12 | Immune system cell activation | Liver cancer H22 and MethA ascites models | Han et al., 2014 |
| | | Mouse model bearing subcutaneous SKOV3 (ovarian carcinoma) tumor explants | Zhao et al., 2011 |
| | | Xenograft model of human glioma | Hong et al., 2009; Ryu et al., 2011 |
| IL-21 | Immunostimulation | Mouse model of B-cell lymphoma | Kim et al., 2015 |
| | | A2780 (ovarian cancer) xenograft model | Hu et al., 2011 |
| PTEN | Induction of G(1)-phase cell cycle arrest | *In vitro* glioma cell line | Yang Z.S. et al., 2014; Guo et al., 2016 |
| CX3CL1 | Cytotoxic T cells and NK cells activation | Mice bearing lung metastases of C26 (colon carcinoma) and B16F10 (skin melanoma) cells | Xin et al., 2007 |
| HSV-TK/GCV | Drug precursors transformation | 9L (glioma) xenograft model | Uchibori et al., 2009 |
| | | *In vitro* glioma cell lines 8-MG-BA, 42-MG-BA and U-118 MG | Matuskova et al., 2010 |
| CD/5-FC | Drug precursors transformation | Subcutaneous model of melanoma or colon cancer | Kucerova et al., 2007, 2008 |
| | | Cal72 (osteosarcoma) xenograft model | NguyenThai et al., 2015 |
| NK4 | Apoptosis induction, angiogenesis and lymphangiogenesis suppression | C-26 lung metastasis model | Kanehira et al., 2007 |
| | | Nude mice bearing gastric cancer xenografts | Zhu et al., 2014 |
| | | MHCC-97H (liver carcinoma) xenograft model | Cai et al., 2017 |
| Oncolytic viruses | Tumor destruction by virus replication | Orthotopic breast and lung tumors | Hakkarainen et al., 2007 |
| | | Mouse glioblastoma multiforme models | Duebgen et al., 2014 |
| | | A375N (melanoma) tumor xenografts | Bolontrade et al., 2012 |
| PEDF | Inhibiting tumor angiogenesis, inducing apoptosis, and restoring the VEGF-A/sFLT-1 ratio | Lewis lung carcinoma (LLC) xenograft model | Chen et al., 2012 |
| | | Mice bearing U87 gliomas | Su et al., 2013 |
| | | CT26 CRPC model | Yang et al., 2016 |
| Apoptin | Tumor destruction, caspase 3 activation | HepG2 (hepatocellular carcinoma) tumor xenografts | Zhang et al., 2016 |
| | | Lung carcinoma xenograft model | Du et al., 2015 |
| HNF4-α | Wnt/β-catenin pathway inhibition | SK-Hep-1 (hepatocellular carcinoma) tumor xenografts | Wu et al., 2016 |
| miR-124 | Increase the differentiation of glioma stem cells by targeting SCP-1 or CDK6 | Glioma tumor cells in a spheroid cell culture system | Lee et al., 2013 |
| | | *In vitro* human glioblastoma multiforme cell line | Sharif et al., 2017 |
| miR-145 | Sox2 and Oct4 expression inhibition | Glioma tumor cells in a spheroid cell culture system | Lee et al., 2013 |

It was further shown that MSCs efficiently absorb and release paclitaxel (PTX) in an active form (Pascucci et al., 2014), DOX, and gemcitabine (GCB), all having an inhibitory effect on tongue squamous cell carcinoma (SCC154) cells growth *in vitro* (Cocce et al., 2017b).

Pessina et al. (2013) found that the maximum concentration of PTX which did not affect MSC viability was 10 000 ng/mL. The concentration is sufficient to decrease the viability of certain types of tumor cells, for example, human leukemia cells. *In vivo* investigations show that PTX-primed MSCs

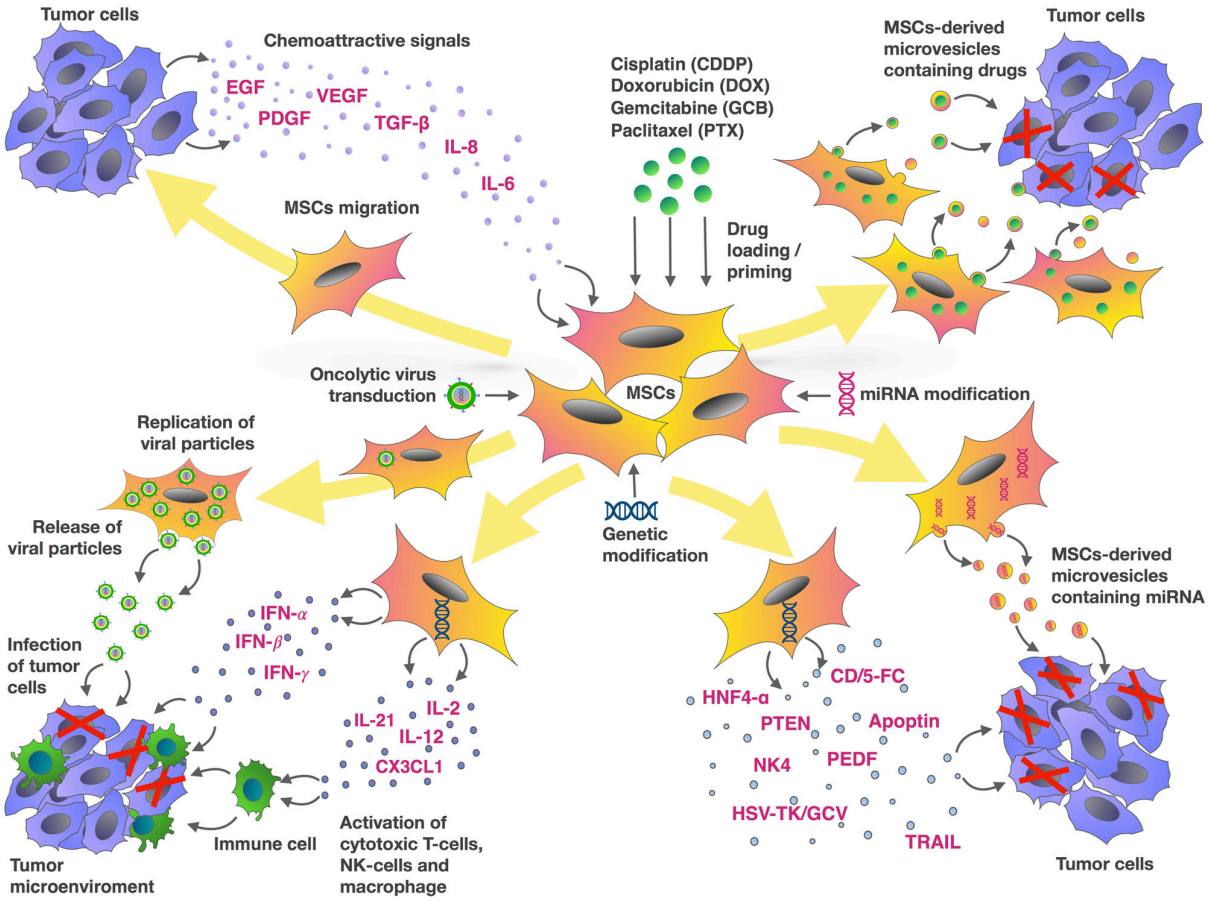


**FIGURE 1 |** Mesenchymal stem cells and tumor cells interaction as an MSC-based approach for cancer therapy. The chemotactic movement of MSCs toward a tumor niche is driven by soluble factors, such as VEGF, PDGF, IL-8, IL-6, bFGF or FGF2, SDF-1, G-CSF, GM-CSF, MCP1, HGF, TGF-β, and UPAR. Genetic modification of MSCs can be used to deliver a range of tumor-suppressing cargos directly into the tumor niche. These cargos include tumor suppressor (TRAIL, PTEN, HSV-TK/GCV, CD/5-FC, NK4, PEDF, apoptin, HNF4-α), oncolytic viruses, immune-modulating agents (IFN-α, IFN-γ, IL-2, IL-12, IL-21, IFN-β, CX3CL1), and regulators of gene expression (miRNAs and other non-coding RNAs). MSCs are also capable of delivering therapeutic drugs such as DOX, PTX, GCB, and CDDP within the tumor site. In addition to using MSCs directly, microvesicles (MVs) isolated from MSCs represent an alternative approach to delivering these agents.

(MSCs-PTX) demonstrate strong antitumor activity inhibiting the growth of tumor cells and vascularization of the tumor in a MOLT-4 (leukemia) xenograft mouse model (Pessina et al., 2013). The anti-tumor activity of primed MSCs is currently being investigated on the different types of tumor cells. For instance, Bonomi et al. (2017b) showed that MSCs-PTX suppress the proliferation of human myeloma cells RPMI 8226 in *in vitro* 3D dynamic culture system. The anti-cancer activity of MSCs-PTX has been further shown in relation to pancreatic carcinoma cells *in vitro* (Brini et al., 2016).

Nicolay et al. (2016) showed that cisplatin (CDDP) had no significant effect on cell morphology, adhesion or induction of apoptosis in MSCs, nor does it affect their immunophenotype or differentiation potential of MSCs once primed with CDDP. This has been confirmed using CDDP at concentrations of 2.5 μg/ml and 5.0 μg/ml (Gilazieva et al., 2016). Thus, MSCs are promising vectors for CDDP delivery toward the tumor sites.

Beside chemical drugs in soluble form, MSCs can absorb nanomaterials containing chemotherapeutic agents. For instance, MSCs primed with silica nanoparticle-encapsulated DOX promoted a significant increase in the apoptosis of U251 glioma cells *in vivo* (Li et al., 2011).

Bonomi et al. (2017a) in their work used MSCs from two sources: dog adipose tissue and bone marrow, to study MSCs-PTX antitumor activity on human glioma cells (T98G and U87MG). The investigation once again showed the pronounced antitumor effect of MSCs-PTX and opens new perspectives for oncological disease therapy not only in humans but also in animals (Bonomi et al., 2017a).

## MSC-DERIVED MICROVESICLES

Extracellular vesicles (EVs) [microvesicles (MVs) and exosomes] released by a large number of cells play an important role in intercellular communication. MVs from different cell types

contain biologically active functional proteins, and nucleic acids including mRNA and microRNA (Pokharel et al., 2016). It was shown that MSC-derived MVs can promote progression of various types of tumors. For instance, MSC-derived MVs have been found to facilitate the migration of MCF7 breast cancer cells by activating the Wnt signaling pathway (Lin et al., 2013), promote the progression of nasopharyngeal carcinoma cells (Shi et al., 2016) and increase the proliferation and metastatic potential of gastric cancer cells (Gu et al., 2016). MSC-derived MVs can also increase tumor cell resistance to drugs. For example, MSC-derived MVs can induce resistance to 5-fluorouracil in gastric cancer cells by activating the CaM-Ks/Raf/MEK/ERK pathway (Ji et al., 2015). Bliss et al. (2016) showed that a possible cause of increased resistance to chemotherapy are micro-RNAs which are included in MVs, such as miR-222/223, which support the resistance of the breast cancer cells in the bone marrow. However, there are conflicting results, for example Del Fattore et al. (2015) reported that MVs isolated from bone marrow and cord blood-derived MSCs suppressed division and induced apoptosis in glioblastoma cells. However, MVs isolated from adipose tissue-derived MSCs showed the opposite effect and stimulated tumor cell proliferation (Del Fattore et al., 2015). As mentioned above, such differences might be explained by activation status of parental MSCs from which the MVs are generated.

One of the possible approaches to use MSCs-isolated MVs in therapy is via the priming/loading of these structures with therapeutic agents. Pascucci et al. (2014) demonstrated that the antitumor activity of MSCs-PTX may be due to the release of a large number of MVs by the MScs. Loaded with PTX MSCs demonstrate vacuole-like structures and accumulation of MVs in extracellular space without significant change in cell morphology. Presence of PTX in MVs was confirmed by Fourier spectroscopy. The release of PTX containing MVs were found to exert anti-cancer activity which was confirmed using the human pancreatic adenocarcinoma cell line CFPAC-1 *in vitro* (Pascucci et al., 2014). This finding was supported by the recent studies of Cocce et al. (2017a) which showed antitumor activity of MVs derived from MSCs-PTX and MSCs-GCB on pancreatic cancer cells *in vitro*.

Yuan et al. (2017) investigated antitumor activity of MSC-derived MVs carrying recombinant TRAIL (rTRAIL) on their surface. Cultivation of M231 breast cancer cells in the presence of MVs led to the induction of apoptosis in cancer cells. At the same time, MVs did not induce apoptosis in normal human bronchial epithelial cells (HBECs). The use of MSC-derived MVs bearing rTRAIL on their surface proved to be more effective than using pure rTRAIL (Yuan et al., 2017).

Kalimuthu et al. (2016) developed bioluminescent EVs using *Renilla luciferase* (Rluc)-expressing MSCs (EV-MSC/Rluc) and showed that these vesicles migrate at tumor sites in the Lewis lung carcinoma (LLC) model *in vivo*. Significant cytotoxic effect of EV-MSC/Rluc on LLC and 4T1 cells *in vitro* was also noticed. Moreover, EV-MSC/Rluc inhibited LLC tumor growth *in vivo* (Kalimuthu et al., 2016).

## CONCLUSION

Tumor development and response to therapy depends not only on tumor cells, but also on different cell types which form the stroma and microenvironment. These include immune cells, vascular endothelial cells and tumor-associated stromal cells such as TAF and MSCs. Due to tropism to the tumor microenvironment, MSCs can be considered as promising vectors for the delivery of antitumor agents (**Figure 1**). To date, there are large number of experimental studies that confirm the anti-oncogenic potential of MSCs modified with therapeutic genes and/or loaded with chemotherapeutic drugs. Thus, the approach of therapeutic agent delivery to the tumor sites using MSCs is promising. However, since it is known that native MSCs can exhibit not only anticancer but also pro-oncogenic properties, further research is needed to improve the safety of this approach. An alternative to using intact MSCs to deliver anti-tumor agents, is the use of MSC-derived MVs which can also be loaded with the same antitumor agents. Further research is needed to evaluate the safety and efficiency of the different therapeutic approaches described in this review to harness the promising potential of MSCs as therapeutic vectors.

## AUTHOR CONTRIBUTIONS

DC wrote the manuscript and made the table. KK and VJ collected the data of homing of MSCs. LT collected the information of MSCs priming. KK made the figure. DC, VS, and AR conceived the idea and edited the manuscript, figure, and table.

## FUNDING

This study was supported by the Russian Foundation for Basic Research grant 16-34-60201. The work was performed according to the Russian Government Program of Competitive Growth of Kazan Federal University. AR was supported by state assignment 20.5175.2017/6.7 of the Ministry of Education and Science of Russian Federation.

## REFERENCES

Ahn, J., Lee, H., Seo, K., Kang, S., Ra, J., and Youn, H. (2013). Anti-tumor effect of adipose tissue derived-mesenchymal stem cells expressing interferon-beta and treatment with cisplatin in a xenograft mouse model for canine melanoma. *PLoS One* 8:e74897. doi: 10.1371/journal.pone.0074897

Arvelo, F., Sojo, F., and Cotte, C. (2016). Tumour progression and metastasis. *Ecancermedicalscience* 10:617. doi: 10.3332/ecancer.2016.617

Birnbaum, T., Roider, J., Schankin, C. J., Padovan, C. S., Schichor, C., Goldbrunner, R., et al. (2007). Malignant gliomas actively recruit bone marrow stromal cells by secreting angiogenic cytokines. *J. Neurooncol.* 83, 241–247. doi: 10.1007/s11060-007-9332-4

Blatt, N. L., Mingaleeva, R. N., Khaiboullina, S. F., Kotlyar, A., Lombardi, V. C., and Rizvanov, A. A. (2013a). In vivo screening models of anticancer drugs. *Life Sci. J.* 10, 1892–1900.

Blatt, N. L., Mingaleeva, R. N., Khaiboullina, S. F., Lombardi, V. C., and Rizvanov, A. A. (2013b). Application of cell and tissue culture systems for anticancer drug screening. *World Appl. Sci. J.* 23, 315–325. doi: 10.5829/idosi.wasj.2013.23.03.13064

Bliss, S. A., Sinha, G., Sandiford, O. A., Williams, L. M., Engelberth, D. J., Guiro, K., et al. (2016). Mesenchymal stem cell-derived exosomes stimulate cycling quiescence and early breast cancer dormancy in bone marrow. *Cancer Res.* 76, 5832–5844. doi: 10.1158/0008-5472.CAN-16-1092

Bolontrade, M. F., Sganga, L., Piaggio, E., Viale, D. L., Sorrentino, M. A., Robinson, A., et al. (2012). A specific subpopulation of mesenchymal stromal cell carriers overrides melanoma resistance to an oncolytic adenovirus. *Stem Cells Dev.* 21, 2689–2702. doi: 10.1089/scd.2011.0643

Bonomi, A., Ghezzi, E., Pascucci, L., Aralla, M., Ceserani, V., Pettinari, L., et al. (2017a). Effect of canine mesenchymal stromal cells loaded with paclitaxel on growth of canine glioma and human glioblastoma cell lines. *Vet. J.* 223, 41–47. doi: 10.1016/j.tvjl.2017.05.005

Bonomi, A., Steimberg, N., Benetti, A., Berenzi, A., Alessandri, G., Pascucci, L., et al. (2017b). Paclitaxel-releasing mesenchymal stromal cells inhibit the growth of multiple myeloma cells in a dynamic 3D culture system. *Hematol. Oncol.* 35, 693–702. doi: 10.1002/hon.2306

Brini, A. T., Cocce, V., Ferreira, L. M., Giannasi, C., Cossellu, G., Gianni, A. B., et al. (2016). Cell-mediated drug delivery by gingival interdental papilla mesenchymal stromal cells (GinPa-MSCs) loaded with paclitaxel. *Expert Opin. Drug Deliv.* 13, 789–798. doi: 10.1517/17425247.2016.1167037

Cafforio, P., Viggiano, L., Mannavola, F., Pelle, E., Caporusso, C., Maiorano, E., et al. (2017). pIL6-TRAIL-engineered umbilical cord mesenchymal/stromal stem cells are highly cytotoxic for myeloma cells both in vitro and in vivo. *Stem Cell Res. Ther.* 8:206. doi: 10.1186/s13287-017-0655-6

Cai, C., Hou, L., Zhang, J., Zhao, D., Wang, Z., Hu, H., et al. (2017). The inhibitory effect of mesenchymal stem cells with rAd-NK4 on liver cancer. *Appl. Biochem. Biotechnol.* 183, 444–459. doi: 10.1007/s12010-017-2456-x

Chanda, D., Isayeva, T., Kumar, S., Hensel, J. A., Sawant, A., Ramaswamy, G., et al. (2009). Therapeutic potential of adult bone marrow-derived mesenchymal stem cells in prostate cancer bone metastasis. *Clin. Cancer Res.* 15, 7175–7185. doi: 10.1158/1078-0432.CCR-09-1938

Chen, Q., Cheng, P., Yin, T., He, H., Yang, L., Wei, Y., et al. (2012). Therapeutic potential of bone marrow-derived mesenchymal stem cells producing pigment epithelium-derived factor in lung carcinoma. *Int. J. Mol. Med.* 30, 527–534. doi: 10.3892/ijmm.2012.1015

Chen, X., Lin, X., Zhao, J., Shi, W., Zhang, H., Wang, Y., et al. (2008). A tumor-selective biotherapy with prolonged impact on established metastases based on cytokine gene-engineered MSCs. *Mol. Ther.* 16, 749–756. doi: 10.1038/mt.2008.3

Choi, S. A., Hwang, S. K., Wang, K. C., Cho, B. K., Phi, J. H., Lee, J. Y., et al. (2011). Therapeutic efficacy and safety of TRAIL-producing human adipose tissue-derived mesenchymal stem cells against experimental brainstem glioma. *Neuro Oncol.* 13, 61–69. doi: 10.1093/neuonc/noq147

Cocce, V., Balducci, L., Falchetti, M. L., Pascucci, L., Ciusani, E., Brini, A. T., et al. (2017a). Fluorescent immortalized human adipose derived stromal cells (hASCs-TS/GFP+) for studying cell drug delivery mediated by microvesicles. *Anticancer Agents Med. Chem.* 17, 1578–1585. doi: 10.2174/1871520617666170327113932

Cocce, V., Farronato, D., Brini, A. T., Masia, C., Gianni, A. B., Piovani, G., et al. (2017b). Drug loaded gingival mesenchymal stromal cells (GinPa-MSCs) inhibit in vitro proliferation of oral squamous cell carcinoma. *Sci. Rep.* 7:9376. doi: 10.1038/s41598-017-09175-4

Cousin, B., Ravet, E., Poglio, S., De Toni, F., Bertuzzi, M., Lulka, H., et al. (2009). Adult stromal cells derived from human adipose tissue provoke pancreatic cancer cell death both in vitro and in vivo. *PLoS One* 4:e6278. doi: 10.1371/journal.pone.0006278

Del Fattore, A., Luciano, R., Saracino, R., Battafarano, G., Rizzo, C., Pascucci, L., et al. (2015). Differential effects of extracellular vesicles secreted by mesenchymal stem cells from different sources on glioblastoma cells. *Expert Opin. Biol. Ther.* 15, 495–504. doi: 10.1517/14712598.2015.997706

Doi, C., Maurya, D. K., Pyle, M. M., Troyer, D., and Tamura, M. (2010). Cytotherapy with naive rat umbilical cord matrix stem cells significantly attenuates growth of murine pancreatic cancer cells and increases survival in syngeneic mice. *Cytotherapy* 12, 408–417. doi: 10.3109/14653240903548194

Du, J., Zhang, Y., Xu, C., and Xu, X. (2015). Apoptin-modified human mesenchymal stem cells inhibit growth of lung carcinoma in nude mice. *Mol. Med. Rep.* 12, 1023–1029. doi: 10.3892/mmr.2015.3501

Du, W., Seah, I., Bougazzoul, O., Choi, G., Meeth, K., Bosenberg, M. W., et al. (2017). Stem cell-released oncolytic herpes simplex virus has therapeutic efficacy in brain metastatic melanomas. *Proc. Natl. Acad. Sci. U.S.A.* 114, E6157–E6165. doi: 10.1073/pnas.1700363114

Duebgen, M., Martinez-Quintanilla, J., Tamura, K., Hingtgen, S., Redjal, N., Wakimoto, H., et al. (2014). Stem cells loaded with multimechanistic oncolytic herpes simplex virus variants for brain tumor therapy. *J. Natl. Cancer Inst.* 106:dju090. doi: 10.1093/jnci/dju090

Dvorak, H. F. (1986). Tumors: wounds that do not heal. Similarities between tumor stroma generation and wound healing. *N. Engl. J. Med.* 315, 1650–1659. doi: 10.1056/NEJM198612253152606

Gilazieva, Z. E., Tazetdinova, L. G., Arkhipova, S. S., Solovyeva, V. V., and Rizvanov, A. A. (2016). Effect of cisplatin on ultrastructure and viability of adipose-derived mesenchymal stem cells. *BioNanoScience* 6, 534–539. doi: 10.1007/s12668-016-0283-0

Gu, H., Ji, R., Zhang, X., Wang, M., Zhu, W., Qian, H., et al. (2016). Exosomes derived from human mesenchymal stem cells promote gastric cancer cell growth and migration via the activation of the Akt pathway. *Mol. Med. Rep.* 14, 3452–3458. doi: 10.3892/mmr.2016.5625

Guiho, R., Biteau, K., Grisendi, G., Taurelle, J., Chatelais, M., Gantier, M., et al. (2016). TRAIL delivered by mesenchymal stromal/stem cells counteracts tumor development in orthotopic Ewing sarcoma models. *Int. J. Cancer* 139, 2802–2811. doi: 10.1002/ijc.30402

Guo, X. R., Hu, Q. Y., Yuan, Y. H., Tang, X. J., Yang, Z. S., Zou, D. D., et al. (2016). PTEN-mRNA engineered mesenchymal stem cell-mediated cytotoxic effects on U251 glioma cells. *Oncol. Lett.* 11, 2733–2740. doi: 10.3892/ol.2016.4297

Hakkarainen, T., Sarkioja, M., Lehenkari, P., Miettinen, S., Ylikomi, T., Suuronen, R., et al. (2007). Human mesenchymal stem cells lack tumor tropism but enhance the antitumor activity of oncolytic adenoviruses in orthotopic lung and breast tumors. *Hum. Gene Ther.* 18, 627–641. doi: 10.1089/hum.2007.034

Han, J., Zhao, J., Xu, J., and Wen, Y. (2014). Mesenchymal stem cells genetically modified by lentivirus-mediated interleukin-12 inhibit malignant ascites in mice. *Exp. Ther. Med.* 8, 1330–1334. doi: 10.3892/etm.2014.1918

Herberts, C. A., Kwa, M. S., and Hermsen, H. P. (2011). Risk factors in the development of stem cell therapy. *J. Transl. Med.* 9:29. doi: 10.1186/1479-5876-9-29

Hong, X., Miller, C., Savant-Bhonsale, S., and Kalkanis, S. N. (2009). Antitumor treatment using interleukin- 12-secreting marrow stromal cells in an invasive glioma model. *Neurosurgery* 64, 1139–1146; discussion 1146–1147. doi: 10.1227/01.NEU.0000345646.85472.EA

Hu, W., Wang, J., He, X., Zhang, H., Yu, F., Jiang, L., et al. (2011). Human umbilical blood mononuclear cell-derived mesenchymal stem cells serve as interleukin-21 gene delivery vehicles for epithelial ovarian cancer therapy in nude mice. *Biotechnol. Appl. Biochem.* 58, 397–404. doi: 10.1002/bab.63

Huang, W. H., Chang, M. C., Tsai, K. S., Hung, M. C., Chen, H. L., and Hung, S. C. (2013). Mesenchymal stem cells promote growth and angiogenesis of tumors in mice. *Oncogene* 32, 4343–4354. doi: 10.1038/onc.2012.458

Ji, R., Zhang, B., Zhang, X., Xue, J., Yuan, X., Yan, Y., et al. (2015). Exosomes derived from human mesenchymal stem cells confer drug resistance in gastric cancer. *Cell Cycle* 14, 2473–2483. doi: 10.1080/15384101.2015.1005530

Kalimuthu, S., Gangadaran, P., Li, X. J., Oh, J. M., Lee, H. W., Jeong, S. Y., et al. (2016). In Vivo therapeutic potential of mesenchymal stem cell-derived extracellular vesicles with optical imaging reporter in tumor mice model. *Sci. Rep.* 6:30418. doi: 10.1038/srep30418

Kalimuthu, S., Oh, J. M., Gangadaran, P., Zhu, L., Lee, H. W., Rajendran, R. L., et al. (2017). In vivo tracking of chemokine receptor CXCR4-engineered mesenchymal stem cell migration by optical molecular imaging. *Stem Cells Int.* 2017:8085637. doi: 10.1155/2017/8085637

Kanehira, M., Xin, H., Hoshino, K., Maemondo, M., Mizuguchi, H., Hayakawa, T., et al. (2007). Targeted delivery of NK4 to multiple lung tumors by bone marrow-derived mesenchymal stem cells. *Cancer Gene Ther.* 14, 894–903. doi: 10.1038/sj.cgt.7701079

Khakoo, A. Y., Pati, S., Anderson, S. A., Reid, W., Elshal, M. F., and Rovira, I. I., et al. (2006). Human mesenchymal stem cells exert potent antitumorigenic effects in a model of Kaposi's sarcoma. *J. Exp. Med.* 203, 1235–1247. doi: 10.1084/jem.20051921

Khorashadizadeh, M., Soleimani, M., Khanahmad, H., Fallah, A., Naderi, M., and Khorramizadeh, M. (2015). Bypassing the need for pre-sensitization of cancer cells for anticancer TRAIL therapy with secretion of novel cell penetrable form of Smac from hA-MSCs as cellular delivery vehicle. *Tumour Biol.* 36, 4213–4221. doi: 10.1007/s13277-015-3058-2

Kidd, S., Caldwell, L., Dietrich, M., Samudio, I., Spaeth, E. L., Watson, K., et al. (2010). Mesenchymal stromal cells alone or expressing interferon-beta suppress pancreatic tumors in vivo, an effect countered by anti-inflammatory treatment. *Cytotherapy* 12, 615–625. doi: 10.3109/14653241003631815

Kim, N., Nam, Y. S., Im, K. I., Lim, J. Y., Lee, E. S., Jeon, Y. W., et al. (2015). IL-21-expressing mesenchymal stem cells prevent lethal B-cell lymphoma through efficient delivery of IL-21, which redirects the immune system to target the tumor. *Stem Cells Dev.* 24, 2808–2821. doi: 10.1089/scd.2015.0103

Kim, S. M., Oh, J. H., Park, S. A., Ryu, C. H., Lim, J. Y., Kim, D. S., et al. (2010). Irradiation enhances the tumor tropism and therapeutic potential of tumor necrosis factor-related apoptosis-inducing ligand-secreting human umbilical cord blood-derived mesenchymal stem cells in glioma therapy. *Stem Cells* 28, 2217–2228. doi: 10.1002/stem.543

Klopp, A. H., Spaeth, E. L., Dembinski, J. L., Woodward, W. A., Munshi, A., Meyn, R. E., et al. (2007). Tumor irradiation increases the recruitment of circulating mesenchymal stem cells into the tumor microenvironment. *Cancer Res.* 67, 11687–11695. doi: 10.1158/0008-5472.CAN-07-1406

Kucerova, L., Altanerova, V., Matuskova, M., Tyciakova, S., and Altaner, C. (2007). Adipose tissue-derived human mesenchymal stem cells mediated prodrug cancer gene therapy. *Cancer Res.* 67, 6304–6313. doi: 10.1158/0008-5472.CAN-06-4024

Kucerova, L., Matuskova, M., Pastorakova, A., Tyciakova, S., Jakubikova, J., Bohovic, R., et al. (2008). Cytosine deaminase expressing human mesenchymal stem cells mediated tumour regression in melanoma bearing mice. *J. Gene Med.* 10, 1071–1082. doi: 10.1002/jgm.1239

Lathrop, M. J., Sage, E. K., Macura, S. L., Brooks, E. M., Cruz, F., Bonenfant, N. R., et al. (2015). Antitumor effects of TRAIL-expressing mesenchymal stromal cells in a mouse xenograft model of human mesothelioma. *Cancer Gene Ther.* 22, 44–54. doi: 10.1038/cgt.2014.68

Lee, H. K., Finniss, S., Cazacu, S., Bucris, E., Ziv-Av, A., Xiang, C., et al. (2013). Mesenchymal stem cells deliver synthetic microRNA mimics to glioma cells and glioma stem cells and inhibit their cell migration and self-renewal. *Oncotarget* 4, 346–361. doi: 10.18632/oncotarget.868

Lejmi, E., Perriraz, N., Clement, S., Morel, P., Baertschiger, R., Christofilopoulos, P., et al. (2015). Inflammatory chemokines MIP-1delta and MIP-3alpha are involved in the migration of multipotent mesenchymal stromal cells induced by hepatoma cells. *Stem Cells Dev.* 24, 1223–1235. doi: 10.1089/scd.2014.0176

Li, L., Guan, Y., Liu, H., Hao, N., Liu, T., Meng, X., et al. (2011). Silica nanorattle-doxorubicin-anchored mesenchymal stem cells for tumor-tropic therapy. *ACS Nano* 5, 7462–7470. doi: 10.1021/nn202399w

Li, L., Li, F., Tian, H., Yue, W., Li, S., and Chen, G. (2014). Human mesenchymal stem cells with adenovirus-mediated TRAIL gene transduction have antitumor effects on esophageal cancer cell line Eca-109. *Acta Biochim. Biophys. Sin.* 46, 471–476. doi: 10.1093/abbs/gmu024

Li, X., Lu, Y., Huang, W., Xu, H., Chen, X., Geng, Q., et al. (2006). In vitro effect of adenovirus-mediated human Gamma Interferon gene transfer into human mesenchymal stem cells for chronic myelogenous leukemia. *Hematol. Oncol.* 24, 151–158. doi: 10.1002/hon.779

Lin, R., Wang, S., and Zhao, R. C. (2013). Exosomes from human adipose-derived mesenchymal stem cells promote migration through Wnt signaling pathway in a breast cancer cell model. *Mol. Cell. Biochem.* 383, 13–20. doi: 10.1007/s11010-013-1746-z

Ling, X., Marini, F., Konopleva, M., Schober, W., Shi, Y., Burks, J., et al. (2010). Mesenchymal stem cells overexpressing IFN-beta inhibit breast cancer growth and metastases through Stat3 signaling in a syngeneic tumor model. *Cancer Microenviron.* 3, 83–95. doi: 10.1007/s12307-010-0041-8

Liu, S., Ginestier, C., Ou, S. J., Clouthier, S. G., Patel, S. H., Monville, F., et al. (2011). Breast cancer stem cells are regulated by mesenchymal stem cells through cytokine networks. *Cancer Res.* 71, 614–624. doi: 10.1158/0008-5472.CAN-10-0538

Ma, F., Chen, D., Chen, F., Chi, Y., Han, Z., Feng, X., et al. (2015). Human umbilical cord mesenchymal stem cells promote breast cancer metastasis by interleukin-8- and interleukin-6-dependent induction of $CD44^{+}/CD24^{-}$ cells. *Cell Transplant.* 24, 2585–2599. doi: 10.3727/096368915X687462

Marini, I., Siegemund, M., Hutt, M., Kontermann, R. E., and Pfizenmaier, K. (2017). Antitumor activity of a mesenchymal stem cell line stably secreting a tumor-targeted TNF-related apoptosis-inducing ligand fusion protein. *Front. Immunol.* 8:536. doi: 10.3389/fimmu.2017.00536

Martinez-Quintanilla, J., Bhere, D., Heidari, P., He, D., Mahmood, U., and Shah, K. (2013). Therapeutic efficacy and fate of bimodal engineered stem cells in malignant brain tumors. *Stem Cells* 31, 1706–1714. doi: 10.1002/stem.1355

Matuskova, M., Hlubinova, K., Pastorakova, A., Hunakova, L., Altanerova, V., Altaner, C., et al. (2010). HSV-tk expressing mesenchymal stem cells exert bystander effect on human glioblastoma cells. *Cancer Lett.* 290, 58–67. doi: 10.1016/j.canlet.2009.08.028

Mohammadpour, H., Pourfathollah, A. A., Nikougoftar Zarif, M., and Shahbazfar, A. A. (2016). Irradiation enhances susceptibility of tumor cells to the antitumor effects of TNF-alpha activated adipose derived mesenchymal stem cells in breast cancer model. *Sci. Rep.* 6:28433. doi: 10.1038/srep28433

Mohr, A., Lyons, M., Deedigan, L., Harte, T., Shaw, G., Howard, L., et al. (2008). Mesenchymal stem cells expressing TRAIL lead to tumour growth inhibition in an experimental lung cancer model. *J. Cell Mol. Med.* 12, 2628–2643. doi: 10.1111/j.1582-4934.2008.00317.x

Nakamura, K., Ito, Y., Kawano, Y., Kurozumi, K., Kobune, M., Tsuda, H., et al. (2004). Antitumor effect of genetically engineered mesenchymal stem cells in a rat glioma model. *Gene Ther.* 11, 1155–1164. doi: 10.1038/sj.gt.3302276

NguyenThai, Q. A., Sharma, N., Luong do, H., Sodhi, S. S., Kim, J. H., Kim, N., et al. (2015). Targeted inhibition of osteosarcoma tumor growth by bone marrow-derived mesenchymal stem cells expressing cytosine deaminase/5-fluorocytosine in tumor-bearing mice. *J. Gene Med.* 17, 87–99. doi: 10.1002/jgm.2826

Nicolay, N. H., Lopez Perez, R., Ruhle, A., Trinh, T., Sisombath, S., Weber, K. J., et al. (2016). Mesenchymal stem cells maintain their defining stem cell characteristics after treatment with cisplatin. *Sci. Rep.* 6:20035. doi: 10.1038/srep20035

Nwabo Kamdje, A. H., Kamga, P. T., Simo, R. T., Vecchio, L., Seke Etet, P. F., Muller, J. M., et al. (2017). Mesenchymal stromal cells' role in tumor microenvironment: involvement of signaling pathways. *Cancer Biol. Med.* 14, 129–141. doi: 10.20892/j.issn.2095-3941.2016.0033

Otsu, K., Das, S., Houser, S. D., Quadri, S. K., Bhattacharya, S., and Bhattacharya, J. (2009). Concentration-dependent inhibition of angiogenesis by mesenchymal stem cells. *Blood* 113, 4197–4205. doi: 10.1182/blood-2008-09-176198

Pascucci, L., Cocce, V., Bonomi, A., Ami, D., Ceccarelli, P., Ciusani, E., et al. (2014). Paclitaxel is incorporated by mesenchymal stromal cells and released in exosomes that inhibit in vitro tumor growth: a new approach for drug delivery. *J. Control. Release* 192, 262–270. doi: 10.1016/j.jconrel.2014.07.042

Pessina, A., Cocce, V., Pascucci, L., Bonomi, A., Cavicchini, L., Sisto, F., et al. (2013). Mesenchymal stromal cells primed with Paclitaxel attract and kill leukaemia cells, inhibit angiogenesis and improve survival of leukaemia-bearing mice. *Br. J. Haematol.* 160, 766–778. doi: 10.1111/bjh.12196

Pessina, A., Piccirillo, M., Mineo, E., Catalani, P., Gribaldo, L., Marafante, E., et al. (1999). Role of SR-4987 stromal cells in the modulation of doxorubicin toxicity to in vitro granulocyte-macrophage progenitors (CFU-GM). *Life Sci.* 65, 513–523. doi: 10.1016/S0024-3205(99)00272-6

Pinilla, S., Alt, E., Abdul Khalek, F. J., Jotzu, C., Muehlberg, F., Beckmann, C., et al. (2009). Tissue resident stem cells produce CCL5 under the influence of cancer cells and thereby promote breast cancer cell invasion. *Cancer Lett.* 284, 80–85. doi: 10.1016/j.canlet.2009.04.013

Pokharel, D., Wijesinghe, P., Oenarto, V., Lu, J. F., Sampson, D. D., Kennedy, B. F., et al. (2016). Deciphering cell-to-cell communication in acquisition of cancer traits: extracellular membrane vesicles are regulators of tissue biomechanics. *OMICS* 20, 462–469. doi: 10.1089/omi.2016.0072

Ponte, A. L., Marais, E., Gallay, N., Langonne, A., Delorme, B., Herault, O., et al. (2007). The in vitro migration capacity of human bone marrow mesenchymal stem cells: comparison of chemokine and growth factor chemotactic activities. *Stem Cells* 25, 1737–1745. doi: 10.1634/stemcells.2007-0054

Qiao, L., Xu, Z., Zhao, T., Zhao, Z., Shi, M., Zhao, R. C., et al. (2008). Suppression of tumorigenesis by human mesenchymal stem cells in a hepatoma model. *Cell Res.* 18, 500–507. doi: 10.1038/cr.2008.40

Ramdasi, S., Sarang, S., and Viswanathan, C. (2015). Potential of mesenchymal stem cell based application in cancer. *Int. J. Hematol. Oncol. Stem Cell Res.* 9, 95–103.

Rattigan, Y., Hsu, J. M., Mishra, P. J., Glod, J., and Banerjee, D. (2010). Interleukin 6 mediated recruitment of mesenchymal stem cells to the hypoxic tumor milieu. *Exp. Cell Res.* 316, 3417–3424. doi: 10.1016/j.yexcr.2010.07.002

Ren, C., Kumar, S., Chanda, D., Chen, J., Mountz, J. D., and Ponnazhagan, S. (2008a). Therapeutic potential of mesenchymal stem cells producing interferon-alpha in a mouse melanoma lung metastasis model. *Stem Cells* 26, 2332–2338. doi: 10.1634/stemcells.2008-0084

Ren, C., Kumar, S., Chanda, D., Kallman, L., Chen, J., Mountz, J. D., et al. (2008b). Cancer gene therapy using mesenchymal stem cells expressing interferon-beta in a mouse prostate cancer lung metastasis model. *Gene Ther.* 15, 1446–1453. doi: 10.1038/gt.2008.101

Ringe, J., Strassburg, S., Neumann, K., Endres, M., Notter, M., Burmester, G. R., et al. (2007). Towards in situ tissue repair: human mesenchymal stem cells express chemokine receptors CXCR1, CXCR2 and CCR2, and migrate upon stimulation with CXCL8 but not CCL2. *J. Cell. Biochem.* 101, 135–146. doi: 10.1002/jcb.21172

Rivera-Cruz, C. M., Shearer, J. J., Figueiredo Neto, M., and Figueiredo, M. L. (2017). The immunomodulatory effects of mesenchymal stem cell polarization within the tumor microenvironment niche. *Stem Cells Int.* 2017:4015039. doi: 10.1155/2017/4015039

Rustad, K. C., and Gurtner, G. C. (2012). Mesenchymal stem cells home to sites of injury and inflammation. *Adv. Wound Care* 1, 147–152. doi: 10.1089/wound.2011.0314

Ryu, C. H., Park, S. H., Park, S. A., Kim, S. M., Lim, J. Y., Jeong, C. H., et al. (2011). Gene therapy of intracranial glioma using interleukin 12-secreting human umbilical cord blood-derived mesenchymal stem cells. *Hum. Gene Ther.* 22, 733–743. doi: 10.1089/hum.2010.187

Sage, E. K., Kolluri, K. K., McNulty, K., Lourenco Sda, S., Kalber, T. L., Ordidge, K. L., et al. (2014). Systemic but not topical TRAIL-expressing mesenchymal stem cells reduce tumour growth in malignant mesothelioma. *Thorax* 69, 638–647. doi: 10.1136/thoraxjnl-2013-204110

Sasaki, M., Abe, R., Fujita, Y., Ando, S., Inokuma, D., and Shimizu, H. (2008). Mesenchymal stem cells are recruited into wounded skin and contribute to wound repair by transdifferentiation into multiple skin cell type. *J. Immunol.* 180, 2581–2587. doi: 10.4049/jimmunol.180.4.2581

Schar, M. O., Diaz-Romero, J., Kohl, S., Zumstein, M. A., and Nesic, D. (2015). Platelet-rich concentrates differentially release growth factors and induce cell migration in vitro. *Clin. Orthop. Relat. Res.* 473, 1635–1643. doi: 10.1007/s11999-015-4192-2

Sharif, S., Ghahremani, M. H., and Soleimani, M. (2017). Delivery of exogenous miR-124 to glioblastoma multiform cells by Wharton's jelly mesenchymal stem cells decreases cell proliferation and migration, and confers chemosensitivity. *Stem Cell Rev.* doi: 10.1007/s12015-017-9788-3

Shi, S., Zhang, Q., Xia, Y., You, B., Shan, Y., Bao, L., et al. (2016). Mesenchymal stem cell-derived exosomes facilitate nasopharyngeal carcinoma progression. *Am. J. Cancer Res.* 6, 459–472.

Smith, C. L., Chaichana, K. L., Lee, Y. M., Lin, B., Stanko, K. M., O'Donnell, T., et al. (2015). Pre-exposure of human adipose mesenchymal stem cells to soluble factors enhances their homing to brain cancer. *Stem Cells Transl. Med.* 4, 239–251. doi: 10.5966/sctm.2014-0149

Son, B. R., Marquez-Curtis, L. A., Kucia, M., Wysoczynski, M., Turner, A. R., Ratajczak, J., et al. (2006). Migration of bone marrow and cord blood mesenchymal stem cells in vitro is regulated by stromal-derived factor-1-CXCR4 and hepatocyte growth factor-c-met axes and involves matrix metalloproteinases. *Stem Cells* 24, 1254–1264. doi: 10.1634/stemcells.2005-0271

Sordi, V., Malosio, M. L., Marchesi, F., Mercalli, A., Melzi, R., Giordano, T., et al. (2005). Bone marrow mesenchymal stem cells express a restricted set of functionally active chemokine receptors capable of promoting migration to pancreatic islets. *Blood* 106, 419–427. doi: 10.1182/blood-2004-09-3507

Srinivasula, S. M., Hegde, R., Saleh, A., Datta, P., Shiozaki, E., Chai, J., et al. (2001). A conserved XIAP-interaction motif in caspase-9 and Smac/DIABLO regulates caspase activity and apoptosis. *Nature* 410, 112–116. doi: 10.1038/35065125

Studeny, M., Marini, F. C., Champlin, R. E., Zompetta, C., Fidler, I. J., and Andreeff, M. (2002). Bone marrow-derived mesenchymal stem cells as vehicles for interferon-beta delivery into tumors. *Cancer Res.* 62, 3603–3608.

Su, H., Li, J., Osinska, H., Li, F., Robbins, J., Liu, J., et al. (2013). The COP9 signalosome is required for autophagy, proteasome-mediated proteolysis, and cardiomyocyte survival in adult mice. *Circ. Heart Fail.* 6, 1049–1057. doi: 10.1161/CIRCHEARTFAILURE.113.000338

Szegezdi, E., O'Reilly, A., Davy, Y., Vawda, R., Taylor, D. L., Murphy, M., et al. (2009). Stem cells are resistant to TRAIL receptor-mediated apoptosis. *J. Cell Mol. Med.* 13, 4409–4414. doi: 10.1111/j.1582-4934.2008.00522.x

Tsukamoto, S., Honoki, K., Fujii, H., Tohma, Y., Kido, A., Mori, T., et al. (2012). Mesenchymal stem cells promote tumor engraftment and metastatic colonization in rat osteosarcoma model. *Int. J. Oncol.* 40, 163–169. doi: 10.3892/ijo.2011.1220

Uchibori, R., Okada, T., Ito, T., Urabe, M., Mizukami, H., Kume, A., et al. (2009). Retroviral vector-producing mesenchymal stem cells for targeted suicide cancer gene therapy. *J. Gene Med.* 11, 373–381. doi: 10.1002/jgm.1313

Volarevic, V., Markovic, B. S., Gazdic, M., Volarevic, A., Jovicic, N., Arsenijevic, N., et al. (2018). Ethical and safety issues of stem cell-based therapy. *Int. J. Med. Sci.* 15, 36–45. doi: 10.7150/ijms.21666

Wang, G. X., Zhan, Y. A., Hu, H. L., Wang, Y., and Fu, B. (2012). Mesenchymal stem cells modified to express interferon-beta inhibit the growth of prostate cancer in a mouse model. *J. Int. Med. Res.* 40, 317–327. doi: 10.1177/147323001204000132

Wang, X. J., Xiang, B. Y., Ding, Y. H., Chen, L., Zou, H., Mou, X. Z., et al. (2017). Human menstrual blood-derived mesenchymal stem cells as a cellular vehicle for malignant glioma gene therapy. *Oncotarget* 8, 58309–58321. doi: 10.18632/oncotarget.17621

Wu, N., Zhang, Y. L., Wang, H. T., Li, D. W., Dai, H. J., Zhang, Q. Q., et al. (2016). Overexpression of hepatocyte nuclear factor 4alpha in human mesenchymal stem cells suppresses hepatocellular carcinoma development through Wnt/beta-catenin signaling pathway downregulation. *Cancer Biol. Ther.* 17, 558–565. doi: 10.1080/15384047.2016.1177675

Xia, L., Peng, R., Leng, W., Jia, R., Zeng, X., Yang, X., et al. (2015). TRAIL-expressing gingival-derived mesenchymal stem cells inhibit tumorigenesis of tongue squamous cell carcinoma. *J. Dent. Res.* 94, 219–228. doi: 10.1177/0022034514557815

Xie, C., Yang, Z., Suo, Y., Chen, Q., Wei, D., Weng, X., et al. (2017). Systemically infused mesenchymal stem cells show different homing profiles in healthy and tumor mouse models. *Stem Cells Transl. Med.* 6, 1120–1131. doi: 10.1002/sctm.16-0204

Xin, H., Kanehira, M., Mizuguchi, H., Hayakawa, T., Kikuchi, T., Nukiwa, T., et al. (2007). Targeted delivery of CX3CL1 to multiple lung tumors by mesenchymal stem cells. *Stem Cells* 25, 1618–1626. doi: 10.1634/stemcells.2006-0461

Xu, W. T., Bian, Z. Y., Fan, Q. M., Li, G., and Tang, T. T. (2009). Human mesenchymal stem cells (hMSCs) target osteosarcoma and promote its growth and pulmonary metastasis. *Cancer Lett.* 281, 32–41. doi: 10.1016/j.canlet.2009.02.022

Yan, C., Song, X., Yu, W., Wei, F., Li, H., Lv, M., et al. (2016). Human umbilical cord mesenchymal stem cells delivering sTRAIL home to lung cancer mediated by MCP-1/CCR2 axis and exhibit antitumor effects. *Tumour Biol.* 37, 8425–8435. doi: 10.1007/s13277-015-4746-7

Yan, Z., Zhuansun, Y., Chen, R., Li, J., and Ran, P. (2014a). Immunomodulation of mesenchymal stromal cells on regulatory T cells and its possible mechanism. *Exp. Cell Res.* 324, 65–74. doi: 10.1016/j.yexcr.2014.03.013

Yan, Z., Zhuansun, Y., Liu, G., Chen, R., Li, J., and Ran, P. (2014b). Mesenchymal stem cells suppress T cells by inducing apoptosis and through PD-1/B7-H1 interactions. *Immunol. Lett.* 162(1 Pt A), 248–255. doi: 10.1016/j.imlet.2014.09.013

Yang, L., Zhang, Y., Cheng, L., Yue, D., Ma, J., Zhao, D., et al. (2016). Mesenchymal stem cells engineered to secrete pigment epithelium-derived factor inhibit tumor metastasis and the formation of malignant ascites in a murine colorectal

peritoneal carcinomatosis model. *Hum. Gene Ther.* 27, 267–277. doi: 10.1089/hum.2015.135

Yang, X., Du, J., Xu, X., Xu, C., and Song, W. (2014). IFN-gamma-secreting-mesenchymal stem cells exert an antitumor effect in vivo via the TRAIL pathway. *J. Immunol. Res.* 2014:318098. doi: 10.1155/2014/318098

Yang, Z. S., Tang, X. J., Guo, X. R., Zou, D. D., Sun, X. Y., Feng, J. B., et al. (2014). Cancer cell-oriented migration of mesenchymal stem cells engineered with an anticancer gene (PTEN): an imaging demonstration. *Onco Targets Ther.* 7, 441–446. doi: 10.2147/OTT.S59227

You, Q., Yao, Y., Zhang, Y., Fu, S., Du, M., and Zhang, G. (2015). Effect of targeted ovarian cancer therapy using amniotic fluid mesenchymal stem cells transfected with enhanced green fluorescent protein-human interleukin-2 in vivo. *Mol. Med. Rep.* 12, 4859–4866. doi: 10.3892/mmr.2015.4076

Yuan, Z., Kolluri, K. K., Gowers, K. H., and Janes, S. M. (2017). TRAIL delivery by MSC-derived extracellular vesicles is an effective anticancer therapy. *J. Extracell. Vesicles* 6:1265291. doi: 10.1080/20013078.2017.1265291

Yuan, Z., Kolluri, K. K., Sage, E. K., Gowers, K. H., and Janes, S. M. (2015). Mesenchymal stromal cell delivery of full-length tumor necrosis factor-related apoptosis-inducing ligand is superior to soluble type for cancer therapy. *Cytotherapy* 17, 885–896. doi: 10.1016/j.jcyt.2015.03.603

Zhang, B., Shan, H., Li, D., Li, Z. R., Zhu, K. S., and Jiang, Z. B. (2012). The inhibitory effect of MSCs expressing TRAIL as a cellular delivery vehicle in combination with cisplatin on hepatocellular carcinoma. *Cancer Biol. Ther.* 13, 1175–1184. doi: 10.4161/cbt.21347

Zhang, J., Hou, L., Wu, X., Zhao, D., Wang, Z., Hu, H., et al. (2016). Inhibitory effect of genetically engineered mesenchymal stem cells with Apoptin on hepatoma cells in vitro and in vivo. *Mol. Cell. Biochem.* 416, 193–203. doi: 10.1007/s11010-016-2707-0

Zhao, W. H., Cheng, J. X., Shi, P. F., and Huang, J. Y. (2011). Human umbilical cord mesenchymal stem cells with adenovirus-mediated interleukin 12 gene transduction inhibits the growth of ovarian carcinoma cells both in vitro and in vivo. *Nan Fang Yi Ke Da Xue Xue Bao* 31, 903–907.

Zhu, Y., Cheng, M., Yang, Z., Zeng, C. Y., Chen, J., Xie, Y., et al. (2014). Mesenchymal stem cell-based NK4 gene therapy in nude mice bearing gastric cancer xenografts. *Drug Des. Dev. Ther.* 8, 2449–2462. doi: 10.2147/DDDT.S71466

**Conflict of Interest Statement:** The authors declare that the research was conducted in the absence of any commercial or financial relationships that could be construed as a potential conflict of interest.

frontiers in Oncology

REVIEW
published: 12 April 2018
doi: 10.3389/fonc.2018.00106

# DNA Damage Inducible Transcript 4 Gene: The Switch of the Metabolism as Potential Target in Cancer

*Indira Tirado-Hurtado[1], Williams Fajardo[2] and Joseph A. Pinto[1]**

[1]*Unidad de Investigación Básica y Traslacional, Oncosalud-AUNA, Lima, Peru,* [2]*Escuela de Medicina Humana, Universidad Privada San Juan Bautista, Lima, Peru*

DNA damage inducible transcript 4 (*DDIT4*) gene is expressed under stress situations turning off the metabolic activity triggered by the mammalian target of rapamycin (mTOR). Several *in vitro* and *in vivo* works have demonstrated the ability of *DDIT4* to generate resistance to cancer therapy. The link between the metabolism suppression and aggressiveness features of cancer cells remains poorly understood since anti-mTOR agents who are part of the repertoire of drugs used for systemic treatment of cancer achieving variable results. Interestingly, the high *DDIT4* expression is associated with worse outcomes compared to tumors with low *DDIT4* expression, seen in a wide variety of solid and hematological tumors, which suggests the driver role of this gene and provide the basis to target it as part of a new therapeutic strategy. In this review, we highlight our current knowledge about the biology of *DDIT4* and its role as a prognostic biomarker, encompassing the motives for the development of target drugs against *DDIT4* as a better target than mTOR inhibitors.

**Keywords: DNA damage inducible transcript 4, mammalian target of rapamycin, malignant tumors, biomarkers, targeted therapies**

OPEN ACCESS

***Edited by:***
*Karine A. Cohen-Solal, Rutgers University, United States*

***Reviewed by:***
*Chakrabhavi Dhananjaya Mohan, University of Mysore, India*
*Alessandro Rufini, University of Leicester, United Kingdom*

****Correspondence:***
*Joseph A. Pinto*
*jpinto@gecoperu.org*

***Specialty section:***
*This article was submitted to Cancer Molecular Targets and Therapeutics, a section of the journal Frontiers in Oncology*

***Received:*** *22 November 2017*
***Accepted:*** *26 March 2018*
***Published:*** *12 April 2018*

***Citation:***
*Tirado-Hurtado I, Fajardo W and Pinto JA (2018) DNA Damage Inducible Transcript 4 Gene: The Switch of the Metabolism as Potential Target in Cancer. Front. Oncol. 8:106. doi: 10.3389/fonc.2018.00106*

## BACKGROUND

Cancer is a complex disease arising from the gradual accumulation of genetic changes resulting in the reprogramming of key cellular processes well described in "The Hallmarks of Cancer" written by Hanahan and Weinberg (1). Structural and functional alterations in driver genes and entire pathways to fulfill the nutritional requirements are responsible for this reprogramming, and although their mechanisms are not fully known, various drugs have been developed to target actionable mutations (2, 3).

One attractive therapeutic strategy is the inhibition of the mammalian target of rapamycin (mTOR), as well as various downstream and upstream signaling molecules (4). The mTOR pathway has evolved as nutrient sensing to promote cell proliferation under adequate nutritional and environmental conditions (5). The activation of mTOR depends on the formation of two complexes called mTOR complex 1 (mTORC1) and mTOR complex 2 (mTORC2) that are activated in distinct ways. mTORC1 controls the protein synthesis and cell survival through the phosphorylation of its substrates, 4EBP1, p70S6K and factor 4G. mTORC1 is inactivated by rapamycin but is activated by growth factors, nutrients, energy and stress signals, and essential signaling pathways (PI3K, MAPK, and AMPK). In contrast to mTORC1, mTORC2 is not inactivated by rapamycin and generally, it is not affected by nutrients and energy signals. mTORC2 regulates cytoskeleton organization and promotes cell survival through the phosphorylation of protein kinase B (Akt) and protein kinase C (6–8). The key role of mTOR in these processes explains its association in pathologies such as cancer (9, 10).

Several works and recent cancer genomic projects described high rates of mutations in genes involved in the mTOR pathway, including *PI3K*, *PTEN*, *AKT*, and *S6K1, 4EBP1,* and *EIF4E*. Based

in this data, mTOR inhibitors (rapamycin and its analogs) have become attractive therapeutic agents tested in several clinical trials, as single agents or in combination with other types of systemic treatment (9). Unfortunately, some inhibitors of mTOR have shown lack of efficacy, including the rapamycin (11).

The DNA damage inducible transcript 4 (*DDIT4*) is induced by cellular stress conditions and regulates the mTOR activity (12), and also its abnormal expression has been linked to multiple diseases, including malignant tumors (13–18).

## *DDIT4* GENE

This gene was simultaneously discovered and cloned in 2002 by two independent research groups. Shoshani et al. using a microarray hybridization technique to investigate the hypoxia-dependent gene expression in rat glioma C6 cells reported a gene highly upregulated in response to hypoxia-inducible factor 1 (HIF-1) and regulating the generation of cellular reactive oxygen species (ROS). This gene was designated *RTP801* (19). Concurrently, Ellisen et al. identified a new p53 target induced by DNA damage and regulated by p63 during embryogenesis and epidermal differentiation. In this study, this gene was alternatively designated *REDD1* (regulated in development and DNA damage response 1), which was also involved in the generation of ROS (20).

Contemporarily with these works, Wang et al. analyzed which genes are potentially involved in regulating glucocorticoid-induced apoptosis in lymphoid cells. Through an oligonucleotide microarray analysis, they discovered a novel dexamethasone-induced gene designated *Dig2* whose expression is significantly induced in cell lines of murine T-cell lymphoma and in normal mouse thymocytes (21). The official name given by the HUGO Gene Nomenclature Committee was *DDIT4*.

*DDIT4* is located on chromosome 10 (10q22.1) and has a length of 2.1 kb, containing three exons and two introns (19, 20). *DDIT4* has three splice variants (one it is the protein coding with 232 amino acids and the others are retained introns), 95 orthologs, one paralog (*DDIT4L*, DNA damage inducible transcript 4 like) and is associated with one phenotype (22). Because of this, it is presumed that it was present in the common ancestor of animals (23).

*DDIT4* is ubiquitously expressed at low levels in most adult tissues (**Figure 1**) (19). The *DDIT4* expression is induced by multiple cellular stresses, such as hypoxia (19, 24), ionizing radiation (IR) (20), methyl methane sulfonate (MMS) (25), heat shock (21), and energy depletion (12). Moreover, it is also upregulated by other chemical molecules, such as glucocorticoids (21, 26, 27), dopaminergic neurotoxins (28), endoplasmic reticulum stress inducers (21, 29), DNA damage agent etoposide (21), and arsenite (30). Conversely, *DDIT4* expression decreases by testosterone, acute resistance exercise, refeeding/nutrient consumption, and suppressed mTORC1 (31).

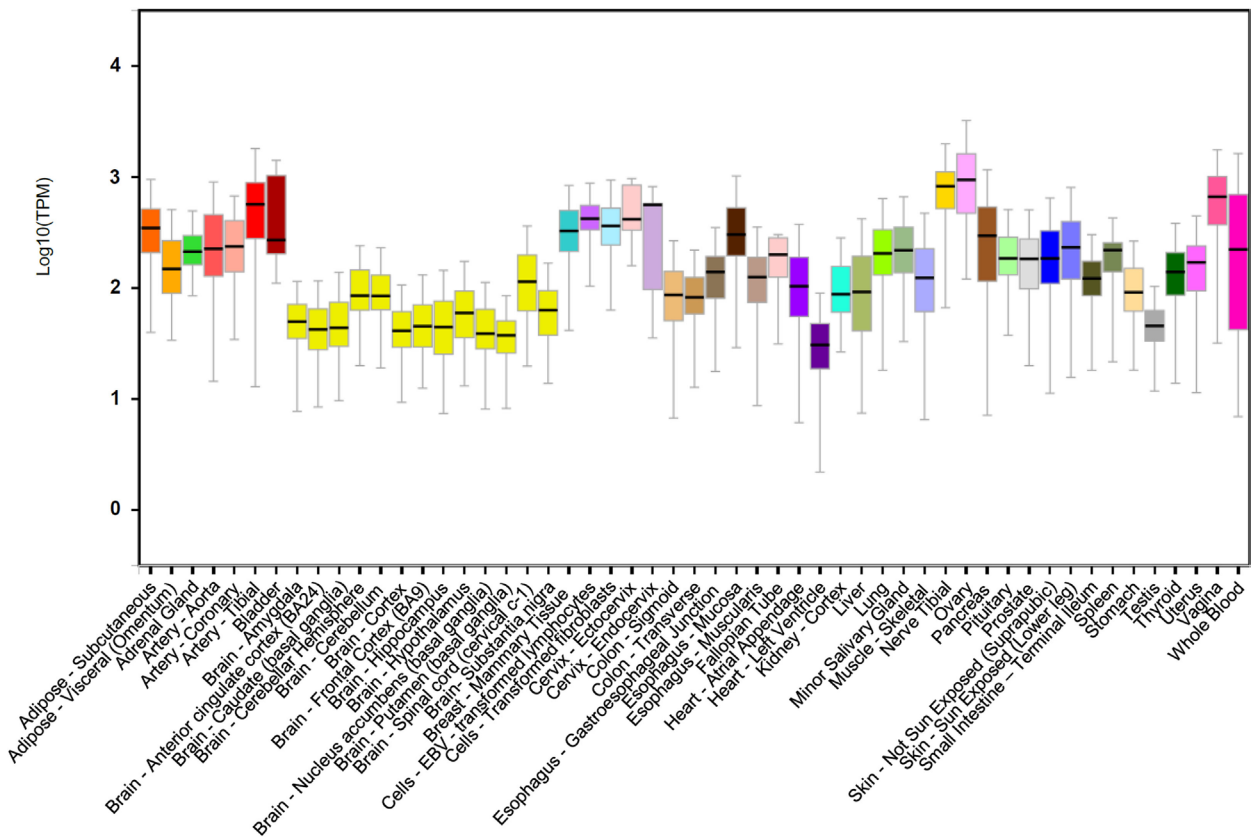


**FIGURE 1** | DNA damage inducible transcript 4 (*DDIT4*) gene expression. *DDIT4* is ubiquitously expressed in multiple human tissues (32).

## DDIT4 PROTEIN

With an estimated half-life of approximately 5 min (33, 34), DDIT4 is a highly conserved protein composed of 232 amino acids, rich in leucine (17%) and contains conserved 9- or 10-serine stretches at its N-terminal end. Its molecular weight is 25 kDa, but it migrates around 35 kDa on Western blot because of its multiple lysine residues at the carboxyl terminus (19, 20). In addition, DDIT4 is mainly present in the cytoplasm and the nucleus (20, 30), but it has also been observed in membranes (35).

The crystal structure of DDIT4 (PDB ID# 3LQ9) shows that this protein has two chains (A and B), where each chain has antiparallel α-helices followed by four β-strands with two highly conserved residues (residues 138–141 and 218–225) that might be essential for the activity of the protein (**Figure 2**). Amino acids in position 85–193 and 207–225 correspond to linear segments required for its function, separated by a dispensable region. The extreme N-terminus has 84 amino acids residues poorly preserved among species and dispensable for the function of the protein. By contrast, the C-terminal region is highly conserved and essential for the correct function of DDIT4. Internal deletions and NAAIRS (the sequence Asn–Ala–Ala–Ile–Arg–Ser) substitutions are poorly tolerated because this causes the protein to change to an unphysiological conformation (36).

## REGULATION OF DDIT4

*DDIT4* expression is upregulated by several transcription factors in response to different stressors (37). For example, under hypoxic conditions, HIF-1 increases the transcription of *DDIT4* by binding to a hypoxia response element of the *DDIT4* promoter causing downregulation of mTOR (19, 24). Telomere destabilization by DNA-damaging agents also increases *DDIT4* expression through multiple pathways. In mouse embryo fibroblasts (MEFs), IR induces *DDIT4* expression through p53 pathway in a dependent manner (20). Similarly, in HaCaT human keratinocytes, MMS induces *DDIT4* expression through Elk-1 pathway and CCAAT/enhancer-binding protein (C/EBP) but in a p53-independent manner (25). Another transcription factor is the nuclear factor of activated T-cells 3, whose overexpression increases c-Myc (mTOR downstream target) and MUC2 expression (a marker of goblet cell differentiation) through the induction of *DDIT4* expression; important process to the regulation of intestinal cell differentiation (38).

**FIGURE 2** | Crystal structure of the human protein DNA damage inducible transcript 4 (PDB ID# 3LQ9). Both of their chains have antiparallel α-helices followed by four β-strands.

MicroRNAs, small and highly conserved non-coding RNA molecules, are also involved in tumorigenesis by regulating (at posttranscriptional level) specific oncogenes and tumor suppressor genes (39–41), such as *DDIT4*. miR-221 overexpression contributes to liver tumorigenesis through the cyclin-dependent kinase inhibitor p27 (Kip1-CDKN1B) and/or *DDIT4* downregulation (42). miR-495, directly upregulated by the transcription factors E12/E47 in breast cancer stem cells promotes oncogenesis and hypoxia resistance *via* downregulation of E-cadherin and *DDIT4* (43). miR-30c plays a key role in radiation-induced cell damage because, maybe in part, it downregulates *DDIT4* expression in human hematopoietic and osteoblast cells after gamma-irradiation (44). miR-630 has a bimodal role in the regulation of apoptosis in response to DNA damage; it promotes apoptosis by downregulation of cell cycle kinase 7 kinase, and on the other hand, it reduces apoptosis by downregulating apoptotic activators, such as DDIT4, PARP3, EP300, and p53 (45).

At posttranslational level, DDIT4 is quickly degraded by the ubiquitin-proteasome system to allow cells to restore mTOR signaling once the stress conditions have been mitigated. One of the models reported by Katiyar et al. consists in the phosphorylation of DDIT4 by GSK3-β, which causes the recruitment of the Cullin 4A (CUL4A)–DNA damage-binding protein 1–regulator of cullins 1–β-transducin repeat containing protein (β-TRCP) E3 ligase complex, that results in DDIT4 ubiquitination and degradation by the proteasome (34). Amplification and overexpression of *CUL4A* have been observed in primary breast cancers (46) and others types of cancers such as hepatocellular carcinomas (47), so it could be considered as a potential predictive and prognostic indicator of some cancers. In addition, increased β-TRCP mRNA and protein expression have also been found in colorectal and pancreatic cancers (48, 49). By contrast, Tan and Hagen reported that there is an alternative E3 ligase (currently unknown) responsible for both basal DDIT4 ubiquitination and ubiquitination that is induced upon mTORC1 inhibition (50). These processes sustain that the dysregulation of DDIT4 degradation could be a common event that elevates mTOR signaling during tumor development.

## *DDIT4* INHIBITS THE ACTIVITY OF mTOR *VIA* TUBEROUS SCLEROSIS COMPLEX (TSC1/TSC2 COMPLEX)

All the stressors mentioned above, *via* different transcription factors, elevate the *DDIT4* expression to fulfill its main function, inhibit mTORC1 to regulate key cellular processes, such as cell

growing, proliferation, and survival (12, 24). This inhibitory effect was initially identified in *Drosophila*, where expression of *Scylla* (homologous protein of DDIT4 in *Drosophila*) suppress the phosphorylation of S6K (a known substrate of TOR) (51); a similar process that was later confirmed in mammalian cells (52). In addition, TSC1/TSC2 complex does not interact directly with mTORC1, but it functions as a GTPase, inactivating to Rheb, converting Rheb-GTP into Rheb-GDP, unable to activate the mTORC1 complex (53).

Gordon et al. proposed two models of the effect of DDIT4 in the mTOR pathway. One model proposes that DDIT4 competes with TSC2 to bind with the 14-3-3 proteins. DDIT4 expression increases causing the dissociation of the 14-3-3 proteins with TSC2, so TSC2 is released to form a functional TSC1/TSC2 complex that inhibits mTORC1 activity (31, 35). However, functional and structural analysis has concluded that it is unlikely that DDIT4 interacts directly with 14-3-3 proteins, discarding this model (36). The other model proposes that phosphatase-2A recruit to Akt causing the reduction of Akt phosphorylation, which in turn causes the reduction of phosphorylation of TSC2 and its induction. The TSC1/TSC2 complex is formed and subsequently represses mTORC1 activity. By contrast, TSC1/TSC2 complex positively regulates mTORC2 through association with rapamycin-insensitive companion of mTOR (31) (**Figures 3** and **4**).

## DDIT4 AND AUTOPHAGY

Autophagy is a catabolic mechanism of cellular adaptation to nutrients deprivation in which cellular components are degraded to its elementary molecules and recycled to promote the cell survival (54). In addition, autophagy participates in the removal of old or damaged cellular organelles and has been associated with the survival of cancer cells (55). Autophagy is the opposite response to cell growth and proliferation induced by mTOR activity. Under favorable nutritional conditions, the complex mTORC1 represses autophagy by phosphorylation of the ULK protein complex turning it in an open structural conformation (inactive form). DDIT4-mediated mTOR repression produces the lack of phosphorylation of the ULK complex, turning the complex in a closed structural conformation (active form) activating the mechanism of autophagy and triggering the formation of the autophagosome (56).

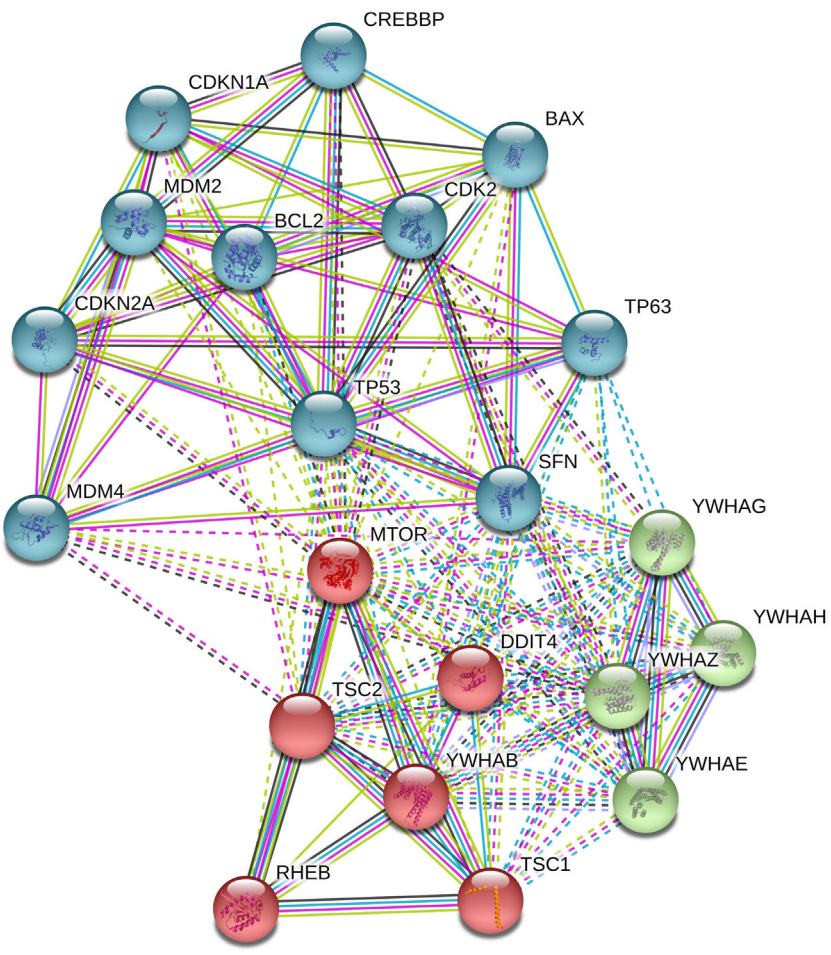


**FIGURE 3** | Analysis in STRING-DB v.10.5 describes that DNA damage inducible transcript 4 (DDIT4) is involved in the regulation of at least three clusters of proteins, (i) mammalian target of rapamycin (mTOR) pathway proteins (in red), (ii) p53 pathway (in sky blue), and (iii) 14-3-3 proteins (in green).

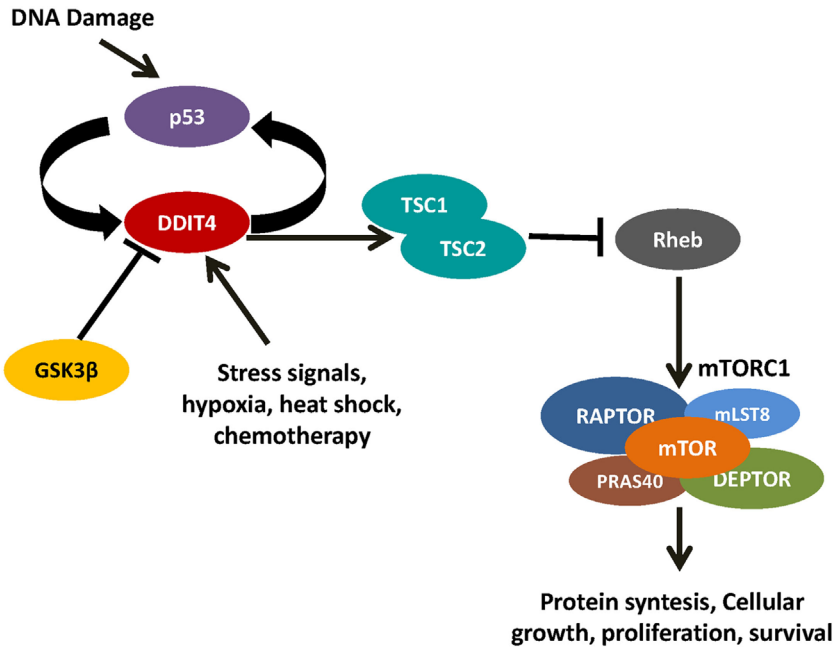


**FIGURE 4** | DNA damage inducible transcript 4 (DDIT4) controls mammalian target of rapamycin (mTOR) by the activation of the TSC1/TSC2 complex. When the TSC1/TSC2 complex inactivates Rheb, it is unable to activate mTOR complex 1.

## ROLE OF *DDIT4* IN CANCER

Dysfunction of *DDIT4* has been associated with multiple diseases, such as neurodegenerative disorders (28, 57), ischemic proliferative retinopathy (58), preeclampsia (59), diabetes, and other degenerative pathologies, such as cancer (10). Results of *in vitro* studies suggest that *DDIT4* could have a context-dependent contrasting role in cancer as oncogene or tumor suppressor (19, 60).

Hyperactivation of the PI3K-Akt-mTOR signaling is a common alteration in cancer. This pathway regulates cellular processes involved in cell growth, proliferation, motility, survival, and apoptosis (61). In normal cells, PI3K-Akt-mTOR signaling is controlled by PTEN through PI3K dephosphorylation ensuring a transient and controlled activation. On the other hand, PTEN inactivation causes a chronic activation of PI3K and its downstream effectors, such as Akt, promoting the cell cycle progression, survival, and decreased apoptosis (62).

To know which genes are involved in the growth of cancer cells *via* chronically activated PIK-3 (such as in *PTEN*$^{-/-}$ cells), Schwarzer et al. compared *PIK3* expression between cells that have active *PIK-3* versus cells in which it is silenced. They found that *DDIT4* mRNA was significantly downregulated in prostate cancer cells (PC-3) using LY294002 (2-morpholin-4-yl-8-phenylchromen-4-one) or rapamycin, both inhibitors of PI3K, in combination with matrigel-based 3D culture system. By contrast, *DDIT4* was overexpressed under hypoxic conditions in a HIF-1α dependent manner. They also verified their results with other methods, as, for example, inhibiting the function of *DDIT4* employing antisense molecules or interference RNA, which indicates that DDIT4 is a transcriptional downstream target in the PI3K pathway and essential for invasive growth of PC-3 both *in vitro* and *in vivo* (13).

On the other hand, *DDIT4* has a key role in RAS signaling to transform human ovarian epithelial cells. *DDIT4* is overexpressed in RAS-transformed human ovarian epithelial cells lines T29 and T80 promoting cell proliferation and colony formation. *DDIT4* is overexpressed after activation of *RAS* oncogene, increasing levels of anti-apoptotic proteins and at the same time decreasing expression of pro-apoptotic proteins (60, 63).

Several works have described an involvement of *DDIT4* in the breast cancer biology, while its expression seems to have different patterns among breast cancer subtypes. Koo and Jung characterized the expression of proteins involved in mTOR and hypoxia pathway with staining with immunohistochemistry where immunophenotypes of breast cancer were determined by the evaluation of estrogen and progesterone receptors and HER2 while breast papilloma samples were included as controls (64).

In this study, Glut-1 and HIF-1α had higher expression in triple-negative breast cancer (TNBC) and HER2 phenotypes than in the luminal A and B phenotypes. These findings could be explained by the greater hypoxia conditions present in TNBC and HER2 tumors. Likewise, Ki-67 expression in TNBC and HER2 was higher than in other phenotypes or papilloma. Interestingly, downregulation of DDIT4 does not lead to a negative feedback to HIF-1 α, so the tumorigenesis mediated by HIF-1α is constant. Moreover, this study demonstrated that HIF-1α expression was associated with reduced disease-free survival (DFS) and reduced overall survival (OS), concordant with previous studies (65–67).

Concluding that TNBC and HER2 overexpression showed the highest cell proliferation and survival in a hypoxic tumor environment by activation of the mTOR pathway and HIF-1α stabilization *via* DDIT4 downregulation (64).

*DDIT4* participate in an endogenous feedback circuit with p53. When cells and tissues of *DDIT4*$^{-/-}$ mice are exposed to IR and chemotherapy treatment, the genetic loss of *DDIT4* confers an increase in DNA damage-induced apoptosis both *in vitro* and *in vivo*, which is associated with elevated levels of p53 protein following DNA damage. It was proved that deregulation of p53 is not due to increased p53 stabilization or failed DNA repair but, instead, to increased p53 translation. Consistent with this, it was demonstrated that *DDIT4* loss elevates the mTORC1 activity, which explains the increased p53 translation and damage sensitivity in *DDIT4*$^{-/-}$ cells (68).

Under stress conditions mTORC1 is also inhibited by the activation of p53 both dependently and independently of Sertrin1/2, suggesting the existence of more than one pathway to inhibit mTORC1 (69–71). To test this, Cam et al. exposed MEFs and *in vivo* tumor models to drugs that induce DNA damage to analyze the upstream regulation of mTORC1 signaling. They found that inhibition of mTORC1 signaling to 4EBP1 requires the coordinated activity of both p53 and p63; by contrast, the inhibition of S6K1 and rpS6 phosphorylation is Akt-dependent. Concordant with this, the loss of p53 or p63 prevents the suppression of mTORC1 signaling induced by the DNA damage, supporting that both are necessary for the inhibition of mTORC1. Suggesting that there are multiples mechanisms that suppress p53/p63 responses and at the same time suppress the ability of the cancer cell to control mTORC1 (72).

In response to DNA damage, DDIT4 phosphorylates downstream Akt through the TSC1/TSC2 complex to inhibit mTORC1 signaling (73, 74). To investigate the clinical significance of this process, Wei et al. analyzed the DDIT4 and p-Akt expression in ovary cancer (primary ovarian cancer and borderline tumors) and normal fallopian tubes. Both DDIT4 and p-Akt expressions were significantly higher in patients with serous ovarian cancer and late FIGO stage; while only DDIT4 expression was significantly higher in ascites formation and only p-Akt expression was significantly histological grade and chemoresistance. Features of patients with improved outcomes in terms of DFS and OS were low DDIT4 staining or absence of p-Akt. In this work, there was no association between *KRAS* mutations and DDIT4 intensity staining, suggesting that *KRAS* is not involved in the activation of DDIT4 (15).

In contrast to the study performed by Koo and Jung, where they reported that *DDIT4* is downregulated in TNBC and HER2 overexpression types (64), Pinto et al. found that *DDIT4* is associated with poor prognosis in TNBC resistant to neoadjuvant chemotherapy (17).

All these data presented previously show that *DDIT4* has a key role in different types of cancer and its aggressiveness. A recent *in silico* analysis of *DDIT4* expression in several cancer types showed that the high expression of this gene was related to a bad outcome in diverse hematologic and solid tumors, such as acute myeloid leukemia, breast cancer, glioblastoma multiforme, melanoma, lung, and colon cancer. Furthermore, it was shown that response to rapamycin and others mTOR inhibitors were not influenced by *DDIT4* expression (18).

## CONCLUDING REMARKS AND FUTURE PERSPECTIVES

The increasing evidence about the involvement of *DDIT4* in key cellular mechanisms of tumor aggressiveness suggests its driver role in cancer and consequently, its potential not only as prognostic biomarker but also as a therapeutic target. Since mTOR inhibitors have shown disappointing results in the treatment of cancer, where the main issues are the lack of a biomarker to select patients who will benefit from these drugs and the poor knowledge about mechanisms of resistance, a better therapeutic strategy would be *DDIT4* inhibition. In contrast to mTOR expression, the high *DDIT4* expression is related with a poor outcome. We hypothesize DDIT4 targeting could lead to cancer cells to avoid the metabolic suppression needed for cell survival under stress conditions (e.g., treatment with cytotoxic chemotherapy or radiotherapy). Combination of DDIT4 inhibitors with DNA-damaging agents, such as cisplatin, will be interesting, especially in tumors with loss of function of *TP53*, because wild-type p53 repress the expression of DDIT4 in a regulatory loop, potentiating the effects of DDIT4 inhibitors.

## AUTHOR CONTRIBUTIONS

IT-H gathered all the information and wrote the first draft of the manuscript. WF wrote, corrected, and also provided important contributions to the final manuscript. JP contributed to the conception and design of the project, critically reviewing the entire manuscript. All authors contributed to manuscript revision, read and approved the submitted version.

## REFERENCES


1. Hanahan D, Weinberg RA. The hallmarks of cancer. *Cell* (2000) 100(1):57–70. doi:10.1016/S0092-8674(00)81683-9
2. Bianco R, Melisi D, Ciardiello F, Tortora G. Key cancer cell signal transduction pathways as therapeutic targets. *Eur J Cancer* (2006) 42(3):290–4. doi:10.1016/j.ejca.2005.07.034
3. Maiese K. Therapeutic targets for cancer: current concepts with PI 3-K, Akt, & mTOR. *Indian J Med Res* (2013) 137(2):243–6.
4. Mita MM, Mita A, Rowinsky EK. The molecular target of rapamycin (mTOR) as a therapeutic target against cancer. *Cancer Biol Ther* (2003) 2(4 Suppl 1): S169–77. doi:10.4161/cbt.365
5. Laplante M, Sabatini DM. mTOR signaling in growth control and disease. *Cell* (2012) 149(2):274–93. doi:10.1016/j.cell.2012.03.017
6. Wullschleger S, Loewith R, Hall MN. TOR signaling in growth and metabolism. *Cell* (2006) 124(3):471–84. doi:10.1016/j.cell.2006.01.016
7. Hay N, Sonenberg N. Upstream and downstream of mTOR. *Genes Dev* (2004) 18(16):1926–45. doi:10.1101/gad.1212704
8. Loewith R, Jacinto E, Wullschleger S, Lorberg A, Crespo JL, Bonenfant D, et al. Two TOR complexes, only one of which is rapamycin sensitive, have distinct roles in cell growth control. *Mol Cell* (2002) 10(3):457–68. doi:10.1016/S1097-2765(02)00636-6
9. Pópulo H, Lopes JM, Soares P. The mTOR signalling pathway in human cancer. *Int J Mol Sci* (2012) 13(2):1886–918. doi:10.3390/ijms13021886

10. Zoncu R, Efeyan A, Sabatini DM. mTOR: from growth signal integration to cancer, diabetes and ageing. *Nat Rev Mol Cell Biol* (2011) 12(1):21–35. doi:10.1038/nrm3025
11. Thoreen CC, Sabatini DM. Rapamycin inhibits mTORC1, but not completely. *Autophagy* (2009) 5(5):725–6. doi:10.4161/auto.5.5.8504
12. Sofer A, Lei K, Johannessen CM, Ellisen LW. Regulation of mTOR and cell growth in response to energy stress by REDD1. *Mol Cell Biol* (2005) 25(14):5834–45. doi:10.1128/MCB.25.14.5834-5845.2005
13. Schwarzer R, Tondera D, Arnold W, Giese K, Klippel A, Kaufmann J. REDD1 integrates hypoxia-mediated survival signaling downstream of phosphatidylinositol 3-kinase. *Oncogene* (2005) 24(7):1138–49. doi:10.1038/sj.onc.1208236
14. An SJ, Chen JK, Liu LL, Zhao YF, Chen XM. Over-expressed genes detected by suppression subtractive hybridization in carcinoma derived from transformed 16HBE cells induced by BPDE. *Biomed Environ Sci* (2005) 18(5):302–6.
15. Jia W, Chang B, Sun L, Zhu H, Pang L, Tao L, et al. REDD1 and p-AKT over-expression may predict poor prognosis in ovarian cancer. *Int J Clin Exp Pathol* (2014) 7(9):5940–9.
16. Çelik H, Bulut G, Han J, Graham GT, Minas TZ, Conn EJ, et al. Ezrin inhibition up-regulates stress response gene expression. *J Biol Chem* (2016) 291(25):13257–70. doi:10.1074/jbc.M116.718189
17. Pinto JA, Araujo J, Cardenas NK, Morante Z, Doimi F, Vidaurre T, et al. A prognostic signature based on three-genes expression in triple-negative breast tumours with residual disease. *NPJ Genom Med* (2016) 1:15015. doi:10.1038/npjgenmed.2015.15
18. Pinto JA, Rolfo C, Raez LE, Prado A, Araujo JM, Bravo L, et al. In silico evaluation of DNA damage inducible transcript 4 gene (DDIT4) as prognostic biomarker in several malignancies. *Sci Rep* (2017) 7(1):1526. doi:10.1038/s41598-017-01207-3
19. Shoshani T, Faerman A, Mett I, Zelin E, Tenne T, Gorodin S, et al. Identification of a novel hypoxia-inducible factor 1-responsive gene, RTP801, involved in apoptosis. *Mol Cell Biol* (2002) 22(7):2283–93. doi:10.1128/MCB.22.7.2283-2293.2002
20. Ellisen LW, Ramsayer KD, Johannessen CM, Yang A, Beppu H, Minda K, et al. REDD1, a developmentally regulated transcriptional target of p63 and p53, links p63 to regulation of reactive oxygen species. *Mol Cell* (2002) 10(5):995–1005. doi:10.1016/S1097-2765(02)00706-2
21. Wang Z, Malone MH, Thomenius MJ, Zhong F, Xu F, Distelhorst CW. Dexamethasone-induced gene 2 (dig2) is a novel pro-survival stress gene induced rapidly by diverse apoptotic signals. *J Biol Chem* (2003) 278(29):27053–8. doi:10.1074/jbc.M303723200
22. *Gene: DDIT4 (ENSG00000168209) – Summary – Homo sapiens – Ensembl Genome Browser 91 [Internet]*. (2017). Available from: http://www.ensembl.org/Homo_sapiens/Gene/Summary?g=ENSG00000168209;r=10:72273920-72276036 (Accessed: February 19, 2018).
23. *Gene: DDIT4 (ENSG00000168209) – Gene Tree – Homo sapiens – Ensembl Genome Browser 90 [Internet]*. (2017). Available from: http://www.ensembl.org/Homo_sapiens/Gene/Compara_Tree?db=core;g=ENSG00000168209;r=10:72273920-72276036 (Accessed: October 9, 2017).
24. Brugarolas J, Lei K, Hurley RL, Manning BD, Reiling JH, Hafen E, et al. Regulation of mTOR function in response to hypoxia by REDD1 and the TSC1/TSC2 tumor suppressor complex. *Genes Dev* (2004) 18(23):2893–904. doi:10.1101/gad.1256804
25. Lin L, Qian Y, Shi X, Chen Y. Induction of a cell stress response gene RTP801 by DNA damaging agent methyl methanesulfonate through CCAAT/enhancer binding protein. *Biochemistry (Mosc)* (2005) 44(10):3909–14. doi:10.1021/bi047574r
26. Molitoris JK, McColl KS, Swerdlow S, Matsuyama M, Lam M, Finkel TH, et al. Glucocorticoid elevation of dexamethasone-induced gene 2 (Dig2/RTP801/REDD1) protein mediates autophagy in lymphocytes. *J Biol Chem* (2011) 286(34):30181–9. doi:10.1074/jbc.M111.245423
27. Wolff NC, McKay RM, Brugarolas J. REDD1/DDIT4-independent mTORC1 inhibition and apoptosis by glucocorticoids in thymocytes. *Mol Cancer Res* (2014) 12(6):867–77. doi:10.1158/1541-7786.MCR-13-0625
28. Malagelada C, López-Toledano MA, Willett RT, Jin ZH, Shelanski ML, Greene LA. RTP801/REDD1 regulates the timing of cortical neurogenesis and neuron migration. *J Neurosci* (2011) 31(9):3186–96. doi:10.1523/JNEUROSCI.4011-10.2011
29. Whitney ML, Jefferson LS, Kimball SR. ATF4 is necessary and sufficient for ER stress-induced upregulation of REDD1 expression. *Biochem Biophys Res Commun* (2009) 379(2):451–5. doi:10.1016/j.bbrc.2008.12.079
30. Lin L, Stringfield TM, Shi X, Chen Y. Arsenite induces a cell stress-response gene, RTP801, through reactive oxygen species and transcription factors Elk-1 and CCAAT/enhancer-binding protein. *Biochem J* (2005) 392(Pt 1):93–102. doi:10.1042/BJ20050553
31. Gordon BS, Steiner JL, Williamson DL, Lang CH, Kimball SR. Emerging role for regulated in development and DNA damage 1 (REDD1) in the regulation of skeletal muscle metabolism. *Am J Physiol* (2016) 311(1):E157–74. doi:10.1152/ajpendo.00059.2016
32. GTEx Consortium, Laboratory, Data Analysis &Coordinating Center (LDACC)—Analysis Working Group, Statistical Methods Groups—Analysis Working Group, Enhancing GTEx (eGTEx) Groups, NIH Common Fund, NIH/NCI, NIH/NIMH, et al. Genetic effects on gene expression across human tissues. *Nature* (2017) 550(7675):204–13. doi:10.1038/nature24277
33. Kimball SR, Do AND, Kutzler L, Cavener DR, Jefferson LS. Rapid turnover of the mTOR complex 1 (mTORC1) repressor REDD1 and activation of mTORC1 signaling following inhibition of protein synthesis. *J Biol Chem* (2008) 283(6):3465–75. doi:10.1074/jbc.M706643200
34. Katiyar S, Liu E, Knutzen CA, Lang ES, Lombardo CR, Sankar S, et al. REDD1, an inhibitor of mTOR signalling, is regulated by the CUL4A–DDB1 ubiquitin ligase. *EMBO Rep* (2009) 10(8):866–72. doi:10.1038/embor.2009.93
35. DeYoung MP, Horak P, Sofer A, Sgroi D, Ellisen LW. Hypoxia regulates TSC1/2–mTOR signaling and tumor suppression through REDD1-mediated 14–3–3 shuttling. *Genes Dev* (2008) 22(2):239–51. doi:10.1101/gad.1617608
36. Vega-Rubin-de-Celis S, Abdallah Z, Kinch L, Grishin NV, Brugarolas J, Zhang X. Structural analysis and functional implications of the negative mTORC1 regulator REDD1. *Biochemistry (Mosc)* (2010) 49(11):2491–501. doi:10.1021/bi902135e
37. Canal M, Romaní-Aumedes J, Martín-Flores N, Pérez-Fernández V, Malagelada C. RTP801/REDD1: a stress coping regulator that turns into a troublemaker in neurodegenerative disorders. *Front Cell Neurosci* (2014) 8:313. doi:10.3389/fncel.2014.00313
38. Zhou Y, Wang Q, Guo Z, Weiss HL, Evers BM. Nuclear factor of activated T-cell c3 inhibition of mammalian target of rapamycin signaling through induction of regulated in development and DNA damage response 1 in human intestinal cells. *Mol Biol Cell* (2012) 23(15):2963–72. doi:10.1091/mbc.E12-01-0037
39. MacFarlane L-A, Murphy PR. MicroRNA: biogenesis, function and role in cancer. *Curr Genomics* (2010) 11(7):537–61. doi:10.2174/138920210793175895
40. Calin GA, Croce CM. MicroRNA signatures in human cancers. *Nat Rev Cancer* (2006) 6(11):857–66. doi:10.1038/nrc1997
41. Iorio MV, Croce CM. MicroRNAs in cancer: small molecules with a huge impact. *J Clin Oncol* (2009) 27(34):5848–56. doi:10.1200/JCO.2009.24.0317
42. Pineau P, Volinia S, McJunkin K, Marchio A, Battiston C, Terris B, et al. miR-221 overexpression contributes to liver tumorigenesis. *Proc Natl Acad Sci U S A* (2010) 107(1):264–9. doi:10.1073/pnas.0907904107
43. Hwang-Verslues WW, Chang P-H, Wei P-C, Yang C-Y, Huang C-K, Kuo W-H, et al. miR-495 is upregulated by E12/E47 in breast cancer stem cells, and promotes oncogenesis and hypoxia resistance via downregulation of E-cadherin and REDD1. *Oncogene* (2011) 30(21):2463–74. doi:10.1038/onc.2010.618
44. Li XH, Ha CT, Fu D, Xiao M. Micro-RNA30c negatively regulates REDD1 expression in human hematopoietic and osteoblast cells after gamma-irradiation. *PLoS One* (2012) 7(11):e48700. doi:10.1371/journal.pone.0048700
45. Cao J-X, Lu Y, Qi J-J, An G-S, Mao Z-B, Jia H-T, et al. MiR-630 inhibits proliferation by targeting CDC7 kinase, but maintains the apoptotic balance by targeting multiple modulators in human lung cancer A549 cells. *Cell Death Dis* (2014) 5:e1426. doi:10.1038/cddis.2014.386
46. Chen LC, Manjeshwar S, Lu Y, Moore D, Ljung BM, Kuo WL, et al. The human homologue for the *Caenorhabditis elegans* cul-4 gene is amplified and overexpressed in primary breast cancers. *Cancer Res* (1998) 58(16):3677–83.
47. Yasui K, Arii S, Zhao C, Imoto I, Ueda M, Nagai H, et al. TFDP1, CUL4A, and CDC16 identified as targets for amplification at 13q34 in hepatocellular carcinomas. *Hepatology* (2002) 35(6):1476–84. doi:10.1053/jhep.2002.33683
48. Müerköster S, Arlt A, Sipos B, Witt M, Grossmann M, Klöppel G, et al. Increased expression of the E3-ubiquitin ligase receptor subunit betaTRCP1 relates to constitutive nuclear factor-kappaB activation and chemoresistance in pancreatic carcinoma cells. *Cancer Res* (2005) 65(4):1316–24. doi:10.1158/0008-5472.CAN-04-1626
49. Ougolkov A, Zhang B, Yamashita K, Bilim V, Mai M, Fuchs SY, et al. Associations among beta-TrCP, an E3 ubiquitin ligase receptor, beta-catenin, and NF-kappaB in colorectal cancer. *J Natl Cancer Inst* (2004) 96(15):1161–70. doi:10.1093/jnci/djh219

50. Tan CY, Hagen T. mTORC1 dependent regulation of REDD1 protein stability. *PLoS One* (2013) 8(5):e63970. doi:10.1371/journal.pone.0063970
51. Reiling JH, Hafen E. The hypoxia-induced paralogs *Scylla* and *Charybdis* inhibit growth by down-regulating S6K activity upstream of TSC in *Drosophila*. *Genes Dev* (2004) 18(23):2879–92. doi:10.1101/gad.322704
52. Corradetti MN, Inoki K, Guan K-L. The stress-inducted proteins RTP801 and RTP801L are negative regulators of the mammalian target of rapamycin pathway. *J Biol Chem* (2005) 280(11):9769–72. doi:10.1074/jbc.C400557200
53. Long X, Lin Y, Ortiz-Vega S, Yonezawa K, Avruch J. Rheb binds and regulates the mTOR kinase. *Curr Biol* (2005) 15(8):702–13. doi:10.1016/j.cub.2005.02.053
54. Mariño G, Niso-Santano M, Baehrecke EH, Kroemer G. Self-consumption: the interplay of autophagy and apoptosis. *Nat Rev Mol Cell Biol* (2014) 15(2):81–94. doi:10.1038/nrm3735
55. Kimmelman AC. The dynamic nature of autophagy in cancer. *Genes Dev* (2011) 25(19):1999–2010. doi:10.1101/gad.17558811
56. Jung CH, Ro S-H, Cao J, Otto NM, Kim D-H. mTOR regulation of autophagy. *FEBS Lett* (2010) 584(7):1287–95. doi:10.1016/j.febslet.2010.01.017
57. Kim J-R, Lee S-R, Chung HJ, Kim S, Baek S-H, Kim JH, et al. Identification of amyloid beta-peptide responsive genes by cDNA microarray technology: involvement of RTP801 in amyloid beta-peptide toxicity. *Exp Mol Med* (2003) 35(5):403–11. doi:10.1038/emm.2003.53
58. Brafman A, Mett I, Shafir M, Gottlieb H, Damari G, Gozlan-Kelner S, et al. Inhibition of oxygen-induced retinopathy in RTP801-deficient mice. *Invest Ophthalmol Vis Sci* (2004) 45(10):3796–805. doi:10.1167/iovs.04-0052
59. Hu YY, Liu JC, Xing AY, You Y, Wang XD. REDD1 expression in placenta during human gestation. *Reprod Sci* (2012) 19(9):995–1000. doi:10.1177/1933719112440054
60. Chang B, Liu G, Yang G, Mercado-Uribe I, Huang M, Liu J. REDD1 is required for RAS-mediated transformation of human ovarian epithelial cells. *Cell Cycle* (2009) 8(5):780–6. doi:10.4161/cc.8.5.7887
61. Porta C, Paglino C, Mosca A. Targeting PI3K/Akt/mTOR signaling in cancer. *Front Oncol* (2014) 4:64. doi:10.3389/fonc.2014.00064
62. Khan KH, Yap TA, Yan L, Cunningham D. Targeting the PI3K-AKT-mTOR signaling network in cancer. *Chin J Cancer* (2013) 32(5):253–65. doi:10.5732/cjc.013.10057
63. Smith ER, Xu X-X. REDD1, a new Ras oncogenic effector. *Cell Cycle* (2009) 8(5):675–6. doi:10.4161/cc.8.5.8184
64. Koo JS, Jung W. Alteration of REDD1-mediated mammalian target of rapamycin pathway and hypoxia-inducible factor-1α regulation in human breast cancer. *Pathobiology* (2010) 77(6):289–300. doi:10.1159/000320936
65. Bos R, van der Groep P, Greijer AE, Shvarts A, Meijer S, Pinedo HM, et al. Levels of hypoxia-inducible factor-1alpha independently predict prognosis in patients with lymph node negative breast carcinoma. *Cancer* (2003) 97(6):1573–81. doi:10.1002/cncr.11246
66. Schindl M, Schoppmann SF, Samonigg H, Hausmaninger H, Kwasny W, Gnant M, et al. Overexpression of hypoxia-inducible factor 1alpha is associated with an unfavorable prognosis in lymph node-positive breast cancer. *Clin Cancer Res* (2002) 8(6):1831–7.
67. Trastour C, Benizri E, Ettore F, Ramaioli A, Chamorey E, Pouysségur J, et al. HIF-1α and CA IX staining in invasive breast carcinomas: prognosis and treatment outcome. *Int J Cancer* (2007) 120(7):1451–8. doi:10.1002/ijc.22436
68. Vadysirisack DD, Baenke F, Ory B, Lei K, Ellisen LW. Feedback control of p53 translation by REDD1 and mTORC1 limits the p53-dependent DNA damage response. *Mol Cell Biol* (2011) 31(21):4356–65. doi:10.1128/MCB.05541-11
69. Budanov AV, Karin M. p53 target genes sestrin1 and sestrin2 connect genotoxic stress and mTOR signaling. *Cell* (2008) 134(3):451–60. doi:10.1016/j.cell.2008.06.028
70. Matthew EM, Hart LS, Astrinidis A, Navaraj A, Dolloff NG, Dicker DT, et al. The p53 target Plk2 interacts with TSC proteins impacting mTOR signaling, tumor growth and chemosensitivity under hypoxic conditions. *Cell Cycle* (2009) 8(24):4168–75. doi:10.4161/cc.8.24.10800
71. Feng Z, Hu W, de Stanchina E, Teresky AK, Jin S, Lowe S, et al. The regulation of AMPK beta1, TSC2, and PTEN expression by p53: stress, cell and tissue specificity, and the role of these gene products in modulating the IGF-1-AKT-mTOR pathways. *Cancer Res* (2007) 67(7):3043–53. doi:10.1158/0008-5472.CAN-06-4149
72. Cam M, Bid HK, Xiao L, Zambetti GP, Houghton PJ, Cam H. p53/TAp63 and AKT regulate mammalian target of rapamycin complex 1 (mTORC1) signaling through two independent parallel pathways in the presence of DNA damage. *J Biol Chem* (2014) 289(7):4083–94. doi:10.1074/jbc.M113.530303
73. Dennis MD, McGhee NK, Jefferson LS, Kimball SR. Regulated in DNA damage and development 1 (REDD1) promotes cell survival during serum deprivation by sustaining repression of signaling through the mechanistic target of rapamycin in complex 1 (mTORC1). *Cell Signal* (2013) 25(12):2709–16. doi:10.1016/j.cellsig.2013.08.038
74. Jin H-O, Hong S-E, Kim J-H, Choi H-N, Kim K, An S, et al. Sustained overexpression of REDD1 leads to Akt activation involved in cell survival. *Cancer Lett* (2013) 336(2):319–24. doi:10.1016/j.canlet.2013.03.021


**Conflict of Interest Statement:** The authors declare that the research was conducted in the absence of any commercial or financial relationships that could be construed as a potential conflict of interest.

frontiers in Pharmacology

ORIGINAL RESEARCH
published: 02 October 2018
doi: 10.3389/fphar.2018.01104

# Conventional Anti-glioblastoma Chemotherapy Affects Proteoglycan Composition of Brain Extracellular Matrix in Rat Experimental Model *in vivo*

*Alexandra Y. Tsidulko[1], Cynthia Bezier[2,3], Gabin de La Bourdonnaye[2,4], Anastasia V. Suhovskih[1,2], Tatiana M. Pankova[1], Galina M. Kazanskaya[1,5], Svetlana V. Aidagulova[6] and Elvira V. Grigorieva[1,2]**

[1] Institute of Molecular Biology and Biophysics, Novosibirsk, Russia, [2] Novosibirsk State University, Novosibirsk, Russia, [3] UPMC-Sorbonne Universities, Paris, France, [4] Institut National des Sciences Appliquées de Toulouse, Toulouse, France, [5] Meshalkin Novosibirsk State Research Institute of Circulation Pathology, Novosibirsk, Russia, [6] Novosibirsk State Medical University, Novosibirsk, Russia

OPEN ACCESS

**Edited by:**
*Ahmed Lasfar, Rutgers, The State University of New Jersey, United States*

**Reviewed by:**
*Sujuan Guo, Dana–Farber Cancer Institute, United States*
*Shiv K. Gupta, Mayo Clinic, United States*

***Correspondence:**
*Elvira V. Grigorieva*
*elv_grig@yahoo.com*

**Specialty section:**
*This article was submitted to Cancer Molecular Targets and Therapeutics, a section of the journal Frontiers in Pharmacology*

**Received:** *13 June 2018*
**Accepted:** *10 September 2018*
**Published:** *02 October 2018*

**Citation:**
*Tsidulko AY, Bezier C, de La Bourdonnaye G, Suhovskih AV, Pankova TM, Kazanskaya GM, Aidagulova SV and Grigorieva EV (2018) Conventional Anti-glioblastoma Chemotherapy Affects Proteoglycan Composition of Brain Extracellular Matrix in Rat Experimental Model in vivo. Front. Pharmacol. 9:1104. doi: 10.3389/fphar.2018.01104*

Temozolomide (TMZ) is a conventional chemotherapy drug for adjuvant treatment of glioblastoma multiforme (GBM), often accompanied by dexamethasone (DXM) to prevent brain oedema and alleviate clinical side effects. Here, we aimed to investigate an ability of the drugs to affect normal brain tissue in terms of proteoglycan (PG) composition/content in experimental rat model *in vivo*. Age- and brain zone-specific transcriptional patterns of PGs were demonstrated for 8, 60, and 120 days old rats, and syndecan-1, glypican-1, decorin, biglycan, and lumican were identified as the most expressed PGs. DXM treatment affected both PG core proteins expression (mainly syndecan-1, glypican-1, decorin, biglycan, lumican, versican, brevican, and NG2) and heparan sulphate (HS)/chondroitin sulphate (CS) content in organotypic brain slice culture *ex vivo* and experimental animals *in vivo* in a dose-dependent manner. TMZ treatment did not result in the significant changes in PG core proteins expression both in normal rat brain hippocampus and cortex *in vivo* (although generics did), but demonstrated significant effects onto polysaccharide HS/CS content in the brain tissue. The effects were age- and brain zone-specific and similar with the age-related PGs expression changes in rat brain. Combination of TMZ with DXM resulted in the most profound deterioration in PGs composition and content in the brain tissue both at core protein and glycosaminoglycan levels. Taken together, the obtained results demonstrate that conventional anti-glioblastoma therapy affects proteoglycan structure and composition in normal brain tissue, potentially resulting in deterioration of brain extracellular matrix and formation of the favourable tumorigenic niche for the expansion of the residual glioma cells. During the TMZ chemotherapy, dose and regimen of DXM treatment matter, and repetitive low DXM doses seem to be more sparing treatment compared with high DXM dose(s), which should be avoided where possible, especially in combination with TMZ.

**Keywords: glioblastoma multiforme, temozolomide, dexamethasone, extracellular matrix, proteoglycan, glycosaminoglycan, heparan sulphate, chondroitin sulphate**

## INTRODUCTION

Glioblastoma multiforme (GBM) is the most aggressive malignant brain tumour (Thakkar et al., 2014; Nørøxe et al., 2017). Despite of numerous new strategies for targeted treatment of glioblastoma, progress in the field remains insufficient (Nam and de Groot, 2017; Touat et al., 2017). After the surgical resection of the tumour node, the main purpose of all consequent treatment strategies is to eliminate the remaining glioblastoma cells and prevent the disease relapse being a main cause of the patient's deaths.

However, being concentrated to destroy the glioblastoma cells, one can overlook a danger coming from a significant impairment of the surrounding normal brain tissue during the adjuvant therapy. In fact, the most dangerous trait of glioblastoma is its' active invasion into the surrounding healthy brain tissue (Paw et al., 2015; Diksin et al., 2017), and the invasiveness of GBM cells and tumour development depend on not only migration capabilities of the proliferating glioblastoma cells but also structure of the surrounding normal brain tissue (Song and Dityatev, 2017; Manini et al., 2018). One of the key invasion-related component of normal brain tissue is extracellular matrix (ECM) which occupies near 20% of its volume and serve as a main basic element of tissue structure and physiology (Nicholson and Hrabětová, 2017). ECM is not only a physical non-specific barrier but is actively involved in cell–cell and cell–matrix interactions and signalling through the numerous ligands like chemokines, growth factors, and adhesion molecules (Miyata and Kitagawa, 2017). Unlike in other organs, brain ECM composes mainly of glycosylated molecules such as proteoglycans (PGs) and glycosaminoglycans (GAGs), predominantly chondroitin sulphate PGs (CSPGs) (Silver et al., 2013; Dyck and Karimi-Abdolrezaee, 2015), hyaluronic acid (HA) (Park et al., 2008; Miyata and Kitagawa, 2017), and heparan sulphate PGs (HSPGs) (Yu et al., 2017).

At present, most of GBM tumours are treated according to a common scheme based on maximally safe surgery, followed by a combination of radiotherapy and chemotherapy with temozolomide (TMZ) and dexamethasone (DXM) as accompanying anti-oedema drug (Seystahl et al., 2016; Reitman et al., 2018). During the adjuvant anti-glioblastoma therapy, both the GBM cancer cells and a surrounding normal brain ECM are exposed to those drugs but their effects towards the brain ECM remain unclear.

TMZ, by definition, is a drug to eliminate cancer cells and its' molecular effects on glioblastoma cells and clinical effects on GBM tumour development are well known (Bei et al., 2010; Yang et al., 2014). However, TMZ effects towards the normal brain tissue surrounding the GBM tumour and its' ECM (especially PGs) remain completely uninvestigated.

More information can be found in the literature on corticosteroid drug DXM, routinely used to prevent/treat peritumoural brain oedema during GBM chemotherapy, despite significant systemic side effects (Murayi and Chittiboina, 2016). DXM do affects glioblastoma cell biology *in vitro* and tumour development *in vivo*, and an overall impression denotes rather negative action of the drug for GBM prognosis and patients survival. DXM use correlates with low overall survival and progression-free survival of GBM patients (Shields et al., 2015); retrospective clinical analyses in three independent patient cohorts and mouse experimental data suggest that DXM may decrease the effectiveness of treatment and shorten patients' survival in glioblastoma, highlighting the importance of identifying alternative agents and substantiating the request for restricted use of corticosteroids in glioblastoma (Pitter et al., 2016). However, as to glioma cells *in vitro*, DXM demonstrates opposite effects as it decreases TMZ-induced apoptosis in human gliobastoma T98G cells (Sur et al., 2005); inhibits glioma cell proliferation in a concentration and species-dependent manner and reduces tumour-induced angiogenesis (Fan et al., 2014), decreases MMP-2 secretion and invasiveness of human U87MG glioma cells (Lin et al., 2008) and suppresses the dispersal of GBM cells through the stimulation of fibronectin secretion and inhibition of the glioma cells motility (Shannon et al., 2015). These data suggest that the negative effect of DXM treatment *in vivo* seem to be related to some unknown molecular mechanisms (possible related to microenvironmental issues) rather then its' direct action towards glioblastoma cells, however, the issue remain uninvestigated.

In this work, we aim to study effects of TMZ and/or DXM treatments on PGs expression and ECM structure in normal rat brain tissue in organotypic system *ex vivo* and animals experimental model *in vivo*.

## MATERIALS AND METHODS

### Animals

Wistar rats aged 8, 60, and 120 days were used in the experiment on age-dependency (totally 15 animals, 5 animals/group). All other experiments *in vivo* were performed on male Wistar rats aged 9–10 weeks and weighing 200–250 g at the beginning of the experiment (totally 35 animals). Animals were housed in polycarbonate cages (36 × 50 × 28 cm) with free access to food and water, natural light/dark cycle, temperature of 25 ± 1°C, humidity of 50–60% and weighed once/day. All the studied animals were adapted to the experimenter for 5 days prior to the start of the experiment. All procedures were conducted in accordance with European Communities Council Directive 2010/63/EU. All efforts were made to minimise animal suffering and to reduce the number of animals used. Animals were sacrificed by decapitation using guillotine according AVMA Guidelines for the Euthanasia of Animals (American Veterinary Medical Association, 2013).

### Organotypic Hippocampal Slice Culture

Organotypic hippocampal slice cultures (OHSCs) were prepared according to the previously described protocols (Gähwiler et al., 1997) with modification (Palyanova et al., 2013). Briefly, neonatal Wistar rat pups (post-natal day 7–8) were decapitated, the brains were rapidly removed under aseptic conditions and placed into ice-cold Hank's balanced solution. The hippocampi were removed and placed into agarose blocks and cut rapidly with a tissue chopper into 400 μm transversal slices. The slices

were transferred to collagen-coated coverslips and placed into Petri dishes containing specialised pedestals. Hank's solution was placed on the bottom of the Petri dishes to supply additional humidity. 100 uL of culture medium, consisting of 25% Hank's balanced solution, 65% DMEM, and 10% foetal bovine serum, was added to each cover slip. The OHSCs were cultivated in a 90% humidified atmosphere with 5% CO2 at 36°C. The medium was changed twice a week; the state of the OHSCs was controlled visually. At day 7 of incubation, DXM was added to the culture medium to final concentrations of 10 nM–200 μM for 24 h. To determine the effects of DXM on OHSC, the cultures were collected into RNAlater solution and used in RT-PCR analysis. All experimental procedures involving rats were approved by the Institutional Animal Care and Use Committee and performed according to the Directive 2010/63/EU.

## Drug Administration

Rats were randomly divided into groups (5 animals/group). The synthetic glucocorticoid agonist DXM (KRKA) was administered subcutaneously (s.c.). Two groups of rats received a single injection of DXM (0.1 or 5 mg/kg) and were sacrificed after 24 h to determine the short-time effects of the drug. Third group received 1 mg/kg of DXM daily for 1 week. TMZ-based drugs (Temodal, Temozolomide-Teva, and Temozolomide-Rus) were administrated peroral 30 mg/kg per day for 5 days. Control group received saline injections (s.c.) of the same volume as the experimental group. Animals were sacrificed by decapitation and one hemisphere from each animal was collected in RNAlater for further RT-PCR analysis, while the other one was fixed in 4% paraformaldehyde and embedded into paraffin blocks.

## RT-PCR Analysis

Total RNA was extracted from the brain samples using the TRIzol Plus RNA Purification Kit (Thermo Fisher Scientific, United States) according to the manufacturer's instructions. cDNA was synthesised from 1 μg of total RNA using a First Strand cDNA Synthesis kit (Fermentas, United States) and 1/10th of the product was subjected to PCR analysis. Quantitative RT-PCR (qRT-PCR) was performed using the CFX96$^{TM}$ Real-Time PCR Detection System (Bio-Rad, United States) and the Taq-pol (IMCB, Russia) Maxima SYBR Green/RO master mix (Thermo Fisher Scientific) under the following conditions: 95°C for 3 min, followed by 40 cycles at 95°C for 10 s, 59°C for 20 s, and 72°C for 30 s. The total reaction volume was 25 μl. The relative amount of mRNA was normalised against Gapdh mRNA, and the fold change for each mRNA was calculated by the $2^{-\Delta Ct}$ method. Primer sequences for rat proteoglycan genes are presented in **Table 1**.

**TABLE 1 |** Sequences of primers used in PCR analysis.

| Gene | Sequence |
|---|---|
| *Sdc1* | 5′-GAACCCACCAGCAGGGATAC-3′ |
| | 5′-CACACTTGGAGGCTGATGGT-3′ |
| *Gpc1* | 5′-GCCAGATCTACGGGGCTAAG - 3′ |
| | 5′-AGACGCAGCTCAGCATACAG-3′ |
| *Hspg2* | 5′-TGATGACGAGGACTTGCTGG-3′ |
| | 5′-ACACCACACTGACAACCTGG-3′ |
| *Vcan* | 5′-ATGTGGATCATCTGGACGGC-3′ |
| | 5′-GTTTCGATGGTGGTTGCCTC-3′ |
| *Bcan* | 5′-AGGGGACCTCACAAGTTCTTC-3′ |
| | 5′-ATTTGACTCGGGGAAAGCCC-3′ |
| *Cspg4* | 5′-ATCTGGGAGGGGGCTATTGT-3′ |
| | 5′-GTACGCCATCAGAGAGGTCG-3′ |
| *Dcn* | 5′-AATGCCATCTCCGAGTGGTG-3′ |
| | 5′-TTGTCGTGGAGTCGAAGCTC-3′ |
| *Bgn* | 5′-GAACAGTGGCTTTGAACCCG-3′ |
| | 5′-CCTCCAACTCGATAGCCTGG-3′ |
| *Lum* | 5′-AATTTGACCGAGTCCGTGGG-3′ |
| | 5′-GCCTTTCAGAGAAGCCGAGA-3′ |
| *Gapdh* | 5′-ATGGCCTTCCGTGTTCCTAC-3′ |
| | 5′-TCCAGGGTTTCTTACTCCTTGG-3′ |

## Immunostaining

For immunohistochemistry, 3,5-μm sections of formalin-fixed paraffin-embedded samples were deparaffinised in xylene twice for 5 min following stepwise rehydration in 100, 95, and 70%, ethanol for 5 min each and 5 min in deionised water. Antigen retrieval was performed at 99°C for 20 min in citrate buffer (pH 6.0). Non-specific binding was blocked with 1% BSA and 10% foetal bovine serum in phosphate buffered saline (PBST) at room temperature for 1 h. After blocking, the slides were incubated with anti-decorin (Abcam ab175404), anti-syndecan-1 (Abcam ab34164), anti-NG2 (Abcam ab83178), anti-HS (Millipore MAB2040), and anti-CS (Sigma-Aldrich C8035) primary antibodies for 1 h at room temperature. After rinsing with PBST three times for 15 min, slides were incubated with secondary antibodies anti-mouse Alexa Fluor 488 (Abcam ab150117) or anti-rabbit Alexa Fluor 647 (Abcam ab 150063) at room temperature for 1 h. After PBST rinse 3 × 10 min, slides were mounted using SlowFade Gold (Thermo Fisher Scientific, Untied States) mounting medium with DAPI and imaged on a Confocal Laser Scanning Biological Microscope Fluoview FV1000 (Olympus, United States). The images were processed using background subtraction to remove shading due to non-uniform illumination and inhomogeneous staining effects and using colour compensation to minimise the effects of spectral bleed-through among the three-color channels (red, green, and blue). Quantitative analysis of the images was performed using CellProfiler 2.2.0 software (Lamprecht et al., 2007).

## Statistical Analysis

Statistical analyses were performed using ORIGIN 8.1 software; a value of $p < 0.05$ was considered to indicate a statistically significant difference. Data are expressed as the means ± SD.

# RESULTS

Conventional anti-glioblastoma chemotherapy includes TMZ as a basic "first-line" drug accompanied by supporting therapy with DXM to prevent brain oedema. In spite of the established effects of the drugs towards cancer cells, their effects to the surrounding

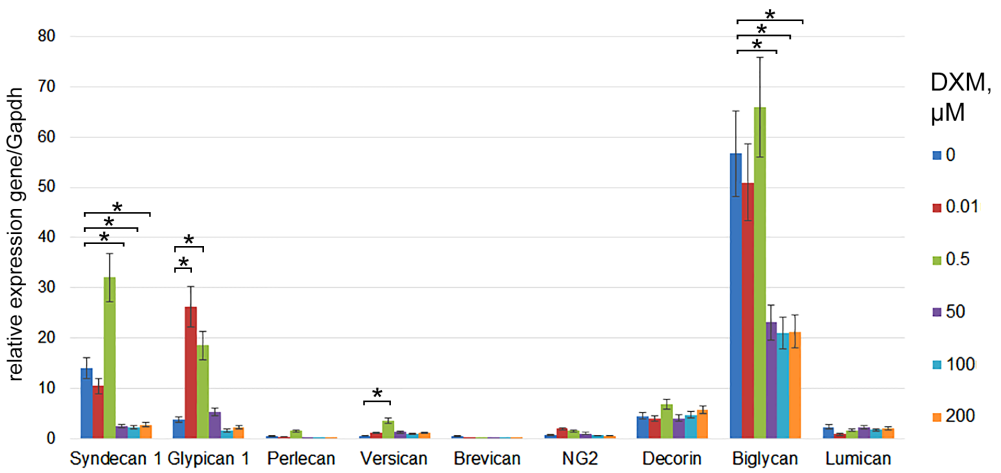


**FIGURE 1 |** PGs expression levels in organotypic rat hippocampus cultures *ex vivo* before and after treatment with various concentrations of DXM. RT-PCR analysis, intensity of the amplified DNA fragments normalised to that of *Gapdh*. Bars represent the mean ± SD from triplicate experiments (OriginPro 8.1). Student's *t*-test, $^{*}p < 0.05$.

normal brain tissue need additional investigation and dictate specific methodological approach. Cultured cross-sections of rat hippocampus *ex vivo* (OHSC) were used instead of GBM cell culture model *in vitro*, as it represents 3D structure of brain tissue and can be used for ECM study (Graber et al., 2012; Minami et al., 2017). In this study, DXM only but not TMZ effects were investigated in the OHSC experimental model *ex vivo* because the last one represents pro-drug and needs to be activated in the entire organism.

## DXM Affects PGs Expression in Organotypic Hippocampal Culture *ex vivo*

Rat brain sections were incubated with various concentrations of DXM (0.01–200 μM) for 24 h. The concentration lies between the minimal (0.001 μM) and maximal (500 μM) concentrations described in the literature (Kuwahara et al., 2003; Mulholland et al., 2005; Graber et al., 2012). Expression of main proteoglycan core proteins in the OHSC samples before and after DXM treatment was determined using RT-PCR (**Figure 1**). Low and high doses of DXM resulted in different changes in the expression of individual PGs compared with the control organotypic culture-low dose (0.01–0.5 μM) treatments increased expression levels of glypican-1 and versican core proteins (5-fold and 10-fold, respectively), whereas high dose (50–200 μM) treatments suppressed syndecan-1 and biglycan expression (5-fold and 3-fold, respectively). The results demonstrate a complex attenuation of PGs expression in normal rat brain by different DXM concentrations in the experimental model *ex vivo* and warrant further investigation of the effects *in vivo*.

## Proteoglycans Expression in Rat Brain Is Age- and Brain Zone-Dependent

As *in vivo* experiments are usually performed using 2-month old rats whereas OHSC study *ex vivo* was performed using hippocampi from 7 to 8 days old rat pups. Age-specificity as well as brain zone-specificity of the PGs expression levels were determined for a correct comparative analysis of the obtained data. Wistar rats aged 8, 60, and 120 days were used in the experiment and expression of main PG core proteins was profiled in various brain zones like hippocampus, cortex, cerebellum, and olfactory bulbs (**Figure 2**). According to the RT-PCR data, PGs demonstrated brain zone-specific expression patterns and overall transcriptional activities of the PGs core proteins in 8-day old rat pups. During post-natal development, significant changes were revealed for both parameters, consisting in continuous overall decrease of the PGs expression in the aged brains mainly due to decorin and biglycan down-regulation and tendency to syndecan-1 and glypican-1 up-regulation (especially at the age of 60 days).

The described effects were characteristic for most of the brain structures studied (hippocampus, cerebellum, and olfactory bulbs) except cortex, where moderate (1.5–2-fold) activation of the PGs expression was observed over 8–120 days development of the animals (**Figure 2**; **Table 2**). Taking into account a long period of drug administration, younger mice (60 days) look more suitable for the planned long-term experiments. So, 2-month old Wistar rats were used for further analysis of DXM and TMZ effects on PGs expression in hippocampus and cortex of normal rat brain *in vivo*.

## High-Dose DXM Treatment Significantly Affects Pattern and Transcriptional Activity of PG-Coding Genes in Rat Brain, Unlike Low DXM Doses or TMZ

The experimental animals were subjected to the treatment with different DXM concentrations (single injection with 0.1 or 2, 5 or 5 mg/kg DXM; repetitive treatment with 1 mg/kg DXM for a week, once/day), or TMZ treatment at

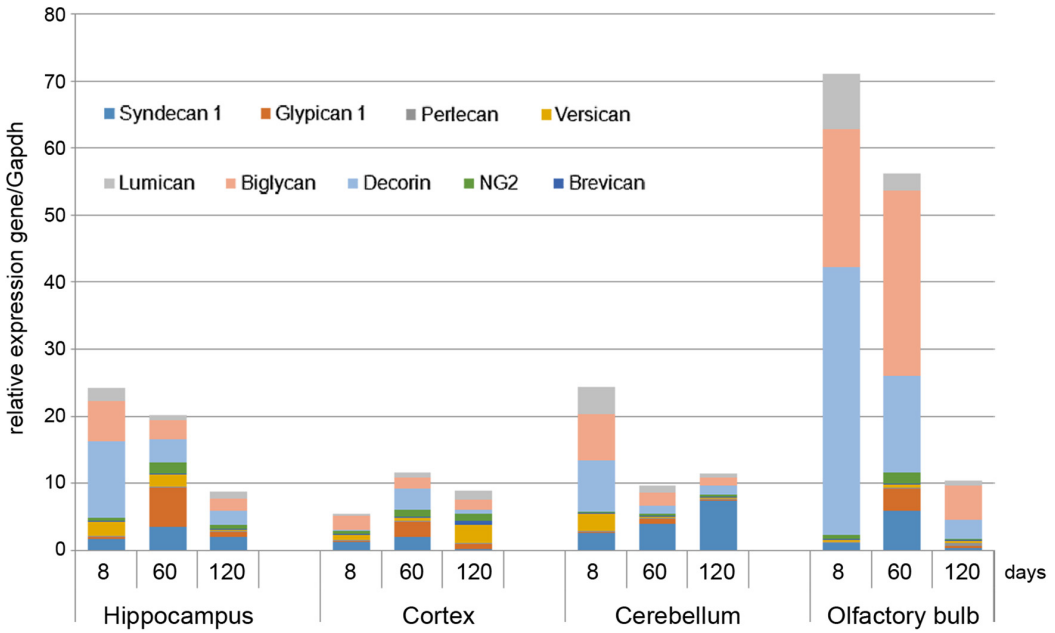


**FIGURE 2 |** Proteoglycans expression in different brain zones of 8, 60, and 120-day old Wistar rats. RT-PCR analysis, intensity of the amplified DNA fragments normalised to that of *Gapdh* from triplicate experiments, Student's *t*-test (OriginPro 8.1). Stacked column compares the contribution of each value to a total across categories.

**TABLE 2 |** Expression of proteoglycans in various Wistar rat brain zones at different age.

| | days | *Sdc1* | *Gpc1* | *Hspg2* | *Vcan* | *Bcan* | *Cspg4* | *Dcn* | *Bgn* | *Lum* |
|---|---|---|---|---|---|---|---|---|---|---|
| Hippocampus | **8** | **1.5** ± 0.2 | **0.33** ± 0.05 | **0.08** ± 0.00 | **2.0** ± 0.2 | NO | **0.52** ± 0.03 | **11.0** ± 0.5 | **5.8** ± 0.3 | **1.92** ± 0.09 |
| | **60** | **3.4** ± 0.1 | **5.9** ± 0.2 | **0.12** ± 0.00 | **1.9** ± 0.7 | **0.06** ± 0.00 | **1.71** ± 0.06 | **3.4** ± 0.1 | **2.93** ± 0.7 | **0.72** ± 0.01 |
| | **120** | **2.4** ± 0.6 | **0.6** ± 0.2 | **0.16** ± 0.00 | **0.34** ± 0.07 | **0.01** ± 0.00 | **0.7** ± 0.2 | **1.9** ± 0.4 | **1.6** ± 0.2 | **1.2** ± 0.3 |
| Cortex | **8** | **1.17** ± 0.06 | **0.2** ± 0.02 | **0.05** ± 0.00 | **0.91** ± 0.04 | NO | **0.37** ± 0.05 | **0.22** ± 0.01 | **1.9** ± 0.2 | **0.31** ± 0.05 |
| | **60** | **1.9** ± 0.7 | **2.24** ± 0.08 | **0.2** ± 0.1 | **0.47** ± 0.03 | **0.21** ± 0.05 | **1.0** ± 0.1 | **3.16** ± 0.01 | **1.69** ± 0.03 | **0.73** ± 0.06 |
| | **120** | **0.14** ± 0.02 | **1.2** ± 0.4 | **0.02** ± 0.01 | **2.4** ± 0.6 | **0.6** ± 0.2 | **1.4** ± 0.4 | **0.55** ± 0.08 | **1.4** ± 0.2 | **1.6** ± 0.4 |
| Cerebellum | **8** | **2.5** ± 0.1 | **0.22** ± 0.00 | **0.05** ± 0.00 | **2.8** ± 0.1 | NO | **0.30** ± 0.04 | **7.63** ± 0.01 | **6.6** ± 0.3 | **4.6** ± 0.7 |
| | **60** | **3.9** ± 0.6 | **0.9** ± 0.1 | **0.05** ± 0.01 | **0.15** ± 0.02 | **0.08** ± 0.01 | **0.30** ± 0.06 | **1.2** ± 0.1 | **2.0** ± 0.2 | **1.1** ± 0.1 |
| | **120** | **6.6** ± 0.9 | **0.25** ± 0.06 | **0.08** ± 0.01 | **0.29** ± 0.04 | NO | **0.3** ± 0.1 | **1.2** ± 0.2 | **1.30** ± 0.01 | **0.7** ± 0.1 |
| Olfactory bulb | **8** | **1.08** ± 0.01 | **0.07** ± 0.01 | **0.08** ± 0.01 | **0.34** ± 0.07 | **0.01** ± 0.00 | **0.52** ± 0.08 | **37.4** ± 3.6 | **20.0** ± 0.9 | **7.9** ± 0.4 |
| | **60** | **5.9** ± 0.7 | **3.4** ± 0.1 | **0.08** ± 0.02 | **0.6** ± 0.03 | **0.01** ± 0.00 | **1.66** ± 0.01 | **14.5** ± 0.5 | **27.7** ± 0.9 | **2.46** ± 0.05 |
| | **120** | **0.30** ± 0.01 | **0.27** ± 0.04 | **0.49** ± 0.05 | **0.47** ± 0.00 | NO | **0.23** ± 0.03 | **3.3** ± 0.6 | **5.03** ± 0.01 | **0.9** ± 0.2 |

*Expression calculated using $2^{dCt}$ method as gene/Gapdh ratio, NO, extremely low PG expression. Average expression levels (bold) ± SD are presented (OriginPro 8.1).*

the regimen close to that used for GBM patients, or both in combination. DXM concentrations range was taken from the literature data and adjusted in each part of the study (*ex vivo* and *in vivo*) because of the significant difference between the tissue level of DXM in human brain tumors and its' cytotoxic concentration in cell culture (Nestler et al., 2002). After that, rat brains were dissected into the different morphological zones, and proteoglycan expression was detected in hippocampus and cortex by RT-PCR analysis (**Figure 3**). Syndecan-1, glypican-1, decorin, biglycan, and lumican were identified as the most expressed proteoglycan-coding genes both in normal rat hippocampus and cortex (**Figure 3A**). High-dose DXM treatments (2.5 and 5 mg/kg) resulted in the increased overall transcriptional activity (**Figure 3B**) and specific expression patterns (**Figure 3C**) of the PGs in hippocampus in dose-dependent manner, mainly due to changes in syndecan-1 (+4-fold), glypican-1 (+3-fold), brevican (+7-fold), CSPG4/NG2 (+2-fold), decorin (-2-fold), and lumican (+3-fold) expression.

Interestingly, the PGs expression in cortex was more resistant to DXM treatment, and only highest DXM concentration (5 mg/kg) significantly increased the transcriptional activity of the genes (**Figure 3B**). In common, long-term treatment by low doses of DXM (1 mg/kg) looks more favourable in terms of PGs expression in normal brain tissue for both hippocampus and cortex than high DXM doses.

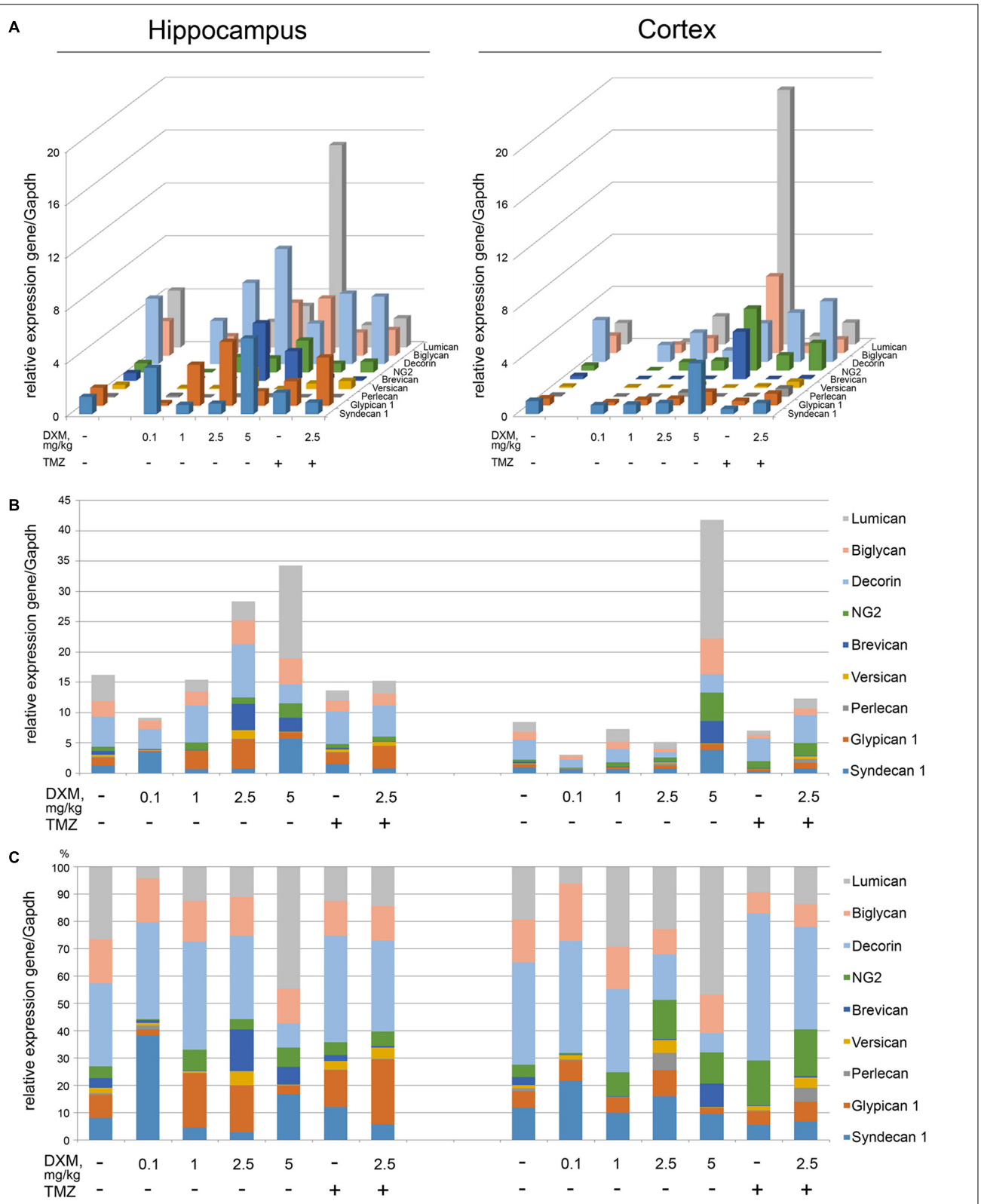


**FIGURE 3 |** Proteoglycan mRNA expression levels in hippocampus and cortex of 2-month Wistar rats before and after treatments with DXM and/or TMZ. **(A)** mRNA expression levels of individual proteoglycan genes. **(B)** Overall transcriptional activity of the total pool of the studied PGs. **(C)** Expression pattern of the individual PG core protein-coding gene as percentage of 100%. RT-PCR analysis, intensity of the amplified DNA fragments normalised to that of *Gapdh*. Bars represent the mean ± SD from triplicate experiments, Student's *t*-test (OriginPro 8.0).

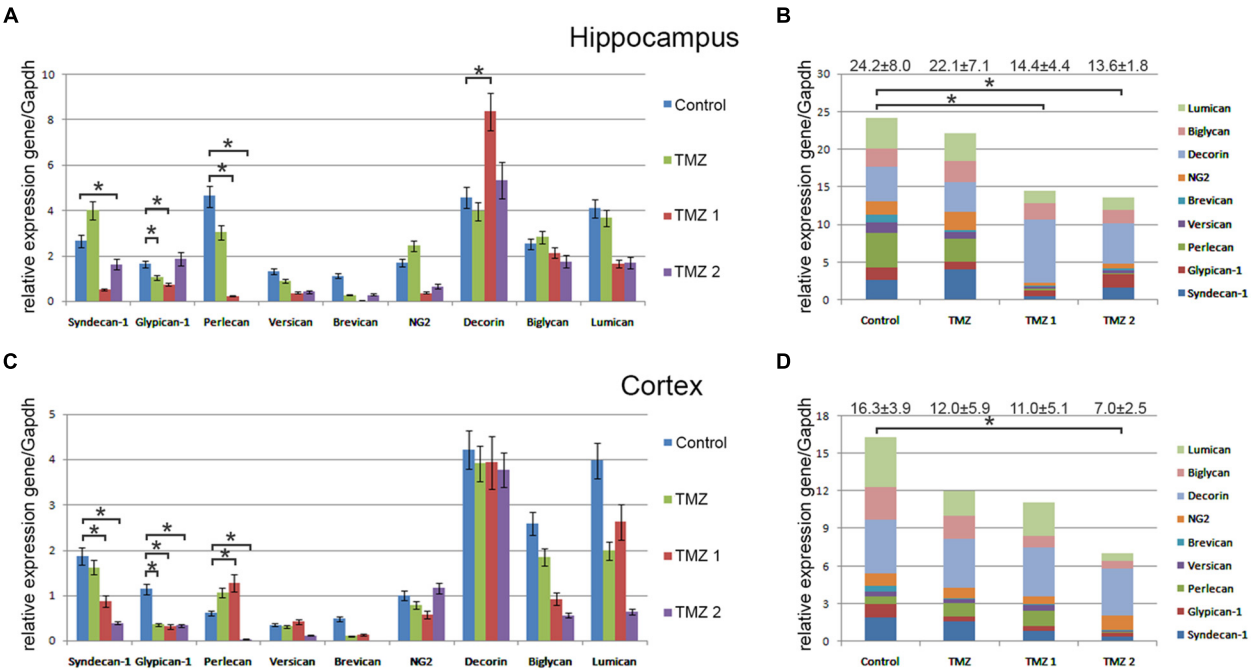


**FIGURE 4 |** Proteoglycan expression levels in hippocampus and cortex of 2-month Wistar rats before and after treatments with different TMZ-based drugs. **(A,B)** Hippocampus, **(C,D)** Cortex. **(A,C)** mRNA expression levels of individual proteoglycan genes. RT-PCR analysis, intensity of the amplified DNA fragments normalised to that of *Gapdh*, bars represent the mean ± SD from triplicate experiments, Student's *t*-test (OriginPro 8.1). **(B,D)** Overall transcriptional activity of PG core proteins in different TMZ-treated groups of animals. Stacked column compares the contribution of each value to a total across categories. Proteoglycan mRNA expression levels in hippocampus and cortex of 2-month Wistar rats before and after treatments with DXM and/or TMZ. mRNA expression levels of individual proteoglycan genes in hippocampus **(A)** and cortex **(C)**. Overall transcriptional activity of the total pool of all studied PGs in hippocampus **(B)** and cortex **(D)**. Expression pattern of the individual PG core protein-coding gene as percentage of 100%. RT-PCR analysis, intensity of the amplified DNA fragments normalised to that of *Gapdh*. Bars represent the mean ± SD from triplicate experiments (OriginPro 8.0). $^*p < 0.05$.

TMZ almost did not affect overall transcriptional activities of the PG core protein-coding genes in both brain zones-neither alone nor in combination with the selected DXM concentration (2.5 mg/kg) (**Figure 3B**), although that modified PG expression patterns both in hippocampus (increase of glypican-1 and decrease of lumican expression levels) and cortex (increase of HSPG2/perlecan and CSPG4/NG2 expression levels) (**Figure 3C**).

Totally, high doses of DXM (5 and 2.5 mg/kg in a less extent) demonstrated pronounced effects towards the activation of transcriptional activity of PG-coding genes and changes in their expression pattern in rat brain tissue, while moderate DXM dose (1 mg/kg) did not affect significantly the mRNA levels of the studied PGs. TMZ alone or in combination with 2.5 mg/kg DXM treatment also did not result in significant changes in the expression of PG core proteins in normal rat brain (both hippocampus and cortex) at the transcriptional level.

## Suppression of the Overall Proteoglycans Expression in Normal Brain Tissue Varies for Different TMZ-Based Drugs

Interestingly, various TMZ-based drugs demonstrated different effects on the overall transcriptional activity and expression pattern of proteoglycan-related genes (**Figure 4**). Common trend was a down-regulation of the overall proteoglycan expression in both hippocampus and cortex, up to 2-fold depending on the drug (TMZ, TMZ1, or TMZ2). The most affected PG type were HSPGs (syndecan-1, glypican-1, and perlecan), being the main contributors in the overall inhibition of the PGs expression by some of the drugs (TMZ1 and TMZ2). The demonstrated effects of the TMZ-based drugs were more pronounced for hippocampus than the cortex of normal rat brain.

## Low Dose of DXM and TMZ Affect Proteoglycan Content in Brain ECM at Core Protein Level

To investigate a potential effect of the treatments onto the PGs expression at the protein level, immunofluorescence analysis of the selected PG core proteins (syndecan-1, decorin and CSPG4/NG2) was performed for control rat brains and those treated with DXM (2.5 mg/kg on days 1 and 4 of the experiment), TMZ (30 mg/kg per day for 5 days) or both (**Figure 5**; **Table 3**). These PGs were chosen from the PGs with the highest expression levels in the normal rat brain tissue (both in hippocampus and cortex), and as representatives from main proteoglycan subtypes (heparan sulphate proteoglycan, chondroitin sulphate proteoglycan and dermatan sulphate proteoglycan). The obtained

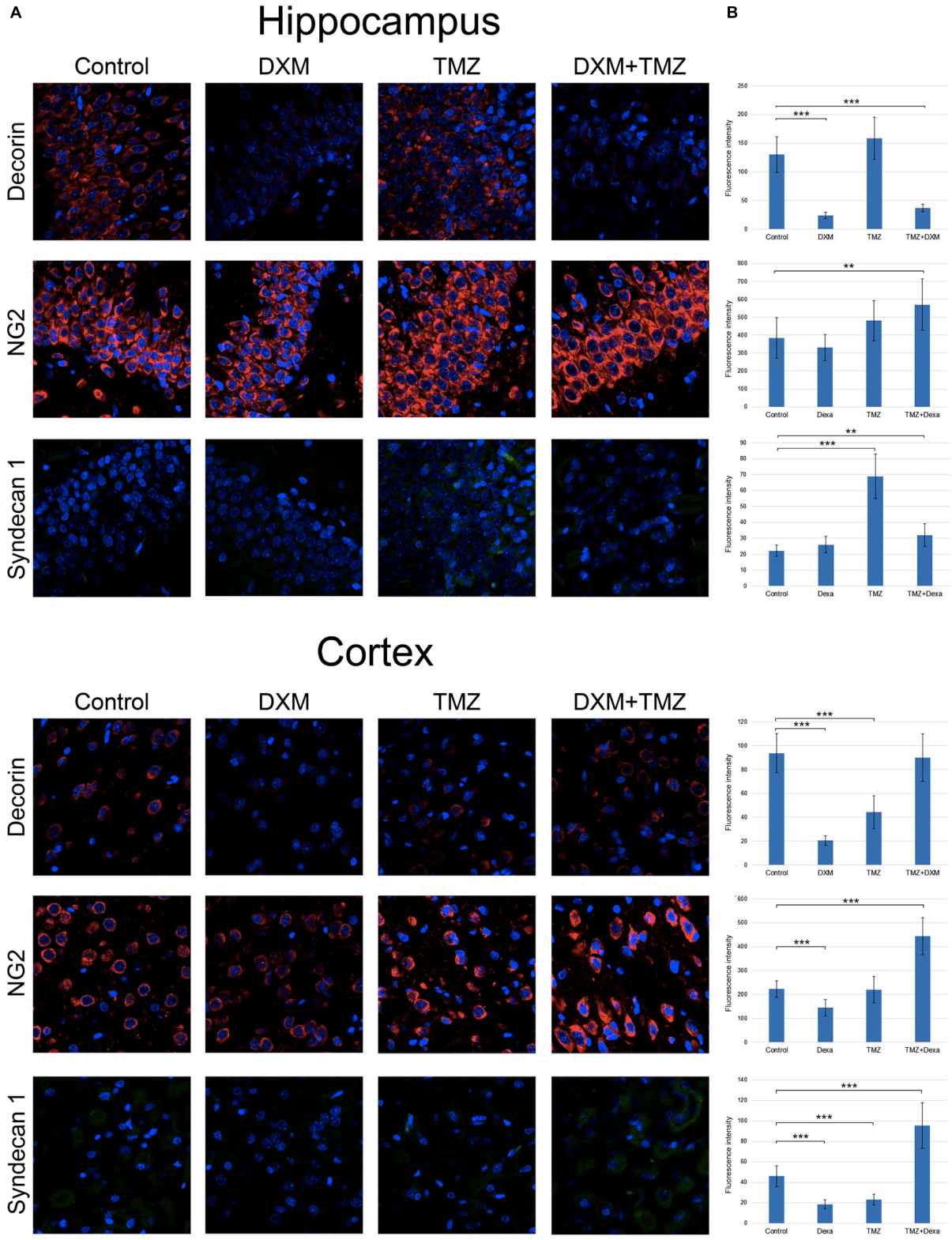


**FIGURE 5 |** Immunofluorescence analysis of PG core proteins content in rat brain before and after treatments with DXM and/or TMZ. **(A)** Immunostaining with anti-decorin, anti-CSPG4/NG2, or anti-syndecan-1 antibodies. Visualization with secondary antibodies Alexa Fluor 647 (red, for decorin and CSPG4/NG2) or Alexa Fluor 488 (green, for syndecan-1). Magnification *400. **(B)**. Quantitative analysis of the PG core proteins content in the control and treated rat brain tissues (CellProfiler 2.2.0 software). Student's *t*-test, $^{*}p < 0.05$, $^{**}p < 0.01$ and $^{***}p < 0.001$.

**TABLE 3 |** Immunofluorescence analysis of individual PG core proteins and GAG content in hippocampi and cortex of control and DXM and/or TMZ-treated Wistar rats.

| | | Decorin | Syndecan-1 | Cspg4/NG2 | HS | CS |
|---|---|---|---|---|---|---|
| Hippocampus | Control | 130.2 ± 8.9 | 22.1 ± 1.9 | 385.4 ± 35.8 | 22.7 ± 2.5 | 36.4 ± 3.2 |
| | DXM | 24.0 ± 1.9 | 25.9 ± 1.8 | 330.9 ± 24.7 | 63.2 ± 5.8 | 63.3 ± 4.5 |
| | TMZ | 158.5 ± 12.4 | 68.9 ± 5.4 | 481.0 ± 36.1 | 53.1 ± 6.3 | 65.0 ± 5.2 |
| | TMZ + DXM | 36.9 ± 3.1 | 32.0 ± 2.3 | 570.4 ± 44.9 | 34.4 ± 2.7 | 86.5 ± 6.2 |
| Cortex | Control | 93.6 ± 11.4 | 45.8 ± 4.7 | 222.4 ± 15.2 | 99.0 ± 13.5 | 41.7 ± 6.2 |
| | DXM | 20.49 ± 1.7 | 18.3 ± 1.8 | 144.3 ± 12.6 | 58.3 ± 6.1 | 20.6 ± 2.0 |
| | TMZ | 44.2 ± 7.4 | 22.9 ± 2.4 | 220.3 ± 21.4 | 41.1 ± 5.3 | 46.9 ± 5.7 |
| | TMZ + DXM | 89.9 ± 10.5 | 95.3 ± 10.9 | 444.6 ± 33.6 | 250.9 ± 34.1 | 202.7 ± 25.1 |

*Average fluorescence intensity calculated using Cell Profiler 2.2.0 software. HS, heparan sulphate and CS, chondroitin sulphate.*

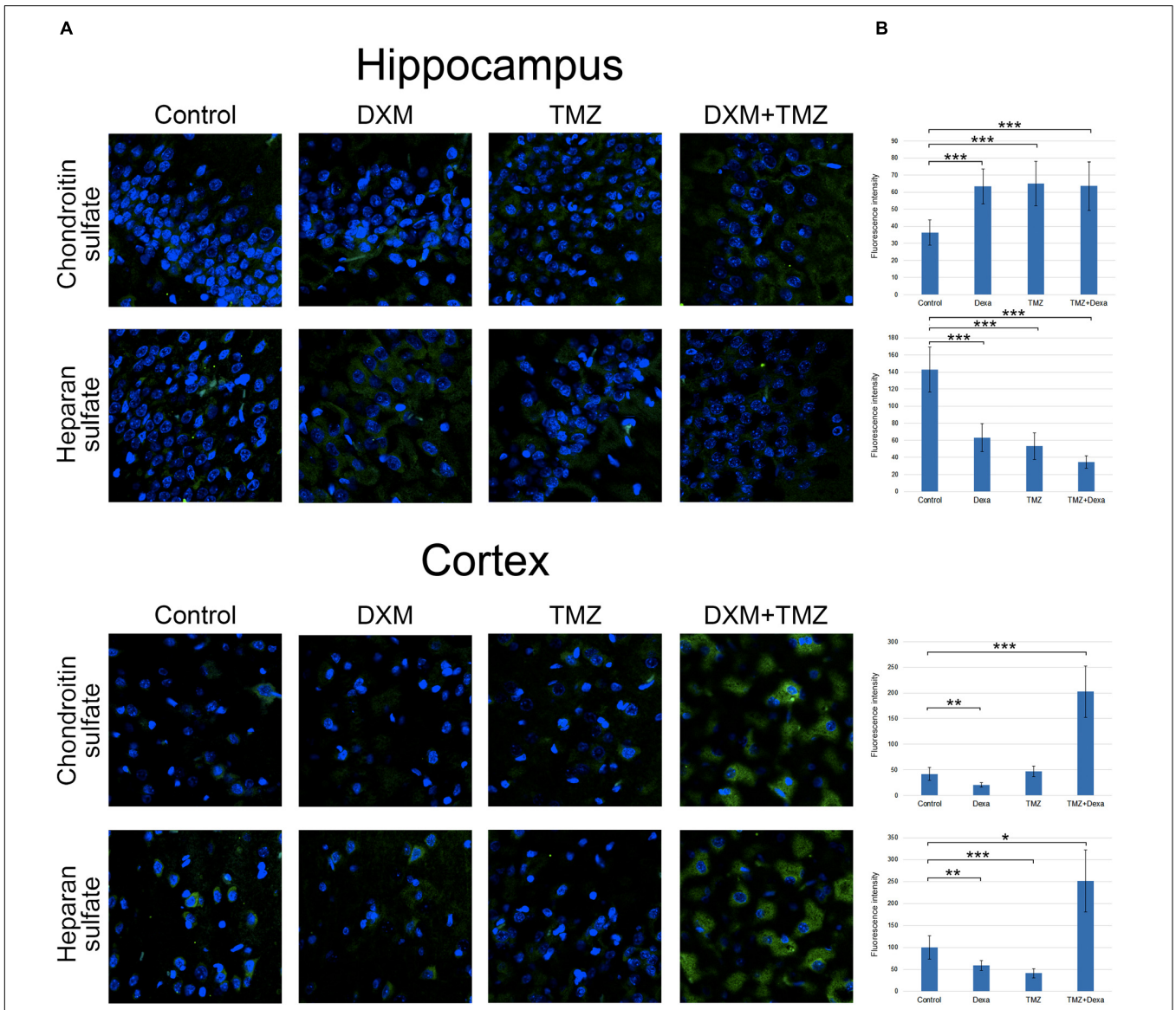


**FIGURE 6 |** Immunofluorescence analysis of GAGs content in rat brain before and after treatments with DXM and/or TMZ. **(A)** Immunofluorescence analysis with anti-HS and anti-chondroitin sulphate antibodies. Visualization with secondary antibodies Alexa Fluor 488 (green). Magnification *400. **(B)** Quantitative analysis of the GAGs content in the control and treated rat brain tissues (CellProfiler 2.2.0 software). Student's *t*-test, $*p < 0.05$, $**p < 0.01$ and $***p < 0.001$.

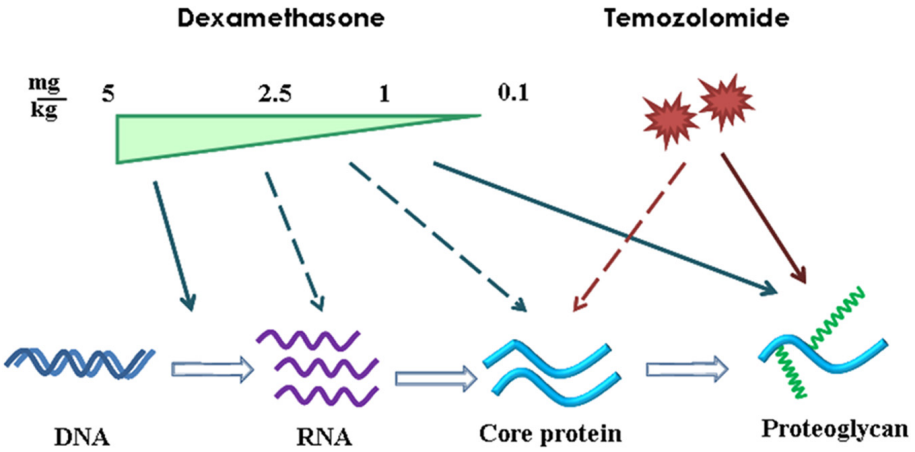


**FIGURE 7 |** Schematic representation of the effects of DXM and TMZ onto PGs expression and content in normal rat brain tissue in the experimental system *in vivo*. Arrows–significant effect and dotted arrows–weak effect.

results revealed differential effects of the drugs onto PG core proteins content in different brain zones. DXM treatment resulted in the decrease of decorin staining both in hippocampus and cortex (5-fold, $p < 0{,}001$ and 4,5-fold, $p < 0{,}001$, respectively), whereas TMZ significantly increased expression of syndecan-1 (3-fold, $p < 0{,}001$) in hippocampus but not cortex. There was a tendency for increased expression of CSPG4/NG2 in hippocampus upon the TMZ treatment as well; however, the change was not statistically significant (**Figure 5**; **Table 3**).

Interesting, the most profound effects were detected for the combined treatment (DXM + TMZ), with brain zone-specific characteristics. In hippocampus, significant decrease of decorin core protein content (3-4-fold, $p < 0{,}001$) along with an evident increase of CSPG4/NG2 (0,5-fold, $p < 0{,}01$) were observed. In cortex, up-regulation of CSPG4/NG2 and syndecan-1 (2-fold, $p < 0{,}001$ and 2-fold, $p < 0{,}001$, respectively) and no changes in decorin content were detected.

The results demonstrate an overall deterioration of the proteoglycan composition in the DXM and/or TMZ treated normal brain tissues at core protein level mainly due to changes in decorin, CSPG4/NG2 and syndecan-1 content. The changes in the proteoglycan core proteins upon DXM/TMZ treatment(s) stay in line with the RT-PCR data on more profound effects of the studied drugs towards hippocampus rather than cortex, and represent side effects of the conventional anti-glioblastoma therapy towards the normal rat brain tissue in the experimental system *in vivo*.

## Both DXM and TMZ Significantly Increase Glycosaminoglycan Content in Rat Brain, Especially in Combination

Along with core proteins, polysaccharide chains of GAGs [heparan sulphate (HS) and chondroitin sulphate (CS)] represent an important structural and functional part of the entire proteoglycan molecules. To determine potential effects of DXM and TMZ onto polysaccharide content of normal brain tissue, specific antibodies to the polysaccharide epitopes on HS and CS molecules were used for immunofluorescence analysis of the control and DXM and/or TMZ treated rat brain tissues (**Figure 6**).

Separate treatment with DXM or TMZ resulted in increase of HS and CS content in hippocampus (2-3-fold and 2-fold, respectively, $p < 0{,}001$) but not cortex. However, the most pronounced effects were observed for the combined DXM/TMZ treatments, which resulted in the significant increase of HS and CS content in hippocampus (1,5-fold, $p < 0{,}01$ and 2-2,5-fold, $p < 0{,}001$, respectively) and especially cortex (2,5-fold and 5-fold, respectively, $p < 0{,}001$).

Taken together, the obtained results for the first time demonstrate an ability of DXM and TMZ to affect PG/GAG expression and composition in normal rat brain tissue in the experimental system *in vivo*. The revealed changes might contribute to transformation of normal brain ECM into tumorigenic niche, susceptible for the enhanced invasion of the residual glioma cells and tumour progression.

# DISCUSSION

The presented results demonstrate that anti-glioblastoma drugs TMZ and DXM affect the content and expression pattern of PGs in normal rat brain tissue *ex vivo* and *in vivo*. As to TMZ, in spite of the known anticancer effects of the drug, there are no published data on its' possible action onto the normal cells or tissues to compare with. A different situation is about DXM, which is often used as anti-oedema drug during anticancer therapy. Its toxic side effects are demonstrated for many different cancers including glioma (Shields et al., 2015; Murayi and Chittiboina, 2016), where DXM may decrease the effectiveness of treatment and shorten survival of GBM patients, substantiating the request for restricted use of corticosteroids in glioblastoma (Pitter et al., 2016). However, molecular mechanisms of the DXM side effects remain unclear.

In the literature, we did not find any direct data about DXM or TMZ effects onto PGs content/composition in normal brain tissue to compare with, unlike their effect towards glioblastoma cells or GBM tumours. It is known that the expression levels of many PGs are changed significantly in glioblastoma cells and during the tumour development. For example, multiple changes occur in gliomas with a common tendency to overall activation of the expression of various PG core proteins: syndecan-1 and perlecan is significantly up-regulated in malignant glioma cell lines and GBM specimens (Watanabe et al., 2006); high expression of glypican-1 in glioma endothelial cells is associated with cell cycle progression (Qiao et al., 2008) and high expression of perlecan is associated with poor GBM prognosis (Kazanskaya et al., 2018); brevican is highly up-regulated in gliomas and promote cancer cells motility in primary brain tumours (Hu et al., 2008); CSPG4/NG2 is expressed in gliomas in oncofoetal manner and is involved in disease progression (Stallcup and Huang, 2008); significant (3–15-fold) up-regulation of CD44 and NG2 expression during the experimental glioma development in mouse glioma model *in vivo* suggest the molecules as possible molecular markers of tumour invasion (Wiranowska et al., 2006), however, human GBM specimens study supports NG2 but not CD44 as a possible prognostic markers of glioblastoma progression (Tsidulko et al., 2017); CSPGs can serve as critical regulators of glioma cells invasion and play an important role in organisation of tumour microenvironment (Silver et al., 2013).

The demonstrated ability of the conventional anti-glioblastoma chemotherapy to modulate PG and GAG expression and/or composition in normal brain tissue, for the first time reveals these brain ECM molecules as potential microenvironmental biomarkers for DXM side effects or molecular targets to search for perspective anti-DXM neuroprotective drugs. From the practical point of view, it underlines a necessity for the possible revision of the current DXM use during the GBM treatment. Moderate dose (1 mg/kg) seems to be the most appropriate in terms of consistency of PGs expression in the brain of the control and treated animals and possibly should be taken as a desirable dose. It means long-term treatment with low dose of DXM could be more appropriate that single high-dose DXM injection to preserve the transcriptional activity of PG-coding genes and resulted structure of brain ECM. The results are indirectly supported by the demonstrated DXM effects in organotypic culture of animal normal brain *ex vivo*: DXM exposure after oxygen-glucose deprivation potentiates oxygen-glucose deprivation-mediated cytotoxicity in organotypic cerebellar slice cultures prepared from neonatal rat pups (Mulholland et al., 2005); DXM is able to suppress transcription of AVP gene during stimulation by cAMP (Kuwahara et al., 2003).

Another interesting finding is that the high or lower doses of DXM have different "targets" on the complex proteoglycan molecules–whether the first one affects transcriptional activity of the PG core proteins, the last one points to polysaccharide GAG chains of the molecule. This fact makes the revealed GAG changes worse detected in the routine research or diagnostic studies, hiding this aspect of the side effects of the widely used drugs like DXM. Important aspect could be related as well to a potential contribution of the DXM-induced changes in normal brain tissue (and especially its ECM) into the neurological, psychological, and social problems for long-term survivors of glioblastoma (Gately et al., 2017). The demonstrated increase of the GAGs content in TMZ/DXM-treated normal brain tissue can be related to an unfavourable transformation of brain ECM into tumourigenic niche supporting glioma cells growth. The data stay in line with the available data on this issue: HS content is significantly increased in the relapsed GBM tumours (Kazanskaya et al., 2018); disruption of cell–cell and cell–ECM interactions by chondroitinase ABC treatment enhances the chemotherapeutic availability and sensitivity of glioma cells to TMZ (Jaime-Ramirez et al., 2017); glioblastoma- and neuroblastome-derived CSC-like cells with high expression of decorin and lumican are resistant to TMZ suggesting a novel pivotal role for the PGs in drug resistance and cell plasticity of glioma stem cells (Farace et al., 2015); blocking of GAG function during anticancer therapy could be a perspective strategy to improve cancer treatment (Belting, 2014).

Comparative analysis of the results, obtained at the transcriptional level of PGs expression (RT-PCR), core proteins expression (IHC) and HS/CS polysaccharide content (IHC with anti-HS/CS antibodies to the polysaccharide epitopes) suggests complex multi-level molecular mechanism of DXM/TMZ effects onto PGs content and distribution in brain tissue in rat experimental model *in vivo* (**Figure 7**). The effects are clearly dose-dependent, high DXM doses result in deregulation of the transcriptional activity of PG-coding genes, whereas low DXM doses and TMZ affect predominantly polysaccharide GAG chains of the molecules.

In summary, the demonstrated disorganization of proteoglycan expression and content in normal rat brain tissue under the DXM/TMZ pressure might contribute to formation of favourable microenvironment for proliferation and invasion of the remaining post-surgery glioblastoma cells, resulting in relapse of the disease. The obtained results extend our knowledge in this field and for the first time reveals the DZM/TMZ-induced changes in PGs expression and ECM organization in normal brain tissue as one of the possible molecular mechanisms of known toxic side effects of the conventional anti-glioblastoma therapy.

## AUTHOR CONTRIBUTIONS

AT and TP carried out organotypic culture experiments *ex vivo*. AT and AS performed the animal experiments. AT and GdLB performed RT-PCR analyses. CB, AS, GK, and SA performed immunostaining. EG and AT designed the experiments and wrote the manuscript.

## FUNDING

This study was funded by the Russian Science Foundation (Grant No. 16-15-10243). AT was supported by scholarship of Russian Federation President for young scientists (SP-5435.2018.4).

## REFERENCES


American Veterinary Medical Association (2013). *AVMA Guidelines for the Euthanasia of Animals*, 2013 Edn. Available: https://www.avma.org/KB/Policies/Documents/euthanasia.pdf

Bei, R., Marzocchella, L., and Turriziani, M. (2010). The use of temozolomide for the treatment of malignant tumors: clinical evidence and molecular mechanisms of action. *Recent Pat. Anticancer Drug Discov.* 5, 172–187. doi: 10.2174/157489210791760526

Belting, M. (2014). Glycosaminoglycans in cancer treatment. *Thromb. Res.* 133(Suppl. 2), S95–S101. doi: 10.1016/S0049-3848(14)50016-3

Diksin, M., Smith, S. J., and Rahman, R. (2017). The molecular and phenotypic basis of the glioma invasive perivascular niche. *Int. J. Mol. Sci.* 18:E2342. doi: 10.3390/ijms18112342

Dyck, S. M., and Karimi-Abdolrezaee, S. (2015). Chondroitin sulfate proteoglycans: key modulators in the developing and pathologic central nervous system. *Exp. Neurol.* 269, 169–187. doi: 10.1016/j.expneurol.2015.04.006

Fan, Z., Sehm, T., Rauh, M., Buchfelder, M., Eyupoglu, I. Y., and Savaskan, N. E. (2014). Dexamethasone alleviates tumor-associated brain damage and angiogenesis. *PLoS One* 9:e93264. doi: 10.1371/journal.pone.0093264

Farace, C., Oliver, J. A., Melguizo, C., Alvarez, P., Bandiera, P., Rama, A. R., et al. (2015). Microenvironmental modulation of decorin and lumican in temozolomide-resistant glioblastoma and neuroblastoma cancer stem-like cells. *PLoS One* 10:e0134111. doi: 10.1371/journal.pone.0134111

Gähwiler, B. H., Capogna, M., Debanne, D., McKinney, R. A., and Thompson, S. M. (1997). Organotypic slice cultures: a technique has come of age. *Trends Neurosci.* 20, 471–477. doi: 10.1016/S0166-2236(97)01122-3

Gately, L., McLachlan, S. A., Dowling, A., and Philip, J. (2017). Life beyond a diagnosis of glioblastoma: a systematic review of the literature. *J. Cancer Surviv.* 11, 447–452. doi: 10.1007/s11764-017-0602-7

Graber, D. J., Hickey, W. F., Stommel, E. W., and Harris, B. T. (2012). Anti-inflammatory efficacy of dexamethasone and Nrf2 activators in the CNS using brain slices as a model of acute injury. *J. Neuroimmune Pharmacol.* 7, 266–278. doi: 10.1007/s11481-011-9338-8

Hu, B., Kong, L. L., Matthews, R. T., and Viapiano, M. S. (2008). The proteoglycan brevican binds to fibronectin after proteolytic cleavage and promotes glioma cell motility. *J. Biol. Chem.* 283, 24848–24859. doi: 10.1074/jbc.M801433200

Jaime-Ramirez, A. C., Dmitrieva, N., Yoo, J. Y., Banasavadi-Siddegowda, Y., Zhang, J., and Relation, T. (2017). Humanized chondroitinase ABC sensitizes glioblastoma cells to temozolomide. *J. Gene Med.* 19:10.1002/jgm.2942. doi: 10.1002/jgm.2942

Kazanskaya, G. M., Tsidulko, A. Y., Volkov, A. M., Kiselev, R. S., Suhovskih, A. V., Kobozev, V. V., et al. (2018). Heparan sulfate accumulation and perlecan/HSPG2 up-regulation in tumour tissue predict low relapse-free survival for patients with glioblastoma. *Histochem. Cell. Biol.* 149, 235–244. doi: 10.1007/s00418-018-1631-7

Kuwahara, S., Arima, H., Banno, R., Sato, I., Kondo, N., and Oiso, Y. (2003). Regulation of vasopressin gene expression by cAMP and glucocorticoids in parvocellular neurons of the paraventricular nucleus in rat hypothalamic organotypic cultures. *J. Neurosci.* 23, 10231–10237. doi: 10.1523/JNEUROSCI.23-32-10231.2003

Lamprecht, M. R., Sabatini, D. M., and Carpenter, A. E. (2007). CellProfiler: free, versatile software for automated biological image analysis. *Biotechniques* 42, 71–75. doi: 10.2144/000112257

Lin, Y. M., Jan, H. J., Lee, C. C., Tao, H. Y., Shih, Y. L., Wei, H. W., et al. (2008). Dexamethasone reduced invasiveness of human malignant glioblastoma cells through a MAPK phosphatase-1 (MKP-1) dependent mechanism. *Eur. J. Pharmacol.* 593, 1–9. doi: 10.1016/j.ejphar.2008.06.111

Manini, I., Caponnetto, F., Bartolini, A., Ius, T., Mariuzzi, L., Di Loreto, C., et al. (2018). Role of microenvironment in glioma invasion: what we learned from in vitro models. *Int. J. Mol. Sci.* 19:E147. doi: 10.3390/ijms19010147

Minami, N., Maeda, Y., Shibao, S., Arima, Y., Ohka, F., Kondo, Y., et al. (2017). Organotypic brain explant culture as a drug evaluation system for malignant brain tumors. *Cancer Med.* 6, 2635–2645. doi: 10.1002/cam4.1174

Miyata, S., and Kitagawa, H. (2017). Formation and remodeling of the brain extracellular matrix in neural plasticity: roles of chondroitin sulfate and hyaluronan. *Biochim. Biophys. Acta* 1861, 2420–2434. doi: 10.1016/j.bbagen.2017.06.010

Mulholland, P. J., Stepanyan, T. D., Self, R. L., Hensley, A. K., Harris, B. R., Kowalski, A., et al. (2005). Corticosterone and dexamethasone potentiate cytotoxicity associated with oxygen-glucose deprivation in organotypic cerebellar slice cultures. *Neuroscience* 136, 259–267. doi: 10.1016/j.neuroscience.2005.07.043

Murayi, R., and Chittiboina, P. (2016). Glucocorticoids in the management of peritumoral brain edema: a review of molecular mechanisms. *Childs Nerv. Syst.* 32, 2293–2302. doi: 10.1007/s00381-016-3240-x

Nam, J. Y., and de Groot, J. F. (2017). Treatment of glioblastoma. *J. Oncol. Pract.* 13, 629–638. doi: 10.1200/JOP.2017.025536

Nestler, U., Winking, M., and Böker, D. K. (2002). The tissue level of dexamethasone in human brain tumors is about 1000 times lower than the cytotoxic concentration in cell culture. *Neurol. Res.* 24, 479–482. doi: 10.1179/016164102101200203

Nicholson, C., and Hrabětová, S. (2017). Brain extracellular space: the final frontier of neuroscience. *Biophys. J.* 113, 2133–2142. doi: 10.1016/j.bpj.2017.06.052

Nørøxe, D. S., Poulsen, H. S., and Lassen, U. (2017). Hallmarks of glioblastoma: a systematic review. *ESMO Open* 1:e000144. doi: 10.1136/esmoopen-2016-000144

Palyanova, N. V., Pankova, T. M., Starostina, M. V., Kicha, A. A., Ivanchina, N. V., and Stonik, V. A. (2013). Neuritogenic and neuroprotective effects of polar steroids from the far east starfishes *Patiria pectinifera* and Distolasterias nipon. *Mar. Drugs* 11, 1440–1445. doi: 10.3390/md11051440

Park, J. B., Kwak, H. J., and Lee, S. H. (2008). Role of hyaluronan in glioma invasion. *Cell Adh. Migr.* 2, 202–207. doi: 10.4161/cam.2.3.6320

Paw, I., Carpenter, R. C., Watabe, K., Debinski, W., and Lo, H. W. (2015). Mechanisms regulating glioma invasion. *Cancer Lett.* 362, 1–7. doi: 10.1016/j.canlet.2015.03.015

Pitter, K. L., Tamagno, I., Alikhanyan, K., Hosni-Ahmed, A., Pattwell, S. S., Donnola, S., et al. (2016). Corticosteroids compromise survival in glioblastoma. *Brain* 139, 1458–1471. doi: 10.1093/brain/aww046

Qiao, D., Yang, X., Meyer, K., and Friedl, A. (2008). Glypican-1 regulates anaphase promoting complex/cyclosome substrates and cell cycle progression in endothelial cells. *Mol. Biol. Cell* 19, 2789–2801. doi: 10.1091/mbc.E07-10-1025

Reitman, Z. J., Winkler, F., and Elia, A. E. H. (2018). New directions in the treatment of glioblastoma. *Semin. Neurol.* 38, 50–61. doi: 10.1055/s-0038-1623534

Seystahl, K., Gramatzki, D., Roth, P., and Weller, M. (2016). Pharmacotherapies for the treatment of glioblastoma - current evidence and perspectives. *Expert Opin. Pharmacother.* 17, 1259–1270. doi: 10.1080/14656566.2016.1176146

Shannon, S., Vaca, C., Jia, D., Entersz, I., Schaer, A., Carcione, J., et al. (2015). Dexamethasone-mediated activation of fibronectin matrix assembly reduces dispersal of primary human glioblastoma cells. *PLoS One* 10:e0135951. doi: 10.1371/journal.pone.0135951

Shields, L. B., Shelton, B. J., Shearer, A. J., Chen, L., Sun, D. A., Parsons, S., et al. (2015). Dexamethasone administration during definitive radiation and temozolomide renders a poor prognosis in a retrospective analysis of newly diagnosed glioblastoma patients. *Radiat. Oncol.* 10:222. doi: 10.1186/s13014-015-0527-0

Silver, D. J., Siebzehnrubl, F. A., Schildts, M. J., Yachnis, A. T., Smith, G. M., Smith, A. A., et al. (2013). Chondroitin sulfate proteoglycans potently inhibit invasion and serve as a central organizer of the brain tumor microenvironment. *J. Neurosci.* 33, 15603–15617. doi: 10.1523/JNEUROSCI.3004-12.2013

Song, I., and Dityatev, A. (2017). Crosstalk between glia, extracellular matrix and neurons. *Brain Res. Bull.* 136, 101–108. doi: 10.1016/j.brainresbull.2017.03.003

Stallcup, W. B., and Huang, F. J. (2008). A role for the NG2 proteoglycan in glioma progression. *Cell Adh. Migr.* 2, 192–201. doi: 10.4161/cam.2.3.6279

Sur, P., Sribnick, E. A., Patel, S. J., Ray, S. K., and Banik, N. L. (2005). Dexamethasone decreases temozolomide-induced apoptosis in human gliobastoma T98G cells. *Glia* 50, 160–167. doi: 10.1002/glia.20168

Thakkar, J. P., Dolecek, T. A., Horbinski, C., Ostrom, Q. T., Lightner, D. D., Barnholtz-Sloan, J. S., et al. (2014). Epidemiologic and molecular prognostic review of glioblastoma. *Cancer Epidemiol. Biomark. Prev.* 23, 1985–1996. doi: 10.1158/1055-9965.EPI-14-0275

Touat, M., Idbaih, A., Sanson, M., and Ligon, K. L. (2017). Glioblastoma targeted therapy: updated approaches from recent biological insights. *Ann. Oncol.* 28, 1457–1472. doi: 10.1093/annonc/mdx106

Tsidulko, A. Y., Kazanskaya, G. M., Kostromskaya, D. V., Aidagulova, S. V., Kiselev, R. S., Volkov, A. M., et al. (2017). Prognostic relevance of NG2/CSPG4, CD44 and Ki-67 in patients with glioblastoma. *Tumour Biol.* 39:1010428317724282. doi: 10.1177/1010428317724282

Watanabe, A., Mabuchi, T., Satoh, E., Furuya, K., Zhang, L., Maeda, S., et al. (2006). Naganuma H. Expression of syndecans, a heparan sulfate proteoglycan, in malignant gliomas: participation of nuclear factor-kappaB in upregulation of syndecan-1 expression. *J. Neurooncol.* 77, 25–32. doi: 10.1007/s11060-005-9010-3

Wiranowska, M., Ladd, S., Smith, S. R., and Gottschall, P. E. (2006). CD44 adhesion molecule and neuro-glial proteoglycan NG2 as invasive markers of glioma. *Brain Cell. Biol.* 35, 159–172. doi: 10.1007/s11068-007-9009-0

Yang, L. J., Zhou, C. F., and Lin, Z. X. (2014). Temozolomide and radiotherapy for newly diagnosed glioblastoma multiforme: a systematic review. *Cancer Invest.* 32, 31–36. doi: 10.3109/07357907.2013.861474

Yu, C., Griffiths, L. R., and Haupt, L. M. (2017). Exploiting heparan sulfate proteoglycans in human neurogenesis-controlling lineage specification and fate. *Front. Integr. Neurosci.* 11:28. doi: 10.3389/fnint.2017.00028

**Conflict of Interest Statement:** The authors declare that the research was conducted in the absence of any commercial or financial relationships that could be construed as a potential conflict of interest.

frontiers in Pharmacology

ORIGINAL RESEARCH
published: 19 October 2018
doi: 10.3389/fphar.2018.01150

# Berberine Attenuated Proliferation, Invasion and Migration by Targeting the AMPK/HNF4α/WNT5A Pathway in Gastric Carcinoma

*Qian Hu[1], Lingli Li[1], Xin Zou[1], Lijun Xu[1] and Ping Yi[1,2]**

*[1] Institute of Integrated Traditional Chinese and Western Medicine, Tongji Hospital, Tongji Medical College, Huazhong University of Science and Technology, Wuhan, China, [2] Department of Integrated Traditional Chinese and Western Medicine, Tongji Hospital, Tongji Medical College, Huazhong University of Science and Technology, Wuhan, China*

**Background:** Recent epidemiologic studies have found that patients with diabetes have a higher risk of gastric cancer (GC), and the long-term use of metformin is associated with a lower risk of gastric cancer. It is believed that blocking tumor energy metabolic alterations is now emerging as a new therapeutic approach of cancer. Berberine, a natural isoquinoline alkaloid, could modulate lipid metabolism and glucose homeostasis by regulating the expression of HNF4α in many metabolic diseases. Here, we investigated the effect of Berberine on GC and its possible molecular mechanism through targeting HNF4α.

**Methods and Results:** (1) AGS and SGC7901 gastric cancer cells were treated with Berberine (BBR). We found that in AGS and SGC7901 cell, BBR inhibited cell proliferation in a time- and dose-dependent manner through downregulating *C-myc.* BBR also induced $G_0$-$G_1$ phase arrest with the decreased expression of cyclin D1. Moreover, BBR attenuated the migration and invasion by downregulating MMP-3. (2) The lentivirus infection was used to silence the expression of HNF4α in SGC7901 cell. The results demonstrated that the knockdown of HNF4α in SGC7901 slowed cells proliferation, induced S phase arrest and dramatically attenuated gastric cancer cells' metastasis and invasion. (3) We performed GC cells perturbation experiments through BI6015 (an HNF4α antagonist), AICAR (an AMPK activator), Compound C (AMPK-kinase inhibitor), metformin and BBR. Our findings indicated that BBR downregulated HNF4α while upregulating p-AMPK. Moreover, the inhibition of HNF4α by BBR was AMPK dependent. (4) Then the LV-HNF4α-RNAi SGC7901 cell model was used to detect the downstream of HNF4α *in vitro*. The results showed that the knockdown of HNF4α significantly decreased WNT5A and cytoplasmic β-catenin, but increased E-cadherin *in vitro*. Berberine also downregulated WNT5A and cytoplasmic β-catenin, the same as LV-HNF4α-RNAi and BI6015 in GC cells. (5) Finally, the SGC7901 and LV-HNF4α-RNAi SGC7901 mouse-xenograft model to evaluate the effect of BBR and HNF4α gene on GC tumor growth. The result illustrated that BBR and knockdown of HNF4α suppressed tumor growth *in vivo*, and BBR decreased HNF4α, WNT5A and cytoplasmic β-catenin levels, the same effect as HNF4α knockout *in vivo*.

OPEN ACCESS

***Edited by:***
*Andrew Zloza,*
*Rutgers Cancer Institute of New Jersey, United States*

***Reviewed by:***
*Harikumar K. B.,*
*Rajiv Gandhi Centre for Biotechnology, India*
*Chakrabhavi Dhananjaya Mohan, University of Mysore, India*

****Correspondence:***
*Ping Yi*
*pyi219@163.com*

***Specialty section:***
*This article was submitted to Cancer Molecular Targets and Therapeutics, a section of the journal Frontiers in Pharmacology*

***Received:*** *18 June 2018*
***Accepted:*** *24 September 2018*
***Published:*** *19 October 2018*

***Citation:***
*Hu Q, Li L, Zou X, Xu L and Yi P (2018) Berberine Attenuated Proliferation, Invasion and Migration by Targeting the AMPK/HNF4α/WNT5A Pathway in Gastric Carcinoma. Front. Pharmacol. 9:1150. doi: 10.3389/fphar.2018.01150*

**Conclusion:** BBR not only had proliferation inhibition effect, attenuated the invasion and migration on GC cell lines, but also suppressed the GC tumor growth *in vivo*. The anti-gastric cancer mechanism of BBR might be involved in AMPK-HNF4α-WNT5A signaling pathway. HNF4α antagonists, such as BBR, could be a promising anti-gastric cancer treatment supplement.

**Keywords: berberine, metformin, gastric cancer, HNF4α, WNT**

## INTRODUCTION

Gastric cancer is one of the leading deadly malignancies in both sexes worldwide, especially in eastern Asia (Torre et al., 2016). In 2017, it is estimated the number of stomach cancer deaths in China will reach 2.21 million, ranking third in the world and second in China (Balakrishnan et al., 2017; Chen et al., 2018). Recent epidemiologic studies have found that patients with diabetes have a higher risk of gastric cancer, and the long-term use of metformin is associated with a lower risk of gastric cancer compared with the lack of use of metformin (Tseng and Tseng, 2014; Li et al., 2018). It is believed that the occurrence of gastric cancer is related to energy metabolism, blocking these metabolic alterations is now emerging as a new therapeutic approach of cancer, and some of metabolic enzymes involved in the glycolytic pathway are currently considered as new therapeutic targets (Song et al., 2015).

Hepatocyte nuclear factor 4α (HNF4α) is a nuclear transcription factor that binds DNA as a homodimer (Jucá et al., 2017). Multiple HNF4α isoforms exist in humans and are suggested to have different physiological roles in development and transcriptional regulation of target genes. Previous studies have found that HNF4α is a key regulator of a number of genes involved in glucose, cholesterol and fatty acid metabolism, and HNF4α mutations cause monogenic type 2 diabetes of the young (Rhee et al., 2006; Love-Gregory and Permutt, 2007). Recent studies have shown that changes in HNF4α gene expression are associated with many types of cancers, such as hepatocellular carcinoma, renal cell carcinoma, gastric adenocarcinoma, small intestine carcinoma, and colorectal cancer (Darsigny et al., 2010). Moreover, many studies have found that HNF4α is highly expressed in gastric cancer tissues, especially in Asia (Chang et al., 2015; Ma et al., 2017). The expression of HNF4α is seen in primary gastric adenocarcinomas and in metastases of gastric carcinoma to the breast, but is absent in primary breast carcinomas, and in metastases of breast carcinomas to the stomach (Van der Post et al., 2014). What's the molecular mechanism of HNF4α, a nuclear receptor that activates the expression of genes involved in glucose, fatty acid and cholesterol metabolism, in the development of gastric cancer?

Berberine (BBR) is a natural isoquinoline alkaloid extracted from plants, such as berberis aquifolium, vulgaris, aristata, and tinospora cordifolia (Tabeshpour et al., 2017). BBR was used to be an antibacterial agent in China for a long time. Over the past decade, It has been reported that BBR could also regulate plasma lipid and glucose levels in type 2 diabetes animal models and humans (Kumar et al., 2015; Pirillo and Catapano, 2015; Tabeshpour et al., 2017; Wang H. et al., 2018). Our previous studies have also indicated that BBR can stimulate insulin secretion and modulate lipids in impaired glucose tolerance rats (Leng et al., 2004), reverse free-fatty-acid-induced insulin resistance in 3T3-L1 adipocytes (Yi et al., 2008), even attenuate intestinal mucosal barrier dysfunction and immune barrier damages in type 2 diabetic rats (Gong et al., 2017). And the molecular mechanism which BBR modulates lipid metabolism, inhibits hepatic gluconeogenesis and enhances insulin secretion is targeting HNF4α (Wang et al., 2008; Wei et al., 2016). Recent studies revealed that BBR can inhibit the growth of gastric tumor, the anti-cancer effect of BBR is through inhibiting glucose uptake and reducing the transcription of glucose metabolism relative genes (Wang et al., 2016; Mao et al., 2018). So does Berberine share same molecular target in metabolism regulation and in anti-tumor developing?

In the present study, firstly, we investigated the anti-gastric cancer effect of BBR on GC cell lines. Secondly, the lentivirus infection was used to silence HNF4α in SGC7901 cell to demonstrate whether HNF4α was a key target for anti-gastric cancer. Then, BI6015 (an HNF4α antagonist), AICAR (an AMPK activator), Compound C (AMPK-kinase inhibitor), metformin and LV-HNF4α-RNAi SGC7901 cell model was used to detect the molecular mechanism of BBR in GC cell lines. Finally, we used SGC7901 and LV-HNF4α-RNAi SGC7901 mouse-xenograft models to demonstrate the effect of BBR and HNF4α *in vivo*. Our results revealed that Berberine, a metabolism-regulated drug, could inhibit GC cells proliferation, migration and invasion and suppress GC tumor growth. The anti-gastric cancer mechanism of BBR might be involved in AMPK- HNF4α-WNT5A signaling pathway and HNF4α is a key molecule target.

## MATERIALS AND METHODS

### Materials

Berberine chloride (BBR), dimethyl sulfoxide (DMSO) and Compound C were obtained from Sigma-Aldrich, United States. BI6015 (an HNF4α antagonist) and AICAR (AMPK activator) were provided by the TOCRIS Bio-Techne. Metformin was purchased from Tongji Hospital. Cultrex PathClear Basement Membrane Extract (BME) was obtained from RDsystems.

**Abbreviations:** AICAR, 5-Aminoimidazole-4-carboxamide1-β-D-ribofurano side; AMPK, adenosine 5′-monophosphate (AMP)-activated protein kinase; BBR, berberine; GC, gastric cancer; GFP, green fluorescent protein; HNF4α, hepatocyte nuclear factor-4α; MET, metformin.

Mouse monoclonal Antibodies against human AMPK, p-AMPK, HNF4α, β-catenin, E-cadherin, cyclin D1, MMP-3, and C-myc were obtained from Cell Signaling Technologies (Boston, MA, United States), WNT5A was purchased from Abgent. Another Antibody against HNF4α (sc-374229) was obtained from Santa Cru Biotechnology (Santa Cruz, CA, United States), which was used for immunohistochemistry of mouse tumor tissue.

## Cell Culture

Hubei Biossci Biological Co., Ltd., supported the GC cell lines SGC7901 and AGS. The SGC7901 and AGS cells were cultured in RPMI 1640 medium (HyClone, China) with 10% fetal bovine serum (FBS) (SiJiQing, China), 1% penicillin-streptomycin-amphotericin solution at 37°C in a humidified chamber with 5% $CO_2$. When cells were in logarithmic growth phase, they were given drug treatment.

## Small Interfering RNA Transfection

Lentiviruses which carried the small interfering human HNF4α RNA (siRNA) were purchased from Gikai Gene and used to transfect cell to silence the expression of HNF4α. Lentiviruses without the siRNA gene were generated as a control and designated as Lenti-GFP. The transfection medium was removed after 12 h, replaced with fresh medium, and the cells then grown in 5% $CO_2$ at 37°C for an additional 48–72 h. Stably transfected cells were selected by puromycin. RT-PCR and western blot analyses were performed to confirm target knockdown by siRNA.

## MTT Assay

Cell growth was assessed with a standard 3-(4,5-dimethyl-2-tetrazolyl)-2,5-diphenyl-2H tetrazolium bromide (MTT) assay. A total of $5 \times 10^3$ cells were seeded in each well of 96-well culture plates. After 8 h, the cells were treated with different concentrations of drugs (Berberine 10∼80 μM, metformin 10∼80 mM). After 24, 48, and 72 h, the culture medium was removed, and 20 μl of a 0.5 mg/ml solution of MTT (Sigma-Aldrich) was added to each well. The plates were then incubated for 4 h at 37°C. The MTT solution was then removed and replaced with 100 μl of DMSO (Wuhan Goodbio Technology Co., Ltd.) per well, and the absorbance at 570 nm was measured using an Enzyme-linked immunoassay (Synergr2 BioTek, United States).

## Migration and Invasion Assays

Cells were trypsinized and resuspended in serum-free medium at a concentration of $1 \times 10^5$ cells/ml. Approximate $2 \times 10^4$ cells were seeded in the upper chamber (Millipore, United States) seated on 24-well plate, and 750 μl complete medium with 10% FBS was added to each well of the plate as the lower chamber. After 16 h of incubation, non-filtered cells were removed using a cotton swab. Migratory cells on the underside of membrane were fixed and stained with 0.1% crystal in five different fields at 200× magnification.

Cell invasion was examined using Corning chamber assays. The bottom of the Transwell membrane was pretreated with 100 μl Cultrex PathClear Basement Membrane Extract (RDsystems) for 2 h at 37°C. Afterward, $5 \times 10^4$ cells re-suspended in serum-free 1640 were plated in the upper chamber of a trans-well apparatus (8.0 um pore, Corning), while 750 μl of 1640 with 10% FBS were provided in the lower chamber. After incubation at 37°C for 24 h, cells that migrated to the bottom of the membrane were attached and fixed, stained with 0.5% crystal violet, and cells in the upper chamber were removed with a cotton sticker. The images were acquired using a light microscope. The cells were examined under a fluorescence microscope. (×200, Nikon).

## Cell Cycle Analysis by Flow Cytometry

Cell cycle distribution assay by flow cytometry. Cell cycle analysis was determined by PI staining. Briefly, AGS and SGC7901 cells were treated with drugs for 48 h, and then were blended with 13-methyl-palmatrubine. Treated and control cells were harvested, washed twice with phosphate buffered saline (PBS) and fixed with pre-cooled 70% ethanol for 24 h at 4°C. Fixed cells were washed, pelleted, re-suspended in 500 μl PBS containing 50 μg RNase A at 37°C and then stained with 5 μg PI in the dark at room temperature for 30 min. Finally, cell cycle distributions were immediately assessed using a FACSort Flow Cytometer (BD Biosciences, San Jose, CA, United States).

## Western Blot Analysis

Cells were washed twice with cold PBS and then were suspended in 100 μl RIPA lysis buffer for 30 min at 4°C, vortexed every 10 min, and then centrifuged at 12000 × *g* for 15 min. The supernatants containing the total protein extracts were collected. Protein concentration was measured by the BCA. Sample proteins (60 μg of protein/lane) on a 10% SDS-polyacrylamide electrophoresis gel (SDS–PAGE).The electrophoresis was carried out first at 80 V for 30 min and followed by 120 V for 60 min. The proteins were separated using SDS–PAGE gel and transferred onto NC membranes (0.4 um, Millipore, United States). The transferred NC membranes were incubated for 1 h with 5% non-fat milk blocking buffer, the primary antibody (1:800 or 1:1000) were incubated overnight with gentle agitation at 4°C. The membranes were washed three times and incubated with the second antibody (1:8000 or 1:10000) at room temperature for 1 h and subsequently were visualized with a near-infrared double color laser imaging system (Odyssey, Lincoln, NE, United States).

## RNA Isolation and Quantitative PCR Analyses

Total RNA was extracted from cultured cells in the exponential phase of growth using the TRIzol Reagent (Magen, Wuhan) according to the manufacturer's instructions. cDNA was synthesized from 2 μg of total RNA using the 5X All-In-One RT MasterMix (abm) at 42°C for 15 min and at 85°C for 5 min. Real-time PCR reactions were performed using EvaGreen 2X qPCR MasterMix at 95°C for 10 min, 95°C for 15 s and 60°C for 60 s, 40 cycles. Relative quantity of HNF4α, WNT5A, C-myc, CyclinD1, β-catenin, MMP-3 and E-cadherin were calculated using the ΔΔCt method with GAPDH as reference control. The

**TABLE 1 |** Primers for RT-PCR assay.

| Gene | Forward (5′-3′) | Reverse (5′-3′) |
|---|---|---|
| AMPKα 2 | CAATCGTTCTGTCGCCACTC | TCTTTCACAGCCTCATC ATCAA |
| HNF4α | TGGTGGACAAAGACAAG AGGAA | GAGCGCATTGATGGAGGG |
| WNT5a | CGACTATGGCTACCGCTTTG | AGGGCATCACCCACCTTG |
| β-catenin | TGCTGAAGGTGCTATCT GTCTG | CCTTCCATCCCTTCC TGTTT |
| CyclinDl | GTGACCACCACCCCAACAA | CCTTTCCCGACCCTGCTA |
| E-cadherin | CCGCCGGCGTCTGTAGGAA | AGGGCTCTTTGACCACCG CTCTC |
| MMP-3 | GGCCTGGAACAGTCTTGGC | TGTCCATCGTTCATCAT CGTCA |
| C-MYC | GGATTCTCTGCTCTCC TCGAC | CTCCAGCAGAAGGTG ATCCA |
| GAPDH | AATCCCATCACCATCT TCCAG | GAGCCCCAGCCTTC TCCAT |

reproducibility of the measurements was assessed by performing triplicate reactions. The primer sequences are listed in **Table 1**.

## Xenograft Model Analysis

Animal experiments were carried out according to the institutional guidelines and regulations. All animal studies were approved by the Huazhong University of Science and Technology Institutional Animal Care and Use Committee (S787). We purchased 18 female athymic mice (BALB/c-nude; 4 weeks old; 13–16 g) from Hunan Slake Jingda Experimental Co., Ltd. (Hunan, China). The animals were maintained under specific pathogen-free condition using a laminar airflow rack and had continuous free access to sterilized flood and autoclaved water. Nine mice were inoculated with SGC7901 cells ($10^7$ cells per animal) subcutaneously on the right flank regions of the mouse. The rest 9 mice were inoculated with normal control ($n$ = 3), Lenti-GFP ($n$ = 3), and LV-HNF4α-RNAi ($n$ = 3) SGC7901 cells ($10^7$ cells per animal), respectively, subcutaneously on the right flank regions of the mouse. Seventy-two hours later, the xenografts were identifiable as a mass of more than 6 mm in maximal diameter in all recipients. The SGC7901 mouse-xenograft models were randomly assigned to three groups (control group, $n$ = 3; BBR group, $n$ = 3; and MET group, $n$ = 3). Mice were gavaged with PBS alone (control), BBR (100 mg/kg/day), MET (250 mg/kg/day) every other day starting on day 3. Tumor volume was calculated every third day as follows: tumor volume ($mm^3$) = [tumor length (mm) × tumor width $(mm)^2$]/2. All animals were sacrificed on day 18 after treatment. All animals were alive during the observation.

## Immunohistochemistry Staining

Solid tumors were removed from sacrificed mice and fixed with 4% formaldehyde. Paraffin-embedded tumors tissue were sliced on 4-μm thick and mounted on APES-coated slides. Slides were deparaffinized in xylene and rehydrated in graded ethanol. Endogenous peroxidase activity was quenched with a 3% hydrogen peroxide solution in methanol at room temperature for 30 min, followed by rinsing in pH 6.0 PBS. After antigen retrieval in a water bash set in a 10 mmol/L citrate buffer (pH 6.0) at 94°C for 8 and 10 min, respectively, the slides were immediately cooled for 20 min at room temperature, Non-specific binding sites were blocked by incubation with wash buffer containing 10% normal goat serum at 37°C for 30 min. The sections were then incubated overnight at 4°C with a primary antibodies against HNF4α (at 1:100; Santa Cruz), WNT5A (at 1:80; abs113167 Abgent), and β-catenin (at 1:100; Cell Signaling Technologies). The positive stains were shown as brown color by peroxidase substrate solution DAB, and samples were lightly counterstained with hematoxylin. Specimens were examined under a light microscope.

## Statistical Analysis

All data were analyzed by Graph Pad Prism 6 software and expressed as the mean ± SD. Significance among groups was analyzed by one-way analysis of variance (ANOVA), followed by Dunnett's multiple comparison post-test. A value with $P < 0.05$ was considered significant.

# RESULTS

## Effect of Berberine on Cell Proliferation in GC Cells

To address the effect of BBR on gastric cancer cells growth, we evaluated GC cell viability using MTT assay. As shown in **Figure 1A**, treatment with increasing concentration of BBR (10–80 μM) resulted in growth inhibition of AGS and SGC7901 cells, also in a time-dependent manner (24, 48, and 72 h), although BBR had an unstable inhibitory effect on SGC7901 cells at 24 h (40–60 μM). Metformin (MET, 10–80 mM) was chosen as positive control (Chang et al., 2015). The result showed that MET had same proliferation inhibition effect on AGS and SGC7901, with a time- and dose-dependent manner, expect for SGC7901 cells at 24 h (**Figure 1B**). Consider reducing the toxicity of drugs to cells and maintaining certain inhibitions against cancer cells, 20 and 30% inhibitory concentration of BBR and MET at 48 h were chosen for the follow-up experiment. The proto-oncogene *C-myc* is closely related to the proliferation of cancer cells. We detected the changes of proliferative gene *C-myc* after treating with BBR and MET by western blotting and RT-PCR. As shown in **Figures 1C,D**, BBR (20 and 30 μM) and MET (30 mM) showed the best inhibitory effect on proto-oncogene *C-myc* in AGS cells ($P < 0.001$). In SGC7901 cells, MET (20 mM) showed a best inhibition ($P < 0.001$). On the whole, treatment with BBR and MET obviously reduced the protein levels of proliferative gene *C-myc*, compared with untreated AGS and SGC7901 cells. As showed in **Figure 1E**, the results showed the same inhibiting trend in mRNA levels after treating with BBR and MET. What's more, the low concentration of BBR and MET had a better effect on inhibiting mRNA expression of proliferative gene *C-myc* than high concentration in both AGS and SGC7901 cells ($P < 0.01$).

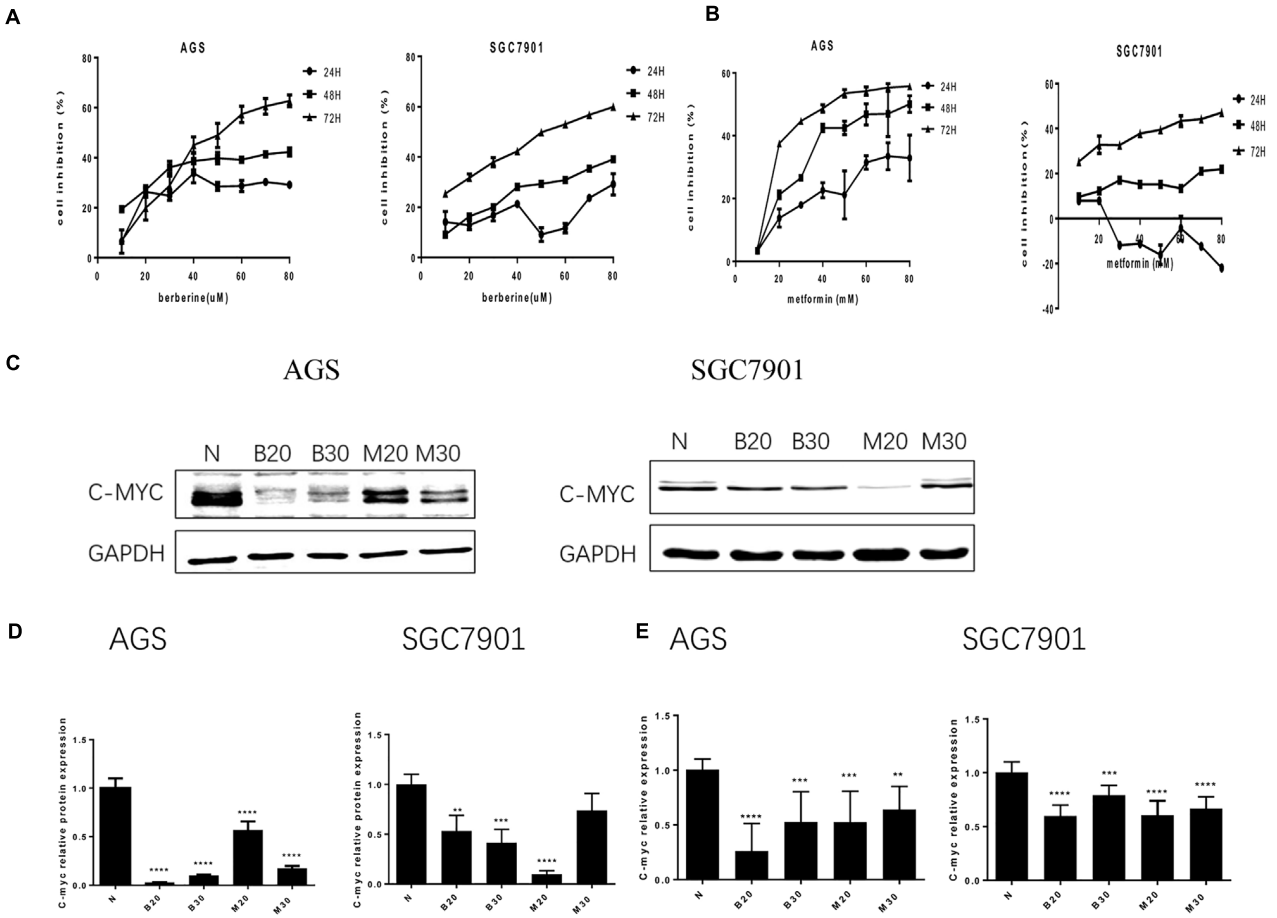


**FIGURE 1 |** Effect of Berberine on proliferation in GC cells. Human gastric cancer AGS and SGC7901 cells were treated with BBR and metformin. **(A)** Effect of BBR on cell inhibition at 24, 48, and 72 h. **(B)** Effect of MET on cell inhibition at 24, 48, and 72 h. **(C)** The protein expression of *C-myc* in AGS and SGC7901 cells 48 h after treatment. **(D)** The quantification of *C-myc* protein levels in AGS and SGC7901 cells. **(E)** The quantification of mRNA expression of *C-myc* in AGS and SGC7901 cells 48 h after treatment. Data were presented as the means ± SD. N, untreated cells (normal control group); B20, Berberine (20 μM); B30, Berberine (30 μM); M20, Metformin (20 μM); M30, Metformin (30 μM); $n = 6$ for MTT and $n = 3$ for western-blot and RT-PCR. $^{**}P < 0.01$, $^{***}P < 0.001$, $^{****}P < 0.0001$ vs. normal control group.

## Berberine Induced $G_0/G_1$ Phase Cell Cycle Arrest

To investigate how BBR influences cancer cell viability, we stained AGS and SGC7901 with PI and quantified the number of cells in $G_0$-$G_1$, S, $G_2$-M period by flow cytometry. We found that the number of cells in $G_0$-$G_1$ period increased in both AGS and SGC7901 cells after treating with BBR and MET ($P < 0.05$, $P < 0.01$, and $P < 0.001$) (**Figures 2A,B** and **Tables 2**, **3**). Cyclin D1 is a key protein implicated in the transition of the $G_0$-$G_1$ phase, a decline in Cyclin D1 level indicates a $G_0$-$G_1$ arrest in cells. We examined both the protein and mRNA levels of Cyclin D1 in AGS and SGC7901 cells separately after the treatment of BBR and MET. The results showed both BBR and MET had negative influence on the protein expression of Cyclin D1 in AGS and SGC7901 cells, and there was a dose-dependent inhibition ($P < 0.05$ and $P < 0.01$) (**Figures 2C,D**). As shown in **Figure 2E**, BBR and MET also downregulated the mRNA level of Cyclin D1 in both AGS and SGC7901 cells, which was consistent with the protein results ($P < 0.001$).

## Berberine Inhibited the Migration and Invasion in GC Cells

Tumor cell invasion and metastasis are the main characteristics of malignant tumor, which are the leading causes of death in patients with malignant tumor. We used the Transwell assay to examine the effect of BBR and MET on GC cells migratory and invasion. As shown in **Figures 3A–C**, the migration numbers of AGS and SGC7901 cells significantly reduced through the Transwell chamber microspores in the treatment group ($P < 0.001$). When chamber was coated with Matrigel, which was used to mimic the extracellular matrix (ECM) around tumors and to detect the invasion ability of cells. As shown in **Figures 3D–F**, The BBR-treated and metformin-treated AGS cells had a significant lower invasion than the untreated cell, the same effect was observed in SGC7901 cells ($P < 0.001$). With the

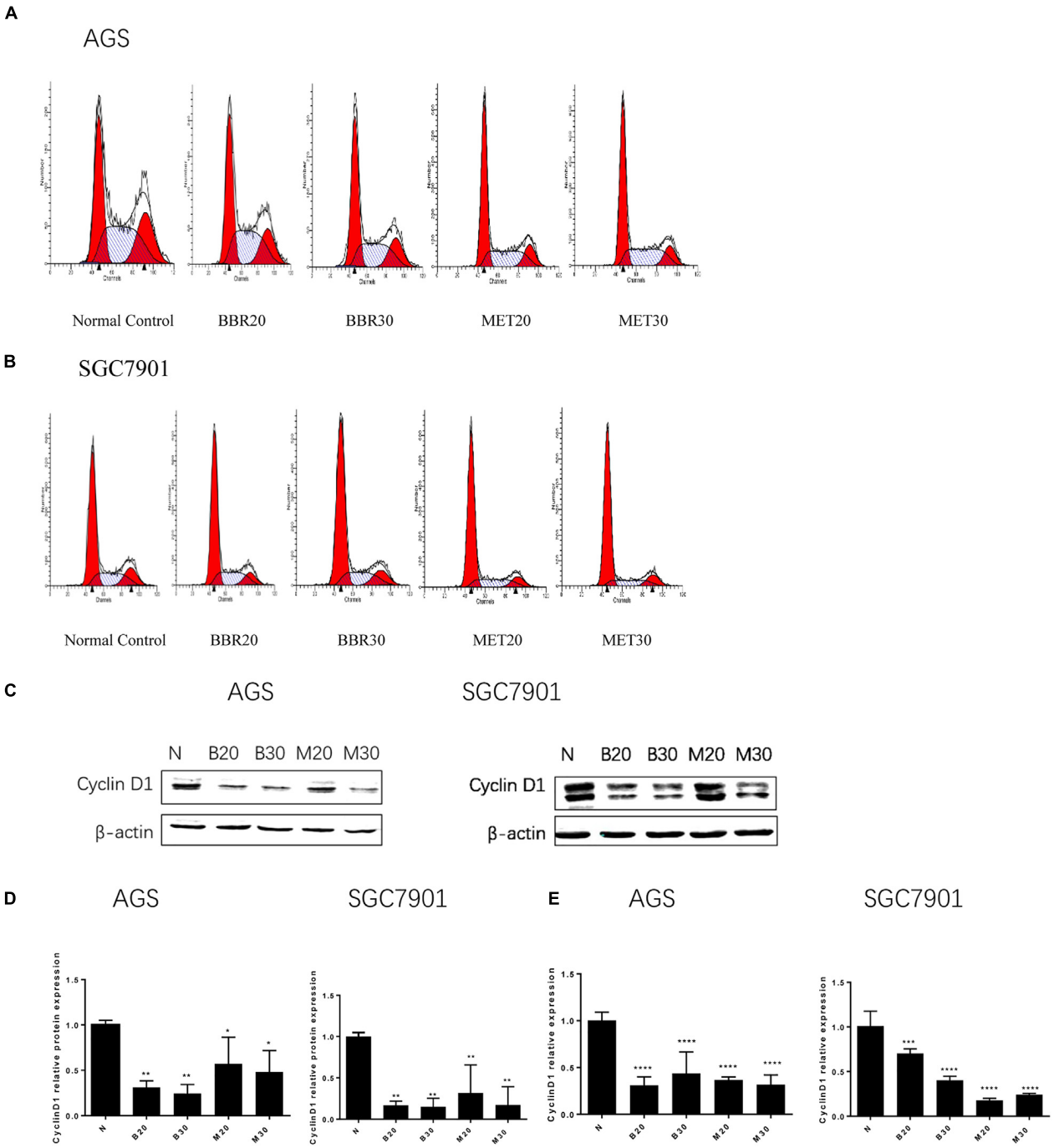


**FIGURE 2 |** Berberine induced G0/G1 phase cell cycle arrest. Human gastric cancer AGS and SGC7901 cells were treated with BBR and MET. At 48 h after treatment, the numbers of cells in $G_0$–$G_1$, S, and $G_2$-M phase were calculated by flow cytometry. **(A)** AGS cells. **(B)** SGC7901 cells. **(C)** The protein expression of Cyclin D1 in AGS and SGC7901 cells 48 h after treatment. **(D)** The quantified western blot of Cyclin D1 in AGS and SGC7901 cells. **(E)** At 48 h after treatment, the quantified mRNA expression of Cyclin D1 in AGS and SGC7901 cells. Data were presented as the means ± SD. $n = 3$ for western-blot and RT-PCR. $^{*}P < 0.05$, $^{**}P < 0.01$, $^{***}P < 0.001$, $^{****}P < 0.0001$ vs. Normal control group.

increase concentration of BBR and MET, the number of gastric cancer cells that invaded and metastasized gradually decreased. Matrix metalloproteinase-3 (MMP-3), known as inducers of EMT, is one of the several MMPs that regulate angiogenesis, invasion and metastasis (Huang et al., 2016; Chu et al., 2018; Simi et al., 2018). It was reported that MMP-3 expression level was negatively correlated with GC development (Xu et al., 2016). We used western-blot and RT-PCR to determine whether BBR

**TABLE 2 |** Cell cycle ratios of BBR on AGS cell (mean + SD) (%).

| Group | G0-G1 | S | G2-M |
|---|---|---|---|
| Control | 42.590 + 5.037 | 40.728 + 4.758 | 18.170 + 4.341 |
| Berberine (20 umol/L) | 44.145 + 3.856*** | 38.118 + 1.223 | 17.735 + 2.673 |
| Berberine (30 umol/L) | 46.720 + 4.365*** | 36.982 + 2.727* | 16.302 + 3.071 |
| Metformin (20 mmol/L) | 47.798 + 2.224*** | 36.217 + 1.052* | 15.972 + 2.156 |
| Metformin (30 mmol/L) | 47.058 + 2.788*** | 36.210 + 1.776* | 16.733 + 4.457 |

*n = 4 for cell cycle analysis vs. Control, *P < 0.05 and ***P < 0.001.*

**TABLE 3 |** Cell cycle ratios of BBR on SGC7901 cell (mean + SD) (%).

| Groups | G0-G1 | S | G2-M |
|---|---|---|---|
| Control | 58.757 + 0.379 | 25.960 + 1.200 | 15.283 + 1.424 |
| Berberine (20 umol/L) | 63.533 + 0.973* | 24.557 + 1.236 | 11.913 + 1.415* |
| Berberine (30 umol/L) | 65.050 + 1.131** | 22.403 + 1.297* | 12.550 + 0.650 |
| Metformin (20 mmol/L) | 69.020 + 1.750*** | 21.283 + 2.182* | 9.663 + 0.686** |
| Metformin (30 mmol/L) | 69.370 + 4.038*** | 18.880 + 2.252** | 11.753 + 2.449* |

*n = 3 for cell cycle analysis vs. Control, *P < 0.05, **P < 0.01, and ***P < 0.001.*

can affect the expression of matrix metalloproteinase-3 (MMP-3). The results showed that BBR (20 and 30 μM) and MET (30 mM) had stable inhibitory effect on MMP-3 protein expression in AGS and SGC7901 cells ($P < 0.01$), MET (20 μM) downregulated the expression of MMP-3 in SGC7901 cells, but had no obvious inhibition in AGS cells (**Figures 3G,H**). As shown in **Figure 3I**, there was a obviously decrease in the mRNA levels of MMP-3 in BBR group compared to untreated group (N) in AGS and SGC7901 cells, MET had similar effect on AGS and SGC7901 cells ($P < 0.01$ and $P < 0.001$).

## Knockdown of HNF4α Attenuated Proliferation, Invasion, and Migration in SGC7901 Cell

Having observed the effect of BBR on gastric cancer, next, we explored the molecular mechanism of BBR against gastric cancer. HNF4α has been reported to be related to malignant tumor formation and metastasis (Xiang et al., 2015; Kato et al., 2018; Maan et al., unpublished). We used lentivirus-mediated transduction of SiRNA-HNF4α to silence the expression of HNF4α in SGC7901 cell, RT-PCR and western blot analyses were performed to confirm target gene knockdown by siRNA. The results showed a 10-fold downregulation of HNF4α expression (**Figures 4A–C**).

MTT assay was added to detect the proliferation in normal control cells (Control), empty vector control cells (GFP) cells and LV-HNF4α-SGC7901 cells. As shown in **Figure 4D**, comparing with the Control and GFP, the knockdown of HNF4α in SGC7901 cells significantly reduced the proliferation ($P < 0.0001$ and $P < 0.001$). Also, we stained normal control cells, GFP and LV-HNF4α-SGC7901 cells with PI and quantified the number of cells in $G_0$-$G_1$, S, $G_2$-M period by flow cytometry. As shown in **Figure 4E** and **Table 4**, we found LV-HNF4α-SGC7901 cells increased S population compared with normal control cells and GFP cells ($P < 0.05$). Moreover, a Transwell assay was used to detect the role of HNF4α in gastric SGC7901 cell migration and invasion. The results showed that knockdown of HNF4α dramatically attenuated the migration and invasion of SGC7901 cell compared with the control cells ($P < 0.001$ and $P < 0.001$) (**Figures 4F,G**).

## Berberine Regulated HNF4α by Activating AMPK in GC Cells

A research has found metformin, a widely used antidiabetic drug, has antitumor activity through modulated HNF4α (Chang et al., 2015). Recent study has shown BBR modulates lipid metabolism and inhibits hepatic gluconeogenesis by decreasing expression of HNF4α in type 2 diabetic mouse (Wei et al., 2016). Our previous study illustrated BBR prevented fructose-induced insulin resistance by promoting the expression HNF4α in rat livers (Wei et al., 2012). In this study, knockdown of HNF4α in SGC7901 cell line slowed its proliferation, induced S phase arrest, dramatically attenuated gastric cancer cells metastasis and invasion and suppressed the tumor growth *in vivo*, the same anti-gastric effect as Berberine. Therefore, we examined how HNF4α was regulated by BBR in GC cell line. BI6015 (an HNF4α antagonist) and AICAR (an AMPK activator) were used and served as positive control.

In AGS cell, BBR and MET significantly decreased the protein level of HNF4α (**Figures 5A,B**). BBR (30 μM), MET (30 mM), and AICAR reduced the mRNA expression of HNF4α (**Figure 5D**). Although there was no obvious decrease in the protein and mRNA levels of HNF4α after BI6015 treatment (**Figures 5B,D**). However, in SGC7901 cell, BI6015 decreased the protein and mRNA expression of HNF4α, the same trend in BBR treatment (**Figures 5C,E**). More thrillingly, the protein levels of HNF4α in BBR group were lower than in BI6015 group ($P < 0.05$). As we expected, MET and AICAR also decreased the protein expression of HNF4α in SGC7901 cells (**Figure 5C**).

As for the expression of p-AMPK and AMPK, we used Metformin and AICAR (an AMPK activator) as the positive control, the results showed that BBR (20 μM) increased the protein level of p-AMPK in both AGS and SGC7901 cells ($P < 0.05$), BBR (30 μM) only upregulated the protein expression of p-AMPK in SGC7901 cell (**Figures 5B,C**). Also, we observed that BBR (30 μM) group increased the mRNA level of p-AMPK in both AGS and SGC7901 cells, but not BBR (20 μM) group (**Figures 5D,E**). Although no statistically significant differences were found in the total level of AMPK after BBR-treated (**Figures 5A–E**).

To explore the interaction between AMPK and HNF4α in gastric cells, we used BBR and Compound C (AMPK inhibitor) to treat two GC cell lines and detected the changes in the protein

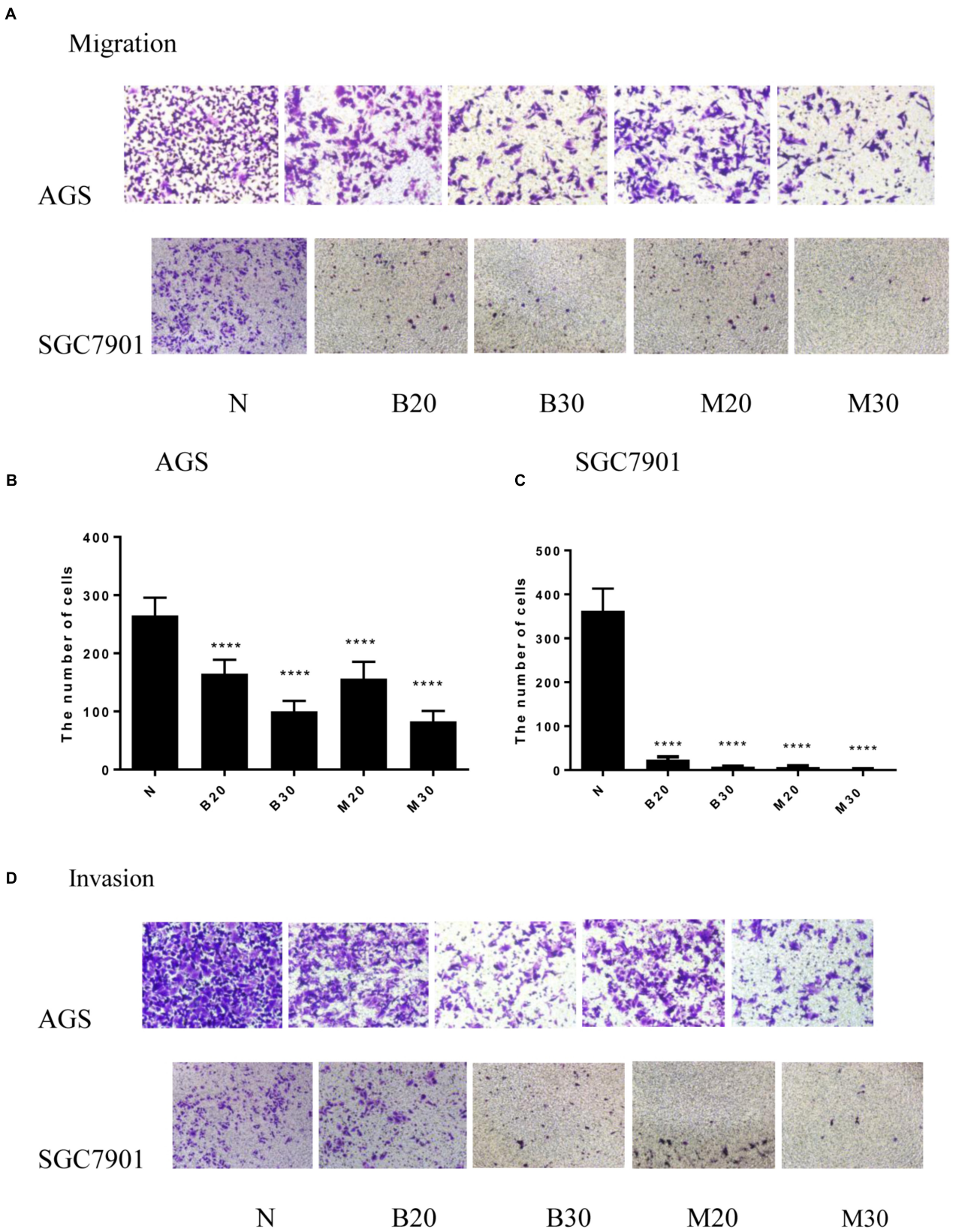


**FIGURE 3 |** Continued

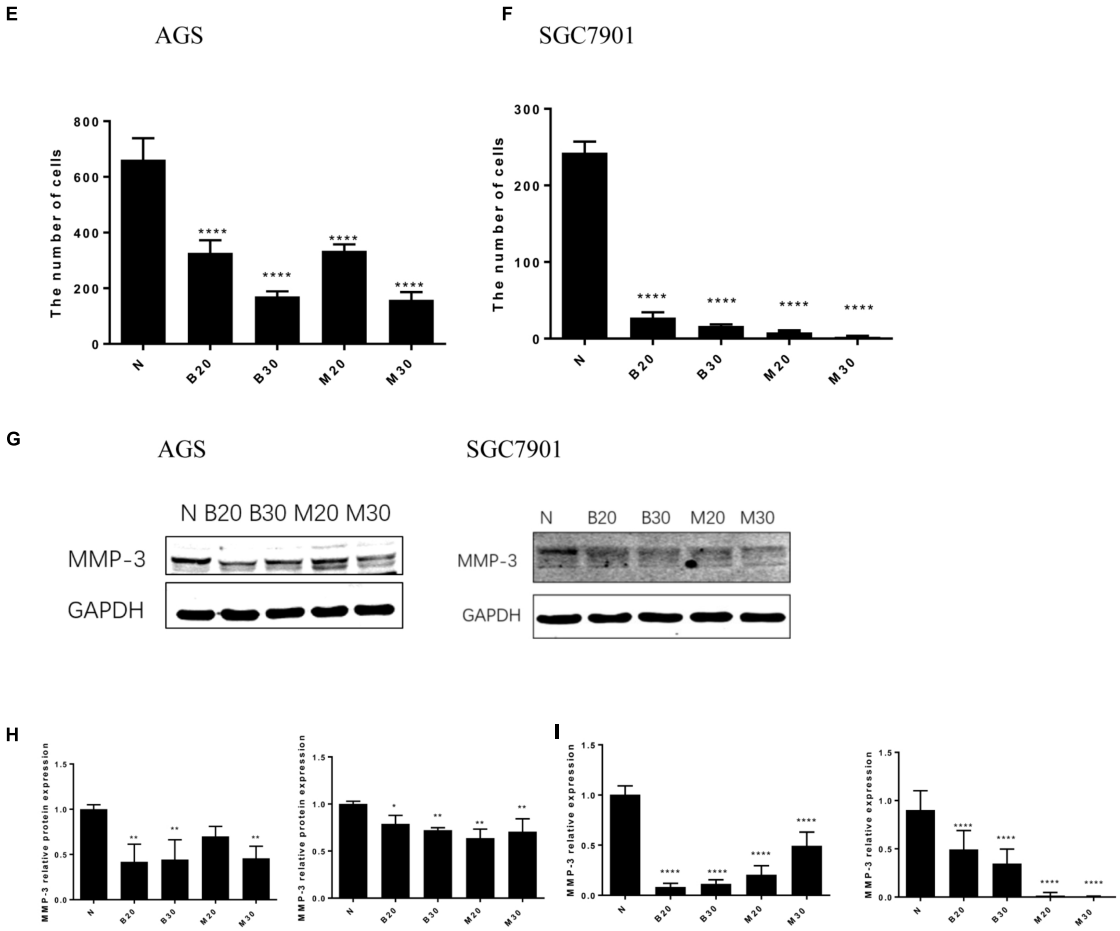


**FIGURE 3 |** Berberine inhibited the migration and invasion of GC cells. Human gastric cancer AGS and SGC7901 cells were treated with BBR and MET. Effect of BBR and MET on migration of GC cells after 48 h treatment. Representative images from experiment **(A)** and quantification of migration cell number (**B**: AGS cells; **C**: SGC7901 cells). Effect of BBR and MET on invasion of GC cells after 48 h treatment. Representative images from experiment **(D)** and quantification of invasion cell number (**E**: AGS cells; **F**: SGC7901 cells). Data were presented as the means ± SD, and representative data from at least three independent experiment are shown. **(G)** Protein expression of MMP-3 in AGS and SGC7901 cells 48 h after BBR and MET treatment. **(H)** The quantified western blot of MMP3 in AGS and SGC7901 cells. **(I)** Quantified mRNA expression of MMP3 in AGS and SGC7901 cells 48 h after BBR and MET treatment. $n = 3$ for western-blot and RT-PCR. $^{*}P < 0.05$, $^{**}P < 0.01$, $^{****}P < 0.0001$ vs. Normal control group.

levels of HNF4α. The results showed, BBR treatment increased p-AMPK expression and decreased HNF4α expression in GC cells, Compound C decreased p-AMPK expression and increased HNF4α expression in GC cells, there was a negative relationship between AMPK and HNF4α in GC cells (**Figures 5F,H,I**). Compound C weakened the inhibition of HNF4α by BBR, suggesting that HNF4α may be the downstream of AMPK in GC cells. Both BBR and Compound C had no effect on the total AMPK protein level (**Figure 5G**).

## Berberine Targeted the WNT/β-Catenin Signaling Through Regulating HNF4α in GC Cells

WNT signaling plays an important role in gastric cancer development, especially WNT5A, a member of the WNT family of secreted lipid-modified glycoproteins, was closely related to the gastric cancer invasion and metastasis (Kanzawa et al., 2013; Ara et al., 2016). Recent research has found that WNT5A is a direct target gene of HNF4α in GC (Nam et al., 2014). To explore how BBR exerts anti-tumor effect by HNF4α acting on downstream targets, Western blot and Real Time PCR were performed to detect the mRNA and protein levels of WNT signaling after BBR-treated. We used BBR, metformin, AICAR (AMPK activator) and BI6015 (an HNF4α antagonist) to interfere with two GC cells. As shown in **Figures 6A–E**, BBR and MET (20 mM) decreased the protein and mRNA expression of WNT5A and cytoplasmic β-catenin in both AGS and SGC7901 cells. MET (30 mM) produced the same inhibitory effect in modulating the WNT signaling pathway as MET (20 mM) in GC cells expect the protein expression of WNT5A in AGS cell. To further investigate the downstream of HNF4α in GC cells, we used SiRNA-HNF4α SGC7901 cell model to detect the WNT pathway.

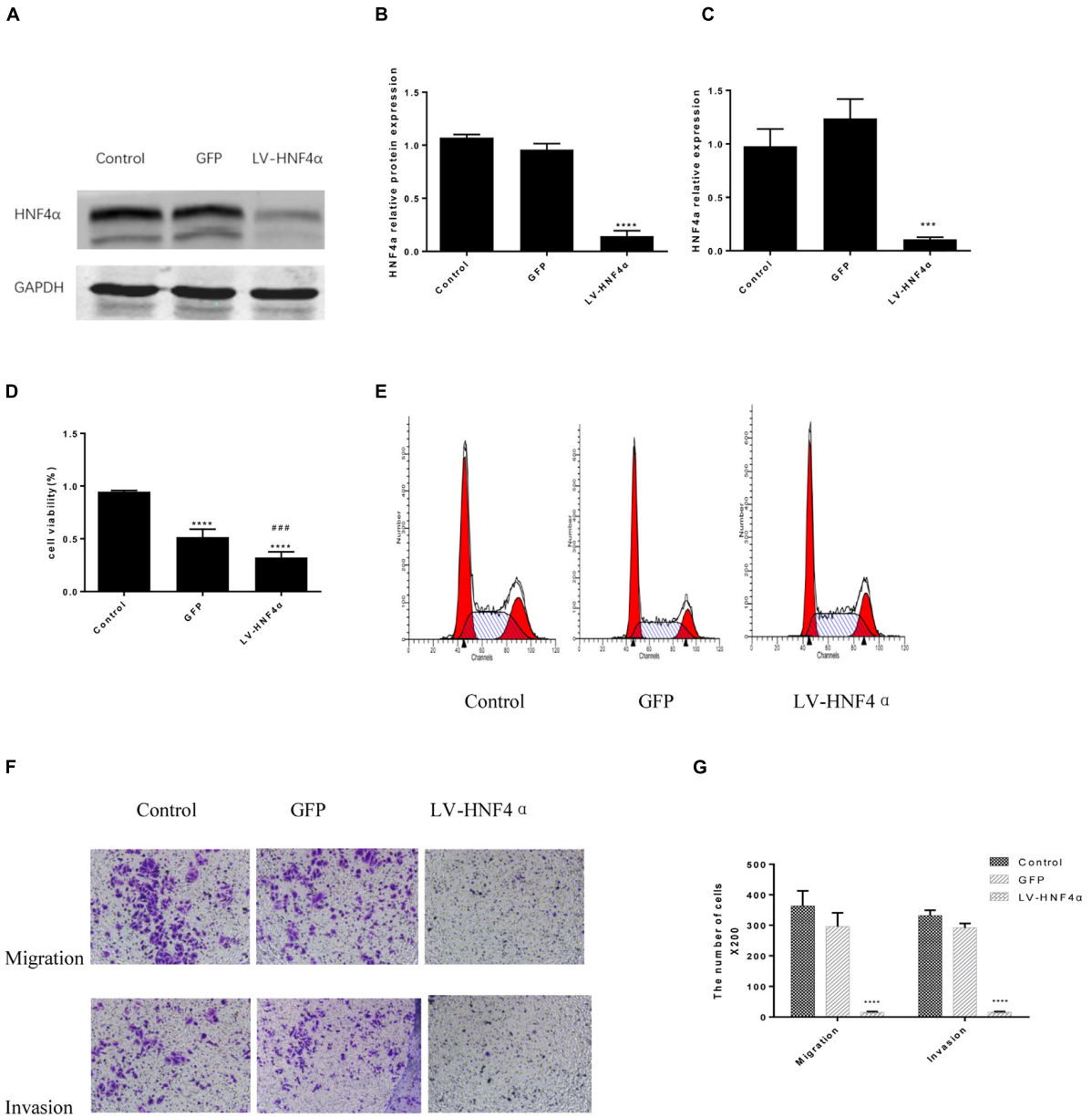


**FIGURE 4 |** Knockdown of HNF4α attenuated proliferation, migration and invasion of SGC7901 cells. Lentivirus-mediated HNF4α siRNA transcript and empty vectors were infected into SGC7901 gastric cancer cells as the Control group and the GFP group respectively. Western-blotting and RT-PCR were used to confirm the knockdown of HNF4α and quantified. **(A)** Representative western-blot images. **(B)** Quantification of Western blot results. **(C)** Quantification of RT-PCR ($n = 3$). We examined the effect of HNF4α knockout on SGC7901 cells. **(D)** Cell proliferation ($n = 3$). **(E)** Cell cycle ($n = 3$). **(F)** Representative images of migration and invasion. **(G)** Quantification of migration and invasion cell number. Data were presented as the means ± SD, with representative data from at least three independent experiments. $^{***}P < 0.05$, $^{****}P < 0.001$ vs. Control group. $^{###}P < 0.001$ vs. GFP group.

Western blot and Real Time PCR separately were used to test the mRNA and protein levels of WNT5A, cytoplasmic β-catenin, E-cadherin and CyclinD1. The WNT/β-catenin, being the canonical WNT pathway, which can induce the expression of CyclinD1 (Larue and Delmas, 2006). E-cadherin, another member of WNT pathway, is lost in some cancers, allowing cellular migration to the stroma (Kobayashi et al., 2018). As shown in **Figures 6F,G**, comparing with normal control cells and Lenti-GFP cells, the protein expression of WNT5A, cytoplasmic β-catenin, and Cyclin D1 decreased while the expression of E-cadherin increased in LV-HNF4α-SGC7901 cell. In mRNA level, there were obvious low levels of WNT5A, cytoplasmic β-catenin, and Cyclin D1 in LV-HNF4α-SGC7901 cell, and the level of E-cadherin in LV-HNF4α-SGC7901 cells was higher in normal control cells and Lenti-GFP cells (**Figure 6H**).

## Knockdown of HNF4α Suppressed Xenograft Tumor Growth *in vivo*

BALB/c nude mouse models with xenografted human SGC7901 cells, Lenti-GFP and LV-HNF4α-SGC7901 cells were employed to evaluate the effect of HNF4α on tumor growth *in vivo*. Eighteen days after inoculation, the body weight remained consistent between these groups (**Figure 7A**). the average final tumor weight and volume in the LV-HNF4α group were 0.01 g and 6.268 $mm^3$, respectively, which was significantly lower than those in normal control group (0.253 g, 234.0571 $mm^3$) and Lenti-GFP group (0.133 g, 71.928 $mm^3$) ($P < 0.05$) (**Figures 7B–D**). There was no statistical difference in tumor weight and volume between normal control group and Lenti-GFP group. Those results suggested that knockdown of HNF4α suppressed gastric cancer tumor growth *in vivo*.

**TABLE 4 |** Cell cycle ratios (mean + SD) (%).

| Groups | $G_0$-$G_1$ | S | $G_2$-M |
|---|---|---|---|
| Normal control | 43.68 + 0.383 | 35.51 + 2.210 | 20.807 + 1.835 |
| GFP | 48. 717 + 2.441* | 35.760 + 3.080 | 15.527 + 0.870* |
| LV-HNF4α | 40.920 + 0.934** | 40.877 + 1. 160* | 18.203 + 0.227 |

We used immunohistochemistry to exam the HNF4α, WNT5A and cytoplasmic β-catenin expression in gastric cancer

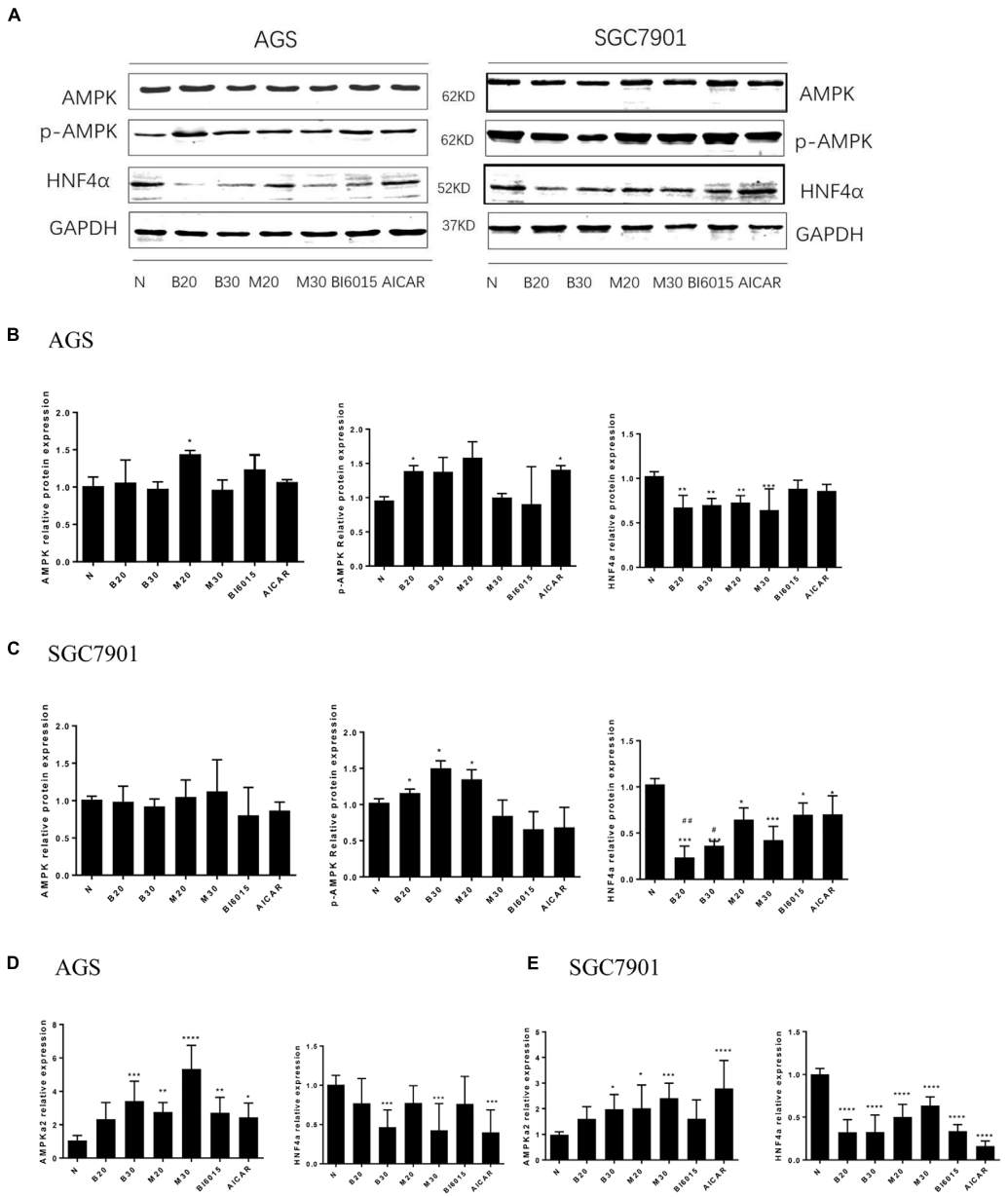


**FIGURE 5 |** Continued

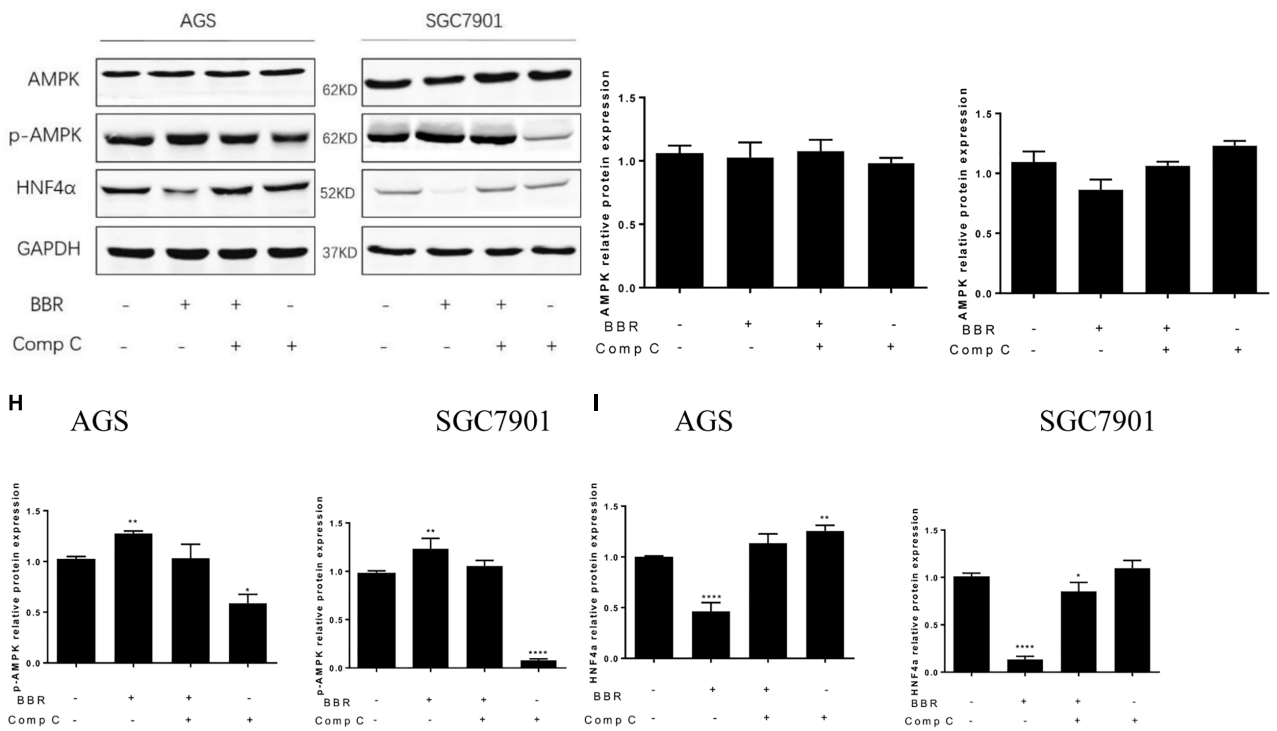


**FIGURE 5 |** Berberine regulated HNF4α by activating AMPK in GC cells. Two GC cell lines, AGS and SGC7901, were treated with BBR (20 μM and 30 μM), metformin (20 mM and 30 mM), BI6015 (an HNF4α antagonist) and AICAR (AMPK agonist). **(A)** The protein expressions of AMPK, p-AMPK and HNF4α in AGS and SGC7901 cells 48 h after treatment. **(B,C)** The quantification of western blot in AGS cells **(B)** and SGC7901 cells **(C)**. **(D,E)** The quantified mRNA expression of AMPK and HNF4α in AGS and SGC7901 cells 48 h after treatment. Two GC cell lines, AGS and SGC7901 cells, were treated with BBR (30 μM) for 24 h, and then with compound C (20 μM) or DMSO for another 24 h. **(F)** The protein expression of AMPK, p-AMPK and HNF4α in AGS and SGC7901 cells after treatment. **(G)** The quantified western blot of AMPK in AGS and SGC7901 cells. **(H)** The quantified western blot of p-AMPK in AGS and SGC7901 cells. **(I)** The quantified western blot of HNF4α in AGS and SGC7901 cells. Data were presented as the means ± SD. $n = 3$ for western-blot and RT-PCR. *T*-test, $^{*}P < 0.05$, $^{**}P < 0.01$, $^{***}P < 0.001$, $^{****}P < 0.0001$ vs. Normal control group. $^{\#}P < 0.05$, $^{\#\#}P < 0.05$ vs. BI6015 group.

tumors of mice. The results showed that the expression of HNF4α decreased in LV-HNF4α group, but did not decrease in normal control group and Lenti-GFP group. The WNT5A and cytoplasmic β-catenin expression were decreased in LV- HNF4α group, which was consistent with previous cell experiments (**Figures 7E–H**) ($P < 0.0001$).

## Berberine Suppressed Xenograft Tumor Growth *in vivo*

The SGC7901 cells were injected subcutaneously into BALB/c nude mouse, normal saline, Berberine and metformin were treated, respectively. During the 18 days treatment, the weight of each group was not statistically significant (**Figure 8A**). As shown in **Figures 8B–D**, 250 mg/kg MET (SGC-M) significantly suppressed the tumor growth *in vivo* compared with normal control group (SGC-N). The average final tumor weight and volume in the SGC-M group were 0.023 g and 68.168 $mm^3$, respectively, which was significantly lower than those in SGC-N group (0.297 g, 278.213 $mm^3$) ($P < 0.001$ and $P < 0.01$). There was also a reduction in tumor weight and volume in the BBR (100 mg/kg) group (SGC-B) compared with normal control group, the average final tumor weight and volume were 0.143 g and 163.955 $mm^3$ ($P < 0.01$ and $P < 0.05$).

To further investigate the insight mechanism of BBR on gastric cancer tumor *in vivo*, immunohistochemistry was used to detect the HNF4α, WNT5A and cytoplasmic β-catenin expression in xenografted tumors. As shown in **Figures 8E–H**, the BBR (100 mg/kg) and MET (250 mg/kg) decreased the HNF4α, WNT5A and cytoplasmic β-catenin expression comparing with the normal control group ($P < 0.0001$). There was no difference between BBR group and MET group in HNF4α, WNT5A and cytoplasmic β-catenin expression.

## DISCUSSION

Berberine (BBR), an isoquinoline alkaloid isolated from Berberis vulgaris, used to be an antibacterial agent in China for a long time. Over the past decade, It has been reported that BBR could also regulate plasma lipid and glucose levels in type 2 diabetes animal models and humans (Kumar et al., 2015;

Pirillo and Catapano, 2015; Tabeshpour et al., 2017; Wang H. et al., 2018). Our previous studies have indicated that BBR can stimulate insulin secretion and modulate lipids in impaired glucose tolerance rats (Leng et al., 2004), reverse free-fatty-acid-induced insulin resistance in 3T3-L1 adipocytes (Yi et al., 2008), even attenuate intestinal mucosal barrier dysfunction and immune barrier damages in type 2 diabetic rats (Gong et al., 2017). In this study, we found that BBR had proliferation inhibition effect on AGS and SGC7901 gastric cancer cell lines in a time and dose-dependent manner. We also detected the proto-oncogene expression of *C-myc*, which frequently upregulates in human cancers and accelerates cell proliferation (Dang, 2012). The results showed that BBR downregulated the mRNA and protein expression of *C-myc* in both GC cell lines, suggesting BBR has potential anti-gastric cancer effect as previous researches have shown (Zhang et al., 2014; Li et al., 2016; Yang et al., 2018).

The balance between cell cycle and cell proliferation often deregulated in cancers (Gérard and Goldbeter, 2014). Then, we detected the effects of BBR on GC cell cycle. After BBR treatment, the number of cells in $G_0$-$G_1$ period increased, and the protein and mRNA expression of CyclinD1 decreased significantly in both AGS and SGC7901 cells. Cyclin D1 is a key protein implicated in the transition of the $G_0$-$G_1$ phase,

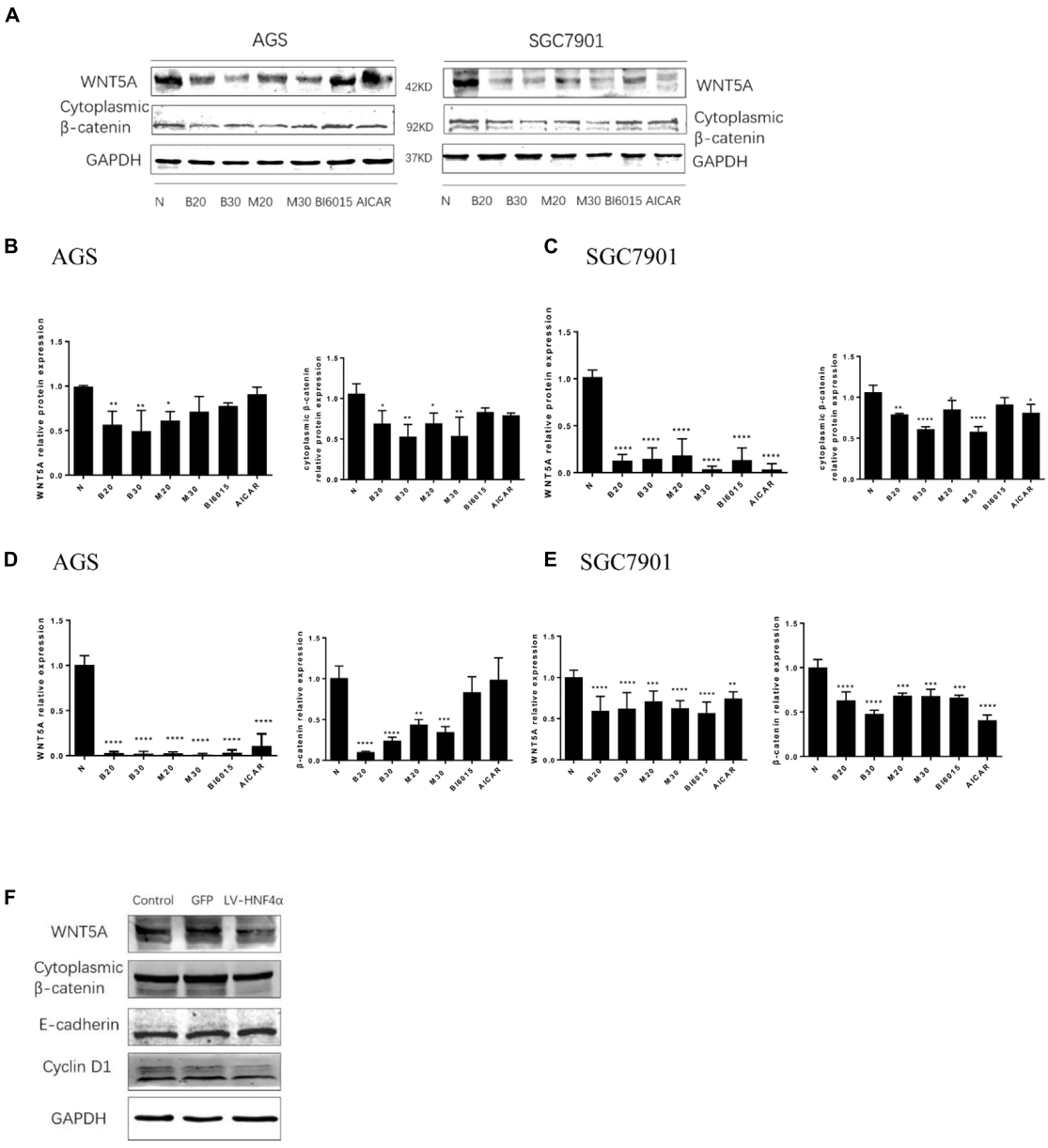


**FIGURE 6 |** Continued

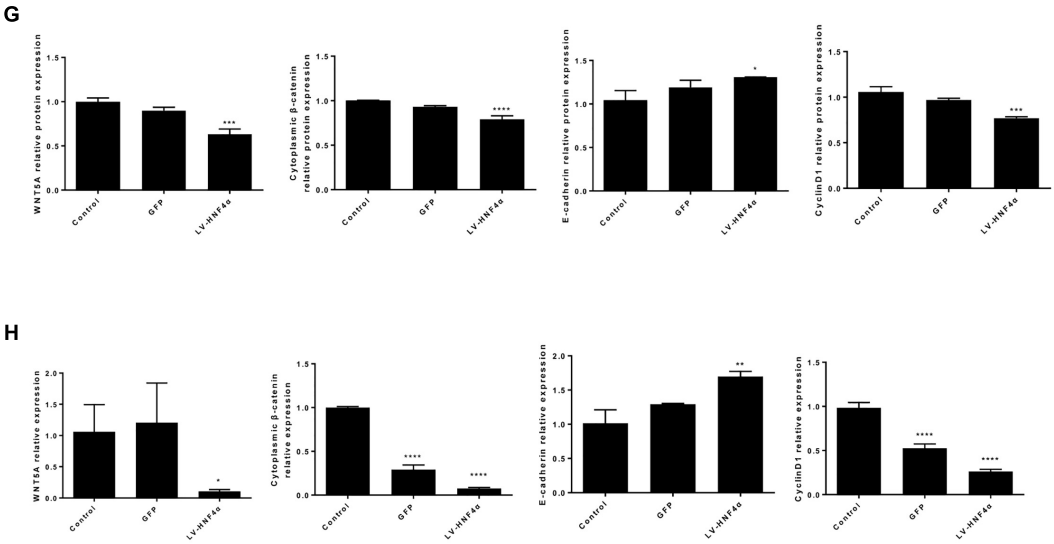


**FIGURE 6 |** Berberine targeted WNT/β -catenin signaling through HNF4α in GC cells. First, two GC cell lines, AGS and SGC7901, were treated with BBR (20 μM and 30 μM), metformin (20 mM and 30 mM), BI6015 (an HNF4α antagonist) and AICAR (AMPK agonist). **(A)** The protein expression of WNT5A and cytoplasmic β-catenin in AGS and SGC7901 cells 48 h after treatment. **(B,C)** The quantified western blot of WNT5A and cytoplasmic β-catenin in AGS and SGC7901 cells. **(D,E)** The quantified mRNA expression of WNT5A and cytoplasmic β-catenin in AGS and SGC7901 cells 48 h after treatment. Next, an siRNA-HNF4α SGC7901 cell model was used to detect the WNT pathway. **(F)** The protein level of WNT5A, cytoplasmic β-catenin, E-cadherin and Cyclin D1 in Control, GFP and LV-HNF4α SGC7901 cell lines. **(G)** The quantified western blot of WNT5A, cytoplasmic β-catenin, E-cadherin and Cyclin D1. **(H)** The quantified mRNA level of WNT5A, cytoplasmic β-catenin, E-cadherin and Cyclin D1 in Control, GFP and LV-HNF4α SGC7901 cell lines. Data were presented as the means ± SD. $n = 3$ for western-blot and RT-PCR. $^{*}P < 0.05$, $^{**}P < 0.01$, $^{***}P < 0.001$, $^{****}P < 0.0001$ vs. Control group.

which allows cells to enter the $G_1$ phase of the cell cycle and promotes cell proliferation (Gérard and Goldbeter, 2014; Wang Q. et al., 2018). The decreased expression of Cyclin D1 indicates a $G_0$-$G_1$ arrest in cells. So the flow cytometry, western blot and RT-PCR results all showed that BBR induced $G_0$-$G_1$ phase arrest in AGS and SGC7901 gastric cancer cell lines.

The depth of tumor invasion and lymph node metastasis are considered as the most important prognostic predictors of gastric cancer (Deng and Liang, 2014). It is essential to explore the mechanisms of invasion and metastasis to improve the survival rate for cancer patients (Zhu et al., 2018). We used the Transwell assay to examine whether BBR affected GC cells' migration and invasion or not. With the increased dose of BBR, the number of gastric cancer cells that invaded and metastasized dramatically decreased. MMP-3, known as inducers of EMT, is one of the several MMPs that regulate angiogenesis, invasion and metastasis (Huang et al., 2016; Chu et al., 2018; Simi et al., 2018).It was reported that MMP-3 expression level was negatively correlated with GC development (Xu et al., 2016). We also found that BBR had stable inhibitory effect on matrix metalloproteinase-3 (MMP-3) protein and mRNA expressions in AGS and SGC7901 cells, which suggested that BBR inhibited the migration and invasion to prevent GC development through downregulating MMP-3 in AGS and SGC7901 GC cells.

Previous researches reported that Metformin (MET) inhibited gastric cancer cells metastatic traits and slowed gastric tumor growth (Courtois et al., 2017; Valaee et al., 2017). In the present study, we also found that BBR, a widely used antibacterial drug, had multiple anti-tumor efficacy on AGS and SGC7901 GC cell lines as MET. We know BBR shares many features in metabolism regulation with MET. Recent researches have demonstrated that MET acted directly on cancer cells by targeting tumor metabolism, and inhibited the migration and invasion of the esophageal carcinoma cell line EC109 (Daugan et al., 2016; He et al., 2018). Among patients with T2DM, some clinical evidences have shown those who took metformin therapy have a lower risk of GC than those who didn't (Zhou et al., 2017; Li et al., 2018). Moreover, it was reported that the anti-gastric cancer effect of metformin was related with the HNF4α inhibition through AMPK signaling (Chang et al., 2015). AMPK directly or indirectly inhibits HNF4α and its downstream HIF-1α, which is consistent with a proposed role for AMPK in suppressing the 'Warburg effect' anaerobic metabolism characteristic of the malignant phenotype (Kato et al., 2018).

Hepatocyte nuclear factor 4α is a nuclear receptor that activates the expression of genes involved in endoderm development and glucose, fatty acid and cholesterol metabolism (Darsigny et al., 2010). Previous studies suggested HNF4α is a potential direct or indirect target for pharmacological drugs that act on the intestinal epithelium, which is a primary site of metabolic control (Cattin et al., 2009). Recent studies have found that HNF4α is related to malignant tumor formation and metastasis (Xiang et al., 2015; Kato et al., 2018; Maan et al., unpublished). It was significantly upregulated in multidrug-resistant GC cells (Ma et al., 2017). To assess the function of HNF4α in GC cells, we used siRNA to silence the expression of HNF4α and tested the proliferation, cell cycles, migration and

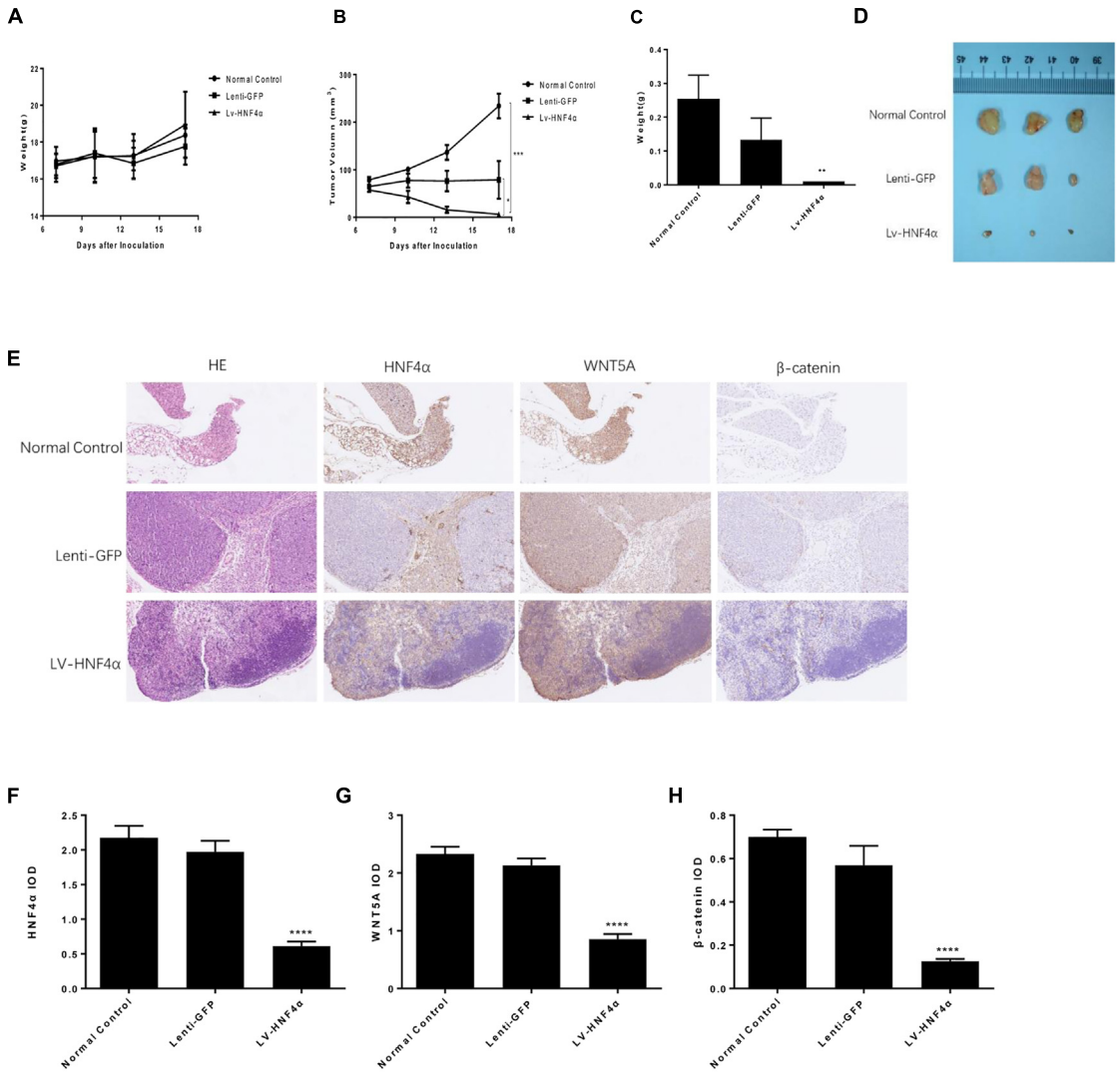


**FIGURE 7 |** Effect of HNF4α on SGC7901 xenograft tumor growth *in vivo*. The normal control, Lenti-GFP, and LV-HNF4α SGC7901 cells were injected subcutaneously into the right scapular region of nude mice. **(A)** Body weight. **(B)** The average tumor volume is shown as the mean ± SD ($mm^3$). **(C)** Tumor weight. **(D)** The tumors removed from mice are shown. **(E)** Representative images from immunohistochemical staining of HNF4α, WNT5A and β-catenin in tumors from each group (50x Lenti). **(F–H)** The quantified immunohistochemistry of HNF4α, WNT5A and β-catenin. Data were expressed as the means ± SD. $^*P < 0.05$, $^{**}P < 0.01$, $^{***}P < 0.001$, $^{****}P < 0.0001$ vs. normal control group.

invasion in SGC7901 cell. We found that knockdown of HNF4α in SGC7901 cell line slowed its proliferation, induced S phase arrest and dramatically attenuated gastric cancer cells' metastasis and invasion. It demonstrated that HNF4α was involved in the growth, invasion and metastasis capacity of gastric cancer. HNF4α gene could serve as a "proto-oncogene" in gastric cancer development.

Our previous studies have indicated that BBR modulates lipid metabolism and inhibits hepatic gluconeogenesis by targeting HNF4α in type 2 diabetic rats (Gao et al., 2008; Wang et al., 2008; Yan et al., 2008). Is the anti-gastric cancer effect of Berberine related with tumor metabolism? How is HNF4α regulated by BBR in GC cell line? We performed GC cell perturbation experiments through BI6015 (an HNF4α antagonist), AICAR (an AMPK activator), metformin, and Berberine. The results showed that BBR downregulated the expression of HNF4α in two GC cells. Given that AMPK mediated the phosphorylation of HNF4α, and prevented transcription factor HNF4α from entering the nucleus to form dimer and DNA binding to improve the degradation of HNF4α (Leclerc et al., 2001). We also observed that BBR (20 μM) upregulated the protein level of phosphor-AMPK (p-AMPK) and BBR (30 μM) upregulated the mRNA level of total AMPK in GC cells,MET increased the mRNA expression of AMPK in GC cells, although no statistically significant differences were found in the total protein level of AMPK after BBR and MET treatment. To further confirm the AMPK may be the potential upstream of HNF4α in GC cells, we used Compound C (AMPK-kinase inhibitor) and BBR to treat

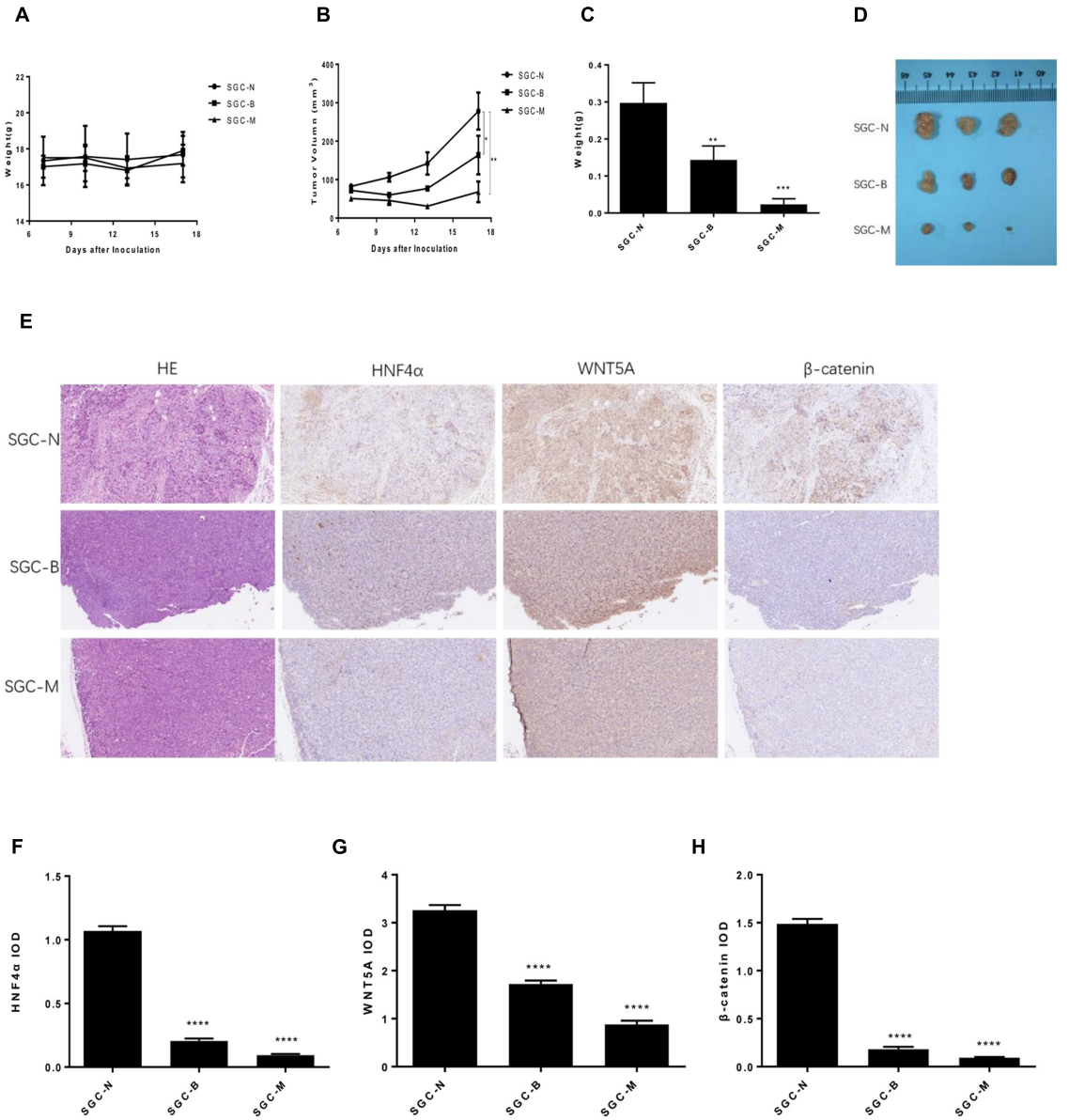


**FIGURE 8 |** Effect of BBR on SGC7901 xenograft tumor growth *in vivo*. The SGC7901 cells were injected subcutaneously into the right scapular region of nude mice, and were given normal saline, Berberine or metformin treatment. **(A)** Body weight. **(B)** The average tumor volume is shown as the means ± SD ($mm^3$). **(C)** Tumor weight. **(D)** The tumors removed from mice are shown. **(E)** Representative images from immunohistochemical staining of HNF4α, WNT5A and $\beta$-catenin in tumors from each group (50× magnification). **(F–H)** The quantified immunohistochemistry of HNF4α, WNT5A and $\beta$-catenin. Data were expressed as the means ± SD. $^*P < 0.05$, $^{**}P < 0.01$, $^{***}P < 0.001$, $^{****}P < 0.0001$ vs. normal group.

two GC cells. We found that BBR downregulated the protein level of HNF4α and Compound C upregulated the expression of HNF4α, Compound C reversed the effect of BBR on the HNF4α, suggesting inhibition of HNF4α by BBR was AMPK dependent. There was a negative correlation between p-AMPK and HNF4α. That means, BBR upregulated the protein of p-AMPK and Compound C downregulated the expression. This phenomenon indicated that HNF4α may be the downstream of AMPK and BBR could regulate the AMPK/HNF4α pathway in gastric cancer cells.

WNT/β-catenin signaling is important for cancer progression, including tumor initiation, tumor growth, cell senescence, cell death, differentiation and metastasis (Anastas and Moon, 2013). It was also reported that HNF4α-WNT5A regulation was the cross-talk between the AMPK metabolic pathway and the WNT signaling pathway (Nam et al., 2014). WNT5A, a member of the WNT family, played an important role in gastric cancer invasion and metastasis (Kanzawa et al., 2013; Ara et al., 2016). Knockdown of WNT5A reduced the metastasis ability of gastric cancer cells (Hanaki et al., 2012). Then, we explored how BBR

acted on WNT/β-catenin signaling pathway in GC cell lines. Our study demonstrated that BBR downregulated the protein and mRNA levels of WNT5A and cytoplasmic β-catenin in AGS and SGC7901 cell lines. To further identify the relationship between HNF4α and WNT signal pathway. SiRNA- HNF4α SGC7901 cell model was used to detect the expression of WNT pathway. The results showed that knockdown of HNF4α decreased significantly the protein and mRNA expression levels of WNT5A, cytoplasmic β-catenin and cyclinD1 *in vitro*, and increased significantly the expression of E-cadherin comparing with control cells. HNF4α was reported to compete with β-catenin for binding to TCF4, regulating Epithelial-to-mesenchymal transition (EMT) (Yao et al., 2016). Loss of E-cadherin is regarded as a major conventional marker of the EMT (Alotaibi et al., 2015; Yamashita et al., 2018). Our study validated that WNT5A was a downstream target gene of HNF4α and showed that knockdown of HNF4α decreased the expression of WNT5A and cytoplasmic β-catenin in GC cell line, which is consistent with the study of Chang et al. (2015). But studies have illustrated, in small intestine and colon cancer, loss of HNF4α activated the WNT/β-catenin signaling pathway. In these cancer tissues, HNF4α was low expressed compared with adjacent normal tissues (Cattin et al., 2009; Yao et al., 2016).

Meanwhile, we analyzed that effect of BBR and HNF4α on gastric cancer tumor *in vivo*. Our results showed that BBR and knockdown of HNF4α suppressed the growth of SGC7901 in nude mice, HNF4α played a critical role in gastric cancer development and might serve as a potential therapy biomarker. Consistent with *in vitro* experiments, BBR downregulated HNF4α, WNT5A, and cytoplasmic β-catenin expression in somatic tumor tissues, the same effect as knocking out HNF4α gene.

Taken together, in the present study, we demonstrated that BBR, an anti-diabetes herb monomer, not only had proliferation inhibition effect on GC cell lines through downregulating cell cycle protein CyclinD1, attenuated the invasion and migration of GC cells by decreasing MMP-3, but also suppressed the growth of gastric tumor. The anti-gastric cancer mechanism of BBR might be involved in AMPK-HNF4α-WNT5A signaling pathway. BBR could modulate HNF4α through AMPK signaling. Moreover, HNF4α could regulate WNT-β-catenin-E-cadherin signaling to attenuate the growth, invasion and metastasis of gastric cancer. Therefore, HNF4α, a nuclear receptor that activated the expression of genes involved in glucose, fatty acid and cholesterol metabolism, was also involved in the development of gastric cancer. HNF4α antagonists, such as BBR, could be a promising anti-gastric cancer treatment supplement.

## ETHICS STATEMENT

The study was carried out in a accordance with the recommendations of Institutional Animal Care and Use Committee at Tongji Medical College (Huazhong University of Science and Technology ACUC No. S787). The study protocol was approved by Institutional Animal Care and Use Committee, Tongji Medical College, Huazhong University of Science and Technology.

## AUTHOR CONTRIBUTIONS

PY designed the study. QH, LL, XZ, and LX conducted the experiments. QH wrote and revised the manuscript. All authors approved the final version to be published.

## FUNDING

This article was supported by the National Natural Science Foundation of China (Nos. 81673757 and 81703886).

## REFERENCES

Alotaibi, H., Basilicata, M. F., Shehwana, H., Kosowan, T., Schreck, I., Braeutigam, C., et al. (2015). Enhancer cooperativity as a novel mechanism underlying the transcriptional regulation of E-cadherin during mesenchymal to epithelial transition. *Biochim. Biophys. Acta* 1849, 731–742. doi: 10.1016/j.bbagrm.2015.01.005

Anastas, J. N., and Moon, R. T. (2013). WNT signalling pathways as therapeutic targets in cancer. *Nat. Rev. Cancer* 13, 11–26. doi: 10.1038/nrc3419

Ara, H., Takagishi, M., Enomoto, A., Asai, M., Ushida, K., Asai, N., et al. (2016). Role for Daple in non-canonical Wnt signaling during gastric cancer invasion and metastasis. *Cancer Sci.* 107, 133–139. doi: 10.1111/cas.12848

Balakrishnan, M., George, R., Sharma, A., and Graham, D. Y. (2017). Changing trends in stomach cancer throughout the world. *Curr. Gastroenterol. Rep.* 19, 36. doi: 10.1007/s11894-017-0575-8

Cattin, A. L., Le Beyec, J., Barreau, F., Saint-Just, S., Houllier, A., Gonzalez, F. J., et al. (2009). Hepatocyte nuclear factor 4 α, a key factor for homeostasis, cell architecture, and barrier function of the adult intestinal epithelium. *Mol. Cell. Biol.* 29, 6294–6308. doi: 10.1128/MCB.00939-09

Chang, H. R., Nam, S., Kook, M., Kim, K., Liu, X., Yao, H., et al. (2015). HNF4α is a therapeutic target that links AMPK to WNT signaling in early-stage gastric cancer. *Gut* 65, 19–32. doi: 10.1136/gutjnl-2014-307918

Chen, W., Sun, K., Zheng, R., Zeng, H., Zhang, S., Xia, C., et al. (2018). Cancer incidence and mortality in China. *Chin. J. Cancer Res.* 30, 1–12. doi: 10.21147/j.issn.1000-9604.2018.01.01

Chu, C., Liu, X., Bai, X., Zhao, T., Wang, M., Xu, R., et al. (2018). MiR-519d suppresses breast cancer tumorigenesis and metastasis via targeting MMP3. *Int. J. Biol. Sci.* 14, 228–236. doi: 10.7150/ijbs.22849

Courtois, S., Durán, R. V., Giraud, J., Sifré, E., Izotte, J., Mégraud, F., et al. (2017). Metformin targets gastric cancer stem cells. *Eur. J. Cancer* 84, 193–201. doi: 10.1016/j.ejca.2017.07.020

Dang, C. V. (2012). MYC on the path to cancer. *Cell* 149, 22–35. doi: 10.1016/j.cell.2012.03.003

Darsigny, M., Babeu, J. P., Seidman, E. G., Gendron, F. P., Levy, E., Carrier, J., et al. (2010). Hepatocyte nuclear factor-4 αpromotes gut neoplasia in mice and protects against the production of reactive oxygen species. *Cancer Res.* 70, 9423–9433. doi: 10.1158/0008-5472.CAN-10-1697

Daugan, M., Dufaÿ Wojcicki, A., d'Hayer, B., and Boudy, V. (2016). Metformin: an anti-diabetic drug to fight cancer. *Pharmacol. Res.* 113, 675–685. doi: 10.1016/j.phrs.2016.10.006

Deng, J. Y., and Liang, H. (2014). Clinical significance of lymph node metastasis in gastric cancer. *World J. Gastroenterol.* 20, 3967–3975. doi: 10.3748/wjg.v20.i14.3967

Gao, Z., Leng, S., Lu, F., Xie, M. J., Xu, L. J., and Wang, K. F. (2008). Effect of berberine on expression of hepatocyte nuclear factor-4alpha in rats with fructose-induced insulin resistance. *J. Huazhong Univ. Sci. Technol.* 28, 261–265. doi: 10.1007/s11596-008-0307-2

Gérard, C., and Goldbeter, A. (2014). The balance between cell cycle arrest and cell proliferation: control by the extracellular matrix and by contact inhibition. *Interface focus* 4:20130075. doi: 10.1098/rsfs.2013.0075

Gong, J., Hu, M., Huang, Z., Fang, K., Wang, D. K., Chen, Q., et al. (2017). Berberine attenuates intestinal mucosal barrier dysfunction in type 2 diabetic rats. *Front. Pharmacol.* 8:42. doi: 10.3389/fphar.2017.00042

Hanaki, H., Yamamoto, H., Sakane, H., Matsumoto, S., Ohdan, H., Sato, A., et al. (2012). An anti-wnt5a antibody suppresses metastasis of gastric cancer cells *in vivo* by inhibiting receptor-mediated endocytosis. *Mol. Cancer Ther.* 11, 298–307. doi: 10.1158/1535-7163.MCT-11-0682

He, Y., Tan, X., Hu, H., Wang, Q., Hu, X., Cai, X., et al. (2018). Metformin inhibits the migration and invasion of esophageal squamous cell carcinoma cells by downregulating the protein kinase B signaling pathway. *Oncol. Lett.* 15, 2939–2945. doi: 10.3892/ol.2017.7699

Huang, J. F., Du, W. X., and Chen, J. J. (2016). Elevated expression of matrix metalloproteinase-3 in human osteosarcoma and its association with tumor metastasis. *J. BUON* 21, 1279–1286.

Jucá, P. C. F. C., Corrêa, S., Vignal, G. M., Accioly, M. T. S., Lustosa, S. A. S., Abdelhay, E., et al. (2017). HNF4A expression as a potential diagnostic tool to discriminate primary gastric cancer from breast cancer metastasis in a Brazilian cohort. *Diagn. Pathol.* 12:43. doi: 10.1186/s13000-017-0635-2

Kanzawa, M., Semba, S., Hara, S., Itoh, T., and Yokozaki, H. (2013). WNT5A is a key regulator of the epithelial-mesenchymal transition and cancer stem cell properties in human gastric carcinoma cells. *Pathobiology* 80, 235–244. doi: 10.1159/000346843

Kato, Y., Maeda, T., Suzuki, A., and Baba, Y. (2018). Cancer metabolism: new insights into classic characteristics. *Jpn. Dent. Sci. Rev.* 54, 8–21. doi: 10.1016/j.jdsr.2017.08.003

Kobayashi, P. E., Fonseca-Alves, C. E., Rivera-Calderón, L. G., Carvalho, M., Kuasne, H., Rogatto, S. R., et al. (2018). Deregulation of E-cadherin, β-catenin, APC and Caveolin-1 expression occurs in canine prostate cancer and metastatic processes. *Res. Vet. Sci.* 118, 254–261. doi: 10.1016/j.rvsc.2018.03.004

Kumar, A., Ekavali, Chopra, K., Mukherjee, M., Pottabathini, R., and Dhull, D. K. (2015). Current knowledge and pharmacological profile of berberine: an update. *Eur. J. Pharmacol.* 761, 288–297. doi: 10.1016/j.ejphar.2015.05.068

Larue, L., and Delmas, V. (2006). The WNT/Beta-catenin pathway in melanoma. *Front. Biosci.* 11, 733–742. doi: 10.2741/1831

Leclerc, I., Lenzner, C., Gourdon, L., Vaulont, S., Kahn, A., and Viollet, B. (2001). Hepatocyte nuclear factor-4alpha involved in type 1 maturity-onset diabetes of the young is a novel target of AMP-activated protein kinase. *Diabetes Metab. Res. Rev.* 50, 1515–1521.

Leng, S. H., Lu, F. E., and Xu, L. J. (2004). Therapeutic effects of berberine in impaired glucose tolerance rats and its influence on insulin secretion. *Acta Pharmacol. Sin.* 25, 496–502.

Li, H. L., Wu, H., Zhang, B. B., Shi, H. L., and Wu, X. J. (2016). MAPK pathways are involved in the inhibitory effect of berberine hydrochloride on gastric cancer MGC 803 cell proliferation and IL-8 secretion *in vitro* and *in vivo*. *Mol. Med. Rep.* 14, 1430–1438. doi: 10.3892/mmr.2016.5361

Li, P., Zhang, C., Gao, P., Chen, X. W., Ma, B., Yu, D., et al. (2018). Metformin use and its effect on gastric cancer in patients with type 2 diabetes: a systematic review of observational studies. *Oncol. Lett.* 15, 1191–1199. doi: 10.3892/ol.2017.7370

Love-Gregory, L., and Permutt, M. A. (2007). HNF4A genetic variants: role in diabetes. *Curr. Opin. Clin. Nutr. Metab. Care* 10, 397–402. doi: 10.1097/MCO.0b013e3281e3888d

Ma, Y., Wei, X., and Wu, Z. J. (2017). HNF-4α promotes multidrug resistance of gastric cancer cells through the modulation of cell apoptosis. *Oncol. Lett.* 14, 6477–6484. doi: 10.3892/ol.2017.7095

Mao, L., Chen, Q., Gong, K., Xu, X. L., Xie, Y. R., Zhang, W. Q., et al. (2018). Berberine decelerates glucose metabolism via suppression of mTOR-dependent HIF-1α protein synthesis in colon cancer cells. *Oncol. Rep.* 39, 2436–2442. doi: 10.3892/or.2018.6318

Nam, S., Chang, H. R., Kim, K. T., Kook, M. C., Hong, D., Kwon, C. H., et al. (2014). PATHOME: an algorithm for accurately detecting differentially expressed subpathways. *Oncogen* 33, 4941–4951. doi: 10.1038/onc.2014.80

Pirillo, A., and Catapano, A. L. (2015). Berberine, a plant alkaloid with lipid- and glucose-lowering properties: from *in vitro* evidence to clinical studies. *Atherosclerosis* 243, 449–461. doi: 10.1016/j.atherosclerosis.2015.09.032

Rhee, J., Ge, H., Yang, W., Fan, M., Handschin, C., Cooper, M., et al. (2006). Partnership of PGC-1alpha and HNF4alpha in the regulation of lipoprotein metabolism. *J. Biol. Chem.* 281, 14683–14690. doi: 10.1074/jbc.M512636200

Simi, A. K., Anlas, A. A., Stallings-Mann, M., Zhang, S., Hsia, T., Cichon, M. A., et al. (2018). A soft microenvironment protects from failure of midbody abscission and multinucleation downstream of the EMT-promoting transcription factor Snail. *Cancer Res.* 78, 2277–2289. doi: 10.1158/0008-5472.CAN-17-2899

Song, I. S., Han, J., and Lee, H. K. (2015). Metformin as an anticancer drug: a commentary on the metabolic determinants of cancer cell sensitivity to glucose limitation and biguanides. *J. Diabetes Investig.* 6, 516–518. doi: 10.1111/jdi.12300

Tabeshpour, J., Imenshahidi, M., and Hosseinzadeh, H. (2017). A review of the effects of Berberis vulgaris and its major component, berberine, in metabolic syndrome. *Iran. J. Basic Med. Sci.* 20, 557–568. doi: 10.22038/IJBMS.2017.8682

Torre, L. A., Siegel, R. L., Ward, E. M., and Jemal, A. (2016). Global cancer incidence and mortality rates and trends–an update. *Cancer Epidemiol. Biomarkers* 25, 16–27. doi: 10.1158/1055-9965.EPI-15-0578

Tseng, C. H., and Tseng, F. H. (2014). Diabetes and gastric cancer: the potential links. *World J Gastroenterol.* 20, 701–1711. doi: 10.3748/wjg.v20.i7.1701

Valaee, S., Yaghoobi, M. M., and Shamsara, M. (2017). Metformin inhibits gastric cancer cells metastatic traits through suppression of epithelial-mesenchymal transition in a glucose-independent manner. *PLoS One* 12:e0174486. doi: 10.1371/journal.pone.0174486

Van der Post, R. S., Bult, P., Vogelaar, I. P., Ligtenberg, M. J. L., Hoogerbrugge, N., and van Krieken, J. H. (2014). HNF4A immunohistochemistry facilitates distinction between primary and metastatic breast and gastric carcinoma. *Virchows Arch.* 464, 673–679. doi: 10.1007/s00428-014-1574-x

Wang, H., Zhu, C., Ying, Y., Luo, L., Huang, D., and Luo, Z. (2018). Metformin and berberine, two versatile drugs in treatment of common metabolic diseases. *Oncotarget* 9, 10135–10146. doi: 10.18632/oncotarget.20807

Wang, J., Yang, S., Cai, X., Dong, J., Chen, Z. Q., Wang, R., et al. (2016). Berberine inhibits EGFR signaling and enhances the antitumor effects of EGFR inhibitors in gastric cancer. *Oncotarget* 7, 76076–76086. doi: 10.18632/oncotarget.12589

Wang, Q., He, G., Hou, M., Chen, L. T., Chen, S. W., Xu, A., et al. (2018). Cell cycle regulation by alternative polyadenylation of CCND1. *Sci. Rep.* 8:6824. doi: 10.1038/s41598-018-25141-0

Wang, Z. Q., Lu, F. E., Leng, S. H., Fang, X. S., Chen, G., Wang, Z. S., et al. (2008). Facilitating effects of berberine on rat pancreatic islets through modulating hepatic nuclear factor 4 alpha expression and glucokinase activity. *World J. Gastroenterol.* 14, 6004–6011. doi: 10.3748/wjg.14.6004

Wei, S., Zhang, M., Yu, Y., Lan, X., Yao, F., Yan, X., et al. (2016). Berberine attenuates development of the hepatic gluconeogenesis and lipid metabolism disorder in type 2 diabetic mice and in palmitate-incubated HepG2 cells through suppression of the HNF-4α miR122 pathway. *PLoS One* 11:e0152097. doi: 10.1371/journal.pone.0152097

Wei, W., Zhao, H., Wang, A., Sui, M., Liang, K., Deng, H. Y., et al. (2012). A clinical study on the short-term effect of berberine in comparison to metformin on the metabolic characteristics of women with polycystic ovary syndrome. *Eur. J. Endocrinol.* 166, 99–105. doi: 10.1530/EJE-11-0616

Xiang, X., Zhao, X., Qu, H., Li, D., Yang, D., Pu, J., et al. (2015). Hepatocyte nuclear factor 4 alpha promotes the invasion, metastasis and angiogenesis of neuroblastoma cells via targeting matrix metalloproteinase 14. *Cancer Lett.* 359, 187–197. doi: 10.1016/j.canlet.2015.01.008

Xu, J., Changyong, E., Yao, Y., Ren, S., Wang, G., and Jin, H. (2016). Matrix metalloproteinase expression and molecular interaction network analysis in gastric cancer. *Oncol. Lett.* 12, 2403–2408. doi: 10.3892/ol.2016.5013

Yamashita, N., Tokunaga, E., Iimori, M., Inoue, Y., Tanaka, K., Kitao, H., et al. (2018). Epithelial paradox: clinical significance of coexpression of e-cadherin and vimentin with regard to invasion and metastasis of breast cancer. *Clin. Breast Cancer* 18, e1003–e1009. doi: 10.1016/j.clbc.2018.02.002

Yan, Z. Q., Leng, S. H., Lu, F. E., Lu, X. H., Dong, H., and Gao, Z. Q. (2008). [Effects of berberine on expression of hepatocyte nuclear factor 4alpha and glucokinase activity in mouse primary hepatocytes]. *Zhongguo Zhong yao za zhi Zhongguo zhongyao zazh China J. Chin. Mat. Med.* 33, 2105–2109.

Yang, Y., Zhang, N., Li, K., Chen, J., Qiu, L., and Zhang, J. F. (2018). Integration of microRNA-mRNA profiles and pathway analysis of plant isoquinoline alkaloid berberine in SGC-7901 gastric cancers cells. *Drug Des. Dev. Ther.* 12, 393–408. doi: 10.2147/DDDT.S155993

Yao, H. S., Wang, J., Zhang, X. P., Wang, L. Z., Wang, Y., Li, X. X., et al. (2016). Hepatocyte nuclear factor 4α suppresses the aggravation of colon carcinoma. *Mol. Carcinogens* 55, 458–472. doi: 10.1002/mc.22294

Yi, P., Lu, F. E., Xu, L. J., Chen, G., Dong, H., and Wang, K. F. (2008). Berberine reverses free-fatty-acid-induced insulin resistance in 3T3-L1 adipocytes through targeting IKKbeta. *World J. Gastroenterol.* 14, 876–883. doi: 10.3748/wjg.14.876

Zhang, X. Z., Wang, L., Liu, D. W., Tang, G. Y., and Zhang, H. Y. (2014). Synergistic inhibitory effect of berberine and d-limonene on human gastric carcinoma cell line MGC803. *J. Med. Food* 17, 955–962. doi: 10.1089/jmf.2013.2967

Zhou, X. L., Xue, W. H., Ding, X. F., Li, L. F., Dou, M. M., Zhang, W. J., et al. (2017). Association between metformin and the risk of gastric cancer in patients with type 2 diabetes mellitus: a meta-analysis of cohort studies. *Oncotarget* 8, 55622–55631. doi: 10.18632/oncotarget.16973

Zhu, T., Hu, X., Wei, P., and Shan, G. Z. (2018). Molecular background of the regional lymph node metastasis of gastric cancer. *Oncol. Lett.* 15, 3409–3414. doi: 10.3892/ol.2018.7813

**Conflict of Interest Statement:** The authors declare that the research was conducted in the absence of any commercial or financial relationships that could be construed as a potential conflict of interest.

frontiers in Oncology

ORIGINAL RESEARCH
published: 17 December 2018
doi: 10.3389/fonc.2018.00611

# PCK1 Downregulation Promotes TXNRD1 Expression and Hepatoma Cell Growth via the Nrf2/Keap1 Pathway

*Lin Tuo[1†], Jin Xiang[1†], Xuanming Pan[1], Qingzhu Gao[1], Guiji Zhang[1], Yi Yang[1], Li Liang[1], Jie Xia[1], Kai Wang[1,2*] and Ni Tang[1*]*

[1] *Key Laboratory of Molecular Biology for Infectious Diseases (Ministry of Education), Department of Infectious Diseases, Institute for Viral Hepatitis, The Second Affiliated Hospital, Chongqing Medical University, Chongqing, China,* [2] *Department of Pathogenic Biology, Basic Medical College, Chongqing Medical University, Chongqing, China*

OPEN ACCESS

**Edited by:**
*Andrew Zloza, Rutgers Cancer Institute of New Jersey, United States*

**Reviewed by:**
*Harikumar KB, Rajiv Gandhi Centre for Biotechnology, India*
*Muthu Kumaraswamy Shanmugam, National University of Singapore, Singapore*

***Correspondence:**
*Kai Wang*
*wangkai@cqmu.edu.cn*
*Ni Tang*
*nitang@cqmu.edu.cn*

[†] *These authors have contributed equally to this work*

**Specialty section:**
*This article was submitted to Cancer Molecular Targets and Therapeutics, a section of the journal Frontiers in Oncology*

**Received:** *30 August 2018*
**Accepted:** *28 November 2018*
**Published:** *17 December 2018*

**Citation:**
*Tuo L, Xiang J, Pan X, Gao Q, Zhang G, Yang Y, Liang L, Xia J, Wang K and Tang N (2018) PCK1 Downregulation Promotes TXNRD1 Expression and Hepatoma Cell Growth via the Nrf2/Keap1 Pathway. Front. Oncol. 8:611. doi: 10.3389/fonc.2018.00611*

Gluconeogenesis, generates glucose from small carbohydrate substrates, and drives the metabolic flux in parallel but opposite to glycolysis. The cytoplasmic isoform of phosphoenolpyruvate carboxykinase (PCK1 or PEPCK-C), a rate-limiting enzyme in gluconeogenesis, initiates the gluconeogenesis process and is reportedly dysregulated in multiple types of cancer. Gluconeogenesis mainly occurs in the liver during fasting, and previous studies have demonstrated that PCK1 acts as a tumor suppressor in hepatocellular carcinoma (HCC); however, the role of PCK1 in cancer progression remains incompletely understood. In the current study, we found that PCK1 expression was decreased in HCC as compared to adjacent normal liver tissues, and low PCK1 expression correlated with poor patient prognosis. Furthermore, overexpression of PCK1 suppressed reactive oxygen species (ROS) production and nuclear translocation of Nrf2 in hepatoma cells. In addition, thioredoxin reductase 1 (TXNRD1), an antioxidant enzyme regulated by the Nrf2/Keap1 pathway, was downregulated upon overexpression of PCK1 in HCC cell lines. Furthermore, we verified this axis using nude mouse xenograft model. Finally, we found that auranofin, a TXNRD1 inhibitor, enhanced the sensitivity of PCK1-knockout hepatoma cells to sorafenib-induced apoptosis. Taken together, our findings suggest that PCK1 deficiency promotes hepatoma cell proliferation via the induction of oxidative stress and the activation of transcription factor Nrf2, and that targeting the TXNRD1 antioxidant pathway sensitizes PCK1-knockout hepatoma cells to sorafenib treatment *in vitro*.

**Keywords: phosphoenolpyruvate carboxylase kinase 1, thioredoxin reductase 1, hepatocellular carcinoma, reactive oxygen species, nuclear factor erythroid 2-related factor 2**

## INTRODUCTION

Hepatocellular carcinoma (HCC), the fifth most common cancer worldwide and the third cause of cancer-related mortality (1), is liable to developing malignant and drug-resistant tumors, with high risk of recurrence. A thorough understanding of the molecular pathogenesis of HCC and novel therapeutic strategies are highly needed. Metabolic reprogramming is a hallmark of cancer (2). In normal cells, energy is obtained primarily through mitochondrial oxidative phosphorylation.

However, tumor cells undergo glycolysis even in the presence of oxygen, known as the "Warburg effect," which supports tumor growth by accumulating glycolytic intermediates for anabolic biosynthesis (3).

The changed glucose metabolism endows tumor cells with metabolic flexibility for biosynthesis requirements. The dysregulation of gluconeogenesis and glycolysis causes a metabolic reprogramming that might be essential for supporting the growth, proliferation, and survival of tumor cells. Meanwhile, emerging evidence is linking altered expression of gluconeogenic enzymes, in particular, phosphoenolpyruvate carboxykinase (PCK, also known as PEPCK, EC number 4.1.1.32), with tumorigenesis (4). PCK1, as the first rate-limiting enzyme of gluconeogenesis, catalyzes the conversion of oxaloacetate (OAA) to phosphoenolpyruvate (PEP), and its dysfunction has been related to diabetes, obesity, insulin resistance, fatty liver, and other metabolic diseases (5, 6). Elevated expression of PCK1 has been reported to benefit tumor growth in certain cancers by maintaining anabolic metabolism (7, 8). In contrast, in HCC, PCK1 is downregulated (9), and a functional study indicated that forced PCK1 expression retards hepatoma cell proliferation (10), however, the underlying mechanism remains to be clarified.

Reactive oxygen species (ROS), such as hydrogen peroxide ($H_2O_2$), hydroxyl radical (HO•), and superoxide anion ($O_2^-$), are formed by the partial reduction of oxygen and are generated as normal byproducts of numerous cellular processes (11). Under physiological conditions, ROS are maintained at low levels, and act as signaling molecules to activate cell proliferation and survival pathways (12). However, excessive ROS production induces oxidative stress, causing cell death or apoptosis, and plays an important role in tumor initiation and progression (13). The nuclear factor erythroid 2-related factor 2 (Nrf2)/Kelch-like ECH-associated protein 1 (Keap1) signaling pathway is one of the crucial defense systems against oxidative stress in tumor tissues and cells (14). ROS production induces Nrf2 translocation from the cytoplasm to nucleus, where it forms heterodimers with small MAF proteins and binds the antioxidant response element (ARE) in the promoters of target genes to activate their transcription to protect against oxidative stress.

Thioredoxin reductase 1 (TXNRD1), an antioxidant enzyme regulated by Nrf2, catalyzes reduction of the active site disulfide of thioredoxin 1 (Trx1), and several other substrates and plays a key role in antioxidant defense, redox regulation, cell proliferation, and cell signaling events (15). TXNRD1 is highly expressed in many cancers, and has been linked with tumor development (3, 13, 16). Recent studies aimed to suppress TXNRD1 as a novel therapeutic target in the treatment of cancers by using various molecules, such as microRNA-124 (17), auranofin (18), and gambogic acid (19). Mechanically, the Trx1 system senses and responds to ROS generated by cellular respiration, metabolism, and immune response, and then regulates the redox status, function, and activity of its target signal pathway (20). However, it is not clear whether PCK1 modulates the expression of TXNRD1 by influencing the ROS levels.

In this study, we aimed to investigate the role of PCK1 in HCC development *in vitro* and *in vivo*. We explored whether PCK1 plays a role in oxidative stress and Nrf2/Keap1 pathway. We also investigated the antitumor effect of auranofin combined with sorafenib in PCK1 knockout hepatoma cells *in vitro*. Our results implicate that PCK1 acts as a tumor suppressor in HCC and combination therapy of sorafenib and TXNRD1 inhibitors may be a novel strategy for HCC treatment.

# MATERIALS AND METHODS

## Patient Samples

Surgically resected samples of HCC tumor tissues and adjacent non-tumorous tissues were obtained from 28 patients at the Department of Hepatobiliary Surgery of the Second Affiliated Hospital of Chongqing Medical University (Chongqing, China). Twenty-eight freshly collected paired HCC tissues were frozen immediately and stored in liquid nitrogen for further research. The patients enrolled in this study did not receive preoperative radiotherapy or chemotherapy.

## Cell Cultures and Drug Treatment

The human hepatoma cell line PLC/PRF/5 was obtained from the American Type Culture Collection (Manassas, VA, USA). Huh7 cells were obtained from the Cell Bank of the Chinese Academy of Sciences (Shanghai, China). All cell lines used in this study were recently authenticated by short tandem repeat profiling (Beijing Microread Gene Technology Co., China). Cells were cultured in Dulbecco's modified Eagle's medium (Hyclone, Logan, UT, USA) containing 10% fetal bovine serum (Gibco, Rockville, MD, USA), 100 IU penicillin, and 100 mg/ml streptomycin at 37°C in a humidified atmosphere containing 5% $CO_2$.

For cell proliferation assay, immunoblotting, and apoptosis-inducing factor studies, cells were plated in triplicate and incubated with sorafenib (5 μmol/L, Cat# S7397; Selleck, Houston, TX, USA), auranofin (0.6 μmol/L, Cat# HY-B1123; MedChem Express, Princeton, NJ, USA), or both sorafenib and auranofin for 72 h and then collected for analysis.

## Plasmid Constructs and Adenovirus Production

The full-length cDNA of PCK1 (coding sequence of NM_002591) was subcloned from plasmid pOTB7-PCK1 (Cat# FL07339; GeneCopoeia, Guangzhou, China) and inserted into the shuttle vector pAdTrack-TO4 (kindly gifted by Dr. Tong-Chuan He, University of Chicago, USA). Primers are shown in **Table S1**. Adenoviral recombinant AdPCK1 was generated using the AdEasy system, as described previously (7). Green fluorescent protein-expressing analogous adenovirus (AdGFP) was used as a control.

## RNA Extraction and Reverse Transcription Real-Time (RT-q)PCR

Huh7 cells were infected with AdPCK1 or AdGFP for 36 h. Total RNA was extracted from cultured cells or fresh tissue samples using TRIzol reagent (Invitrogen, Rockville, MD, USA), following the manufacturer's instructions. The RNA was reverse transcribed using Moloney murine leukemia virus reverse transcriptase (Promega) and random hexamers (Promega,

Madison, WI, USA). SYBR Green was used for quantitative PCR in a CFX Real-Time PCR Detection System (Bio-Rad, Hercules, CA, USA). The relative mRNA levels were calculated using the $2^{-\Delta\Delta Ct}$ method. Each in triplicate. All primers are shown in **Table S1**. The actin beta gene (*ACTB*) was used as reference gene for normalization in both cells and tissues.

## Western Blotting Analysis

Cells and tissue samples were harvested and treated with lysis buffer (Beyotime, Shanghai, China) containing 1 mM phenylmethylsulfonyl fluoride (Beyotime). Protein concentrations were determined using a BCA protein assay kit (Beyotime). Comparable amounts of proteins were subjected to 10% sodium dodecyl sulfate polyacrylamide gel electrophoresis and electrotransferred to polyvinylidene difluoride membranes (Millipore, Billerica, MA, USA). The membranes were probed with antibodies against PCK1 (1:1000; Cat# BS6870; Bioworld, Atlanta, GA, USA), TXNRD1 (1:500; Cat# 15140; Cell Signaling), or NRF2 (1:1000; Cat# 12721; Cell Signaling). Secondary antibodies conjugated to horseradish peroxidase were purchased from Abcam (Cambridge, MA, USA). Protein bands were visualized using Super Signal West Pico Chemiluminescent Substrate Kit (Millipore) and quantified using ImageJ software (National Institutes of Health, Bethesda, MA, USA, http://imagej.nih.gov/ij/). GAPDH (Cat# AF0006; Beyotime), β-actin (Cat# BL005B; Biosharp), laminB1 (Cat# AP6001; Bioworld), and β-tubulin (Cat# AP0064; Bioworld) were used as normalization controls. Nuclear and cytoplasmic extracts of cells were collected using a Nuclear and Cytoplasmic Protein Extraction Kit (Beyotime). All experiments were repeated three times independently.

## Immunohistochemistry

Paraffin-embedded liver tissue samples were obtained from the same 28 patients described above, and then sliced and deparaffinized according to standard procedures. The slides were incubated with anti-PCK1 antibody at 4°C overnight. After washing with PBS, the sections were incubated with secondary anti-rabbit IgG (ZSGB-BIO, Beijing, China) and stained with 3,3'-diaminobenzidine (ZSGB-BIO). For immunohistochemical assessment, the staining images of 3 pairs of HCC and adjacent non-tumor tissues were quantified using integrated optical density (IOD) by Image-Pro Plus 6.0 software.

## RNA-Sequencing (RNA-Seq) and Expression Analysis

For RNA sequencing, Huh7 cells were infected with AdGFP ($n = 3$) or AdPCK1 ($n = 3$) for 36 h. Total RNA was extracted using Trizol reagent (Invitrogen), and quantified using a NanoDrop ND-1000 spectrophotometer (Thermo Fisher Scientific, Wilmington, DE, USA) and a Bioanalyzer 2,200 (Agilent Technologies, CA, USA). Then, 5 μg RNA with a RNA Integrity Number (RIN) above 8.0 was used for cDNA library construction. RNA-seq and bioinformatic data analysis were performed by Shanghai Novel Bio Ltd. Briefly, strand-specific RNA-seq libraries were prepared using the Total RNA-seq (H/M/R) Library Prep Kit (Vazyme Biotech, Nanjing, China) and were sequenced on an Ion Torrent Proton Sequencer (Life Technologies, Carlsbad, CA, USA) according to Ion PI Sequencing 200 Kit v2.0 (Life Technologies). Raw reads in FASTQ format were subjected to quality control using FastQC (http://www.bioinformatics.babraham.ac.uk/projects/fastqc/). RNA-seq reads were aligned to the reference genome using Bowtie (http://bowtie-bio.sourceforge.net). Uniquely mapped reads were used for further analysis. Gene expression levels are expressed as RPKM (reads per kilobase per million reads) and differences in gene expression were calculated with rSeq (http://www-personal.umich.edu/~jianghui/rseq).

The RNA-seq data generated in this study have been deposited in the National Center for Biotechnology Information (NCBI) Gene Expression Omnibus database (GEO, http://www.ncbi.nlm.nih.gov/geo) under accession number GSE117822.

## CRISPR/Cas9-Mediated Knockout of PCK1

The CRISPR/Cas9 plasmids lentiCRISPR v2, pMD2.G, and psPAX2 were kindly provided by Prof. Ding Xue from the School of Life Sciences, Tsinghua University (Beijing, China). Single-guide RNAs (sgRNAs) targeting human PCK1 were designed by using the E-CRISP online tool (http://www.e-crisp.org/E-CRISP/designcrispr.html). The DNA oligonucleotides were annealed and cloned into the lentiCRISPR v2 vector digested with *BsmB*I (Thermo Fisher Scientific, Waltham, MA, USA). HEK293T cells were co-transfected with PCK1 sgRNAs or empty lentiCRISPR v2 as a control, envelop plasmid pMD2.G, and packaging plasmid psPAX2 using Lipofectamine 2,000 (Thermo Fisher Scientific, Waltham, MA, USA), following the manufacturer's protocol. Medium containing lentiviral particles and 5 μg/mL polybrene were used to infect PLC/PRF/5 cells. Two days post infection, cells were selected in medium containing 2 μg/mL puromycin. Then, the cells were trypsinized from the plates and seeded into a 96-well plate (1 cell/well, theoretically). The culture medium was replaced with fresh, puromycin-containing medium every 2 days until drug-resistant single colonies were identified by western blot analysis. For genotyping, clonal cell genomic DNA was extracted with Genomic DNA Purification Kit (Genloci Biotechnologies Inc, Jiangsu, China) according to the manufacturer's instructions. The genomic region flanking the gRNA target site was amplified by touch down PCR, and then subsequently cloned into the pMD19-T TA cloning vector (Takara, Kyoto, Japan) and sequenced (**Figure S1**). PCK1 knockout efficiency was confirmed by western blotting. PCK1-knockout cells and control cells were defined as KO 1/KO 2 cells and parental cells, respectively. All primers are shown in **Table S1**.

## Cell Proliferation Assay

The IncuCyte ZOOM Live-Cell Imaging system (Essen BioScience, Ann Arbor, Michigan, USA) was used for monitoring cell proliferation. Cells were seeded in 96-well plates at $1 \times 10^3$ cells/well and were cultured for 5 days. The plate was scanned and phase-contrast images were acquired in real time every 24 h post treatment, and quantified time-lapse curves were generated by IncuCyte ZOOM software. The medium was replaced with

fresh medium containing the respective reagents at 3-day intervals.

## Cell Apoptosis Assay

Cells were seeded at a density of $1.0 \times 10^6$ cells/mL and treated with different reagents. After washing twice with PBS, the cells detached with trypsin, collected by centrifugation and incubated with reagents from the Annexin-V-FITC Apoptosis Detection Kit (Biotool, Shanghai, China) according to the manufacturer's protocol. Then the cells were analyzed by FACS Vantage SE flow cytometer (BD Biosciences, San Jose, CA, USA). The experiment was repeated three times independently.

## Measurement of NADP/NADPH

NADPH and $NADP^+$ levels were measured using a NADP/NADPH Assay Kit (ab65349, Abcam, Cambridge, UK) according to the manufacturer's instructions. Cell lysates were extracted with provided buffer, then mixed with NADP cycling solution and with the NADPH developer. The absorbances of NADP and NADPH were measured at OD450 nm, and the concentrations were calculated by comparison with the standard curve.

## ROS Assay

Huh7 cells were infected with AdGFP or AdPCK1 in 6-well plates. Frozen tumors were sectioned at 10 μm. Tissues sections, infected Huh7, KO, and parental cells were incubated with 5μM of CellROX Deep Red Reagent (Thermo Fisher Scientific) for 30 min. The tissues and cells were washed 3 times with PBS and then, the nuclei were stained with 1 μg/mL DAPI (Sigma, St. Louis, MO, USA) for 3 min. The fixed tissues and cells were imaged under a confocal laser-scanning microscope (Leica, Heidelberg, Germany). The proportions of ROS-positive to total tissues or cells were determined by fluorescence microscopy in five random fields (magnification, 50× or 200×) in three wells.

## Xenograft Tumor Formation Assay

For the subcutaneous xenograft tumor model, 18 BALB/c nude mice (male, 5–6 weeks of age) were randomly divided into Mock, AdGFP and AdPCK1 groups (6 mice per group). MHCC-97H cells were mock-infected or infected with AdGFP, AdPCK1 for 24 h, collected and subcutaneously injected into the flanks of nude mice ($1 \times 10^5$ cells/injection). Tumor volumes were measured at 4-day intervals and calculated as length [cm] × (square of width [cm])/2. Mice were sacrificed after 4 weeks, and tumor tissues were removed for assessment. The protocol of animal experiments was approved by the Institutional Animal Care and Use Committee at Chongqing Medical University, and adhere to National Regulations for the administration of laboratory animal.

## Statistical Analysis

Data are presented as the mean ± standard deviation (SD). Survival rates were calculated using the Kaplan-Meier method and statistical significance was evaluated using the log-rank test. Statistical significance was determined using Student's *t*-test when comparing 2 groups or one-way analysis of variance (ANOVA) when comparing more than 2 groups. Statistical analysis was conducted using GraphPad Prism 7.0 software (La Jolla, CA, USA). *P*-values $< 0.05$ were considered statistically significant.

# RESULTS

## PCK1 Expression Is Downregulated in HCC

To clarify the function of PCK1 during the carcinogenesis of HCC, we first analyzed PCK1 expression levels in an independent cohort of 373 HCC samples (including 50 paired HCC tissues and para-tumor tissues) from The Cancer Genome Atlas (TCGA) database. The data showed that PCK1 expression was significantly lower in tumor tissues than in normal liver tissues (**Figure 1A**). In addition, we interpreted 72 cases as "PCK1 High" or "PCK1 Low" depending on the PCK1 expression level. Survival curve analysis demonstrated that patients with low expression of PCK1 had lower overall survival than patients with high expression of PCK1 (median survival, 835 vs. 1,630 days; **Figure 1B**). We further detected the PCK1 expression levels in 20 pairs of HCC and adjacent non-cancerous tissues from patients at the second affiliated Hospital of Chongqing Medical University. PCK1 mRNA levels were downregulated in HCC tissues compared to adjacent normal tissues ($P < 0.01$, **Figure 1C**). In addition, PCK1 protein levels were markedly lower in 16 out of the 20 HCC tissues (85%, **Figure 1D**). Immunohistochemical staining showed that PCK1 expression levels were significantly lower in HCC than in para-tumor tissues ($P < 0.01$, **Figure 1E**). Collectively, these data indicated that PCK1 is generally downregulated in HCC tissues, which is correlated with poorer prognosis.

## PCK1 Represses TXNRD1 Expression in Hepatoma Cells

Huh7 PCK1-overexpressing as well as PLC/PRF/5 PCK1-knockout cell lines were used to investigate the potential function of PCK1 in hepatoma cell proliferation. RNA-seq analysis demonstrated that the expression of 498 genes was significantly changed in AdPCK1- vs. AdGFP-infected Huh7 cells. Among these differentially expressed genes, *TXNRD1*, encoding a critical antioxidant enzyme, was remarkably downregulated ($P < 0.05$, **Figure 2A** and **Table S2**). Suppression of both TXNRD1 mRNA and protein expression was verified in PCK1-overexpressing Huh7 cells by RT-qPCR and immunoblot analysis (**Figures 2B,C**). In PCK1-KO PLC/PRF/5 cells, both TXNRD1 mRNA and protein levels were enhanced (**Figures 2B,D**). In addition, we examined the protein levels of PCK1 and TXNRD1 in eight cases of paired HCC and adjacent non-cancerous tissues. Downregulation of PCK1 (8/8) and upregulation of TXNRD1 (6/8) in HCC tissues were observed by immunoblotting (**Figure 2E**). These results indicated that PCK1 significantly downregulated TXNRD1 expression in hepatoma cells, and that the expression levels of PCK1 were negatively correlated with TXNRD1 expression in HCC tissues.

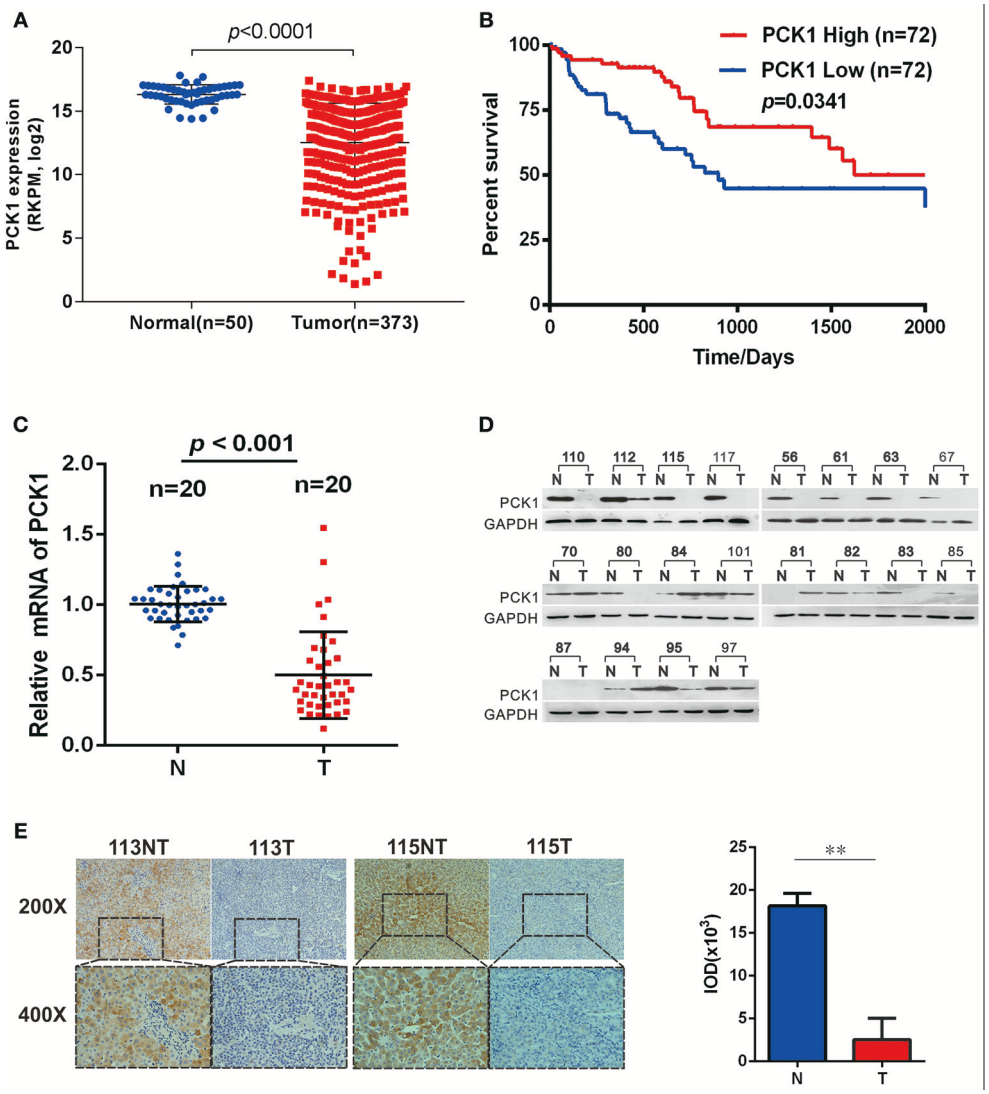


**FIGURE 1 |** PCK1 is generally decreased in hepatocellular carcinoma (HCC) tissues and correlates with poorer patient prognosis. **(A)** Expression of PCK1 in patients with HCC in the TCGA Liver Hepatocellular Carcinoma (LIHC) dataset. **(B)** Kaplan Meier survival curve based on data for 142 HCC patients in the TCGA dataset, divided into two groups by PCK1 expression levels in tumors. N represents paratumor tissues. T represents tumor tissues. **(C)** RT-qPCR analysis of PCK1 expression in 20 paired HCC and adjacent non-tumorous tissues ($P < 0.001$). **(D)** PCK1 protein levels in 20 paired primary HCC tissues and adjacent non-tumor tissues determined by western blotting. β-actin was used as a loading control. **(E)** Representative immunohistochemistry (IHC) images of PCK1 in HCC and adjacent non-tumor tissues. Immunostaining intensity was measured using ImagePro Plus 6.0 software. ($^{**}P < 0.01$); magnification: 400×,200×. Statistical analysis of PCK1 protein levels from 4 pairs of HCC and adjacent non-tumor tissues as determined by IHC staining. The cropped blots are used in the figure and full length blots are presented in **Figure S2**.

## PCK1 Suppresses Oxidative Stress in Hepatoma Cells

Previous studies have indicated TXNRD1 plays an important role in redox homoeostasis, and its expression could be induced by ROS production. (11, 13, 21) Furthermore, NADPH/$NADP^+$, which is necessary for redox balance, can be regulated by the pentose phosphate pathway (PPP) (22). Thus, we examined NADPH/$NADP^+$ ratio and ROS levels in hepatoma cells upon PCK1 expression. As expected, the ratio of NADPH/$NADP^+$ was increased in PCK1-overexpressing hepatoma cells (**Figure 3A**), while decreased in PCK1-KO PLC/PRF/5 cells (**Figure 3B**), compared to control cells. Specifically, we found that the ROS production was significantly reduced in PCK1-overexpressing Huh7 cells, while compared to parental cells, higher production of ROS was detected in PCK1-KO PLC/PRF/5 cells (**Figures 3C,D**). As Nrf2 is a key transcription factor in triggering ROS-induced gene expression, (13, 23) the regulatory effect of PCK1 on Nrf2 cellular distribution was also investigated. Immunoblot results revealed a remarkably increased cytoplasmic but decreased nuclear level

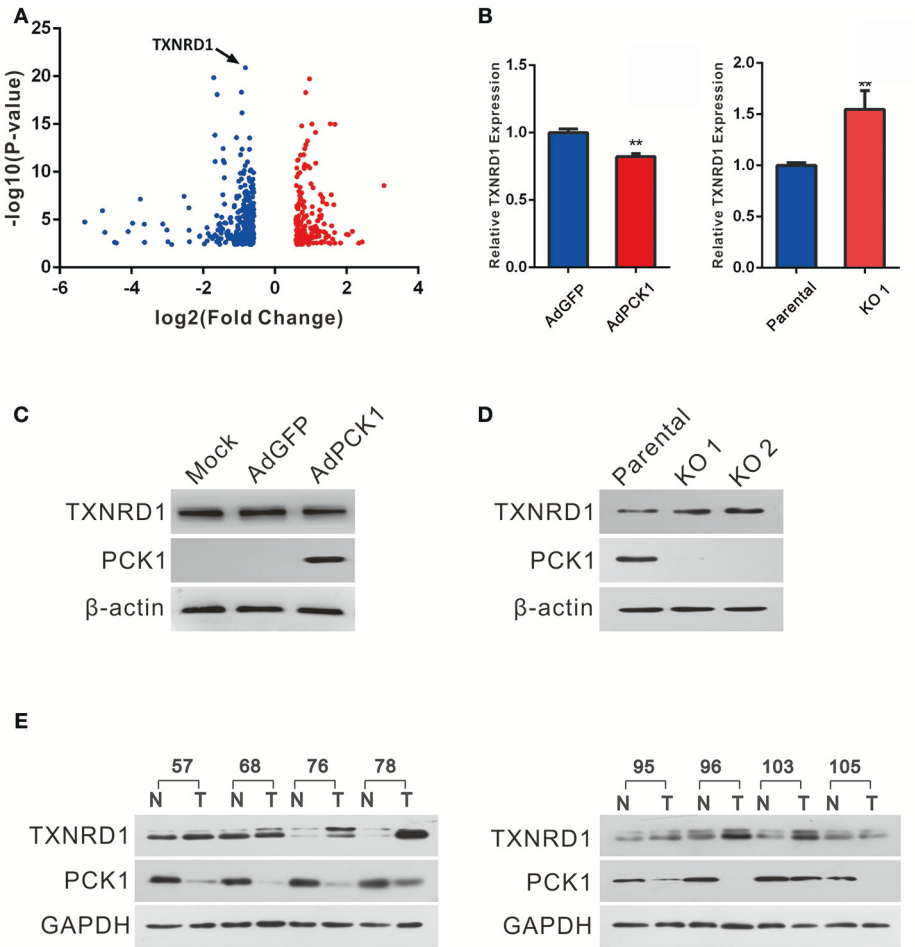


**FIGURE 2 |** PCK1 represses TXNRD1 expression in hepatoma cells and hepatic tissues**. (A)** Volcano plot of RNA-seq data from Huh7 cells infected with adenoviruses expressing PCK1 (AdPCK1) vs. Huh7 cells infected vector control (AdGFP). In total, 498 genes were differentially expressed (fold change >1.5 or < 0.667; FDR < 0.05). TXNRD1 is downregulated in PCK1-overexpressing hepatoma cells. **(B)** RT-qPCR analysis of mRNA levels of TXNRD1 in Huh7 cells infected with AdPCK1 or AdGFP. Total mRNA was isolated at 36 h after infection. Elevated mRNA expression of TXNRD1 in PCK1-KO (endogenous PCK1 was knocked out in PLC/PRF/5 cells by CRISPR-Cas9) compared to parental cells. Data are shown as the mean ± SD ($n = 3$ independent experiments; $^{**}P < 0.01$ by Student's *t*-test). **(C)** Western blot analysis of TXNRD1 in Huh7 cells infected with AdPCK1 or AdGFP. **(D)** Protein levels of TXNRD1 were detected by western blot analysis in PCK1-KO cells and parental cells. **(E)** PCK1 and TXNRD1 protein levels in eight cases of paired primary hepatocellular carcinoma tissues and and adjacent non-tumor tissues. GAPDH was used as a loading control. The cropped blots are used in the figure and full length blots are presented in **Figure S3**.

of Nrf2 in PCK1-overexpressing Huh7 cells (**Figure 3E**). In contrast, the nuclear levels of Nrf2 were elevated in PCK1-KO cells compared to parental cells (**Figure 3F**). These results suggested that overexpression of PCK1 suppresses both ROS production and the nuclear translocation of Nrf2.

## PCK1 Exerts Antitumor Effect by Inhibiting ROS Level and TXNRD1expression *in vivo*

The antitumor effect *in vivo* was evaluated in MHCC-97H xenograft tumor in nude mice. All mice developed xenograft tumors at the injection site. Twenty days after injection, we noticed that the tumors were much smaller in the PCK1-overexpression group than in the mock and the empty vector group (**Figure 4A**). As shown in **Figure 4B**, overexpression of PCK1 significantly reduced the growth rate of MHCC-97H tumor growth compared with the mock and GFP control group by measuring tumor volume every 4 days ($^{*}P < 0.05$, AdPCK1 group vs. AdGFP group, **Figure 4B**). In addition, the average tumor size was smaller in the PCK1-overexpression group than that in the control group (**Figure 4C**). We also found that ROS production was significantly reduced in PCK1-overexpression group (**Figure 4D**). Furthermore, western-blot analysis was used to analyze the expression levels of PCK1 and TXNRD1 in the xenograft tumor tissues. Immunoblotting results revealed higher expression of PCK1 and lower expression of TXNRD1 in tumor tissues derived from the PCK1-overexpressing hepatoma cells than in GFP control group (**Figure 4E**). Together, these results suggested that PCK1 could inhibit hepatoma cell growth *in vivo* by decreasing ROS level and TXNRD1 expression.

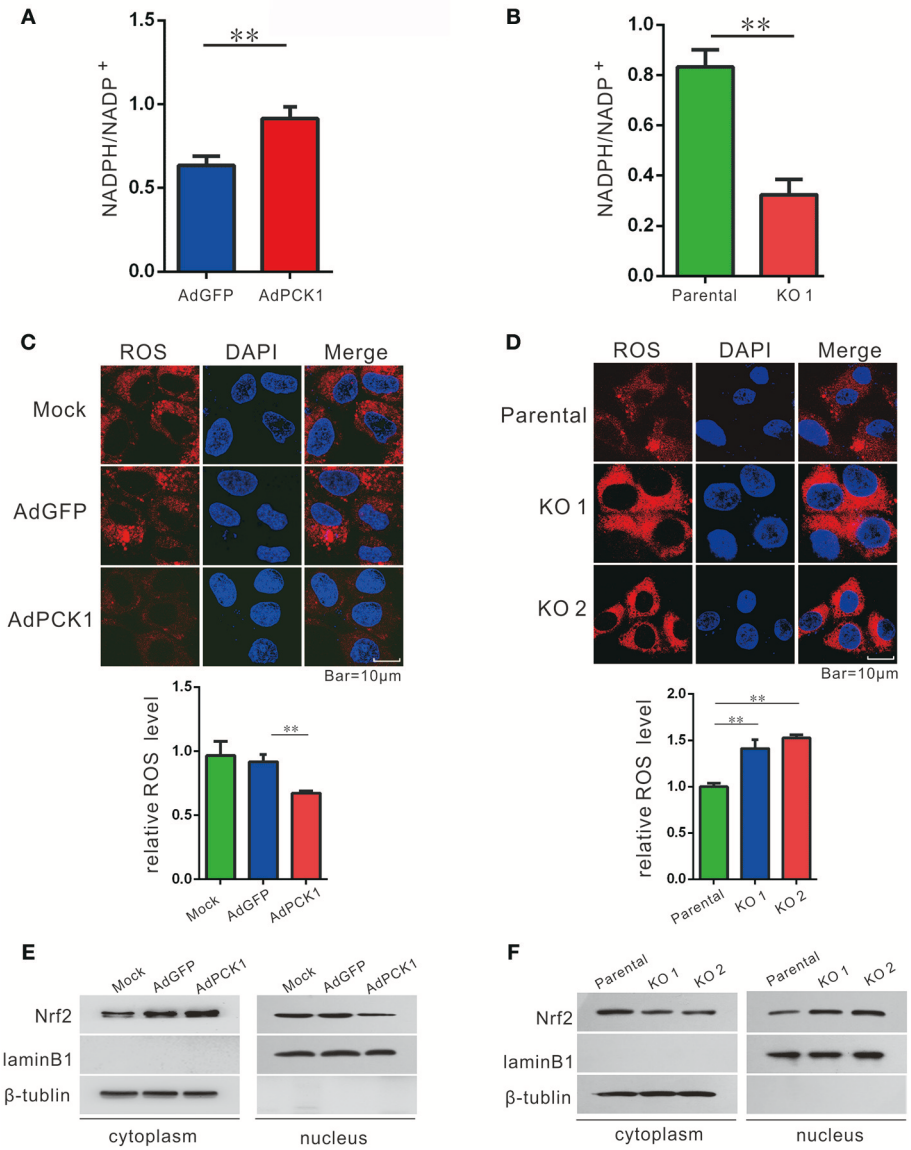


**FIGURE 3 |** PCK1 suppresses oxidative stress in liver cancer cells. Relative ratios of NADPH to total NADP in PCK1-overexpressing cells **(A)**, and PCK1-KO cells **(B)** were measured by using an NADP/NADPH quantification kit (Abcam). Fluorescent labeling of ROS (red) in the cytoplasm, nuclei were stained with DAPI (blue). Scale bar = 10 μm. ROS levels in PCK1-overexpressing cells **(C)**, and PCK1-KO cells **(D)** were detected, and the relative fluorescence intensities were determined after normalization to mock-infected or parental cells. Data are represented as the mean ± SD ($n = 3$, technical replicates; $^{**}P < 0.01$ by Student's $t$-test). **(E)** Protein expression of Nrf2. Huh7 cells were treated as described in **Figure 2**. Two days post infection, nuclear and cytoplasmic fractions were obtained and analyzed by western blotting. LaminB1 and β-tubulin were used as internal loading controls. **(F)** Nuclear accumulation of Nrf2 in PCK1-KO cells. Nuclear and cytoplasmic fractions were obtained and analyzed by western blotting. LaminB1 and β-tubulin were used as internal loading controls for western blotting. The cropped blots are used in the figure and full length blots are presented in **Figure S4**.

## Auranofin Enhances the Sensitivity to Apoptosis Induced by Sorafenib Treatment via Inhibition of TXNRD1 in PCK1-KO Cells *in vitro*

To explore a potential treatment strategy for HCC, we tested the apoptosis-inducing effect of sorafenib (the first drug approved for advanced HCC treatment) in combination with auranofin (an inhibitor of thioredoxin reductase) *in vitro*. PCK1-KO PLC/PRF/5 cells were treated with 0.6 μmol/L auranofin or 5 μmol/L sorafenib, alone or in combination. The cell proliferation rate was increased in PCK1-KO cells as compared to parental cells. Furthermore, combined treatment with sorafenib and auranofin induced a synergistic inhibitory effect on cell proliferation in PCK1-KO cells (**Figure 5A**). In addition, excess ROS accumulation were observed in PCK1-KO cells treated with auranofin plus sorafenib (**Figure 5B**). Apoptosis is one of the most important factors affecting cell proliferation. To

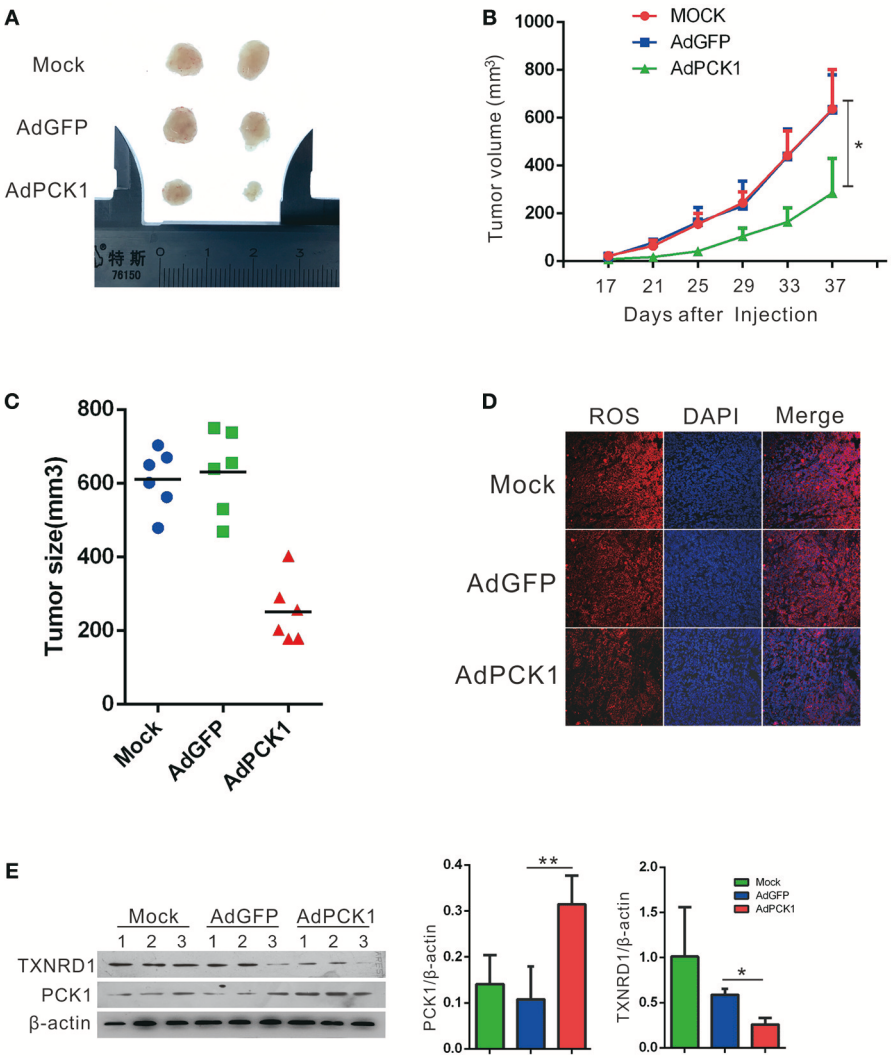


**FIGURE 4 |** PCK1 inhibits tumor growth and oxidative stress in xenograft tumors. MHCC-97H cells were infected with AdGFP or AdPCK1 or mock-infected for 24 h, then subcutaneous injected into nude mice ($n = 6$). **(A)** Representative image of tumor in all groups (presented two tumors each group). **(B)** The growth curve of subcutaneous xenograft tumor. Tumor volumes were measured every 4 days and calculated as length × (square of width)/2 (repeated-measures analysis of variance, $^*P < 0.05$ compared to AdGFP group, error bars represent mean ± SD, $n = 6$). **(C)** Tumor size of subcutaneous xenografts after dissected. **(D)** ROS monitored by immunofluorescent labeling (red) and nuclei by DAPI (blue) staining in xenografts. Scale bar = 200 μm. **(E)** Expression of PCK1 and TXNRD1 checked by western blot assay in xenograft tumor samples. Semi-quantitative densitometry graphs of immunoblots (arbitrary densitometry units) for PCK1 and TXNRD1 levels normalized to β-actin expression are shown. ($^*P < 0.05$, $^{**}P < 0.01$, AdPCK1 group vs. AdGFP group). The cropped blots are used in the figure and full length blots are presented in **Figure S5**.

investigate the effects of sorafenib and auranofin on apoptosis, we detected the protein levels of Caspase3/9, Cleaved caspase 3/9, Bax and Bcl-2, and analyzed the Bax/Bcl-2 ratio, which indicates apoptosis occurrence. PCK1-KO cells treated with sorafenib exhibited increased Cleaved caspase3, Cleaved caspase9 and Bax levels, while cells treated with auranofin plus sorafenib showed significantly increased these proteins expression as compared to cells treated with sorafenib alone. The Bax/Bcl-2 ratio was markedly increased in the PCK1-KO cell exposed to combination treatment as compared to parental cells or each PCK1-KO exposed to single treatments. Furthermore, the protein levels of TXNRD1 were decreased in cells treated with auranofin plus sorafenib, compared to those in PCK1-KO cells treated with auranofin alone (**Figure 5C**). Flow-cytometric analysis revealed that treatment with auranofin or sorafenib induced cell apoptosis. Cells treated with auranofin plus sorafenib showed significantly higher apoptosis ($P < 0.001$; **Figures 5D,E**). Taken together, these *in vitro* data suggested auranofin could increase the sensitivity of PCK1-KO cells to sorafenib.

## DISCUSSION

Metabolic reprogramming is a hallmark of cancer, plays an important role in tumor proliferation, metastasis and drug-resistance by providing essential cellular components such as energy equivalents, redox cofactors and biomass building blocks.

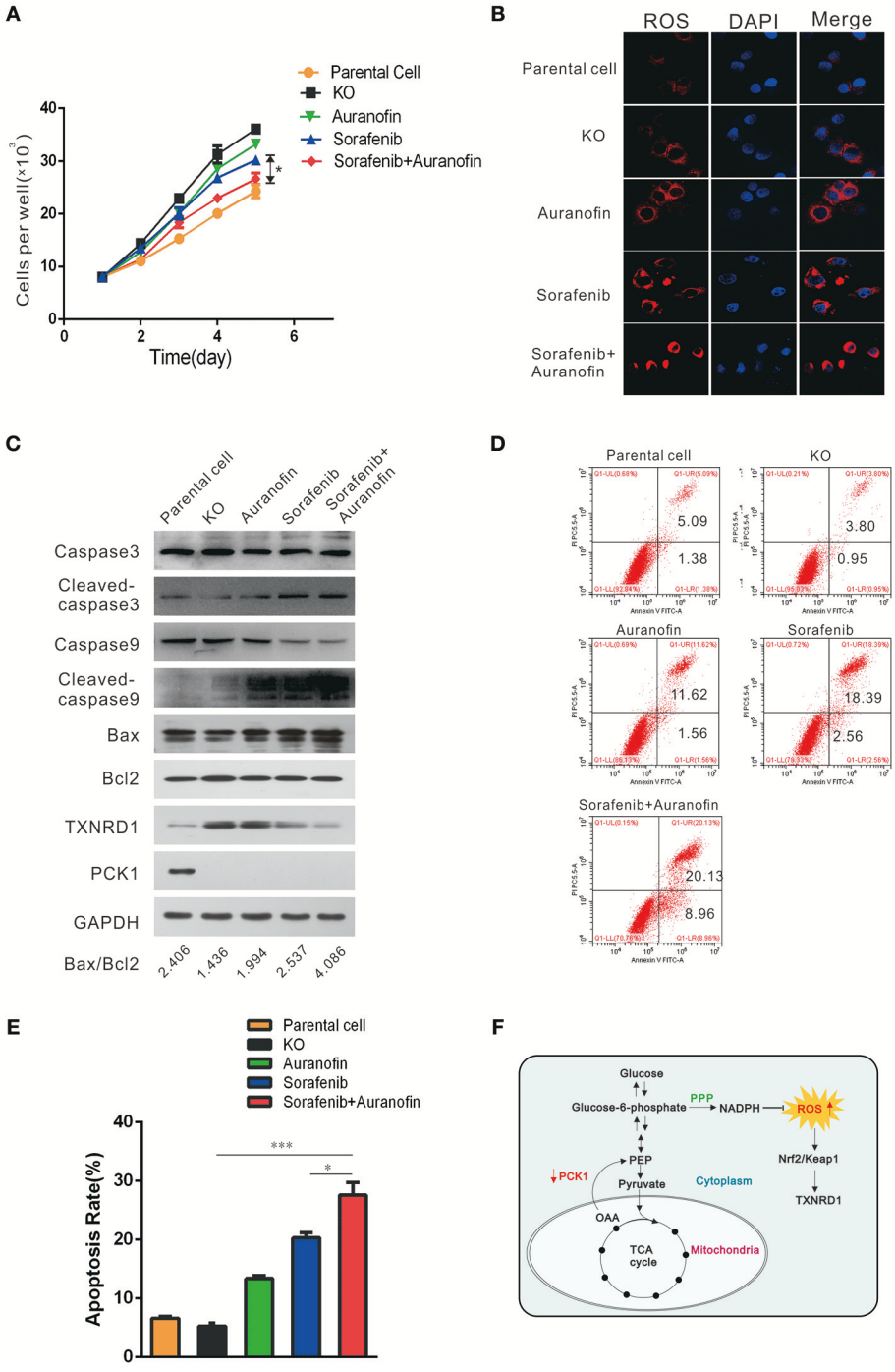


**FIGURE 5 |** Auranofin enhances the sensitivity to sorafenib-induced apoptosis via inhibition of TXNRD1 in PCK1-KO cells *in vitro*. **(A)** Cell proliferation curves. PCK1-KO hepatoma cells were treated with 0.6 μmol/L auranofin or 5 μmol/L sorafenib alone or in combination. Cells were plated into 96-well plates at $1 \times 10^3$ cells/well and were counted every 24 h in triplicate. Data are presented as the mean ± SD; $^*P < 0.05$ vs. Sorafenib alone. **(B)** ROS were monitored by fluorescent labeling (red) and nuclei were stained by DAPI (blue) in cells treated with sorafenib and auranofin alone or in combination. Scale bar = 10 μm. **(C)** Protein expression of Caspase3/9, Cleaved caspase3/9, Bax, Bcl2, TXNRD1, and PCK1. PCK1-KO hepatoma cells were treated as in **Figure 4A** for 48 h and the proteins were isolated and analyzed by western blotting. GAPDH expression served as an internal control. **(D)** Flow-cytometric analysis of apoptosis was performed after treatments with sorafenib and/or auranofin. **(E)** Quantification of cell death detected in **Figure 4C**. Cell apoptosis as detected by PI staining. Values represent the mean percentage of dead cells ± SD from three samples ($^*P < 0.05$,$^{***}P < 0.001$). **(F)** Schematic illustration showing the PCK1–NADPH–ROS-TXNRD1 axis. In HCC, decreased PCK1 suppressed the generation of NADPH via pentose phosphate pathway (PPP). Subsequently, ROS, which is quenched by NADPH, was increased, further promoted nuclear translocation of Nrf2 and the expression of TXNRD1. The cropped blots are used in the figure and full length blots are presented in **Figure S6**.

(24–27) Our results demonstrated that PCK1 was significantly decreased in HCC tumor tissues compared with adjacent normal tissues, which was verified by analysis of data obtained from the TCGA database. Furthermore, lower PCK1 expression correlated with poorer prognosis. Consistent with previous studies (4, 9), our data suggest a tumor-suppressor function of PCK1 in HCC.

However, elevated PCK1 expression has also been found in other types of cancers, such as melanoma (8), breast cancer (26), and colorectal cancer (7), where it supports anabolic pathways and cell proliferation. The distinct expression profile of PCK1 in HCC tissues compared to other solid tumors can be explained by the fact that in the liver, which accounts for approximately 90% of gluconeogenesis, the upregulation of gluconeogenesis by PCK1 results in the suppression of hepatoma proliferation. Specifically, PCK1-induced promotion of gluconeogenesis enhances energy consumption and attenuates energy production, including glycolysis, and mitochondrial respiration, which results in ATP depletion. Decreased aerobic glycolysis and mitochondrial respiration pathway also suppresses the generation of metabolic intermediates as building blocks for cells (28). Forced PCK1 expression in glucose-starved hepatoma cells reportedly induces tricarboxylic acid cycle cataplerosis, leading to energy crisis, oxidative stress, and cell apoptosis (4).

In cancer cells, excess ROS are generated through increased anabolism, decreased catabolism, or mitochondrial dysfunction. Previous studies have shown that glucose metabolism-related enzymes, such as PKM and FBP1 (29–31), can participate in the regulation of ROS production. In our study, low expression of PCK1 resulted in elevated intracellular ROS level *in vitro* and *in vivo*. PCK1 plays a crucial role in hepatic anabolism and catabolism (4, 22, 32). Thus, PCK1 is likely to regulate the ROS level through altering the metabolism of HCC. Ko et al. reported that PCK1 deletion in myeloid cells increases the intracellular ROS level (33). Ma et al. reported that 3-MPA, an inhibitor of PCK1, could increase ROS in $CD8^+$ memory T cells through the abrogation of the PCK1-glycogen-pentose phosphate pathway (PPP) (34). Since NADPH is a key product of PPP, and plays an essential role in the ROS generation via glutathione (GSH) system, we hypothesized that glucose-6-phosphate which indirectly catalyzed by PCK1 is channeled to PPP. Our results demonstrate that PCK1 overexpression increases the ratio of $NADPH/NADP^+$, and further decreases ROS production. However, it has been reported that forced PCK1 expression in glucose-starved HCC cells induces a high ROS level (4). Thus, the specific mechanism of PCK1 affecting ROS through metabolic regulation under different culture conditions requires further investigation.

Our data further showed that overexpression of PCK1 abrogated the nuclear translocation of Nrf2 and the expression of its downstream gene TXNRD1. The transcription factor Nrf2 is considered a major transcriptional regulator in the defense against ROS (35, 36). TXNRD1 is a critical antioxidant enzyme that catalyzes the NADPH-dependent reduction of thioredoxin to regulate cellular redox homeostasis (37, 38). TXNRD1 is upregulated in many human malignancies, and inhibition of the TXN pathway causes hepatoma cell death (17, 39–41). Furthermore, auranofin, a TXNRD1 inhibitor, has been reported to induce apoptosis and to enhance the anticancer activities of chemotherapeutic agents (16, 42, 43). In line herewith, we observed that TXNRD1 may be related to drug resistance of hepatoma cells. Sorafenib, a multi-kinase inhibitor, is the first-line therapy for patients with advanced HCC (1). However, considering the sorafenib resistance crisis in HCC, the development of new combination therapies with sorafenib is urgently required. Recent studies reported that synergistic combination of sorafenib and uracil-tegafur or octreotide can improve the sensitivity toward sorafenib in the treatment of HCC (44, 45). This study confirmed that sorafenib in combination with auranofin exhibits a stronger pro-apoptotic effect *in vitro*.

In conclusion, our study demonstrated that PCK1 is significantly downregulated in HCC, and PCK1 deficiency decreases NADPH/NADP+ ratio, increases cellular ROS levels, which results in activation of Nrf2 and expression of TXNRD1(**Figure 5F**). In addition, auranofin enhances the sensitivity to sorafenib via inhibition of TXNRD1 in PCK1-knockout cells *in vitro*. Our finding provides new insights into the mechanism of antioxidant enzyme gene TXNRD1 mediated by altered metabolism in liver cancer, and might offers a potential therapy for HCC.

## ETHICS STATEMENT

All patients provided informed consent, and this study was conducted with the approval of Institutional Ethical Review Board of Chongqing Medical University (project license number: 2017012). All animal experiments were carried out according to the guidelines of the Institutional Animal Care and Use Committee at Chongqing Medical University (The project license number: 2017012), and protocols of animal care and use adhere to National Regulations for the administration of laboratory animals.

## AUTHOR CONTRIBUTIONS

KW and NT conceived and designed the study. LT, JX, XP, QG, GZ, and YY performed experimental work. LL and JX performed data analysis. LT prepared the manuscript. KW and NT provided administrative support and funded experiments. All authors read and approved the final manuscript.

## FUNDING

This study was supported by research grants from China National Natural Science Foundation (grant nos. 81572683, 81371827, 81872270, and 31171307 to NT, 81602417 to KW, and 81602045 to JX), the Major National S&T program (2017ZX10202203-004, 2012ZX10002005-003-002 to NT), Natural Science Foundation Project of CQ CSTC (grant no. cstc2015jcyjBX0011 to NT), the Program for Innovation Team of Higher Education in Chongqing (grant no. CXTDX201601015), the Leading Talent Program of CQ CSTC (grant no. CSTCCXLJRC201719 to NT), the Scientific Research Innovation Project for Postgraduate

in Chongqing (grant no. YB17116), and Talent Development Program of CQMU for Postgraduate (grant no. BJRC201705).

## ACKNOWLEDGMENTS

We would like to thank Dr. Tong-Chuan He (University of Chicago, USA) for providing the AdEasy system. We are also grateful to Prof. Ding Xue (School of Life Sciences, Tsinghua University) for providing the CRISPR/Cas9 system, lentiCRISPR v2, pMD2.G and psPAX2.

## SUPPLEMENTARY MATERIAL

The Supplementary Material for this article can be found online at: https://www.frontiersin.org/articles/10.3389/fonc.2018.00611/full#supplementary-material

## REFERENCES

1. Marrero JA, Kulik LM, Sirlin C, Zhu AX, Finn RS, Abecassis MM, et al. Diagnosis, Staging and Management of Hepatocellular Carcinoma: 2018 Practice Guidance by the American Association for the Study of Liver Diseases. *Hepatology* (2018) 68:723–50. doi: 10.1002/hep.29913
2. Hanahan D, Weinberg RA. Hallmarks of cancer: the next generation. *Cell* (2011) 144:646–74. doi: 10.1016/j.cell.2011.02.013
3. Tardito S, Oudin A, Ahmed SU, Fack F, Keunen O, Zheng L, et al. Glutamine synthetase activity fuels nucleotide biosynthesis and supports growth of glutamine-restricted glioblastoma. *Nat Cell Biol*. (2015) 17:1556–68. doi: 10.1038/ncb3272
4. Liu M-X, Jin L, Sun S-J, Liu P, Feng X, Cheng Z-L, et al. Metabolic reprogramming by PCK1 promotes TCA cataplerosis, oxidative stress and apoptosis in liver cancer cells and suppresses hepatocellular carcinoma. *Oncogene* (2018) 37:1637–53. doi: 10.1038/s41388-017-0070-6
5. Beale EG, Harvey BJ, Forest C. PCK1 and PCK2 as candidate diabetes and obesity genes. *Cell Biochem Biophys*. (2007) 48:89–95. doi: 10.1007/s12013-007-0025-6
6. Satapati S, Kucejova B, Duarte JAG, Fletcher JA, Reynolds L, Sunny NE, et al. Mitochondrial metabolism mediates oxidative stress and inflammation in fatty liver. *J Clin Invest*. (2016) 126:1605. doi: 10.1172/JCI86695
7. Park J-W, Kim SC, Kim WK, Hong JP, Kim K-H, Yeo HY, et al. Expression of phosphoenolpyruvate carboxykinase linked to chemoradiation susceptibility of human colon cancer cells. *BMC Cancer* (2014) 14:160. doi: 10.1186/1471-2407-14-160
8. Li Y, Luo S, Ma R, Liu J, Xu P, Zhang H, et al. Upregulation of cytosolic phosphoenolpyruvate carboxykinase is a critical metabolic event in melanoma cells that repopulate tumors. *Cancer Res.* (2015) 75:1191–6. doi: 10.1158/0008-5472.CAN-14-2615
9. Gingold JA, Zhu D, Lee D-F, Kaseb A, Chen J. Genomic profiling and metabolic homeostasis in primary liver cancers. *Trends Mol Med.* (2018) 24:395–411. doi: 10.1016/j.molmed.2018.02.006
10. Bian X-L, Chen H-Z, Yang P-B, Li Y-P, Zhang F-N, Zhang J-Y, et al. Nur77 suppresses hepatocellular carcinoma via switching glucose metabolism toward gluconeogenesis through attenuating phosphoenolpyruvate carboxykinase sumoylation. *Nat Commun*. (2017) 8:14420. doi: 10.1038/ncomms14420
11. Ray PD, Huang B-W, Tsuji Y. Reactive oxygen species (ROS) homeostasis and redox regulation in cellular signaling. *Cell Signal.* (2012) 24:981–90. doi: 10.1016/j.cellsig.2012.01.008
12. Sena LA, Chandel NS. Physiological roles of mitochondrial reactive oxygen species. *Mol Cell* (2012) 48:158–67. doi: 10.1016/j.molcel.2012.09.025
13. Rodriguez-Garcia A, Hevia D, Mayo JC, Gonzalez-Menendez P, Coppo L, Lu J, et al. Thioredoxin 1 modulates apoptosis induced by bioactive compounds in prostate cancer cells. *Redox Biol.* (2017) 12:634–47. doi: 10.1016/j.redox.2017.03.025
14. Yu X, Kensler T. Nrf2 as a target for cancer chemoprevention. *Mutat Res.* (2005) 591:93–102. doi: 10.1016/j.mrfmmm.2005.04.017
15. Peng X, Giménez-Cassina A, Petrus P, Conrad M, Rydén M, Arnér ESJ. Thioredoxin reductase 1 suppresses adipocyte differentiation and insulin responsiveness. *Sci Rep.* (2016) 6:28080. doi: 10.1038/srep28080
16. Bhatia M, McGrath KL, Di Trapani G, Charoentong P, Shah F, King MM, et al. The thioredoxin system in breast cancer cell invasion and migration. *Redox Biol.* (2016) 8:68–78. doi: 10.1016/j.redox.2015.12.004
17. Hao C, Xu X, Ma J, Xia J, Dai B, Liu L, et al. MicroRNA-124 regulates the radiosensitivity of non-small cell lung cancer cells by targeting TXNRD1. *Oncol Lett.* (2017) 13:2071–8. doi: 10.3892/ol.2017.5701
18. Marzano C, Gandin V, Folda A, Scutari G, Bindoli A, Rigobello MP. Inhibition of thioredoxin reductase by auranofin induces apoptosis in cisplatin-resistant human ovarian cancer cells. *Free Radic Biol Med*. (2007) 42:872–81. doi: 10.1016/j.freeradbiomed.2006.12.021
19. Duan D, Zhang B, Yao J, Liu Y, Sun J, Ge C, et al. Gambogic acid induces apoptosis in hepatocellular carcinoma SMMC-7721 cells by targeting cytosolic thioredoxin reductase. *Free Radic Biol Med*. (2014) 69:15–25. doi: 10.1016/j.freeradbiomed.2013.12.027
20. Matsuzawa A. Thioredoxin and redox signaling: Roles of the thioredoxin system in control of cell fate. *Arch Biochem Biophys.* (2017) 617:101–5. doi: 10.1016/j.abb.2016.09.011
21. Richter K, Konzack A, Pihlajaniemi T, Heljasvaara R, Kietzmann T. Redox-fibrosis: Impact of TGFβ1 on ROS generators, mediators and functional consequences. *Redox Biol.* (2015) 6:344–52. doi: 10.1016/j.redox.2015.08.015
22. Patra KC, Hay N. The pentose phosphate pathway and cancer. *Trends Biochem Sci.* (2014) 39:347–54. doi: 10.1016/j.tibs.2014.06.005
23. Khan AUH, Allende-Vega N, Gitenay D, Garaude J, Vo D-N, Belkhala S, et al. Mitochondrial Complex I activity signals antioxidant response through ERK5. *Sci Rep*. (2018) 8:7420. doi: 10.1038/s41598-018-23884-4
24. Yoshida GJ. Metabolic reprogramming: the emerging concept and associated therapeutic strategies. *J Exp Clin Cancer Res*. (2015) 34:111. doi: 10.1186/s13046-015-0221-y
25. Xiong Y, Lei Q-Y, Zhao S, Guan K-L. Regulation of glycolysis and gluconeogenesis by acetylation of PKM and PEPCK. *Cold Spring Harb Symp Quant Biol.* (2011) 76:285–9. doi: 10.1101/sqb.2011.76.010942
26. Dong C, Yuan T, Wu Y, Wang Y, Fan TWM, Miriyala S, et al. Loss of FBP1 by Snail-mediated repression provides metabolic advantages in basal-like breast cancer. *Cancer Cell* (2013) 23:316–31. doi: 10.1016/j.ccr.2013.01.022
27. Méndez-Lucas A, Li X, Hu J, Che L, Song X, Jia J, et al. Glucose catabolism in liver tumors induced by c-MYC Can Be Sustained by Various PKM1/PKM2 ratios and pyruvate kinase activities. *Cancer Res*. (2017) 77:4355–64. doi: 10.1158/0008-5472.CAN-17-0498
28. Koppenol WH, Bounds PL, Dang CV. Otto Warburg's contributions to current concepts of cancer metabolism. *Nat Rev Cancer* (2011) 11:325–37. doi: 10.1038/nrc3038
29. Chen M, Zhang J, Li N, Qian Z, Zhu M, Li Q, et al. Promoter hypermethylation mediated downregulation of FBP1 in human hepatocellular carcinoma and colon cancer. *PLoS ONE* (2011) 6:e25564. doi: 10.1371/journal.pone.0025564
30. Dai J, Ji Y, Wang W, Kim D, Fai LY, Wang L, et al. Loss of fructose-1,6-bisphosphatase induces glycolysis and promotes apoptosis resistance of cancer stem-like cells: an important role in hexavalent chromium-induced carcinogenesis. *Toxicol Appl Pharmacol*. (2017) 331:164–73. doi: 10.1016/j.taap.2017.06.014
31. Shinohara H, Taniguchi K, Kumazaki M, Yamada N, Ito Y, Otsuki Y, et al. Anti-cancer fatty-acid derivative induces autophagic cell death through modulation of PKM isoform expression profile mediated by bcr-abl in chronic myeloid leukemia. *Cancer Lett.* (2015) 360:28–38. doi: 10.1016/j.canlet.2015.01.039
32. Montal ED, Dewi R, Bhalla K, Ou L, Hwang BJ, Ropell AE, et al. PEPCK coordinates the regulation of central carbon metabolism to promote cancer cell growth. *Mol Cell* (2015) 60:571–83. doi: 10.1016/j.molcel.2015.09.025
33. Ko C-W, Counihan D, Wu J, Hatzoglou M, Puchowicz MA, Croniger CM. Macrophages with a deletion of the phosphoenolpyruvate carboxykinase 1

(Pck1) gene have a more proinflammatory phenotype. *J Biol Chem*. (2018) 293:3399–409. doi: 10.1074/jbc.M117.819136
34. Ma R, Ji T, Zhang H, Dong W, Chen X, Xu P, et al. A Pck1-directed glycogen metabolic program regulates formation and maintenance of memory CD8+ T cells. *Nat Cell Biol.* (2018) 20:21–7. doi: 10.1038/s41556-017-0002-2
35. Hayes JD, Dinkova-Kostova AT. The Nrf2 regulatory network provides an interface between redox and intermediary metabolism. *Trends Biochem Sci.* (2014) 39:199–218. doi: 10.1016/j.tibs.2014.02.002
36. Levonen A-L, Hill BG, Kansanen E, Zhang J, Darley-Usmar VM. Redox regulation of antioxidants, autophagy, and the response to stress: implications for electrophile therapeutics. *Free Radic Biol Med.* (2014) 71:196–207. doi: 10.1016/j.freeradbiomed.2014.03.025
37. Fu B, Meng W, Zeng X, Zhao H, Liu W, Zhang T. TXNRD1 Is an unfavorable prognostic factor for patients with hepatocellular carcinoma. *BioMed Res Int*. (2017) 2017:1–8. doi: 10.1155/2017/4698167
38. Iverson SV, Eriksson S, Xu J, Prigge JR, Talago EA, Meade TA, et al. A Txnrd1-dependent metabolic switch alters hepatic lipogenesis, glycogen storage, and detoxification. *Free Rad Biol Med.* (2013) 63:369–80. doi: 10.1016/j.freeradbiomed.2013.05.028
39. Fernandes AP, Capitanio A, Selenius M, Brodin O, Rundlöf A-K, Björnstedt M. Expression profiles of thioredoxin family proteins in human lung cancer tissue: correlation with proliferation and differentiation. *Histopathology* (2009) 55:313–20. doi: 10.1111/j.1365-2559.2009.03381.x
40. Cañas A, López-Sánchez LM, Valverde-Estepa A, Hernández V, Fuentes E, Muñoz-Castañeda JR, et al. Maintenance of S-nitrosothiol homeostasis plays an important role in growth suppression of estrogen receptor-positive breast tumors. *Breast Cancer Res*. (2012) 14:R153. doi: 10.1186/bcr3366
41. Esen H, Erdi F, Kaya B, Feyzioglu B, Keskin F, Demir LS. Tissue thioredoxin reductase-1 expression in astrocytomas of different grades. *J Neurooncol*. (2015) 121:451–8. doi: 10.1007/s11060-014-1661-5
42. Dai B, Yoo S-Y, Bartholomeusz G, Graham RA, Majidi M, Yan S, et al. KEAP1-dependent synthetic lethality induced by AKT and TXNRD1 inhibitors in lung cancer. *Cancer Res*. (2013) 73:5532–43. doi: 10.1158/0008-5472.CAN-13-0712
43. Lee J-E, Kwon Y-J, Baek H-S, Ye D-J, Cho E, Choi H-K, et al. Synergistic induction of apoptosis by combination treatment with mesupron and auranofin in human breast cancer cells. *Arch Pharm Res*. (2017) 40:746–59. doi: 10.1007/s12272-017-0923-0
44. Prete SD, Montella L, Caraglia M, Maiorino L, Cennamo G, Montesarchio V, et al. Sorafenib plus octreotide is an effective and safe treatment in advanced hepatocellular carcinoma: multicenter phase II So.LAR. study. *Cancer Chemother Pharmacol.* (2010) 66:837–44. doi: 10.1007/s00280-009-1226-z
45. Hsu C-H, Shen Y-C, Lin Z-Z, Chen P-J, Shao Y-Y, Ding Y-H, et al. Phase II study of combining sorafenib with metronomic tegafur/uracil for advanced hepatocellular carcinoma. *J Hepatol.* (2010) 53:126–31. doi: 10.1016/j.jhep.2010.01.035

**Conflict of Interest Statement:** The authors declare that the research was conducted in the absence of any commercial or financial relationships that could be construed as a potential conflict of interest.

frontiers in Pharmacology

ORIGINAL RESEARCH
published: 22 February 2019
doi: 10.3389/fphar.2019.00134

# Cycling Quiescence in Temozolomide Resistant Glioblastoma Cells Is Partly Explained by microRNA-93 and -193-Mediated Decrease of Cyclin D

*Jessian L. Munoz[1,2†], Nykia D. Walker[2†], Satvik Mareedu[1,2], Sri Harika Pamarthi[1], Garima Sinha[1,2], Steven J. Greco[1] and Pranela Rameshwar[1,2*]*

[1] Rutgers New Jersey Medical School, Rutgers University, Newark, NJ, United States, [2] Rutgers School of Graduate Studies at New Jersey Medical School, Rutgers University, Newark, NJ, United States

OPEN ACCESS

**Edited by:**
Murugabaskar Balan,
Boston Children's Hospital, Harvard Medical School, United States

**Reviewed by:**
Shree Ram Singh,
National Cancer Institute at Frederick, United States
Pere Gascon,
Hospital Clínic de Barcelona, Spain

***Correspondence:**
Pranela Rameshwar
rameshwa@njms.rutgers.edu

[†] These authors have contributed equally to this work

**Specialty section:**
This article was submitted to Cancer Molecular Targets and Therapeutics, a section of the journal Frontiers in Pharmacology

**Received:** 01 October 2018
**Accepted:** 05 February 2019
**Published:** 22 February 2019

**Citation:**
Munoz JL, Walker ND, Mareedu S, Pamarthi SH, Sinha G, Greco SJ and Rameshwar P (2019) Cycling Quiescence in Temozolomide Resistant Glioblastoma Cells Is Partly Explained by microRNA-93 and -193-Mediated Decrease of Cyclin D. Front. Pharmacol. 10:134. doi: 10.3389/fphar.2019.00134

Glioblastoma multiforme (GBM) is a fatal malignancy of the central nervous system, commonly associated with chemoresistance. The alkylating agent Temozolomide (TMZ) is the front-line chemotherapeutic agent and has undergone intense studies on resistance. These studies reported on mismatch repair gene upregulation, ABC-targeted drug efflux, and cell cycle alterations. The mechanism by which TMZ induces cell cycle arrest has not been well-established. TMZ-resistant GBM cells have been linked to microRNA (miRNA) and exosomes. A cell cycle miRNA array identified distinct miRNAs only in exosomes from TMZ-resistant GBM cell lines and primary spheres. We narrowed the miRs to miR-93 and -193 and showed in computational analyses that they could target Cyclin D1. Since Cyclin D1 is a major regulator of cell cycle progression, we performed cause-effect studies and showed a blunting effects of miR-93 and -193 in Cyclin D1 expression. These two miRs also decreased cell cycling quiescence and induced resistance to TMZ. Taken together, our data provide a mechanism by which GBM cells can exhibit TMZ-induced resistance through miRNA targeting of Cyclin D1. The data provide a number of therapeutic approaches to reverse chemoresistance at the miRNA, exosomal and cell cycle points.

**Keywords: glioblastoma, cell cycle, chemoresistance, microRNA, Cyclin D**

## INTRODUCTION

Glioblastoma multiforme (GBM) is the most common adult primary brain tumor. In addition, GBM is also the most lethal brain cancer with a 5-year survival rate of ∼8% (Naydenov et al., 2011). GBMs uniformly acquire resistance to the front-line alkylating chemotherapeutic agent, Temozolomide (TMZ) (Jiang et al., 2011). Multiple mechanisms of TMZ resistance have been previously described such as an increase in the Multiple Drug Resistance (MDR) efflux, base pair excision, gene methylation and cell cycle arrest (Johannessen and Bjerkvig, 2012).

Cell cycle progression requires the concerted activity of a number of factors both positive and negative (Louis, 2006). Cyclin D1 is a G1 phase protein that facilitates the progression of cells into S phase. The expression and degradation of Cyclin D1 is highly regulated to coordinate the temporal role of Cyclin D1 (Freemantle et al., 2007). Since microRNAs (miRs) have been linked to

chemoresistance, we studied if miRNAs, through the regulation of Cyclin D1, affected the response of GBM cells to TMZ.

miRNA are small RNA molecules (18–22 base pairs) that regulate protein expression by binding to the non-coding regions of mRNA to inhibit translation (Sen et al., 2014). Increasing evidence has shown roles for miRNAs in development, differentiation and malignancy (Di Leva et al., 2014). In addition, miRNAs have been shown to have a key role in the acquisition and maintenance of chemoresistance (Tezcan et al., 2014). miRNAs can also target multiple regulators of cell cycle progression including Cyclin D1 (Zhao et al., 2014; Huang et al., 2015).

Exosomes are endosomal in origin and can function as a mediator of contact-independent communication among cells (Pant et al., 2012). The exosomes contain RNA including non-coding miRNA, DNA and proteins (Thery et al., 2002). Due to their ability to mediate intercellular communication, exosomes could also serve as vehicles for miRNA-based therapy (Munoz et al., 2013). An understanding of how miRNAs affect GBM pathophysiology will offer opportunities for novel therapeutic approaches. This study shows describes roles for two miRNAs, miR-93 and -193, in regulating Cyclin D1 expression. We also demonstrated that the regulation of Cyclin D1 by these two miRNAs led to TMZ resistance in GBM cells.

## MATERIALS AND METHODS

### Cell Lines

U87 and T98G cells were purchased from American Type Culture Collection (ATCC; Manassas, VA) and then expanded as per manufacturer's instructions.

### Reagents and Antibodies

All tissue culture media were purchased Life Technologies Gibco (Grand Island, NY), fetal calf serum (FCS) from Hyclone Laboratories (Logan, UT), TMZ from Sigma Aldrich (St. Louis, MO) and, anti-Cyclin D1, anti-β-actin, HRP-anti-rabbit and HRP-anti-mouse IgG from Cell Signaling (Danvers, MA).

### Real-Time RT-PCR

RNA was extracted with Trizol reagent (Invitrogen). Reverse transcription with 200 ng of cDNA was performed with the High Capacity cDNA Reverse Transcription Kit (Applied Biosystems) in accordance with the manufacturer's recommendation. Real-time PCR was performed on 7300 Real-Time PCR System (Life Technologies Applied Biosystems, Grand Island, NY) using the following cycling profile: an initial incubation of 50°C for 2 min, 95°C for 10 min, 40 cycles at 95°C for 15 s and 60°C for 60 s. All primers were purchased from Sigma. The relative expression was calculated using the 2(–Delta Delta C(T)), as previously described (Lim et al., 2011).

### Western Blot

Temozolomide resistant GBM cells were prepared as previously described (Munoz et al., 2014b). Briefly, GBM cells were incubated with 200 μM of TMZ or vehicle (control). At different times during treatment with TMZ, whole cell extracts were isolated with M-PER Mammalian Protein Extraction Reagent (Thermo Fisher Scientific, Danvers, MA). The cell extracts (10 μg) were analyzed by western blots, as previously described (Park et al., 2013). Briefly, the samples were electrophoresed on 12% SDS-PAGE gels (Bio-Rad, Hercules, CA). The proteins were transferred onto PVDF membranes (Perkin Elmer, Boston, MA). The membranes were incubated overnight with primary antibodies at a final dilution of 1/1000. Primary antibodies were detected during a 2-h incubation period with HRP-conjugated IgG at 1/2000 final dilution. HRP activity was detected by chemiluminescence using SuperSignal West Femto Maximum Sensitivity Substrate (Thermo Fisher Scientific, Danvers, MA). Membranes were stripped with Restore Stripping Buffer (Thermo Fisher Scientific) prior to being reprobed with other antibodies.

### Short Interference RNA (siRNA) Targeted Knockdown

Dicer1 targeting-siRNA pooled duplexes (Dharmacon, Lafayette, CO) knocked down Dicer1 in GBM cells using methods, previously described (Munoz et al., 2014c). Briefly, GBMs ($10^4$) were seeded in 12-well plates. After 24 h, 30 nM siRNA was delivered into the cells using Lipofectamine RNAiMax (Life Technologies). Control cells were transfected from non-targeting siRNA duplexes (Dharmacon).

### miRNA Analyses

Stem Cell miRNA Profiling Panel with 95 miRNAs were purchased from System Biosciences (Palo Alto, CA). The analyses followed manufacturer's protocol. Total RNA was isolated from exosomes using Trizol® and then analyzed by qPCR. Since nuclear U6 internal control would not be detected in exosomes we selected the miRNAs with absolute changes between vehicle and TMZ-resistant cells. In this regard, the selected miRs were undetectable in vehicle-treated cells and detectable in with TMZ resistance.

### Cell Cycle Analyses

Cell cycle analyses were performed by labeling with propidium iodide (PI) or 7-AAD, as described (Lim et al., 2011). GBM cells ($10^6$) were washed in PBS and then resuspended in 0.1% hypotonic sodium citrate solution containing 5 μg/ml PI and 200 μg/ml DNase-free RNase A. Cells were incubated for 30 min at room temperature and then immediately acquired on FACSCalibur (Becton Dickson, San Jose, CA) and then analyzed with the ModFit software (Verity Software House). 7-AAD labeling were done with 1 μg/mL for 20 min. After this, the cells were washed and then immediately analyzed as for PI labeling.

### Caspase Activity

GBM cells ($10^4$) were studied for caspase activity using Vybrant® FAM Caspase-3 and -7 Assay Kit (Thermo Fisher Scientific). The method was performed according to the manufacturer's protocol. The cells were evaluated by flow cytometry using the FACS Calibur (Becton Dickinson).

## Exosome Isolation and Characterization

Exosomes were isolated using a multi-step process. First, large particles were removed by sequential centrifugation up to 50,000 *g* (Lim et al., 2011). The remaining particles were pelleted by ultracentrifugation (Sorvall mTx 150, Thermo Fisher Scientific, Springfield, NJ) at 100,000 *g* for 18 h. The recovered vesicles were analyzed for tetraspaninins (CD63 and CD81) by western blot and flow cytometry. The latter method used CD63 magnetic bead isolation. The exosomes were captured onto the beads and then labeled with CD63-FITC and anti-CD81-APC (BD Biosciences).

The recovered particle size was verified by Nanoparticle tracking analysis (NTA) using a NanoSight NS300 instrument (Amesbury, United Kingdom) as described (Bliss et al., 2016). The data were analyzed with the NTA software (NANOSight version 2.3) using dilutions with deionized water.

## Statistical Analyses

Data were analyzed using the students *t*-test using two comparable groups (control/experimental). A $p$ value of less than 0.05 was considered significant.

# RESULTS

## Analyses of GBM Cell-Derived Exosomes

Prior to testing the role for exosome-containing miRNA in TMZ-resistance, we studied the exosomes by phenotype and size to ensure no contamination with other microvesicles such as apoptotic bodies. Exosomes were isolated from the culture media of GBM cells, treated with vehicle (DMSO) or with TMZ (induced resistant cells). The latter was achieved with 200 μM TMZ for 72 h, as described (Munoz et al., 2014a). Due to the endosomal origin of exosomes, they were characterized for two tetraspanin proteins, CD63 and CD81. Western blot showed bands for CD63 and CD81 with a relatively light band for vehicle-treated U87-derived exosomes (**Figure 1A**). A second set of analyses used metallic microbeads with bound anti-CD63 to capture all exosomes (**Figure 1B**, top). The exosomes were detected by double labeling with anti-CD63-FITC and anti-CD81-APC. Flow cytometric analyses indicated expressions of CD63 and CD81, although with varied fluorescence intensities (**Figure 1B**, lower panels). The size of exosomes were analyzed by NTA, which showed a narrow histogram with average size of 100 nm, indicating homogeneity of the exosome size (**Figure 1C**; Beach et al., 2014).

## Selected miRNAs in TMZ-Resistant Exosomes

Next, we asked if the contents of exosomes might begin to explain the cyclin state of GBM resistance. We compared the exosomal miRNAs from TMZ-resistant U87 and T98G cells with vehicle (DMSO)- treatment using a PCR-based array with 95 miRNAs linked to cell cycle. We selected those that showed an absolute increase from vehicle for each cell line. Next, we narrowed the selection for those that showed consistency in both cells lines. This resulted in five miRNAs (miR-19b, 23a, 93, 193b, and 373) (**Figure 1D**). The left bar was included to show that these five miRNAs were undetected in the untreated and vehicle-treated GBM cells (#ND = not detected).

We next validated the array studies by real-time PCR using RNA from naïve (untreated and vehicle treatment) and TMZ-resistant U87 and T98G cells. The resistant cells were acquired by treating with 200 μM TMZ for 72 h. In addition to the five miRNAs shown in **Figure 2A**, we also included miR23b. The values obtained with exosomes from vehicle and untreated GBM cells were similar and were arbitrarily assigned values of 1. The changes in miRNAs from TMZ-resistant exosomes were presented as fold change over vehicle/untreated exosomes. MiR-19b, 23a/b, 93, 193b, and 373 expressions ranged between 2 and 8 folds (**Figure 2A**). Based on these results, we experimentally assigned these miRNAs as the signature profile for TMZ-resistant GBM cells.

## Narrowing the Signature miRNA Profile in Early Passage Primary GBM Cells

U87 and T98G cells were long-term passaged cells that were artificially established as chemoresistance GBM cells. We therefore asked whether the identified profile of miRNA was similar to low-passage GBM cells from patients. We used two primary cells that were established as neurospheres from GBM patients. These cell lines were previously described (Munoz et al., 2014a). BT145 was derived from a patient that never received TMZ therapy and BT164, from a patient refractory to TMZ treatment. Both cell lines retained similar properties in culture with regard to TMZ sensitivity.

RNA from neurosphere cultures (BT145 and BT164) were analyzed by TaqMan® qPCR for miR-19b, 23a/b, 93, 193b, and 373. The results showed >2 fold increases in miR-93b, 193 and 373 in BT164 cells (TMZ resistant) as compared to BT145 cells (TMZ sensitive) (**Figure 2B**). MiR-19 was <2 fold in BT164/BT145 cells. MiR-23a and MiR-23b were undetected in both cell lines. Based on these results, further analyses on TMZ resistance focused on miR-93b, 193 and 373.

## Predicted Function for miR-93b, 193 and 373

We used Ingenuity® miRNA target analyses from reports in the literature and identified miR-19, 23a/b, 93b, 193 and 373 as individual target of CCND1 (Cyclin D1) (**Figure 2C**; **Supplementary Material**). We therefore mapped these miRNAs on the CCND1 3′ UTR of Cyclin D1 (*CCND1*) using TargetScan®. The analyses revealed a cluster of miR-93 and miR-193 in the 3′ UTR of CCND1 (**Figure 2D**). We next examined previous information from >500 Agilent arrays from The Cancer Genome Atlas (TCGA) and also noted increases in miR-93b and miR-193 (Munoz et al., 2014a). Based on these we narrowed the number of miRNAs to -93 and -193 in further studies.

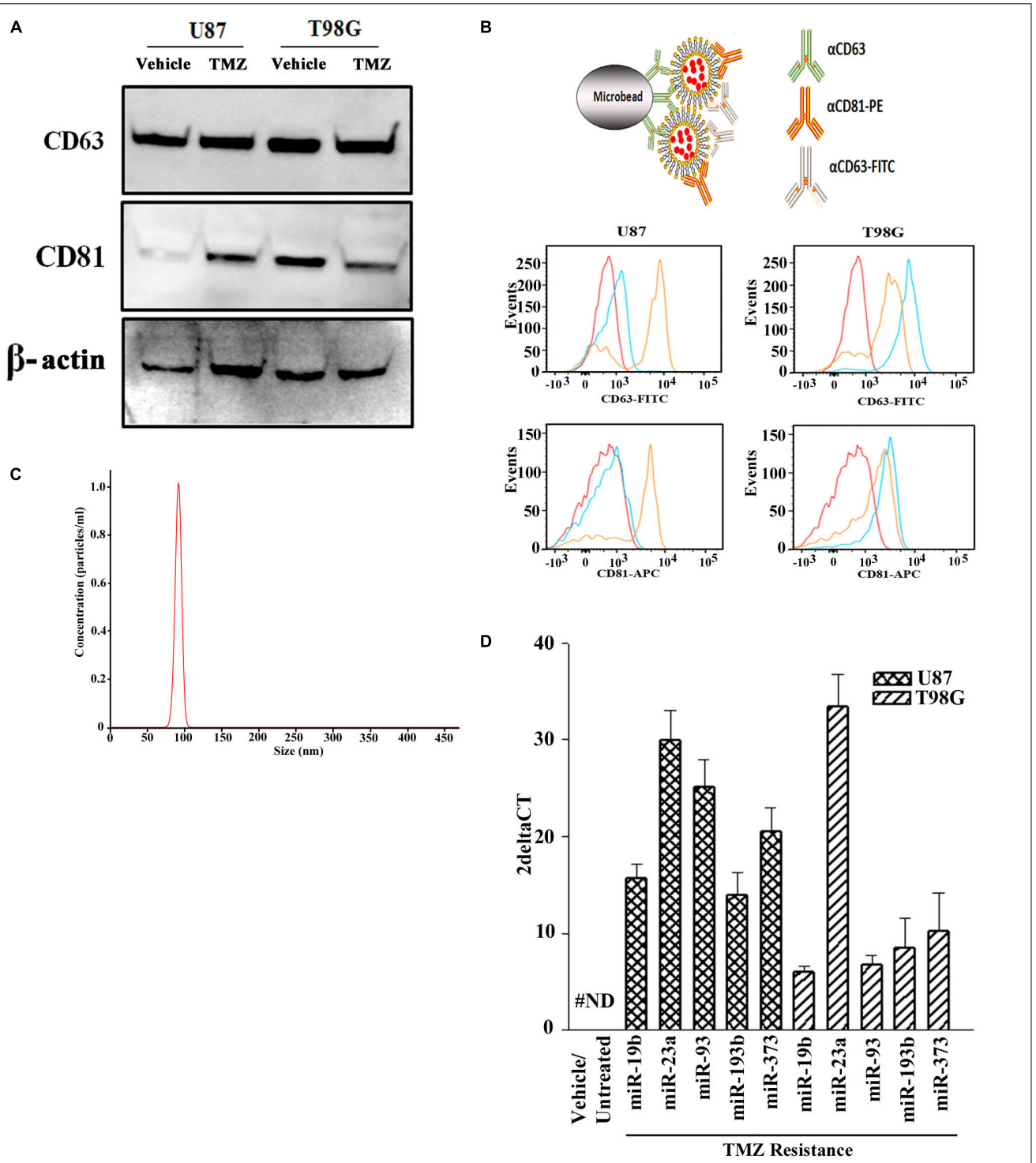


**FIGURE 1 |** miRNA profile in TMZ resistant GBM cells (U87 and T98G). **(A)** Exosomes were collected from vehicle- and TMZ-treated GBM cells and then analyzed for CD63 and CD81 by western blot. The membrane was stripped and reprobed for β-actin. **(B)** The carton (top) demonstrates how exosomes were immunoprecipitated with microbeads conjugated to anti-CD63. The microbeads were incubated with exosomes from vehicle- or TMZ-resistant GBM cells. After this, the beads were incubated with anti-CD81-PE and anti-CD63-FITC. Control beads were incubated with isotype control. The beads were analyzed by flow cytometry: red, negative/isotype control, blue untreated, yellow TMZ-treated). **(C)** Additional analyses of the exosomes were done by NTA. A represented histogram is shown demonstrating the average size of 100 nm. **(D)** The miRNAs from the arrays in TMZ-resistant cells and naïve (untreated and vehicle treatment) GBM cells. The results are presented as $2^{\Delta}$CT ($n$ = 3, ±SD).

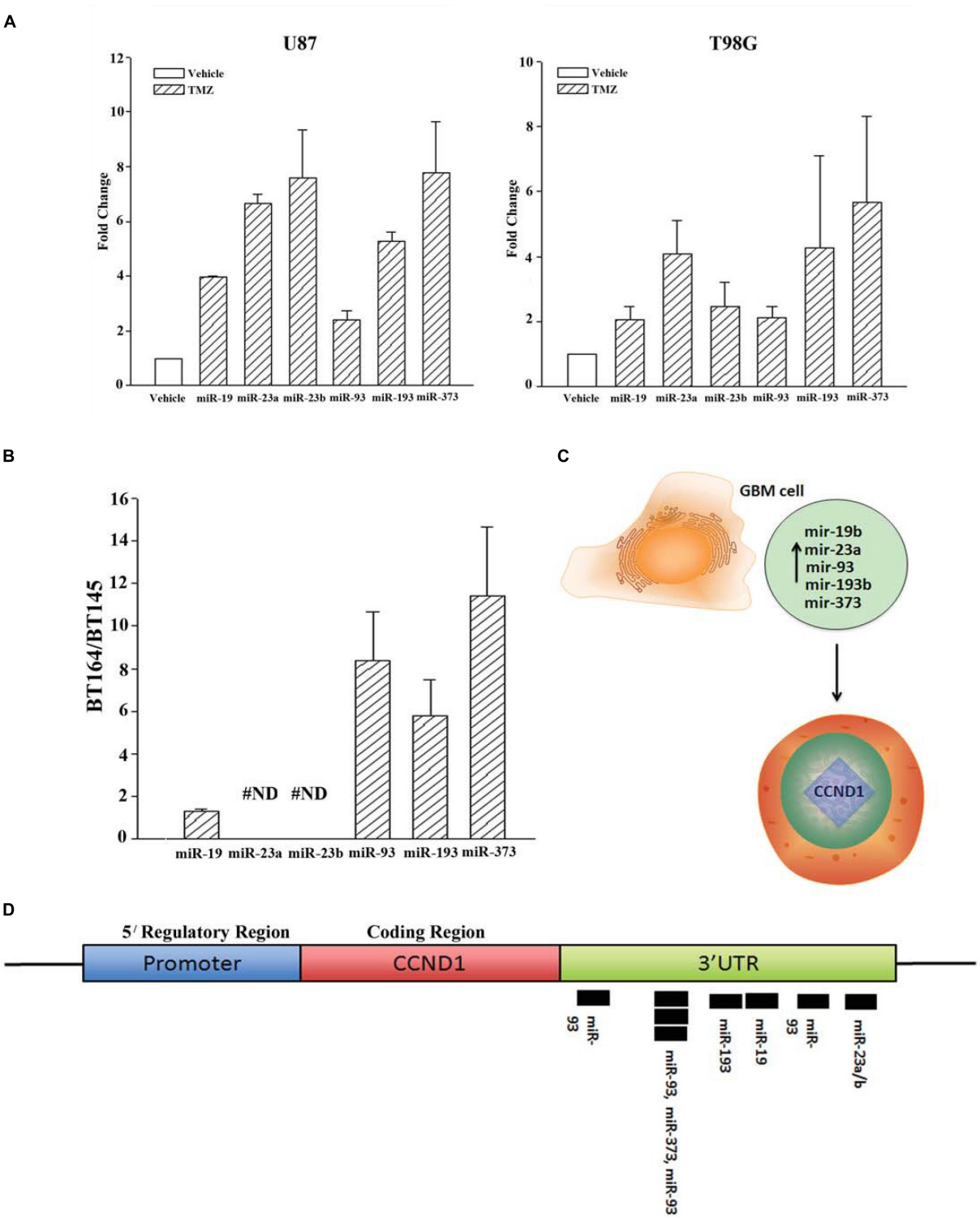


**FIGURE 2 |** Validation of miRNAs from TMZ-resistant GBM cells and identifying the target. **(A)** Real time PCR was performed for the miRNAs shown to be increased in array studies (**Figure 1D**). Real-time PCR for miR-19, -23a/b, -93, -193 and -373 was performed with RNA from vehicle-treated and TMZ-resistant U87 and T98G cells. The values for vehicle were assigned 1 to calculate fold changes in the TMZ-resistant GBM cells ($n = 4 \pm$ SD). **(B)** Real time PCR was performed for the miRNAs studied in "A" using RNA from low-passage BT164 (TMZ resistant) and BT145 (TMZ naïve). The results are presented as the ratio of normalized Ct values of BT164/BT145 ($n = 4$, ±SD). ND = none detected. **(C)** Ingenuity® miRNA analyses identified specific miRNAs as targets for *CCND1* (Cyclin D1). **(D)** The miRNAs, identified in "C," are shown for predictive binding sites on the 3′UTR of cyclin D1 (CCND1).

## Decreased Cyclin D1 in TMZ-Resistant GBM Cells

The results shown in **Figure 2** predicted miR-23, -93 and 193 as targets of Cyclin D1. However, we did not pursue studies on miR-23 since it was not detected in primary resistant GBM spheres. First, we studied the expression of Cyclin D1 in vehicle and TMZ-resistant GBM cells by real-time PCR and western blot. Real time PCR showed a significant ($p < 0.05$) reduction in Cyclin D1 mRNA in TMZ-treated cells (**Figure 3A**). Western blots also showed a significant ($p < 0.05$) reduction in Cyclin D1 in the TMZ-resistant GBM cells as compared to untreated/naïve GBM cells (**Figure 3B**, normalized densities in lower panel). In summary, the results showed decreased expression of Cyclin D1 in TMZ-resistant GBM cells.

## Cell Cycle Analyses of Naïve and TMZ-Resistant GBM Cells

The decrease in Cyclin D1 at the levels of mRNA and protein did not indicate function. We therefore performed cell cycle analyses using Propidium Iodide (PI) DNA labeling. Vehicle-treated U87 showed 57.3% cycling (G2+S+M), which was reduced to 14.4% in the TMZ-resistant cells (**Figure 3C**). Vehicle-treated T98G cells showed 48.3% cycling cells (G2+S+M), which was reduced to 32.9% in the TMZ-resistant cells. Since TMZ generally resulted in cells in G2 phase of the cell cycle, we repeated the cell cycle analyses with 7-AAD labeling. In three independent experiments, the percentages of cells in G2 phase of the cell cycle after TMZ treatment doubled as compared to vehicle (**Figure 3C**). In summary, the results indicated a correlation between TMZ resistant with reduced expression of Cyclin D1.

## Dicer1 Knockdown in TMZ Resistant GBM Cells Prevented a Decrease in Cyclin D1

The studies shown in **Figure 3** did not prove that the miRNAs were involved in the reduction of Cyclin D or even cycling quiescence. Prior to studies on the specific miRNAs, we first asked if miRNAs are involved in cycling quiescence of TMZ resistant GBM cells. This was addressed by knockdown of Dicer, which is a type III RNase and a key enzyme in the maturation of miRNAs (Adams and Eischen, 2014; van den Beucken et al., 2014). We established resistant GBM cells in which Dicer 1 was knocked down, as previously described (Munoz et al., 2014a). U87 and T98G cells were transfected with control oligonucleotides or Dicer-targeting siRNA and then treated with 200 μM TMZ for 72 h.

Real time PCR for cyclin D1 indicated ∼2-fold increase in the Dicer1 knockdown/TMZ-resistant U87 and T98G cells over control siRNA (**Figure 4A**). The values for control Dicer siRNA were normalized to 1 (**Figure 4A**). Western blot for Cyclin D1 indicated a significant ($p < 0.05$) increase (∼3 fold) in band densities in the knockdown/TMZ-resistant GBM cells, as compared to control siRNA (**Figure 4B**). Since dicer is needed for maturation of pre-miRs, its knockdown supported a role for miRNA in controlling the expression/decease of Cyclin D1 in TMZ-resistant GBM cells.

## Pre-miR-93 and -193 Reduced Cyclin D1 in GBM Cells

MiR-93 and -193 were increased in exosomes from TMZ-resistant cell lines and in resistant GBM spheres from a patient (short-term passage cells) (**Figure 2**). Furthermore, miR-93 and -193 were also increased in primary GBM tissues, based on the data deposited in TCGA [13]. Since TMZ led to a decrease in cycling cells (**Figure 3C**), and Dicer knockdown caused an increase in the levels of Cyclin D1 (**Figure 4**), we asked if miR-93 and -193 could decrease the expression of cyclin D1 in U87 and T98G cells.

U87 and T98G cells were transfected with control precursor (pre)-miR, pre-miR-93 or pre-miR-193. Real-time PCR validated the efficiency of transfection, as indicated by >500-fold increase of the transfected pre-miRNAs over control pre-miRs, whose values were assigned 1 (**Figure 5A**). Real time PCR for Cyclin D1 indicated a significant ($p < 0.05$) decrease in Cyclin D1 mRNA in the pre-miR-93 and pre-miR-193 transfectants (**Figure 5B**).

Next, we investigated if pre-miR-93 and pre-miR-193 can decrease Cyclin D1 protein in the TMZ-treated GBM cells by western blots. U87 and T98G were transfected with pre-miR-93, pre-miR-193, control pre-miR or untransfected. After this, the cells were treated with 200 μM TMZ for 72 h. The cell extracts were then studied for Cyclin D1. As compared to untransfected and cells transfected with control miRNA, there was a significant ($p < 0.05$) decrease in Cyclin D1 protein in the pre-miR-93 and pre-miR-193 transfectants (**Figure 5C**, normalized band densities shown below for three independent experiments). In summary, this section showed pre-miR-93 and -193 as mediators of cyclin D1 expression.

## MiR-93 and -193 Enhanced TMZ-Mediated Cycling Quiescence of GBM Cells

TMZ treatment increased miR-93 and -193 levels with concomitant decrease in the cycling of GBM cells (**Figures 2**, **3**). Also, transfection with miR-93 and -193 decreased Cyclin D1 (**Figure 5**). We therefore asked if miR-93 and -193 can decrease GBM cell cycle, and whether this can be enhanced by TMZ.

U87 and T98G cells were transfected with pre-miR-93, pre-miR-193 or control pre-miRNA, and then treated with vehicle or 200 μM TMZ. At 72 h, the cells were studied for cycling phase by PI or 7-AAD labeling. Vehicle-treated U87 cells, transfected with control pre-miRNA showed 15.3% cells in cycling phase (G2+S+M), which was increased to 56.6% by TMZ, indicating arrest (**Figure 6A**). Transfection with pre-miR-93 led to a change in 59.1 to 13.7% cycling with TMZ (**Figure 6C**, left panels). Similar studies with pre-miR-193 reduced cell cycling from 41.7 to 11.1% following TMZ treatment (**Figure 6C**, right panels).

Studies with T98G showed similar changes with regards to cell cycle. Vehicle-treated T98G cells, transfected with control pre-miRNA, showed 19.4% cycling (G2+S+M), which was increased

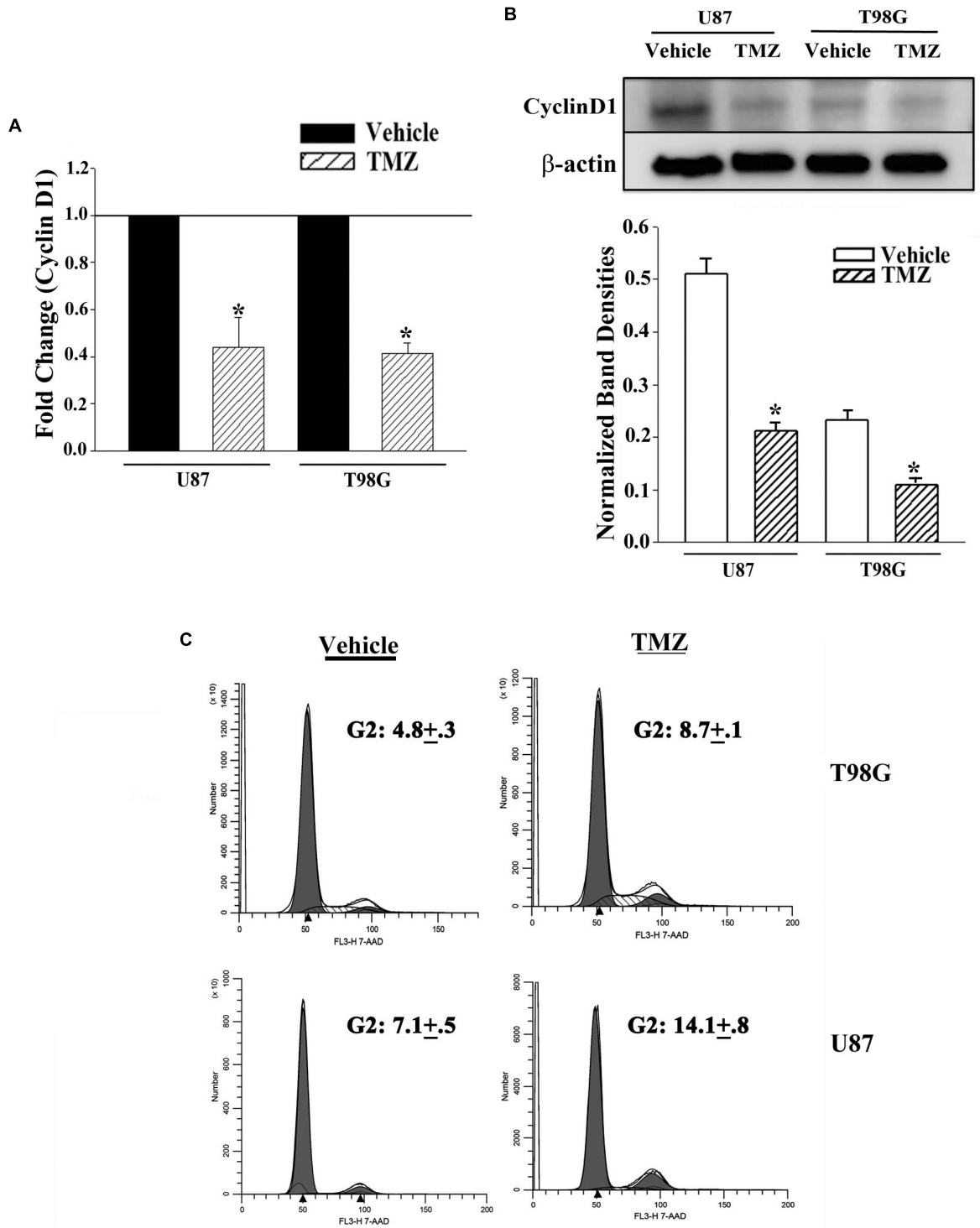


**FIGURE 3 |** Decrease in Cyclin D1 in TMZ resistant GBM cells and cycling quiescence. **(A)** Real time PCR was performed with RNA from vehicle- and TMZ-treated U87 and T98G for Cyclin D1 mRNA. The normalized values for vehicle treatment are assigned 1 and the treated cells are presented as fold change (±SD, $n = 4$). **(B)** Western blots were performed with cell extracts from vehicle and TMZ-treated U87 and T98G for Cyclin D1. The blot was stripped and reprobed for β-actin. The normalized band densities are presented as the mean ± SD of three different experiments. **(C)** U87 and T98G cells were labeled with 7-AAD in three independent experiments. The figure shows representative histograms. * $p < 0.05$ vs. vehicle treatment.

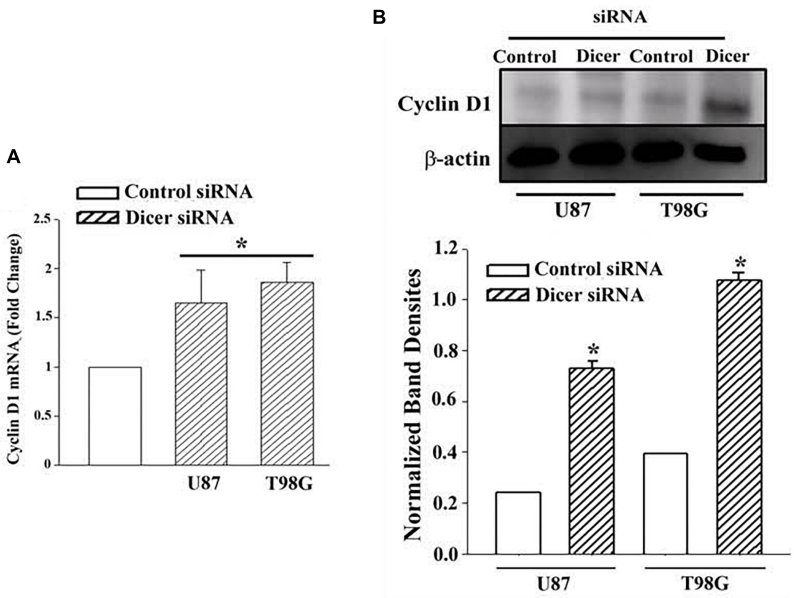


**FIGURE 4 |** Cyclin D1 in TMZ-resistant, Dicer knockdown GBM cells. U87 and T98G cells were transfected with Dicer siRNA or control siRNA. After this, the cells were treated with 200 μM TMZ for 72 h and then analyzed for Cyclin D1 mRNA by real time PCR **(A)** and western blot **(B)**. Normalized band densities for three western blots (±SD) are shown in the graph of "A." *$p < 0.05$ vs. control siRNA.

to 58% by TMZ treatment (**Figure 6B**). Vehicle-treated pre-miR-93 transfectants resulted in 41.8% cycling cells and this was reduced to 12.9% by TMZ (**Figure 6D**, left panels). Similarly, pre-miR-193 with vehicle showed 43.2% and decrease to 11% cycling in TMZ-treated cells (**Figure 6D**, right panels). In summary, in the presence of TMZ, miR-93 and -193 independently enhanced cell cycle quiescence of GBM cells.

## MiR-93 and miR-193 Induced Chemoresistance in GBM Cells

Thus far, we showed miR-93 and -193 could enhance cell cycle quiescence in GBM cells and this correlated with a decrease in Cyclin D1 (**Figures 5**, **6**). In this set of studies, we asked if the increases in miR-93 and -193 could contribute to TMZ resistance. To address this question, we studied the cells for total and cleaved caspase 3. U87 and T98G were untransfected or transfected with control pre-miR, miR-93 or miR-193. The cells were treated with 200 μM TMZ for 72 h or with vehicle. Cell lysates were analyzed for total and cleaved caspase 3 by western blot. The percent caspase 3 activity was calculated as the band densities of cleaved caspase 3/(cleaved + total caspase 3).

Treatment of untransfected GBM cells with TMZ showed intense caspase activity and this was comparable to control pre-miR (**Figure 7A**, two left diagonal bars). Parallel studies with pre-miR-93 and -193 transfectants showed marked decrease in band densities (**Figure 7A**, two right diagonal bars). This decrease was not noted for vehicle-treated cells (**Figure 7B**, open bars).

Next, caspase 3 activity was studied by fluorescent DEVD (Caspase cleavage sequence). The analyses used the Vybrant® FAM™ caspase-3 and -7 assay. GBM cells were transfected with control pre-miR, pre-miR-93 or pre-miR-193 and then treated with 200 μM TMZ. After 72 h, the cells were analyzed by flow cytometry. The results showed reduced caspase 3 activity in U87 and T98G cells, transfected with pre-miR-93 and -193 and treated with TMZ (green histogram) as compared to vehicle (solid purple histogram) (**Figure 7B**). Taken together, the two approaches used to study caspase activity in GBM cells transfected with miR-93 and miR-193 indicated induced TMZ resistance.

# DISCUSSION

GBM has continued to present with a poor prognosis for patients despite surgical intervention, chemo- and radiotherapy. Resistance to chemotherapy occurs uniformly and the mechanisms underlying this resistance are an area of extensive research (Spinelli et al., 2012). Yet, no therapies circumventing TMZ resistance have progressed to clinical therapy and improved patient outcome. This may be partially due to the diverse and numerous mechanisms employed by GBM cells to resist TMZ therapy. We have previously described three mechanisms of resistance in GBM cells treated with TMZ, increased intracellular communication (Munoz et al., 2014a), miRNA regulation of Sonic Hedgehog signaling (Munoz et al., 2014a), and EGFR regulation of the MDR1 gene (Munoz et al., 2014a). This study analyzed the changes in the miRNA content of exosomes from TMZ resistant GBM cells and then determine how this regulated Cyclin D1. These findings reveal yet another mechanism by which GBM cells resist TMZ, similar to another report (Chen et al., 2016).

Recently exosomes have become an important area of research (Beach et al., 2014). Exosomes serve as a functional method

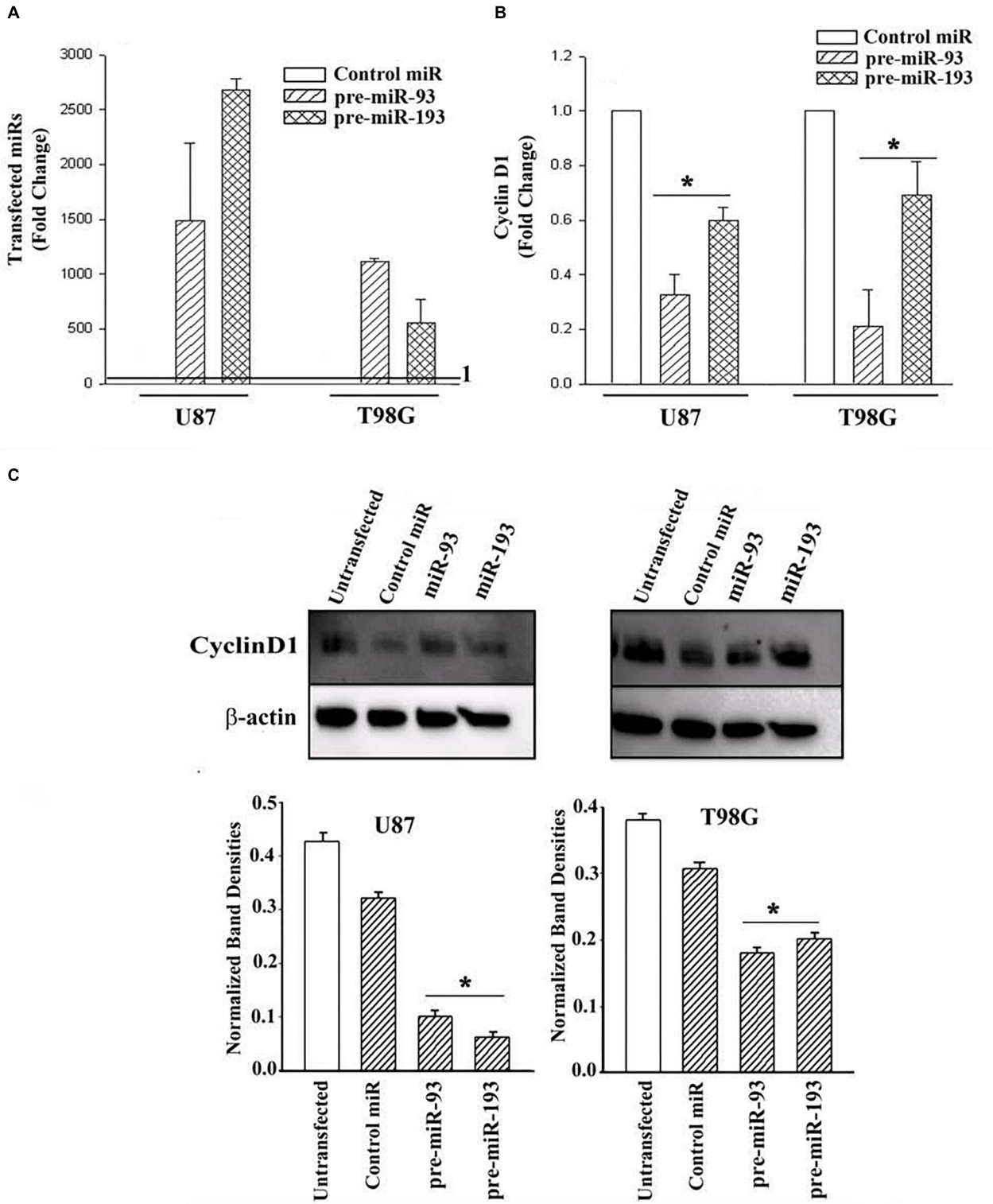


**FIGURE 5 |** Cyclin D1 expression in miR-93/-193 GBM transfectants treated with TMZ. **(A)** Real time PCR for control miR, miR-93 and miR193 with RNA from U87 and T98G, transfected with the respective pre-miRs. The results are presented as the mean (±SD, $n = 3$) fold change of control. The controls for both primers are set at values of 1. **(B)** The transfectants in "A" were studied for cyclin D1 and the results are presented as mean fold change (±SD, $n = 3$) over the transfectants with control pre-miR. The control pre-miR was assigned values of 1. **(C)** The transfectants in "A" were treated with 200 μM TMZ. After 72 h, the viable cells were studied for Cyclin D1. An additional control with untransfected cells was included in the blot. The mean (±SD, $n = 3$) normalized band densities are shown in the graphs.
* $p < 0.05$ vs. control miR.

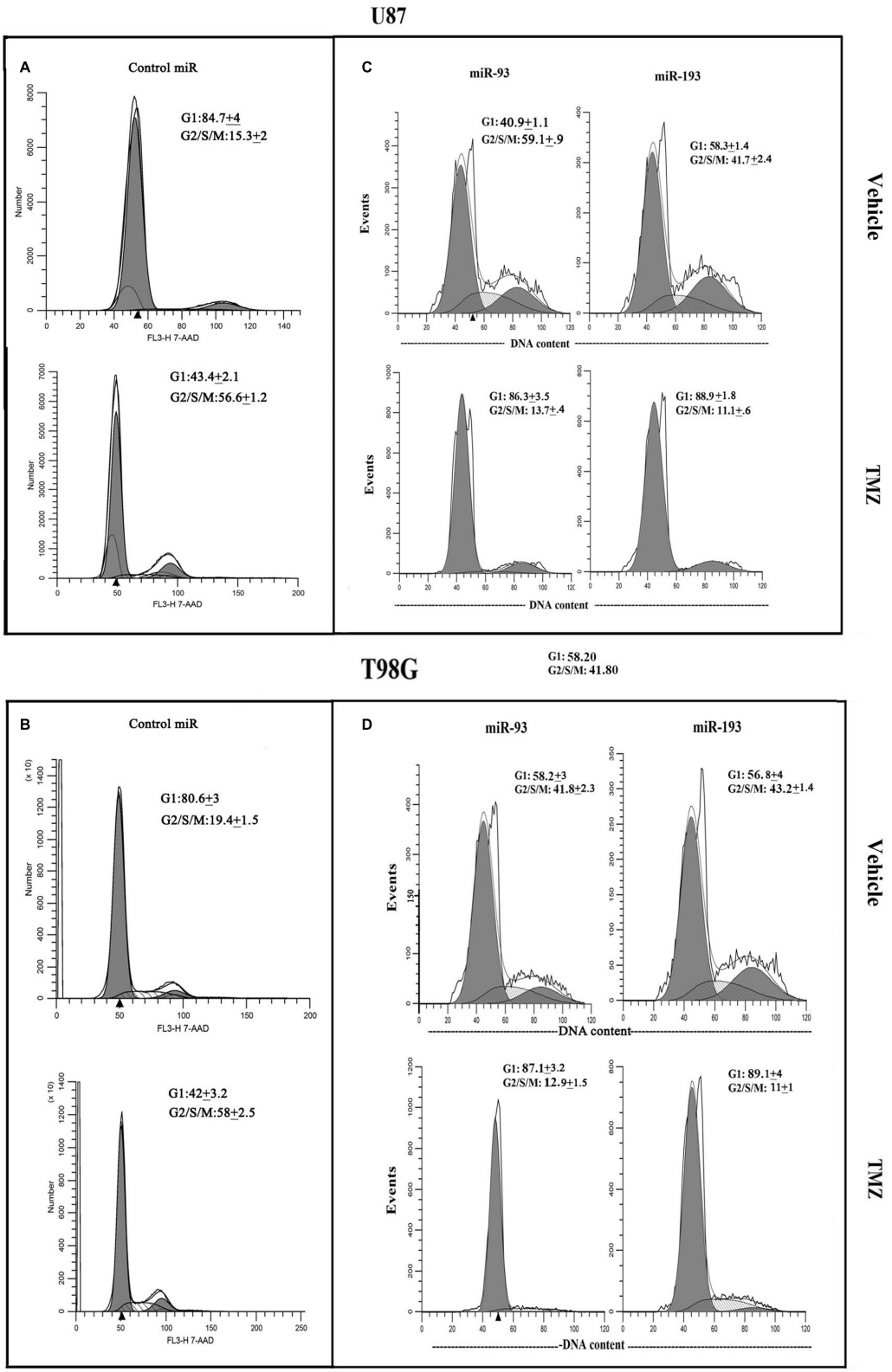


**FIGURE 6 |** Cell cycle phase of TMZ-treated GBM cells, transfected with pre-miRs. U87 (**A** and **C**) and T98G (**B** and **D**) cells were transfected with control pre-miRs, pre-miR-93 or pre-miR-193. The cells were treated with vehicle or 200 μM TMZ. After 72 h the cells were analyzed for cell cycle by propidium iodide (miR-93 and -193) treatment and 7-AAD for control miR. The results represent three independent experiments.

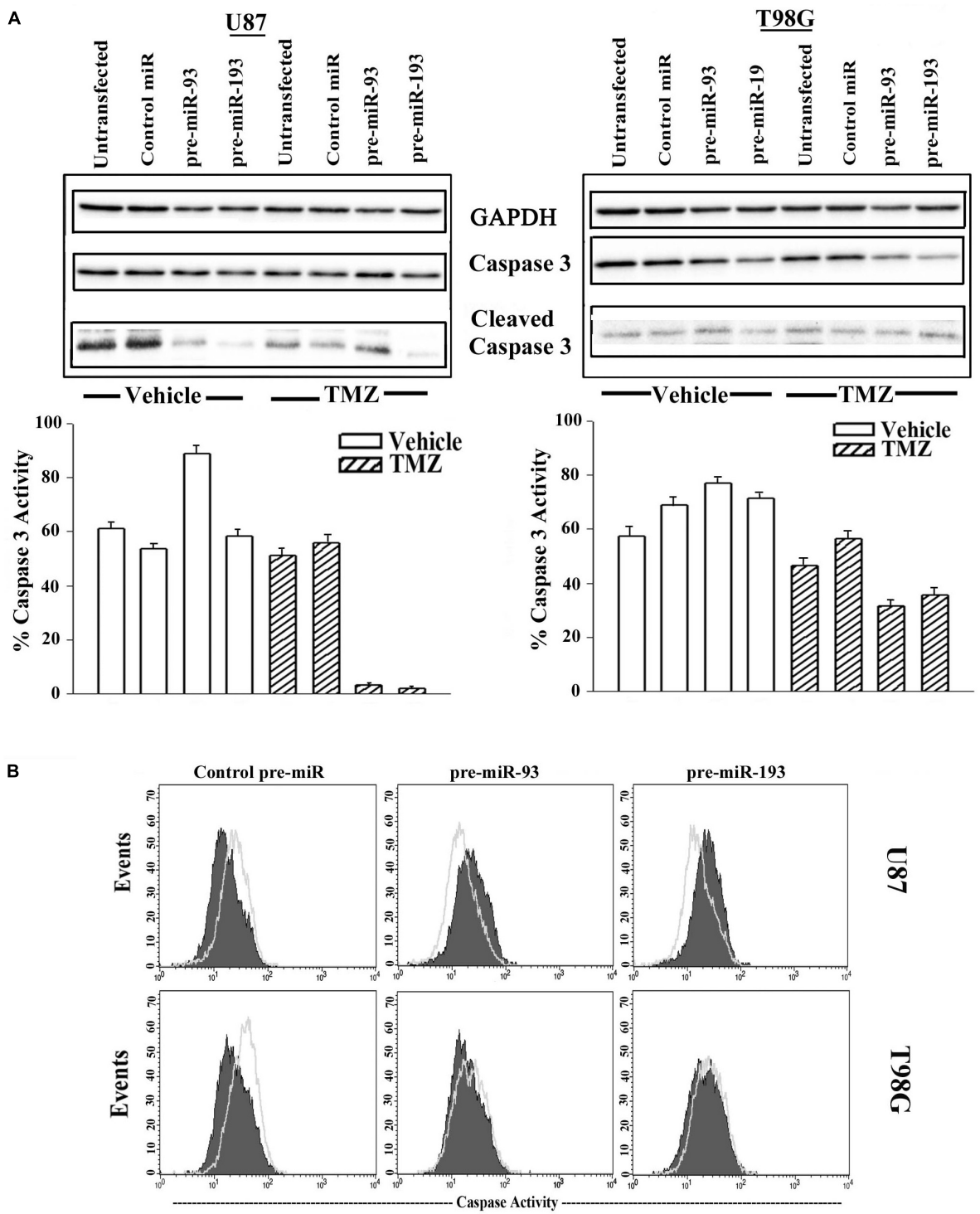


**FIGURE 7 |** Active caspase 3 in TMZ and pre-miR-93 and -193 transfected GBM cells. **(A)** U87 and T98G cells were untransfected for transfected with control pre-miR, pre-miR-93 or -193. The cells were treated with vehicle or 200 μM TMZ for 72 h. Whole cell extracts were analyzed in western blots for total caspase 3 and cleaved caspase 3. The normalized band densities were presented as the % caspase activity ((cleaved caspase/total + cleaved caspase) × 100%) (lower graphs). **(B)** U87 and T98G were transfected with control pre-miR, pre-miR-93 or -193. The cells were treated with vehicle or 200 M TMZ for 72 h. The cells were labeled intracellularly for cleaved caspase 3 (open histogram) and total caspase (solid histogram).

of contact-independent communication between cells and can function as a tool for cellular-based therapy (Munoz et al., 2013). Thus, we isolated exosomal miRNA from vehicle and TMZ- treated GBM cells. A miRNA array was then performed and validated with both whole cell RNA samples and neurosphere lines derived from TMZ-sensitive and –resistant patient samples (**Figure 1**). At that time four miRNAs were identified as solely present in TMZ resistant cells (**Figure 2**). When compared to data from TCGA, miR-93 and -193 were upregulated in >500 TCGA samples. Interestingly, miR-93 has been shown to regulate AKT signaling in Cisplatin-resistant Ovarian Cancer cells (Fu et al., 2012) and miR-193 has been shown to be upregulated in TMZ- resistant GBM cells, but no target has been identified (Hiddingh et al., 2014). Also, similar to our findings, miR-93 have been shown to promote the malignancy of GBM partly via TMZ resistance (Chen et al., 2016). This was an interesting report as it confirms our findings shown a link between miR-93 and Cyclin D.

miRNA Pathway analyses with Ingenuity® revealed published data showing regulation of Cyclin D1 by miR-93 and miR-193 (Chen et al., 2010; Yu et al., 2011). We then looked at expression of Cyclin D1 RNA and protein in TMZ treated GBM cells and noted a significant ($p < 0.05$) reduction in its expression as compared to vehicle (DMSO)-treated cells (**Figures 3A,B**). Cell cycle analyses by flow cytometry also showed retention of the cells in G1/0 phase following TMZ exposure (**Figure 3C**). miRNA biosynthesis requires cleavage by the RNase type III, Dicer1. To evaluate a role for miRNA regulation of Cyclin D1, Dicer1 was knocked down by targeting siRNA. Dicer1 knockdown restored Cyclin D1 expression in TMZ treated cells, indicating a role for miRNA in the cycling quiescence of TMZ-treated GBM cells. Dicer1 knockdown has also been shown to increase GBM sensitivity to TMZ (Munoz et al., 2014a). We then transfected GBM cells with precursor miRNA-93 and -193 and this caused resulted in a significant ($p < 0.05$) decrease in Cyclin D1 with concomitant cycling quiescence (**Figures 5C**, **6**). These two miRNAs also protected the GBM cells from cell death, despite the presence of TMZ (**Figure 7A**). Taken together, these experiments showed a role for miRNA in the regulation of Cyclin D1 in TMZ-exposed GBM cells.

miRNAs have become an area of research with great potential. miRNA not only regulate important cellular processes, but also offer an avenue of therapeutic intervention (Shibata et al., 2015). This study shows how two miRNAs, working in concert, to target Cyclin D1 to induce cycling quiescence of GBM cells. Cellular proliferation is a hallmark trait of cancer; yet, cancers cells have shown reduction of cell cycle progression as a method to evade chemotherapies depending on DNA synthesis such as alkylating agents (Miwa et al., 2015). Thus, the findings in this paper allow for the development of miRNA targeting therapy as an option to overcome this mechanism of TMZ resistance in GBM, a malignancy known to show uniform resistant to TMZ and poor patient outcome. Non-coding RNA such as miRNA can be used in clinical application via several methods. They can be expressed in mesenchymal stem cells for delivery to the tumor as exosomes. Additionally, they can be packaged into nanoparticle or even in microvesicles. The limitation of this paper is the omission of *in vivo* studies, which will be corrected in ongoing research.

## AUTHOR CONTRIBUTIONS

JM and PR conceptualized and designed the study. JM, NW, SG, GS, and SM involved in development of methodology. JM, NW, SG, SM, and SP acquired the data. All authors analyzed and interpreted the data, and wrote and edited the manuscript.

## FUNDING

This study was supported by the National Academy of Science.

## SUPPLEMENTARY MATERIAL

The Supplementary Material for this article can be found online at: https://www.frontiersin.org/articles/10.3389/fphar.2019.00134/full#supplementary-material

## REFERENCES

Adams, C. M., and Eischen, C. M. (2014). Cell survival is dicey without dicer. *Mol. Cell. Oncol.* 1:e961825. doi: 10.4161/23723548.2014.961825

Beach, A., Zhang, H. G., Ratajczak, M. Z., and Kakar, S. S. (2014). Exosomes: an overview of biogenesis, composition and role in ovarian cancer. *J. Ovarian Res.* 7:14. doi: 10.1186/1757-2215-7-14

Bliss, S. A., Sinha, G., Sandiford, O. A., Williams, L. M., Engelberth, D. J., Guiro, K., et al. (2016). Mesenchymal stem cell-derived exosomes stimulate cycling quiescence and early breast cancer dormancy in bone marrow. *Cancer Res.* 76, 5832–5844. doi: 10.1158/0008-5472.CAN-16-1092

Chen, J., Feilotter, H. E., Pare, G. C., Zhang, X., Pemberton, J. G., Garady, C., et al. (2010). MicroRNA-193b represses cell proliferation and regulates cyclin D1 in melanoma. *Am. J. Pathol.* 176, 2520–2529. doi: 10.2353/ajpath.2010.091061

Chen, R., Liu, Q., Cheng, H., Jiang, B., Peng, R., Zou, Q., et al. (2016). MicroRNA-93 promotes the malignant phenotypes of human glioma cells and induces their chemoresistance to temozolomide. *Biol. Open* 5, 669–677. doi: 10.1242/bio.015552

Di Leva, G., Garofalo, M., and Croce, C. M. (2014). MicroRNAs in cancer. *Annu. Rev. Pathol.* 9, 287–314. doi: 10.1146/annurev-pathol-012513-104715

Freemantle, S. J., Liu, X., Feng, Q., Galimberti, F., Blumen, S. D., Sekula, D., et al. (2007). Cyclin degradation for cancer therapy and chemoprevention. *J. Cell. Biochem.* 102, 869–877. doi: 10.1002/jcb.21519

Fu, X., Tian, J., Zhang, L., Chen, Y., and Hao, Q. (2012). Involvement of microRNA-93, a new regulator of PTEN/Akt signaling pathway, in regulation of chemotherapeutic drug cisplatin chemosensitivity in ovarian cancer cells. *FEBS Lett.* 586, 1279–1286. doi: 10.1016/j.febslet.2012.03.006

Hiddingh, L., Raktoe, R. S., Jeuken, J., Hulleman, E., Noske, D. P., Kaspers, G. J., et al. (2014). Identification of temozolomide resistance factors in glioblastoma via integrative miRNA/mRNA regulatory network analysis. *Sci. Rep.* 4:5260. doi: 10.1038/srep05260

Huang, S., Zou, X., Zhu, J. N., Fu, Y. H., Lin, Q. X., Liang, Y. Y., et al. (2015). Attenuation of microRNA-16 derepresses the cyclins D1, D2 and E1 to provoke cardiomyocyte hypertrophy. *J. Cell. Mol. Med.* 19, 609–619. doi: 10.1111/jcmm.12445

Jiang, G., Wei, Z. P., Pei, D. S., Xin, Y., Liu, Y. Q., and Zhen, N. J. (2011). A novel approach to overcome temozolomide resistance in glioma and melanoma: inactivation of MGMT by gene therapy. *Biochem. Biophys. Res. Commun.* 406, 311–314. doi: 10.1016/j.bbrc.2011.02.042

Johannessen, T. C., and Bjerkvig, R. (2012). Molecular mechanisms of temozolomide resistance in glioblastoma multiforme. *Expert Rev. Anticancer Ther.* 12, 635–642. doi: 10.1586/era.12.37

Lim, P. K., Bliss, S. A., Patel, S. A., Taborga, M., Dave, M. A., Gregory, L. A., et al. (2011). Gap junction-mediated import of microRNA from bone marrow stromal cells can elicit cell cycle quiescence in breast cancer cells. *Cancer Res.* 71, 1550–1560. doi: 10.1158/0008-5472.CAN-10-2372

Louis, D. N. (2006). Molecular pathology of malignant gliomas. *Annu. Rev. Pathol.* 1, 97–117. doi: 10.1146/annurev.pathol.1.110304.100043

Miwa, S., Yano, S., Kimura, H., Yamamoto, M., Toneri, M., Matsumoto, Y., et al. (2015). Cell-cycle fate-monitoring distinguishes individual chemosensitive and chemoresistant cancer cells in drug-treated heterogeneous populations demonstrated by real-time fucci imaging. *Cell Cycle* 4, 621–629. doi: 10.4161/15384101.2014.991604

Munoz, J. L., Bliss, S. A., Greco, S. J., Ramkissoon, S. H., Ligon, K. L., and Rameshwar, P. (2013). Delivery of functional anti-miR-9 by mesenchymal stem cell-derived exosomes to glioblastoma multiforme cells conferred chemosensitivity. *Mol. Ther. Nucleic Acids* 2:e126. doi: 10.1038/mtna.2013.60

Munoz, J. L., Rodriguez-Cruz, V., Greco, S. J., Nagula, V. K., Scotto, W., and Rameshwar, P. (2014a). Temozolomide induces the production of epidermal growth factor to regulate MDR1 expression in glioblastoma cells. *Mol. Cancer Ther.* 13, 2399–2411. doi: 10.1158/1535-7163.MCT-14-0011

Munoz, J. L., Rodriguez-Cruz, V., Greco, S. J., Ramkissoon, S. H., Ligon, K. L., and Rameshwar, P. (2014b). Temozolomide resistance in glioblastoma cells occurs partly through epidermal growth factor receptor-mediated induction of connexin 43. *Cell Death Dis.* 5:e1145. doi: 10.1038/cddis.2014.111

Munoz, J. L., Rodriguez-Cruz, V., Ramkissoon, S. H., Ligon, K. L., Greco, S. J., and Rameshwar, P. (2014c). Temozolomide resistance in glioblastoma occurs by miRNA-9-targeted PTCH1, independent of sonic hedgehog level. *Oncotarget* 6, 1190–1201.

Naydenov, E., Tzekov, C., Minkin, K., Nachev, S., Romansky, K., and Bussarsky, V. (2011). Long-term survival with primary glioblastoma multiforme: a clinical study in bulgarian patients. *Case Rep. Oncol.* 4, 1–11. doi: 10.1159/000323432

Pant, S., Hilton, H., and Burczynski, M. E. (2012). The multifaceted exosome: biogenesis, role in normal and aberrant cellular function, and frontiers for pharmacological and biomarker opportunities. *Biochem. Pharmacol.* 83, 1484–1494. doi: 10.1016/j.bcp.2011.12.037

Park, J. M., Munoz, J. L., Won, B. W., Bliss, S. A., Greco, S. J., Patel, S. A., et al. (2013). Exogenous CXCL12 activates protein kinase C to phosphorylate connexin 43 for gap junctional intercellular communication among confluent breast cancer cells. *Cancer Lett.* 331, 84–91. doi: 10.1016/j.canlet.2012.12.007

Sen, R., Ghosal, S., Das, S., Balti, S., and Chakrabarti, J. (2014). Competing endogenous RNA: the key to posttranscriptional regulation. *Sci. World J.* 2014:896206. doi: 10.1155/2014/896206

Shibata, C., Otsuka, M., Kishikawa, T., Ohno, M., Yoshikawa, T., Takata, A., et al. (2015). Diagnostic and therapeutic application of noncoding RNAs for hepatocellular carcinoma. *World J. Hepatol.* 7, 1–6. doi: 10.4254/wjh.v7.i1.1

Spinelli, G. P., Miele, E., Lo Russo, G., Miscusi, M., Codacci-Pisanelli, G., Petrozza, V., et al. (2012). Chemotherapy and target therapy in the management of adult high- grade gliomas. *Curr. Cancer Drug Targets* 12, 1016–1031. doi: 10.2174/156800912803251207

Tezcan, G., Tunca, B., Bekar, A., Preusser, M., Berghoff, A. S., Egeli, U., et al. (2014). microRNA expression pattern modulates temozolomide response in GBM tumors with cancer stem cells. *Cell. Mol. Neurobiol.* 34, 679–692. doi: 10.1007/s10571-014-0050-0

Thery, C., Zitvogel, L., and Amigorena, S. (2002). Exosomes: composition, biogenesis and function. *Nat. Rev. Immunol.* 2, 569–579. doi: 10.1038/nri855

van den Beucken, T., Koch, E., Chu, K., Rupaimoole, R., Prickaerts, P., Adriaens, M., et al. (2014). Hypoxia promotes stem cell phenotypes and poor prognosis through epigenetic regulation of dicer. *Nat. Commun.* 5:5203. doi: 10.1038/ncomms6203

Yu, X. F., Zou, J., Bao, Z. J., and Dong, J. (2011). miR-93 suppresses proliferation and colony formation of human colon cancer stem cells. *World J. Gastroenterol.* 17, 4711–4717. doi: 10.3748/wjg.v17.i42.4711

Zhao, Z., Liu, J., Wang, C., Wang, Y., Jiang, Y., and Guo, M. (2014). MicroRNA-25 regulates small cell lung cancer cell development and cell cycle through cyclin E2. *Int. J. Clin. Exp. Pathol.* 7, 7726–7734.

**Conflict of Interest Statement:** The authors declare that the research was conducted in the absence of any commercial or financial relationships that could be construed as a potential conflict of interest.

frontiers in Pharmacology

ORIGINAL RESEARCH
published: 27 March 2019
doi: 10.3389/fphar.2019.00200

# The Coincidence Between Increasing Age, Immunosuppression, and the Incidence of Patients With Glioblastoma

*Erik Ladomersky[1], Denise M. Scholtens[1,2], Masha Kocherginsky[2,3], Elizabeth A. Hibler[2], Elizabeth T. Bartom[4], Sebastian Otto-Meyer[1], Lijie Zhai[1], Kristen L. Lauing[1], Jaehyuk Choi[4,5], Jeffrey A. Sosman[6], Jennifer D. Wu[7,8], Bin Zhang[6,8], Rimas V. Lukas[9,10] and Derek A. Wainwright[1,6,8,9]**

[1] Department of Neurological Surgery, Northwestern University Feinberg School of Medicine, Chicago, IL, United States, [2] Department of Preventive Medicine, Northwestern University Feinberg School of Medicine, Chicago, IL, United States, [3] Department of Obstetrics and Gynecology, Northwestern University Feinberg School of Medicine, Chicago, IL, United States, [4] Department of Biochemistry and Molecular Genetics, Northwestern University Feinberg School of Medicine, Chicago, IL, United States, [5] Department of Dermatology, Northwestern University Feinberg School of Medicine, Chicago, IL, United States, [6] Department of Medicine-Hematology and Oncology, Northwestern University Feinberg School of Medicine, Chicago, IL, United States, [7] Department of Urology, Northwestern University Feinberg School of Medicine, Chicago, IL, United States, [8] Department of Microbiology-Immunology, Northwestern University Feinberg School of Medicine, Chicago, IL, United States, [9] Robert H. Lurie Comprehensive Cancer Center, Northwestern University Feinberg School of Medicine, Chicago, IL, United States, [10] Department of Neurology, Northwestern University Feinberg School of Medicine, Chicago, IL, United States

OPEN ACCESS

**Edited by:**
*Andrew Zloza, Rush University Medical Center, United States*

**Reviewed by:**
*Praveen Bommareddy, Rutgers, The State University of New Jersey, United States*
*Tomas Garzon-Muvdi, Thomas Jefferson University Hospitals, United States*

***Correspondence:**
*Derek A. Wainwright*
*Derekwainwright@northwestern.edu*

**Specialty section:**
*This article was submitted to Cancer Molecular Targets and Therapeutics, a section of the journal Frontiers in Pharmacology*

**Received:** *12 January 2019*
**Accepted:** *18 February 2019*
**Published:** *27 March 2019*

**Citation:**
*Ladomersky E, Scholtens DM, Kocherginsky M, Hibler EA, Bartom ET, Otto-Meyer S, Zhai L, Lauing KL, Choi J, Sosman JA, Wu JD, Zhang B, Lukas RV and Wainwright DA (2019) The Coincidence Between Increasing Age, Immunosuppression, and the Incidence of Patients With Glioblastoma. Front. Pharmacol. 10:200. doi: 10.3389/fphar.2019.00200*

**Background:** Glioblastoma (GBM) is the most aggressive primary brain tumor in adults and is associated with a median overall survival (mOS) of 16–21 months. Our previous work found a negative association between advanced aging and the survival benefit after treatment with immunotherapy in an experimental brain tumor model. Given the recent phase III clinical success of immunotherapy in patients with many types of cancer, but not for patients with GBM, we hypothesize that aging enhances immunosuppression in the brain and contributes to the lack of efficacy for immunotherapy to improve mOS in patients with malignant glioma. Herein, we compare epidemiological data for the incidence and mortality of patients with central nervous system (CNS) cancers, in addition to immune-related gene expression in the normal human brain, as well as peripheral blood immunological changes across the adult lifespan.

**Methods:** Data were extracted from the National Cancer Institute's surveillance, epidemiology, and end results (SEER)-, the Broad Institute's Genotype Tissue Expression project (GTEx)-, and the University of California San Francisco's 10k Immunomes-databases and analyzed for associations with aging.

**Results:** The proportion of elderly individuals, defined as ≥65 years of age, has predominantly increased for more than 100 years in the United States. Over time, the rise in elderly United States citizens has correlated with an increased incidence and mortality rate associated with primary brain and other CNS cancer. With advanced aging, human mRNA expression for factors associated with immunoregulation including immunosuppressive indoleamine 2,3 dioxygenase 1 (IDO) and programmed

death-ligand 1 (PD-L1), as well as the dendritic cell surface marker, CD11c, increase in the brain of normal human subjects, coincident with increased circulating immunosuppressive Tregs and decreased cytolytic $CD8^+$ T cells in the peripheral blood. Strikingly, these changes are maximally pronounced in the 60–69 year old group; consistent with the median age of a diagnosis for GBM.

**Conclusion:** These data demonstrate a significant association between normal human aging and increased immunosuppression in the circulation and CNS; particularly late in life. Our data raise several hypotheses including that, aging: (i) progressively suppresses normal immunosurveillance and thereby contributes to GBM cell initiation and/or outgrowth; (ii) decreases immunotherapeutic efficacy against malignant glioma.

**Keywords: aging, biomarker, IDO, immunosuppression, PD-L1, immunotherapy, Treg, IDH**

## INTRODUCTION

Glioblastoma (GBM) is the most common primary malignant brain tumor in adults. Despite the aggressive standard of care regimen that includes maximal surgical resection followed by radiation therapy and chemotherapy with temozolomide, and more recently tumor treating fields, the median overall survival (mOS) remains at 16–21 months post-diagnosis, with just 43% of patients surviving for 2 years post-diagnosis (Stupp et al., 2005, 2009, 2017; Johnson and O'Neill, 2012). A major factor contributing to the poor GBM patient prognosis is the potent immunosuppression, found systemically and locally in the brain tumor microenvironment (Chongsathidkiet et al., 2018). High intratumoral expression of immunosuppressive mediators including programmed cell death protein-1 (PD-1) and indoleamine 2,3 dioxygenase 1 (IDO), is prognostic for decreased GBM patient survival (Wainwright et al., 2012; Nduom et al., 2016; Zhai et al., 2017). Immune checkpoint inhibitor treatment has demonstrated a survival benefit in patients with non-small cell lung carcinoma (Antonia et al., 2016), renal cell cancer (Motzer et al., 2015), end-stage melanoma (Larkin et al., 2015), and other aggressive malignancies arising outside of the central nervous system (CNS). In contrast, this benefit has yet to translate into patients with GBM in phase III clinical trials to-date (Bristol-Myers Squibb, 2017; Filley et al., 2017).

Age is one of the primary risk factors for cancer, with individuals $\geq$65 years of age accounting for 60% of newly diagnosed malignancies and 70% of all cancer-related deaths (Ries et al., 2006). A similar report highlighted an age adjusted cancer mortality rate for persons $\geq$65 at $\sim$16 times higher than the mortality rate for those <65 (Berger et al., 2006). Care for these individuals is challenging due to the number of diseases elderly subjects are at high risk for, which also raises the likelihood of presenting multiple comorbidities during advanced aging (Yancik et al., 1998, 2001). Similarly, the incidence and mortality rate of GBM increases during advanced aging with a median diagnosis at 64 years old (Young et al., 2017). Aging is a complex process that affects nearly all aspects of the immune system (Nikolich-Zugich, 2018). In general, advanced aging decreases immune system effectiveness, as is evidenced in elderly individuals who receive the influenza vaccine (McElhaney and Dutz, 2008). Aging also negatively impacts apoptotic cell clearance (Aprahamian et al., 2008), the numbers of naïve T cells (Cambier, 2005), and the wound healing response (Wick et al., 2010). T cell senescence increases with progressive aging through the induction of p16 (Liu et al., 2009). Aging also affects T cell receptor (TCR) signaling in $CD4^+$ T cells, due in part to decreased miR-181a; a microRNA highly expressed in normal T cells (Adachi and Davis, 2011; Li et al., 2012; Chen et al., 2013). Both aged mice (Rossi et al., 2005) and human (Pang et al., 2011) hematopoietic stem cells (HSC) possess a myeloid-biased differentiation potential as compared with HSC from young subjects. Moreover, macrophages from donor subjects with advanced age possess decreased capacity for antigen presentation as compared to young donors (Davila et al., 1990; Gon et al., 1996). Neuro-immune interactions are also affected by aging in the brain (Carson et al., 2006) that include a significant upregulation of MHCII and CD11b on microglia (Rogers et al., 1988; Perry et al., 1993), as well as an accumulation of brain-resident dendritic cells (Bulloch et al., 2008; D'Agostino et al., 2012; Kaunzner et al., 2012). However, it is not yet clear as to whether aging possesses a distinct impact on immunosuppressive gene expression across select tissues that contribute to a microenvironment permissive for oncogenesis, tumor progression, and/or resistance to immunoregulatory-based therapies.

Our laboratory previously demonstrated a negative impact of advanced age on the survival of animals engrafted with syngeneic experimental brain tumors (Ladomersky et al., 2016). C57BL/6 mice intracranially injected with murine GL261 glioma cells at 72–74 weeks old, which is similar in humans to a time frame associated with the median age of a GBM patient diagnosis (Fox et al., 2007; Dutta and Sengupta, 2016), have a decreased mOS as compared to animal subjects with an age of 6–8 weeks old (27.5 and 21.5 days, respectively, $P = 0.029$, $n = 10$–12/group); the latter of which is similar in age to a human teenager. The negative impact of advanced aging was coincident with increased immunosuppressive IDO1 gene expression in the normal, non-malignant mouse brain. More recently, we discovered that a substantial proportion of C57BL/6 mice intracranially injected with GL261 at 6–8 weeks of age experience long-term survival when simultaneously treated with

radiation (RT), anti-PD-1 mAb, and IDO1 enzyme inhibitor (Ladomersky et al., 2018). The brain tumor survival benefit provided by this treatment, however, was negatively affected by animal subjects with advanced age as compared with young subjects (Ladomersky et al., 2018). Importantly, there was no significant difference in tumor infiltrating leukocyte populations between the young and aged subjects within treatment groups. To our knowledge, this is the first preclinical primary brain cancer study to demonstrate a negative impact of aging on survival after treatment with immunotherapy.

Further supporting the hypothesis that, advanced aging mediates suppression of immune system efficacy against a tumor challenge event, previous work showed that splenocytes isolated from young, but not old immunized subjects, were able to eradicate subcutaneous tumors in mice (Schreiber et al., 2012). Specifically, immunodeficient recombination activating gene knockout mice ($Rag^{-/-}$) were subcutaneously engrafted 8101 cells arising from mice treated with UV-irradiation, and possessing a somatic mutation in the T cell-recognized antigen RNA helicase, p68. Splenocytes isolated from 5 month old mice and immunized with live 8101 cells, but not those from immunized 29 month old mice, eradicated 8101 cell-based tumors post-adoptive transfer into $Rag^{-/-}$ mice. Interestingly, melanoma patients ≥62 years of age show increased responsiveness to anti-PD-1 mAb treatment as compared with younger human subjects (Kugel et al., 2018). Recapitulating this clinical observation, 10 month old animal subjects, which roughly correlate to the human age of 38–47 years and engrafted with murine BSC9AJ2 melanoma cells, show decreased tumor growth as compared to 2 month old engrafted mice after treatment with anti-PD-1 mAb (Kugel et al., 2018). This highlights an interesting dichotomy suggesting that, the productivity of an anti-tumor immune response during treatment with immunotherapy likely depends on both the cancer type and age of the host. These combined findings may suggest that GBM is an outlier when considering its place in cancer immunology and immunotherapy. Accordingly, we previously found an inverse association between high CD3ε and CD8α gene expression with GBM patient survival (Zhai et al., 2017), which is a diametrically opposite finding as compared with non-small cell lung cancer and melanoma (Zeng et al., 2016; Zhai et al., 2018).

In our current study, we explored the associations between human: (i) aging; (ii) levels of gene expression associated with immunoregulation inside the brain; (iii) immunological changes in the peripheral blood; and (iv) incidence and mortality of patients with primary brain and other CNS tumors. Epidemiological analyses of GBM patient characteristics were compared across the Surveillance, Epidemiology, and End Results (SEER) database, age-dependent gene expression levels of normal human brain from the GTEx database, and age-associated changes in normal human peripheral blood leukocytes from the 10k Immunomes database. Our study confirms the striking observation that the brain cancer mortality rate is actively rising, with a particular enrichment among the elderly population in the United States. The incidence of GBM is 3.4× higher among individuals ≥65 years old, as compared to those <65, while the mortality rate for individuals ≥65 years old with GBM is 7× higher as compared to GBM patients <65. Gene expression levels of immunosuppressive IDO1 increased in the normal human brain and was maximal among individuals aged 60–69 years old. As compared to younger subjects, there was a maximal incidence of circulating immunosuppressive regulatory T cells (Tregs) and a significantly decreased cytolytic $CD8^+$ T cell population among the 60–69 year old age group. Our study found a cumulative peak index for immunosuppressive and/or immunoregulatory mediators during the time frame associated with the median age of a GBM patient diagnosis. These data raise the intriguing possibility that aging suppresses mechanisms of immunosurveillance and responsiveness to immunotherapy, which is associated with the increasing number of elderly patients with brain cancer and the failure of immunotherapy to benefit GBM patients in phase III clinical trials to-date, respectively.

# MATERIALS AND METHODS

## Data

### Life Expectancy Data

Life expectancy data were analyzed from the Center for Disease Control and Prevention. Data were accessed through the National Center for Health Statistics portal[1]. The filename used was *Life expectancy at birth and at age 65, and at age 75, by sex, race, and Hispanic origin: United States, selected years 1900–2016*.

### Surveillance of Epidemiology and End Results Database (SEER)

All population, incidence, and mortality data from the SEER database were accessed through SEER*Stat (Version 8.3.5[2]). Population-level data were accessed through a Frequency Session. Variables examined were: (1) Age recode with <1 year olds; and (2) year. Incidence and mortality data were accessed through a Rate Session. Variables examined for incidence include: (1) age recode with <1 year olds; (2) year of diagnosis; (3) histology recode – broad groupings; (4) histology recode – brain groupings; and (5) COD to site recode. The COD to site recode was used to analyze the mortality rate of GBM. Variables examined for mortality include: (1) age recode with <1 year old; (2) year of death; and (3) cause of death recode. All rate data were crude/non-age-adjusted. Data were accessed on 12-05-2018.

### NCI 2018 Estimates

Estimated incidence and mortality data were retrieved from the NCI Cancer Stat Facts website[3]. The top 16 causes of cancer were analyzed for both incidence and mortality. Comparison across the 16 cancers for the mortality to incidence ratio estimate were calculated by dividing the estimated mortality with the estimated incidence in the year 2018. Cost data were accessed through the NCI Cancer Prevalence and Cost of Care Projections website[4]. Cost per patient was calculated by taking the 2018 estimated

[1]https://www.cdc.gov/nchs/hus/contents2017.htm#015

[2]https://seer.cancer.gov/seerstat/

[3]https://seer.cancer.gov/statfacts/html/common.html

[4]https://costprojections.cancer.gov/graph.php#

total charges for each type of cancer and dividing it by the 2018 estimated incidence of each cancer type.

### TCGA

Survival data for GBM patients were analyzed from the cancer genome atlas. The data were accessed using the UCSC Xena portal. Data were accessed on 02-01-2019.

### 10k Immunomes

Normal human peripheral blood cell data were analyzed from the 10k Immunomes database. The data were accessed through the UCSF portal[5]. All data analyzed were CyTOF data plotted by age. Data were accessed on 06-22-2018.

### GTEx

Gene expression data for normal human tissues were analyzed from the GTEx database. Data were accessed through the dbGaP portal. All data were represented as log-transformed fragments per kilobase of transcript per million mapped reads (FPKM). These data were then plotted by subject age.

## Statistical Analysis

10k Immunomes and TCGA expression data are represented as the mean ± SEM. GTEx data are represented by each individual value. The statistical significance of differences in cell counts (CyTOF) and gene expression (log-transformed FPKM) between two groups was determined by Student *t*-test. Differences among multiple groups were assessed using ANOVA with *post-hoc* Tukey test. The statistical significance of TCGA survival data was determined by Log-rank test. Data were analyzed using Prism software (GraphPad Software). A *P*-value less than 0.05 was considered significant.

# RESULTS

## The Rate of Cancer Incidence Increases With Age

Over the past 40 years in the United States, improved healthcare systems and enhanced awareness of proper nutrition and exercise have led to substantial increases in mean life expectancy, rising from 72.6 years of age in 1975, to 78.8 years of age in 2015 (**Figure 1A**). Coincident with the increasing life expectancy in the United States, the proportion of elderly (≥65 years) individuals is rising. The elderly age group represented 10.6% of the total population in 1975, and increased to 14.9% in 2015 (**Figure 1B**). Both the incidence and mortality rates associated with cancer diagnoses are higher among the elderly population as compared to individuals <65 years of age (**Figures 1C,D**). In the year 1975, the incidence and mortality rate within the elderly population for all malignancies was 1,732/100,000 people and 942/100,000, respectively, whereas in the year 2015, the incidence rate for all malignancies in the elderly population was 1,876/100,000 and the mortality rate was 879/100,000. Compared to the population <65, these incidence and mortality rates were 9.6 and 12.1 times higher, respectively, in 1975, and 7.1 and 13.6 times higher, respectively, in 2015. The slight decrease in mortality rate between 1975 and 2015 is most likely due to improved detection and treatment techniques in select cancers. However, due to the increasing elderly population, the absolute numbers of cancer related mortalities in this population has risen from 214,173 in 1975, to 419,389 in 2015. Together, these data suggest an association between the aging population and an absolute increase of cancer-related deaths in the elderly population of the United States.

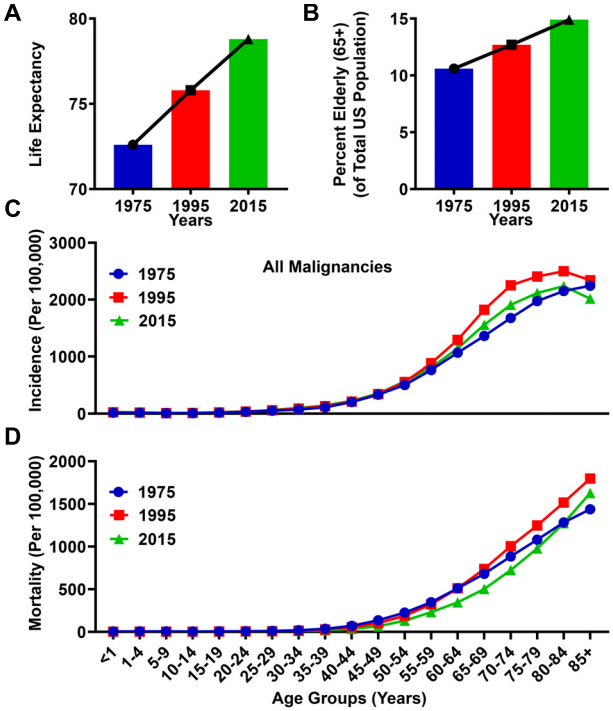


**FIGURE 1 |** Progressive aging is associated with an increased rate of cancer incidence and mortality. **(A)** Life expectancy from the Center for Disease Control and Prevention (CDC) database for an average lifespan in the United States between the years 1975 and 2015. **(B)** Population data from the Surveillance, Epidemiology, and Ends Results (SEER) database representing the total number of elderly human subjects (ages ≥65) divided by the total population in the United States for the years 1975, 1995, and 2015. **(C)** Incidence and **(D)** mortality rates from the SEER database for all malignancies in the years 1975, 1995, and 2015. Rates are defined as number of cases and deaths, respectively, divided by the population in each age category and multiplied by 100,000 people (per 100,000).

## Brain Cancer Diagnoses Pose a Growing Challenge to the United States Healthcare System

Primary brain tumors arising from a transformed cell within the CNS is a relatively rare form of cancer, with the 16th highest rate of incidence among all cancers, and an estimated 23,880 new patient diagnoses in 2018 (**Figure 2A**). Dwarfing this number is the estimated 266,120 new diagnoses for patients with breast cancer in the year 2018. The overall ratio of estimated breast

[5]http://10kimmunomes.ucsf.edu/

cancer incidence, as compared with brain cancer, is 11:1. In contrast, the estimated mortality rate for patients diagnosed with CNS cancer is 16,830 in 2018 (**Figure 2B**), and is 40,920 for individuals diagnosed with breast cancer. The overall ratio of breast cancer-associated mortalities, as compared to mortality due to CNS cancer, is only 2.4:1. Aggressiveness of cancer diagnoses can also be calculated with the mortality-to-incidence ratio (MIR), which is determined by dividing overall mortality with the number of new diagnoses in a given year (Choi et al., 2017). CNS cancer as a group possesses the third highest MIR of 0.70, which is only exceeded by pancreatic and liver cancer, with MIR scores of 0.80 and 0.72, respectively (**Figure 2C**). Leading all other groups, treatment for CNS cancers is the most costly on a per patient basis, with an average cost estimated to be $225,364 in 2018 (**Figure 2D**).

## Brain Cancer Incidence/Mortality Is Rising and Enriched in the Elderly

Although there has only been a small change in the incidence and mortality rates of all malignancies (**Figures 1C,D**) from 1975 to 2015, analysis of incidence data for brain and other CNS cancer shows a different trend (**Figure 3A**). The incidence rate has increased overall from 5.4/100,000 in 1975, to 7.0/100,000 in 2015. The overall increase, however, is primarily attributable to the elderly population. In 1975 the incidence rate for individuals with brain and other CNS malignancies ≥65 years of age was 14.2/100,000, which increased nearly 37% to 19.4/100,000 in 2015. In that same time span, the incidence rate for those <65 years of age only slightly increased from 4.4/100,000 in 1975 to 5.0/100,000 in 2015. When comparing other malignancy types including breast, pancreatic, and lung, a similar trend of increased incidence was observed. Breast cancer incidence rates increased from 47.4/100,000 to 78.0/100,000 in the total population over the same time span, and from 192.4/100,000 to 242.6/100,000 among the elderly population (**Figure 3B**). Pancreatic cancer incidence rates rose more slightly, from 9.4/100,000 to 14.5/100,000 in the total population and from 63.3/100,000 to 68.8/100,000 among the elderly over the past 40 years (**Figure 3C**). The incidence of melanoma increased from 6.8/100,000 to 28.4/100,000 in the total population and from 16.7/100,000 to 97.7/100,000 within the elderly population from 1975 to 2015 (**Figure 3D**). Overall, more people were diagnosed with malignancies in 2015 as compared with 1975.

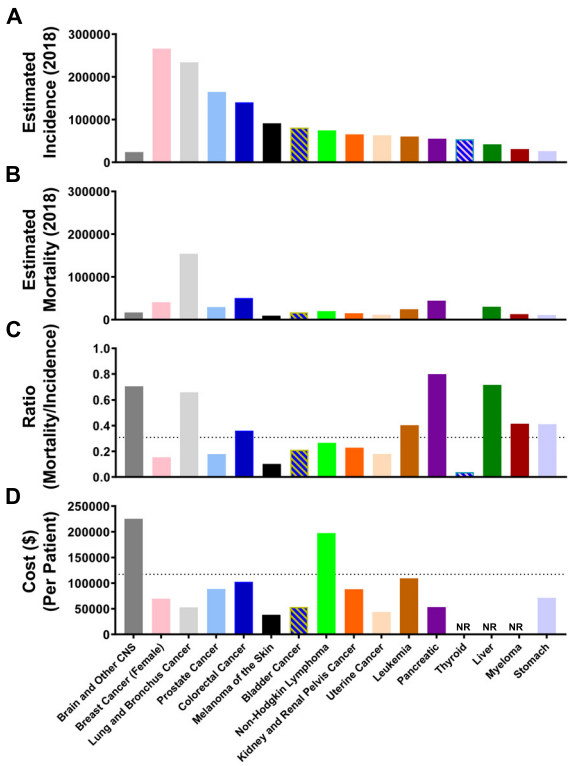


**FIGURE 2 |** Brain and other CNS cancer is associated with a high mortality/incidence ratio and is expensive to treat. The estimated total **(A)** incidence and **(B)** mortality rate for the top 16 cancer types according to NCI Cancer Stat Facts. **(C)** The calculated mortality to incidence ratio (estimated mortality/estimated incidence) for the top 16 cancer sites according to NCI Cancer Stat Facts. The dotted line represents an average across all 16 cancer types. **(D)** Cost (United States dollars) per patient for each of the top 16 cancer types. Dotted line represents the average for all 16 cancer types. NR, Not reported.

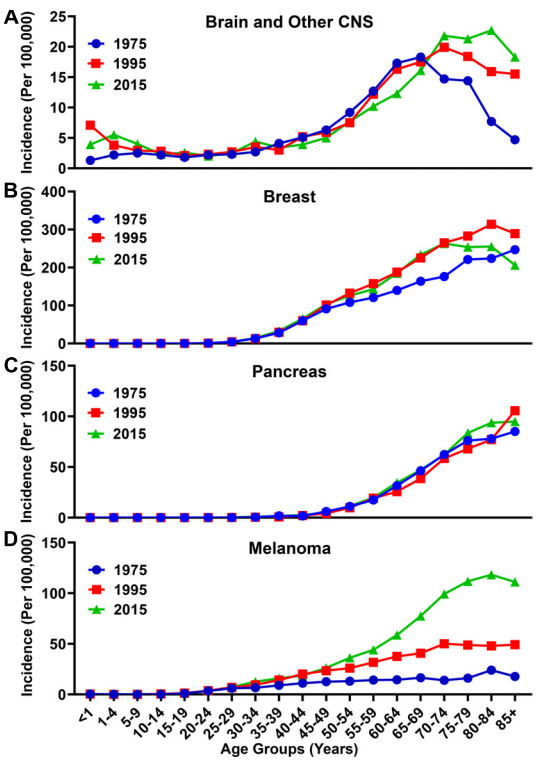


**FIGURE 3 |** Incidence rate for brain, breast, pancreatic, and melanoma malignancies over time. Incidence rates for **(A)** brain and other CNS, **(B)** breast, **(C)** pancreatic, and **(D)** melanoma malignancies analyzed from the SEER database for the years 1975, 1995, and 2015. Rates defined as number of cases divided by the population in each age category multiplied by 100,000 people (per 100,000).

Similar to the increased rate of incidence, the overall mortality rate among individuals with brain and other CNS cancers increased in the total population from 3.8/100,000 in 1975 to 5.1/100,000 in 2015 (**Figure 4A**) The mortality rate for individuals with brain and other CNS malignancies ≥65 years old was 11.6/100,000 in 1975, and increased by 56% to 18.1/100,000 in 2015. In contrast, the mortality rate for individuals <65 years of age rose slightly from 2.8/100,000 in 1975 to 2.9/100,000 in 2015. The overall mortality rate for individuals with breast cancer decreased from 15.1/100,000 in 1975 to 13.1/100,000 in 2015, and from 66.8/100,000 to 52.9/100,000 among individuals ≥65 years of age during the same time periods, respectively (**Figure 4B**). The overall mortality rate for individuals with pancreatic cancer rose from 9.0/100,000 to 13/100,000 from 1975 to 2015, but only increased slightly from 56.2/100,000 to 63.0/100,000 among individuals ≥65 years of age during the same time periods, respectively (**Figure 4C**). The overall mortality rate increased for patients with melanoma from 1.8/100,000 to 2.8/100,000 from 1975 to 2015 and increased from 6.2/100,000 in 1975 to 12.2 in 2015 among individuals ≥65 years of age during the same time periods, respectively (**Figure 4D**).

When analyzing the MIR as a function of aging, there were differences in trends among the malignancies analyzed. While the overall MIR for individuals with brain cancer increased slightly from 0.70 in 1975 to 0.73 in 2015 (**Figure 5A**), there is a larger increase from 0.82 in 1975 to 0.93 in 2015 among individuals ≥65. In contrast, the overall MIR for individuals with breast cancer decreased over the same time span from 0.32 in 1975 to 0.17 in 2015 (**Figure 5B**), with a similar decrease of 0.35 in 1975 to 0.22 in 2015 among individuals ≥65. The overall MIR for individuals with pancreatic cancer was 0.96 in 1975 and slightly decreased to 0.90 in 2015 (**Figure 5C**), whereas this figure is relatively unchanged within the elderly population at 0.89 in 1975 to 0.90 in 2015. The overall MIR for individuals with melanoma decreased from 0.26 to 0.10 in 2015, and from 0.37 to 0.12 among individuals ≥65, respectively (**Figure 5D**). Taken together, these data show substantially different trends of aggressiveness, historically and currently, with brain cancer and other CNS cancers demonstrating a substantial increase in overall incidence, mortality, and MIR among the elderly portion of the United States population.

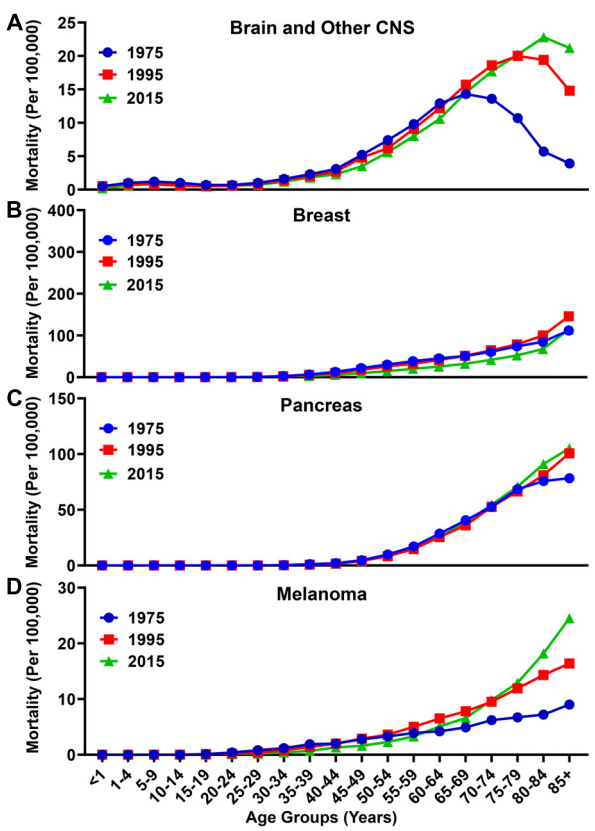


**FIGURE 4 |** Mortality rate for brain, breast, pancreatic, and melanoma malignancies over time. Mortality rates for **(A)** brain and other CNS, **(B)** breast, **(C)** pancreatic, and **(D)** melanoma malignancies analyzed from the SEER database for the years 1975, 1995, and 2015. Rates defined as number of deaths divided by the population in each age category multiplied by 100,000 people (per 100,000).

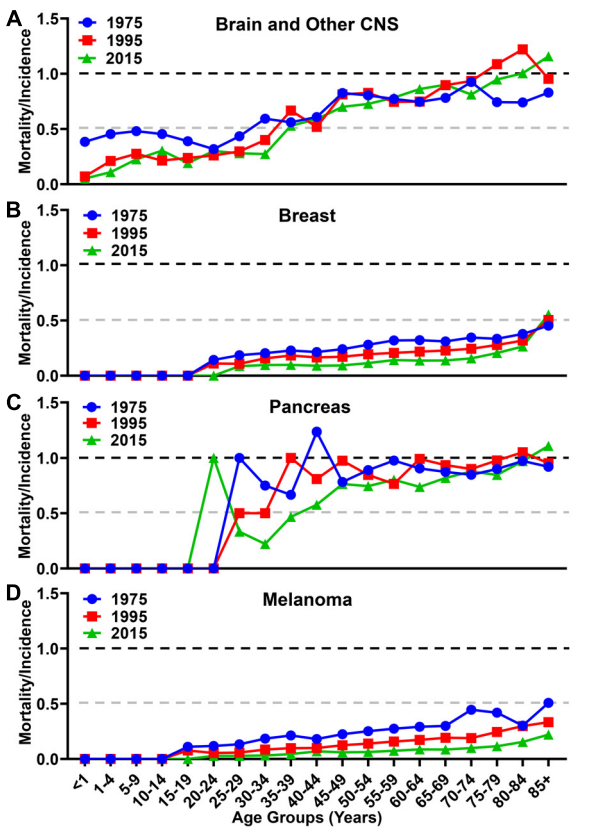


**FIGURE 5 |** Mortality to incidence ratio for brain, breast, pancreatic, and melanoma malignancies over time. The calculated mortality to incidence ratio of **(A)** brain and other CNS, **(B)** breast, **(C)** pancreatic, and **(D)** melanoma malignancies for each year calculated from SEER incidence and mortality data. Instances where the ratio is over 1.0 are due to the lag time between diagnosis and mortality in GBM and pancreatic cancer.

## The Incidence and Mortality of Individuals With GBM Is Progressively Enriched With Aging

Glioblastoma (GBM; grade IV) is the most common primary malignant brain tumor in adults and accounts for 54% of malignant glioma diagnoses (Wen and Kesari, 2008). Among total glioma incidence, the rate of a GBM diagnosis is substantially higher as compared with grade II and grade III glioma (**Figure 6A**). The rate of a GBM patient diagnosis and mortality is enriched among the elderly population (**Figure 6**) and the MIR for individuals ≥65 years of age is 1.00.

Not only is GBM enriched among the elderly population, but the prognosis for these patients is substantially worse as compared with individuals <65 years of age. We analyzed overall survival and expression data from the cancer genome atlas (TCGA) for individuals with GBM who possessed corresponding patient data, expression data, and a reported IDH status ($n = 144$). There were only 8 patients within the dataset reporting the presence of mutant IDH (mIDH), all of which were <65 years of age. There is a significantly shorter mOS of 11.3 months among individuals ≥65 years of age as compared with individuals <65 years of age (14.5 months; $P = 0.019$) (**Figure 7A**). In contrast, mOS for the eight individuals with mIDH GBM is a striking 27.9 months. Intratumoral gene expression levels for the immunosuppressive enzyme, IDO1, is similar for individuals <65 and ≥65 with wild-type IDH status, and significantly decreased among mIDH GBM (**Figures 7B,C**) as was previously reported (Zhai et al., 2017). While a majority of individuals with wild-type IDH GBM were diagnosed later in life, 50 percent of individuals with mIDH GBM were diagnosed before the age of 35 (**Figure 7D**). Not surprisingly, overall survival time decreased with progressively increasing age among individuals with GBM (**Figure 7E**). Taken together, the data indicate that individuals with a wild-type IDH GBM, which constitute the majority of new diagnoses, possess substantial comorbidity with advanced aging.

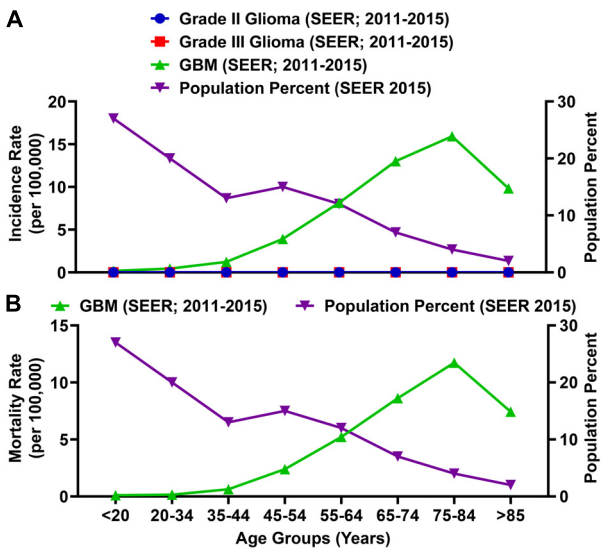


**FIGURE 6 |** The incidence and mortality rates for glioblastoma (GBM) patients are enriched among the elderly population. **(A)** SEER incidence rates (per 100,000) for grade II glioma, grade III glioma, and GBM (grade IV glioma; all left axis) compared to the percent of the total population represented for each age group. Grade II and III glioma incidence rates calculated by SEER were >0.015 (per 100,000) for each age category. **(B)** The SEER mortality rate for GBM as compared to the percent of the total population represented for each age group. Incidence and mortality data is represented as a summation for the years 2011–2015.

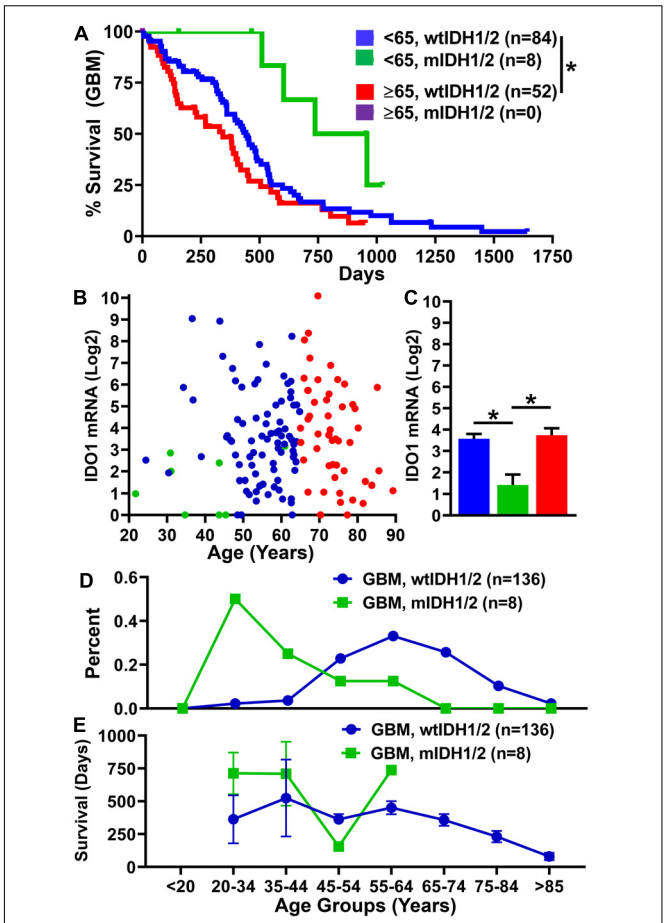


**FIGURE 7 |** Prognosis is worse for individuals with GBM ≥65. Analysis of GBM data for individuals with corresponding patient data, gene expression (HiSeq) data, and a reported mIDH1/2 status from the TCGA. **(A)** Survival data of individuals with wild-type IDH1/2 <65 ($n = 84$), ≥65 ($n = 52$), and those with mIDH1/2 ($n = 8$). IDO1 gene expression **(B)** dot plot and **(C)** bar graph of individuals with wild-type IDH1/2 <65 (blue), ≥65 (red), and those with mIDH1/2 (green). **(D)** The percentage of GBM diagnoses within each age category for individuals with wtIDH1/2 (blue) and mIDH1/2 (green). **(E)** Survival time in days of individuals diagnosed in each age category. $^*P < 0.05$.

## The Median Age of a GBM Patient Diagnosis Is Coincident With Enhanced Global Immunosuppression

Although GBM is generally considered as a disease initiated by genetic mutations, it may also arise due to immunological dysfunction (Shurin, 2012); although it is not clear which event(s) precede(s) the other in contributing to GBM cell

initiation/outgrowth. While immunosuppression is routinely analyzed in GBM patients following a diagnosis (Beatty and Gladney, 2015), few studies have prospectively investigated the correlation between progressive aging and the level of immunosuppression in human subjects. With the hypothesis that the suppression of the normal immune system contributes to the microenvironment necessary to facilitate GBM cell initiation, the 10k Immunomes database was profiled for immune system status among healthy human subjects. There were substantial changes in the peripheral immune system associated with aging. While there were no noticeable trends among total lymphocytes (**Figure 8A**) and $CD19^+$ B cell (**Figure 8B**) levels, analysis of T cell subpopulations revealed an interesting phenotypic trend. As demonstrated in **Figure 8C**, $CD4^+$ T cell levels are maximal in the 60–69 age range. Drilling down into the $CD4^+$ T cell subset revealed that the maximal increase was primarily attributable to the increase of immunosuppressive regulatory T cells (Tregs; $CD3^+CD4^+FoxP3^+$) within the same 60–69 age group (**Figure 8D**). Strikingly, the cytotoxic $CD8^+$ T cells coincidently decreased with progressive aging (**Figure 8E**). Since a high $CD8^+$ T/Treg ratio is associated with improved overall survival, (Yue et al., 2014; Shang et al., 2015) and because there is a decreased $CD8^+$ T/Treg ratio during advanced aging of normal human healthy individuals that is maximal in the 60–69 age group, the data collectively demonstrate a trend for increased immunosuppression in the peripheral blood coincident with the median age of a GBM patient diagnosis.

We previously demonstrated that immunosuppressive IDO1 is significantly increased in the normal healthy brain of 72–74 week old mice as compared with young 6–8 week old counterparts; independent of tumor burden (Ladomersky et al., 2016, 2018). To determine whether this observation is generalizable to humans, RNA-sequencing data from the GTEx database was analyzed for mRNA expression levels of established immunoregulatory genes in normal human brain (**Figure 9A**). Similar to our analysis of increased IDO1 expression levels in the brain of mice during advanced aging, IDO1 is also increased in the normal human brain among the 60–69 age group as compared to human subjects in the 50–59 age group ($P$ = 0.02; **Figure 9A**; **Supplementary Figure S1**). Although this trend remained when comparing the 60–69 age group to other age cohorts, it did not achieve statistical significance due to insufficient human samples for comparison. Similar to increased IDO1 mRNA expression, gene expression for immunosuppressive PD-L1 was also highest in the 60–69 year old age group as compared with the 20–29 year old age group ($P$ = 0.01). Unexpectedly, CD11c mRNA levels, a marker traditionally associated with immune sentinel dendritic cells, was also increased in the 60–69 age group as compared with human subjects in the 50–59 age group ($P$ = 0.02; **Figure 9A**). Interestingly, samples containing the highest IDO1 gene expression (**Figure 9A**; green) also showed high PD-L1 and CD11c levels, possibly suggesting an immunosuppressive phenotype with dendritic cell accumulation in those samples. In contrast to the enrichment of select immunosuppressive factors significantly increased in the normal human brain, IDO1 mRNA levels do not significantly change in pancreatic, skin, or thyroid tissues across age groups (**Figure 9B**; **Supplementary Figure S2**), nor any other human tissue analyzable in the GTEx database. Collectively, these

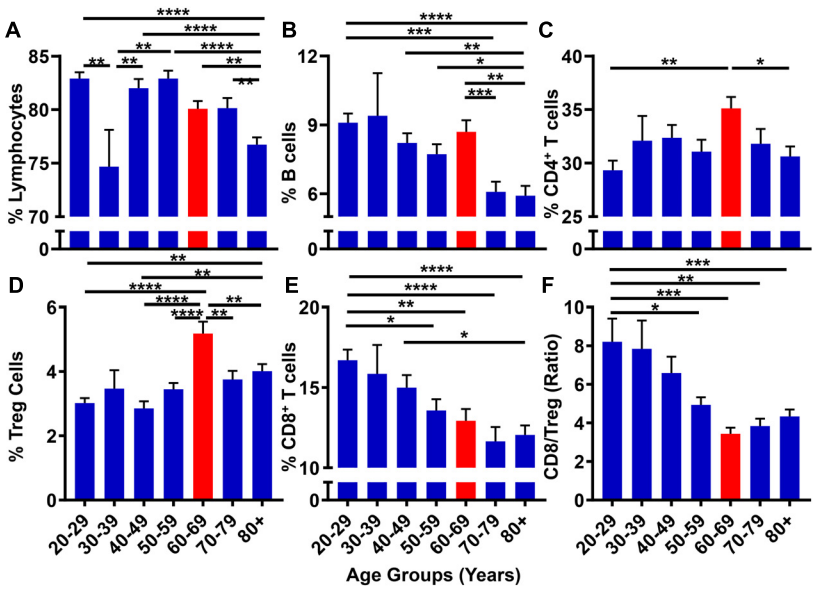


**FIGURE 8 |** The peripheral blood $CD8^+$ T/Treg ratio decreases with progressive aging in healthy human subjects. 10k immunomes CyTOF data from the peripheral blood of healthy patients analyzed for **(A)** total lymphocytes, **(B)** B cells, **(C)** $CD4^+$ T cells, **(D)** $CD8^+$ T cells, **(E)** Tregs ($CD4^+CD25^+FoxP3^+$), and **(F)** $CD8^+$ T/Treg ratio. Data was analyzed among age groups including 20–29 ($n$ = 110), 30–39 ($n$ = 14), 40–49 ($n$ = 76), 50–59 ($n$ = 78), 60–69 ($n$ = 72), 70–79 ($n$ = 57), 80+ ($n$ = 127). $^*P < 0.05$; $^{**}P < 0.01$; $^{***}P < 0.001$; $^{****}P < 0.0001$.

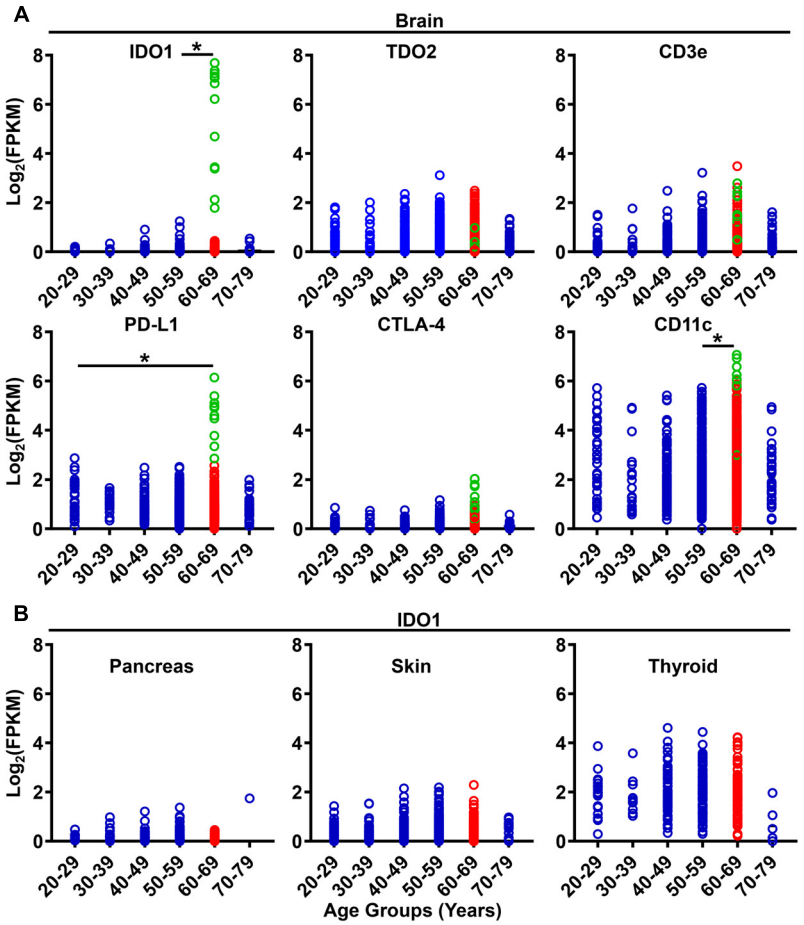


**FIGURE 9 |** Gene expression for immunosuppressive and immunoregulatory factors increase in the normal human brain with aging. **(A)** GTEx gene expression analysis of IDO1, TDO2, CD3ε, PD-L1, CTLA-4, and CD11c in the brain. Data was analyzed among age groups including 20–29 ($n$ = 38), 30–39 ($n$ = 19), 40–49 ($n$ = 123), 50–59 ($n$ = 386), 60–69 ($n$ = 549), 70–79 ($n$ = 37). Green circles across gene panels share the same sample IDs. **(B)** GTEx gene expression analysis of IDO1 in the normal human pancreas ($n$ = 167), skin ($n$ = 812), and thyroid ($n$ = 280). *$P < 0.05$.

data confirm that systemic and brain-specific immunoregulatory factors favoring immunosuppression are maximal during the time frame associated with the median age of a GBM patient diagnosis.

## DISCUSSION

The Director of the National Cancer Institute, Dr. Normal E. Sharpless, M.D., formerly an investigator within the National Institute of Aging, has highlighted the importance of the relationship between cancer and aging (Sharpless, 2018). Cancer is a disease enriched among the elderly and is often associated with deficits in normal immunosurveillance (Dunn et al., 2004; Zhong et al., 2016). Aging is associated with progressive immunological changes throughout the body, including involution of the thymus, a critical site for pre-T cell education and development into mature naïve T cells, a shift of the circulating T cell repertoire from a naïve to memory phenotype, an absolute decrease in the number of naïve T and B cells, a reduction in cytokine signaling, and reduced uptake of antigens and/or microbes by dendritic cells. To further understand the immunological changes that occur during aging, and whether these differences provide for preventative or therapeutic applications to individuals that will be diagnosed with malignant primary brain cancer, we comprehensively studied multiple bioinformatic database repositories for aging-related associations between GBM patient incidence and mortality, changes in the peripheral immune response of normal healthy human subjects, and gene expression throughout the normal healthy human body for immunoregulatory factors. Accordingly, the scientific premise of our investigation aimed to identify meaningful relationships between the ages of a GBM patient diagnosis, with differences in the immune system that are potentially therapeutically targetable.

During our investigation, we discovered that the United States rate of incidence and mortality for brain and other CNS malignancies has been rising over the past 40 years, and due to its

enrichment among the elderly population, may reflect the increased number of individuals that have a higher propensity for brain cancer diagnoses as compared with younger subjects (**Figures 1**, **3**, **4**, **5**). This differs from the trend for all malignancies, where the incidence and mortality rates decline between the years 1995 and 2015 (**Figures 1C,D**). This may be due to an increase in the number of effective therapies for treating other types of cancer, as well as improved prevention and detection techniques for high incidence malignancies including breast cancer and melanoma. According to a 2018 projection by the NCI (see text footnote 3), brain and other CNS malignancies have the third highest mortality:incidence (MIR) ratio when comparing across major cancer subtypes, which reflects a high degree of aggressiveness. Strikingly, brain cancer and other CNS malignancies were predicted to be the most expensive cancer on a per patient basis in the year 2018 (**Figure 2**). Further investigation of glioma incidence data revealed that GBM diagnoses are highly enriched among the elderly. When the mortality data was accounted for, the MIR for individuals with GBM between the years 2011–2015 was 1.00 (**Figure 6**). Analysis of TCGA data revealed that not only are the elderly at a higher risk for GBM, but this cohort of individuals also have a significantly worse prognosis when diagnosed with GBM (**Figure 7**). Further evaluation revealed a peak GBM patient incidence/mortality rate that corresponded to the maximal levels of immunosuppressive IDO1 and PD-L1 mRNA expression in the CNS, as well as immunosuppressive peripheral Treg abundance (**Figures 8**, **9**). Interestingly, the $CD4^+FoxP3^-$ T cells were less affected by aging (**Figure 8**). A hypothesis for the increased immunosuppressive markers in the 60–69 age group, but not among even older age groups, is that only a subset of individuals experience this increase. It's also possible that the transient increase in local immunosuppression synergizes with peripheral mechanisms during a timeframe of substantial hormonal imbalance (i.e., menopause). Interestingly, CD11c mRNA expression also increased in the elderly human brain, which may be associated with the accumulation of brain-resident cells (Bulloch et al., 2008; D'Agostino et al., 2012; Kaunzner et al., 2012).

Since cancer is enriched among the elderly, combined with the increasing size of the population with advanced age (**Figures 1A,B**), it was surprising to find that not all malignancies had an associated increased mortality rate when comparing data between 1975 and 2015. Several hypotheses may explain the rise in mortality of primary malignant brain cancer as compared to other malignancies including: (i) the lack of effective treatment options for patients diagnosed with incurable brain tumors as compared to therapeutic improvements for non-CNS malignancies; (ii) a steady enrichment in factors that promote the development of more malignant primary brain tumors; (iii) a more aggressive natural history in established primary brain tumors; (iv) an absolute increase in the number of elderly individuals that have a higher chance for developing primary malignant glioma; (v) an increase over time of elderly patients diagnosed with malignant brain tumors due to more aggressive patient work ups providing for a larger pool of individuals contributing to the mortality statistics; or (vi) a combination of all stated potential conferring factors.

The CNS is a potently immunosuppressive and immunospecialized organ, as compared with peripheral tissues (Carson et al., 2006). Through normal human subject gene expression analysis, we found increased immunosuppressive IDO1 in the brain that was maximally enhanced in the 60–69 year old subgroup, which is complementary to our previous work demonstrating increased IDO1 in the normal brain of mice during advanced aging (Ladomersky et al., 2016, 2018). Unexpectedly, IDO1 enzyme activity was not increased in the aged brain, questioning the functionality of the increased brain IDO1 expression. Recent studies in our laboratory and others have hypothesized that the immunosuppressive function of IDO1 may be, in-part, independent of its associated enzyme activity (Pallotta et al., 2011; Wainwright et al., 2012; Zhai et al., 2017). Although additional studies are required to fully understand the relationship between increased human brain IDO1 expression and advanced aging, a hypothesis that currently fits the available data is that IDO1 expression increases CNS immunosuppression through non-enzyme activity. Whether the basal increase of brain IDO1 expression contributes to the microenvironment required for GBM cell initiation is also an intriguing consideration.

Another factor for considering the effects of aging on immunosuppression and GBM onset is the differences between primary, or *de novo* GBM, and secondary GBM; the latter of which develops from lower grade II or III glioma. Primary GBM represents a majority of all malignant glioma cases (>90%) (Ohgaki and Kleihues, 2007). Primary GBM is routinely associated with mutation of PTEN (Ohgaki et al., 2004), EGFR amplification (Ekstrand et al., 1992), and $p16^{INK4a}$ deletion (Biernat et al., 1997). Secondary GBM, which accounts for <10% of GBM diagnoses, tends to arise in younger individuals and is characterized by the presence of mutated isocitrate dehydrogenase (mIDH) and TP53 (Kohanbash et al., 2017). The median age of diagnosis for patients with a secondary GBM is ∼45 years old (Ohgaki and Kleihues, 2005). The different ages at which primary and secondary GBMs arise may reflect different microenvironmental CNS conditions that contribute to GBM cell initiation. Highlighting this plurality, GBM presenting with a mIDH is often associated with immune cell exclusion and almost totally absent of tumor cell-killing cytolytic $CD8^+$ T cells (Kohanbash et al., 2017). Despite the minimal infiltration of immune cells, the presence of mIDH is associated with a favorable prognosis in GBM, as compared with primary GBM that predominantly contain wild-type IDH (Yan et al., 2009).

Our comprehensive analysis across multiple databases provides a unique perspective for assessing the risk of GBM in the elderly. While the data show interesting trends, a prospective analysis of a large patient cohort is warranted to validate the hypotheticals proposed by our current study. Some of these considerations will be built into an upcoming prospective phase I/II trial evaluating newly diagnosed GBM patients, before and after treatment with standard radiation, nivolumab (anti-PD-1 mAb) and BMS986205 (IDO1 enzyme inhibitor), led by our group. Further analysis of TCGA survival data

allows for a valuable comparison of prognostic criteria between elderly and younger individuals, but still does not account for major differences of tumor biology. Future studies aimed at evaluating aging-related mechanisms and increased immunosuppression will allow for a validation of whether there are therapeutically targetable changes that potentially prevent brain tumor incidence and/or enhance the effectiveness of immunotherapeutic treatments.

Taken together, these data suggest that immunosuppressive changes in the brain are affected by processes mediated by aging and may contribute to the significantly increased brain cancer mortality rate enriched within the elderly population. The median age of a GBM diagnosis coincides with an immunosuppressive phenotype in the peripheral blood and inside the brain parenchyma. Potentially, subsets of individuals with altered expression of immunoregulatory genes possess an enhanced risk for developing GBM. A high priority must be placed on determining whether these gene expression changes contribute to tumor cell initiation and/or progression, as well as the ability to detect increases in CNS immunosuppression through a peripheral (i.e., outside of the CNS) biomarker. Further research in this area will not only allow for a better understanding of elderly GBM patient treatment, but also potentially contribute to the ability of identifying individuals at a higher risk for developing the terminal disease.

## DATA AVAILABILITY

All datasets generated for this study are included in the manuscript and/or the **Supplementary Files**.

## AUTHOR CONTRIBUTIONS

EL performed a majority of the data mining associated with this submitted work. Data analysis was performed by EL, with statistical input from DS. All data were reviewed by DMS, MK, EAH, ETB, SO, LZ, KLL, JC, JAS, JDW, BZ, and RVL. EL and DAW prepared the figures and wrote the manuscript.

## FUNDING

EL was supported by PHS grant number T32CA070085. DAW was supported by PHS grant number R01NS097851 awarded by the NIH/NINDS, United States Department of Health and Human Services. RVL and DAW are supported by PHS grant number P50CA221747 awarded by the NIH/NCI, United States Department of Health and Human Services; the Gail Boyter Magness Foundation; the Grace Giving Foundation. ETB was supported by PHS grant 5R50CA221848-02 awarded by the NCI.

## SUPPLEMENTARY MATERIAL

The Supplementary Material for this article can be found online at: https://www.frontiersin.org/articles/10.3389/fphar.2019.00200/full#supplementary-material

**FIGURE S1 |** GTEx Analysis. GTEx gene expression analysis of IDO1, TDO2, CD3e, and PD-L1 in the brain, pancreas, skin, and thyroid.

**FIGURE S2 |** GTEx Analysis. GTEx gene expression analysis of CTLA-4, CD11c, PTGS2, and SLC6A4 in the brain, pancreas, skin, and thyroid.

## REFERENCES

Adachi, K., and Davis, M. M. (2011). T-cell receptor ligation induces distinct signaling pathways in naive vs. antigen-experienced T cells. *Proc. Natl. Acad. Sci. U.S.A.* 108, 1549–1554. doi: 10.1073/pnas.1017340108

Antonia, S. J., Lopez Martin, J. A., Bendell, J., Ott, P. A., Taylor, M., Eder, J. P., et al. (2016). Nivolumab alone and nivolumab plus ipilimumab in recurrent small-cell lung cancer (CheckMate 032): a multicentre, open-label, phase 1/2 trial. *Lancet Oncol.* 17, 883–895. doi: 10.1016/S1470-2045(16)30098-5

Aprahamian, T., Takemura, Y., Goukassian, D., and Walsh, K. (2008). Ageing is associated with diminished apoptotic cell clearance in vivo. *Clin. Exp. Immunol.* 152, 448–455. doi: 10.1111/j.1365-2249.2008.03658.x

Beatty, G. L., and Gladney, W. L. (2015). Immune escape mechanisms as a guide for cancer immunotherapy. *Clin. Cancer Res.* 21, 687–692. doi: 10.1158/1078-0432.CCR-14-1860

Berger, N. A., Savvides, P., Koroukian, S. M., Kahana, E. F., Deimling, G. T., Rose, J. H., et al. (2006). Cancer in the elderly. *Trans. Am. Clin. Climatol. Assoc.* 117, 147–55; discussion 155–156.

Biernat, W., Tohma, Y., Yonekawa, Y., Kleihues, P., and Ohgaki, H. (1997). Alterations of cell cycle regulatory genes in primary (de novo) and secondary glioblastomas. *Acta Neuropathol.* 94, 303–309. doi: 10.1007/s004010050711

Bristol-Myers Squibb (2017). *Bristol-Myers Squibb Announces Results from CheckMate -143, a Phase 3 Study of Opdivo (nivolumab) in Patients with Glioblastoma Multiforme*. Available at: https://news.bms.com/press-release/bmy/bristol-myers-squibb-announces-results-checkmate-143-phase-3-study-opdivo-nivoluma

Bulloch, K., Miller, M. M., Gal-Toth, J., Milner, T. A., Gottfried-Blackmore, A., Waters, E. M., et al. (2008). CD11c/EYFP transgene illuminates a discrete network of dendritic cells within the embryonic, neonatal, adult, and injured mouse brain. *J. Comp. Neurol.* 508, 687–710. doi: 10.1002/cne.21668

Cambier, J. (2005). Immunosenescence: a problem of lymphopoiesis, homeostasis, microenvironment, and signaling. *Immunol. Rev.* 205, 5–6. doi: 10.1111/j.0105-2896.2005.00276.x

Carson, M. J., Doose, J. M., Melchior, B., Schmid, C. D., and Ploix, C. C. (2006). CNS immune privilege: hiding in plain sight. *Immunol. Rev.* 213, 48–65. doi: 10.1111/j.1600-065X.2006.00441.x

Chen, C. Z., Schaffert, S., Fragoso, R., and Loh, C. (2013). Regulation of immune responses and tolerance: the microRNA perspective. *Immunol. Rev.* 253, 112–128. doi: 10.1111/imr.12060

Choi, E., Lee, S., Nhung, B. C., Suh, M., Park, B., Jun, J. K., et al. (2017). Cancer mortality-to-incidence ratio as an indicator of cancer management outcomes in organization for economic cooperation and development countries. *Epidemiol. Health* 39:e2017006. doi: 10.4178/epih.e2017006

Chongsathidkiet, P., Jackson, C., Koyama, S., Loebel, F., Cui, X., Farber, S. H., et al. (2018). Sequestration of T cells in bone marrow in the setting of glioblastoma and other intracranial tumors. *Nat. Med.* 24, 1459–1468. doi: 10.1038/s41591-018-0135-2

D'Agostino, P. M., Gottfried-Blackmore, A., Anandasabapathy, N., and Bulloch, K. (2012). Brain dendritic cells: biology and pathology. *Acta Neuropathol.* 124, 599–614. doi: 10.1007/s00401-012-1018-0

Davila, D. R., Edwards, C. K. III, Arkins, S., Simon, J., and Kelley, K. W. (1990). Interferon-gamma-induced priming for secretion of superoxide anion and tumor necrosis factor-alpha declines in macrophages from aged rats. *FASEB J.* 4, 2906–2911. doi: 10.1096/fasebj.4.11.2165948

Dunn, G. P., Old, L. J., and Schreiber, R. D. (2004). The immunobiology of cancer immunosurveillance and immunoediting. *Immunity* 21, 137–148. doi: 10.1016/j.immuni.2004.07.017

Dutta, S., and Sengupta, P. (2016). Men and mice: relating their ages. *Life Sci.* 152, 244–248. doi: 10.1016/j.lfs.2015.10.025

Ekstrand, A. J., Sugawa, N., James, C. D., and Collins, V. P. (1992). Amplified and rearranged epidermal growth factor receptor genes in human glioblastomas reveal deletions of sequences encoding portions of the N- and/or C-terminal tails. *Proc. Natl. Acad. Sci. U.S.A.* 89, 4309–4313. doi: 10.1073/pnas.89.10.4309

Filley, A. C., Henriquez, M., and Dey, M. (2017). Recurrent glioma clinical trial, CheckMate-143: the game is not over yet. *Oncotarget* 8, 91779–91794. doi: 10.18632/oncotarget.21586

Fox, J. G., Davisson, M. T., and Smith, A. L. (2007). *The Mouse in Biomedical Research*. New York, NY: Academic Press.

Gon, Y., Hashimoto, S., Hayashi, S., Koura, T., Matsumoto, K., and Horie, T. (1996). Lower serum concentrations of cytokines in elderly patients with pneumonia and the impaired production of cytokines by peripheral blood monocytes in the elderly. *Clin. Exp. Immunol.* 106, 120–126.

Johnson, D. R., and O'Neill, B. P. (2012). Glioblastoma survival in the United States before and during the temozolomide era. *J. Neurooncol.* 107, 359–364. doi: 10.1007/s11060-011-0749-4

Kaunzner, U. W., Miller, M. M., Gottfried-Blackmore, A., Gal-Toth, J., Felger, J. C., McEwen, B. S., et al. (2012). Accumulation of resident and peripheral dendritic cells in the aging CNS. *Neurobiol. Aging* 33, 681.e1–693.e1. doi: 10.1016/j.neurobiolaging.2010.06.007

Kohanbash, G., Carrera, D. A., Shrivastav, S., Ahn, B. J., Jahan, N., and Mazor, T. (2017). Isocitrate dehydrogenase mutations suppress STAT1 and CD8+ T cell accumulation in gliomas. *J. Clin. Invest.* 127, 1425–1437. doi: 10.1172/JCI90644

Kugel, C. H. III, Douglass, S. M., Webster, M. R., Kaur, A., Liu, Q., Yin, X., et al. (2018). Age correlates with response to anti-PD1, reflecting age-related differences in intratumoral effector and regulatory T-cell populations. *Clin. Cancer Res.* 24, 5347–5356. doi: 10.1158/1078-0432.CCR-18-1116

Ladomersky, E., Zhai, L., Gritsina, G., Genet, M., Lauing, K. L., Wu, M., et al. (2016). Wainwright, advanced age negatively impacts survival in an experimental brain tumor model. *Neurosci. Lett.* 630, 203–208. doi: 10.1016/j.neulet.2016.08.002

Ladomersky, E., Zhai, L., Lenzen, A., Lauing, K. L., Qian, J., Scholtens, D. M., et al. (2018). IDO1 inhibition synergizes with radiation and PD-1 blockade to durably increase survival against advanced Glioblastoma. *Clin. Cancer Res.* 24, 2559–2573. doi: 10.1158/1078-0432.CCR-17-3573

Larkin, J., Chiarion-Sileni, V., Gonzalez, R., Grob, J. J., Cowey, C. L., Lao, C. D., et al. (2015). Combined nivolumab and ipilimumab or monotherapy in untreated melanoma. *N. Engl. J. Med.* 373, 23–34. doi: 10.1056/NEJMoa1504030

Li, G., Yu, M., Lee, W. W., Tsang, M., Krishnan, E., Weyand, C. M., et al. (2012). Decline in miR-181a expression with age impairs T cell receptor sensitivity by increasing DUSP6 activity. *Nat. Med.* 18, 1518–1524. doi: 10.1038/nm.2963

Liu, Y., Sanoff, H. K., Cho, H., Burd, C. E., Torrice, C., Ibrahim, J. G., et al. (2009). Expression of p16(INK4a) in peripheral blood T-cells is a biomarker of human aging. *Aging Cell* 8, 439–448. doi: 10.1111/j.1474-9726.2009.00489.x

McElhaney, J. E., and Dutz, J. P. (2008). Better influenza vaccines for older people: what will it take? *J. Infect. Dis.* 198, 632–634. doi: 10.1086/590435

Motzer, R. J., Escudier, B., McDermott, D. F., George, S., Hammers, H. J., Srinivas, S., et al. (2015). Nivolumab versus everolimus in advanced renal-cell carcinoma. *N. Engl. J. Med.* 373, 1803–1813. doi: 10.1056/NEJMoa1510665

Nduom, E. K., Wei, J., Yaghi, N. K., Huang, N., Kong, L. Y., Gabrusiewicz, K., et al. (2016). PD-L1 expression and prognostic impact in glioblastoma. *Neuro Oncol.* 18, 195–205. doi: 10.1093/neuonc/nov172

Nikolich-Zugich, J. (2018). The twilight of immunity: emerging concepts in aging of the immune system. *Nat. Immunol.* 19, 10–19. doi: 10.1038/s41590-017-0006-x

Ohgaki, H., Dessen, P., Jourde, B., Horstmann, S., Nishikawa, T., Di Patre, L. P., et al. (2004). Genetic pathways to glioblastoma: a population-based study. *Cancer Res.* 64, 6892–6899. doi: 10.1158/0008-5472.CAN-04-1337

Ohgaki, H., and Kleihues, P. (2005). Population-based studies on incidence, survival rates, and genetic alterations in astrocytic and oligodendroglial gliomas. *J. Neuropathol. Exp. Neurol.* 64, 479–489. doi: 10.1093/jnen/64.6.479

Ohgaki, H., and Kleihues, P. (2007). Genetic pathways to primary and secondary glioblastoma. *Am. J. Pathol.* 170, 1445–1453. doi: 10.2353/ajpath.2007.070011

Pallotta, M. T., Orabona, C., Volpi, C., Vacca, C., Belladonna, M. L., Bianchi, R., et al. (2011). Indoleamine 2,3-dioxygenase is a signaling protein in long-term tolerance by dendritic cells. *Nat. Immunol.* 12, 870–878. doi: 10.1038/ni.2077

Pang, W. W., Price, E. A., Sahoo, D., Beerman, I., Maloney, W. J., Rossi, D. J., et al. (2011). Human bone marrow hematopoietic stem cells are increased in frequency and myeloid-biased with age. *Proc. Natl. Acad. Sci. U.S.A.* 108, 20012–20017. doi: 10.1073/pnas.1116110108

Perry, V. H., Matyszak, M. K., and Fearn, S. (1993). Altered antigen expression of microglia in the aged rodent CNS. *Glia* 7, 60–67. doi: 10.1002/glia.440070111

Ries, L. A. G., Harkins, D., Krapcho, M., Mariotto, A., Miller, B. A., Feuer, E. J., et al. (2006). *SEER Cancer Statistics Review, 1975-2003*. Behtesda, MD: National Cancer Institute.

Rogers, J., Luber-Narod, J., Styren, S. D., and Civin, W. H. (1988). Expression of immune system-associated antigens by cells of the human central nervous system: relationship to the pathology of Alzheimer's disease. *Neurobiol. Aging* 9, 339–349. doi: 10.1016/S0197-4580(88)80079-4

Rossi, D. J., Bryder, D., Zahn, J. M., Ahlenius, H., Sonu, R., Wagers, A. J., et al. (2005). Cell intrinsic alterations underlie hematopoietic stem cell aging. *Proc. Natl. Acad. Sci. U.S.A.* 102, 9194–9199. doi: 10.1073/pnas.0503280102

Schreiber, K., Arina, A., Engels, B., Spiotto, M. T., Sidney, J., Sette, A., et al. (2012). Spleen cells from young but not old immunized mice eradicate large established cancers. *Clin. Cancer Res.* 18, 2526–2533. doi: 10.1158/1078-0432.CCR-12-0127

Shang, B., Liu, Y., Jiang, S. J., and Liu, Y. (2015). Prognostic value of tumor-infiltrating FoxP3+ regulatory T cells in cancers: a systematic review and meta-analysis. *Sci. Rep.* 5:15179. doi: 10.1038/srep15179

Sharpless, N. (2018). *The Challenging Landscape of Cancer and Aging: Charting a Way Forward*. Available at: https://www.cancer.gov/news-events/cancer-currents-blog/2018/sharpless-aging-cancer-research

Shurin, M. R. (2012). Cancer as an immune-mediated disease. *Immunotargets Ther.* 1, 1–6. doi: 10.2147/ITT.S29834

Stupp, R., Hegi, M. E., Mason, W. P., van den Bent, M. J., Taphoorn, M. J., Janzer, R. C., et al. (2009). Effects of radiotherapy with concomitant and adjuvant temozolomide versus radiotherapy alone on survival in glioblastoma in a randomised phase III study: 5-year analysis of the EORTC-NCIC trial. *Lancet Oncol.* 10, 459–466. doi: 10.1016/S1470-2045(09)70025-7

Stupp, R., Mason, W. P., van den Bent, M. J., Weller, M., Fisher, B., Taphoorn, M. J., et al. (2005). Radiotherapy plus concomitant and adjuvant temozolomide for glioblastoma. *N. Engl. J. Med.* 352, 987–996. doi: 10.1056/NEJMoa043330

Stupp, R., Taillibert, S., Kanner, A., Read, W., Steinberg, D., Lhermitte, B., et al. (2017). Effect of tumor-treating fields plus maintenance temozolomide vs maintenance temozolomide alone on survival in patients with glioblastoma: a randomized clinical trial. *JAMA* 318, 2306–2316. doi: 10.1001/jama.2017.18718

Wainwright, D. A., Balyasnikova, I. V., Chang, A. L., Ahmed, A. U., Moon, K. S., Auffinger, B., et al. (2012). IDO expression in brain tumors increases the recruitment of regulatory T cells and negatively impacts survival. *Clin. Cancer Res.* 18, 6110–6121. doi: 10.1158/1078-0432.CCR-12-2130

Wen, P. Y., and Kesari, S. (2008). Malignant gliomas in adults. *N. Engl. J. Med.* 359, 492–507. doi: 10.1056/NEJMra0708126

Wick, G., Backovic, A., Rabensteiner, E., Plank, N., Schwentner, C., and Sgonc, R. (2010). The immunology of fibrosis: innate and adaptive responses. *Trends Immunol.* 31, 110–119. doi: 10.1016/j.it.2009.12.001

Yan, H., Parsons, D. W., Jin, G., McLendon, R., Rasheed, B. A., Yuan, W., et al. (2009). IDH1 and IDH2 mutations in gliomas. *N. Engl. J. Med.* 360, 765–773. doi: 10.1056/NEJMoa0808710

Yancik, R., Wesley, M. N., Ries, L. A., Havlik, R. J., Edwards, B. K., and Yates, J. W. (2001). Effect of age and comorbidity in postmenopausal breast cancer patients aged 55 years and older. *JAMA* 285, 885–892. doi: 10.1001/jama.285.7.885

Yancik, R., Wesley, M. N., Ries, L. A., Havlik, R. J., Long, S., Edwards, B. K., et al. (1998). Comorbidity and age as predictors of risk for early mortality of male and female colon carcinoma patients: a population-based study. *Cancer* 82, 2123–2134. doi: 10.1002/(SICI)1097-0142(19980601)82:11<2123::AID-CNCR6>3.0.CO;2-W

Young, J. S., Chmura, S. J., Wainwright, D. A., Yamini, B., Peters, K. B., and Lukas, R. V. (2017). Management of glioblastoma in elderly patients. *J. Neurol. Sci.* 380, 250–255. doi: 10.1016/j.jns.2017.07.048

Yue, Q., Zhang, X., Ye, H. X., Wang, Y., Du, Z. G., Yao, Y., et al. (2014). The prognostic value of Foxp3+ tumor-infiltrating lymphocytes in patients with glioblastoma. *J. Neurooncol.* 116, 251–259. doi: 10.1007/s11060-013-1314-0

Zeng, D. Q., Yu, Y. F., Ou, Q. Y., Li, X. Y., Zhong, R. Z., Xie, C. M., et al. (2016). Prognostic and predictive value of tumor-infiltrating lymphocytes for clinical

therapeutic research in patients with non-small cell lung cancer. *Oncotarget* 7, 13765–13781. doi: 10.18632/oncotarget.7282

Zhai, L., Ladomersky, E., Lauing, K. L., Wu, M., Genet, M., and Gritsina, G. (2017). Infiltrating T cells increase IDO1 expression in glioblastoma and contribute to decreased patient survival. *Clin. Cancer Res.* 23, 6650–6660. doi: 10.1158/1078-0432.CCR-17-0120

Zhai, L., Ladomersky, E., Lenzen, A., Nguyen, B., Patel, R., Lauing, K. L., et al. (2018). Wainwright, IDO1 in cancer: a Gemini of immune checkpoints. *Cell. Mol. Immunol.* 15, 447–457. doi: 10.1038/cmi.2017.143

Zhong, Z., Sanchez-Lopez, E., and Karin, M. (2016). Autophagy, inflammation, and immunity: a troika governing cancer and its treatment. *Cell* 166, 288–298. doi: 10.1016/j.cell.2016.05.051

**Conflict of Interest Statement:** The authors declare that the research was conducted in the absence of any commercial or financial relationships that could be construed as a potential conflict of interest.

frontiers in Oncology

ORIGINAL RESEARCH
published: 02 April 2019
doi: 10.3389/fonc.2019.00197

# Bronchoalveolar Lavage Fluid-Derived Exosomes: A Novel Role Contributing to Lung Cancer Growth

*Yibao Yang[1†], Ping Ji[1†], Xuan Wang[2], Hao Zhou[2], Junlu Wu[1], Wenqing Quan[1], Anquan Shang[1], Junjun Sun[1], Chenzheng Gu[1], Jenni Firrman[3], Weidong Xiao[4], Zujun Sun[1*] and Dong Li[1*]*

[1] Department of Clinical Laboratory, Shanghai Tongji Hospital, Tongji University School of Medicine, Shanghai, China, [2] Department of Pharmacy, Putuo People's Hospital, Shanghai, China, [3] Dairy and Functional Foods Research Unit, Agriculture Research Service, Eastern Regional Research Center, United States Department of Agriculture, Wyndmoor, PA, United States, [4] Sol Sherry Thrombosis Research Center, Temple University, Philadelphia, PA, United States

OPEN ACCESS

**Edited by:**
Andrew Zloza,
Rush University Medical Center,
United States

**Reviewed by:**
Praveen Bommareddy,
Rutgers University, The State University of New Jersey,
United States
Prakash Gangadaran,
Kyungpook National University,
South Korea
Susanne Gabrielsson,
Karolinska Institutet (KI), Sweden

***Correspondence:**
Zujun Sun
14111010030@fudan.edu.cn
Dong Li
lidong@tongji.edu.cn

[†]These authors have contributed equally to this work

**Specialty section:**
This article was submitted to Cancer Molecular Targets and Therapeutics, a section of the journal Frontiers in Oncology

**Received:** 03 January 2019
**Accepted:** 07 March 2019
**Published:** 02 April 2019

**Citation:**
Yang Y, Ji P, Wang X, Zhou H, Wu J, Quan W, Shang A, Sun J, Gu C, Firrman J, Xiao W, Sun Z and Li D (2019) Bronchoalveolar Lavage Fluid-Derived Exosomes: A Novel Role Contributing to Lung Cancer Growth. Front. Oncol. 9:197. doi: 10.3389/fonc.2019.00197

Exosomes are nanovesicles produced by a number of different cell types and regarded as important mediators of cell-to-cell communication. Although bronchoalveolar lavage fluid (BALF) has been shown to be involved in the development of tumors, its role in lung cancer (LC) remains unclear. In this article, we systemically studied BALF-derived exosomes in LC. C57BL/6 mice were injected with Lewis lung carcinoma cells and exposed to non-typeable *Haemophilus influenza* (NTHi) lysate. The analysis showed that the growth of lung tumors in these mice was significantly enhanced compared with the control cohort (only exposure to air). Characterization of the exosomes derived from mouse BALF demonstrated elevated levels of tumor necrosis factor alpha and interleukin-6 in mice exposed to NTHi lysates. Furthermore, abnormal BALF-derived exosomes facilitated the development of LC *in vitro* and *in vivo*. The internalization of the BALF-derived exosomes contributed to the development of LC tumors. Collectively, our data demonstrated that exosomes in BALF are a key factor involved in the growth and progression of lung cancer.

**Keywords: exosomes, lung cancer, bronchoalveolar lavage fluid, non-typeable *Haemophilus influenza*, tumor necrosis factor alpha**

## INTRODUCTION

Lung cancer (LC) is a serious public health problem and a major cause of cancer-related death worldwide. Owing to the difficulties in the early detection of LC, the mortality rate among patients remains high, with a 5-year survival rate of merely 18% after diagnosis (1). Pulmonary adenocarcinoma is the major histological type of lung tumors (2). Emerging evidence indicates that the tumor microenvironment (TME) is closely associated with tumor progression (3). Studies investigating the communication between the TME and tumor cells have mostly been limited to soluble factors produced by inflammatory cells in the TME, which may contribute to the development of cancer (4, 5). A growing body of evidence suggests that exosomes mediate cell-to-cell communication (6, 7), and play an important role in tumor progression and metastasis (8–10).

Exosomes are nanoscale vesicles with a size ranging from 30 nm to 150 nm (11–13). In 1983, Johnstone identified these vesicles termed exosomes in culture supernatant and regarded them as a waste product released by erythrocytes (14). Exosomes are secreted by various living cells, including macrophages (15), dendritic cells (16), B cells (17), platelets (18), and tumor cells (19). In addition, exosomes have been found in body fluids, such as saliva (20), urine (21), breast milk (22), plasma (23), and the bronchoalveolar lavage fluid (BALF) (24). Increasing evidence indicates that exosomes play a key role in disease development *in vivo*. Recently, research suggested that BALF-derived exosomes may contribute to inflammation by increasing the level of cytokines (such as interleukin-13, interferon-γ) and the production of leukotriene C4 (24, 25). In addition, Edward et al. demonstrated that exosomes found in breast milk at different periods of time can promote the epithelial-mesenchymal transition of breast cancer cells (26). However, the role of BALF-derived exosomes in LC remains poorly understood.

In the present study, we investigated the contribution of BALF-derived exosomes to the progression of LC using *in vitro* and *in vivo* models.

## MATERIALS AND METHODS

### Cell Culture and Reagents

Mouse Lewis lung carcinoma (LLC) cells were purchased from the American Type Culture Collection and cultured in Dulbeccos's modified Eagle's medium (DMEM) (Hyclone Laboratories, Inc., South, UT, USA) supplemented with 10% fetal bovine serum (FBS) (Invitrogen, Grand Island, NY, USA), 100 U/mL penicillin and 100 U/mL streptomycin (Hyclone Laboratories, Inc., South, UT, USA), and maintained in a humidified 5% $CO_2$ atmosphere at 37°C.

### Construction of Mouse Lung Cancer Model

C57BL/6 male mice (aged 6–8 weeks) were purchased from Shanghai Experimental Animal Slack limited Ltd, qualified SCXK (Shanghai, China) 2012-0002, and maintained at the pathogen-free Central Animal Facility of the Tongji Hospital of Tongji University. Animal experiments were strictly performed according to the Guidelines for the animal care and use issued by the Animals of the National Institutes of Health in Bethesda, MD, USA. All experiments involving animals were approved by the Ethics Committee of Tongji Hospital of Tongji University. A mouse model of LC was generated as previously described (27) with some modifications. In brief, $2 \times 10^5$ LLC cells per mouse were injected through the tail vein. After 1 week, the mice were exposed to non-typeable *Haemophilus influenza* (NTHi) lysates or filtered air. The mice were exposed to NTHi lysates for 20 min per time, once per week, for 3 weeks. After anesthesia, the animals were sacrificed, and the lungs were removed and fixed for further experiments.

### Measurement of Inflammatory Cells

Bronchoalveloar lavage fluids (BALF) were collected from mice as previously described (28, 29). The total number of leukocytes in the BALF of mice was counted using a hemocytometer, 50 μL of BALF were centrifugated at 12000 rpm, 4 min by cytospin (Thermo-Fischer, Waltham, MA, USA) to determine the percentage of leukocyte populations through Wright-Giemsa staining.

### Exosome Isolation and Labeling

After tracheal intubation of the mice, the lungs were gently lavaged thrice with 1 mL of ice cold, sterile phosphate-buffered saline (PBS). The fluids collected from mice were maintained at −80°C and immediately processed for exosome isolation.

Exosome isolation was performed through differential ultracentrifugation as previously described (28, 29). The concentration of protein in exosome pellets was measured using the bicinchoninic acid assay (Beyotime, Shanghai, China). For the *in vitro* uptake experiment, exosomes were labeled using a PKH67 green fluorescent cell linker mini kit (Sigma Aldrich, St. Louis, MO, USA) according to the instructions provided by the manufacturer. Ten random fields were counted. For the *in vivo* uptake study, the labeling procedure was identical to that used in the *in vitro* analysis. The labeled exosomes were delivered into the mice, and 18 h later the lungs were removed and embedded in OCT compound, and stored at −80°C. Photographs were captured using an immunofluorescence microscope (Nikon, Tokyo, Japan).

## PREPARATION OF NTHI LYSATES

The NTHi lysate was produced from *Haemophilus haemolyticus* as previously described (30). First, the NTHi was inoculated on chocolate agar for 24 h in 5% $CO_2$ at 37°C. Then they were grown in 1 L of brain-heart infusion broth (Sigma-Aldrich, St. Louis, MO) containing 3.5 μg/mL NAD (Sigma-Aldrich, St. Louis, MO). Next, the medium was centrifuged at 2500 × g for 10 min at 4°C, washed and resuspended in 20 mL PBS. The culture was transferred to the 100 mm dish and ultraviolet irradiated. Last, the culture was transferred to a 50 mL tube and sonicated three times for 30 s. The concentration of protein was quantified by a bicinchoninic assay (Beyotime, Shanghai, China) and then adjusted to 2.5 mg/mL in PBS and frozen at −80°C.

### Transmission Electron Microscopy (TEM)

A 10 μL aliquote of the exosome suspension was added onto a 200-mesh carbon-coated copper grid for 1 min. Subsequently, the grid was negatively stained with 2% uranyl acetate for 1 min. The sample was observed using a FEI Tecnai G2 spirit transmission electron microscope (Thermo-Fischer, Waltham, MA, USA).

### Nanosight Particle Tracking Analysis (NTA)

For NTA, the size distribution of the purified exosomes was analyzed using the NanoSight LM10 system (Malvern

**Abbreviations:** LC, lung cancer; IL-6, interleukin-6; TNF-α, tumor necrosis factor alpha; TME, tumor microenvironment; EMT, epithelial-mesenchymal transition; COPD, chronic obstructive pulmonary disease; BALF, bronchoalveolar lavage fluid; LLC, Lewis lung carcinoma; NTHi, non-typeable *Haemophilus influenza*; air-Exos, exosomes from mice exposed to air; NTHi-Exos, exosomes from mice exposed to NTHi lysates.

Instruments Ltd. Malvern, UK). In brief, exosome suspension was diluted in PBS. Subsequently, the software of the NanoSight LM10 system was used to determine the concentration and particle size of exosomes.

## Western Blotting Analysis

Western blotting analysis was carried out as previously described (31). Briefly, exosomes were lysed by radio immunoprecipitation assay buffer (RIPA) (CST, Boston, USA) containing protease and phosphatase inhibitor cocktails (Roche). Equal amounts of exosomes were loaded on a 10% SDS polyacrylamide gel. The antibodies used for western blot are as following: CD63, CD9, HSP70, and TSG101 purchased from Santa Cruz (Santa Cruz Biotechnology, Inc., Texas, USA), Calnexin (Abcam plc, Cambridge, UK), PCNA (CST, Boston, USA) HRP-conjugated goat anti-rabbit (Santa Cruz Biotechnology, Inc., Texas, USA) or rabbit-anti-mouse (Dako, Carpinteria. CA, USA) was used as secondary antibody.

## Cell Proliferation Assay

A cell proliferation assay was performed using the cell count kit-8 (DojinDo, Tokyo, Japan). In brief, 1,000 LLC cells were seeded into a 96-well plate and treated with exosomes (5 μg/mL) for 0, 24, 48, and 72 h. Absorbance at 450 nm was measured using a microplate reader (ThermoFisher Scientific, Waltham, MA, USA).

## Cell Migration and Invasion Assay

Invasion and migration assays were performed using a 24-well transwell insert, with 8 μm pores, with or without pre-coated Matrigel (Corning, USA). The LLC cells were trypsinized and washed thrice with serum-free DMEM. A total of $2 \times 10^4$ cells were suspended in 100 μL of serum-free DMEM and added to the upper inserts. Exosomes (10 μg/mL), or PBS (control) were added to wells containing DMEM with 2% FBS. The invasion assay was performed in a similar manner, with minor modification. The LLC cells were co-cultured with exosomes (10 μg/mL) or PBS for 24 h, and subsequently trypsinized and washed for the migration assay. A total of $2 \times 10^4$ cells were suspended in 500 μL of serum-free DMEM and added to the upper inserts. Seven hundred fifty microliter DMEM containing 10% FBS (750 μL) was added to the wells. After 24 h, the LLC cells on the upper surface of the chamber were removed using a cotton swab, whereas those at the lower membrane surface were fixed with 4% paraformaldehyde and stained with 0.1% crystal violet. Ten random fields were counted.

## Enzyme-Linked Immunosorbent Assay (ELISA)

The levels of tumor necrosis factor-α (TNF-α) and interleukin-6 (IL-6) in the exosomes obtained from mouse BALF were measured using ELISA kits (USCN Life Science & Technology, Missouri City, TX, USA) according to the instructions provided by the manufacturer. In brief, before the ELSIA assay, we used RIPA lysis buffers to lysis exosomes and then we adjusted the concentration of exosome. The remaining steps follow the instructions.

## Animal Experiments

LLC cells ($2 \times 10^5$ cells per mouse) were injected into C57BL/6 mice via the tail vain. One week later, purified exosomes (5 μg) or PBS were delivered into the mice twice per week for 2 weeks. All mice were sacrificed 4 weeks after injection. Tumor volume ($mm^3$) was calculated as $(a^2 \times b)/2$, where "a" and "b" represent the width and length, respectively.

## Histology and Immunohistochemistry

Lungs were fixed in 10% formalin and embedded in paraffin. Tumor tissues were cut into 4 μm thick sections and stained using a hematoxylin and eosin (H&E) kit, according to the instructions provided by the manufactures. For the immunohistochemical experiment, tumor tissue was incubated with primary antibodies against proliferating cell nuclear antigen (PCNA) overnight at 4°C. Subsequently, the tumor tissues were washed using PBS, and the analysis was performed using the GTvision IHC kit (Gene Tech, Shanghai, China) according to the instructions provided by the manufacture.

## Statistical Analysis

Values are presented as means ± standard error of the mean (SEM). Student's *t*-test (two-sided) was applied for the analysis of differences between two groups. $P < 0.05$ denoted statistical significance. All data were analyzed using the SPSS 22 statistical software (SPSS Inc, Chicago, IL, USA).

# RESULTS

## NTHi Lysates Promote Lung Tumor Growth

Inflammation plays a key role in tumor progression (32). We established a metastatic mouse model of LC to better understand the mechanism through which NTHi lysates induce the development of lung neoplasma. Mice were exposed to either 2.5 mg/mL NTHilysates (**Figure 1A**) or clean air. After 3 weeks, we found that the mice exposed to NTHi lysates exhibited a significant increase in lung tumor growth compared with those exposed to air. H&E staining demonstrated that the tumor nodules were significantly increased, and the diameter of the tumor was larger in mice exposed to NTHi lysates vs. air-exposed mice (**Figure 1B**). The maximum diameter and number of lung tumor nodules greatly increased in mice treated with NTHi lysates compared with those observed in mice exposed to air (**Figures 1C,D**). In addition, we found that the number of total leukocyte cells, neutrophils, and macrophages in the BALF increased in mice exposed to NTHi compared with those reported in those exposed to air (**Figures 2A–C**). However, the number of lymphocytes remained unchanged (**Figure 2D**). Significant differences were also found in exosomal protein concentration after NTHi exposure vs. air exposure due to the large increase in cell numbers (**Figure 2E**).

## Characterization of Exosomes From the BALF of Mice

Exosomes in the BALF of mice exposed to NTHi lysates or air were purified through differential ultracentrifugation—an established method for the isolation of exosomes (31).

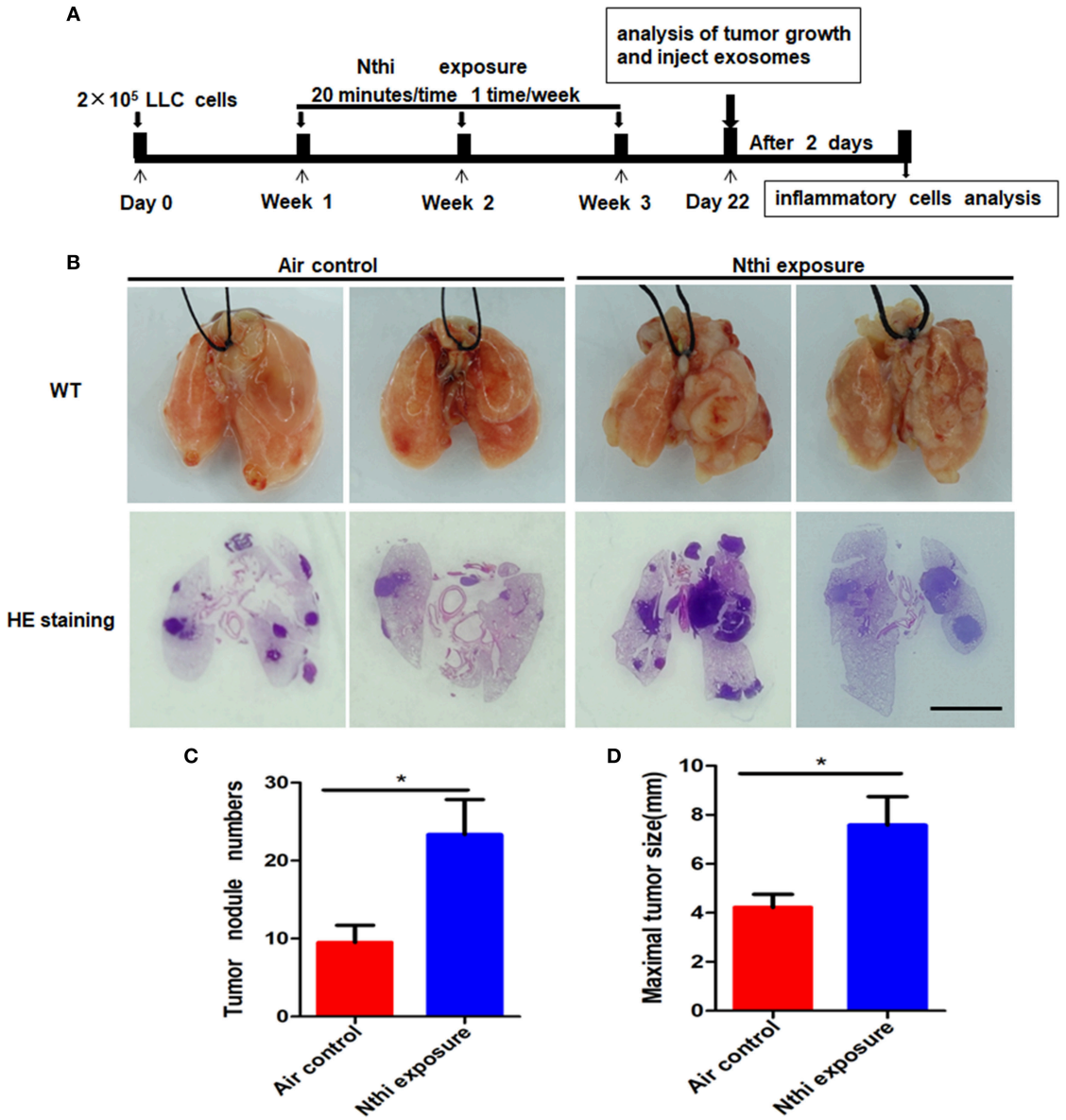


**FIGURE 1 |** Exposure to NTHi lysate promotes the development of lung tumor. **(A)** Scheme of experimental protocols for the promotion of NTHi-induced lung cancer. **(B)** Lung appearance and histology in WT mice 3 weeks after initiation of the NTHi lysate exposure protocol. Scar bar = 100 μm. **(C,D)** The number of tumor nodules and the maximal tumor diameter detectable on the surface were determined. Results are means ± SEM ($n = 7$), $^*P < 0.05$.

The morphology of exosomes was analyzed using TEM. Both BALF-derived air-Exos (i.e., exosomes obtained from mice exposed to air) and NTHi-Exos (i.e., exosomes obtained from mice exposed to NTHi) were typical rounded vesicles ranging from 30 to 150 nm in size (**Figure 3A**). Western blotting analysis demonstrated that the exosomes were positive for the hallmark exosome proteins, including CD63, CD9, Hsp70, and Tsg101 (28, 29) (**Figure 3B**). The NTA showed that the peak sizes of air-Exos and NTHi-Exos were 63 nm and 41 nm, respectively (**Figure 3C**). Collectively, these data indicated that BALF-derived vesicles exhibit the general features associated with exosomes.

## Proinflammatory Cytokines Were Upregulated in NTHi-Exos

Subsequently, we investigated the cytokine content (i.e., TNF-α and IL-6) of exosomes released in response to exposure to NTHi lysates. The results showed that the levels of TNF-α and IL-6 were upregulated in NTHi-Exos compared vs. air-Exos (**Figures 4A,B**).

## NTHi-Exos Promote the Proliferation, Migration, and Invasion of LLC Cells

We labeled the exosomes obtained from the BALF of mice using the green fluorescent marker PKH67 and co-cultured them with

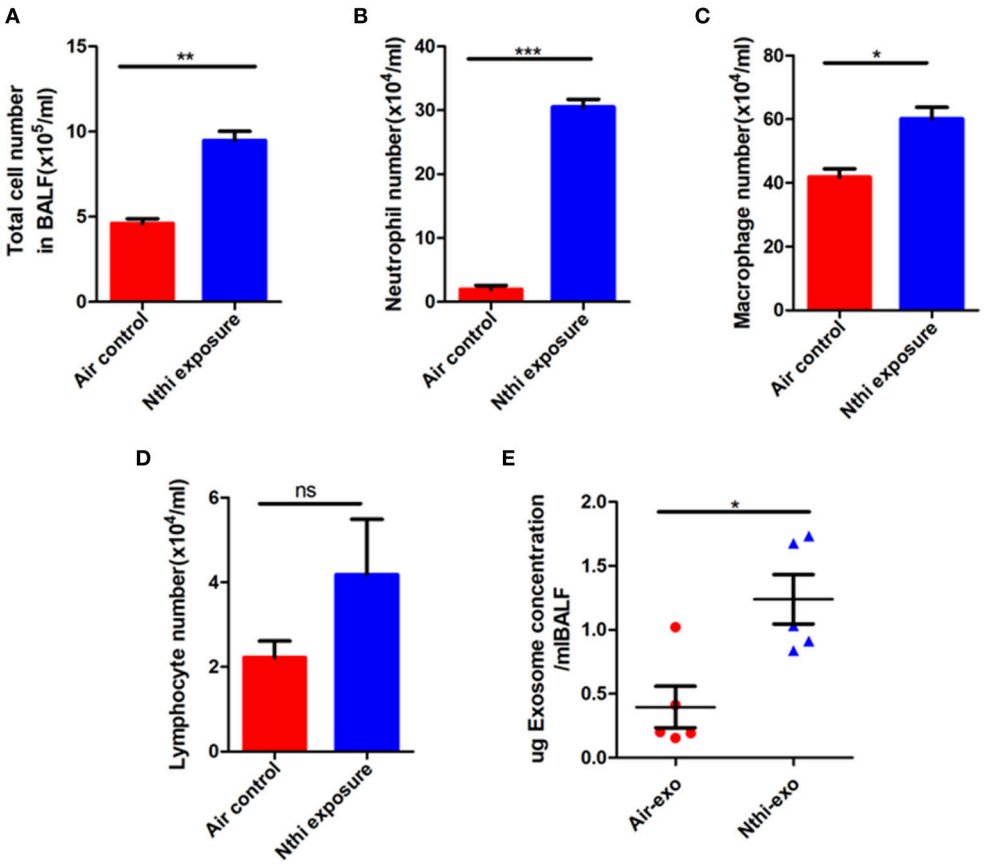


**FIGURE 2 |** Analysis of the cells and exosomal protein concentration in the bronchoalveolar lavage fluid (BALF). **(A)** Total cell numbers in the BALF of mice exposed to NTHi lysate or air. **(B–D)** The composition of cells was evaluated through cytospin preparations. The number of **(B)** neutrophils, **(C)** macrophages, and **(D)** lymphocytes in the BALF of mice exposed to NTHi lysate or air. **(E)** Concentration of exosomal protein (μg) from BALF of NTHi- and air-induced mice. Results are means ± SEM ($n = 5$), $^*P < 0.05$, $^{**}P < 0.01$, $^{***}P < 0.001$.

LLC cells for 24 h to determine the uptake of exosomes by LC cells. The results showed that LLC cells can uptake exosomes (**Figure 5A**). Meanwhile, we found that the percentage of LLC cells engulfing NTHi-exo is much higher than that of Air-exo (**Figure 5B**). In order to examine whether BALF-derived NTHi-Exos or air-Exos exerted an effect on LLC cells, we investigated the effect of BALF-derived NTHi-Exos and air-Exos on their proliferation, migration, and invasion. LLC cells co-cultured with NTHi-Exos exhibited higher proliferation rates than those co-cultured with air-Exos or control (**Figure 6A**). In addition, LLC cells treated with NTHi-Exos showed higher motility than those treated with air-Exos or control (**Figure 6B**). Similar to the results of migration, cellular invasion was also enhanced in response to the NTHi-Exos condition (**Figure 6C**). These results revealed that BALF-derived NTHi-Exoscan promote the proliferation, migration, and invasion of LLC cells.

## NTHi-Exos Promote LC Growth *in vivo*

We used a metastatic mouse model of LC for animal experiments to further examine the role of BALF-derived exosomes on tumor growth *in vivo*. We delivered PKH67-labeled exosomes into C57BL/6 mice using a new intubation method (33). After 18 h, we observed that the exosomes were internalized by tumor cells (**Figure 7A**). Subsequently, according to the experimental flow chart (**Figure 7B**), mice were sacrificed 4 weeks later, and the lungs were removed for further analysis. H&E staining showed that the tumor nodules were significantly increased, and the diameter of the tumors was larger in mice treated with NTHi-Exos than in mice treated with air-Exos or control (**Figure 7C**). The results showed that the number of tumor nodules and volume of the tumors in mice treated with NTHi-Exos were significantly larger vs. those observed in mice treated with air-Exos or control (**Figures 7D,E**). Moreover, the expression level of PCNA—a marker of proliferation—was highly increased in mice treated with NTHi-Exos (**Figures 7F,G**). These results suggest that NTHi-Exos can facilitate tumor growth *in vivo*.

## DISCUSSION

The present study identified and characterized BALF-derived exosomes from mice. The data obtained using TEM, NanoSight NTA, and western blotting analysis, clearly demonstrated that

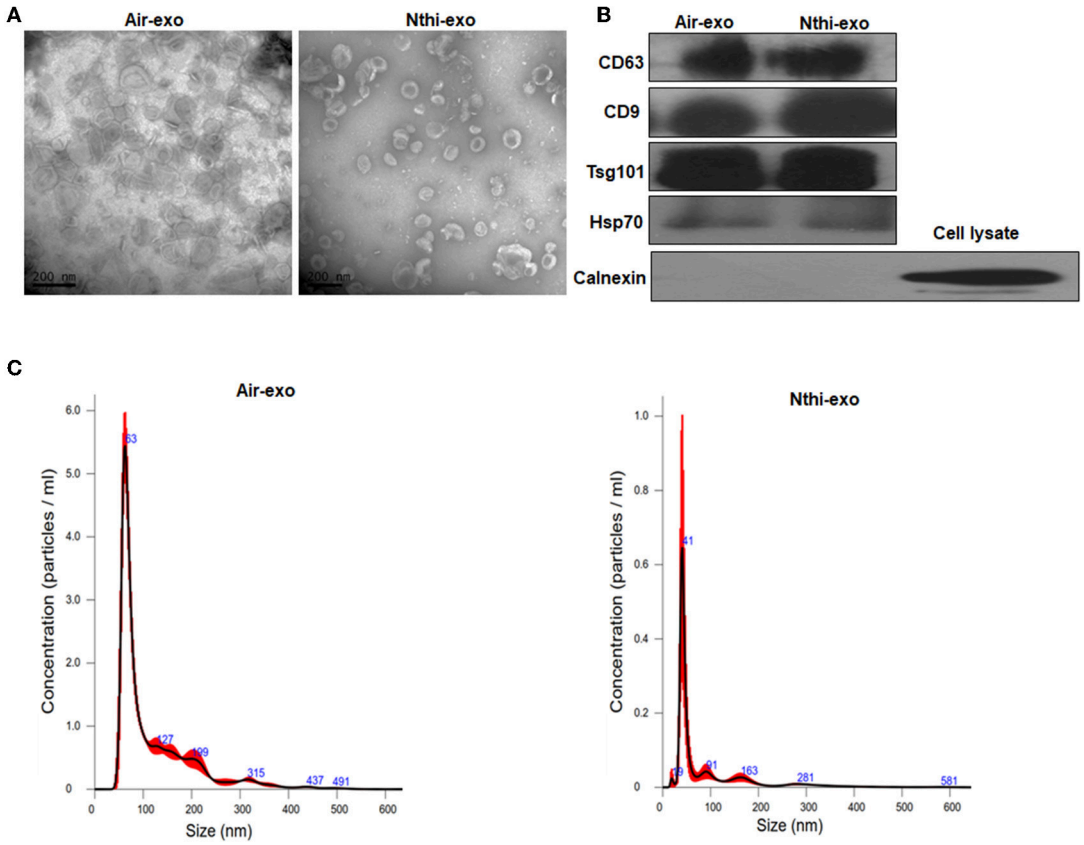


**FIGURE 3 |** Characterization of exosomes from the BALF of mice exposed to NTHi lysate or air. **(A)** Transmission electron microscopy images of NTHi-Exos and air-Exos. **(B)** Western blotting analysis of exosomal markers CD63, CD9, Hsp70, Tsg101, and negative biomarkers Calnexin. **(C)** Nanoparticle tracking analysis determined the size distribution of NTHi-Exos and air-Exos. Results are presented as means ± SEM of three independent experiments.

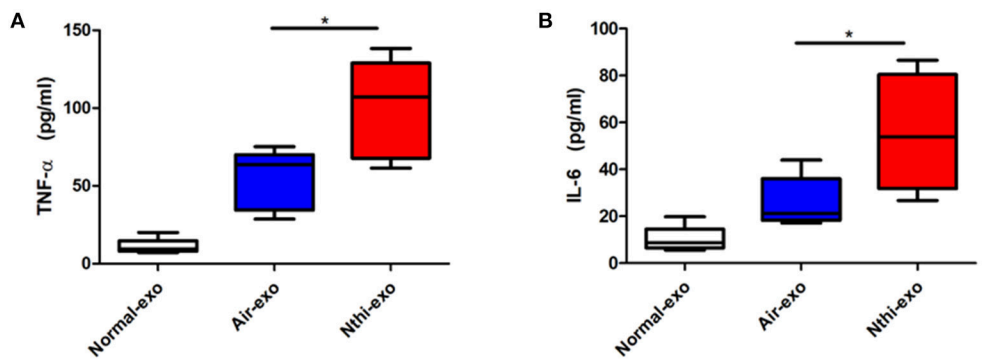


**FIGURE 4 |** The expression of TNF-αand IL-6in exosomes from the BALF. **(A)** The levels of TNF-α and **(B)** IL-6 were analyzed using ELISA. Results are means ± SEM ($n = 5$, $^*P < 0.05$).

BALF-derived exosomes exhibit the typical size, morphology, and markers associated with exosomes. Interestingly, we found that, in mice treated with NTHi lysates, BALF-derived exosomes enhanced the growth, migration, and invasion of LLC cells. Chronic obstructive pulmonary disease (COPD) is an important risk factor for lung cancer, and bacterial pathogens frequently colonize in COPD patients, which always induce chronic inflammation of lung. NTHi—a small Gram-negative bacterium—is most often localized in the airways of patients with chronic obstructive pulmonary disease (30). Therefore, we used NTHi lysates to induce chronic inflammation to investigate how bacterial pathogens contribute to the development of lung

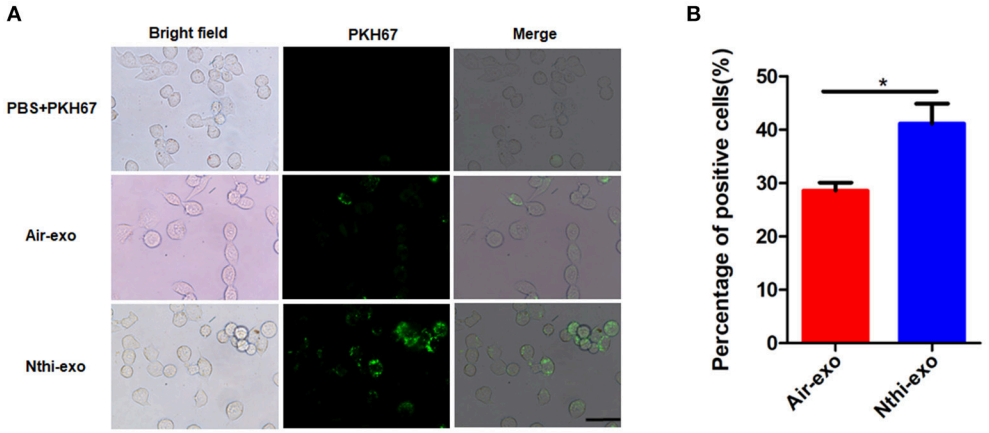


**FIGURE 5 |** Internalization of exosomes from the BALF of mice exposed to NTHi lysate or air. **(A)** LLC cells demonstrated uptake of labeled-exosomes (green fluorescent dye), images are taken at 24 h co-culture with LC cells. Scar bar=100 μm. **(B)** the percentage of positive LLC cells engulfing labeled-exosomes ($n = 10$). Results are presented as means ± SEM. (*$P < 0.05$).

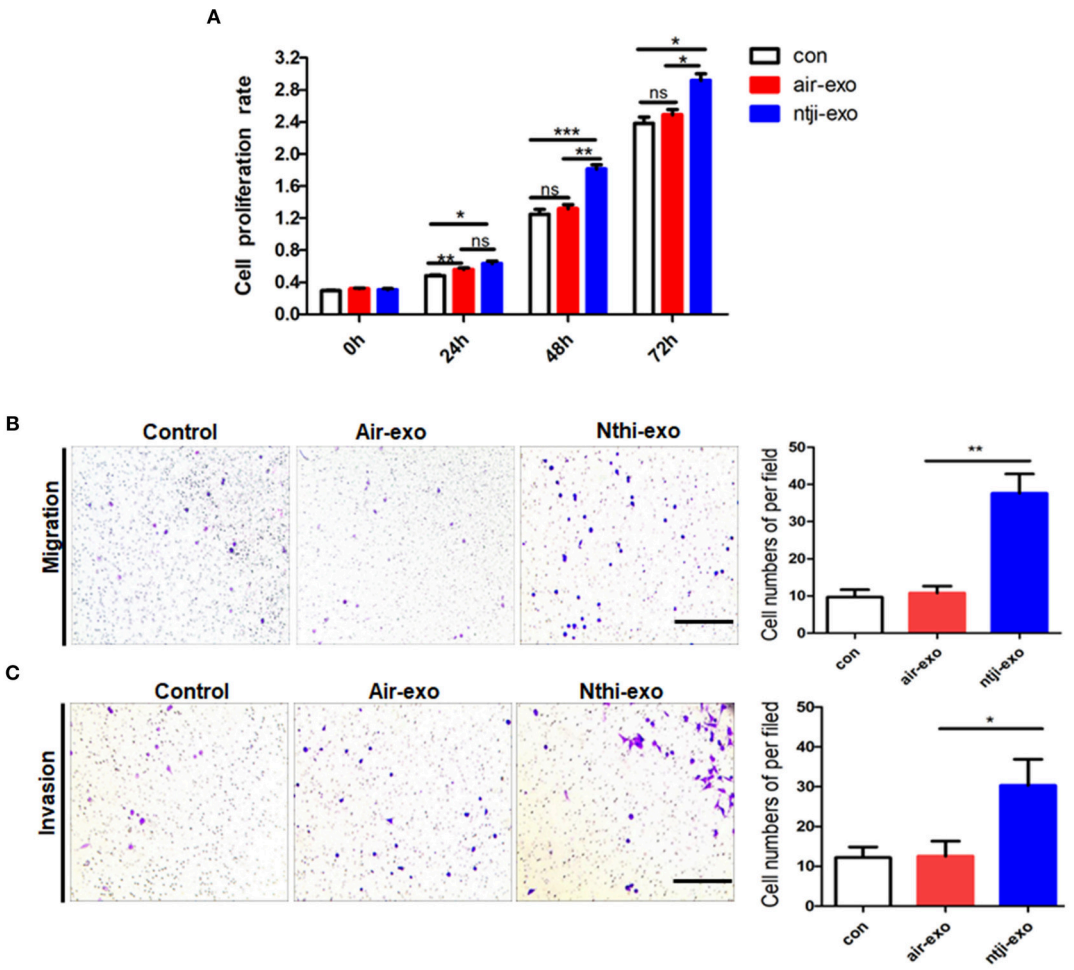


**FIGURE 6 |** Roles of exosomes from the BALF of mice exposed to NTHi lysate or air. **(A)** Cell proliferation assay was performed in LLC cells incubated with PBS, air-Exosor NTHi-Exos ($n = 4$). **(B)** Migration assay was performed in LLC cells co-cultured with PBS, air-Exos or NTHi-Exos ($n = 10$). **(C)** Invasion assay was performed in LLC cells co-cultured with PBS, air-Exos or NTHi-Exos ($n = 10$). Scar bar = 200 μm. Results are presented as means ± SEM of three independent experiments. (*$P < 0.05$, **$P < 0.01$, ***$P < 0.001$).

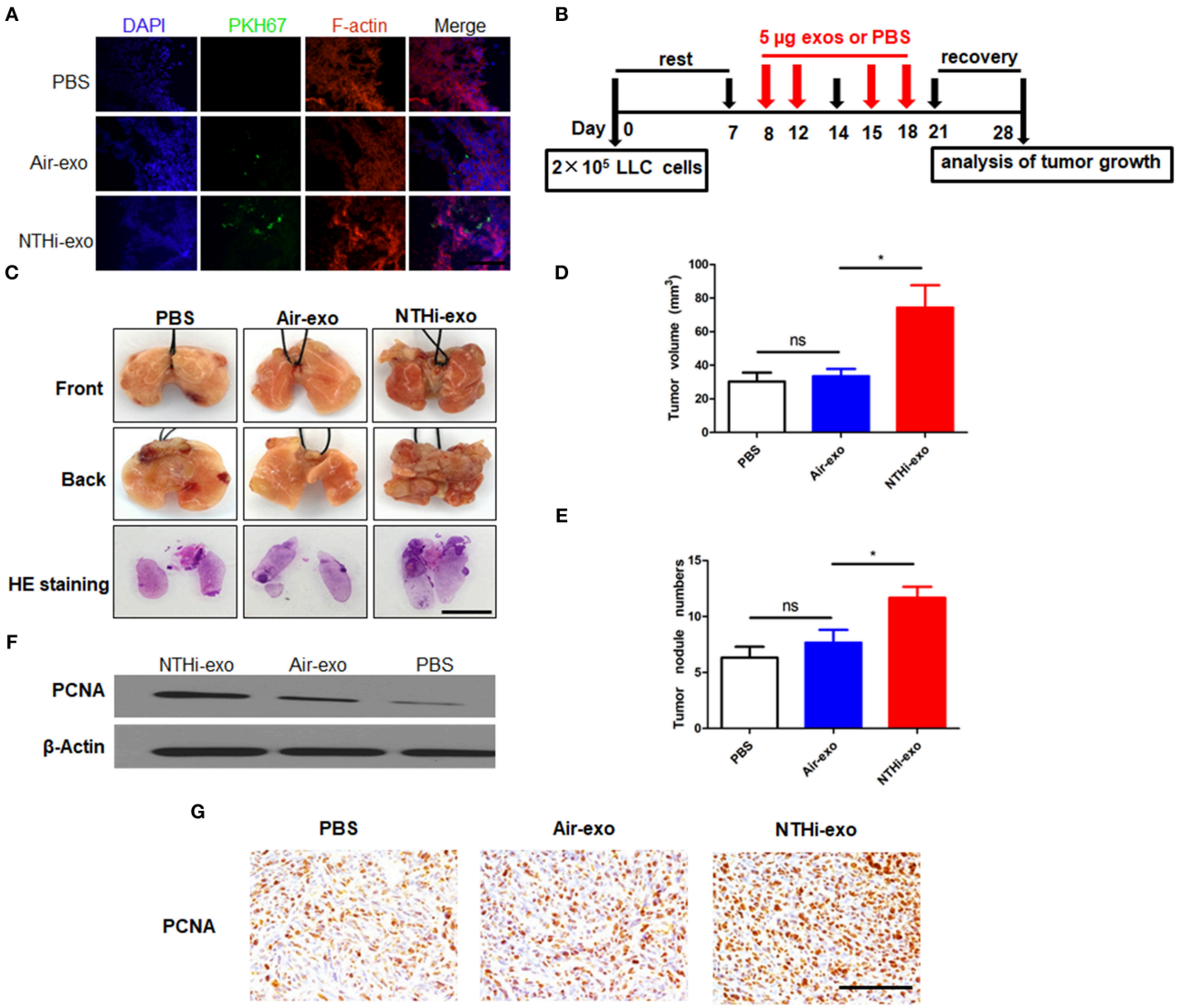


**FIGURE 7 |** NTHi-Exos promote tumor growth *in vivo*. **(A)** Tumor cells demonstrated uptake ofPKH-67 labeled exosomes from the BALF. Scar bar = 100 μm. **(B)** Scheme of experimental protocols for animal experiment. **(C)** Microscopic and macroscopic analysis of lung cancer after injection of exosomes or PBS control (*n* = 5) Scar bar=100 μm. **(D–E)** Lung tumor nodules and volume detectable on the surface were determined. **(F)** Western blotting analysis of PCNA protein levels in excised lung tumors treated with NTHi-Exos, air-Exos, and PBS control. **(G)** Immunohistochemical analysis of PCNA protein levels in tumor tissues. Scar bar=200 μm. Results are presented as means ± SEM of three independent experiments. *$P < 0.05$.

cancer. Evidence has shown that inflammation induced by NTHi resulted in lung tumor progression in *KRAS*-dependent mouse models and *Gprc5a*-knockout mouse models (34, 35). In the present study, we stimulated mice with NTHi lysates to simulate the microenvironment of chronic obstructive pulmonary disease. Our analysis yielded a similar phenomenon regarding the progression of lung cancer (**Figure 1**). The development of tumors in mice stimulated by NTHi-induced inflammation was faster than that observed in mice exposed to air.

Exposure to NTHi lysates led to a significant increase in the number of inflammatory cells and the expression of inflammatory factors in the BALF of mice (36). Moreover, in our study, there was a large increase in the number of inflammatory cells in the BALF of mice following exposure to NTHi, especially neutrophils (**Figure 2**). Notably, the production of exosomes was highly increased in mice exposed to NTHi lysates. We hypothesize that the increase in exosomes is the result of the observed increase in inflammatory cells infiltrating the lungs.

We showed that exosomes from the BALF of mice can be detected in a mouse model of LC. TEM and NanoSight NTA demonstrated that these exosomes were similar to those reported in previous studies, in terms of morphology and size. Notably, the size of BALF-derived exosomes in this study was slightly smaller than those previously reported (i.e., 41–63 nm vs. 100–150 nm,

respectively) (**Figure 3C**). However, these values were consistent with those reported by other groups (12, 29). Furthermore, consistent with previous studies (29), BALF-derived exosomes contained the hallmark protein components of exosomes, such as tetraspanin CD63, CD9, Hsp70, and Tsg101 (**Figure 3B**). Collectively, these data clearly demonstrate that exosomes were successfully isolated from the BALF of mice.

Recently, several groups have shown that exosomes play key roles in cancer progression and metastasis (37). To our knowledge, few studies have shown the relationship between BALF-derived exosomes and LC. Different from previous studies in animals and patients, which have focused on the role of single populations or mixed populations of exosomes in BALF in the inflammatory disease of the lung (24, 38), we focused on whether BALF-derived exosomes can have an effect on lung carcinoma. Therefore, we investigated the functional role of BALF-derived exosomes in LLC cells and animals. We found that BALF-derived exosomes are easily internalized by LLC cells (**Figure 5A**). Our data suggest that the mixed exosomes in the BALF of NTHi-exposed mice can activate LLC cells, resulting in higher cell viability, motility, and invasiveness (**Figure 6**). Moreover, our *in vivo* analysis yielded similar results. With regard to the molecular level—macroscopic or microscopic—the development of tumor in the mice treated with NTHi-Exos was faster than that observed in mice treated with air-Exos or control (**Figures 7C,B,E**). The expression level of PCNA was highly increased in the mice treated with NTHi-Exos (**Figures 7F,G**). We have tested the LLC cells treated directly with NTHi lysate. However, the results showed that there is no effect in migration and invasion of LLC cells stimulated with NTHi lysate (2.5, 5, and 10 μg/μL) (**Figure S1**). These results suggest that NTHi-Exos can facilitate tumor growth *in vivo*.

Although the mechanism involved in this process remains unknown, exosomes are able to modify the microenvironment by potentiating inflammation (24, 25, 39), which plays a critical role in the development of carcinoma (4). Meanwhile, we found that the levels of TNF-α and IL-6 in exosomes were significantly elevated (**Figure 4**). These cytokines are important inflammatory factors involved in the progression of tumor formation. Therefore, we speculate that BALF-derived exosomes affect the TME through their proinflammatory cargo, leading to initial tumorigenesis and tumor progression. Of note, exosomes were pelleted at a speed of 100,000 g (31), it is possible that debris from NTHi co-isolated with the exosomes. The tumor progression may be the result of the co-stimulatory effect.

This study clearly demonstrated that purified exosomes from BALF-derived mice exposed to NTHi lysates can facilitate the growth and progression of LC *in vitro* and *in vivo*. Importantly, our findings further stress the role of exosomes as key elements in the course of lung tumor development and as potential new therapeutic targets.

## AUTHOR CONTRIBUTIONS

DL and ZS designed the study and interpreted the data and amended the manuscript. YY and PJ performed the experiments and drafted the manuscript. XW, HZ, and AS participated in animal testing and flow cytometry analysis. JW, WQ, and CG helped to do the analysis. JF and WX amended the manuscript. All authors read and approved the final version of this manuscript.

## FUNDING

This work was supported by the National Natural Science Foundation of China (81472179, 81873975), the Excellent Academic Leader Training Program of Shanghai Health System (2018BR31), the Clinical Research and Cultivation Project of Shanghai Tongji Hospital [ITJ(ZD)1803], the National Natural Science Foundation Training Program of Tongji Hospital (GJPY1804), and the Project of Shanghai health and family planning commission (20164Y0071).

## SUPPLEMENTARY MATERIAL

The Supplementary Material for this article can be found online at: https://www.frontiersin.org/articles/10.3389/fonc.2019.00197/full#supplementary-material

**Figure S1 |** LLC treated directly with NTHi lysate. **(A)** Proliferation, **(B)** Migration, **(C)** Invasion.

## REFERENCES

1. Siegel RL, Miller KD, Jemal A. Cancer statistics. *CA Cancer J Clin*. (2018) 68:7–30. doi: 10.3322/caac.21442
2. Toh CK. The changing epidemiology of lung cancer. *Methods Mol Biol*. (2009) 472:397–1. doi: 10.1007/978-1-60327-492-0_19
3. Rowley DR. Reprogramming the tumor stroma: a new paradigm. *Cancer Cell*. (2014)26:451–2. doi: 10.1016/j.ccell.2014.09.016
4. Grivennikov SI, Greten FR, Karin M. Immunity, inflammation, and cancer. Cell. (2010)140:883–99. doi: 10.1016/j.cell.2010.01.025
5. Shalapour S, Karin M. Immunity, inflammation, and cancer: an eternal fight between good and evil. *J Clin Invest*. (2015) 125:3347–55. doi: 10.1172/JCI80007
6. A. Becker, BK. Thakur, JM. Weiss, HS. Kim, H. Peinado, D. Lyden, et al. Extracellular vesicles in cancer: cell-to-cell mediators of metastasis. cancer cell (2016) 30:836–8. doi: 10.1016/j.ccell.2016.10.009
7. Tkach M, Thery C. Communication by extracellular vesicles: where we are and where we need to go. *Cell*. (2016)164:1226–32. doi: 10.1016/j.cell.2016.01.043
8. Melo SA, Sugimoto HO', Connell JT, Kato N, Villanueva A, Vidal A, et al. Cancer exosomes perform cell-independent microRNA biogenesis and promote tumorigenesis. *Cancer Cell*. (2014) 26:707–1. doi: 10.1016/j.ccell.2014.09.005
9. Lazar I, Clement E, Dauvillier S, Milhas D, Ducoux-Petit M, LeGonidec S, et al. Adipocyte exosomes promote melanoma aggressiveness through fatty acid oxidation: a novel mechanism linking obesity and cancer. *Cancer Res*. (2016) 76:4051–57. doi: 10.1158/0008-5472.CAN-16-0651
10. HoshinoA, Costa-SilvaB, ShenTL, RodriguesG, HashimotoA, Tesic MarkM,et al. Tumour exosome integrins determine organotropic metastasis. *Nature*. (2015) 527:329–5. doi: 10.1038/nature15756
11. TheryC, ZitvogelL, AmigorenaS. Exosomes: composition, biogenesis and function. *Nat Rev Immunol*. (2002)2:569–9. doi: 10.1038/nri855
12. TheryC, OstrowskiM, SeguraE. Membrane vesicles as conveyors of immune responses. *Nat Rev Immunol*. (2009) 9:581–3. doi: 10.1038/nri2567

13. ColomboM, RaposoG, Thery C. Biogenesis, secretion, and intercellular interactions of exosomes and other extracellular vesicles. *Annu Rev Cell Dev Biol*. (2014) 30:255–9. doi: 10.1146/annurev-cellbio-101512-122326
14. Johnstone RM, Adam M, Hammond JR, Orr L, Turbide C. Vesicle formation during reticulocyte maturation. Association of plasma membrane activities with released vesicles (exosomes). *J Biol Chem*. (1987) 262:9412–20.
15. Binenbaum Y, Fridman E, Yaari Z, Milman N, Schroeder A, Ben David G,et al. Transfer of miRNA in macrophages-derived exosomes induces drug resistance of pancreatic adenocarcinoma. Cancer Res (2018) 78:5287–99.doi: 10.1158/0008-5472.CAN-18-0214
16. Thery C, Duban L, Segura E, Veron P, Lantz O, Amigorena S, et al. Indirect activation of naive CD4+ T cells by dendritic cell-derived exosomes. *Nat Immunol*. (2002) 3:1156–62.doi: 10.1038/ ni854
17. MeckesDG Jr, GunawardenaHP, DekroonRM, HeatonPR, EdwardsRH, OzgurS, et al. Modulation of B-cell exosome proteins by gamma herpesvirus infection. *Proc Natl Acad Sci USA*. (2013) 110:E2925–33. doi: 10.1073/pnas.1303906110
18. Heijnen HF, Schiel AE, Fijnheer R, Geuze HJ, Sixma JJ. Activated platelets release two types of membrane vesicles: microvesicles by surface shedding and exosomes derived from exocytosis of multivesicular bodies and alpha-granules. *Blood*. (1999) 94:3791–99.
19. Gao L, Wang L, Dai T, Jin K, Zhang Z, Wang S, et al. Tumor-derived exosomes antagonize innate antiviral immunity. *Nat Immunol*. (2018) 19:233–5. doi: 10.1038/s41590-017-0043-5
20. Katsiougiannis S, Chia D, Kim Y, Singh RP, Wong DT. Saliva exosomes from pancreatic tumor-bearing mice modulate NK cell phenotype and antitumor cytotoxicity. *FASEB J*. (2017) 31:998–1010.doi: 10.1096/fj.201600984R
21. Rodriguez M, Bajo-Santos C,Hessvik NP, Lorenz S, Fromm B, Berge V, et al. Identification of non-invasive miRNAs biomarkers for prostate cancer by deep sequencing analysis of urinary exosomes. *Mol Cancer*. (2017) 16:156. doi: 10.1186/s12943-017-0726-4
22. Torregrosa Paredes P, Gutzeit C, Johansson S, Admyre C, Stenius F, Alm J, et al. Differences in exosome populations in human breast milk in relation to allergic sensitization and lifestyle. *Allergy*. (2014) 69:463–1.doi: 10.1111/all.12357
23. Vicencio JM, Yellon DM, Sivaraman V, Das D, Boi-Doku C, Arjun S, et al. Plasma exosomes protect the myocardium from ischemia-reperfusion injury. *J Am Coll Cardiol*. (2015) 65:1525–36. doi: 10.1016/j.jacc.2015.02.026
24. Torregrosa Paredes P, Esser J, Admyre C, Nord C,Rahman QK, Lukic A, et al. Bronchoalveolar lavage fluid exosomes contribute to cytokine and leukotriene production in allergic asthma. Allergy (2012) 67:911–9. doi: 10.1111/j.1398-95.2012.02835.x
25. Qazi KR, Torregrosa Paredes P, Dahlberg B, Grunewald J, Eklund A, Gabrielsson S, et al. Proinflammatory exosomes in bronchoalveolar lavage fluid of patients with sarcoidosis. *Thorax*. (2010) 65:1016–24. doi: 10.1136/thx.2009.132027
26. Qin W, Tsukasaki Y, Dasgupta S, Mukhopadhyay N, Ikebe M,Sauter ER, et al. Exosomes in human breast milk promote EMT. *Clin Cancer Res*. (2016) 22:4517–24. doi: 10.1158/1078-0432.CCR-16- 0135
27. Li D, Beisswenger C, Herr C, Schmid RM, Gallo RL, Han G, et al. Expression of the antimicrobial peptide cathelicidin in myeloid cells is required for lung tumor growth. *Oncogene*. (2014) 33:2709–16. doi: 10.1038/onc.2013.248
28. Maroto R, Zhao Y, Jamaluddin M, Popov VL, Wang H, Kalubowilage M, et al. Effects of storage temperature on airway exosome integrity for diagnostic and functional analyses. *J Extracell Vesicles*. (2017) 6:1359478. doi: 10.1080/20013078.2017.1359478
29. Prado N, Marazuela EG, Segura E, Fernandez-Garcia H, Villalba M, Thery C, et al. Exosomes from bronchoalveolar fluid of tolerized mice prevent allergic reaction. *J Immunol*. (2008) 181:1519–25. doi: 10.4049/jimmunol.181.2.1519
30. Murphy TF, Brauer AL, Sethi S, Kilian M, Cai X, Lesse AJ, et al. Haemophilus haemolyticus: a human respiratory tract commensal to be distinguished from Haemophilus influenzae. *J Infect Dis*. (2007) 195:81–9. doi: 10.1086/509824
31. Thery C, Amigorena S, Raposo G, Clayton A. Isolation and characterization of exosomes from cell culture supernatants and biological fluids. *Curr Protoc Cell Biol*. (2006) Chapter3: Unit3.22. doi: 10.1002/0471143030.cb0322s30
32. Zitvogel L, Pietrocola F, Kroemer G. Nutrition, inflammation and cancer. *Nat Immunol*. (2017)18:843–50. doi: 10.1038/ni.3754
33. Nambiar MP, Gordon RK, Moran TS, Richards SM, Sciuto AM. A simple method for accurate endotracheal placement of an intubation tube in Guinea pigs to assess lung injury following chemical exposure. *Toxicol Mech Methods*. (2007) 17:385–2. doi: 10.1080/15376510601094131
34. Moghaddam SJ, Li H, Cho SN, Dishop MK, Wistuba II, Ji L, et al. Promotion of lung carcinogenesis by chronic obstructive pulmonary disease-like airway inflammation in a K-ras-induced mouse model. *Am J Respir Cell Mol Biol*. (2009) 40:443-453. doi: 10.1165/rcmb.2008-0198OC
35. Barta P, Van Pelt C, Men T, Dickey BF, Lotan R, Moghaddam SJ, et al. Enhancement of lung tumorigenesis in a Gprc5a Knockout mouse by chronic extrinsic airway inflammation. *Mol Cancer*. (2012) 11:4. doi: 10.1186/1476-4598-11-4
36. Moghaddam SJ, Clement CG, De la Garza MM, Zou X, Travis EL, Young HW, et al. Haemophilus influenzae lysate induces aspects of the chronic obstructive pulmonary disease phenotype. *Am J Respir Cell Mol Biol*. (2008) 38:629–8. doi: 10.1165/rcmb.2007-0366OC
37. An T, Qin S, Xu Y, Tang Y, Huang Y, Situ B, et al. Exosomes serve as tumour markers for personalized diagnostics owing to their important role in cancer metastasis. *J Extracell Vesicles*. (2015) 4:27522. doi: 10.3402/jev.v4.27522.eCollection 2015
38. Kulshreshtha A, Ahmad T, Agrawal A, Ghosh B. Proinflammatory role of epithelial cell-derived exosomes in allergic airway inflammation. *J Allergy Clin Immunol*. (2013) 131:1194–03,1203.e1-14. doi: 10.1016/j.jaci.2012.12.1565
39. Bhatnagar S, Shinagawa K, Castellino FJ, Schorey JS. Exosomes released from macrophages infected with intracellular pathogens stimulate a proinflammatory response *in vitro* and *in vivo*. *Blood*. (2007) 110:3234–44. doi: 10.1182/blood-2007-03-079152


**Conflict of Interest Statement:** The authors declare that the research was conducted in the absence of any commercial or financial relationships that could be construed as a potential conflict of interest.

frontiers in Pharmacology

ORIGINAL RESEARCH
published: 04 April 2019
doi: 10.3389/fphar.2019.00291

# NEDD9 Facilitates Hypoxia-Induced Gastric Cancer Cell Migration via MICAL1 Related Rac1 Activation

*Shuo Zhao[1], Pengxiang Min[1], Lei Liu[2,3], Lin Zhang[2,3], Yujie Zhang[1,2], Yueyuan Wang[1], Xuyang Zhao[2,3], Yadong Ma[1], Hui Xie[3,4], Chenchen Zhu[5], Haonan Jiang[5], Jun Du[1,2]* and Luo Gu[1,2,3]**

[1] Department of Physiology, Nanjing Medical University, Nanjing, China, [2] Jiangsu Key Lab of Cancer Biomarkers, Prevention and Treatment, Collaborative Innovation Center For Cancer Personalized Medicine, Nanjing Medical University, Nanjing, China, [3] Department of Biochemistry and Molecular Biology, Nanjing Medical University, Nanjing, China, [4] Department of Implantology, Changzhou Stomatological Hospital, Changzhou, China, [5] School of Basic Medical Science, Nanjing Medical University, Nanjing, China

OPEN ACCESS

**Edited by:**
Ahmed Lasfar,
Rutgers University, The State University of New Jersey, United States

**Reviewed by:**
Shiv K. Gupta,
Mayo Clinic, United States
Berta Nieves Vázquez,
Biomedical Research Institute of Bellvitge, Spain

***Correspondence:**
Jun Du
dujun@njmu.edu.cn
Luo Gu
lgu@njmu.edu.cn

**Specialty section:**
This article was submitted to Cancer Molecular Targets and Therapeutics, a section of the journal Frontiers in Pharmacology

**Received:** 31 October 2018
**Accepted:** 11 March 2019
**Published:** 04 April 2019

**Citation:**
Zhao S, Min P, Liu L, Zhang L, Zhang Y, Wang Y, Zhao X, Ma Y, Xie H, Zhu C, Jiang H, Du J and Gu L (2019) NEDD9 Facilitates Hypoxia-Induced Gastric Cancer Cell Migration via MICAL1 Related Rac1 Activation. Front. Pharmacol. 10:291. doi: 10.3389/fphar.2019.00291

**Aims and Hypothesis:** NEDD9 is highly expressed in gastric cancer and has a significant involvement in its pathogenesis. However, the mechanism behind hypoxia-promoted cancer cell migration and its regulation because of NEDD9 is still unknown. The aim of this study is to investigate the involvement of NEDD9 in gastric cancer cell migration under hypoxia and explore the underlying potential molecular mechanisms.

**Methods:** Cell motility was measured by wound healing and transwell assay. NEDD9 and MICAL1 expressions were examined by western blot analysis. Interaction between NEDD9 and MICAL1 was assessed by immunohistochemistry and co-immunoprecipitation assay, respectively. Cells were transfected with plasmids or siRNA to upregulate or downregulate the expression of NEDD9 and MICAL1. Rac1, Cdc42, and RhoA activation was assessed by pulldown assay.

**Results:** The mRNA and protein level of NEDD9 increased as a result of hypoxia in gastric cancer cell lines BGC-823 and SGC-7901 while decreased levels of NEDD9 caused reduced cell migratory potential in response to hypoxia. Hypoxia also caused the enhancement of MICAL1 expression. Furthermore, it was revealed that there is a positive correlation between NEDD9 and MICAL1 protein while hypoxia played role in increasing their interaction. Under hypoxic conditions, silencing of NEDD9 caused reduction in the stability of MICAL1 protein, while depletion of MICAL1 also inhibited the migration of NEDD9-overexpressing gastric cancer cells. In addition, silencing of NEDD9 or MICAL1 expression reversed the increased GTP forms of Rac1 and Cdc42 in hypoxic cells. However, only the upregulation of Rac1-GTP level was observed in gastric cancer cells that were already overexpressed by MICAL1.

**Conclusion:** In all, it is concluded that MICAL1 is regulated by NEDD9 that facilitates hypoxia-induced gastric cancer cell migration via Rac1-dependent manner.

**Keywords: MICAL1, NEDD9, migration, gastric cancer, Rac1**

## INTRODUCTION

Neural precursor cell expressed developmentally downregulated protein 9 (NEDD9) also known as HEF1, Cas-L, CASS2 is a member of the Crk-associated substrate (CAS) protein family. NEDD9 was first described to be expressed in the brain of the mouse in embryonic stage—where its expression was seen developmentally downregulated (Kumar et al., 1992). As a non-catalytic scaffolding protein containing multiple docking sites, NEDD9 is involved in connecting external stimulus signals with downstream signaling molecules. Therefore, it plays a critical role in assembling signaling cascades and regulating multiple cellular processes including tumor progression (Nikonova et al., 2014; Shagisultanova et al., 2015).

It has been documented that NEDD9 is strongly associated with development of multiple types of cancer (Jin et al., 2014; Wang et al., 2014; Zhou et al., 2017). NEDD9 is overexpressed in gastric cancer tissues (Liu et al., 2014). The upregulation of NEDD9 can lead to malignant transformation of normal human gastric epithelial cells (Feng et al., 2015). Growing evidence suggests that overexpression of NEDD9 can increase the risk of metastasis of cancer cells. For example, NEDD9 is highly enriched in focal adhesion and interacts with FAK and Src, which can initiate cell migration and invasion (Sima et al., 2013; Bradbury et al., 2014). Upregulation of NEDD9 is reported to activate Rac1 GTPase and drive mesenchymal-mode movement of cancer cells (Sanz-Moreno et al., 2008). In addition, NEDD9 is positively correlated with the expression of mesenchymal-type marker proteins such as vimentin and Zeb, while E-cadherin is opposite (Feng et al., 2015). NEDD9 is also involved in canonical Wnt/β-catenin pathway-mediated colonic cell migration and cancer progression (Li et al., 2011). Understanding the NEDD9 regulatory pathway in cell migration will provide not only new insights into cancer metastasis but also therapeutic targets for gastric cancer. However, the mechanism underlying the effect of NEDD9 on gastric cancer cell motility has not been fully investigated.

Hypoxia is a powerful selective driver of aggressive tumor behavior (Bertout et al., 2008). One of the key regulators of cellular response to hypoxia is the increased expression level of hypoxia-inducible factor 1α (HIF-1α). Stable HIF1α expression can modulate cellular metabolism and increase angiogenesis (Hockel and Vaupel, 2001). NEDD9 has been identified as a novel HIF-1α-regulated gene which can mediate hypoxia-induced colorectal cancer cell migration (Kim et al., 2010). In addition, NEDD9 was also found selectively induced in neurons after transient global ischemia (Sasaki et al., 2005). However, involvement of NEDD9 with gastric cancer cell motility and relative mechanisms under hypoxic condition is still unknown. Molecules interacting with Cas L (MICALs) are redox enzymes that are crucial for cytoskeleton dynamics (Vanoni, 2017; Yoon and Terman, 2018). Our previous work identified a novel link between MICAL1 and RAB upon EGF stimulation and found that MICAL1 was essential for maintaining invasive phenotype of breast cancer cells (Deng et al., 2016b). Unfortunately, the regulator(s) of MICAL1 in gastric cancer is still unclear. NEDD9 was identified to interact with MICAL1 by far western screening analysis (Suzuki et al., 2002) providing a basis for further exploring the role of MICAL1 in NEDD9-induced alteration of cancer cell function.

The present study is a continuation of our previous study where we have proven that MICAL1 exerts a significant growth and invasion-promoting effects on breast cancer cells (Deng et al., 2016b, 2018). The results here demonstrated that hypoxia promoted gastric cancer cell migration by positively regulating the expression of NEDD9 and its subsequent binding to MICAL1. In addition, NEDD9/MICAL1 also promotes cell migration in Rac1-dependent manner. These findings revealed a novel relationship between NEDD9 and MICAL1 in the context of hypoxia-induced gastric cancer cell migration.

## MATERIALS AND METHODS

### Ethics Statement

All immunohistochemistry assays with human tumor specimens were conducted under the institutional guidelines of Jiangsu Province.

### Cell Culture

Human gastric cancer cell lines (BGC-823, SGC-7901) and HEK-293T cells were obtained from the Cell Biology Institute of Chinese Academy of Sciences (Shanghai, China). Cells were cultured in Dulbecco's modified Eagle's medium (DMEM, high glucose) (Hyclone, Thermo Scientific, Waltham, MA, United States) supplemented with 10% (v/v) fetal bovine serum (FBS) (Gibco, Carlsbad, CA, United States) and antibiotics (100 U/mL streptomycin and 100 μg/mL penicillin) (Invitrogen, Carlsbad, CA, United States) in a humidified incubator at 37°C with 5% $CO_2$. Cells were grown on coverslips for fluorescence staining and on plastic dishes for protein extraction.

For hypoxia, cells were exposed to a continuous flow of a humidified mixture of 1% O2, 5% CO2, and 94% N2 at 37°C for the indicated time.

### Plasmids and siRNAs

Human full-length NEDD9 cDNA was amplified from pBluescriptR-NEDD9 plasmid (Youbio, Hunan, China) using the following primer set, sense: 5′-AAGGGTACCG AGCTGGATCCATGAAGTATAAGAATCTTATGGCA-3′ and antisense: 5′-TGCTGGATATCTGCAGAATTCTCAGAACGTT GCCATCTC-3′. In these primers, BamHI and EcoRI restriction site sequences have been underlined. The full-length MICAL1 DNA was amplified from pOTB7-MICAL1 plasmid using the following primer set, sense: 5′-CCC AAGCTTGCCACCATGGCTTCACCTACCTCCA-3′, antisence: 5′-CCAACTCGAGGCCCTGGGCCCCTGTCCCCAAGGCCA-3′. In these primers, HindIII and XhoI restriction site sequences have been underlined. The PCR products were cloned into the pCMV-C-HA vector (Clontech, Palo Alto, CA, United States). All constructions were ensured by sequencing. The cells were grown in six-well plates until approximately 80% confluence, and then transiently transfected with those plasmids by using

FuGENE HD Transfection Reagent (Promega, Madison, WI, United States) according to the manufacturer's instructions.

The siRNAs were synthesized and purified by GenePharma (Shanghai, China), and the siRNAs specifically targeting NEDD9 were as follows: #1, 5′-GAGGCGUUCAGUUUCUUGAdTdT-3′, #2, 5′-CCAAGAACAAGAGGUAUAUd TdT-3′, and #3, 5′-GAUG GGAUCAACCGAUUGUdTdT-3′. siRNAs specifically targeting MICAL1 were as follows: 5′-CUCGGUGCUA AGAAGUUCUdTdT-3′. Cells were transfected with siRNA using Lipofectamine 2000 (Thermo Fisher Scientific, Waltham, MA, United States) according to the transfection method provided by the manufacturer. After transfection with plasmid or siRNA for 36 h, the cells were cultured in hypoxia, and then treated with cycloheximide (CHX) (Sigma, St. Louis, MO, United States) at the indicated time points.

## Cell Wound Healing and Transwell Assay

After transfection with indicated exogenous materials when the cells reached approximately 95–100% confluent, a scratch was made manually in the monolayer of cells by using a 10 μL pipette tip. The cells were washed with PBS and then incubated in fresh medium with or without hypoxia. The wounded cellular monolayer was permitted to heal for 12 h. Photographs of wound healing were taken using microscope (Carl Zeiss Meditec, Jena, Germany).

Transwell assay were performed using a 24-well cell culture insert with 8 μm pores (Millipore, Billerica, MA, United States). Cells were harvested, washed, and suspended in DMEM without FBS, then seeded on the upper chamber with density of $4 \times 10^4$/200 μL. Cells were allowed to get attached to the membrane for about 30 min. The lower chamber was filled with 600 μL DMEM with 10% FBS. After incubation for 12 h, the cells were fixed, and stained with 0.1% crystal violet for 5 min. Then the cells on the upper surface of the membrane were removed and the number of stained cells on the lower surface of the membrane was counted in photos taken under an inverted microscope (TS100; Nikon, Tokyo, Japan).

## Co-immunoprecipitation Assay

Co-immunoprecipitation assay were performed as previously described (Deng et al., 2016a). Briefly, cell lysates were incubated with antibody at 4°C for 4 h. Antibody-bound complexes were precipitated with protein A+G agarose beads (Beyotime, Nantong, China) and rinsed with PBS. Then agarose-associated protein complexes were dissolved in SDS loading buffer and analyzed by immunoblotting analysis.

## Immunoblotting Analysis

Protein extraction from the sample and concentration determination of whole cells was performed as previously described (Duan et al., 2016). Briefly, the cells were lyzed in RIPA buffer containing phenylmethanesulfonyl fluoride (PMSF) and protease inhibitor cocktail. Equal amounts of proteins were resolved on SDS polyacrylamide gels and transferred to nitrocellulose membrane. The resulting blots were blocked with 5% non-fat dry milk and probed with antibodies. The following antibodies were used: GAPDH (KangChen, Shanghai, China), β-actin (Santa Cruz, Santa Cruz, CA, United States), MICAL1 (proteintech, Hubei, China), NEDD9 (Santa Cruz), FLAG (Abways, Shanghai, China), Rac1 (BD, Franklin Lakes, NJ, United States), RhoA, Cdc42, and HA antibodies (Cell Signaling, Danvers, MA, United States). Protein bands were detected by incubating with HRP-conjugated antibodies (Santa Cruz) and developed using ECL reagent (Millipore). Digital images of the positive bands were obtained and analyzed with Quantity One (Bio-Rad, Hercules, CA, United States).

## Pulldown Assay

Rac1, Cdc42, and RhoA activity was measured by pulldown assay (Chen et al., 2018). Active RhoA was pulldown by GST-RBD beads and active Cdc42/Rac1 was pulldown by PAK-CRIB beads. In brief, protein lysates were centrifuged, supernatant was collected in new tubes containing beads precoupled with GST–PBD or PAK-CRIB, and incubated under rotation at 4°C for 30 min. Then, the beads were washed and the proteins bound on the beads were separated by SDS-PAGE. The amounts of active RhoA, Cdc42, and Rac1 were determined by immunoblotting analysis.

## Measurement of ROS

2′,7′-Dichlorofluorescein diacetate (CM-H2DCFDA) (Invitrogen, Carlsbad, CA, United States), a ROS-specific fluorescent probe, was used to determine the intracellular ROS levels. After exposing it to hypoxia for 4 h, the cells were stained with 5 μM CM-H2DCFDA for 15 min at 37°C. After washing with PBS, the cover slips were mounted on glass slides. Images were collected using an Olympus BX51 microscope coupled with an Olympus DP70 digital camera.

## Immunohistochemistry

Tumor specimens were obtained from Outdo biotech (Shanghai, China). Thirty primary human gastric tumor samples and their corresponding paracancerous tissue samples were used for immunohistological staining in our study. The sections were deparaffinized and rehydrated. Peroxidase blocking was done with 3% $H_2O_2$ in methanol for 15 min at 37°C. Antigen retrieval was performed by transferring the sections into EDTA buffer (pH 8.0). The sections were then blocked by goat serum and applied with MICAL1 (proteintech, Hubei, China) or NEDD9 (absin, Shanghai, China) antibody at 4°C overnight. Next, the sections were treated with the secondary antibody (MXB, Fujian, China) for 1 h at room temperature. After counterstaining with hematoxylin, the slides were mounted and photographs were obtained using an Olympus BX51 microscope. Reagents for immunohistochemistry were all obtained from ZSGB-BIO (Beijing, China). The Immuno Reactive Score (IRS) was calculated as intensity of the staining reaction multiplied by the percentage of the number of positive cells as previously described (Dumitru et al., 2013; Medale-Giamarchi et al., 2013).

## CCK8 Assay

Cell proliferation was determined by using cell counting kit-8 kits (bimake, Houston, TX, United States) according to the

manufacturer's instructions. Cells were seeded at a density of $5 \times 10^3$ cells per well into 96-well plate (Corning), 10 μL of the CCK-8 solution was added to each well of the plate. After 1 h, the absorbance was conducted at 450 nm using a microplate absorbance reader (Bio-Tek, Elx800, United States).

## RT-qPCR

Total RNAs were prepared using TRIzol reagent (Invitrogen). cDNA was synthesized using equal amounts of RNA (0.5 μg) from each sample. qPCR was performed on the ABI StepOne$^{TM}$ Real-Time PCR System (Applied Biosystems, Foster City, CA, United States) using GoTaq qPCR Master Mix assay (Promega). The gene expression levels were calculated with Rt ($2^{-\Delta\Delta CT}$) values by StepOne Software v 2.1 (Applied Biosystems). The following primers were used to amplify: β-actin: 5′-CATGTACGTTGCTATCCAGGC-3′ (sense) and 5′-CTCCTTAATGTCACGCACGAT-3′ (antisense); MICAL1:5′GGCACTCGGTGCTAAGAAGTT-3′ (sense) and 5′-CCCCAGTGAATTTCCACCCC-3′ (antisense); NEDD9: 5′-GACCGTCATAGAGCAGAACAC-3′ (sense) and 5′-TGCAT GGGACCAATCAGAAGC-3′ (antisense).

## Statistical Analysis

All experiments were repeated at least three times and whole data are presented as mean ± SD. The significance of difference in two groups was analyzed by Student's *t*-test. $P < 0.05$ represents statistical significance and $P < 0.01$ represents sufficiently statistical significance (two-tailed). Pearson correlation test was used indicate the association between MICAL1 and NEDD9 protein expressions in immunohistochemistry analysis.

# RESULTS

## Hypoxia Promotes NEDD9 Protein Accumulation in Gastric Cancer Cells

To assess the effect of hypoxia on NEDD9 expression in gastric cancer cells, SGC-7901 and BGC-823 cells were cultured under hypoxia for the indicated time. As it has been previously shown in other cell types, NEDD9 protein usually appears as 105 and 115 kD isoforms (Latasa et al., 2016). The results in **Figure 1A** show that hypoxia induced an increase in both NEDD9 isoforms in gastric cancer cells within 2 h and peaked at 4 h of hypoxia, then returned to the basal level at 12 h. The whole western blot picture of NEDD9 is available in **Supplementary Figure S1**. The elevated levels of NEDD9 mRNA were detected by qPCR (**Supplementary Figure S2**). Although hypoxia increased both bands in each doublet, modified their proportion and changed the ratio between them. In BGC-823 cells, p115 isoform accounted for about 50% of total NEDD9 in resting cells. While hypoxia incubation caused lowering of p115 isoform proportion as compared to control group, therefore the proportion of p105 isoform became higher in BGC-823. In contrast, more proportion of p115 isoform produced in SGC-7901 cells under hypoxic condition (**Figures 1B,C**). These results confirmed that hypoxia is an inducer of NEDD9 expression in gastric cancer cells.

## Hypoxia Stimulates Gastric Cancer Cell Migration Through NEDD9

As shown in **Figure 2A**, knockdown of NEDD9 with siRNA reduced the NEDD9 expression in both SGC-7901 and BGC-823 cells, indicating the efficiency of the siRNA targeting NEDD9 in the present study. We noticed that siRNA #3 was most effective among the three NEDD9 siRNAs; therefore, it was selected for the following study. To further examine whether hypoxia stimulates gastric cancer cell migration in NEDD9-dependent manner, we investigated SGC-7901 and BGC-823 cell migration using wound closure assay after transfecting these cells with NEDD9 siRNA. Under hypoxia, the cell migration rate got increased significantly as compared to the cells under normal condition. However, in NEDD9-silenced cells, such stimulatory effect of hypoxia on cell migration was greatly inhibited (**Figure 2B**). Cell migration was also assessed by transwell migration assay. The migrated cell number was increased two folds in hypoxia treated cultures as compared to control group of cells. Knockdown of NEDD9 significantly decreased the cell migration rate in both normoxia- or hypoxia-treated gastric cancer cells (**Figure 2C**). NEDD9 knockdown had no significant effect on proliferative capacity in gastric cancer cells under hypoxia for 12 h, evidenced by the CCK8 assay (**Supplementary Figure S3**), ruling out the effect of proliferation on cell migration in the indicated time period. In all, the results above indicated that the increased expression of NEDD9 was essential for hypoxia-stimulated gastric cancer cell migration.

## MICAL1 Is Required for Hypoxia-Induced Cell Migration

It has been found that EGF-induced breast cancer cell invasion is MICAL1-dependent, which forms complexes with RAB35 (Deng et al., 2016b). Based on the finding that NEDD9 interacts with MICAL1 by far western screening (Suzuki et al., 2002), we further investigated whether MICAL1 was also involved in hypoxia-stimulated gastric cancer cell migration. The levels of MICAL1 mRNA were not changed significantly under hypoxia by qPCR analysis (**Supplementary Figure S2**). Immunoblotting analysis showed that, in both gastric cancer cells, the amount of MICAL1 was increased significantly after hypoxia incubation with maximal activation at 4 h, and it declined toward basal levels after 8 h (**Figure 3A**). Furthermore, knockdown of MICAL1 repressed the hypoxia-promoted gastric cancer cell migratory phenotype (**Figures 3B,C**).

## NEDD9 Prevents MICAL1 Degradation

Immunohistochemistry analysis in the gastric cancer tissue microarray showed a positive correlation between NEDD9 and MICAL1 expressions ($r = 0.55$) (**Figures 4A,B**). The result suggests a possibility that the upregulation of NEDD9 may contribute to the MICAL1 expression in gastric cancer cells.

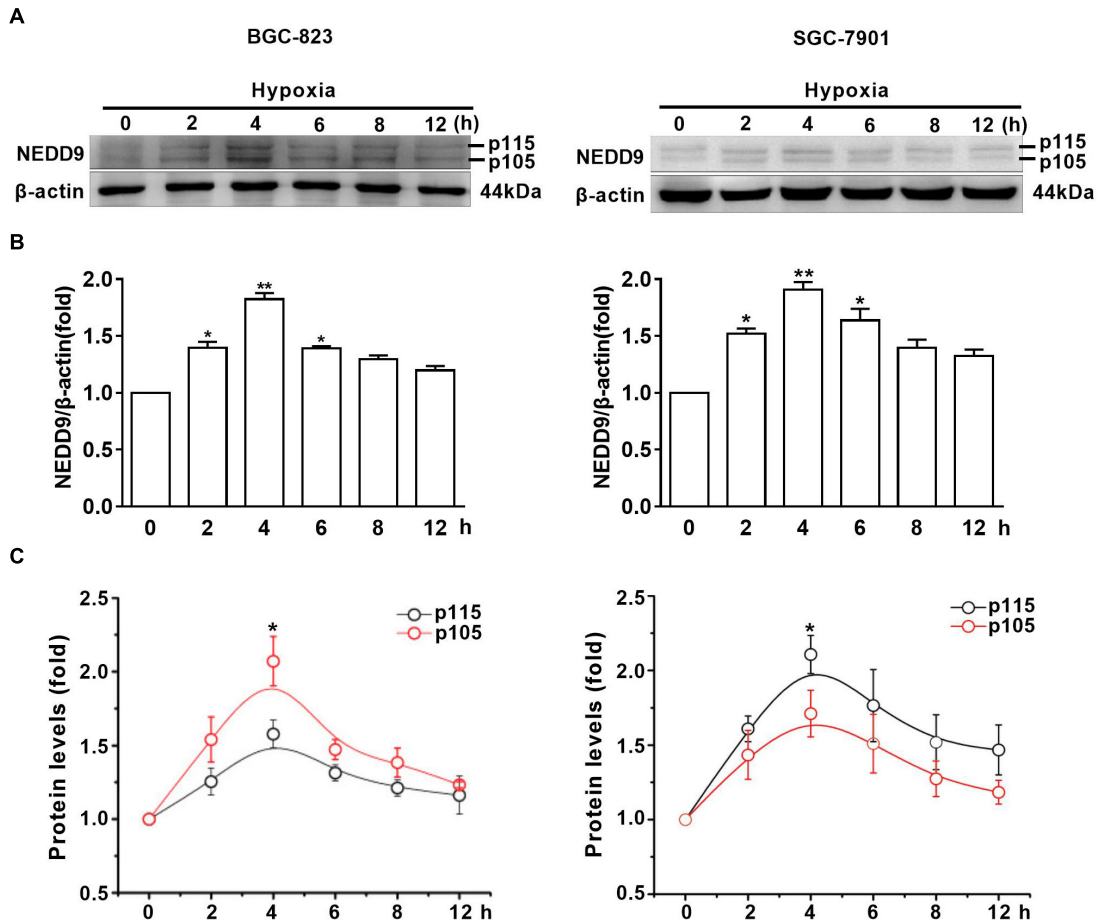


**FIGURE 1 |** Hypoxia increases NEDD9 protein expression. **(A)** Gastric cancer cell lines BGC-823 and SGC-7901 were exposed to hypoxia for 12h and NEDD9 protein levels were determined by immunoblotting analysis. **(B)** NEDD9 was quantified and normalized against β-actin. $^{*}P < 0.05$, $^{**}P < 0.01$, referring to the difference between cells treated with and without hypoxia. **(C)** Quantification of p105 and p115 isoforms of NEDD9 during hypoxia incubation.$^{*}P < 0.05$, referring to the difference between p105 and p115 isoforms during hypoxia.

It is reported that NEDD9 overexpression correlates with poor prognosis of gastric cancer (Liu et al., 2014; Zhang et al., 2015), However, in our study, due to the limited number of samples, we were unable to demonstrate the significant interaction between NEDD9, MICAL1, and gastric cancer progression (data not shown). MICAL1 is a redox enzyme that is crucial for ROS generation. Knockdown of either NEDD9 or MICAL1 in gastric cancer cells inhibited hypoxia-induced ROS production (**Supplementary Figure S4**). Furthermore, the co-immunoprecipitation study on both Flag-NEDD9 and HA-MICAL1 overexpressed in HEK293 cells indicated the direct binding of MICAL1 and NEDD9 (**Supplementary Figure S5A**). The interaction between MICAL1 and NEDD9 was also confirmed by co-immunoprecipitation assay, which showed the endogenous MICAL1 interacted with NEDD9 in SGC-7901 and BGC-823 cells. Moreover, under hypoxic conditions, the interaction increased in those gastric cancer cells (**Supplementary Figure S5B**). To determine whether NEDD9 could regulate stability of MICAL1, we blocked the protein synthesis by CHX. As shown in **Figure 4C**, under hypoxia, the expression levels of MICAL1 were dramatically decreased over the course of 8 h by depleted NEDD9 expression in comparison with control cells. In all, these data suggested that by interaction with the MICAL1, NEDD9 maintained MICAL1 stability under hypoxia by reducing its degradation in gastric cancer cells.

## Silencing of NEDD9/MICAL1 Blocks Hypoxia-Induced Rho GTPases Activation

The members of Rho GTPases, Rac1, Cdc42, and RhoA, have been considered as classical cytoskeleton regulators associated with cancer cell migratory phenotype. To verify that NEDD9 and MICAL1 could impact hypoxia-mediated activity of those Rho GTPases, we transfected cells with NEDD9 siRNA or MICAL1 siRNA, and then examined their effects on Rac1, Cdc42, and RhoA. The efficiency of the siRNA targeting NEDD9 or MICAL1 is presented in **Supplementary Figure S6**. Results from pulldown assay showed

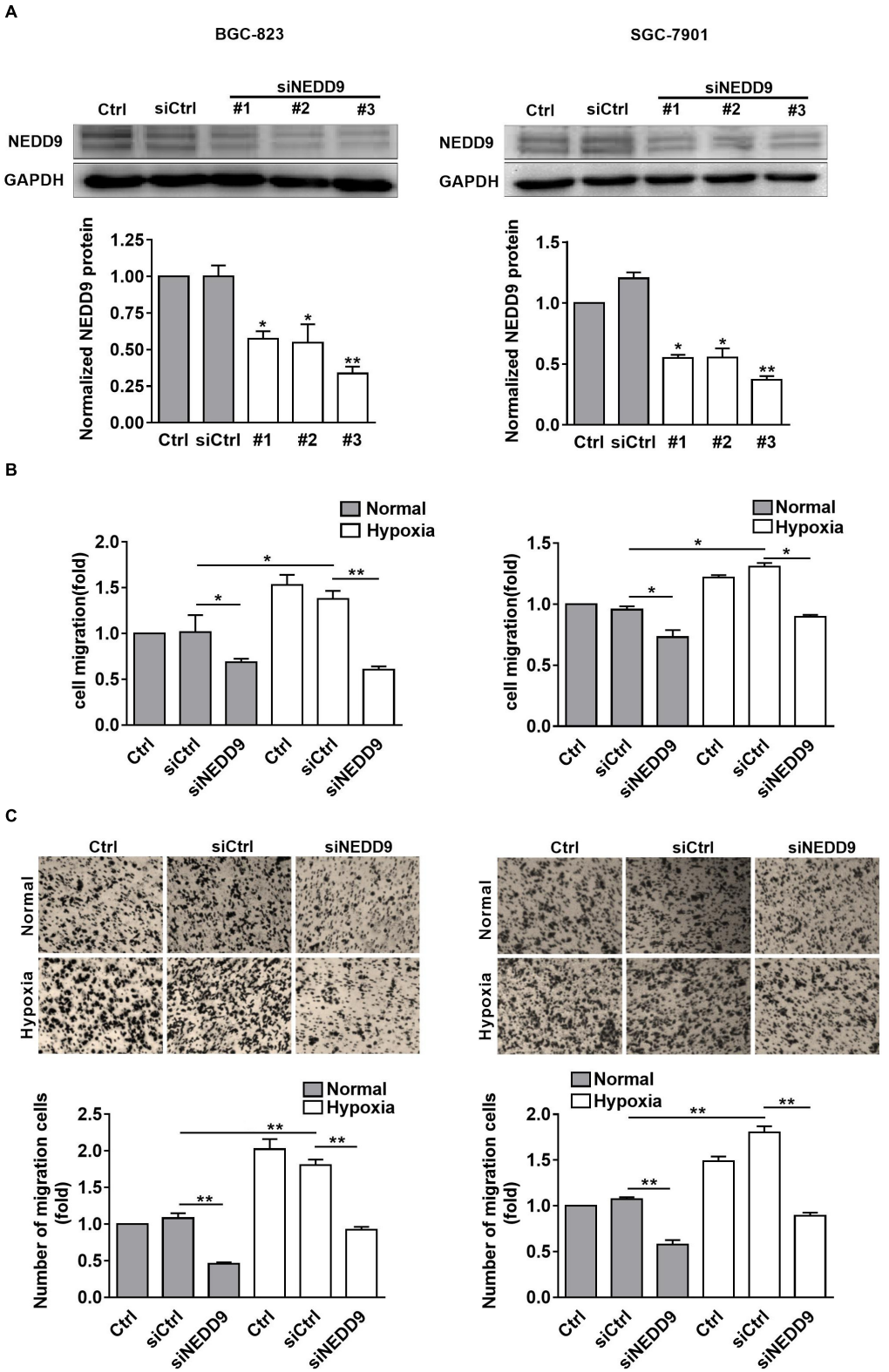


**FIGURE 2 |** Effect of NEDD9 on hypoxia-induced gastric cancer cell migration. **(A)** BGC-823 cells (left) and SGC-7901 cells (right) were transfected with control siRNA or NEDD9 siRNA. After 48 h, immunoblotting analysis was performed to detect the expression of NEDD9 and GAPDH. The bands were quantified and normalized against GAPDH. $^{*}P < 0.05$, $^{**}P < 0.01$, referring to the difference between cells transfected with control siRNA or NEDD9 siRNA. The migratory capacity of those cells transfected with NEDD9 siRNA under hypoxia were evaluated by wound healing assay **(B)** and transwell assay **(C)**. $^{*}P < 0.05$, $^{**}P < 0.01$.

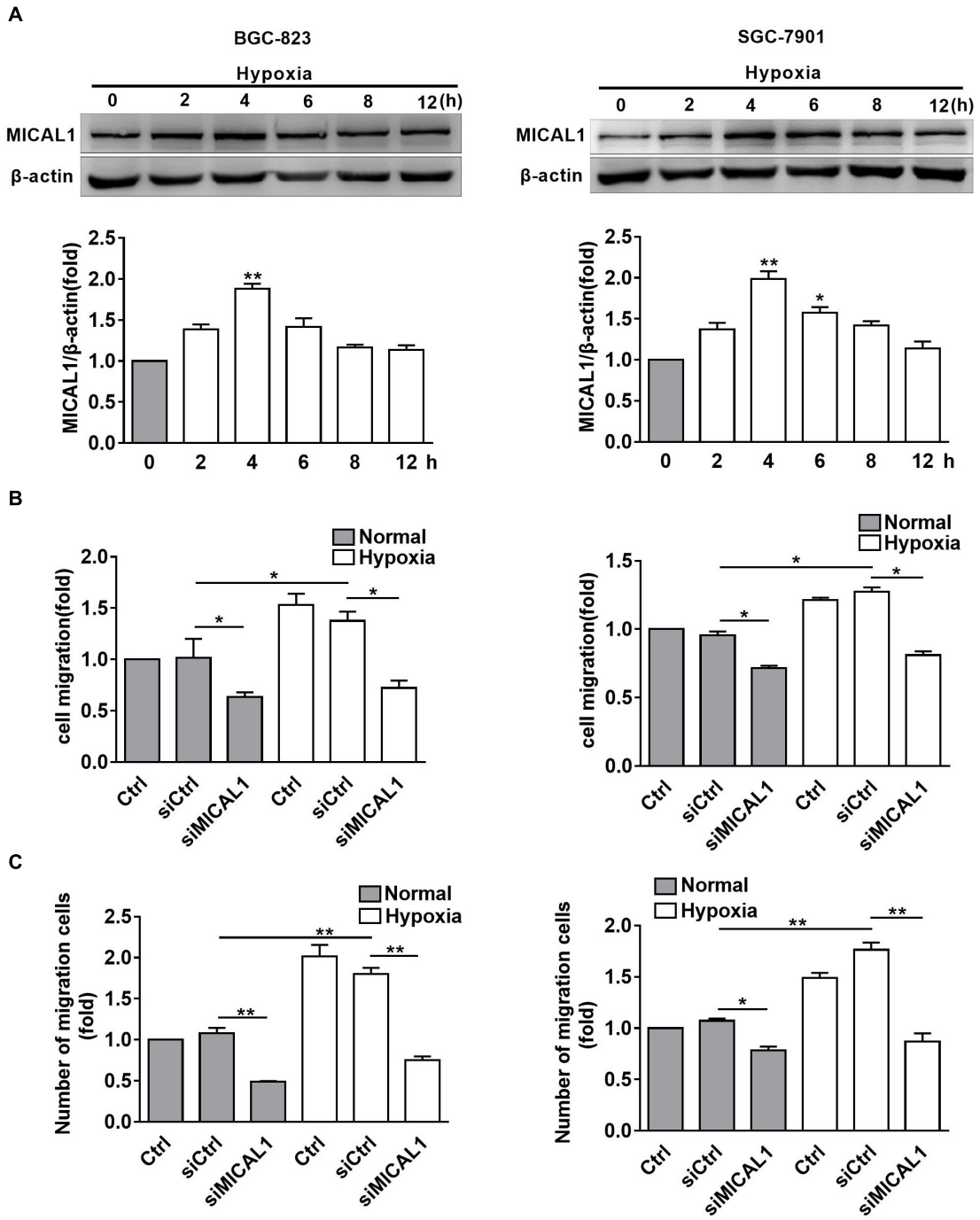


**FIGURE 3 |** MICAL1 is essential for hypoxia-induced cell migration. **(A)** BGC-823 cells (left) and SGC-7901 cells (right) were treated with hypoxia for 12 h and the expression of MICAL1 protein levels was determined by immunoblotting analysis. The bands were quantified and normalized against β-actin. $^{*}P < 0.05$, $^{**}P < 0.01$ referring to the difference between cells treated with and without hypoxia. The migratory capacity of those cells transfected with MICAL1 siRNA under hypoxia was evaluated by wound healing assay **(B)** and transwell assay **(C)**. $^{*}P < 0.05$, $^{**}P < 0.01$.

that hypoxia incubation increased both Rac1 and Cdc42 activation in SGC-7901 and BGC-823 cells. Furthermore, increased activation of Rac1 and Cdc42 under hypoxia was attenuated by either NEDD9 or MICAL1 depletion (**Figures 5A,B**). Since RhoA activation in BGC-823 cells was not significantly affected by hypoxia as well as NEDD9 or MICAL1 depletion, we did not test it again in SGC-7901 cells (**Figure 5C**). Collectively, these data indicated that NEDD9 and MICAL1 contribute to hypoxia-induced Rac1 and Cdc42 activation.

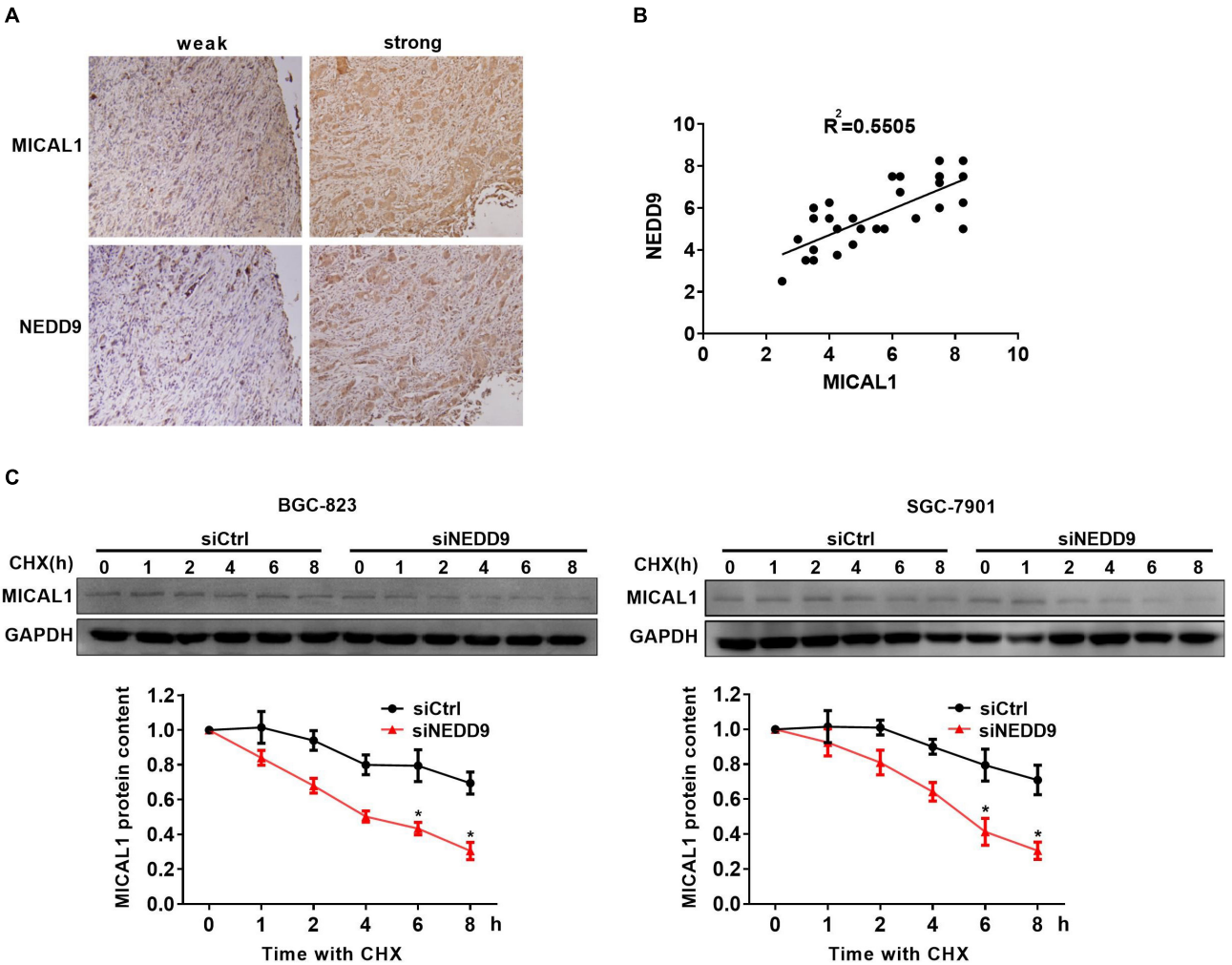


**FIGURE 4 |** NEDD9 binds to MICAL1 and prevents its degradation. **(A)** Using serial sections of the same sample, representative gastric cancer tissue stained for MICAL1 and NEDD9 (weak and strong staining) are shown. **(B)** The scatterplot of correlated protein levels between MICAL1 and NEDD9 were shown ($n$ = 30). **(C)** After blocking protein synthesis with CHX (10 μg/mL) for the indicated times, the hypoxic cells transfected with control siRNA or NEDD9 siRNA were lyzed and MICAL1 levels were determined by immunoblotting analysis. GAPDH was used as control. *$P$ < 0.05 referring to the difference between cells treated with control siRNA or NEDD9 siRNA.

## Rac1 Mediates NEDD9/MICAL1 Induced Gastric Cancer Migration

MICAL1 plasmid significantly increased the MICAL1 expression in gastric cancer cells, confirming the efficiency of the MICAL1 overexpression protocol in the present study (**Figure 6A**). It is noted that MICAL1 overexpression only increased Rac1 activation rather than Cdc42 activation (**Figure 6A**), suggesting that the role of MICAL1 in mediating cell migration may depend on Rac1 activation. The role of MICAL1 in regulating cell migration was further confirmed by the facts that MICAL1 overexpression promoted gastric cell migration rate (**Figure 6B**). As shown in **Figure 6C**, Rac1 activation was increased in NEDD9-overexpressed gastric cancer cells. Rac1-GTP levels were increased by 1.27-folds in BGC-823 cells and by 1.38-folds in SGC-7901 cells However, knockdown of MICAL1 attenuated NEDD9-induced Rac1 activation, Rac1-GTP levels were decreased to 0.93-folds in BGC-823 cells and 0.70-folds in SGC-7901 cells when compared with control group. Knockdown of MICAL1 also prevented NEDD9-stimulated cell migration in both BGC-823 and SGC-7901 cells (**Figure 6D**). Collectively, these results revealed that NEDD9/MICAL1 may act on Rac1 to affect hypoxia-induced gastric cancer cell migration.

## DISCUSSION

Globally, gastric cancer is the fifth most-common cancer and the third leading cause of death (McGuire, 2016). The prognosis of gastric cancer is poor, due to the fact that the tumor has already metastasized by the time of diagnosis. Emerging evidence indicated that hypoxia is one of the major factors for gastric cancer progression (Fujikuni et al., 2014). However, the molecular mechanisms underlying metastasis in gastric cancer cell under hypoxia were not fully understood. It is

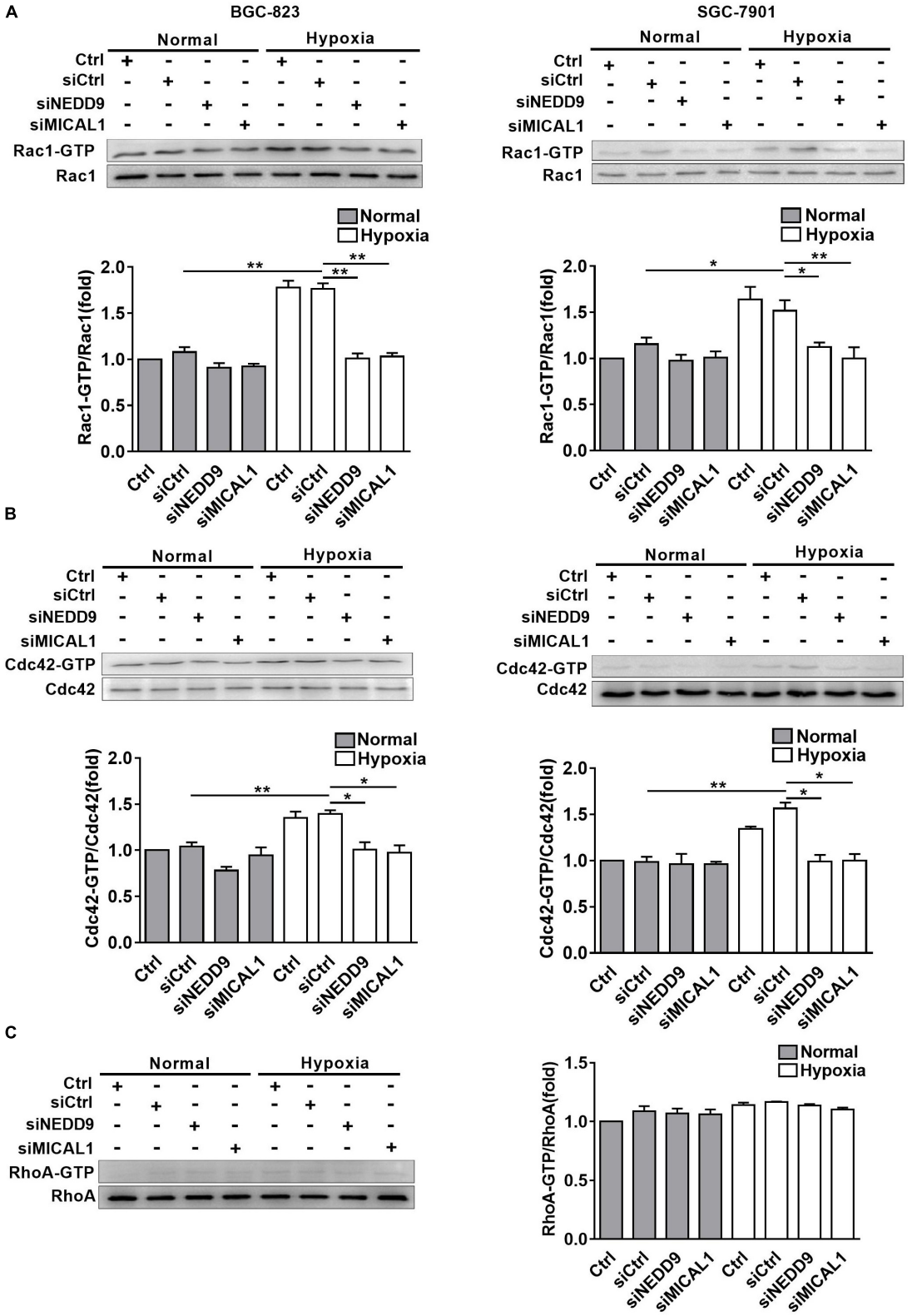


**FIGURE 5 |** Effect of NEDD9 and MICAL1 on hypoxia-induced Rho-GTPases activation. **(A–C)** BGC-823 and SGC-7901 cells were transfected with MICAL1 siRNA or NEDD9 siRNA, and then those cells were exposed to hypoxia for 4 h. Protein extraction from cells was analyzed by immunoblotting analysis. The GTP-bound form of endogenous Rac1 **(A)**, Cdc42 **(B)**, and RhoA **(C)** were precipitated and examined by immunoblotting analysis. All the experiments were repeated thrice. $^{*}P < 0.05$, $^{**}P < 0.01$.

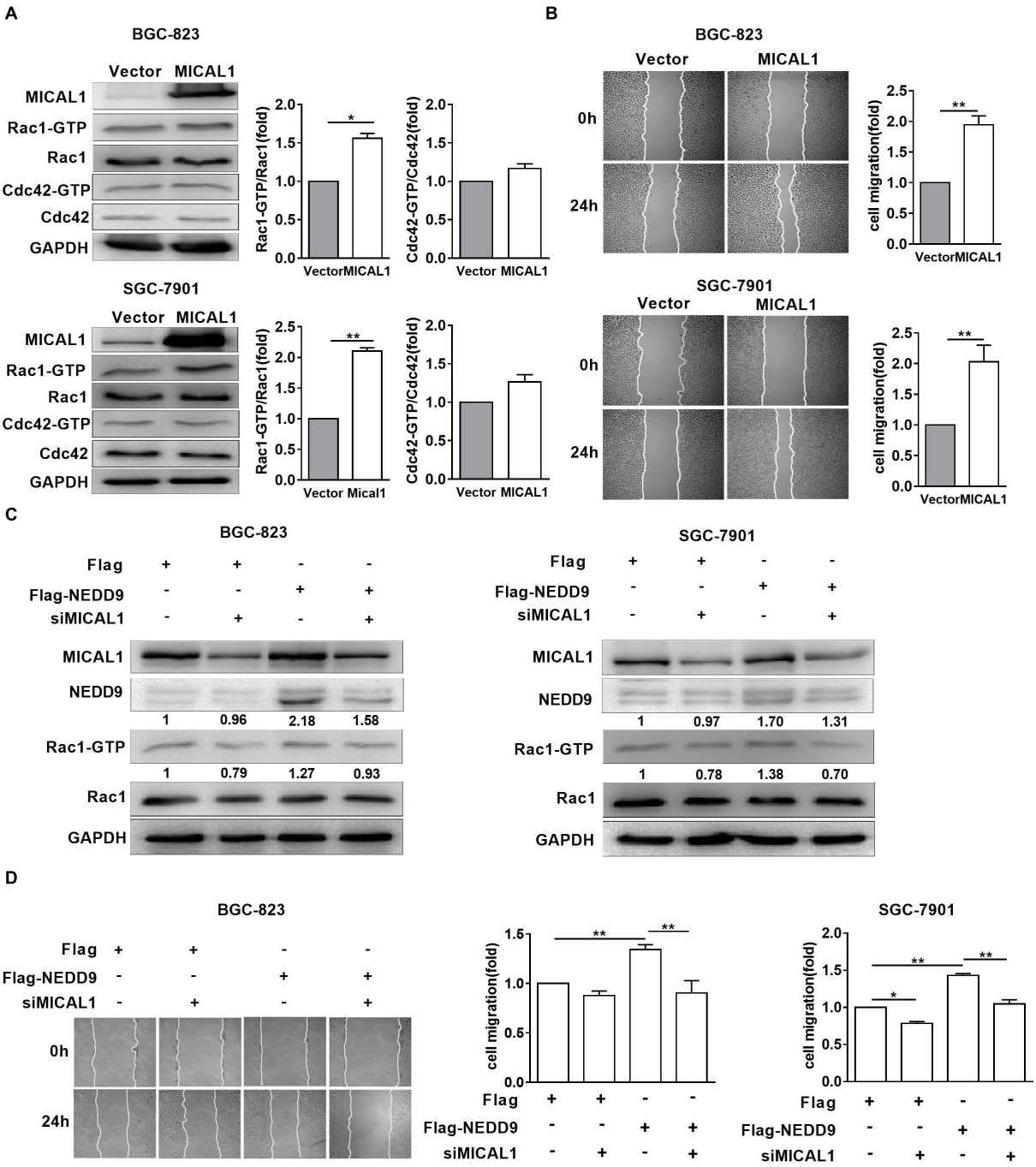


**FIGURE 6 |** Rac1 mediates MICAL1/NEDD9 induced gastric cancer migration. **(A)** BGC-823 and SGC-7901 cells were transfected with MICAL1 plasmids where total cellular proteins were extracted and analyzed for GTP-bound form of Rac1 and Cdc42. $^{*}P < 0.05$, $^{**}P < 0.01$. **(B)** Cells were transfected with MICAL1 plasmids or empty vectors, and then wound healing assay were performed to evaluate the migration of both cells. $^{**}P < 0.01$. **(C)** BGC-823 and SGC-7901 cells were transfected with NEDD9 plasmids and/or MICAL1 siRNA. After 48 h, extracted protein from cells was analyzed for NEDD9 and Rac1-GTP expressions. **(D)** Results of wound healing assay showed that knockdown of MICAL1 delayed cell migration in BGC-823 and SGC-7901 cells which overexpressed NEDD9. $^{*}P < 0.05$, $^{**}P < 0.01$.

well accepted that NEDD9 expression is sensitive to multiple stimuli such as TGF-beta (Morimoto et al., 2014), retinoic acid (Latasa et al., 2016), estrogen (Bradshaw et al., 2011), and progesterone receptor overexpression (Richer et al., 2002). NEDD9 mRNA was also confirmed to be upregulated by hypoxia in stem cells derived from umbilical cord blood and bone marrow (Martin-Rendon et al., 2007). NEDD9 was overexpressed in gastric cancer patients (Karabulut et al., 2015;

Zhang et al., 2015). The present study provides evidence that hypoxia promotes NEDD9 protein expression in gastric cancer cells. Meanwhile, silencing of NEDD9 suppressed the increased cell migration stimulated by hypoxia, confirming that NEDD9 was involved in the migration of gastric cancer cells under hypoxia. Moreover, we noticed here that NEDD9 appeared as two main protein phospho-forms of 105 and 115 kDa. Both phospho-forms were identified to be highly expressed by retinoic acid stimulation (Latasa et al., 2016); 105 kDa NEDD9 is already tyrosine phosphorylated and undergoes further phosphorylation modifications to produce a 115 kDa hyper-phosphorylated protein that is tyrosine and serine phosphorylated. The increase in the proportion of the 105 kDa isoform in BGC-823 and 115 kDa isoform in SGC-7901 indicated a relative different increment of NEDD9 phosphorylation status in various types of gastric cancer cells under hypoxia.

By far western screening analysis, MICAL interacts with SH3 domain of NEDD9 through its proline-rich PPKPP sequence (Suzuki et al., 2002). However, least data are available about the relationship between NEDD9 and MICAL1 in gastric cancer cells. MICAL1, a multidomain flavoenzyme, is strongly involved in the mechanisms that promote breast cancer cell proliferation and invasion (Deng et al., 2016b, 2018). By interacting with cytoskeletal components, MICAL1 has also been proven to be involved in the terminal steps of cytokinesis (Fremont et al., 2017). Recent study highlighted that MICAL1 deficiency in oral squamous cell carcinoma arrested MMP9 secretion, vimentin, and E-cadherin levels, consistent with increased N-cadherin (Grauzam et al., 2018). It suggests the possibility that MICAL1 participated in the control of gastric cancer cell migration. By analysis of gastric cancer specimens, we noticed a positive correlation between NEDD9 and MICAL1 protein expressions. So it is interesting to investigate the role of NEDD9 and MICAL1 in hypoxia-treated gastric cancer cells. *In vitro*, hypoxia induced MICAL1 protein level in a time-dependent fashion in gastric cancer cells. Silencing of NEDD9 significantly accelerated MICAL1 degradation and reduced cell migration rate under hypoxia. In contrast, MICAL1 deletion inhibited NEDD9-mediated migration in gastric cancer cell lines. Therefore, it was identified that hypoxia-induced NEDD9 expression has the ability to maintain MICAL1 protein level by reducing its degradation, thereby maintaining gastric cancer cell migratory properties. In the present work, we observed that NEDD9 bound directly to MICAL1 in gastric cancer cells and this interaction increased under hypoxic condition. The results suggested that NEDD9 might enhance its binding to MICAL1 and therefore decrease its degradation under hypoxia. The precise mechanisms by which NEDD9 regulates MICAL1 levels still needed to be identified.

Next we examined the potential effectors under NEDD9/MICAL1 for cell migration under hypoxia. Cdc42, Rac1, and RhoA, members of Rho GTPase family, are the most common regulators of actin cytoskeleton dynamics and cell movement. Similar to others findings (Xue et al., 2006; Du et al., 2011), here we found that hypoxia elevated both Rac1-GTP and Cdc42-GTP levels, but not RhoA-GTP in gastric cancer cells. Furthermore, knockdown of NEDD9 or MICAL1 prevented hypoxia-induced upregulation of Rac1 and Cdc42 activity and cell migration. Interestingly, only Rac1 activity was increased in MICAL1-overexpressed gastric cancer cells. Rac1 cycles between active GTP-bound and inactive GDP-bound states. In its active state, it promotes cell migration by driving cell polarization and lamellipodia formation (Raftopoulou and Hall, 2004; Parri and Chiarugi, 2010). NEDD9 plays an essential role in mesenchymal-mode cell migration via Rac1 activation (Jones et al., 2017), and MICAL has the ability to induce redox changes in Rho GTPase family (Ventura and Pelicci, 2002). It may be reasonable to speculate that NEDD9/MICAL1-enhanced hypoxic gastric cancer cell motility is mediated at least in part through Rac1 activation.

It remains unclear how MICAL1 causes the activation of Rac1 upon hypoxia. Hypoxia is able to upregulate PI3K/Akt signaling activation in breast cancer cells (Du et al., 2011). We previously demonstrated that MICAL1 enhanced PI3K/Akt activation (Deng et al., 2016b), and PI3K/Akt has been identified as a upstream activator of mTOR, p70S6K1, as well as GSK-3β. All of the above are linked with Rac1 activation (Aslan et al., 2011; Rom et al., 2012; Hall et al., 2018). As we know that the structure of MICAL1 contains monooxygenase domain, therefore, it participates in controlling intracellular ROS generation. Many studies suggested that ROS-mediated cancer cell migration is associated with PI3K/Akt activation (Yang et al., 2011; Huang et al., 2013). Therefore, it is understood that MICAL1 might stimulate Rac1 activation via PI3K/Akt signaling in gastric cancer cells. In all, we identified a novel link between NEDD9 and MICAL1 in accelerating gastric cancer cell motility under hypoxia. Hypoxia increased NEDD9 expression and its interaction with MICAL1, thereby preventing MICAL1 degradation. Furthermore, we observed that hypoxia stimulated Rac1 activation, which may serve as an important mediator for NEDD9/MICAL1-facilitated gastric cancer cell migration. The function and regulation of NEDD9/MICAL1 expression may be of major clinical importance and may provide new insights for the discovery of novel therapeutic targets.

## AUTHOR CONTRIBUTIONS

JD designed the study. SZ, PM, LL, LZ, YZ, YW, XZ, YM, and HJ performed the experiments. SZ, HX, and CZ performed the statistical analysis. JD and LG drafted the manuscript and supervised the experimental work. All authors read and approved the final manuscript.

## FUNDING

This work was supported by the National Natural Science Foundation of China (No. 81773107) to JD, the National Natural Science Foundation of China (No. 81372319), a Project Funded by Jiangsu Collaborative Innovation Center for Cancer

Personalized Medicine to LG, the National Natural Science Foundation of China (No. 81602561) to YZ, a Project Funded by the Priority Academic Program Development of Jiangsu Higher Education Institutions (PAPD), and the Training Programs of Innovation and Entrepreneurship for Undergraduates by Jiangsu province (201810312018Z).

## ACKNOWLEDGMENTS

We are thankful to our colleague Maria Bibi for critically reading the paper.

## SUPPLEMENTARY MATERIAL

The Supplementary Material for this article can be found online at: https://www.frontiersin.org/articles/10.3389/fphar.2019.00291/full#supplementary-material

**FIGURE S1 |** Raw data of NEDD9 expression under hypoxia. The membranes were exposed for protein bands. NEDD9 expression was detected three times **(A–C)**.

**FIGURE S2 |** Effect of hypoxia on **(A)** NEDD9 and **(B)** MICAL1 mRNA expressions. Gastric cancer cells BGC-823 and SGC-7901 were exposed to hypoxia for 12 h and NEDD9 and MICAL1 mRNA levels were determined by qPCR. Afterward, NEDD9 and MICAL1 mRNAs were quantified and normalized against β-actin. $^{*}P < 0.05$, $^{**}P < 0.01$, referring to the difference between cells treated with and without hypoxia.

**FIGURE S3 |** Effect of NEDD9 and MICAL1 on cell proliferation under hypoxia. **(A)** BGC-823 and **(B)** SGC-7901 cells were transfected with MICAL1 siRNA and NEDD9 siRNA and then they were exposed to hypoxia for 12 h. The cells were incubated with CCK8 and analyzed for cell proliferation.

**FIGURE S4 |** Effect of NEDD9 and MICAL1 on ROS production under hypoxia. **(A)** BGC-823 and **(B)** SGC-7901 cells were transfected with MICAL1 siRNA or NEDD9 siRNA and then exposed to hypoxia for 4 h. Afterward, the cells were incubated with CM-H2DCFDA and analyzed for ROS generation. $^{*}P < 0.05$, $^{**}P < 0.01$.

**FIGURE S5 |** NEDD9 interacts with MICAL1 in gastric cancer cells. **(A)** Immunoprecipitation assay was performed in HEK293T cells that co-transfected with HA-tagged MICAL1 or/and FLAG-tagged NEDD9. **(B)** Co-immunoprecipitation assay was performed which shows binding of endogenous NEDD9 to MICAL1 in BGC-823 and SGC-7901 cells under hypoxia.

**FIGURE S6 |** Knockout efficiency of NEDD9 and MICAL1. **(A)** BGC-823 and **(B)** SGC-7901 cells were transfected with MICAL1 siRNA or NEDD9 siRNA, and then exposed to hypoxia for 4 h. Protein extracted from cells was analyzed by immunoblotting analysis.

## REFERENCES

Aslan, J. E., Tormoen, G. W., Loren, C. P., Pang, J., and McCarty, O. J. (2011). S6K1 and mTOR regulate Rac1-driven platelet activation and aggregation. *Blood* 118, 3129–3136. doi: 10.1182/blood-2011-02-331579

Bertout, J. A., Patel, S. A., and Simon, M. C. (2008). The impact of O2 availability on human cancer. *Nat. Rev. Cancer* 8, 967–975. doi: 10.1038/nrc2540

Bradbury, P., Bach, C. T., Paul, A., and O'Neill, G. M. (2014). Src kinase determines the dynamic exchange of the docking protein NEDD9 (neural precursor cell expressed developmentally down-regulated gene 9) at focal adhesions. *J. Biol. Chem.* 289, 24792–24800. doi: 10.1074/jbc.M113.544106

Bradshaw, L. N., Zhong, J., Bradbury, P., Mahmassani, M., Smith, J. L., Ammit, A. J., et al. (2011). Estradiol stabilizes the 105-kDa phospho-form of the adhesion docking protein NEDD9 and suppresses NEDD9-dependent cell spreading in breast cancer cells. *Biochim. Biophys. Acta* 1813, 340–345. doi: 10.1016/j.bbamcr.2010.11.018

Chen, Y., Zhang, L., Liu, L., Sun, S., Zhao, X., Wang, Y., et al. (2018). Rasip1 is a RUNX1 target gene and promotes migration of NSCLC cells. *Cancer Manag. Res.* 10, 4537–4552. doi: 10.2147/CMAR.S168438

Deng, W., Gu, L., Li, X., Zheng, J., Zhang, Y., Duan, B., et al. (2016a). CD24 associates with EGFR and supports EGF/EGFR signaling via RhoA in gastric cancer cells. *J. Transl. Med.* 14:32. doi: 10.1186/s12967-016-0787-y

Deng, W., Wang, Y., Gu, L., Duan, B., Cui, J., Zhang, Y., et al. (2016b). MICAL1 controls cell invasive phenotype via regulating oxidative stress in breast cancer cells. *BMC Cancer* 16:489. doi: 10.1186/s12885-016-2553-1

Deng, W., Wang, Y., Zhao, S., Zhang, Y., Chen, Y., Zhao, X., et al. (2018). MICAL1 facilitates breast cancer cell proliferation via ROS-sensitive ERK/cyclin D pathway. *J. Cell. Mol. Med.* 22, 3108–3118. doi: 10.1111/jcmm.13588

Du, J., Xu, R., Hu, Z., Tian, Y., Zhu, Y., Gu, L., et al. (2011). PI3K and ERK-induced Rac1 activation mediates hypoxia-induced HIF-1alpha expression in MCF-7 breast cancer cells. *PLoS One* 6:e25213. doi: 10.1371/journal.pone.0025213

Duan, B., Cui, J., Sun, S., Zheng, J., Zhang, Y., Ye, B., et al. (2016). EGF-stimulated activation of Rab35 regulates RUSC2-GIT2 complex formation to stabilize GIT2 during directional lung cancer cell migration. *Cancer Lett.* 379, 70–83. doi: 10.1016/j.canlet.2016.05.027

Dumitru, C. A., Bankfalvi, A., Gu, X., Zeidler, R., Brandau, S., and Lang, S. (2013). AHNAK and inflammatory markers predict poor survival in laryngeal carcinoma. *PLoS One* 8:e56420. doi: 10.1371/journal.pone.0056420

Feng, J., Zhao, J., Xie, H., Yin, Y., Luo, G., Zhang, J., et al. (2015). Involvement of NEDD9 in the invasion and migration of gastric cancer. *Tumour Biol.* 36, 3621–3628. doi: 10.1007/s13277-014-2999-1

Fremont, S., Hammich, H., Bai, J., Wioland, H., Klinkert, K., Rocancourt, M., et al. (2017). Oxidation of F-actin controls the terminal steps of cytokinesis. *Nat. Commun.* 8:14528. doi: 10.1038/ncomms14528

Fujikuni, N., Yamamoto, H., Tanabe, K., Naito, Y., Sakamoto, N., Tanaka, Y., et al. (2014). Hypoxia-mediated CD24 expression is correlated with gastric cancer aggressiveness by promoting cell migration and invasion. *Cancer Sci.* 105, 1411–1420. doi: 10.1111/cas.12522

Grauzam, S., Brock, A. M., Holmes, C. O., Tiedeken, J. A., Boniface, S. G., Pierson, B. N., et al. (2018). NEDD9 stimulated MMP9 secretion is required for invadopodia formation in oral squamous cell carcinoma. *Oncotarget* 9, 25503–25516. doi: 10.18632/oncotarget.25347

Hall, G., Lane, B. M., Khan, K., Pediaditakis, I., Xiao, J., Wu, G., et al. (2018). The human FSGS-causing ANLN R431C mutation induces dysregulated PI3K/AKT/mTOR/Rac1 signaling in podocytes. *J. Am. Soc. Nephrol.* 29, 2110–2122. doi: 10.1681/ASN.2017121338

Hockel, M., and Vaupel, P. (2001). Tumor hypoxia: definitions and current clinical, biologic, and molecular aspects. *J. Natl. Cancer Inst.* 93, 266–276. doi: 10.1093/jnci/93.4.266

Huang, J. S., Cho, C. Y., Hong, C. C., Yan, M. D., Hsieh, M. C., Lay, J. D., et al. (2013). Oxidative stress enhances Axl-mediated cell migration through an Akt1/Rac1-dependent mechanism. *Free Radic. Biol. Med.* 65, 1246–1256. doi: 10.1016/j.freeradbiomed.2013.09.011

Jin, Y., Li, F., Zheng, C., Wang, Y., Fang, Z., Guo, C., et al. (2014). NEDD9 promotes lung cancer metastasis through epithelial-mesenchymal transition. *Int. J. Cancer* 134, 2294–2304. doi: 10.1002/ijc.28568

Jones, B. C., Kelley, L. C., Loskutov, Y. V., Marinak, K. M., Kozyreva, V. K., Smolkin, M. B., et al. (2017). Dual targeting of mesenchymal and amoeboid motility hinders metastatic behavior. *Mol. Cancer Res.* 15, 670–682. doi: 10.1158/1541-7786.MCR-16-0411

Karabulut, M., Alis, H., Afsar, C. U., Karabulut, S., Kocatas, A., Oguz, H., et al. (2015). Serum neural precursor cell-expressed, developmentally down regulated 9 (NEDD9) level may have a prognostic role in patients with gastric cancer. *Biomed. Pharmacother.* 73, 140–146. doi: 10.1016/j.biopha.2015.06.010

Kim, S. H., Xia, D., Kim, S. W., Holla, V., Menter, D. G., and Dubois, R. N. (2010). Human enhancer of filamentation 1 is a mediator of hypoxia-inducible

factor-1alpha-mediated migration in colorectal carcinoma cells. *Cancer Res.* 70, 4054–4063. doi: 10.1158/0008-5472.CAN-09-2110

Kumar, S., Tomooka, Y., and Noda, M. (1992). Identification of a set of genes with developmentally down-regulated expression in the mouse brain. *Biochem. Biophys. Res. Commun.* 185, 1155–1161. doi: 10.1016/0006-291X(92)91747-E

Latasa, M. J., Jimenez-Lara, A. M., and Cosgaya, J. M. (2016). Retinoic acid regulates Schwann cell migration via NEDD9 induction by transcriptional and post-translational mechanisms. *Biochim. Biophys. Acta* 1863(7 Pt A), 1510–1518. doi: 10.1016/j.bbamcr.2016.04.009

Li, Y., Bavarva, J. H., Wang, Z., Guo, J., Qian, C., Thibodeau, S. N., et al. (2011). HEF1, a novel target of Wnt signaling, promotes colonic cell migration and cancer progression. *Oncogene* 30, 2633–2643. doi: 10.1038/onc.2010.632

Liu, Y., Wang, D., Zhao, K. L., Zhu, J. W., Yin, H. B., Wei, Y. Z., et al. (2014). NEDD9 overexpression correlates with poor prognosis in gastric cancer. *Tumour Biol.* 35, 6351–6356. doi: 10.1007/s13277-014-1839-7

Martin-Rendon, E., Hale, S. J., Ryan, D., Baban, D., Forde, S. P., Roubelakis, M., et al. (2007). Transcriptional profiling of human cord blood CD133+ and cultured bone marrow mesenchymal stem cells in response to hypoxia. *Stem Cells* 25, 1003–1012. doi: 10.1634/stemcells.2006-0398

McGuire, S. (2016). World cancer report 2014. Geneva, Switzerland: World Health Organization, International Agency for Research on Cancer, WHO Press, 2015. *Adv. Nutr.* 7, 418–419. doi: 10.3945/an.116.012211

Medale-Giamarchi, C., Lajoie-Mazenc, I., Malissein, E., Meunier, E., Couderc, B., Berge, Y., et al. (2013). RhoB modifies estrogen responses in breast cancer cells by influencing expression of the estrogen receptor. *Breast Cancer Res.* 15:R6. doi: 10.1186/bcr3377

Morimoto, K., Tanaka, T., Nitta, Y., Ohnishi, K., Kawashima, H., and Nakatani, T. (2014). NEDD9 crucially regulates TGF-beta-triggered epithelial-mesenchymal transition and cell invasion in prostate cancer cells: involvement in cancer progressiveness. *Prostate* 74, 901–910. doi: 10.1002/pros.22809

Nikonova, A. S., Gaponova, A. V., Kudinov, A. E., and Golemis, E. A. (2014). CAS proteins in health and disease: an update. *IUBMB Life* 66, 387–395. doi: 10.1002/iub.1282

Parri, M., and Chiarugi, P. (2010). Rac and Rho GTPases in cancer cell motility control. *Cell Commun. Signal.* 8:23. doi: 10.1186/1478-811X-8-23

Raftopoulou, M., and Hall, A. (2004). Cell migration: Rho GTPases lead the way. *Dev. Biol.* 265, 23–32. doi: 10.1016/j.ydbio.2003.06.003

Richer, J. K., Jacobsen, B. M., Manning, N. G., Abel, M. G., Wolf, D. M., and Horwitz, K. B. (2002). Differential gene regulation by the two progesterone receptor isoforms in human breast cancer cells. *J. Biol. Chem.* 277, 5209–5218. doi: 10.1074/jbc.M110090200

Rom, S., Fan, S., Reichenbach, N., Dykstra, H., Ramirez, S. H., and Persidsky, Y. (2012). Glycogen synthase kinase 3beta inhibition prevents monocyte migration across brain endothelial cells via Rac1-GTPase suppression and down-regulation of active integrin conformation. *Am. J. Pathol.* 181, 1414–1425. doi: 10.1016/j.ajpath.2012.06.018

Sanz-Moreno, V., Gadea, G., Ahn, J., Paterson, H., Marra, P., Pinner, S., et al. (2008). Rac activation and inactivation control plasticity of tumor cell movement. *Cell* 135, 510–523. doi: 10.1016/j.cell.2008.09.043

Sasaki, T., Iwata, S., Okano, H. J., Urasaki, Y., Hamada, J., Tanaka, H., et al. (2005). Nedd9 protein, a Cas-L homologue, is upregulated after transient global ischemia in rats: possible involvement of Nedd9 in the differentiation of neurons after ischemia. *Stroke* 36, 2457–2462. doi: 10.1161/01.STR.0000185672.10390.30

Shagisultanova, E., Gaponova, A. V., Gabbasov, R., Nicolas, E., and Golemis, E. A. (2015). Preclinical and clinical studies of the NEDD9 scaffold protein in cancer and other diseases. *Gene* 567, 1–11. doi: 10.1016/j.gene.2015.04.086

Sima, N., Cheng, X., Ye, F., Ma, D., Xie, X., and Lu, W. (2013). The overexpression of scaffolding protein NEDD9 promotes migration and invasion in cervical cancer via tyrosine phosphorylated FAK and SRC. *PLoS One* 8:e74594. doi: 10.1371/journal.pone.0074594

Suzuki, T., Nakamoto, T., Ogawa, S., Seo, S., Matsumura, T., Tachibana, K., et al. (2002). MICAL, a novel CasL interacting molecule, associates with vimentin. *J. Biol. Chem.* 277, 14933–14941. doi: 10.1074/jbc.M111842200

Vanoni, M. A. (2017). Structure-function studies of MICAL, the unusual multidomain flavoenzyme involved in actin cytoskeleton dynamics. *Arch. Biochem. Biophys.* 632, 118–141. doi: 10.1016/j.abb.2017.06.004

Ventura, A., and Pelicci, P. G. (2002). Semaphorins: green light for redox signaling? *Sci. STKE* 2002:pe44. doi: 10.1126/stke.2002.155.pe44

Wang, H., Mu, X., Zhou, S., Zhang, J., Dai, J., Tang, L., et al. (2014). NEDD9 overexpression is associated with the progression of and an unfavorable prognosis in epithelial ovarian cancer. *Hum. Pathol.* 45, 401–408. doi: 10.1016/j.humpath.2013.10.005

Xue, Y., Bi, F., Zhang, X., Zhang, S., Pan, Y., Liu, N., et al. (2006). Role of Rac1 and Cdc42 in hypoxia induced p53 and von Hippel-Lindau suppression and HIF1alpha activation. *Int. J. Cancer* 118, 2965–2972. doi: 10.1002/ijc.21763

Yang, Y., Du, J., Hu, Z., Liu, J., Tian, Y., Zhu, Y., et al. (2011). Activation of Rac1-PI3K/Akt is required for epidermal growth factor-induced PAK1 activation and cell migration in MDA-MB-231 breast cancer cells. *J. Biomed. Res.* 25, 237–245. doi: 10.1016/S1674-8301(11)60032-8

Yoon, J., and Terman, J. R. (2018). MICAL redox enzymes and actin remodeling: new links to classical tumorigenic and cancer pathways. *Mol. Cell Oncol.* 5:e1384881. doi: 10.1080/23723556.2017.1384881

Zhang, S. S., Wu, L. H., Liu, Q., Chen, K. S., and Zhang, X. F. (2015). Elevated expression of NEDD9 is associated with metastatic activity in gastric cancer. *Onco Targets Ther.* 8, 633–640. doi: 10.2147/OTT.S77904

Zhou, S., Xu, M., Shen, J., Liu, X., Chen, M., and Cai, X. (2017). Overexpression of NEDD9 promotes cell invasion and metastasis in hepatocellular carcinoma. *Clin. Res. Hepatol. Gastroenterol.* 41, 677–686. doi: 10.1016/j.clinre.2017.04.011

**Conflict of Interest Statement:** The authors declare that the research was conducted in the absence of any commercial or financial relationships that could be construed as a potential conflict of interest.

frontiers in Pharmacology

ORIGINAL RESEARCH
published: 16 April 2019
doi: 10.3389/fphar.2019.00400

# Novel 3,4-Dihydroisocoumarins Inhibit Human P-gp and BCRP in Multidrug Resistant Tumors and Demonstrate Substrate Inhibition of Yeast Pdr5

*Julia Sachs[1], Katja Döhl[2], Anja Weber[3], Michele Bonus[4], Ferdinand Ehlers[1], Edmond Fleischer[5], Anette Klinger[5], Holger Gohlke[4,6], Jörg Pietruszka[3,7], Lutz Schmitt[2] and Nicole Teusch[1]**

[1] Bio-Pharmaceutical Chemistry and Molecular Pharmacology, Faculty of Applied Natural Sciences, Technische Hochschule Köln, Leverkusen, Germany, [2] Institute of Biochemistry, Heinrich-Heine-Universität Düsseldorf, Düsseldorf, Germany, [3] Institute of Bioorganic Chemistry, Heinrich-Heine-Universität Düsseldorf im Forschungszentrum Jülich, Jülich, Germany, [4] Institute for Pharmaceutical and Medicinal Chemistry, Heinrich-Heine-Universität Düsseldorf, Düsseldorf, Germany, [5] MicroCombiChem GmbH, Wiesbaden, Germany, [6] John von Neumann Institute for Computing, Jülich Supercomputing Centre and Institute for Complex Systems – Structural Biochemistry, Forschungszentrum Jülich GmbH, Jülich, Germany, [7] IBG-1: Biotechnology, Forschungszentrum Jülich, Jülich, Germany

OPEN ACCESS

**Edited by:**
*Ahmed Lasfar, Rutgers University – The State University of New Jersey, United States*

**Reviewed by:**
*Chun Hei Antonio Cheung, National Cheng Kung University, Taiwan*
*Murugabaskar Balan, Boston Children's Hospital, Harvard Medical School, United States*
*Akash Sabarwal, Harvard Medical School, United States*

***Correspondence:**
*Nicole Teusch*
*nicole.teusch@uni-osnabrueck.de*

**Specialty section:**
*This article was submitted to Cancer Molecular Targets and Therapeutics, a section of the journal Frontiers in Pharmacology*

**Received:** *26 September 2018*
**Accepted:** *01 April 2019*
**Published:** *16 April 2019*

**Citation:**
*Sachs J, Döhl K, Weber A, Bonus M, Ehlers F, Fleischer E, Klinger A, Gohlke H, Pietruszka J, Schmitt L and Teusch N (2019) Novel 3,4-Dihydroisocoumarins Inhibit Human P-gp and BCRP in Multidrug Resistant Tumors and Demonstrate Substrate Inhibition of Yeast Pdr5. Front. Pharmacol. 10:400. doi: 10.3389/fphar.2019.00400*

Multidrug resistance (MDR) in tumors and pathogens remains a major problem in the efficacious treatment of patients by reduction of therapy options and subsequent treatment failure. Various mechanisms are described to be involved in the development of MDR with overexpression of ATP-binding cassette (ABC) transporters reflecting the most extensively studied. These membrane transporters translocate a wide variety of substrates utilizing energy from ATP hydrolysis leading to decreased intracellular drug accumulation and impaired drug efficacy. One treatment strategy might be inhibition of transporter-mediated efflux by small molecules. Isocoumarins and 3,4-dihydroisocoumarins are a large group of natural products derived from various sources with great structural and functional variety, but have so far not been in the focus as potential MDR reversing agents. Thus, three natural products and nine novel 3,4-dihydroisocoumarins were designed and analyzed regarding cytotoxicity induction and inhibition of human ABC transporters P-glycoprotein (P-gp), multidrug resistance-associated protein 1 (MRP1) and breast cancer resistance protein (BCRP) in a variety of human cancer cell lines as well as the yeast ABC transporter Pdr5 in *Saccharomyces cerevisiae*. Dual inhibitors of P-gp and BCRP and inhibitors of Pdr5 were identified, and distinct structure-activity relationships for transporter inhibition were revealed. The strongest inhibitor of P-gp and BCRP, which inhibited the transporters up to 80 to 90% compared to the respective positive controls, demonstrated the ability to reverse chemotherapy resistance in resistant cancer cell lines up to 5.6-fold. In the case of Pdr5, inhibitors were identified that prevented substrate transport and/or ATPase activity

with $IC_{50}$ values in the low micromolar range. However, cell toxicity was not observed. Molecular docking of the test compounds to P-gp revealed that differences in inhibition capacity were based on different binding affinities to the transporter. Thus, these small molecules provide novel lead structures for further optimization.

**Keywords: multidrug resistance, cancer chemotherapy, 3,4-dihydroisocoumarin, P-glycoprotein, breast cancer resistance protein, Pdr5**

## INTRODUCTION

Cancer remains the second most common cause of death worldwide with 8.7 million deaths in 2015 (Fitzmaurice et al., 2017). Despite constant progress in antitumor drug development, multidrug resistance (MDR) poses a major problem in effective patient treatment. MDR is estimated to cause treatment failure in about 90% of patients with recurrent tumors (Longley and Johnston, 2005). Additionally, it becomes a more and more severe problem in the treatment of pathogens. In general, MDR encompasses intrinsic or acquired resistance of cancer cells or pathogens to a spectrum of drugs, finally leading to reduction of treatment options and to therapy failure. Several mechanisms mediating MDR have been described, including mutations in drug targets, alterations in drug metabolism, decreased uptake or increased efflux of the drug (Kaye and Kaye, 2000; Gillet and Gottesman, 2010).

Probably the most prominent and widespread mechanism in eukaryotic cells is covered by increased drug transport from the cytoplasm through overexpression of ATP-binding cassette (ABC) transporters (El-Awady et al., 2016). The ABC transporter superfamily, representing one of the oldest and largest protein families, is expressed from archaea to human. The common mechanism for all ABC transporters encompasses the active membrane translocation of a broad spectrum of substrates using energy from ATP hydrolysis (Szöllősi et al., 2017).

Regarding MDR development accompanying antitumor therapy, three ABC transporters were identified as the main contributors in humans. P-glycoprotein (P-gp, ABCB1), multidrug resistance-associated protein 1 (MRP1, ABCC1) and breast cancer resistance protein (BCRP, ABCG2) are frequently overexpressed in chemotherapy-resistant tumors, where they facilitate resistance to wide varieties of drugs commonly used in clinical practice (Bugde et al., 2017). Furthermore, recent studies have shown a pronounced influence of ABC transporters in drug resistance mechanisms controlled by cancer stem cells, mainly responsible for recurrence of the disease (Begicevic and Falasca, 2017).

The ABC transporter Pdr5 from *Saccharomyces cerevisiae* is located in the plasma membrane (PM) and acts in combination with other exporter pumps as a first line of defense against structurally unrelated xenobiotic compounds forming the pleitropic drug resistance (PDR) network (Ernst et al., 2005). Pdr5 is the most abundant exporter pump in yeast and highly homologous to multidrug mediating transporters of clinical relevant fungi such as *Candida albicans*. Each year billions of people become infected with pathogenic fungi and 1.5 million people are killed because of that (Brown et al., 2012). One of the largest problems is the evolving resistance shift of several fungi against azoles, which prevent one of the most efficient treatments. Therefore, the development of new antifungal drugs is of great importance.

Since the discovery of ABC transporter and characterization of their significant contribution to MDR, pharmacological strategies to overcome transporter-mediated MDR have been in the focus of various drug discovery approaches (Szakács et al., 2006; Tillotson and Theriault, 2013). One focus is the development of small molecule inhibitors interfering with transporter activity in combination with chemotherapeutic drugs, thereby increasing intracellular drug accumulation and efficacy by reversing resistance (Zhang and Ma, 2010; Spengler et al., 2017; Tran-Nguyen et al., 2017). ABC transporters involved in MDR often have overlapping substrate spectra. For example, several tyrosine kinase inhibitors including dasatinib and imatinib were demonstrated to become translocated to the extracellular space by P-gp and BCRP (Dohse et al., 2010). This leads to reduced efficacy of those drugs and subsequent therapy failure.

In most tumors, MDR is not only mediated by overexpression of one ABC transporter, but by expression of several transporters. Furthermore, P-gp and BCRP are co-expressed at the blood–brain barrier and prevent effective treatment of brain tumors (Agarwal et al., 2011). Hence, the design of dual transporter inhibitors appears to be more efficacious in mentioned cases. To date, several dual inhibitors of P-gp and BCRP have been identified including tariquidar and derivatives, aurones and chalcones (Sim et al., 2011; Gu et al., 2014; Li et al., 2015). Tariquidar entered clinical trials up to phase II to circumvent P-gp mediated MDR, but did not reveal sufficient clinical activity (Pusztai et al., 2005).

Natural compounds and their derivatives play an important role in drug discovery and development (Newman and Cragg, 2016; Guo, 2017). In this context, various ABC transporter inhibitors from natural sources were identified and characterized in the last decades (Karthikeyan and Hoti, 2015). Early natural product P-gp inhibitors such as cyclosporine A or its synthetic derivative PSC833 were tested in clinical trials up to phase III, but failed due to toxicity or other unintended side effects (Warner et al., 1995; Baer et al., 2002). Among them were several dual inhibitors of P-gp and BCRP, for example some aurones, chalcones or flavonoids (Boumendjel et al., 2009; Sim et al., 2011; Yuan et al., 2012; Iriti et al., 2017).

Isocoumarins, isomers of coumarin, represent a large class of secondary metabolites, which can be found in bacteria, fungi, lichens, marine sponges and to a lesser extent in higher plants (Saeed, 2016). To date, several 100 different isocoumarins and dihydroisocoumarins from nature have been identified and

derivatives have been synthesized. Owing to their great structural diversity, diverse biological and pharmacological activities of isocoumarins including cytotoxicity and antimetastatic effects against various cancer types including breast, colon, melanoma (Cichewicz et al., 2004; Abid et al., 2012; Guimarães et al., 2016; Zhang et al., 2017), inhibition of inflammation (Liang et al., 2011; Ramanan et al., 2016) or different enzymes including aromatase and kallikrein peptidases as potential cancer targets (Endringer et al., 2008; Teixeira et al., 2011) as well as antibacterial, antifungal and antimalarial activities (Hoepfner et al., 2012; Lai et al., 2016; Simic et al., 2016) could be identified. Several natural or synthetic coumarins were identified as inhibitors of either P-gp, BCRP or both, yet activities were mostly moderate, and compound concentrations between 10 and 100 μM had to be applied for transporter inhibition (Barthomeuf et al., 2005; Raad et al., 2006; Combes et al., 2011; Bisi et al., 2017; Sjöstedt et al., 2017). In contrast, isocoumarins have to our knowledge not been characterized as potential MDR-reversing agents to date.

In this study, the three natural compounds 6-methoxymellein (**3**), angelicoin B (**4**) and ellagic acid as well as nine novel 3,4-dihydroisocoumarins (**Figure 1**) were analyzed regarding their cytotoxicity in cancer cells and inhibition of the endogenously expressed human ABC transporters P-gp, BCRP, and MRP1 and of the yeast transporter Pdr5. For further insights into the mechanism of action, Pdr5 ATPase and substrate transport assays were performed. These results were complemented with molecular docking studies that indicate that differences in the inhibitory power of the investigated 3,4-dihydroisocoumarins with respect to P-gp-mediated transport result from differences in the compounds' binding affinities to P-gp.

# MATERIALS AND METHODS

## Chemicals and Reagents

A549 and HCT-15 cells were purchased from the German Collection of Microorganisms and Cell Cultures (Braunschweig, Germany) and H69AR cells from the American Type Culture Collection (Manassas, VA, United States). Dr. Erasmus Schneider (Wadsworth Center, New York State Department of Health, Albany, NY, United States) kindly provided the MCF-7/MX cells. Cell culture media and supplements were purchased from Thermo Fisher Scientific (Waltham, MA, United States). Yeast extract, peptone, and D-glucose were purchased from Carl Roth (Karlsruhe, Germany). Hoechst 33342, rhodamine 6G (R6G) and adenosine 5′-triphosphate (ATP) were purchased from Sigma-Aldrich (St. Louis, MO, United States) and dissolved in water. Calcein-AM, PSC833, Ko143, MK-571, doxorubicin, mitoxantrone, and ketoconazole (Sigma-Aldrich, St. Louis, MO, United States) were dissolved in dimethyl sulfoxide (DMSO; Carl Roth, Karlsruhe, Germany or Acros Organics, Geel, Belgium). Hepes buffer was purchased from Lonza (Basel, Switzerland). CellTiter-Glo Luminescent Cell Viability Assay was purchased from Promega (Madison, WI, United States). Microtiter plates were purchased from Greiner Bio-One (Kremsmünster, Austria) or Falcon (Corning, NY, United States).

## Test Compounds

3,4-Dihydroisocoumarins were synthesized in three steps starting from α,β-unsaturated δ-lactones (Fischer and Pietruszka, 2007; Böse et al., 2014) and freshly prepared Brassard's diene. The reaction was catalyzed by AlMe3 as Lewis acid and Tf2CH2 as Brønsted acid leading to the major vinylogous (E)-configured Michael-product and the minor cyclic product. The isolated (E)-configured Michael-product was cyclized with the strong base lithium bis(trimethylsilyl)amide (LHMDS) at −78°C to room temperature for 16 h. Both fractions of the isochromenones from the first and second step were oxidized with 2,3-dichloro-5,6-dicyano-1,4-benzoquinone (DDQ) in toluene at room temperature for 4 h to the desired end product. Overall yields were between 30 and 84%.

Deprotection of isocoumarins (***R*)-19** and (***S*)-19** by boron trifluoride diethyl ether in dichloromethane at 0°C gave (***R*)-19a** and (***S*)-19a** in good to moderate yields between 36 and 47%. The free hydroxy-groups of the pentyl-derivative **16** and the unsubstituted isocoumarin **14** were protected by dimethylsulfate. This procedure gave 66% of the corresponding methyl-protected pentyl-isocoumarin **16a** and 51% of the methyl-protected isocoumarin **14a**.

**Ellagic acid** was provided by MicroCombiChem GmbH (Wiesbaden, Germany). All test compounds were dissolved in DMSO.

## Cell Culture

### Human Cancer Cell Lines

The human lung adenocarcinoma cell line A549 was cultured in DMEM medium supplemented with 10% fetal bovine serum (FBS), 100 U/mL penicillin and 100 μg/mL streptomycin. P-gp-expressing human colon adenocarcinoma cells HCT-15 were cultured in RPMI 1640 medium supplemented with 10% FBS, 100 U/mL penicillin and 100 μg/mL streptomycin. BCRP-expressing MCF-7/MX human breast adenocarcinoma cells were cultured in DMEM medium supplemented with 10% FBS, 100 U/mL penicillin and 100 μg/mL streptomycin. MRP1-expressing H69AR human small cell lung cancer cells were cultured in RPMI 1640 medium (ATCC modification) supplemented with 20% FBS, 100 U/mL penicillin and 100 μg/mL streptomycin. All cancer cell lines employed have been systematically characterized regarding their respective ABC transporter expression profile (Sachs et al., 2019).

Cells were maintained in a humidified atmosphere at 37°C and 5% $CO_2$ and subcultured when confluency reached 80 to 90%.

### Yeast Strain

The following *S. cerevisiae* yeast strain was used: YRE1001 (*MATa ura3-52 trp1-1 leu2-3,112 his3-11,15 ade2-1 pdr1-3 pdr5pdr5prom*Δ*::TRP1*). *S. cerevisiae* was cultured in YPD medium (10 g/L yeast extract, 20 g/L peptone, 2% glucose) at 30°C and 200 rpm. The yeast strain has been described previously (Ernst et al., 2008; Gupta et al., 2014). Based on these studies it is evident that Pdr5 localizes to the PM and is present in approximately 10% of the overall membrane protein content of the PM.

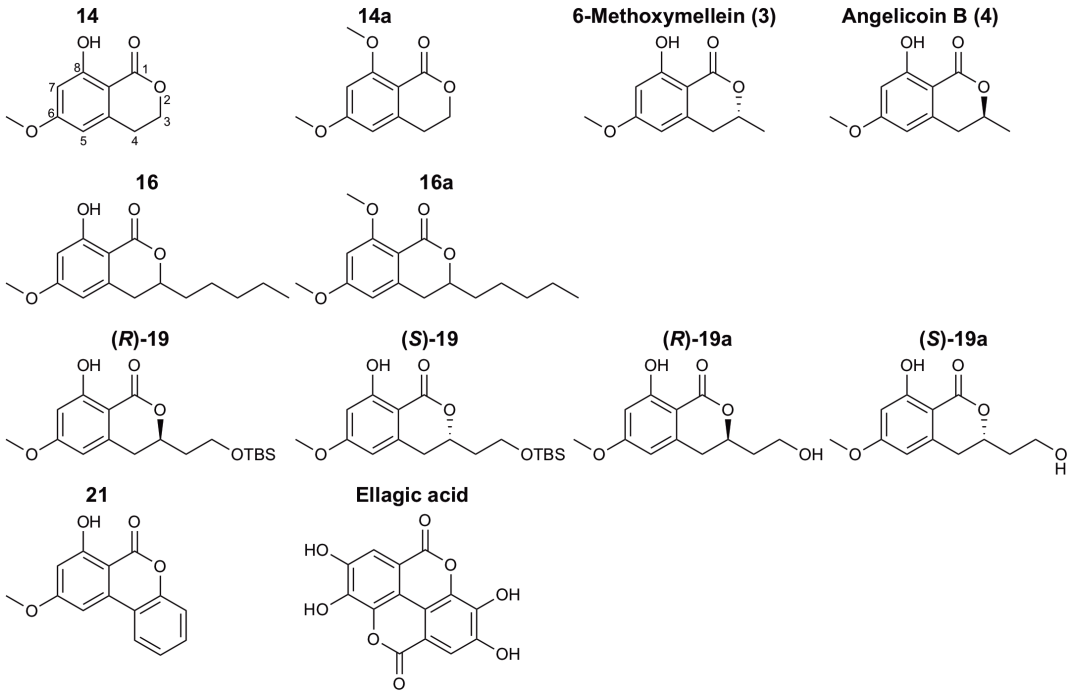


**FIGURE 1 |** Structures of natural and synthetic 3,4-dihydroisocoumarins.

## Cell Viability Assay

Cytotoxic activity of test compounds was analyzed after 48 h using the CellTiter-Glo Luminescent Cell Viability Assay published previously (Weber et al., 2017) in 384-well plates with the following cell densities: A549, MCF-7/MX: $2 \times 10^3$ cells/well; HCT-15: $3 \times 10^3$ cells/well; H69AR: $5 \times 10^3$ cells/well. Pipetting was conducted with the CyBi-Well 96-channel simultaneous pipettor (Analytik Jena AG, Jena, Germany). For generation of dose-response curves and calculation of $IC_{50}$ values, the four-parameter logistic model was applied.

The ability of identified inhibitors of P-gp and BCRP to sensitize HCT-15 or MCF-7/MX cells to chemotherapy was analyzed by co-treatment with test compounds and doxorubicin or mitoxantrone, respectively. Cells were incubated with a serial dilution of the chemotherapeutic drug alone or in combination with fixed concentrations of the test compounds or positive controls (2.5 μM PSC833 and 1 μM Ko143, respectively). Fold change of drug $IC_{50}$ was calculated with the formula $IC_{50}$ (drug alone)/$IC_{50}$ (drug with modulator).

## Liquid Drug Assay

The liquid drug assay was carried out in sterile 96-well plates. 50 μl of yeast cell culture at an $OD_{600}$ of 0.15 were mixed with 193.75 μl YPD and 6.25 μl of the test compound or DMSO as a negative control. To distinguish between cytotoxic compounds and those which inhibit Pdr5 WT specifically, the Pdr5 substrate ketoconazole was added only to cultures expressing wild-type Pdr5 in a final concentration of 1 μg/ml. At this concentration, inhibition of Pdr5 would result in ketoconazole-mediated cell death. After 48 h at 30°C the growth was measured with an ELISA plate reader (BioRad, Hercules, CA, United States) at 595 nm.

## Isolation of Pdr5 Containing Plasma Membranes

*Saccharomyces cerevisiae* cells expressing Pdr5 WT or the E1036Q (EQ) mutant were cultured to an $OD_{600}$ of 1.5 in YPD-media at 25°C. The nitrogen source was replenished by addition of a $10^{th}$ volume of 5x YP (50 g/l yeast extract, 100 g/l peptone). The cells were grown to an OD of 3.5 and harvested (5000 × *g* at 4°C for 15 min). The isolation of Pdr5 containing PMs was performed as described (Kolaczkowski et al., 1996; Ernst et al., 2008).

## Inhibition of ABC Transporter Activities

### P-gp Transport Assay

The transport of calcein-AM by P-gp and its modulation by test compounds was analyzed in the P-gp-expressing HCT-15 cell line. $5 \times 10^4$ cells were seeded in black 96-well plates and incubated at 37°C and 5% $CO_2$ for 24 h. The culture medium was removed and replaced by Hank's balanced salt solution supplemented with 10 mM HEPES. Test compounds, 2.5 μM PSC833 (positive control) or 0.5% DMSO (negative control) were added in triplicates and incubated for 30 min at 37°C and 5% $CO_2$. The substrate calcein-AM was added (final concentration 0.5 μM) and the fluorescence (excitation 485 nm, emission 520 nm) was measured over 3 h with the Infinite m1000 pro microplate reader (Tecan Group AG, Männedorf, Switzerland) at 37°C. The transport activity of P-gp was analyzed

by determining the slope of the linear part of the fluorescence-time curve (0–30 min) using linear regression. Normalization of the data to PSC833 (100% inhibition) and DMSO (0% inhibition) was performed.

### BCRP Transport Assay

Breast cancer resistance protein transport activity was determined in the BCRP-expressing MCF-7/MX cell line. Hoechst 33342 was applied as transporter substrate and 1 μM Ko143 as positive control or 0.5% DMSO as negative control and the assay was performed according to the P-gp assay. Fluorescence was measured at an excitation wavelength of 355 nm and emission wavelength of 460 nm. The transport activity of BCRP was analyzed by determining the plateau of the fluorescence-time curve by using non-linear regression (one-phase exponential fit). Normalization of the data to Ko143 (100% inhibition) and DMSO (0% inhibition) was performed.

### MRP1 Transport Assay

Transport activity of MRP1 was determined in MPR1-expressing H69AR cells using the substrate calcein-AM and 20 μM MK-571 as the positive control or 0.5% DMSO as negative control. Experimental procedure was according to the P-gp assay, except that $7.5 \times 10^4$ cells were seeded per well. The transport activity of MRP1 was analyzed by determining the slope of the linear part of the fluorescence-time curve (0–20 min) using linear regression. Normalization of the data to MK-571 (100% inhibition) and DMSO (0% inhibition) was performed.

### Pdr5 Transport Assay

Active transport of R6G was measured according to the protocol developed by Kolaczkowski et al. (1996), using a Tecan Infinite 200 pro reader (Tecan Group AG, Männedorf, Switzerland). 6 μg of the isolated PM containing Pdr5 were resuspended in 200 μl of the transport buffer (50 mM HEPES, pH 7.0, 5 mM $MgCl_2$, 10 mM $NaN_3$, and 150 nM R6G) and incubated in a black 96-well plate at 30°C. 5 μl of the test compound were added at the indicated concentrations. Active transport was initiated by the addition of 10 μl 200 mM ATP and fluorescence intensity was recorded in 15 s-intervals for 20 min (excitation wavelength at 524 nm, emission wavelength at 558 nm, number of flashes 30, integration time 2000 μs). $IC_{50}$ determination was performed with a serial dilution of the test compounds.

## Pdr5 ATPase Assay

Oligomycin (OM)-sensitive ATPase activity was measured from 0.8 μg PM containing Pdr5 incubated with 2 mM ATP, 5 mM $MgCl_2$ in 270 mM TRIS-glycine buffer (pH 9.5) and 2.5 μl of the test compounds or DMSO as a control in a total volume of 100 μl. To reduce the background activities, 0.2 mM ammonium molybdate, 10 mM $NaN_3$ and 50 mM $KNO_3$, respectively, were added (Dufour et al., 1988; Goffeau and Dufour, 1988). In a second assay, OM (20 μg/ml) was added to an otherwise identical setup. After incubation at 30°C for 20 min, the reaction was stopped by adding 25 μl of the reaction to 175 μl 40 mM $H_2SO_4$. The amount of released inorganic phosphate was determined by a colometric assay in 96-well plates (Goffeau and Dufour, 1988; Decottignies et al., 1994; Wada et al., 2002). The difference of both assays ( ± OM) corresponds to the specific ATPase activity of Pdr5 (Ernst et al., 2008).

## Molecular Docking Studies

The cryo-EM structure of P-gp (PDB ID: 6FN1, chains A and B) (Alam et al., 2018) was prepared for molecular docking using the Protein Preparation Wizard (Sastry et al., 2013) as implemented in the Maestro GUI[1] of the Schrödinger Suite version 2018-2[1]. Protonation states for Asp, Glu, His and Lys, tautomers for His and chi flips for Asp, Glu, and His were calculated at pH 7.4 with the PROPKA (Olsson et al., 2011; Søndergaard et al., 2011) implementation in Maestro. Subsequently, a restrained energy minimization was performed on all hydrogen atoms. To be able to use the structure for later MM-GBSA calculations with implicit membrane, the coordinates of the prepared structure were superimposed onto the coordinates of its respective OPM (Lomize et al., 2012) entry. The membrane region was then defined in the Maestro GUI, using the membrane dimensions of 31.4 Å calculated by the PPM server (Lomize et al., 2012).

Molecular docking was performed using the Glide XP docking protocol (Friesner et al., 2004, 2006) of the Schrödinger Suite version 2018-2. To allow more poses to pass through the initial Glide screens, the initial number of poses per ligand was increased from 5,000 to 50,000 and the scoring window was widened from 100.0 to 500.0. In addition, the number of minimized poses per ligand was increased from 400 to 1,000 and the 'expanded sampling' option was enabled. Post-docking minimization was performed on 100 poses, and the resulting best 10 poses per ligand were kept for further evaluation.

Four re-docking experiments were performed to assess the suitability of the selected docking approach: two re-dockings were performed in the presence of the respective other ligand entity (re-docking 1), and two re-dockings were performed in which both ligand entities were docked sequentially (re-docking 2). For re-docking 1, the size of the region in which the geometric center of the ligand can move during docking ('inner box') was set to 10 Å, and the size of the region in which ligand atoms may be placed during docking ('outer box') was set such that it expands the size of the inner box by 17 Å. For re-docking 2, the center and size of the inner box was set to match the center and size of the smallest possible cuboid that encloses both ligands in the cryo-EM complex. The size of the outer box was set such that it expands the size of the inner box by 15 Å. The same box as for re-docking 2 was also used for the docking of the 3,4-dihydroisocoumarins. Since this docking procedure produced favorably scored poses in two different binding sites, the dockings were repeated for each of these binding sites individually, using docking boxes centered on the geometric center of the poses generated in the corresponding binding pocket. For these dockings, the box sizes were set as for re-docking 1.

In order to obtain a more reliable estimate of the relative affinities of the 3,4-dihydroisocoumarins, for each of the two binding sites, the best scored pose of each docked ligand

[1]https://www.schrodinger.com/citations

was post-processed using the MM-GBSA implementation in Prime (see footnote number 1) with the VSGB 2.1 solvation model (Jianing et al., 2011). During this procedure, protein flexibility was taken into account for all residues within 8 Å of the ligand pose. Contributions due to changes in the configurational entropy of the ligand or the receptor upon complex formation were neglected, in order to avoid introducing uncertainty in the computations (Gohlke and Case, 2004; Weis et al., 2006; Hou et al., 2011). For compounds **16** and **16a**, the final effective binding energy was expressed as the average over the effective binding energies for both enantiomers. All effective binding energies were then converted to relative effective binding energies.

## Data Analysis and Statistics

All experiments were performed in at least three independent replicates. Data were analyzed with GraphPad Prism v. 6.07 (GraphPad Software, Inc., La Jolla, CA, United States) and results are presented as mean ± SEM. Different groups were compared statistically using one-way ANOVA followed by Dunnett's multiple comparisons test. Differences were considered significant when $p < 0.05$.

# RESULTS

## Cytotoxic Activity of 3,4-Dihydroisocoumarins in Human Cancer Cell Lines

Cytotoxicity of 12 3,4-dihydroisocoumarins was analyzed in the sensitive lung cancer cell line A549 as well as in three resistant cell lines HCT-15 (colon carcinoma), MCF-7/MX (breast carcinoma) and H69AR (lung carcinoma) either expressing the ABC transporter P-gp, BCRP, or MRP1, respectively. Cells were incubated for 48 h with test compounds and cell viability was assessed.

$IC_{50}$ values of the tested 3,4-dihydroisocoumarins are summarized in **Table 1**. Most compounds did not display significant cytotoxic activities in the cancer cell lines and $IC_{50}$ values were above the highest concentrations applied in the assay. However, one exception were the enantiomers **(*R*)-19** and **(*S*)-19**. Both compounds displayed comparable cytotoxicity in sensitive A549 cells and the BCRP-overexpressing MCF-7/MX cells. In A549 cells, $IC_{50}$ value of compound **(*R*)-19** was 47.5 ± 3.2 μM (mean ± SEM) and $IC_{50}$ value of **(*S*)-19** was 42.0 ± 3.9 μM. In MCF-7/MX cells, both compounds were slightly more toxic with $IC_{50}$ values of 28.1 ± 0.7 μM and 33.5 ± 7.5 μM, respectively. In contrast, in P-gp expressing HCT-15 cells, only **(*R*)-19** demonstrated a cytotoxic effect, whereas **(*S*)-19** was not toxic. Furthermore, the unprotected derivatives of **(*R*)-19** and **(*S*)-19**, **(*R*)-19a** and **(*S*)-19a**, were analyzed. In both cases, removal of the protecting TBS group led to complete or near complete loss of cytotoxic activity in all cell lines.

Compound **16** was not cytotoxic in P-gp expressing HCT-15 cells and BCRP-expressing MCF-7/MX cells. In MRP1-expressing H69AR cells and sensitive A549 cells, only minor cytotoxic activity was observed. $IC_{50}$ values were 88.5 ± 4.6 μM and 78.6 ± 2.2 μM, respectively. Remarkably, the derivative **16a**, which differs from **16** by the methoxy group instead of the hydroxy group at position 8, displayed slightly improved activity in A549 cells with an about 1.5-fold lower $IC_{50}$ value and a clearly improved activity in BCRP-expressing MCF-7/MX cells. In those cells, the $IC_{50}$ value was 10.6 ± 0.9 μM. In P-gp or MRP1-expressing cell lines, no cytotoxicity could be observed.

The known natural products 6-methoxymellein (**3**), angelicoin B (**4**) and **ellagic acid** did not show any cytotoxic effects against the tested cancer cell lines.

**TABLE 1 |** Cytotoxicity of 3,4-dihydroisocoumarins on human tumor cell lines.

| Compound | $IC_{50}$ (μM) | | | |
|---|---|---|---|---|
| | A549 | HCT-15 | MCF-7/MX | H69AR |
| 14 | >100 | >100 | >100 | >100 |
| 14a | >100 | >100 | >100 | >100 |
| 16 | 78.6 ± 2.2 | >100 | >100 | 88.5 ± 4.6 |
| 16a | 53.6 ± 5.6 | >100 | 10.6 ± 0.9 | >100 |
| (*R*)-19 | 47.5 ± 3.2 | 57.1 ± 7.5 | 28.1 ± 0.7 | >100 |
| (*R*)-19a | >100 | >100 | >100 | >100 |
| (*S*)-19 | 42.0 ± 3.9 | >100 | 33.5 ± 7.5 | 86.8 ± 9.2 |
| (*S*)-19a | >100 | >100 | 89.8 ± 4.9 | >100 |
| 6-Methoxymellein (3) | >100 | >100 | >100 | >100 |
| Angelicoin B (4) | >100 | >100 | >100 | >100 |
| 21 | >50 | >50 | >50 | >50 |
| Ellagic acid | >50 | >50 | >50 | >50 |

*Data represent mean ± SEM of at least three independent experiments performed in quadruplicates.*

## Identification of 3,4-Dihydroisocoumarins as Dual Inhibitors of P-gp and BCRP

The 12 3,4-dihydroisocoumarins were tested for their ability to inhibit the transport activity of the human ABC transporters P-gp, BCRP, and MRP1 in cell lines overexpressing the respective transporter. Therefore, intracellular fluorescence of the transporter substrates calcein-AM and Hoechst 33341 were measured over time after cells had been treated with different concentrations of the test compounds. Inhibition rates of the compounds were normalized to the positive controls 2.5 μM PSC833, 1 μM Ko143, and 20 μM MK-571, respectively. As a result, three compounds were identified as dual inhibitors of transport activity of P-gp and BCRP (**Figures 2A,B**).

Pentyl-derivative **16** was the strongest dose-dependent inhibitor of P-gp and BCRP among the tested compounds. Relative inhibition of P-gp was 36.3 ± 5.3% at a concentration of 10 μM, 52.6 ± 3.1% at 20 μM and 81.2 ± 2.7% at 50 μM (mean ± SEM). Regarding inhibition of BCRP, the rates were comparable to P-gp with relative values between 35.3 ± 3.4% at 10 μM and 89.1 ± 4.6% at 50 μM. Interestingly, derivative **16a**, which differs from **16** only by the methoxy group instead of the hydroxy group at position 8, showed reduced inhibition rates against both transporters with a more pronounced effect

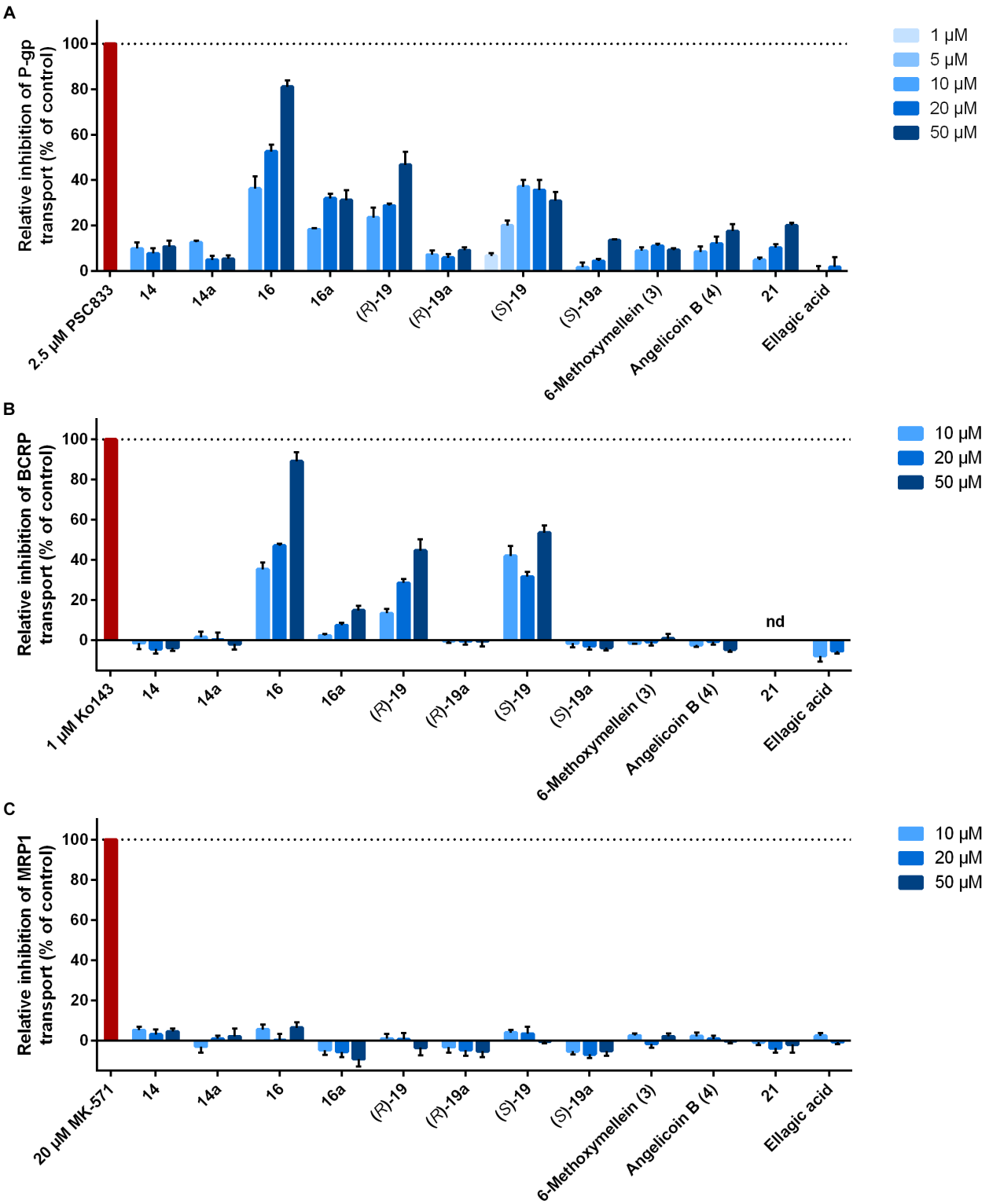


**FIGURE 2 |** Influence of 3,4-dihydroisocoumarins on ABC transporter activity. Cancer cell lines overexpressing **(A)** P-gp (HCT-15), **(B)** BCRP (MCF-7/MX), or **(C)** MRP1 (H69AR) were incubated with test compounds and intracellular fluorescence of the substrates calcein-AM (P-gp, MRP1) or Hoechst 33342 (BCRP) was measured over 3 h. Data were normalized to DMSO (0% inhibition) and the positive controls PSC833, Ko143, and MK-571, respectively (100% inhibition). Bars represent mean ± SEM of at least three independent experiments. nd, not determined because of intrinsic fluorescence.

for BCRP. Relative inhibition was between 18.4 ± 0.5 and 31.9 ± 2.2% for P-gp and 2.3 ± 0.9 and 14.9 ± 2.2% for BCRP.

Two additional compounds were identified as dual P-gp and BCRP inhibitors, **(*R*)-19** and **(*S*)-19**, but with lower activities compared to derivative **16**. Derivative **(*R*)-19** inhibited P-gp with relative rates between 23.6 ± 4.2 and 46.8 ± 5.7%. Regarding **(*S*)-19**, highest P-gp inhibition was achieved at 10 μM (37.1 ± 2.9%). Inhibition of BCRP was comparable. As both compounds contain protective groups at the hydroxy group at the ethyl chain at position 3, inhibition rates were compared to the deprotected derivatives **(*R*)-19a** and **(*S*)-19a**. In both cases, the deprotected compounds showed clearly reduced inhibitory ability of P-gp with values between about 5 and 15% and completely abolished inhibitory ability of BCRP.

Two compounds without substitution at position 3 were analyzed, **14** and **14a**. They only differ in the substituent at position 8, which is either a hydroxy group **14** or methoxy group **14a**. Both compounds did not inhibit BCRP and displayed only minor inhibitory activity against P-gp up to about 10% relative inhibition.

Furthermore, the two natural products and enantiomers 6-methoxymellein (**3**) and angelicoin B (**4**) were studied. They share the same structure with compound **14**, but are substituted with a methyl group at position 3. Relative rates of P-gp inhibition of 6-methoxymellein (**3**) and angelicoin B (**4**) did not differ significantly from those of derivative **14**. In case of BCRP, no inhibitory activity could be observed, as was the case for derivative **14**.

Compound **21**, a tricyclic derivative, weakly inhibited P-gp with a relative inhibition rate of 20.0 ± 1.2% at the highest concentration used. Its ability to inhibit BCRP could not be determined due to inherent fluorescence. The natural product **ellagic acid** did not display any inhibitory activity against P-gp or BCRP. It has to be noted that this compound could not be employed at a concentration of 50 μM due to its low solubility.

Regarding inhibition of MRP1 transport function in H69AR cells, none of the test compounds demonstrated any activity (**Figure 2C**).

## Sensitization of Resistant Cancer Cells to Chemotherapy by 3,4-Dihydroisocoumarins

Cancer cells overexpressing MDR related ABC transporters are characterized by reduced susceptibility to chemotherapeutic drugs, which are substrates of the respective transporters. These are for example doxorubicin (P-gp) and mitoxantrone (BCRP). To determine if the identified P-gp and BCRP inhibitor derivative **16** is able to re-sensitize resistant cancer cells to chemotherapy, P-gp expressing HCT-15 cells and BCRP-expressing MCF-7/MX cells were co-treated with doxorubicin or mitoxantrone and different concentrations of compound **16**. $IC_{50}$ values were determined after 48 h and compared to single treatment with the chemotherapeutic drugs. PSC833 (2.5 μM) and Ko143 (1 μM) served as respective positive controls for P-gp and BCRP, respectively.

In both cases, compound **16** was able to significantly sensitize the resistant cancer cells to chemotherapy. In HCT-15 cells, doxorubicin alone had an $IC_{50}$ value of 8.5 ± 0.7 μM (mean ± SEM; **Figure 3A** and **Table 2**). Addition of 20 μM of compound **16** did not lead to a change in $IC_{50}$, whereas the combination with 50 μM of the compound lead to a 3.7-fold decrease in $IC_{50}$ to 2.3 ± 0.1 μM. In contrast, compound **14**, which displayed minor P-gp inhibiting activity, did not sensitize the cells to doxorubicin. The positive control PSC833 reduced the $IC_{50}$ of doxorubicin around 28-fold to a value of 0.35 ± 0.08 μM.

In BCRP-expressing MCF-7/MX cells, $IC_{50}$ value of the drug mitoxantrone alone was 19.6 ± 2.4 μM (**Figure 3B** and **Table 3**). Addition of compound **16** revealed a dose-dependent decrease in $IC_{50}$ up to 5.6-fold at 50 μM to 3.5 ± 0.9 μM. As observed above, compound **14**, which did not inhibit BCRP transport function, did not have a significant influence on the sensitivity of the cells to mitoxantrone. The positive control Ko143 was able to increase the cytotoxicity of mitoxantrone around 65-fold to an $IC_{50}$ value of 0.33 ± 0.07 μM.

## Cytotocity of 3,4-Dihydroisocoumarins on Pdr5 Wild-Type and Pdr5 EQ Expressing Yeast Strains and Their Ability to Inhibit Transport and ATPase Activity of Pdr5 Wild-Type

The 12 3,4-dihydroisocoumarins were tested on two different *S. cerevisiae* strains to determine their cytotoxicity on yeast. Therefore, a Pdr5 WT and a Pdr5 EQ mutant overexpressing strain were incubated with serial dilutions of the test compounds and $OD_{600}$ was measured after 48 h of cell growth at 30°C. None of the tested 3,4-dihydroisocoumarins showed an effect on the growth of the cells (**Figure 4**), except compound **16a**, which inhibited the growth of the mutant strain slightly at the highest tested concentration (**Figure 4D**). However, it had no effect on the wild-type strain (**Figure 4C**).

In a first initial screen, the effect of the highest concentrations (10 mM) of the 3,4-dihydroisocoumarins on R6G transport and ATPase activity of Pdr5 in PM preparations was analyzed (**Figure 5**). In the case of the transport assay, Pdr5 containing PM preparations were incubated simultaneously with R6G and the test compound. If Pdr5 actively transports R6G, the concentration of the substrate increases in one of the membrane leaflets, which leads to a self-quenching effect. This can be measured as a decrease of fluorescence intensity in real time. Compound **14**, 6-methoxymellein (**3**) and angelicoin B (**4**) did not interfere with Pdr5-mediated R6G transport (**Figure 5A**) as the observed changes in fluorescence were comparable to R6G transport of the wild-type protein in the absence of the compound. In contrast, compounds **21**, ***(R)*-19a** and ***(S)*-19a** inhibited transport activity to 49, 43, and 37%, respectively. Only compound ***(R)*-19**, ***(S)*-19**, **16** and **16a** were able to inhibit the transport of R6G completely.

**Figure 5B** summarizes the effect of the 3,4-dihydroisocoumarins on ATPase activity of Pdr5 WT. Again, compound **14**, 6-methoxymellein (**3**) and angelicoin B (**4**) had

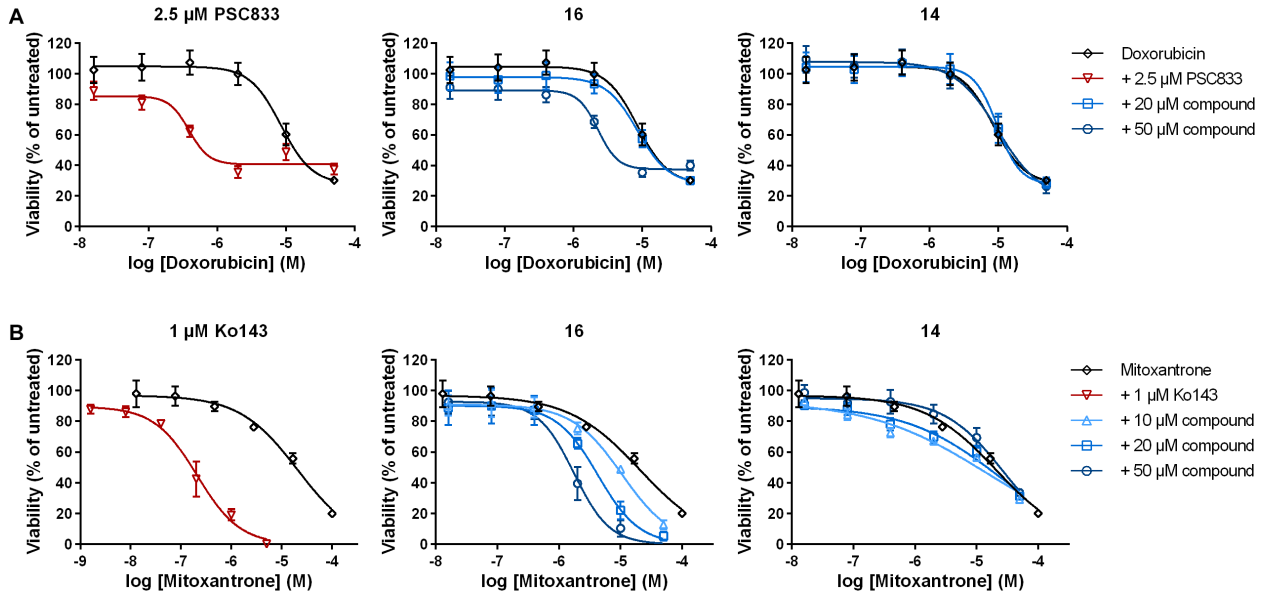


**FIGURE 3 |** Sensitization of resistant cancer cells to chemotherapy by selected 3,4-dihydroisocoumarins. **(A)** P-gp expressing HCT-15 and **(B)** BCRP-expressing MCF-7/MX were treated with either doxorubicin or mitoxantrone alone, in combination with positive controls PSC833 or Ko143 or in combination with varying concentrations of test compounds **16** and **14**. Cell viability was determined after 48 h. Data represent mean ± SEM normalized to untreated cells of at least three independent experiments performed in quadruplicates.

no inhibitory effect. In contrast to the capability of **(R)-19a** and **(S)-19a** to inhibit transport of R6G, no inhibition of the ATPase activity was observed. **Ellagic acid** and compound **21** inhibited the ATPase activity to 56 and 54%, respectively. Compounds ***(R)*-19**, ***(S)*-19**, **16,** and **16a** showed the highest inhibition potential on the Pdr5 WT ATPase activity.

Finally, $IC_{50}$ values were determined for those inhibitors that displayed the highest potential in the transport and the ATPase assay (***(R)*-19**, ***(S)*-19**, **16,** and **16a**) (**Figures 6**, **7**). **Figure 6** summarizes the $IC_{50}$ measurements of the transport assays.

**TABLE 2 |** Sensitization of HCT-15 cells to doxorubicin treatment by selected 3,4-dihydroisocoumarins.

| Compound | $IC_{50}$ (µM) | *p*-Value | Fold change |
|---|---|---|---|
| Doxorubicin | 8.5 ± 0.7 | – | 1.00 |
| +2.5 µM PSC833 | 0.3 ± 0.03** | 0.0017 | 28.33 |
| +20 µM 16 | 8.7 ± 1.6 | 0.9999 | 0.98 |
| +50 µM 16 | 2.3 ± 0.08* | 0.0129 | 3.70 |
| +20 µM 14 | 9.6 ± 1.0 | 0.9498 | 0.89 |
| +50 µM 14 | 10.6 ± 2.1 | 0.6313 | 0.80 |

*PSC833 was used as positive control. Fold change of cytotoxicity was determined by dividing the $IC_{50}$ value of cells treated with doxorubicin alone by the $IC_{50}$ value of cells treated with doxorubicin in combination with the respective test compound. Data show mean ± SEM of three independent experiments performed in quadruplicates. *$p < 0.05$; **$p < 0.01$ compared to doxorubicin alone (one-way ANOVA followed by Dunnett's multiple comparisons test).*

The lowest $IC_{50}$ was determined for compound ***(S)*-19** with 5.3 ± 0.6 µM. Compound **16** and **16a** showed $IC_{50}$ values of 15.1 ± 2.1 and 14.6 ± 3.9 µM, respectively. The highest $IC_{50}$ value was detected for compound ***(R)*-19** with 26.0 ± 3.5 µM. **Figure 7** summarizes the $IC_{50}$ measurements with respect to inhibition of ATPase activity. Due to the solubility limit of these compounds, no reliable determination of $IC_{50}$ values could be performed.

## Binding Mode Prediction and Effective Binding Energy Calculations on Complexes of P-Glycoprotein and 3,4-Dihydroisocoumarins

The selected docking protocol was able to reproduce the binding modes of Zosuquidar (ZQU) in P-gp, regardless of whether the second ligand entity was retained in the structure ($RMSD_{ZQU1304}$: 0.93 Å, $RMSD_{ZQU1305}$: 1.14 Å, **Figure 8A**) or not ($RMSD_{ZQU1305}$: 1.53 Å, $RMSD_{ZQU1304}$: 3.21 Å, **Figure 8B**), suggesting that it is also suitable for predicting the binding modes of other molecules, such as the 3,4-dihydroisocoumarins. When two molecules of ZQU were sequentially docked to the P-gp structure, all poses obtained during the first run corresponded to the binding mode of ZQU1305 in the cryo-EM structure (**Figure 8B**), indicating that the subpocket occupied by this ligand entity has a higher affinity toward ZQU than the subpocket occupied by the ligand entity ZQU1304. In line with this, the pose obtained for re-docking of ZQU1305 with ZQU1304 present was scored markedly better than the pose obtained for re-docking of ZQU1304 with ZQU1305 present (Glide Docking Scores: −10.40 and −8.60 kcal $mol^{-1}$, respectively). Similarly, initial docking

**TABLE 3 |** Sensitization of MCF-7/MX cells to mitoxantrone treatment by selected 3,4-dihydroisocoumarins.

| Compound | $IC_{50}$ (μM) | *p*-Value | Fold change |
|---|---|---|---|
| Mitoxantrone | 19.6 ± 2.4 | – | 1.00 |
| +1 μM Ko143 | 0.3 ± 0.07**** | < 0.0001 | 65.33 |
| +10 μM 16 | 21.1 ± 1.4 | 0.9795 | 0.93 |
| +20 μM 16 | 5.3 ± 1.1**** | < 0.0001 | 3.70 |
| +50 μM 16 | 3.5 ± 0.9**** | < 0.0001 | 5.60 |
| +10 μM 14 | 19.4 ± 2.6 | > 0.9999 | 1.01 |
| +20 μM 14 | 25.5 ± 1.0 | 0.0942 | 0.77 |
| +50 μM 14 | 25.0 ± 1.3 | 0.0988 | 0.78 |

*Ko143 was used as positive control. Fold change of cytotoxicity was determined by dividing the $IC_{50}$ value of cells treated with mitoxantrone alone by the $IC_{50}$ value of cells treated with mitoxantrone in combination with the respective test compound. Data show mean ± SEM of three independent experiments performed in quadruplicates. ****p < 0.0001 compared to doxorubicin alone (one-way ANOVA followed by Dunnett's multiple comparisons test).*

of the 3,4-dihydroisocoumarins revealed two spatially distinct binding sites (BS1 and BS2) overlapping with those of ZQU1304 and ZQU1305, respectively, to which all ligands were docked separately during the final docking experiment (**Figure 8C**). Since, on average, the calculated effective binding energies were 7.44 ± 3.45 kcal $mol^{-1}$ (21.64 ± 6.01 kcal $mol^{-1}$ for the active molecules **16**, **(*R*)-19** and **(*S*)-19**) more favorable in BS2 (**Table 4**), only the poses in BS2 were used for the final evaluation.

The calculated effective binding energies of the 3,4-dihydroisocoumarins agree very well with their ability to inhibit P-gp-mediated transport: Compounds **16**, **16a**, **(*R*)-19** and **(*S*)-19**, which all inhibited substrate transport by > 20% at concentrations of 20 μM (**Figure 2A**), also showed significantly more favorable effective binding energies than the inactive compounds ($\Delta G_{eff}$ = −48.16 ± 0.73 kcal $mol^{-1}$ versus $\Delta G_{eff}$ = −31.81 ± 1.79 kcal $mol^{-1}$, $p < 10^{-4}$) (**Figure 8C** and **Table 4**). Note, though, that configurational entropy differences were neglected here, such that the difference in the binding free energies of the two classes may be smaller due to enthalpy-entropy compensation effects. These results validate the obtained binding modes for the 3,4-dihydroisocoumarins in P-gp and corroborate the experimental findings on the compounds' ability to inhibit P-gp-mediated substrate transport.

## DISCUSSION

In this study, 3,4-dihydroisocoumarins, which have so far not been in the focus as potential MDR reversing agents, were evaluated as potential inhibitors of human and yeast ABC transporters. Notably, among the tested derivatives, three novel

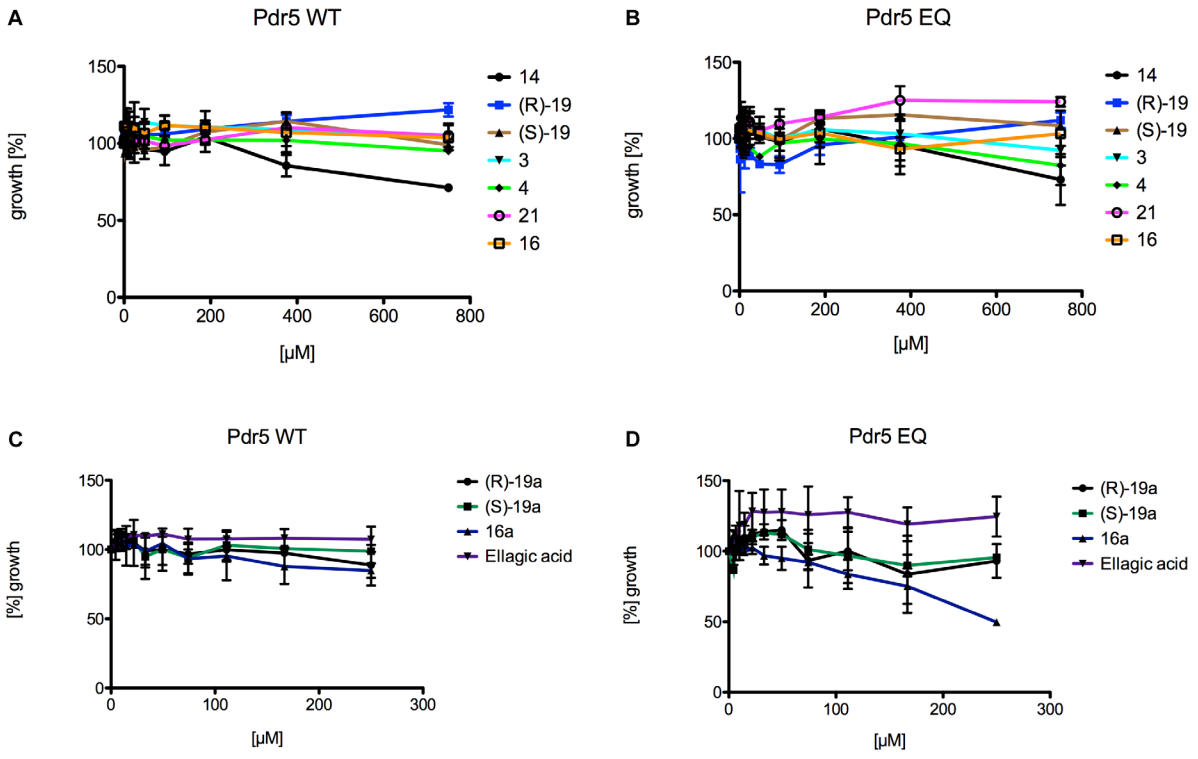


**FIGURE 4 |** Liquid drug assays of the 12 3,4-dihydroisocoumarins and *S. cerevisiae* strains expressing Pdr5 WT or the mutant Pdr5 EQ. **(A)** The influence of **14**, ***(R)*-19**, ***(S)*-19**, **3**, **4**, **21**, and **16** on growth of strains expressing Pdr5 WT. **(B)** The influence of **14**, ***(R)*-19**, ***(S)*-19**, **3**, **4**, **21**, and **16** on growth of strains expressing Pdr5 EQ. **(C)** The influence of ***(R)*-19a**, ***(S)*-19a**, **16a** and **ellagic acid** on growth of strains expressing Pdr5 WT. **(D)** The influence of ***(R)*-19a**, ***(S)*-19a**, **16a** and **ellagic acid** on growth of strains expressing Pdr5 EQ. Cells were incubated at different concentrations of the compounds for 48 h at 30 °C and $OD_{600}$ was determined.

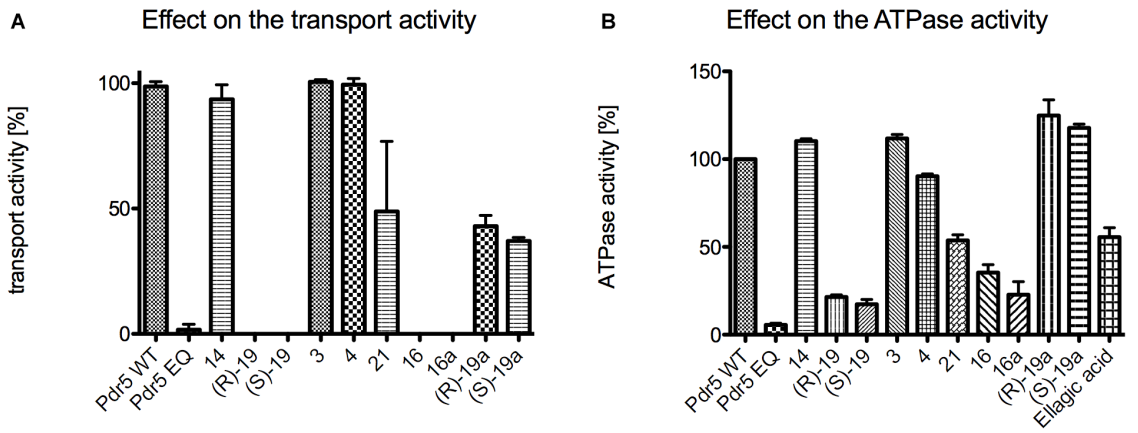


**FIGURE 5 |** Initial screening of the 12 test compounds to determine their effect on **(A)** the transport activity of Pdr5 WT and **(B)** their effect on the ATPase activity. Within the transport assay compound **14**, **3** and **4** had no effect on both activities. Compound **21**, ***(R)*-19a** and ***(S)*-19a** were able to inhibit the transport activity to around 50%. Only compound ***(R)*-19**, ***(S)*-19**, **16** and **16a** were able to inhibit the transport activity of Pdr5 WT completely. In contrast, compounds **14**, **3**, **4**, ***(R)*-19a** and ***(S)*-19a** had nearly no effect on the ATPase activity. Compound **21** and **ellagic acid** were able to inhibit the ATPase activity of Pdr5 WT to 50%. Only compound ***(R)*-19**, ***(S)*-19**, **16** and **16a** were able to inhibit ATPase activity below 40% in comparison to Pdr5 WT in the absence of any compound.

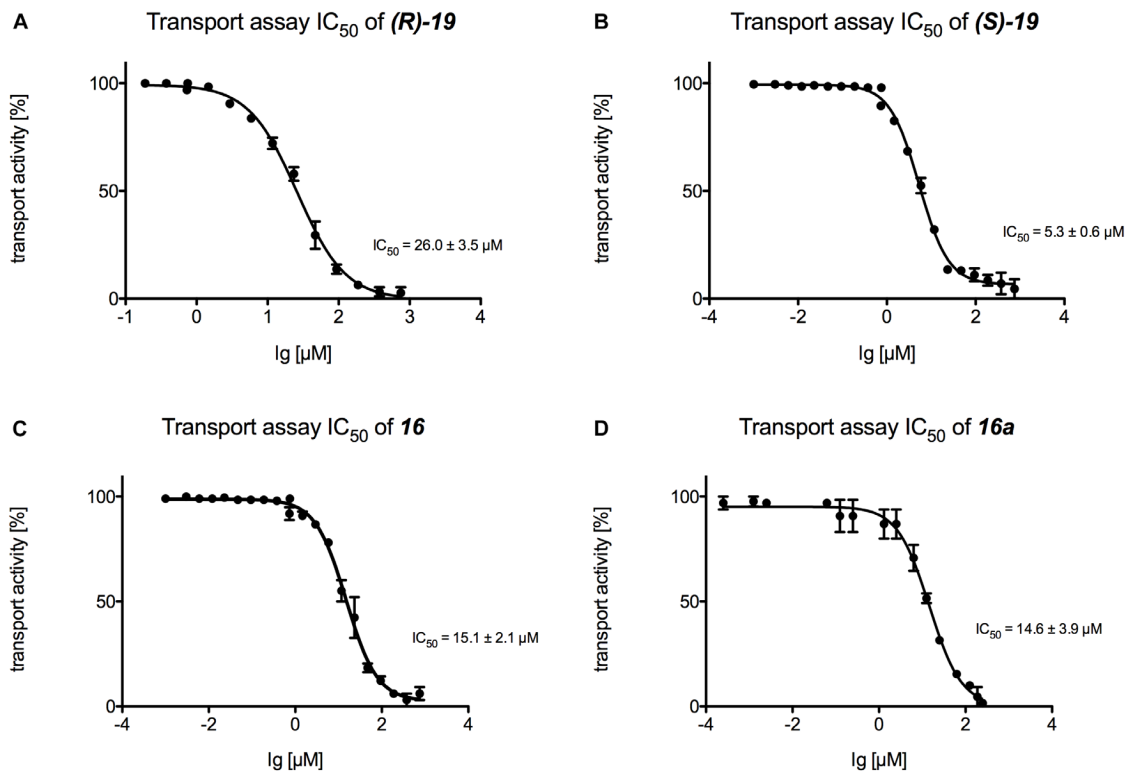


**FIGURE 6 |** Determination of the transport $IC_{50}$ values for **(A)** compound ***(R)*-19**, **(B)** compound ***(S)*-19**, **(C)** compound **16** and **(D)** compound **16a**. For each compound a serial dilution was used to determine the $IC_{50}$ curve. Membranes were incubated with the compound and active transport was detected with the Tecan Infinite M200.

3,4-dihydroisocoumarins were identified as dual inhibitors of two human transporters, P-gp and BCRP. Furthermore, the most potent inhibitor, derivative **16**, demonstrated inhibition of both transporters between 80 and 90% compared to the respective positive controls at the highest test concentration (50 µM). As proof of concept, P-gp expressing HCT-15 cells and BCRP-expressing MCF-7/MX cells (Sachs et al., 2019) were treated with compound **16** in combination with the chemotherapeutic drugs doxorubicin and mitoxantrone, broadly described as transporter substrates for P-gp and

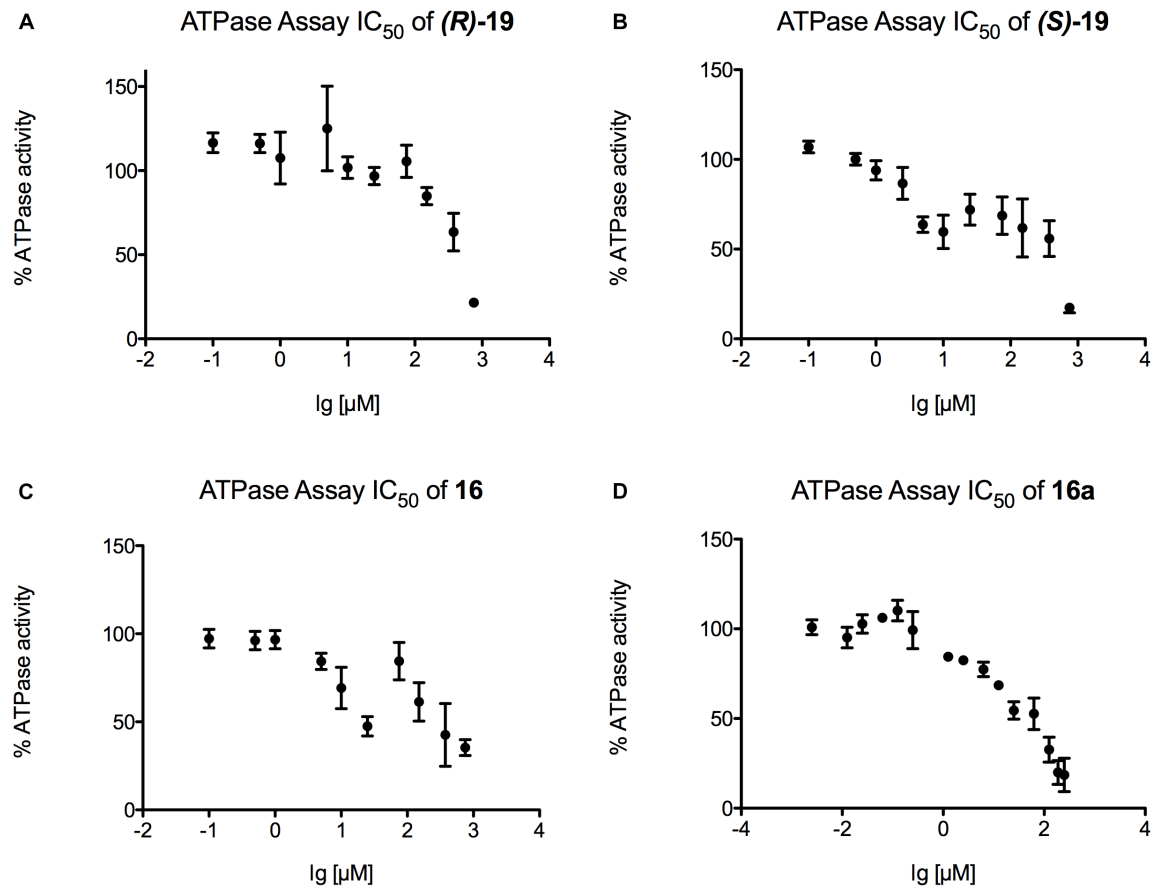


**FIGURE 7 |** Determination of the ATPase $IC_{50}$ values for **(A)** compound ***(R)*-19**, **(B)** compound ***(S)*-19**, **(C)** compound **16** and **(D)** compound **16a**. For each compound a serial dilution was used to display the $IC_{50}$ curve. Pdr5 plasma membranes (PMs) were incubated with the compound for 20 min and release of inorganic phosphate was detected with an Elisa PlateReader at 595 nm.

BCRP. Subsequently, co-treatment with 50 µM of derivative **16** sensitized chemotherapy-resistant cancer cells HCT-15 colon carcinoma cells to doxorubicin by decreasing the $IC_{50}$ value of doxorubicin-induced cytotoxicity by 3.7-fold and sensitized MCF-7/MX breast carcinoma cells to mitoxantrone by decreasing the $IC_{50}$ value of mitoxantrone-induced cytotoxicity by 5.6-fold. Moreover, enantiomers (***R*)-19** and (***S*)-19** inhibited transport function of P-gp and BCRP, but with lower potency compared to derivative **16**. Noteworthy, distinct structure-activity relationships for transporter inhibition could be identified, and they run in parallel for P-gp and BCRP: our data show that the hydroxy group at position 6 is mandatory for transporter inhibition and substitution by a methoxy group clearly reduces activity. Furthermore, a hydrophobic carbon chain at position 3 is indispensable for inhibition and this substituent seems to need a certain chain length. Compounds without alkyl substituent (derivative **14**) or with a methyl group [6-methoxymellein (**3**) and angelicoin B (**4**)] as well as compounds with a hydrophilic chain (derivatives (***R*)-19a** and (***S*)-19a**) demonstrated significantly decreased inhibition of both transporters. Those effects were more pronounced in BCRP inhibition than in P-gp inhibition.

Molecular docking can provide an explanation at the atomistic level for the observed structure-activity relationship. Here, we focused on docking of 3,4-dihydroisocoumarins to P-gp because for this system it was possible to validate the suitability of our docking protocol. The predicted binding modes of the active molecules **16**, (***R*)-19** and (***S*)-19** close to the binding sites of ZQU are largely identical (**Figures 8D,E**, **9A,B**) and reveal that the hydroxy group at position 8 stabilizes the binding mode via hydrogen bonding to the hydroxy group in Y306. Introduction of a bulky methyl group, as realized in **16a**, not only abolishes this interaction, but also leads to a steric clash with Y306, forcing the molecule to invert its orientation (**Figure 9B**). Furthermore, the hydrophobic OTBS moiety in (***R*)-19** and (***S*)-19** protrudes into a predominantly hydrophobic subpocket, formed by residues M298, N720, F769, Q772, Q837, and V990. Removal of this group, as realized in (***R*)-19a** and (***S*)-19a**, leads to an unsatisfied hydrogen bond donor in this subpocket, which disfavors binding. Finally, compounds **3**, **4**, **14**, **14a**, and **21** adopt binding modes that either resemble the inverted orientation of **16a**, or are dissimilar to those of the active molecules **16**, (***R*)-19** and (***S*)-19** (**Figure 9C**). Taken together, these results indicate that differences in the inhibitory power of

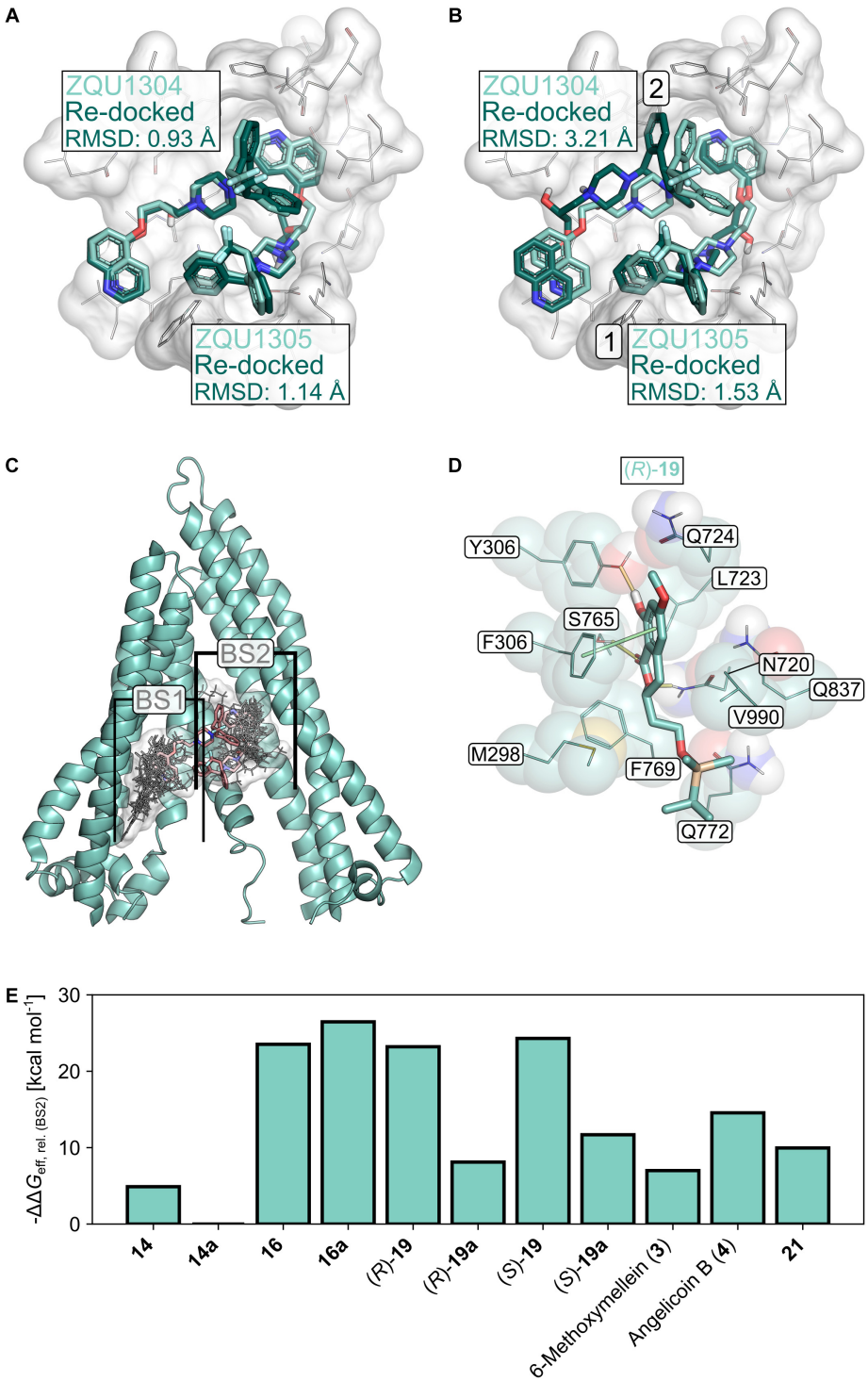


**FIGURE 8 |** Molecular docking studies. **(A)** Re-docking of Zosuquidar (ZQU, darker turquoise, sticks representation) into the cryo-EM structure (PDB ID: 6FN1; Alam et al., 2018) of P-gp (white, sticks and cartoon representation, only part of the protein is shown for clarity) while the coordinates of the respective second ZQU molecule (lighter turquoise) were retained from the cryo-EM structure. **(B)** Sequential re-docking of ZQU into the cryo-EM structure of P-gp. The result of the first and second runs are indicated with a *1* and *2*, respectively. Colors and representations are as in **(A)**. **(C)** Binding sites (denoted as BS1 and BS2) for 3,4-dihydroisocoumarins found during docking. The molecular structures of the 3,4-dihydroisocoumarins are displayed as lines, and their joint molecular surface is rendered in white. Zosuquidar is shown as red sticks. The relevant region in the transmembrane domain of P-gp is shown in cartoon representation **(D)** Binding mode of ***(R)*-19** in BS2 of P-gp. Hydrogen bonds are displayed as yellow lines, $\pi$-stacking interactions as green lines. **(E)** Relative effective binding energies for 3,4-dihydroisocoumarins in P-gp, calculated by the MM-GBSA approach. To allow for a better comparison with the P-gp transport assay, the energies are expressed as $-\Delta\Delta G_{eff}$.

**TABLE 4 |** Relative effective energies of 3,4-dihydroisocoumarins binding to P-gp.[1]

| Compound | $\Delta\Delta G_{eff}$[2] | |
|---|---|---|
| | BS1 | BS2 |
| 14 | −10.04 (−24.55) | −14.16 (−28.67) |
| 14a | −14.85 (−29.36) | −9.27 (−23.78) |
| 16 | −13.46 (−27.97) | −32.80 (−47.31) |
| 16a | −24.12 (−38.63) | −35.74 (−50.25) |
| (*R*)-19 | −20.48 (−34.99) | −32.48 (−46.99) |
| (*R*)-19a | −22.61 (−37.12) | −17.38 (−31.89) |
| (*S*)-19 | 0.00 (−14.51) | −33.57 (−48.08) |
| (*S*)-19a | −14.41 (−28.92) | −20.96 (−35.47) |
| 6-Methoxymellein (3) | −12.62 (−27.13) | −16.27 (−30.78) |
| Angelicoin B (4) | −20.66 (−35.17) | −23.83 (−38.34) |
| 21 | −20.56 (−35.02) | −19.23 (−33.74) |

*[1]All values are relative to the effective binding energy of (S)-19 in BS1. [2]In kcal mol$^{-1}$.*

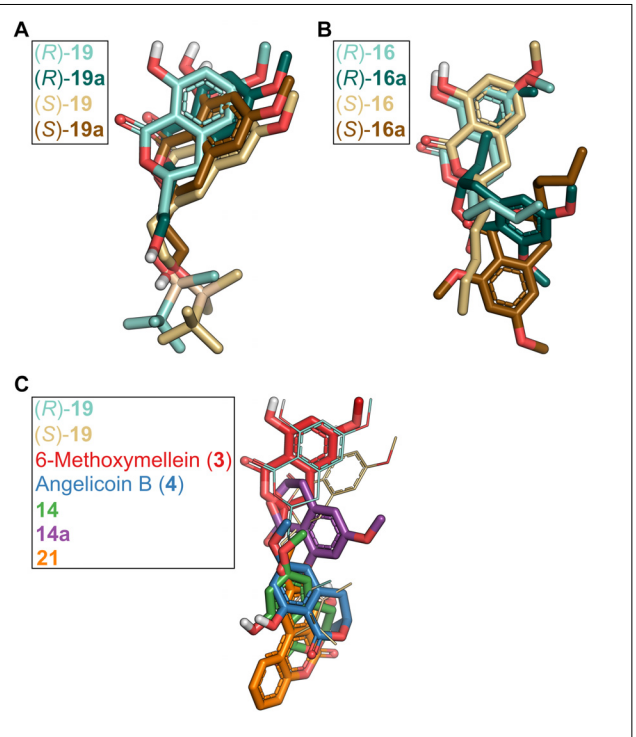


**FIGURE 9 |** Comparison of binding poses of 3,4-dihydroisocoumarins in P-gp obtained by molecular docking. **(A)** Binding poses of compounds carrying a TBS group in the side chain [**(*R*)-19**, **(*S*)-19**] versus compounds in which the TBS group was removed [**(*R*)-19a**, **(*S*)-19a**]. **(B)** Binding poses of compounds that carry a hydroxy group at position 8 [**(*R*)-16**, **(*S*)-16**] versus compounds that carry a methoxy group at position 8 [**(*R*)-16a**, **(*S*)-16a**]. **(C)** Binding modes of compounds **3**, **4**, **14**, **14a,** and **21** in comparison to **(*R*)-19** and **(*S*)-19**.

the investigated 3,4-dihydroisocoumarins with respect to P-gp-mediated transport result from differences in the compounds' binding affinities to P-gp rather than their ability to modulate P-gp's transport cycle or to affect P-gp function via a different mechanism. They further support the recent finding (Alam et al., 2018) that the central cavity in P-gp can accommodate multiple molecules in different subpockets and, thereby, substantiate the concept of a binding site with high plasticity (Wise, 2012; McCormick et al., 2015).

Regarding these results, the 3,4-dihydroisocoumarin derivatives that we identified as dual P-gp and BCRP inhibitors with moderate activity might serve as a promising starting point for further development of novel inhibitors for overcoming cancer MDR. In future work, it will be important to identify additional substituents at other positions of the molecule to significantly improve the potency of the current chemical lead structure.

In a first initial screening ***(R)*-19**, ***(S)*-19**, **16** and **16a** were identified as potential inhibitors of the yeast ABC transporter Pdr5. With these four compounds $IC_{50}$ measurements with respect to R6G transport as well as the ATPase activity were performed. In the case of the transport assay the highest $IC_{50}$ value was determined for ***(R)*-19** with 26.0 ± 3.5 μM. Interestingly the lowest $IC_{50}$ was detected for its enantiomer ***(S)*-19** with 5.3 ± 0.6 μM. The transport $IC_{50}$ values for **16** and **16a** were nearly similar with 15.1 ± 2.1 and 14.6 ± 3.9 μM, respectively. For the ATPase activity it was not possible to reliably determine any $IC_{50}$ value because of the limited solubility of the compounds. The highest ATPase activity inhibition of Pdr5 wild-type was detected for ***(S)*-19** with an inhibition down to 17.3% activity in comparison to Pdr5 WT without any compound. For ***(R)*-19** the ATPase activity was inhibited to 21.5% and for **16** and **16a** the activity was inhibited to 35.4 and 22.8%, respectively. Our data furthermore suggest that these four coumarins are substrates of Pdr5, which are transported in competition to the fluorophore R6G and become inhibitory at higher concentrations, a phenomena often observed for P-gp (Al-Shawi et al., 2003) and Pdr5 (Ernst et al., 2008). In contrast to P-gp, it is obviously not important if there is a hydroxy or methoxy group at position 6, but it seems important that a longer hydrophobic side chain is present at position 3. The two natural substrates 6-methoxymellein (**3**) and angelicoin (**4**) with only a small methyl group at position 3 or compound **14** with no alkyl side chain at all displayed no effect on neither transport nor ATPase activity. Furthermore, in comparison to that the two compounds with a longer alkyl side chain with a hydrophilic group (***(R)*-19a** and ***(S)*-19a**) showed only inhibition to around 40%. In addition to transporter inhibition, the cytotoxic activity of the test compounds was analyzed in sensitive A549 lung carcinoma cells as well as resistant HCT-15 colon carcinoma, H69AR lung carcinoma and MCF-7/MX breast carcinoma cells. Most compounds did not exhibit any toxic effects in cancer cells. One exception was derivative **16a**, which proved to be selectively cytotoxic in BCRP-expressing MCF-7/MX cells with an $IC_{50}$ value of 10.6 μM, but not in P-gp or MRP1-expressing cells. In sensitive A549, cytotoxicity was significantly lower with an $IC_{50}$ value of 53.6 μM. At this point, it would be interesting to further characterize if compound **16a** specifically kills multidrug-resistant cells by analyzing its activity in parental, sensitive MCF-7 cells. If this is the case, gaining insights into the mechanism of action and target would be helpful to find out more about

collateral sensitivity in BCRP-overexpressing cancer cells and how to exploit this feature in tumor therapy (Pluchino et al., 2012; Rao et al., 2014).

## AUTHOR CONTRIBUTIONS

JS, KD, and MB performed experiments, analyzed data, and wrote the manuscript. AW synthesized test compounds. EF and AK provided ellagic acid. NT, LS, HG, JP, EF, and AK contributed to study conception and design and received funding. All authors revised the manuscript.

## FUNDING

This work was funded by the German Federal Ministry for Economic Affairs and Energy ('ZIM Kooperationsprojekt' KF3279X01AJ3 to EF, AK, JP, LS, and NT) and supported by a scholarship of the Studienstiftung des Deutschen Volkes for AW. The Ph.D. training of JS was financed by the graduate program in Pharmacology and Experimental Therapeutics at the University of Cologne, which is financially and scientifically supported by Bayer. Funding by Deutsche Forschungsgemeinschaft (DFG) (INST 208/704-1 FUGG) to purchase the hybrid computer cluster used in this study is gratefully acknowledged.

## ACKNOWLEDGMENTS

We would like to thank Dr. Erasmus Schneider (Wadsworth Center, New York State Department of Health, Albany, NY, United States) for kindly providing the MCF-7/MX cell line and Janina Betz and Vanessa Mundorf for excellent technical assistance. We are grateful for computational support by the "Zentrum für Informations und Medientechnologie" at the Heinrich Heine University and the computing time provided by the John von Neumann Institute for Computing (NIC) to HG on the supercomputer JURECA at Jülich Supercomputing Centre (JSC) (user ID: HKF7).

## REFERENCES

Abid, O. U. R., Khalid, M., Hussain, M. T., Hanif, M., Qadeer, G., Rama, N. H., et al. (2012). Synthesis and anti-cancer, anti-metastatic evaluation of some new fluorinated isocoumarins and 3,4-dihydroisocoumarins. *J. Fluor. Chem.* 135, 240–245. doi: 10.1016/j.jfluchem.2011.11.011

Agarwal, S., Hartz, A. M. S., Elmquist, W. F., and Bauer, B. (2011). Breast cancer resistance protein and P-glycoprotein in brain cancer: two gatekeepers team up. *Curr. Pharm. Des.* 17, 2793–2802. doi: 10.2174/138161211797440186

Alam, A., Küng, R., Kowal, J., McLeod, R. A., Tremp, N., Broude, E. V., et al. (2018). Structure of a zosuquidar and UIC2-bound human-mouse chimeric ABCB1. *Proc. Natl. Acad. Sci.* 115, E1973–E1982. doi: 10.1073/pnas.1717044115

Al-Shawi, M. K., Polar, M. K., Omote, H., and Figler, R. A. (2003). Transition state analysis of the coupling of drug transport to ATP hydrolysis by P-glycoprotein. *J. Biol. Chem.* 278, 52629–52640. doi: 10.1074/jbc.M308175200

Baer, M. R., George, S. L., Dodge, R. K., O'Loughlin, K. L., Minderman, H., Caligiuri, M. A., et al. (2002). Phase 3 study of the multidrug resistance modulator PSC-833 in previously untreated patients 60 years of age and older with acute myeloid leukemia: Cancer and leukemia group B Study 9720. *Blood* 100, 1224–1232.

Barthomeuf, C., Grassi, J., Demeule, M., Fournier, C., Boivin, D., and Béliveau, R. (2005). Inhibition of P-glycoprotein transport function and reversion of MDR1 multidrug resistance by cnidiadin. *Cancer Chemother. Pharmacol.* 56, 173–181. doi: 10.1007/s00280-004-0914-y

Begicevic, R.-R., and Falasca, M. (2017). ABC transporters in cancer stem cells: beyond chemoresistance. *Int. J. Mol. Sci.* 18:2362. doi: 10.3390/ijms18112362

Bisi, A., Cappadone, C., Rampa, A., Farruggia, G., Sargenti, A., Belluti, F., et al. (2017). Coumarin derivatives as potential antitumor agents: growth inhibition, apoptosis induction and multidrug resistance reverting activity. *Eur. J. Med. Chem.* 127, 577–585. doi: 10.1016/j.ejmech.2017.01.020

Böse, D., Niesobski, P., Lübcke, M., and Pietruszka, J. (2014). A diastereoselective one-pot, three-step cascade toward α-substituted allylboronic esters. *J. Org. Chem.* 79, 4699–4703. doi: 10.1021/jo5004168

Boumendjel, A., McLeer-Florin, A., Champelovier, P., Allegro, D., Muhammad, D., Souard, F., et al. (2009). A novel chalcone derivative which acts as a microtubule depolymerising agent and an inhibitor of P-gp and BCRP in in-vitro and in-vivo glioblastoma models. *BMC Cancer* 9:242. doi: 10.1186/1471-2407-9-242

Brown, G. D., Denning, D. W., Gow, N. A. R., Levitz, S. M., Netea, M. G., and White, T. C. (2012). Hidden killers: human fungal infections. *Sci. Transl. Med.* 4:165rv13. doi: 10.1126/scitranslmed.3004404

Bugde, P., Biswas, R., Merien, F., Lu, J., Liu, D.-X., Chen, M., et al. (2017). The therapeutic potential of targeting ABC transporters to combat multi-drug resistance. *Expert Opin. Ther. Targets* 21, 511–530. doi: 10.1080/14728222.2017.1310841

Cichewicz, R. H., Valeriote, F. A., and Crews, P. (2004). Psymberin, a potent sponge-derived cytotoxin from *Psammocinia* distantly related to the pederin family. *Org. Lett.* 6, 1951–1954. doi: 10.1021/ol049503q

Combes, S., Barbier, P., Douillard, S., McLeer-Florin, A., Bourgarel-Rey, V., Pierson, J.-T., et al. (2011). Synthesis and biological evaluation of 4-arylcoumarin analogues of combretastatins. Part 2. *J. Med. Chem.* 54, 3153–3162. doi: 10.1021/jm901826e

Decottignies, A., Kolaczkowski, M., Balzi, E., and Goffeau, A. (1994). Solubilization and characterization of the overexpressed PDR5 multidrug resistance nucleotide triphosphatase of yeast. *J. Biol. Chem.* 269, 12797–12803.

Dohse, M., Scharenberg, C., Shukla, S., Robey, R. W., Volkmann, T., Deeken, J. F., et al. (2010). Comparison of ATP-binding cassette transporter interactions with the tyrosine kinase inhibitors imatinib, nilotinib, and dasatinib. *Drug Metab. Dispos.* 38, 1371–1380. doi: 10.1124/dmd.109.031302

Dufour, J.-P., Amory, A., and Goffeau, A. (1988). Plasma membrane ATPase from the yeast *Schizosaccharomyces pombe*. *Methods Enzymol.* 157, 513–528. doi: 10.1016/0076-6879(88)57100-8

El-Awady, R., Saleh, E., Hashim, A., Soliman, N., Dallah, A., Elrasheed, A., et al. (2016). The role of eukaryotic and prokaryotic abc transporter family in failure of chemotherapy. *Front. Pharmacol.* 7:535. doi: 10.3389/fphar.2016.00535

Endringer, D. C., Guimarães, K. G., Kondratyuk, T. P., Pezzuto, J. M., and Braga, F. C. (2008). Selective inhibition of aromatase by a dihydroisocoumarin from *Xyris pterygoblephara*. *J. Nat. Prod.* 71, 1082–1084. doi: 10.1021/np800098f

Ernst, R., Klemm, R., Schmitt, L., and Kuchler, K. (2005). Yeast ATP-binding cassette transporters: cellular cleaning pumps. *Methods Enzymol.* 400, 460–484. doi: 10.1016/S0076-6879(05)00026-1

Ernst, R., Kueppers, P., Klein, C. M., Schwarzmueller, T., Kuchler, K., and Schmitt, L. (2008). A mutation of the H-loop selectively affects rhodamine transport by the yeast multidrug ABC transporter Pdr5. *Proc. Natl. Acad. Sci.* 105, 5069–5074. doi: 10.1073/pnas.0800191105

Fischer, T., and Pietruszka, J. (2007). Efficient synthesis of either enantiomer of ethyl 5-hydroxyhept-6-enoate. *Adv. Synth. Catal.* 349, 1533–1536. doi: 10.1002/adsc.200700086

Fitzmaurice, C., Allen, C., Barber, R. M., Barregard, L., Bhutta, Z. A., Brenner, H., et al. (2017). Global, regional, and national cancer incidence, mortality, years of life lost, years lived with disability, and disability-adjusted life-years for 32 cancer groups, 1990 to 2015: a systematic analysis for the global burden of disease study. *JAMA Oncol.* 3, 524–548. doi: 10.1001/jamaoncol.2016.5688

Friesner, R. A., Banks, J. L., Murphy, R. B., Halgren, T. A., Klicic, J. J., Mainz, D. T., et al. (2004). Glide: a new approach for rapid, accurate docking and scoring.

1. method and assessment of docking accuracy. *J. Med. Chem.* 47, 1739–1749. doi: 10.1021/jm0306430

Friesner, R. A., Murphy, R. B., Repasky, M. P., Frye, L. L., Greenwood, J. R., Halgren, T. A., et al. (2006). Extra precision glide: docking and scoring incorporating a model of hydrophobic enclosure for protein-ligand complexes. *J. Med. Chem.* 49, 6177–6196. doi: 10.1021/jm051256o

Gillet, J.-P., and Gottesman, M. M. (2010). "Mechanisms of Multidrug Resistance in Cancer," in *Multi-Drug Resistance in Cancer*, ed. J. Zhou (Totowa, NJ: Humana Press), 47–76. doi: 10.1007/978-1-60761-416-6_4

Goffeau, A., and Dufour, J.-P. (1988). Plasma membrane ATPase from the yeast Saccharomyces cerevisiae. *Methods Enzymol.* 157, 528–533. doi: 10.1016/0076-6879(88)57101-X

Gohlke, H., and Case, D. A. (2004). Converging free energy estimates: MM-PB(GB)SA studies on the protein-protein complex Ras-Raf. *J. Comput. Chem.* 25, 238–250. doi: 10.1002/jcc.10379

Gu, X., Ren, Z., Peng, H., Peng, S., and Zhang, Y. (2014). Bifendate-chalcone hybrids: A new class of potential dual inhibitors of P-glycoprotein and breast cancer resistance protein. *Biochem. Biophys. Res. Commun.* 455, 318–322. doi: 10.1016/j.bbrc.2014.11.016

Guimarães, K. G., Freitas, R. P., de Ruiz, A. L. T. G., Fiorito, G. F., Carvalho, J. E., de da Cunha, E. F. F., et al. (2016). Synthesis, antiproliferative activities, and computational evaluation of novel isocoumarin and 3,4-dihydroisocoumarin derivatives. *Eur. J. Med. Chem.* 111, 103–113. doi: 10.1016/j.ejmech.2016.01.051

Guo, Z. (2017). The modification of natural products for medical use. *Acta. Pharm. Sin. B* 7, 119–136. doi: 10.1016/j.apsb.2016.06.003

Gupta, R. P., Kueppers, P., Hanekop, N., and Schmitt, L. (2014). Generating symmetry in the asymmetric ABC transporter Pdr5 from *Saccharomyces cerevisiae*. *J. Biol. Chem.* 289, 15272–15279. doi: 10.1074/jbc.M114.553065

Hoepfner, D., McNamara, C. W., Lim, C. S., Studer, C., Riedl, R., Aust, T., et al. (2012). Selective and specific inhibition of the *Plasmodium falciparum* lysyl-tRNA synthetase by the fungal secondary metabolite cladosporin. *Cell Host Microbe* 11, 654–663. doi: 10.1016/j.chom.2012.04.015

Hou, T., Wang, J., Li, Y., and Wang, W. (2011). Assessing the performance of the MM/PBSA and MM/GBSA methods. 1. the accuracy of binding free energy calculations based on molecular dynamics simulations. *J. Chem. Inf. Model.* 51, 69–82. doi: 10.1021/ci100275a

Iriti, M., Kubina, R., Cochis, A., Sorrentino, R., Varoni, E. M., Kabała-Dzik, A., et al. (2017). Rutin, a quercetin glycoside, restores chemosensitivity in human breast cancer cells. *Phytother. Res.* 31, 1529–1538. doi: 10.1002/ptr.5878

Jianing, L., Robert, A., Kai, Z., Yixiang, C., Suwen, Z., and Richard, A. F. (2011). The VSGB 2.0 model: A next generation energy model for high resolution protein structure modeling. *Proteins* 79, 2794–2812. doi: 10.1002/prot.23106

Karthikeyan, S., and Hoti, S. (2015). Development of fourth generation ABC inhibitors from natural products: a novel approach to overcome cancer multidrug resistance. *Anticancer Agents Med. Chem.* 15, 605–615. doi: 10.2174/1871520615666150113103439

Kaye, K. S., and Kaye, D. (2000). Multidrug-resistant pathogens: mechanisms of resistance and epidemiology. *Curr. Infect. Dis. Rep.* 2, 391–398. doi: 10.1007/s11908-000-0065-1

Kolaczkowski, M., van der Michel, R., Cybularz-Kolaczkowska, A., Soumillion, J.-P., Konings, W. N., and André, G. (1996). Anticancer drugs, ionophoric peptides, and steroids as substrates of the yeast multidrug transporter Pdr5p. *J. Biol. Chem.* 271, 31543–31548. doi: 10.1074/jbc.271.49.31543

Lai, D., Wang, A., Cao, Y., Zhou, K., Mao, Z., Dong, X., et al. (2016). Bioactive dibenzo-α-pyrone derivatives from the endophytic fungus *Rhizopycnis vagum* Nitaf22. *J. Nat. Prod.* 79, 2022–2031. doi: 10.1021/acs.jnatprod.6b00327

Li, X.-Q., Wang, L., Lei, Y., Hu, T., Zhang, F.-L., Cho, C.-H., et al. (2015). Reversal of P-gp and BCRP-mediated MDR by tariquidar derivatives. *Eur. J. Med. Chem.* 101, 560–572. doi: 10.1016/j.ejmech.2015.06.049

Liang, Q., Wu, Q., Jiang, J., Duan, J. A., Wang, C., Smith, M. D., et al. (2011). Characterization of sparstolonin B, a Chinese herb-derived compound, as a selective Toll-like receptor antagonist with potent anti-inflammatory properties. *J. Biol. Chem.* 286, 26470–26479. doi: 10.1074/jbc.M111.227934

Lomize, M. A., Pogozheva, I. D., Joo, H., Mosberg, H. I., and Lomize, A. L. (2012). OPM database and PPM web server: resources for positioning of proteins in membranes. *Nucleic Acids Res.* 40, D370–D376. doi: 10.1093/nar/gkr703

Longley, D. B., and Johnston, P. G. (2005). Molecular mechanisms of drug resistance. *J. Pathol.* 205, 275–292. doi: 10.1002/path.1706

McCormick, J. W., Vogel, P. D., and Wise, J. G. (2015). Multiple drug transport pathways through human p-glycoprotein. *Biochemistry* 54, 4374–4390. doi: 10.1021/acs.biochem.5b00018

Newman, D. J., and Cragg, G. M. (2016). Natural poducts as sources of new drugs from 1981 to 2014. *J. Nat. Prod.* 79, 629–661. doi: 10.1021/acs.jnatprod.5b01055

Olsson, M. H. M., Søndergaard, C. R., Rostkowski, M., and Jensen, J. H. (2011). PROPKA3: consistent treatment of internal and surface residues in empirical pKa predictions. *J. Chem. Theory Comput.* 7, 525–537. doi: 10.1021/ct100578z

Pluchino, K. M., Hall, M. D., Goldsborough, A. S., Callaghan, R., and Gottesman, M. M. (2012). Collateral sensitivity as a strategy against cancer multidrug resistance. *Drug Resist. Updat.* 15, 98–105. doi: 10.1016/j.drup.2012.03.002

Pusztai, L., Wagner, P., Ibrahim, N., Rivera, E., Theriault, R., Booser, D., et al. (2005). Phase II study of tariquidar, a selective P-glycoprotein inhibitor, in patients with chemotherapy-resistant, advanced breast carcinoma. *Cancer* 104, 682–691. doi: 10.1002/cncr.21227

Raad, I., Terreux, R., Richomme, P., Matera, E.-L., Dumontet, C., Raynaud, J., et al. (2006). Structure-activity relationship of natural and synthetic coumarins inhibiting the multidrug transporter P-glycoprotein. *Bioorg. Med. Chem.* 14, 6979–6987. doi: 10.1016/j.bmc.2006.06.026

Ramanan, M., Sinha, S., Sudarshan, K., Aidhen, I. S., and Doble, M. (2016). Inhibition of the enzymes in the leukotriene and prostaglandin pathways in inflammation by 3-aryl isocoumarins. *Eur. J. Med. Chem.* 124, 428–434. doi: 10.1016/j.ejmech.2016.08.066

Rao, D. K., Liu, H., Ambudkar, S. V., and Mayer, M. (2014). A combination of curcumin with either gramicidin or ouabain selectively kills cells that express the multidrug resistance-linked ABCG2 transporter. *J. Biol. Chem.* 289, 31397–31410. doi: 10.1074/jbc.M114.576819

Sachs, J., Kadioglu, O., Weber, A., Mundorf, V., Betz, J., Efferth, T., et al. (2019). Selective inhibition of P-gp transporter by goniothalamin derivatives sensitizes resistant cancer cells to chemotherapy. *J. Nat. Med.* 73, 226–235. doi: 10.1007/s11418-018-1230-x

Saeed, A. (2016). Isocoumarins, miraculous natural products blessed with diverse pharmacological activities. *Eur. J. Med. Chem.* 116, 290–317. doi: 10.1016/j.ejmech.2016.03.025

Sastry, G. M., Adzhigirey, M., Day, T., Annabhimoju, R., and Sherman, W. (2013). Protein and ligand preparation: parameters, protocols, and influence on virtual screening enrichments. *J. Comput. Aid. Mol. Des.* 27, 221–234. doi: 10.1007/s10822-013-9644-8

Sim, H. M., Loh, K. Y., Yeo, W. K., Lee, C. Y., and Go, M. L. (2011). Aurones as modulators of ABCG2 and ABCB1: synthesis and structure-activity relationships. *ChemMedChem* 6, 713–724. doi: 10.1002/cmdc.201000520

Simic, M., Paunovic, N., Boric, I., Randjelovic, J., Vojnovic, S., Nikodinovic-Runic, J., et al. (2016). Functionalised isocoumarins as antifungal compounds: synthesis and biological studies. *Bioorg. Med. Chem. Lett.* 26, 235–239. doi: 10.1016/j.bmcl.2015.08.086

Sjöstedt, N., Holvikari, K., Tammela, P., and Kidron, H. (2017). Inhibition of breast cancer resistance protein and multidrug resistance associated protein 2 by natural compounds and their derivatives. *Mol. Pharma.* 14, 135–146. doi: 10.1021/acs.molpharmaceut.6b00754

Søndergaard, C. R., Olsson, M. H. M., Rostkowski, M., and Jensen, J. H. (2011). Improved treatment of ligands and coupling effects in empirical calculation and rationalization of pka values. *J. Chem. Theory Comput.* 7, 2284–2295. doi: 10.1021/ct200133y

Spengler, G., Kincses, A., Gajdács, M., and Amaral, L. (2017). New roads leading to old destinations: efflux pumps as targets to reverse multidrug resistance in bacteria. *Molecules* 22:468. doi: 10.3390/molecules22030468

Szakács, G., Paterson, J. K., Ludwig, J. A., Booth-Genthe, C., and Gottesman, M. M. (2006). Targeting multidrug resistance in cancer. *Nat. Rev. Drug. Discov.* 5, 219–234. doi: 10.1038/nrd1984

Szöllősi, D., Rose-Sperling, D., Hellmich, U. A., and Stockner, T. (2017). Comparison of mechanistic transport cycle models of ABC exporters. *Biochim. Biophys. Acta* 1860, 818–832. doi: 10.1016/j.bbamem.2017.10.028

Teixeira, T. S. P., Freitas, R. F., Abrahão, O., Devienne, K. F., Souza, L. R., de Blaber, S. I., et al. (2011). Biological evaluation and docking studies of natural isocoumarins as inhibitors for human kallikrein 5 and 7. *Bioorg. Med. Chem. Lett.* 21, 6112–6115. doi: 10.1016/j.bmcl.2011.08.044

Tillotson, G. S., and Theriault, N. (2013). New and alternative approaches to tackling antibiotic resistance. *F1000Prime Rep.* 5:51. doi: 10.12703/P5-51

Tran-Nguyen, V.-K., Prasad, R., Falson, P., and Boumendjel, A. (2017). Modulators of the efflux pump Cdr1p of *Candida albicans*: mechanisms of action and chemical features. *Curr. Med. Chem.* 24, 3242–3253. doi: 10.2174/0929867324666170523102244

Wada, S. I., Niimi, M., Niimi, K., Holmes, A. R., Monk, B. C., Cannon, R. D., et al. (2002). Candida glabrata ATP-binding cassette transporters Cdr1p and Pdh1p expressed in a *Saccharomyces cerevisiae* strain deficient in membrane transporters show phosphorylation-dependent pumping properties. *J. Biol. Chem.* 277, 46809–46821. doi: 10.1074/jbc.M207817200

Warner, E., Tobe, S. W., Andrulis, I. L., Pei, Y., Trachtenberg, J., and Skorecki, K. L. (1995). Phase I-II study of vinblastine and oral cyclosporin A in metastatic renal cell carcinoma. *Am. J. Clin. Oncol.* 18, 251–256. doi: 10.1097/00000421-199506000-00013

Weber, A., Döhl, K., Sachs, J., Nordschild, A. C. M., Schröder, D., Kulik, A., et al. (2017). Synthesis and cytotoxic activities of goniothalamins and derivatives. *Bioorg. Med. Chem.* 25, 6115–6125. doi: 10.1016/j.bmc.2017.02.004

Weis, A., Katebzadeh, K., Söderhjelm, P., Nilsson, I., and Ryde, U. (2006). Ligand affinities predicted with the MM/PBSA method: Dependence on the simulation method and the force field. *J. Med. Chem.* 49, 6596–6606. doi: 10.1021/jm0608210

Wise, J. G. (2012). Catalytic transitions in the human MDR1 P-glycoprotein drug binding sites. *Biochemistry* 51, 5125–5141. doi: 10.1021/bi300299z

Yuan, J., Wong, I. L. K., Jiang, T., Wang, S. W., Liu, T., Wen, B. J., et al. (2012). Synthesis of methylated quercetin derivatives and their reversal activities on P-gp- and BCRP-mediated multidrug resistance tumour cells. *Eur. J. Med. Chem.* 54, 413–422. doi: 10.1016/j.ejmech.2012.05.026

Zhang, G.-J., Li, B., Chen, L., Tian, Y., Liu, S.-J., Cui, H.-M., et al. (2017). Isocoumarin derivatives and monoterpene glycoside from the seeds of *Orychophragmus violaceus*. *Fitoterapia* 125, 111–116. doi: 10.1016/j.fitote.2017.12.025

Zhang, L., and Ma, S. (2010). Efflux pump inhibitors: a strategy to combat P-glycoprotein and the NorA multidrug resistance pump. *ChemMedChem* 5, 811–822. doi: 10.1002/cmdc.201000006

**Conflict of Interest Statement:** EF and AK were employed by company MicroCombiChem GmbH.

The remaining authors declare that the research was conducted in the absence of any commercial or financial relationships that could be construed as a potential conflict of interest.

# Advantages of publishing in Frontiers

**OPEN ACCESS**
Articles are free to read for greatest visibility and readership

**FAST PUBLICATION**
Around 90 days from submission to decision

**HIGH QUALITY PEER-REVIEW**
Rigorous, collaborative, and constructive peer-review

**TRANSPARENT PEER-REVIEW**
Editors and reviewers acknowledged by name on published articles

**Frontiers**
Avenue du Tribunal-Fédéral 34
1005 Lausanne | Switzerland

**Visit us:** www.frontiersin.org
**Contact us:** info@frontiersin.org | +41 21 510 17 00

**REPRODUCIBILITY OF RESEARCH**
Support open data and methods to enhance research reproducibility

**DIGITAL PUBLISHING**
Articles designed for optimal readership across devices

**FOLLOW US**
@frontiersin

**IMPACT METRICS**
Advanced article metrics track visibility across digital media

**EXTENSIVE PROMOTION**
Marketing and promotion of impactful research

**LOOP RESEARCH NETWORK**
Our network increases your article's readership